

## Computational Researches on Damage and Failure Mechanics of CFRP T-joints under Pulling Load

XUESHI MA<sup>\*</sup>, YI WANG<sup>\*\*</sup>, QINGDA YANG<sup>\*\*\*</sup>, KE XIONG<sup>\*\*\*\*</sup>

<sup>\*</sup>State Key Laboratory of Mechanics and Control of Mechanical Structures, Nanjing University of Aeronautics and Astronautics, <sup>\*\*</sup>State Key Laboratory of Mechanics and Control of Mechanical Structures, Nanjing University of Aeronautics and Astronautics, <sup>\*\*\*</sup>Department of Mechanical and Aerospace Engineering, University of Miami, <sup>\*\*\*\*</sup>State Key Laboratory of Mechanics and Control of Mechanical Structures, Nanjing University of Aeronautics and Astronautics

### ABSTRACT

Abstract As a typical case of co-cured connection of composite structural components, T-joints represent potentially a vulnerable section affecting the overall integral structure reliability and efficiency. In this study, filler cracking and interface debonding of Carbon Fiber Reinforced Polymer (CFRP) T-joints (T700/QY8911) under pulling have been numerically investigated by Augmented Finite Element Method (AFEM) [1] – Cohesive Zone Model (CZM) as well as Extended Finite Element Method (XFEM) – Cohesive Zone Model (CZM), respectively. The two numerical and experimental results have been obtained and compared, describing the major failure modes (filler crack &&& interface debond) of the typical T-joints during pulling process. In addition, load-displacement responses of the T-joints have also been separately obtained from AFEM-CZM, XFEM-CZM and experimental pulling test. Comparing with the experiment data, there are good performances for AFEM-CZM and XFEM-CZM in predicting damage paths and failure status of the T-joints. From the results, it can be demonstrated that filler crack initiation occurs at early stage of pull-off and initiates at the top region which reveals that stress generally concentrates around top region under pulling load. Upon continuous pulling, tensile load subjected to the T-joint will increase until structural ultimate failure. During the whole tensile process, filler seems to make little contribution on load-bearing for the structure. However, debond starts to appear at stiffener-to-skin interface and filler-to-skin interface at the moment of onset failure, which means load-bearing capability of the T-joint mainly depends on debond durability of the interface related to skin. Furthermore, fiber-bridge could be considered to adopt for improving load-carrying of T-joints under pull-off based on the stress status predicted by numerical analyses. Key words: CFRP T-joint; AFEM-CZM; XFEM-CZM; Pulling References [1] W. Liu, Q. D. Yang\*, et al. An efficient augmented finite element method for arbitrary cracking and crack interaction in solids. *Int. J. Numer. Meth. Engng* 2014;99:438-468. [2] Yi Sheng, Ke Xiong\*, et al. Fracture behavior of carbon fiber T-joints under tensile load (with English abstract). *Acta Materialiae Composite Sinica* 30(6), (2013) 185-90. [3] X. Ma, K. Bian, K. Xiong\*, et al. Experimental research on detection for interface debond of CFRP T-joints under tensile load. *Compos Struct* 2016;158:359-368.

# Evaluation of FEM analysis model on solar module steel structure design

Yasuhiro MAEDA\*, Yoshihito OZAWA<sup>+</sup>, and Naoto TAKEHANA<sup>^</sup>,  
Wataru TAKANO<sup>^</sup>, Yuta ONODE<sup>^</sup>

\* Graduate School of Fukushima University  
Fukushima, Fukushima, Japan  
[s1671004@ipc.fukushima-u.ac.jp](mailto:s1671004@ipc.fukushima-u.ac.jp)

<sup>+</sup>Fukushima University  
Fukushima, Fukushima, Japan  
[ozawa@sss.fukushima-u.ac.jp](mailto:ozawa@sss.fukushima-u.ac.jp)

<sup>^</sup> Okuji Kensan Co., Ltd  
Osaka, Osaka, Japan  
[n\\_takegahana@okuji.co.jp](mailto:n_takegahana@okuji.co.jp)

**Key word:** FEM Analysis, Photovoltaic System, Support Structure Design, Buckling,

**Abstract.** In recent years, accidents have frequently occurred under the rapid spread of photovoltaic power generation system in Japan. The support structures of the system were deformed or destroyed due to strong wind or heavy snow when the support structure was designed improperly. The main cause is considered to be a mistake in the structural calculation model, especially the model for joint parts. In this study, we conducted a full-scale experiment simulating wind load and snow load on photovoltaic power generation system, furthermore, it was examined that the joint parts model proposed by the Authors is valid for safety design of the support structure. The buckling element was modeled with thin shell element and some reports on the deformation state until buckling were precisely shown from the results of elastoplastic analysis.

## 1 INTRODUCTION

In recent years, the use of renewable energy has been dramatically increased in each country. Especially "photovoltaic power generation system" (hereinafter called "PV system") has been attracting a wide attention around the world, and the scale of market is expanding continuously. In Japan, the introduction of PV system is beginning to be advanced, and then the number of large-scale PV system has rapidly increased because the Feed-in Tariff Law for Renewable Electric Energy (Fit Low) takes effect from July 1, 2012. In order to precede massive introduction of PV system in Japan, it is considered that there are found to be two problems as the current condition. The first is that the power generation cost is higher than that of the other major power supply. The second is that the structural accidents are frequently occurring along with the rapid spread of PV system. In order to solve these problems, it is an urgent issue to realize the safe and reasonable support structure. In addition, in the PV system, the support structures of the PV system were deformed or destroyed due to strong wind or heavy snow when the support structure

was designed improperly [1]. The main cause of inappropriate design is considered to be a mistake in the structural calculation model, especially the model for joint parts.

In this study, we compare the experimental results with the analysis results simulating wind load and snow load applied to the support structure of PV system which is composed of 1.6 mm in thickness thin steel plates as main structural elements [2]. Furthermore, we will examine that the joint parts model proposed by the Authors is valid for safely design of the support structure. The buckling element is modeled with thin shell elements and some reports on the process of buckling are precisely shown from the results of elastoplastic analysis.

## 2 LOADING TEST

### 2.1 Experimental Procedure

The support structure equipped with the solar cell module of four lines and two columns was treated as one unit ground installation of PV system. Then, two units to be simulated were arranged side by side as a specimen. The outline of the specimen is shown in Fig. 1. Table 1 shows the cross-sectional shape of the support structure elements used in the experiments, and Table 2 shows the conditions of wind load experiment [3, 4].

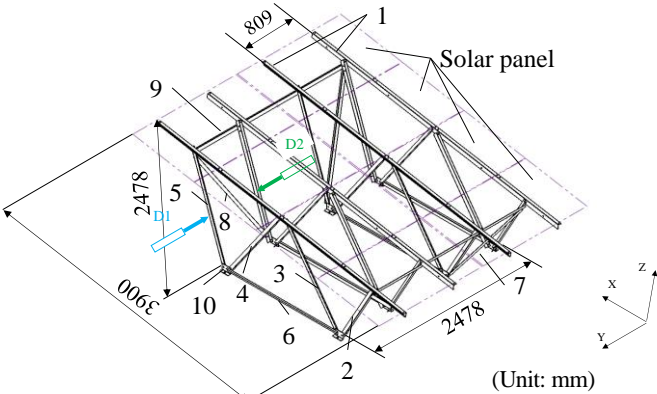


Fig. 1 Support structure of PV system

Table1 Cross-sectional shape of elements

	Cross-section shape [mm]
1	L-66.2×45×11.6×1.6
2	L-45×45×1.6
3	L-45×45×1.6
4	L-45×45×1.6
5	L-45×45×1.6
6	L-45×25×1.6
7	L-45×25×1.6
8	L-45×25×1.6
9	L-45×25×1.6
10	L-85×45×4.5

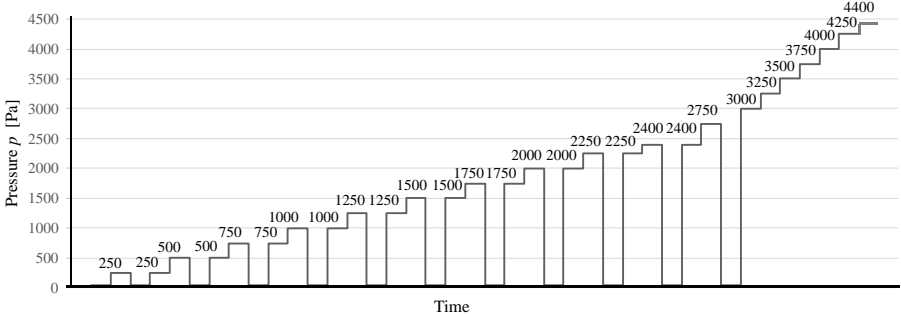


Fig. 2 Pressure step applied to the solar panels

Table 2 Condition of wind load experiment

Load	Design condition	Module surface inclination angle	Calculation method
Wind load	Design standard wind speed 38 m/s Ground roughness classification III	20 degrees	$W/A=C_f \times q=1.25 \times 1540=1925 \text{ Pa}$

In this experiment, we carried out an experiment procedure in order to simulate the positive pressure of the wind load (pressure to depress the PV system) by using a dynamic wind pressure chamber. The pressure step applied to the solar panels is shown in Fig. 2. Pressure  $p$  was applied until the specimen destroyed, and the evaluation of strength, deformation and fracture were conducted for the specimen. In the displacement measurement, since the displacement sensor would be damaged due to the breakage of the specimen, the measurement was continued until the final stage only for D1, but for D2 it was stopped at 2000 Pa.

### 2.3 Experimental result

Figure 3 shows the relationship between the pressure and the displacement at sensor position D1 and D2 shown in Fig. 1. The displacements of pillar element No. 5 from sensor positions D1 have minus value, opposite sign to data from D2 shown in Fig. 3. For pillar element No. 5, it was observed that the element deformed toward inside from visual observation. The relationship

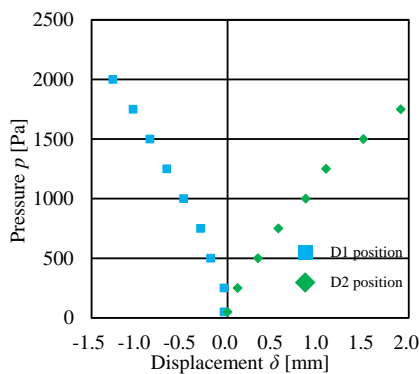


Fig. 3 Relationship between pressure and displacement

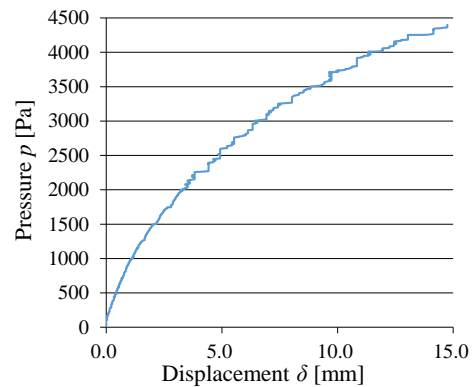


Fig. 4 Relationship between pressure and displacement in position of D3

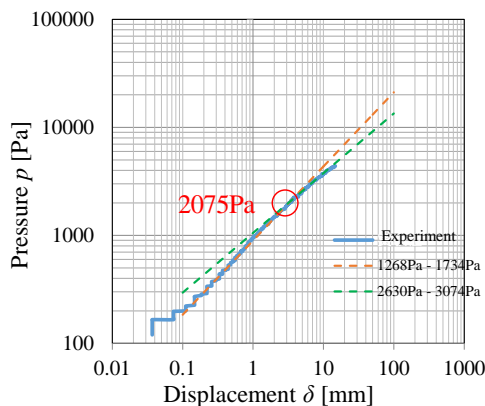


Fig. 5 Relationship between pressure and displacement with logarithm scale of both axis



Fig. 6 Destruction situation of specimen

between the pressure and the displacement up to the destroyed pressure at the position D1 is shown in Fig. 4. In order to evaluate the kink point of the deformation of support structure easily, Fig.5 shows for relationship between the pressure and displacement in logarithm scale of both axes. The point of intersection of the dotted lines indicated by the red circle in Fig. 5 was taken as the inflection point, and this stress level of 2075 Pa could be taken as the kink point of deformation of the pillar element No. 5. After continuing pressure, the specimen was suppressed from 4250 Pa to 4500 Pa, and then the pillar element No. 4 buckled and the specimen of PV system was destroyed as shown in Fig. 6.

In experiments for simulating snow load, experiments were conducted by using same specimens with different tilt angles of array surface. In the case of snow load, the pillar element No. 5 buckled and the breaking pressure was 5038 Pa.

### 3 FINITE ELEMENT METHOD

FEM analysis was carried out in order to examine the important effect of the joint parts model on the destruction accident, and the buckling process of the pillar elements in the experiment.

The mechanical properties used in the analysis are shown in Table 3. In the plastic range, the relationship between the stress and plastic strain is bilinear due to the relation to the yield stress and the tensile strength.

Table 3 Mechanical property of SS400

	Young's modulus [MPa]	Poisson's ratio	Yield stress [MPa]	Tensile strength [MPa]	Elongation
Analysis model	205000	0.3	235	400	33%

#### 3.1.1 Three-dimensional elasticity analysis with beam element

At the joint parts of the support structure with the thin steel plate, the centroid axis of an element with L-shape deviates from that of an adjacent element. Accident occurred due to the lack of conscious on these mismatches. Especially it is important to simulate real joint parts model in FEM analysis by using beam elements. We proposed the joint parts model as follows and examined whether it is effective for the safety support structure design.

The analytical model used in analysis is a three-dimensional elastic beam element model. In order to simulate the joint parts of the actual structure, the joint nodes between two adjacent elements were not set at the along the same line, and the centroids of joint elements remain apart each other. Furthermore, we proposed a model with eccentricity that does not constrain the rotating motion only the bolt axis (Fig. 7 (a)) <sup>[5]</sup>. For the comparison, we also analyzed the non-eccentricity model (Fig. 7 (b)) simulated the joint parts node rigidity. For the initial conditions of the analysis, when simulating a wind load, a uniformly distributed load in the perpendicular direction acts on the element No. 1. And when simulating a snow load, an equally distributed load acts on the element No. 1 however in the vertical direction to the horizon.

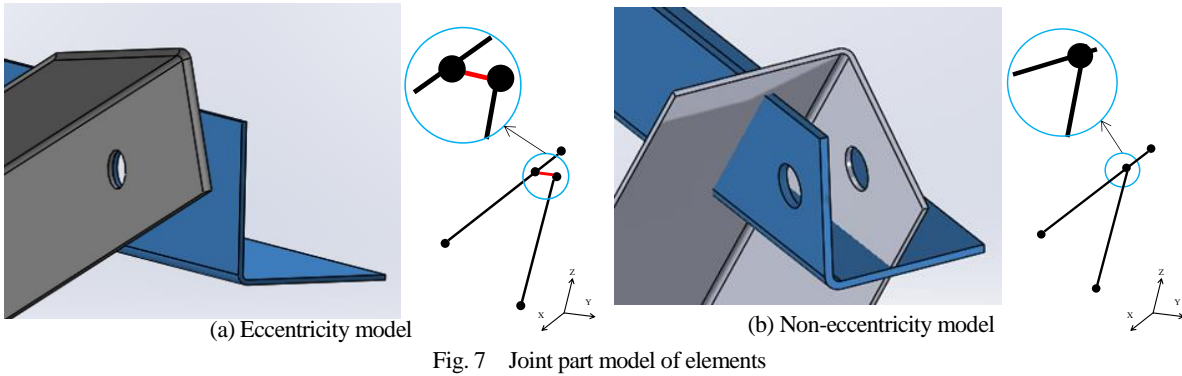


Fig. 7 Joint part model of elements

### 3.1.2 The results of analysis

Figure 8 shows the relationship between the pressure and the displacement at the same measurement position of the experiment shown in Fig.1. Figure 9 shows the deformation behavior by the use of the eccentricity model and the non-eccentricity model, when the wind load is applied. From Fig. 8, in the eccentricity model, the displacement of the pillar elements at D1 position become large as increasing the pressure, the displacement at D1 takes smaller value than that at D2, and with a opposite sign against that at D2. In the non-eccentricity model, the behavior at D1 is inverse relation to the eccentricity model and the displacement at D2 indicates nearly zero. In Fig. 9, the pillar elements No. 5 in the eccentricity model was deformed toward inside, and in the case of the non-eccentricity model, the deformation of the element tilts to one side. The same tendency was also observed for the experiments in the case of snow load.

For the element which experienced buckling in the experiment, the load level is coincided with

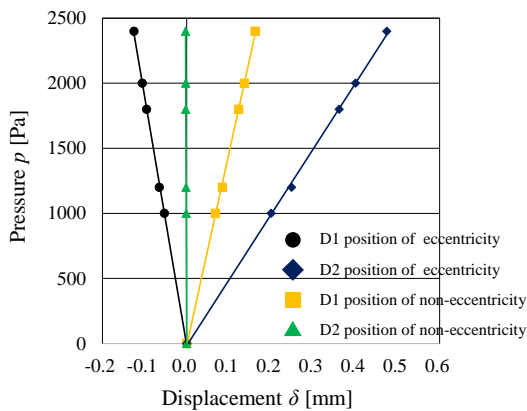


Fig. 8 Relationship between y direction pressure and displacement

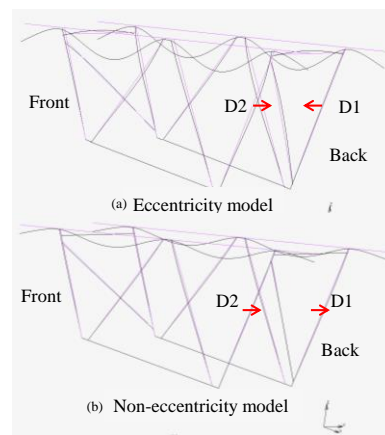


Fig. 9 Deformation diagram

Table 4 Analytical values of axial force and bending moment

		Axial force [N]	Bending moment [N·m]
Wind load	Eccentricity model	-1982.1	8173.6
	Non-eccentricity model	-1986.0	-867.4
Snow Load	Eccentricity model	-1471.8	-9769.6
	Non-eccentricity model	-1256.9	1035.1

the points where the axial force and the bending moment are maximized in the analysis results. Table 4 shows analytical values of axial force and bending moment for the buckled element in the eccentricity model and non-eccentricity mode. From Table 4, it can be seen that the bending moment takes on very large value in the eccentricity model. It can be seen from Figs. 8 and 9 that the bending deformation due to twisting of the joint part can be expressed in the eccentricity model.

**3.2 Three-Dimensional Shell Element Elastoplastic Analysis**

**3.2.1 Shell Element Finite Element Model**

In the experiment, the pillar elements buckled and the support structure was suddenly destroyed. Therefore, it is important to understand the buckling process of the structure and the behavior of a buckled element. In this Chapter, for the purpose to examine the deformation state until the pillar element is buckling, the elastoplastic analysis was conducted for a pillar element which buckled at onset of the support structure destruction.

Let us focus on the pillar element No. 4 buckled at first in the experiment for wind pressure. Figure 10 shows the applied load and the boundary conditions of the model. The model was analyzed with a bilinear thin-shell element. The displacement of lower end was completely constrained at all nodes of the bottom end, and that of upper end was set as a free end. The load was applied to the bolt circle center that is eccentric from the centroid. The axial force P obtained in the analytical result of Section 3.1.2 was applied at the free end as a load.

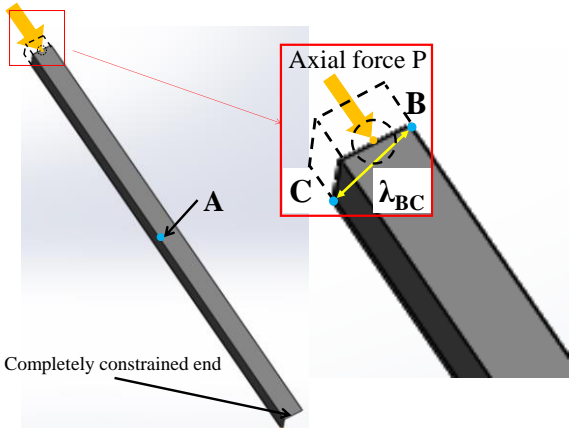


Fig. 10 Analysis model of pillar element No. 4

**3.2.2 Analysis Results**

Elastoplastic analysis was conducted with the pillar elements (No. 2 to 5). The pillar element No. 4 buckled at first in the analytical simulation as well as in the experiment. Therefore, the analytical result of the pillar element No. 4 will be precisely described below.

Figure 11 shows the relationship between the pressure and the displacement at the point A, which

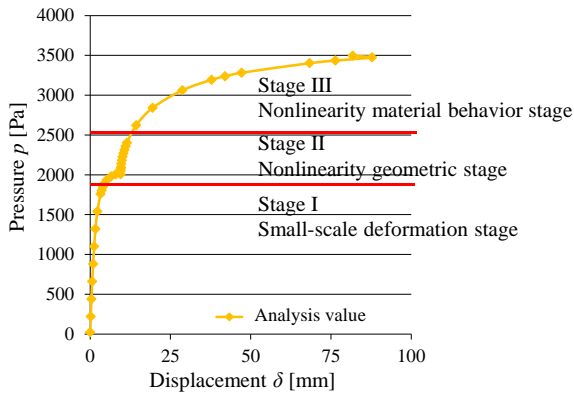


Fig. 11 Relationship between pressure and displacement (shell element model)

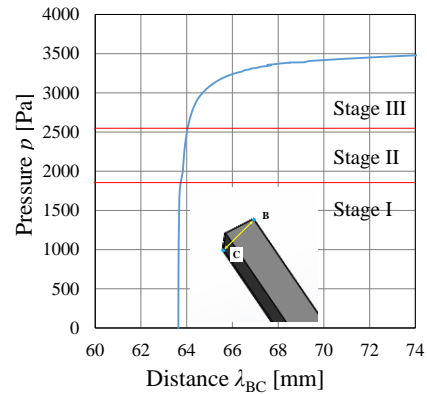


Fig. 12 Relationship between pressure and distance between B and C

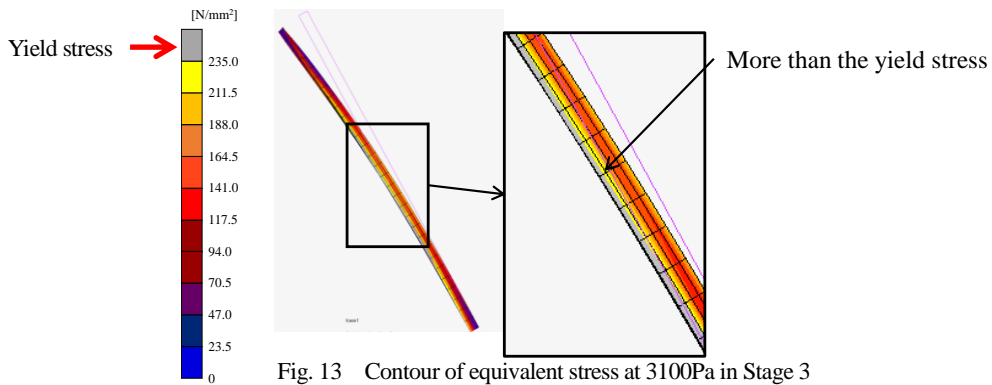


Fig. 13 Contour of equivalent stress at 3100Pa in Stage 3

is the center in the length direction of the element shown in Fig. 10. By examining the results for the kink point appeared in Fig. 11, the deformation state until the structure buckling was divided into three stages. In the Stage I, as a shown Fig. 11, it is a linear relationship between pressure and displacement is observed and in the elastic deformation. Therefore, it was defined as a small-scale deformation stage of the pillar element. The Stage II is a nonlinear deformation stage from in Fig. 11. It is seen that there is a kink point of deformation behavior near 2000Pa. From Fig. 12, the distance between two points B and C  $\lambda_{BC}$  starts to increase, so that the L-shaped of cross section is beginning to be deformed into flat shape in this stage. But the stress of the pillar element was found to be less than the yield stress. This is considered to be caused the reduction in the geometrical rigidity after the cross-sectional shape changes. Therefore, the Stage II was defined as a geometrical nonlinearity deformation stage. In the final Stage, the strong nonlinear behavior was observed as shown in Fig. 11. From the stress distribution of the element in Fig. 13, since the stress in the cross section of the pillar element is equal to be the yield stress or higher than it, the Stage III was defined as a nonlinear material behavior stage and buckling occur.

## 4 DISCUSSION

### 4.1 Evaluation of Joint Part Model of Beam Element Model

In the eccentricity model, the bending deformation of the pillar elements with the geometrical eccentricity at the joint part could be described with the sufficient accuracy correspond to the actual model. In order to evaluate the buckling load of the element No. 4, the procedure is shown in as follows;

The compressive stress of the element was calculated from the axial force and the bending moment of the analytical result by using the Eq. (1) ;

$$\sigma_T = P_y/A + M_y/Z \quad (1)$$

where  $\sigma_T$  is the vertical compressive stress [Pa],  $P_y$  is the axial force [N],  $A$  is sectional area of element [ $\text{mm}^2$ ],  $M_y$  is the bending moment [N·mm] and  $Z$  is section modulus [ $\text{mm}^3$ ]. The compressive load is calculated by multiplying the compressive stress  $\sigma_T$  by the cross-sectional area  $A$ , and then the relationship between the compressive load of pillar element  $\sigma_T A$  and the experimental pressure  $p$  is shown in Figs. 14 (a) wind load and (b) snow load. The buckling load of the element No. 4 and No. 5 in Table 1 is calculated by using the Eq. (2) ;

$$P_{cr} = \pi^2 EI/l^2 \quad (2)$$

where  $P_{cr}$  is Euler buckling load [N],  $E$  is young's modulus [MPa],  $I$  is cross-sectional secondary moment [ $\text{mm}^4$ ] and  $l$  is the length of the beam [mm]. The buckling load of the element No. 4 and No. 5 is shown by the red line in Fig. 14 (a) and (b), respectively. It was seen that the buckling occurs at the intersection of the red line to the straight lines of the analytical results in the

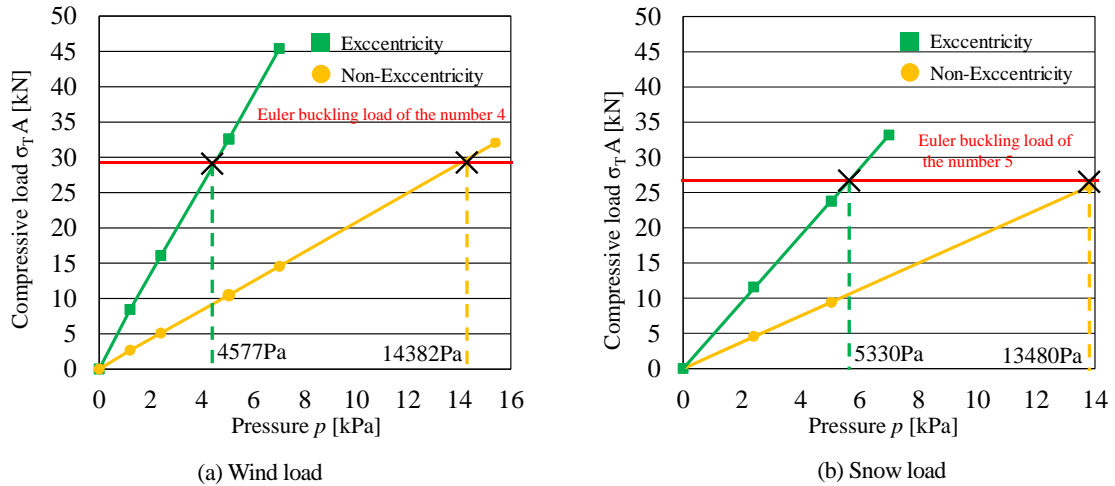


Fig. 14 Relationship between pressure and compressive load

Table 5 Comparison of the buckling stress between experimental results and analytical results

	Experiment	Eccentricity model	Non-Eccentricity model
Wind load [Pa]	4400	4577	14382
Snow load [Pa]	5038	5330	13480

eccentricity model and in the non-eccentricity model. Table 5 shows the comparison of the buckling loads in the experiment with the loads calculated from the simulation for two models. For the case of wind load and snow load, the buckling load with the eccentricity model shows good agreement with the experiments. The bending moment value in Table 4 is large in the eccentricity model and then, the bending deformations due to the twist of the joint part are well described in the analysis. Therefore, in the evaluation of buckling load, it was found that the simulation results that the eccentricity model shows better agreement with the experiments than the results with the non-eccentricity model.

**4.2 Comparison between analysis results and experimental results deformation of a buckling element**

Figure 15 shows comparison of the relationship between the pressure and the displacement in the dynamic wind pressure experiment and in the analysis where the buckling behavior of the pillar element is defined as three stages as in Fig. 11. From Fig. 15, the deformation behavior of the pillar element in the experiment is not in good agreement with in the analysis, however the kink point in the experiment shown in Fig. 11 is indicated about at the starting point of the geometrical nonlinear in the stage 2 of analysis. Although there is slight difference from the boundary conditions of the pillar element in the analysis, it means good suggestion for understanding a kink point observed in the deformation state. For better understanding these deformation behaviors, it is important to set exact boundary conditions of experiment in the further analysis.

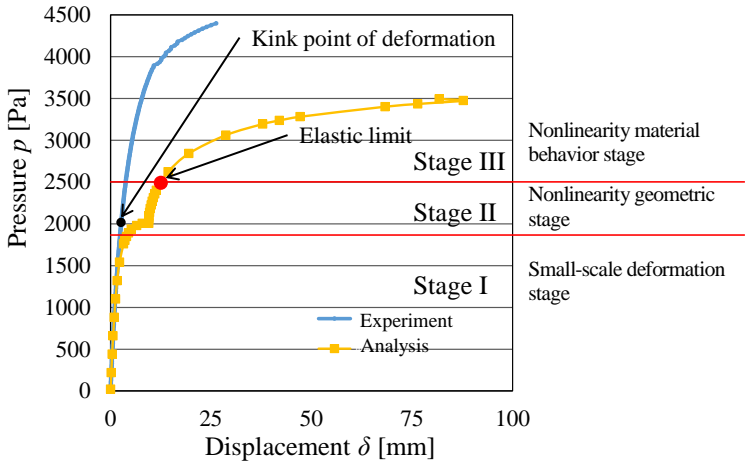


Fig. 15 Comparison of relationship between displacement and pressure in experiment and analysis

**5 CONCLUSIONS**

In order to design the strong and high rigidity support structure of PV system by the thin plate, we analyzed two joint part models in the FEM analysis with three dimensional elastic beam elements, and examined the structure deformation behavior and buckling load from the experiment result and the analytical result. In addition, in order to clarify the deformation behavior

until buckling of the pillar element, we conducted the elastoplastic analysis for the pillar element modeled with the thin shell element. The obtained results in this study are summarized as follows.

- i. From the deformation behavior and the evaluation of the buckling load, the FEM analysis with the eccentric model for the joint part in the actual structure successfully applied to be safety design of PV system.
- ii. The deformation behavior until buckling was clarified from the results of elastoplastic analysis of pillar element model with thin shell element. From this result, the kink point in the experiment was seen to be caused due to the effect of geometrical nonlinearity.
- iii. It was found that the kink point in the experiment is indicated about at the starting point of the geometrical nonlinear in the stage II of analysis. Although there is slight difference from the boundary conditions of the pillar element in the analysis, it means good suggestion for understanding a kink point observed in the deformation state.

In our future work, it might be required to consider not only the axial force but also the influence of the transvers force. In order to examine the stress distribution and deformation state of the entire support structure precisely, we will model the actual support structure by using three-dimensional shell elements and conduct elastoplastic analysis. By conducting a revised analysis, an analytical model which clarifies the buckling load and incorporate it into the whole model could be proposed for safe support structure of PV system.

## **ACKNOWLEDGMENTS**

This paper is based on results obtained from a project commissioned by the New Energy and Industrial Technology Development Organization (NEDO).

## **REFERENCES**

- [1] Takamori, K. Somekawa, D. Okuji, M. and Uematsu, Y. WIND RESISTANCE TEST OF A PHOTOVOLTAIC SYSTEM INSTALLED ON METAL ROOF. Proc. Symp. Wind Engng. 24th. (2016) 319-324 (in Japanese)
- [2] AIJ Design. Standard for Steel Structures Based on Allowable Stress Concept. (2017)
- [3] Somekawa, D. Koizumi, T. Taniguchi, T. and Taniike Y. WIND LOADS ACTING ON THE PHOTOVOLTAIC PANELS ARRAYED NEAR GROUND. Proc. Symp. Wind Engng. 22nd. (2012) 157-160 (in Japanese)
- [4] Somekawa, D. Koizumi, T. Taniguchi, T. and Taniike Y. WIND LOADS ACTING ON PV PANELS AND SUPPORT STRUCTURES WITH VARIOUS LAYOUTS. Proc. The Eighth Asia-Pac. Conf. Wind. Engng. (2013) 235-242
- [5] Mtsuura, M. Hatanaka, A. and Yamaguchi, T. Study on load carrying capacity of a small power transmission tower made of angle steel members. J. Struct. Engng. Vol. 58A., (2012) 50-61

## **Atomic Mixed-Mode Cohesive-Zone Laws of Hydrogen-Embrittled Grain Boundaries in Crystalline Metals via Nanoscale Field Projection Method**

Nghia Trong MAI<sup>\*</sup>, Vinh Phu NGUYEN<sup>\*\*</sup>, Phuoc Quang PHI<sup>\*\*\*</sup>, Seung Tae CHOI<sup>\*\*\*\*</sup>

<sup>\*</sup>Chung-Ang University, <sup>\*\*</sup>Chung-Ang University, <sup>\*\*\*</sup>Chung-Ang University, <sup>\*\*\*\*</sup>Chung-Ang University

### **ABSTRACT**

Grain boundaries of polycrystalline materials can be one of the easiest paths for crack propagations, since atoms at grain boundaries experience less ordered interatomic interactions with neighboring atoms than those in homogeneous crystalline materials. Furthermore, thermodynamically, impurity atoms such as hydrogen, chrome, nickel, copper, and carbon atoms in polycrystalline iron, tend to segregate near grain boundaries, which may cause the degradation of mechanical properties and accelerate intergranular fracture. Recently, a field projection method (FPM) was established to extract the crack-tip cohesive zone law (CZL) from far field data using J- and M-based mutual integrals between the physical field and numerical auxiliary field. In this study, we extend the universality of the FPM for atomic mixed-mode CZL of a crack tip on an interface between two anisotropic solids by using an analytical auxiliary field, as well as the effective use of atomic-level J- and M-based mutual integrals. This augmented FPM has no convergence problems and does not need to find a numerical helper every time, depending on the given problem associated with finite elements solution. The atomic-level field projection is applied to characterize a cohesive crack-tip naturally arising from atomic deformation field, which can be obtained from molecular dynamic simulation of decohesion along the hydrogen-segregated grain boundaries in nickel. Our FPM results enable the development of a qualitative picture of the traction-separation relations and functional form and parameters for a cohesive surface constitutive model consisting of separate normal and shear traction-separation relations.

## Automatic Isogeometric Models Generation from Standard B-REP Models – Application to Reduced Order Modeling

Tristan MAQUART<sup>\*</sup>, Thomas Elguedj<sup>\*\*</sup>, Anthony Gravouil<sup>\*\*\*</sup>, Michel Rochette<sup>\*\*\*\*</sup>

<sup>\*</sup>Université de Lyon, CNRS, INSA-Lyon, LaMCoS UMR5259, France; ANSYS Research & Development, France,  
<sup>\*\*</sup>Université de Lyon, CNRS, INSA-Lyon, LaMCoS UMR5259, France, <sup>\*\*\*</sup>Université de Lyon, CNRS, INSA-Lyon,  
LaMCoS UMR5259, France, <sup>\*\*\*\*</sup>ANSYS Research & Development, France

### ABSTRACT

Key Words: Isogeometric Analysis, NURBS, Global Parameterization, Cross Fields, Parametric geometry, Multiparametric, Singular value decomposition. We present an effective framework to automatically construct trivariate B-spline models of complicated geometry and arbitrary topology required for most mechanical applications and parametric studies. The input is a triangulation of the solid 3D model's boundary provided from B-Rep CAD models or scanned geometry. The boundary surface is decomposed into a set of cuboids [1], approximating the input boundary mesh. Due to its highly regular and trivariate structure, the polycube is suitable for serving as the canonical domain of the volume parameterization required for trivariate NURBS construction. The polycube's nodes and arcs decompose the input model globally into hexahedral domains. Using cross fields and aligned global parameterization [2], optimal compatible trivariate B-spline are reconstructed. For different parametric instances with the same topology (including sharp features) but different geometries, this method allows to have the same representation: i.e., meshes with the same topology (i.e., isotopological meshes : same mesh connectivity) where each point on a mesh have a homologue into another mesh (with possibly homologue sharp features). This method is used to build reduced order models (ROMs) [3]. Real time simulations remain intractable despite the impressive increasing computing power, we present an approach for building geometric multiparametric isogeometric models suitable for ROM construction. The efficiency and the robustness of the proposed approach are illustrated by solving mechanical equations given several geometric parameters. REFERENCES [1] H. Al-Akhras, T. Elguedj, A. Gravouil, and M. Rochette, "3D Isogeometric Analysis Suitable Trivariate NURBS Models from Standard B-Rep CAD", *Computer Methods in Applied Mechanics and Engineering*, doi:10.1016/j.cma.2016.04.028, 2016. [2] Marcel Campen and Leif Kobbelt. "Quad layout embedding via aligned parameterization". In *Computer Graphics Forum*, volume 33, pages 69-81. Wiley Online Library, 2014. [3] Ye Lu, Nawfal Blal, Anthony Gravouil, Multi-parametric space-time computational vademecum for parametric studies: Application to real time welding simulations, In *Finite Elements in Analysis and Design*, Volume 139, 2018, Pages 62-72, ISSN 0168-874X,

## Numerical Modeling of Pull-Out-Tests Using Finite Elements

YADIAN MENENDEZ ROSALES\*, RAUL DURAND\*\*

\*UNIVERSITY OF BRASILIA, \*\*UNIVERSITY OF BRASILIA

### ABSTRACT

During the last decades, several researches have been studying the phenomenon of steel-concrete bond with the purpose of establishing parameters that express the evolution of the bond stress as a function of the rebar slip. This information is useful to develop constitutive models and to obtain material parameters needed for numerical predictions of reinforced concrete structures. In this regard, the pull-out test is one of the experimental tests widely used for these purposes. This work presents a contact model for the mechanical behavior of steel-concrete interface. This model is based on the one proposed by CEB-FIP MODEL CODE (2010) and the plasticity theory. The model was implemented in a finite element code and tested against a battery of experimental pull-out tests in cylindrical specimens of 100, 150 and 200 mm diameter and 200 mm height combined with different steel bars with diameters of 8, 10 and 12 mm and anchorage length of 100 mm. In the finite element model, the rebars were simulated using a novel semi-embedded approach which allows rod elements to cross solid (concrete) elements and, thanks to the contact model, predict rebar slip and contact failure. After the analyses, it was observed that the proposed contact model successfully reproduced the main characteristics of the pull-out-test. Numerical results, as for example load-displacement curves including softening, were in good agreement when compared with experimental results.

## Nonlinear Analysis of Squeal and Whirl Mode Instabilities

Alexy MERCIER<sup>\*</sup>, Louis JEZEQUEL<sup>\*\*</sup>, Sébastien BESSET<sup>\*\*\*</sup>, Abdelbasset HAMDANI<sup>\*\*\*\*</sup>,  
Jean-Frédéric DIEBOLD<sup>\*\*\*\*\*</sup>

<sup>\*</sup>LTDS/Safran Landing Systems, <sup>\*\*</sup>LTDS, <sup>\*\*\*</sup>LTDS, <sup>\*\*\*\*</sup>Safran Landing Systems, <sup>\*\*\*\*\*</sup>Safran Landing Systems

### ABSTRACT

The &quot;Whirl&quot; and &quot;Squeal&quot; modes generate significant vibrations on an aircraft braking system. These vibrations strongly damage the brake structure and generate acoustic discomfort. Nowadays, several types of finite element (FE) models have been developed. In order to test and simply reproduce some important physics in these models (FE), analytical and phenomenological models have been developed. The ultimate goal is to have a tool to model as faithfully as possible braking dynamics. To accelerate computation time, model reductions such as synthesis or double modal synthesis are used. Finally, to ensure the convergence of vibration amplitudes, the major sources of nonlinearities have been identified and integrated into the model (FE). These nonlinearities are located at the different friction interfaces of the system and in the hydro-mechanical part.

## High-Fidelity Seismic Response Analysis of a Nuclear Power Plant Using K computer

Tomoshi MIYAMURA\*, Shinobu YOSHIMURA\*\*, Tomonori YAMADA\*\*\*

\*Nihon University, \*\*University of Tokyo, \*\*\*University of Tokyo

### ABSTRACT

In the earthquake resistant design of a nuclear power plant, mass-spring models are usually used to simulate structural behavior. However, seismic responses of details of the plant cannot be simulated using such macro model. A high-fidelity 3D finite element model of integrated boiling water reactor and reactor building of the Unit 1 at the Fukushima Daiichi Nuclear Power Plants was constructed [1]. In the present study, the results of the seismic response analyses for the Tohoku Off-Pacific Coast Earthquake of 9.0 Mw using the analysis model are presented. The analyses are conducted using a parallel finite element structural analysis code, ADVENTURE\_Solid 2.0 [2] implemented on the K computer that is one of the fastest supercomputers in the world. The finite element model is made of tetrahedral solid elements. Reactor building, pressure boundary including primary containment vessel, suppression chamber, bent pipes, and reactor pressure vessel are modeled precisely and integrated. Total DOFs of the mesh using linear elements (linear element model) is approximately two hundred million, and that of the mesh using quadratic elements (quadratic element model) is approximately fifteen hundred million. The linear element model is verified using the numerical results of the quadratic element model. The elastic seismic response analysis for 65 seconds is conducted using the linear element model. The numerical results including maximum acceleration and maximum stress at a number of points, and floor response spectra (acceleration response spectra) are compared with those of the conventional seismic response analysis using a lumped-mass model [3]. Computation performance of a parallel solution algorithm, that is, the hierarchical domain decomposition method with balancing domain decomposition preconditioner is evaluated on the K computer. Methods of data handling of huge output data such as an offline rendering technique and automatic generation of graphs are presented. A preliminary elastic-plastic seismic response analysis for 55 seconds is also conducted. Steel material of main pressure boundary components are supposed to be elastic-plastic using the von Mises yield criterion. The numerical results and computation performance are presented. References [1] S. Yoshimura, T. Yamada, H. Kawai, T. Miyamura, M. Ogino, and R. Shioya, Petascale coupled simulations of real world's complex structures, IACM Expression, No.37, pp. 9-13, 2015. [2] ADVENTURE project, <http://adventure.sys.t.u-tokyo.ac.jp/> [3] TEPCO report on seismic response analysis results of building and important components and piping in Fukushima Daiichi Nuclear Power Stations utilizing observed data during Tohoku Off-Pacific Coast Earthquake in 2011, 2011 [in Japanese].

## Similarities and Differences between the Thick Level Set and Cohesive Models for Quasi-brittle Failure

Nicolas MOES\*

\*Ecole Centrale de Nantes

### ABSTRACT

Three topics will be summarized in the presentation. They correspond to the three papers listed below. The first topic deals with the equivalence of the cohesive zone model (CZM) and the Thick Level Set approach to fracture (TLS). The TLS is a continuum damage model in which the damage gradient is bounded. In the 1D setting (bar under tension), TLS and CZM parameters may be chosen so that they model the same global behavior. In the 2D setting, the TLS generalizes the CZM approach and offers more capabilities (no extra equations needed for crack growth direction, stress triaxiality taken into account and crack branching made possible). Based on the above equivalence, the TLS parameters have been identified to fit experimental data of size and shape effects. Even though it is continuum damage based, the TLS gives a great capability in fitting the experiments on a large spectrum of size and shapes. Finally, a second version of the TLS (TLS V2), unifies continuum damage and cohesive zone within a unique model. Damage is both surfacic and volumic. The TLS V2 allows to get high numerical performances even for long process zones. References. - Parrilla Gómez, A., Moës, N., & Stolz, C. (2015). Comparison between thick level set (TLS) and cohesive zone models. *Advanced Modeling and Simulation in Engineering Sciences*, 2(1), 18. <http://doi.org/10.1186/s40323-015-0041-9> - Parrilla Gómez, A., Stolz, C., Moës, N., Grégoire, D., & Pijaudier-Cabot, G. (2017). On the capability of the Thick Level Set (TLS) damage model to fit experimental data of size and shape effects. *Engineering Fracture Mechanics*, 184, 75–87. <http://doi.org/10.1016/j.engfracmech.2017.07.014> - B. Le, N. Moës & G. Legrain (2018), Coupling damage and cohesive zone models with the Thick Level Set approach to fracture *Journal: Engineering Fracture Mechanics*, *Engineering Fracture Mechanics*, to appear.

## **A Magnification-based Multi-asperity (MBMA) Model of Rough Contact Where the Greenwood-Williamson and Persson Theories Meet**

Benben Ma<sup>\*</sup>, Xu Guo<sup>\*\*</sup>, Yichao Zhu<sup>\*\*\*</sup>

<sup>\*</sup>Dalian University of Technology, <sup>\*\*</sup>Dalian University of Technology, <sup>\*\*\*</sup>Dalian University of Technology

### **ABSTRACT**

Contact analysis without adhesion is still a challenging problem, mainly owing to the multiscale and self-fractal characteristics of rough surfaces. Up to now, theories for analyzing contact behavior of rough surfaces in literature can be generally categorized into two groups: the asperity-based Hertz contact models initiated by Greenwood and Williamson (G-W model), which is shown more accurate under small indentation distance, and the magnification-based pressure diffusion theory initiated by Persson, which is shown to work well under full contact conditions. The aim of this paper is to propose a theoretical model that can effectively formulate the contact status of rough surfaces during the entire compression process. This is achieved by integrating the idea of magnification, or evolving resolution into an asperity representation of rough surfaces, and a magnification-based multi-asperity model is thus established. In the derived model, the originally complex contact problem is decomposed into a family of sub-problems each defined on a morphologically simpler contact islands. Benefiting from the explicit results given by Greenwood and Williamson, the proposed method is relatively easy for numerical implementation. Compared to other G-W type models, the proposed method has especially shown its strength in the computation of the contact area. Moreover, the G-W and Persson models are found well connected by the proposed approach. For its validation, the proposed model is well compared with existing theoretical, numerical and experimental results. In particular, the proposed model has shown its excellency through comparison with representative theoretical, numerical and experimental data compiled in the "contact challenge" test by Mueser et al.

## Comparative Study on Seismic Design Method of Utility Tunnel

Hongmin Ma\*, Jianxun Ma†

\* Ph.D.Student

99 Yanxiang Road

Xi'an, Shaanxi, China

Email address: mahongmin@stu.xjtu.edu.cn

† Professor

99 Yanxiang Road

Xi'an, Shaanxi, China

Email address: matumu@163.com

**Key words:** Response Displacement Method, Response Acceleration Method, Time History Method, Single Deck Utility Tunnel, Double Deck Utility Tunnel.

**Summary.** *The response displacement method and the response acceleration method were studied and summarized from the principle. Two kinds of sectional utility tunnel models of single deck utility tunnel and double deck utility tunnel are established respectively. Then time history method, response displacement method and response acceleration method were used to carry out the seismic calculation of the two models. In the calculation, the universality of the calculation method was analyzed by changing the 3 types of factors, such as the seismic type and peak acceleration of seismic waves and the stiffness of the structure. The calculation results shows that the two pseudo-static methods all have high accuracy, but the response acceleration method is more accurate. By comparing the calculation results of two different cross-section forms of the utility tunnel, it can be found that the calculation results are the same as the whole, but the specific calculation results are different. Therefore, it should be carried out in accordance with the form of the structure and the factors considered in the seismic calculation of the utility tunnel. Detailed calculation and analysis is needed.*

### 1 INTRODUCTION

With the development of urbanization, people began to develop and utilize the underground space vigorously, and the underground structure engineering technology has also been greatly developed<sup>[1]</sup>. In 1995 Kobe earthquake<sup>[2]</sup> and the 1999 Chi Chi earthquake in Taiwan<sup>[3]</sup> have caused irreparable damage in a large number of subway stations, tunnels and utility tunnels, then raised the seismic research of underground structure in the world. At present, the commonly used pseudo static methods for seismic response analysis of underground structures include seismic

coefficient theory, free field deformation method, soil structure interaction coefficient method, response displacement method (RDM) [4-6], response acceleration method (RAM) [7,8], pushover method and integral response displacement method. Through the previous theoretical research, it is found that the response displacement method (RDM) and the response acceleration method (RAM) are more suitable for the seismic calculation of the utility tunnel. In this paper, the finite element software ABAQUS is used to establish a single deck utility tunnel and double deck utility tunnel model, which are calculated by RDM, RAM and time history method (THM) respectively. The error analysis of the two methods of RDM and RAM is carried out. Finally, based on the calculation results, the recommended method for seismic calculation of utility tunnel is given.

## 2 THE PRINCIPLE OF RDM AND RAM

### 2.1 A brief introduction to RDM

In 1970s, scholars from various countries research underground structural response characteristics under earthquake by field observation, experimental study and theoretical analysis. The results show that the underground structural vibration together with the surrounding soil under earthquake, structural displacement and acceleration are basically the same as the surrounding underground [4]. Then the Japanese scholars through seismic observation data to further understand the vibration characteristics of the underground structure, gradually realize the decisive effect on seismic response of underground structures is the deformation of surrounding soil not the inertial force of structure, then put forward RDM. The calculation model of the RDM is shown in Fig.1.

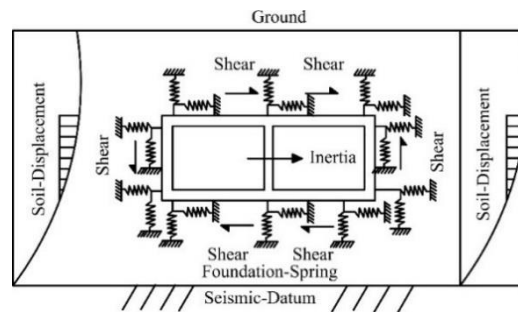


Figure 1. Model of RDM

### 2.2 A brief introduction to RAM

The response acceleration method is used to simulate the interaction between soil and structure by applying the inertial force by the analysis of seismic response of one dimensional soil layer in free field [9]. The calculation model is shown in Fig.2.

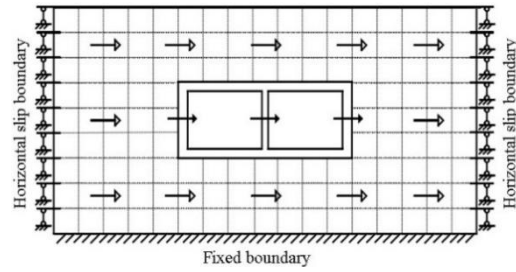


Figure 2. Model of RAM

### 3 CALCULATION MODEL AND CONDITION

#### 3.1 Structure

In this calculation, two typical cross section utility tunnel of single deck utility tunnel (SDUT) and double deck utility tunnel (DDUT) are used. The total width of the single deck utility tunnel is 10m, the height is 4m, the thickness of the top panel, the bottom panel and the side wall are all 0.5m, and the thickness of the middle diaphragm is 0.4m. The total width of the double deck utility tunnel is 6m, the height is 6m, the thickness of the top panel, the bottom panel, the middle diaphragm and the side wall are all 0.3m. The size of the two structures is shown in Fig.3 and Fig.4 respectively.

The concrete material is C40, density  $\rho=2500\text{Kg/m}^3$ , elastic modulus  $E=32.5\text{GPa}$ , Poisson's ratio  $\nu=0.2$ .

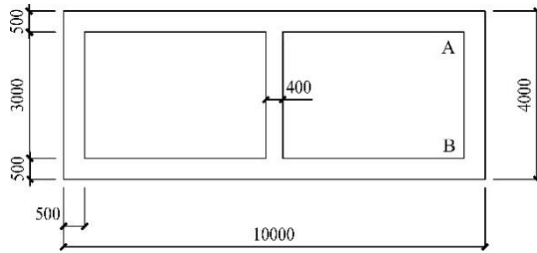


Figure 3. Cross section of SDUT (mm)

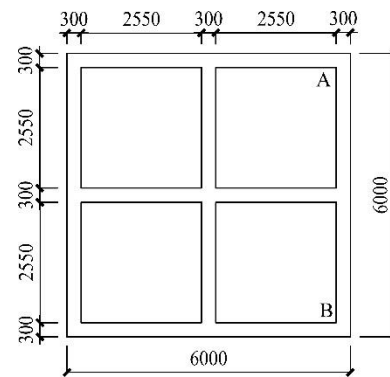


Figure 4. Cross section of DDUT (mm)

### 3.2 Soil

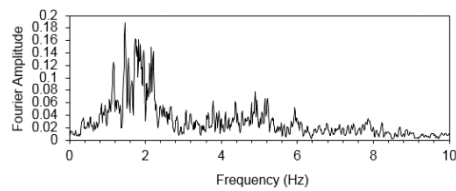
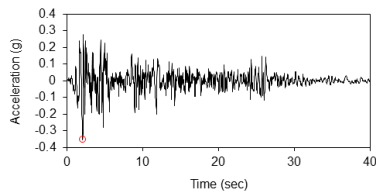
The layered soil is selected for calculation, and the specific soil information is shown in Table 1.

Table 1. Soil parameters

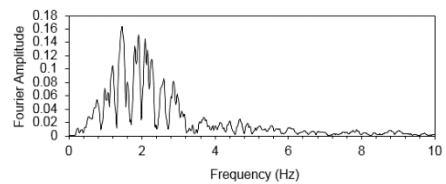
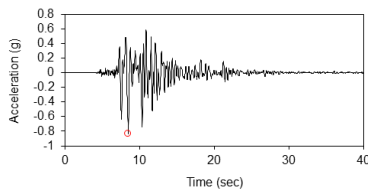
Serial Number	Type	Thickness (m)	$\gamma$ (kN/m <sup>3</sup> )	C (kPa)	$\Phi$ (°)	$V_s$ (m/s)	G (MPa)	$\nu$
1	Backfill	0.5	18.5	10	10	115	26	0.33
2	Fine Sand I	2.5	18.7	7	12	160	36	0.31
3	Fine Sand II	3	19	7	26	200	79.5	0.28
4	Silty Clay	34	20.1	13	20	251	120.3	0.30
5	Round Pebble		22			520		0.25

### 3.3 Seismic wave

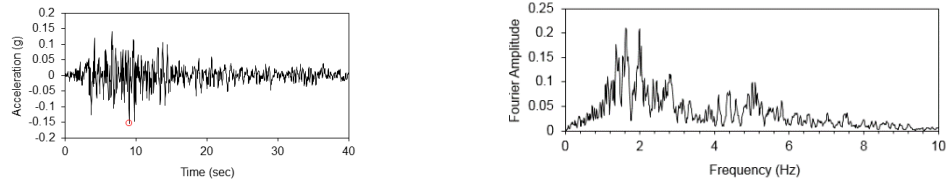
Because different seismic waves have different characteristics, 3 kinds of seismic waves commonly used in seismic calculation of subway stations are selected. The time history curves and fourier spectrum of 3 kinds waves are chosen such as El-Centro wave, Kobe wave and Taft wave and shown in Fig.5.



El-centro wave



Kobe wave



Taft wave

Figure 5. Acceleration time history curve and Fourier spectrum curve of input seismic wave

## 4 RESULTS AND ANALYSIS

When the calculation process to establish two-dimensional finite element model, the depth of utility tunnel is 3m, the width of soil is 7 times the width of the structure, the soil depth calculate to seismic datum (shear wave velocity  $\geq 500\text{m/s}$ ). The calculation is simplified as follows: 1. There is no slip and separation between soil and structure during earthquake, and the structure is coupled with the soil layer. 2. It is assumed that both the soil and the underground structure are in the linear elastic state in the calculation process.

### 4.1 Different input seismic wave

The time history curves of 3 kinds of waves are chosen such as El-Centro wave, Kobe wave and Taft wave and shown in FIG.6. The PGA of these seismic waves is 0.2. The calculation results are shown in Table 4. It can be seen from Table 2 that the calculation error of RAM is smaller than that of RDM, no matter which kind of seismic wave is used in two structure. The maximum value of the relative error of the moment in RDM is 12.04% (Taft Wave), and the maximum relative error of the displacement is 11.50% (Kobe Wave) in SDUT. The maximum value of the relative error of the moment in RDM is 8.53% (Kobe Wave), and the maximum relative error of the displacement is 11.09% (El-Centro Wave) in SDUT. By comparing the relative error of the table, it is obvious that the error of RAM is smaller than that of RDM, no matter what kind of seismic wave.

### 4.2 Different peak ground acceleration

The Kobe wave is used to input the PGA to 0.05g, 0.2g, 0.5g and 0.8g respectively. The calculation results are shown in Fig. 5 and Fig. 6. The PGA of seismic wave is adjusted according to the following formula:

$$a'(t) = \frac{a'_{\max}}{a_{\max}} a(t) \quad (1)$$

Table 2. Calculation results under the different seismic waves

		The Results of RDM		The Results of RAM	
		Results	Relative Error	Results	Relative Error
The bending moment at B of SDUT (kN·m)	El-Centro wave	400.98	7.32%	412.98	4.55%
	Kobe wave	360.59	10.38%	410.23	2.03%
	Taft wave	351.01	12.04%	400.20	1.01%
The bending moment at B of DDUT (kN·m)	El-Centro wave	265.58	7.81%	279.32	3.39%
	Kobe wave	240.65	8.53%	253.21	3.80%
	Taft wave	212.96	5.19%	230.74	2.73%
The displacement of side wall of SDUT (mm)	El-Centro wave	4.91	1.03%	4.95	1.85%
	Kobe wave	4.56	11.50%	4.03	1.47%
	Taft wave	4.36	3.07%	4.38	3.55%
The displacement of side wall of DDUT (mm)	El-Centro wave	10.26	9.68%	12.62	11.09%
	Kobe wave	12.31	4.15%	11.95	1.10%
	Taft wave	8.26	8.42%	9.23	2.33%

The  $a'(t)$  and  $a'_{\max}$  are the adjusted seismic acceleration curves and the PGA.  $a(t)$  and  $a_{\max}$  are the seismic acceleration curves and the PGA of the original ground.

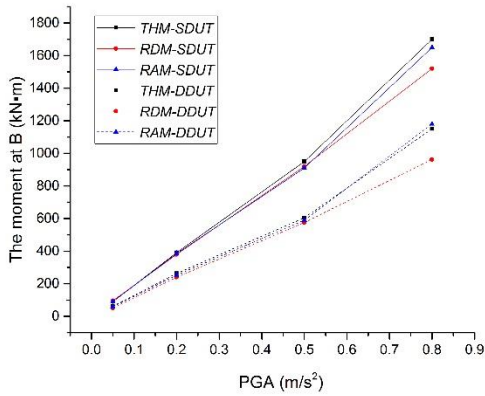


Figure 6. The bending moment at B (kN·m)

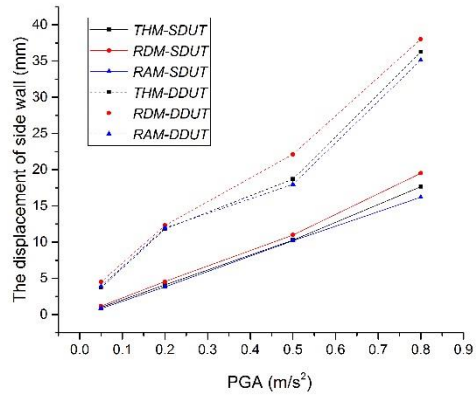


Figure 7. The displacement of side wall (mm)

By observing Fig.6 and Fig.7, we can see that with the increase of PGA, both the moment at B and the displacement of side wall all show an obvious upward trend. Because the thickness of the side plate of DDUT is smaller than that of SDUT, the bending moment of B is smaller than that of SDUT, while the side wall deformation is larger. In Fig.6 and Fig.7, it is found that SDUT and DDUT exhibit different regularity in bending moment and side panel deformation.

### 4.3 Different relative stiffness

Using the Kobe wave with PGA as 0.2g, the structural stiffness is calculated at 0.5 times, 1 times, 2 times and 5 times of the basic stiffness. The calculation results are shown in Fig.8 and Fig. 9.

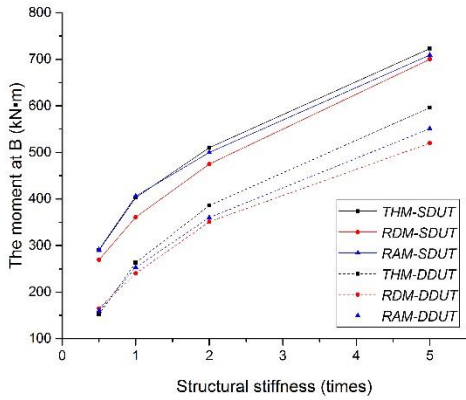


Figure 8. The bending moment at B (kN·m)

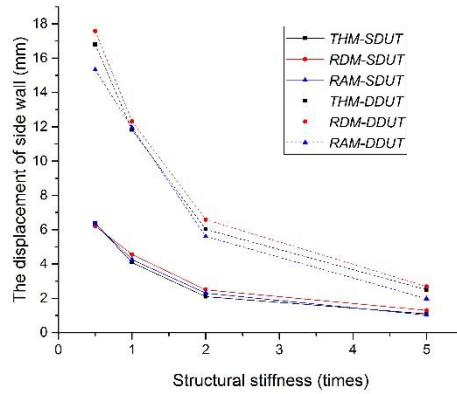


Figure 9. The displacement of side wall (mm)

From the above Fig.8 and Fig.9, it can be seen that the variation trend of the results of the three methods in SDUT and DDUT is the same when the structural stiffness is changed. The result curves of CAM are close to THM, it shows that RAM has higher computation accuracy while RDM has larger discrete type and lower computation accuracy.

## 5 CONCLUSIONS

In this paper, two kinds of sectional utility tunnel models of SDUT and DDUT are established respectively. Then THM, RDM and RAM methods are used to carry out the seismic calculation of the two models. In the calculation, the universality of the calculation method is analyzed by changing the 3 types of factors, such as the type and size of the input seismic waves and the stiffness of the structure. Through the calculation and analysis, the main conclusions are as follows:

- It is found that there are no abrupt changes in the calculation results of RDM and RAM, which show that these two methods are all can used in the seismic calculation of utility tunnel.

- Although the overall change trend of SDUT and DDUT is the same after changing the calculation parameters in the calculation, but the specific aspects are different, so the detailed analysis is needed in the calculation of the utility tunnel of different sections according to the form of the section and the factors considered.
- No matter what kind of calculation conditions, CAM has high accuracy, while CDM calculation results are discrete. Therefore, it is recommended that CAM be used for seismic response calculation of utility tunnel.

## REFERENCES

- [1] Qian, Q.H. The fourth wave of geotechnology. *Underground Space*. (1999) 19: 267-272.
- [2] Zhao, Z.X. and Xv, J.R. In 1995 the Japanese earthquake in Kobe building collapse and the edge of the S wave and surface wave interference on the secondary Basin. *Chinese Science Bulletin*. (2003) 48:2566-2571.
- [3] Hao, M. Xie, L.L. and Xu, L.J. Some considerations on the physical measure of seismic intensity. *Acta Seismologica Sinica*. (2005) 27:245-250.
- [4] Newmark, M. Problems in wave propagation in soil and rock. *Proceedings of the International Symposium on Wave Propagation and Dynamic Properties of Earth Materials*. (1968).
- [5] Wang, N. *Seismic design of tunnels: a simple state of the art design approach*. New York: Parsons Brinckerhoff Quade and Douglas Inc. (1993).
- [6] Liu, J.B. Wang, W.H. and Zhao, D.D. Integral response deformation method for seismic analysis of underground structure. *Chinese Journal of Rock Mechanics and Engineering*. (2013) 32:1618-1624.
- [7] Kawashima, K. *The seismic design of underground structures*. Japan: Kashima Publishing. (1994).
- [8] Li, B. *Theoretical analysis of seismic response of underground subway structures and its application*. Beijing: Tsinghua University. (2005).
- [9] Liu, J.B. Liu, X.Q. and Li, B. A pushover method for seismic response analysis and design of underground structures. *China Civil Engineering Journal*. (2008) 41:73-80.

## Uncertainty Quantification of Finite Element Analysis of Uni-axial Strength Test Holed Composite Laminates

Li Ma<sup>\*</sup>, Jeffrey Fong<sup>\*\*</sup>, Pedro Marcal<sup>\*\*\*</sup>, Robert Rainsberger<sup>\*\*\*\*</sup>, Alan Heckert<sup>\*\*\*\*\*</sup>, James Filliben<sup>\*\*\*\*\*</sup>

<sup>\*</sup>Theiss Research, <sup>\*\*</sup>NIST, <sup>\*\*\*</sup>MPACT Corp., <sup>\*\*\*\*</sup>XYZ Scientific Applications, Inc., <sup>\*\*\*\*\*</sup>NIST, <sup>\*\*\*\*\*</sup>NIST

### ABSTRACT

In the aerospace industry, open hole specimens of composite laminates have been used in standardized tests to generate design allowables. Using finite element method (FEM) based tool MicMac/FEA with ABAQUS code interface and statistical design of experiments, Shah, et al. in 2010 studied average-property-based failure envelope with uncertainty estimates of open hole specimen with quasi-isotropic carbon fiber-epoxy laminate. However, their FEM model is deterministic, without uncertainty analysis. In this paper, based on Shah&apos;s FEM model, we developed FEM model of uni-axial strength test of holed composite laminates using ABAQUS and ANSYS with a series of quadrilateral and triangle shell element designs. The mesh density ranges from the original 8 X 8 (very coarse) to 10x10 (coarse), 12x12 (normal), 14x14 (fine), and 16 X 16 (very fine). For each of the meshes, we compute the failure strength from Hashin failure criteria. Then we use a 4-parameter logistic function nonlinear least squares fit algorithm to obtain an estimate of the failure strength at infinite degrees of freedom (d.o.f) as well as its uncertainty at one-billion-d.o.f. and relative error convergence rates. Our results are then compared with Shah&apos;s with the additional advantage that our results have uncertainty quantification that can be compared with experimental data. The significance and limitation of our method on the uncertainty quantification of FEM model of uniaxial strength test of holed composite laminates are discussed.

## **An Adaptive Kirigami Metamaterial Plate for Broadband Anisotropic Elastic Wave Manipulation on a Subwavelength Scale**

Qian Ma<sup>\*</sup>, Rui Zhu<sup>\*\*</sup>, Yangyang Chen<sup>\*\*\*</sup>, Guoliang Huang<sup>\*\*\*\*</sup>, Gengkai Hu<sup>\*\*\*\*\*</sup>

<sup>\*</sup>Beijing Institute of Technology, <sup>\*\*</sup>Beijing Institute of Technology, <sup>\*\*\*</sup>University of Missouri, <sup>\*\*\*\*</sup>University of Missouri, <sup>\*\*\*\*\*</sup>Beijing Institute of Technology

### **ABSTRACT**

Although metamaterials possess peculiar negative material properties and subwavelength wave manipulation abilities, there are still unfilled gaps between current metamaterial design and engineering standards for practical applications. In fact, the subtractive microstructures and resonance-induced narrow bandgaps significantly prevent elastic metamaterials from successful engineering implementations. In this presentation, we propose an adaptive metamaterial plate with its microstructure consisting of built-on-top kirigami structures and shunted piezoelectric patches with feedback circuit control. First, an analytical model of the proposed metamaterial is developed to explain the mechanism of its adaptive bandgaps and switchable anisotropy for flexural wave propagation. Then, an additive unit cell design is conducted with lightweight kirigami microstructure and strategically positioned piezoelectric patches. Feedback control of the piezoelectric shunts is realized with the help of a semi-analytically determined transfer function, which provides tunable anisotropic mass density in a broad frequency range. Finally, full-wave simulations on the broadband directional flexural wave propagation as well as super-resolution hyperlens effect are conducted to demonstrate the robustness of proposed adaptive kirigami metamaterial in subwavelength-scale flexural wave control. This attachable and adaptive metamaterial opens a new avenue for practical elastic wave control and management in engineering structures.

# High-order Two-scale Asymptotic Analysis and Computation of the Dynamic Piezoelectric Performance for Composite Structures with Axisymmetric Configuration

Qiang Ma<sup>\*</sup>, Junzhi Cui<sup>\*\*</sup>, Zihui Li<sup>\*\*\*</sup>

<sup>\*</sup>College of Mathematics, Sichuan University, Chengdu, 610064, China, <sup>\*\*</sup>LSEC, ICMSEC, The Academy of Mathematics and Systems Science, CAS, Beijing, 100190, China, <sup>\*\*\*</sup>Hypervelocity Aerodynamics Institute, China Aerodynamics Research and Development Center, Mianyang, 621000, China

## ABSTRACT

The high-order asymptotic expansion homogenization method is developed for the dynamic piezoelectric problem of the composite materials with axisymmetric configuration. The structure considered is periodically distributed in only radial and axial directions, while homogeneous in circumferential direction, and the constituent materials are assumed to be orthotropic. By reformulating the governing equations in the compact form, the multi-scale expansion of the displacement and electrical field is performed, the homogenized piezoelectric model is obtained and the second-order asymptotic approximations are also derived. Theoretical results are derived for some simplified problem in both 1-D and 2-D cases. The corresponding high-order finite element algorithm is proposed, and two numerical examples are carried out to demonstrate the effectiveness of our proposed model. It is also indicated that the second-order asymptotic approximations are more accurate to simulate the coupled piezoelectric performance of the composites.

## FLUID-STRUCTURE INTERACTION NUMERTCAL SIMULATION OF DIFFERENTIAL PRESSERE PIPELINE INSPECTION GAUGE PASSING ABILITY

Rui MA<sup>\*</sup>, S Fan ZHU<sup>†</sup>, D Yan SHI<sup>†</sup>,H Xi REN<sup>†</sup>

<sup>\*</sup>College of Mechanical and Electrical Engineering, Harbin Engineering University  
Harbin, Hei Longjiang, China  
Email: [marui1993@hrbeu.edu.cn](mailto:marui1993@hrbeu.edu.cn)

<sup>†</sup>College of Mechanical and Electrical Engineering, Harbin Engineering University  
Harbin, Hei Longjiang, China  
Email: [zhushifan@hrbeu.edu.cn](mailto:zhushifan@hrbeu.edu.cn)  
Email: [shidongyan@hrbeu.edu.cn](mailto:shidongyan@hrbeu.edu.cn)

**Key words:** Pipeline Inspection Gauge; Fluid-Structure Interaction; CEL Method; Mooney-Rivlin Model; Local Deformation

**Summary:** *Differential pressure Pipeline Inspection Gauge(PIG) can accurately scan and detect oil and gas pipelines. In order to achieve the scanning and detection of oil and gas pipelines, It must ensure that the pipeline detector through the oil and gas pipeline smoothly. Based on the method of coupled Euler-Lagrangian (CEL), a fluid-structure interaction model for the operation of the pipeline detector was established. The Mooney-Rivlin model was used to describe the superelastic and non-linear behavior of the polyurethane rubber. Analyzing the complex mechanical behavior of the local deformation of PIG when it passing through the pipeline. Based on the CEL simulation method, calculating the passability of PIG in the actual pipeline and analysising the factors which impact the passability. We have demonstrated in this paper that the amount interference of cup is a very important parameter. When the amount of interference is less than 15.0%, the detector can pass through the pipeline. When the pipe is in the deformation area, the height of the deformation part is less than 6.0 %. The detector can pass through the pipe smoothly. Through the research of this paper, we can provide theoretical basis and reference for the design and use of the detector in the pipeline.*

## 1 INTRODUCTION

At present, as one of the most economical and reliable ways of oil transmission, pipelines play a crucial role in modern industry. Due to the long-time of transmission, pipelines will be subject to corrosion by transmission medium. The detection method commonly used at home and abroad is placing detectors inside the pipeline to complete the scan inspection of the pipeline wall [1-2]. The use of differential pressure Pipeline Inspection Gauge(PIG) is one of the main techniques for pipeline inspection. PIG is exposed to pressure differences at both ends of the fluid medium, thus generating a driving force for the PIG [3-5].

The structure of PIG is a middle cabin with rubber cup at both ends. The number of rubber cup is generally 2 to 3[6]. The rubber cup is an important part that directly contacts the pipe inner wall on the PIG. It is made from a non-linear solid material with characteristics of super-elasticity, volume incompressibility and large deformation. Its' material characteristics have important effect on the dynamic characteristic of PIG [7-9].

In order to further explore the mechanical behavior of PIG encountering pipeline local deformation. Zhang Hang [10-11] established a dynamic theoretical model for the transient migration of PIG passing girth welds in confined spaces of pipelines. The overall dynamics of PIG was analyzed. Liu Baoyu [12] established a geometrical theoretical model for the PIG bendability, and systematically analyzed the different structures of the cup. Durali M [13] established a one-dimensional equivalent spring and damping vibration model of PIG. He studied the vibration characteristics of the PIG passing solder joint deformation. The above research focuses on the one or two-dimensional theory and simplified simulation of the model. It lacks a complete PIG motion process with the inertia of the detector and the influence of friction. It even does not involve the coupling model construction of three-dimensional model and other important research work such as numerical simulation.

This paper is focused on the complex dynamics problem of PIG. Based on the CEL fluid-solid coupling method, study the key technology of fluid-solid coupling numerical simulation for non-linearity of PIG systematically.

## 2 FLUID-SOLID COUPLING MODELS

### 2.1 CEL method

The Coupled Euler-Lagrangian (CEL) method in ABAQUS combines the advantages of Euler method and Lagrangian method. It can handle large deformation, nonlinear, fluid-solid coupling and other issues correctly. In CEL method, the area to be analyzed is divided into an Euler area and a Lagrangian area according to the possibility of large deformation. In these two areas, the Euler finite element method and Lagrange are used respectively. The finite element method is used for calculation. Using CEL method for numerical analysis, the flow state of fluid material can be obtained by calculating the Euler Volume Fraction (EVF). Each Euler cell is assigned a percentage that represents the part of the Euler cell that is filled with material, if a Euler unit is completely filled with material, then  $EVF=1$ , if there is no material in the unit,  $EVF=0$ .

The CEL method in ABAQUS is a general contact based on a penalty function algorithm to solve the contact problem between Euler materials and Lagrangian materials. Creating boundary nodes on the edges and faces of Lagrangian cells, creating fixed reference point on the Euler material surface, and the penalty function contact method approaches the hard pressure-occlusal behavior. This method allows small Euler materials to penetrate into Lagrangian. area.

## 2.2 Geometric models and grids

The force condition of PIG is shown in Fig.1. Setting the length of the pipe to 6m, the diameter is 216mm, the length of the thin pipe section is 5m, and the inner diameter is 200mm. The PIG consists of three polyurethane-driven cups and a central cabin, the diameter of cups are 280mm.

The power received by the inner detector is the driving pressure generated by the fluid medium at the front and rear ends of the detector at different pressures. The pressures at both ends of PIG are  $P_1$  and  $P_2$ . The frictional resistance caused by the contact between cups and wall of pipe is the main resistance against the PIG.

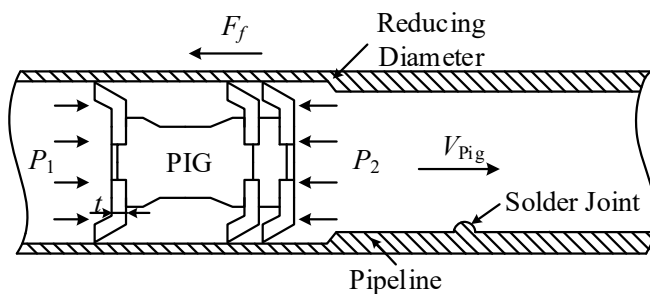


Fig.1 Force condition of Pipeline Inspection Gauge

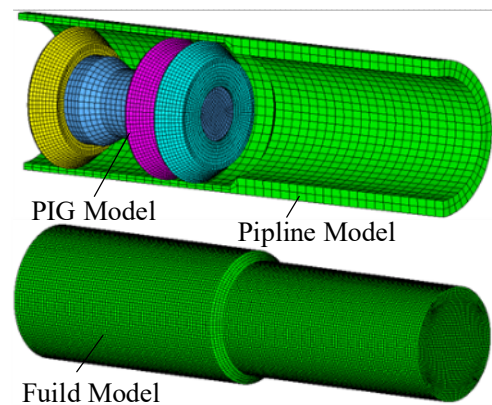


Fig.2 Fluid - Solid Coupling Finite Element Model for PIG

In order to analyze the complex dynamics characteristics of the PIG inside the pipe under the influence of fluid medium, a fluid-solid coupling finite element model is established by using CEL method, as shown in Fig. 2.

In order to ensure the accuracy of finite element analysis, a reasonable selection of cell types, shapes, and grid densities is required in order to maintain a good cell morphology during the analysis. In this paper, a linear reduction integration unit C3D8R is used to divide the PIG and set the grid density of the cup to be twice of the center cabin. The pipeline is set as a rigid body and is also divided by C3D8R units. The mesh density is approximately equal to the center cabin. The fluid is meshed with Euler cells. The cell type is an 8-node linear Euler solid cell EC3D8R. By default, the EC3D8R cell uses viscous hourglass control. In

order to make the simulation result more accurate, the solid grid density needs to be set to 3 to 5 times of the density of the fluid grid. In the numerical simulation process, the Euler material's initial material definition was controlled by the Volume Fraction Tool in ABAQUS which combined with the material's pre-defined field.

The smooth pipeline model and the local deformation pipeline model were established respectively, as shown in Figure 3. The smooth pipeline is used for the analysis of the mechanical motion of the PIG in straight pipeline, mainly to explore the effect of the interference of the cup on passing ability. The local deformation pipeline is used to analyze the mechanical motion of the PIG in irregular pipelines, mainly to explore the effect of the pipeline deformation on the passing ability. The local deformation shape of the pipeline is hemispherical which refer to the actual working conditions for internal processing in the pipeline.

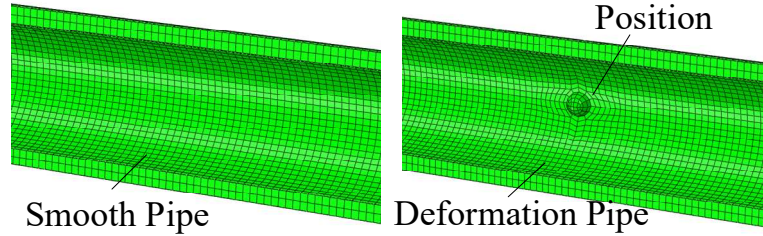


Fig.3 Finite Element Model of Smooth Pipeline and Deformation Pipe

### 2.3 Fluid material model

Based on ABAQUS's CEL method, the fluid material in the pipe is represented by the state equation (EOS) combined by Mie-Grüneisen and Hugoniot<sup>[14-15]</sup>, which defines the volumetric strength of the material and the ratio of pressure to density. The universal fluid Mie-Grüneisen's state equation is expressed as:

$$p = p_H \left( 1 - \frac{\Gamma_0 \eta}{2} \right) + \Gamma_0 \rho_0 E_m \quad (1)$$

Where  $p_H$  and  $E_m$  are Hugoniot pressure and energy per unit mass respectively. They are functions of density  $\rho$ ,  $\rho_0$  is reference density,  $\Gamma_0$  is material constant, and  $\eta$  is nominal volume compressive strain.

The pressure equation that usually satisfies the Hugoniot curve is expressed as:

$$p_H = \frac{\rho_0 c_0^2 \eta}{(1 - s \eta)^2} \quad (2)$$

Where  $c_0$  is sound velocity in fluid,  $s$  is undetermined constant. The linear relationship between fluid impact velocity  $U_s$  and fluid particle velocity  $U_p$ , can be expressed as:

$$U_s = c_0 + s U_p \quad (3)$$

Substituting equation (2) into equation (1) can be expressed as:

$$p = \frac{\rho_0 c_0^2 \eta}{(1-s\eta)^2} \left( 1 - \frac{\Gamma_0 \eta}{2} \right) + \Gamma_0 \rho_0 E_m \quad (4)$$

Based on the above equation, this paper set the density  $\rho = 1000 \text{kg}/\text{m}^3$ , the viscosity  $\mu = 0.001 \text{kg}/(\text{m} \cdot \text{s})$ , the sound speed  $C_0 = 1483 \text{m}/\text{s}$  and  $s = 0, \Gamma_0 = 0$ .

## 2.4 Rubber cup constitutive model

The PIG's cups are made from urethane rubber. The Mooney-Rivlin material model is used to describe the properties of the rubber material. The general form of the strain energy density function for rubber materials can be expressed as:

$$U = C_{10}(\bar{I}_1 - 3) + C_{01}(\bar{I}_2 - 3) + \frac{1}{D_1}(J_{el} - 1)^2 \quad (5)$$

Where  $U$  is the strain energy per unit volume,  $C_{01}$ ,  $C_{10}$  and  $D$  are material parameter which are related to temperature.  $\bar{I}_1$  is the first and  $\bar{I}_2$  is the second invariants of Cauchy-Green deformation tensors, expressed as:

$$\bar{I}_1 = \bar{\lambda}_1^2 + \bar{\lambda}_2^2 + \bar{\lambda}_3^2; \bar{I}_2 = \bar{\lambda}_1^{(-2)} + \bar{\lambda}_2^{(-2)} + \bar{\lambda}_3^{(-2)} \quad (6)$$

Where the offset  $\bar{\lambda}_i = J^{-1/3} \lambda_i$ ,  $J$  is the total volume ratio,  $J_{el}$  is the elastic volume ratio,  $\lambda_i$  is the main extension, the initial shear modulus and bulk modulus are defined as:

$$G = 2(C_{10} + C_{01}) \quad K = \frac{2}{D_1} \quad (7)$$

In order to accurately express the stress-strain relationship of the rubber material, the data obtained through uniaxial tensile test, was fitted by Abaqus/Standard to obtain the hyper-elastic constitutive parameters of the rubber material. The mechanical properties curve of polyurethane materials as shown below:

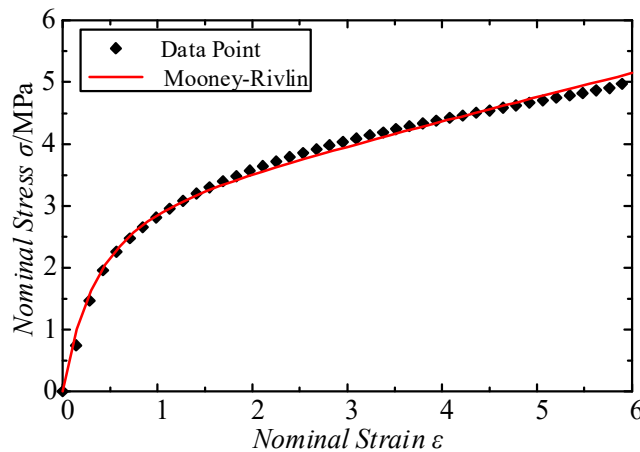


Fig.4 Stress-strain relationship of polyurethane rubber

In this paper, Mooney-Rivlin model is used to describe the mechanical behavior of rubber materials. The experimental results are used to fit the obtained polyurethane rubber cup constitutive model coefficients:  $C_{10} = 1.93e6$ ,  $C_{01} = 0.96e6$ . The material is incompressible.

## 2.5 Boundary conditions and friction coefficients

The boundary conditions include the inlet and outlet boundaries of the pipeline, and the space constraints of the pipeline. In order to satisfy the hydrodynamic equation, the inlet boundary of the pipeline is set as the velocity boundary, and the outlet boundary of the pipeline is the natural flow. During the PIG runs in the pipeline, it is mainly affected by the force of the fluid and the force of the inner wall of the pipeline. The friction coefficient is an important parameter that affects the force. In this paper, the friction coefficient between the inner detector and the pipeline is set to 0.4.

## 3 SIMULATION RESULTS AND ANALYSIS

The PIG is mainly subjected to the action of the driving pressure and the friction force, that maintains a balance between the basic driving force and the friction force at a constant speed. In this paper, the fluid-structure coupled finite element model of the PIG movement in the pipeline is established by the nonlinear finite element software ABAQUS using the CEL method. Friction force and stress are taken as the research objects, and the influencing factors of the in-line detector are analyzed.

### 3.1 Analysis of straight pipe mechanics behavior

For the study of the relationship between the mechanical behavior and the interference of the cups in the operation of the straight pipe, three types of cups with 10mm, 14mm and 18mm thickness were used as the research object, and the pipe was 8-inch (internal diameter 200mm). limited the cups' interference range to 0 to 35mm with an interval of 5mm. Obtained numerical simulation data points, and after three times of polynomial fitting, to obtain the results of Figure 5~7.

Fig. 5 shows the relationship between the friction force and the interference magnitude of the cups. It can be seen that when the interference magnitude increases from 25mm to 35mm, the friction increment is larger and the curve is steeper. When the interference magnitude is from 10mm to 25mm, the increase in friction is smaller and more gradual. The data points from the 14mm and 18mm cup thickness deviate from the fitting curves, and the data points with the thickness of 10mm basically coincided with the fitting curve.

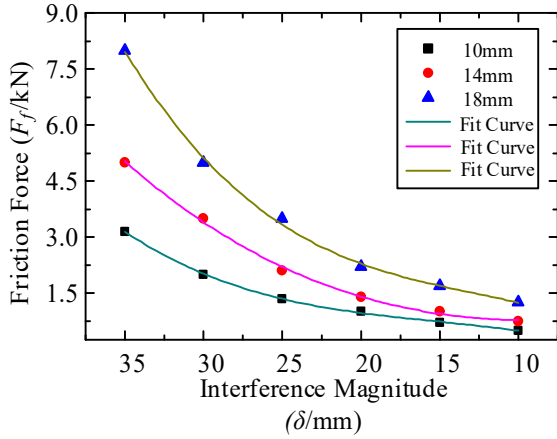


Fig.5 Relation between frictional force  $F$  and magnitude of interference  $\delta$

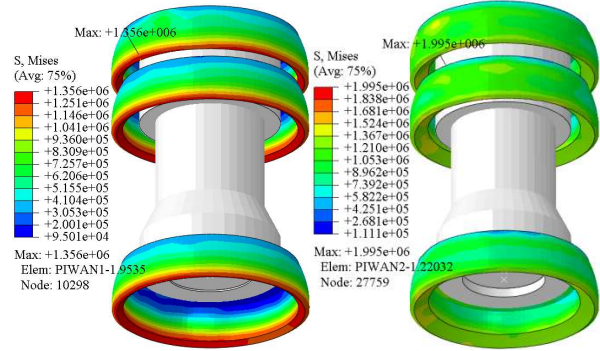


Fig.6 The Mises stress nephogram of PIG

The Mises stress on the detector is shown in Fig. 6. It can be seen that when the detector runs smoothly in a smooth pipe, the stress on the PIG is more uniform and appears at the interface between the cup and the inner wall of the pipe. Comparing the Mises stress cloud map with the thickness of 10mm and 18mm, it can be seen that with the same amount of interference magnitude, the stiffness of the cup increases significantly with the increase of the thickness of the cup.

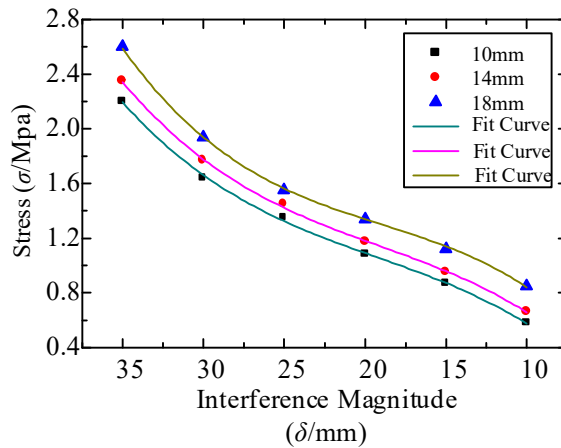


Fig.7 Relation between stress  $\sigma$  and magnitude of interference  $\delta$

Figure 7 shows the relationship between the stress of PIG and the change in the interference of the cup. It can be seen that when the interference increases from 10mm to 15mm, the stress on the detector increases more obviously. When the magnitude of interference is from 15mm to 30mm, the rising trend of the stress on the PIG is slowed down. When the interference magnitude is in the range of 30mm~35mm, the stress is greatly

increased. Exceeded the reasonable range of applications for the cups. As can be seen from the three fitting curves, the change trend of the curve is basically the same, and the coincidence degree between the simulated data point and the fitted curve is high, indicating that the thickness of the cups only has the effect of increasing the stiffness.

### 3.2 Analysis deformation mechanical behavior

To study the mechanical behavior of PIG at the local deformation of the pipe. When it running in the pipe, due to the super elastic and nonlinear characteristics of the sealed cups, when the shape of the pipe is abruptly changed, the complex dynamic behavior will occur great fluctuations. Setting the boundary velocity to 1m/s, 2m/s, and 3m/s respectively, the inner diameter of the pipe to 200mm, and the thickness of the cuvette to 14mm as the research object, to investigate the process of the pipe deformation (half-sphere) height increasing from 4mm to 20mm. The relationship between the friction force, the cup stress, and the deformation height is used to analyze the influence factors of the PIG passing ability.

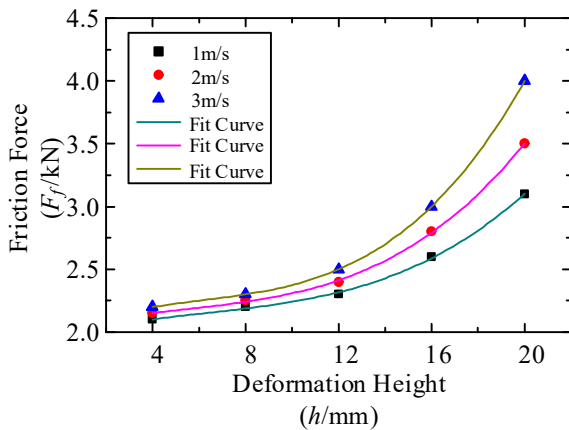


Fig.8 Relation between stress  $\sigma$  and deformation height  $h$

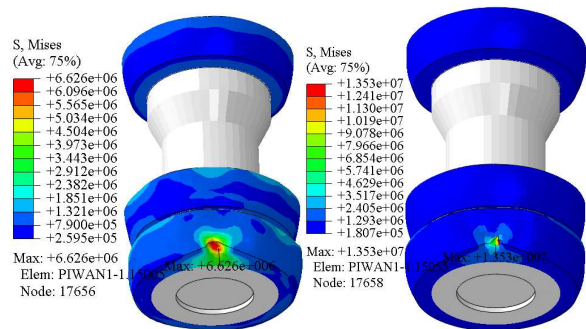


Fig.9 The Mises stress nephogram of PIG

Figure 8 shows the relationship between the friction force and the deformation height. Analysis of Figure 8 shows that when the deformation height changes in the interval of 4-12mm, the friction force of the detector changes more smoothly, and less than 2.5kN, the trend of the three fitting curves is similar; when the deformation height increases from 12mm to 20mm, at that time, friction increased significantly, and the increase of the three curves gradually increased. It shows that the speed will have a certain influence on the friction force that the PIG receives when it passes through the deformation zone of the pipeline, and the speed will lead the friction force to increase.

When PIG passes through the local deformation part of pipeline, the phenomenon of stress concentration will inevitably occur. As shown in Fig. 9, when passing through the local deformation zone of the pipeline, the stress exceeds the reasonable area of the cup, but after

through the deformation zone, due to the polyurethane. The material has a high degree of super-elastic, flying behavior, that will return to normal motion. However, through simulation, it can be seen that when the stress of the cup is very large, the damage to the cup is irreversible.

When the PIG passes through the deformation part of pipeline, due to the presence of the deformation part, the PIG will produce a significant stress concentration phenomenon. Figure 10 shows the relationship between the stress  $\sigma$  of PIG and the deformation height  $h$ . According to the fitting curve, the trend of the maximum stress change experienced by the cup is basically the same as that of the friction force. When the deformation height is less than 12mm, the stress changes less than 10 MPa, which is in line with the reasonable use range of the polyurethane rubber material; the stress change trend is also the same related to the passing speed, the working condition with a speed of 1m/s, the stress is obviously less, and less than 10MPa; the working condition with a speed of 3m/s, when the deformation height is 20mm, the maximum stress reaches 24.8MPa, showing the polyurethane material Strong superelastic, nonlinear behavior.

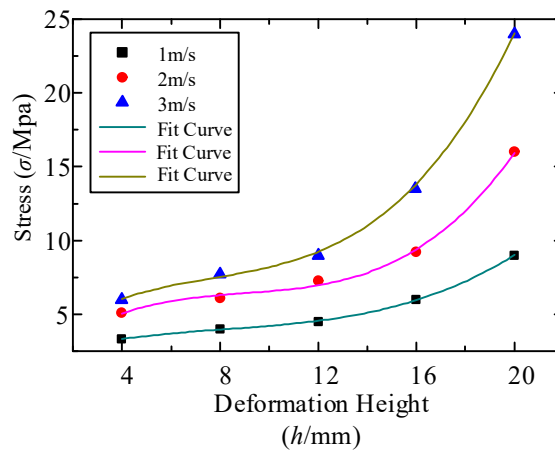


Fig.10 Relation between stress  $\sigma$  and deformation height  $h$

When the PIG passes through the deformation part of pipeline, due to the presence of the deformation part, the PIG will produce a significant stress concentration phenomenon. Figure 10 shows the relationship between the stress  $\sigma$  of PIG and the deformation height  $h$ . According to the fitting curve, the trend of the maximum stress change experienced by the cup is basically the same as that of the friction force. When the deformation height is less than 12mm, the stress changes less than 10 MPa, which is in line with the reasonable use range of the polyurethane rubber material; the stress change trend is also the same related to the passing speed, the working condition with a speed of 1m/s, the stress is obviously less, and less than 10MPa; the working condition with a speed of 3m/s, when the deformation height is 20mm, the maximum stress reaches 24.8MPa, showing the polyurethane material Strong superelastic, nonlinear behavior.

### 3.3 Analysis of Passing Influence Factors

The above simulation method was used to numerically simulate the fluid-structure interaction of the PIG when passing through the smooth straight pipe section and local deformation of the pipe. The difference method [16] was used to do the surface fitting to the stress, and the fitting surface was shown in the Figure.11 and Figure 12.

As can be seen from Figure 11, when the pipe diameter does not change, the stress in the detector increases as the thickness of the cup increases, but the stress increases slowly when the amount of interference is constant. When the thickness of the cup increase from 10mm to 18mm, the stress increase value is less than 0.5MPa; when the cups' interference reaches 30mm, that is the 15.0% of pipe diameter, the stress change obviously increases obviously, indicating that the stress is beyond the range of reasonable use. It can achievable conclusion is in order to ensure that PIG can smoothly pass through the pipeline, the magnitude of interference should be less than 15.0% of the inner pipeline diameter.

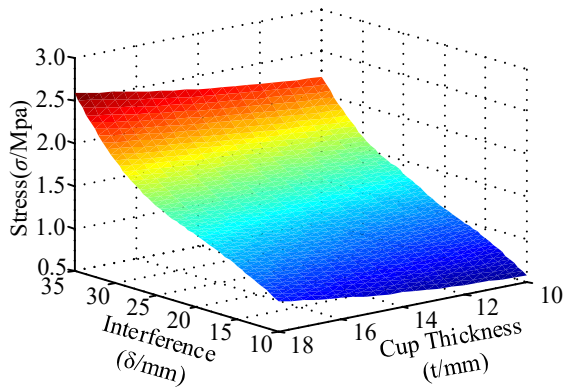


Fig.11 Relation of stress  $\sigma$  versus thickness  $t$  and magnitude of interference  $\delta$

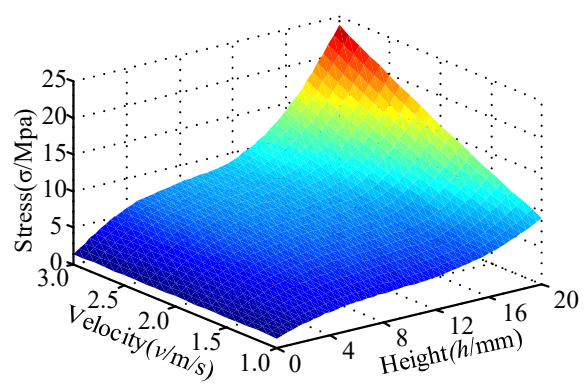


Fig.12 Relation of stress  $\sigma$  versus deformation height  $h$  and boundary velocity  $v$

As can be seen from Fig. 12, when PIG's structure is unchanged, the deformation height is 0, the stress on the cups is basically at 2 MPa and remains unchanged, indicating that in the smooth straight pipeline, the change of velocity has little effect on the stress. But when the speed is less than 2m/s and the pipe deformation height is larger than 8.0% of the pipe inner diameter, the stress on the detector increases significantly, the speed is faster than 2m/s, and the pipe deformation height is bigger than 6.0% of the pipe inner diameter. The stress increases significantly, indicating that the faster the speed is, the larger stress on the cups. In order to ensure the high efficiency of PIG, when the deformation height is less than 12mm, as the 6.0% of the pipeline diameter. The device can pass through the pipeline smoothly.

### 4 Conclusion

In this paper, the CEL method is applied to the in-pipe detector simulation. The fluid-solid coupling model of the detector in the pipeline is established. The coupling effect of the

detector inside the pipeline and the fluid and the pipeline is considered. The dynamic model of the fluid material is established and the polyurethane rubber cup is established. Material experiments were performed using the Mooney-Rivlin hyperelastic constitutive model, and numerical simulations using the CEL method yielded the following conclusions:

1) When the detector is operated in the pipe, the maximum stress in the smooth pipe mainly occurs at the contact surface between the cup and the inner wall of the pipe, and the stress distribution is more uniform under steady state operation. In the local deformation of the pipeline, there is a large stress concentration.

2) The amount of interference of the inner detector tube sealer is a very important parameter for the passage of the inner detector in the pipeline. To ensure that the detector can smoothly pass through the pipeline, the amount of interference should be less than 15.0% of the inner diameter of the pipeline.

3) When the pipe is locally deformed, the height of the deformation determines the level of the passing performance of the detector. When the deformation height is less than 6.0% of the internal diameter of the pipe, the detector can smoothly pass through the pipe.

In addition, the CEL method is applied to the field of fluid-solid coupling dynamics of detectors in pipelines, and nonlinear dynamic analysis of detectors in pipelines is carried out to provide theoretical basis and technical basis for the design and manufacture of detectors in pipelines.

### **Acknowledgement**

This paper is funded by the International Exchange Program of Harbin Engineering University for Innovation-oriented Talents Cultivation.

### **REFERENCES**

- [1] Guan L, Osman A, Gao Y, et al. Analysis of Rolling Motion Effect on SINS Error Modeling in PIG[C]//Ieee/ion Plans. 2016.
- [2] DAI Bo, XU Guang. Analysis of motion state of detectors in pipelines based on effusion holes[J]. Journal of Computers and Applied Chemistry, 2013(8).
- [3] Kandroodi MR, Araabi BN, Bassiri MM, et al. Estimation of Depth and Length of Defects from Magnetic Flux Leakage Measurements: Verification with Simulations, Experiments, and Pigging data[J]. 2016, PP(99):1- 1.
- [4] Dai Bo, Yang Guang, Zhang Xiao, et al. Mathematical model for velocity control of detectors in differential pressure driven pipelines [J]. Journal of Computers and Applied Chemistry, 2016, 33(4).
- [5] Aksenov DV, Shcherbakov VI, Leshchenko V V. Selection of structural parameters of an inspection pig for arterial oil and gas pipelines from conditions of dynamics[J]. Chemical and Petroleum Engineering, 2013, 49(3):265-269.
- [6] Zhang H, Zhang S, Liu S, et al. Chatter vibration phenomenon of pipeline inspection gauges (PIGs) in natural gas pipeline[J]. Journal of Natural Gas Science & Engineering, 2015,

27:1129-1140.

- [7] Zhang Xing, Liu Shuhai, Li Qing, et al. Influence of the interference on the stiffness characteristics of sealed leather bowl of pig 1016mm pig[J]. Chemical Engineering Equipment and Tube, 2015, 52(6):82-86.
- [8] Gu Yaxiong, Zhou Qiongli, Yang Qiang. Design and Simulation of Detector Leakage Device in Gas Pipeline[J]. Instrumentation Users, 2013(3):81-82.
- [9] Zhang H, Zhang S, Liu S, et al. Collisional vibration of PIGs (pipeline inspection gauges) passing through girth welds in pipelines[J]. Journal of Natural Gas Science & Engineering, 2016, 37:15-28.
- [10] Zhang Xing, Zhang Shimin, Guo Shudun, et al. Dynamic simulation of the process of over-weld welding of straight-pipe pig cleaners[J]. Petroleum Mining and Related Machinery, 2015, 44(2):22-27.
- [11] Zhu X, Wang D, Yeung H, et al. Comparison of linear and nonlinear simulations of bidirectional pig contact forces in gas pipelines[J]. Journal of Natural Gas Science & Engineering, 2015, 27:151-157.
- [12] Liu Baoyu. Design and theoretical study of detectors in gas transmission pipelines [D]. China University of Petroleum, 2010.
- [13] Durali M, Fazeli A, Nabi A, et al. Investigation of Dynamics and Vibration of PIG in Oil and Gas Pipelines [C]// ASME 2007 International Mechanical Engineering Congress and Exposition. 2007:2015-2024.
- [14] Sillem A. Feasibility study of a tire hydroplaning simulation in a finite element code using a coupled Eulerian-Lagrangian method [J]. 2008.
- [15] Ahmadzadeh M, Saranjam B, Hoseini Fard A, et al. Numerical simulation of sphere water entry problem using Eulerian–Lagrangian method[J]. Applied Mathematical Modelling, 2014, 38(5–6):1673-1684.
- [16] Chen Shili, Gao Chunqian, Guo Shixu, et al. Research on the Penetration Simulation of Spherical Inner Detector in Submarine Riser[J]. Computer Engineering and Applications, 2015, 51(19): 265-270.

## **A Numerical Model for Calculating Atmospheric Corrosion Rate of Marine Steel Structures**

Rujin Ma<sup>\*</sup>, Chuanjie Cui<sup>\*\*</sup>, Airong Chen<sup>\*\*\*</sup>

<sup>\*</sup>Tongji University, <sup>\*\*</sup>Tongji University, <sup>\*\*\*</sup>Tongji University

### **ABSTRACT**

Atmospheric corrosion is particularly common but hazardous for marine steel structures in civil engineering. Nowadays, a great number of salt spray accelerated corrosion tests have been carry out to illuminate the corrosion rate and corroded structure performance. However the relationship between marine atmospheric corrosion and salt spray environment corrosion is still uncertain. In this research, the electrochemical principle of atmospheric corrosion is analysed and a numerical corrosion model in marine atmospheric environment is developed considering atmospheric humidity, chloride ion concentration and structure stress. The numerical simulation agrees well with the experimental results under same environment condition. At last, based on the numerical model, a parameter analysis of atmospheric humidity, chloride ion concentration and structure stress are studied. The results show that the corrosion rate increases with all of the three parameters. The growth rate increases with atmospheric humidity while decreases with chloride ion concentration and structure stress. This numerical model is certainly helpful for design and maintenance of marine steel structures such as cross-sea bridges, oil platforms and so on .

## Topology Optimization of Cable Domes Based on Genetic Algorithm

Shuo Ma<sup>\*</sup>, Xing-Fei Yuan<sup>\*\*</sup>

<sup>\*</sup>Zhejiang University, <sup>\*\*</sup>Zhejiang University

### ABSTRACT

This study mainly focuses on topology optimization of cable domes based on genetic algorithm, in which the vertical stiffness is set as the objective of optimization. Modified stiffness matrix based form-finding method (mSMFF) is used for form-finding and structural analysis of self-stressed cable domes. An innovative encoding scheme which uses ground structures as well as 0-1 strings to generate connectivity matrix and rest lengths of members are adopted. The mSMFF method is then used to give the initial solution of topology, prestress and configuration. Constraint conditions including constant total mass, yielding and buckling constraints are processed by transforming initial solutions into feasible solutions, in which a nonlinear equation is solved for the coefficient of prestress. The objective function is set as the work done by vertically uniform load, which is a reflection of vertical stiffness. A simple genetic algorithm(SGA) is used for the topology optimization of cable domes. Numerical examples show that the proposed method is efficient in simultaneously searching new topology, prestress and configuration of cable domes with high vertical stiffness. Topology, configuration and prestress are the three main factors that affect the mechanical properties of a tensegrity structure, so the design and optimization of tensegrities can be classified into three categories respectively. There are large amounts of researches focuses on form-finding, force-finding as well as prestress and configuration optimization of tensegrity structures, while the study of topology optimization of tensegrity structures with certain mechanical properties is limited. To this end, the optimization of cable domes with high vertical stiffness is studied. This study proposes a novel encoding scheme to generate new cable domes and uses genetic algorithm to do topology optimization of cable domes with topology, configuration and prestress as variables simultaneously. The numerical results extend the existing forms of cable domes.

## Phase Field Modeling of the Sintering Process

Weixin Ma<sup>\*</sup>, Yongxing Shen<sup>\*\*</sup>, Wentao Yan<sup>\*\*\*</sup>

<sup>\*</sup>University of Michigan-Shanghai Jiao Tong University Joint Institute, Shanghai Jiao Tong University, <sup>\*\*</sup>University of Michigan-Shanghai Jiao Tong University Joint Institute, Shanghai Jiao Tong University, <sup>\*\*\*</sup>Department of Mechanical Engineering, Northwestern University

### ABSTRACT

Modeling of sintering process has been developed in different scales with different methods. Our work focuses on metals at the microscale, which is applicable to the preheat stage of 3D printing. We hope it could help to finding the proper temperature and time in preheating to improve the quality of 3D printing. We consider the sintering process between two metal powders. The governing equation is given by: Cahn-Hilliard Equation for the conserved density field  $c$  [1]  $\frac{\partial c}{\partial t} = \nabla \cdot (M \nabla \cdot \frac{\delta F}{\delta c}(x,t))$  Allen-Cahn Equation for the un-conservative order parameter field  $\phi$  [2]  $\frac{\partial \phi}{\partial t} = -L \nabla \cdot \frac{\delta F}{\delta \phi}(x,t)$  where  $M$  is the concentration mobility tensor,  $F$  is the total free energy and  $L$  is the order parameter scalar mobility.  $x$  and  $t$  represent spatial position vector and time respectively. In our previous work [3], we model the sintering process of metal powder at the nanoscale. Only the grain boundaries at the grain surface are taken into account. However, for micro scale metal powders, each particle is consisted of several grains, which means grain boundaries are within each particles. The evolution of grain boundaries inside the particle and in between two particles now has been added. Representative examples will be included to showcase the method. References: [1] Cahn JW, Hilliard JE. J Chem Phys 1958;28:258. [2] Cahn JW. Acta Metall 1961;9:795. [3] Wentao Yan, Ya Qian, Weixin Ma, Bin Zhou, Yongxing Shen, Feng Lin, Modeling and Experimental Validation of the Electron Beam Selective Melting Process, Engineering, Volume 3, Issue 5, 2017, Pages 701-707.

## Subdivision Stencils around Extraordinary Vertices with Quasi-G2 Continuity and with Applications in Isogeometric Analysis

Weiyin Ma<sup>\*</sup>, Yue Ma<sup>\*\*</sup>

<sup>\*</sup>City University of Hong Kong, <sup>\*\*</sup>City University of Hong Kong

### ABSTRACT

Abstract: This talk presents a novel method to construct subdivision/refinement stencils near extraordinary vertices with limit surfaces having quasi-G2 continuity at extraordinary positions. Most existing subdivision schemes result in unbounded curvature or highly oscillated curvature around an extraordinary vertex. Some researchers minimize the Gaussian curvature variation for a set of central surfaces through tuning the subdivision masks. Some other researchers explicitly optimize the local quadratic precision of eigenvectors corresponding to the subsubdominant eigenvalue utilizing the extra degrees of freedom obtained through tuning the subdivision stencils for triangle control meshes. In our work, we optimize the subdivision stencils to provide the best possible curvature behaviour near extraordinary vertices with respect to G2 requirements for stationary subdivision of quadrilateral meshes. The subdivision stencils include that for one-ring new face vertices, one-ring new edge vertices and updated vertex vertices near an extraordinary vertex similar to that of Catmull-Clark subdivision, but with maximum possible degrees of freedom for further optimizing the stencils. We first construct the subdivision stencils to ensure subdivision properties including G1 continuity with bounded curvature at extraordinary positions. The remaining degrees of freedom of the constructed subdivision stencils are further used to optimize the subdivision towards a scheme with G2 continuity through direct optimization of the eigenbasis functions corresponding to the subsubdominant eigenvalue of the subdivision and to achieve other desired limit surface properties. A systematic evaluation shows that the constructed subdivision stencils produce better limit surfaces in extraordinary regions than that of other similar existing subdivision schemes with respect to a necessary and sufficient criterion for C2 continuity (Peters and Reif 2008) and local curvature behaviour. The resulting subdivision stencils can be integrated with either subdivision schemes for quadrilateral meshes of arbitrary topology or unstructured T-splines (Scott et al. 2013). Applications of the resulting schemes using the proposed refinement stencils in isogeometric analysis (Hughes et al. 2005) are also discussed. References: [1] J. Peters and U. Reif, *Subdivision Surfaces*, Springer-Verlag Berlin Heidelberg, 2008. [2] M. A. Scott, R. N. Simpson, J. A. Evans, S. Lipton, S. P. A. Bordas, T. J. R. Hughes, T. W. Sederberg, *Isogeometric boundary element analysis using unstructured T-splines*. *Computer Methods in Applied Mechanics and Engineering* 254: 197-221, 2013. [3] T. J. R. Hughes, J. A. Cottrell and Y. Bazilevs, *Isogeometric analysis: CAD, finite elements, NURBS, exact geometry and mesh refinement*. *Computer Methods in Applied Mechanics and Engineering* 194(39-41):4135-4195, 2005.

## A Semi-analytical Method for Critical Buckling Analysis of 2D Nano-materials

Yong Ma<sup>\*</sup>, Yuli Chen<sup>\*\*</sup>, Shengtao Wang<sup>\*\*\*</sup>, Yanguang Zhou<sup>\*\*\*\*</sup>

<sup>\*</sup>Institute of Solid Mechanics, Beihang University (BUAA), <sup>\*\*</sup>Institute of Solid Mechanics, Beihang University (BUAA), <sup>\*\*\*</sup>Institute of Solid Mechanics, Beihang University (BUAA), <sup>\*\*\*\*</sup>Aachen Institute for Advanced Study in Computational Engineering Science (AICES), RWTH Aachen University

### ABSTRACT

The performances of 2D nano-materials in micro- and nano-electronics and devices are significantly affected by their morphologies, which depend on the surface features of the supporting substrate. In practical applications, non-developable substrates are widely used, and thus it is of great importance to predict the final morphology of 2D nano-materials on non-developable substrates. To this end, energy-based theoretical models are developed for several substrates with different topographies and a mode-independent energy buckling analysis method (MIEM) is proposed to analyze the final morphology. By molecular dynamics simulations, three typical morphologies of 2D nano-materials, completely conforming, partial delamination and wrinkling, are observed. Based on simulation results, theoretical models are established for spherical, concave and convex substrate, respectively. Applying the principle of minimum energy, the strain in 2D nano-materials can be derived. And then we propose a half-analytical method to predict the critical buckling of structures, named mode-independent energy-based buckling analysis method (MIEM). In MIEM, the pre-knowledge of buckling mode is not required, and the modified Cauchy-Born rule is employed to obtain the equilibrium configuration of atom-structures, which can greatly reduce computation load. Meanwhile, it can take full advantage of the structure characteristics, such as periodicity and flatness, to further reduce the calculation amount so that the method is more suitable for large-scale nanostructures than the atomistic simulations. Besides, it is as accurate as atomic simulation because it is derived directly from the atomic potentials and no additional simplifications are made. With this method, whether the atom-structure buckles can be determined, and finally the critical conditions of different morphologies can be derived. These results can provide guidelines to design high quality graphene-based electronics and can be extended as the surface roughness standard for the supporting substrates. Reference [1] Zhou Y, Chen Y, Liu B, et al. Mechanics of nanoscale wrinkling of graphene on a non-developable surface[J]. Carbon, 2014, 84(1):263-271. [2] Chen Y, Ma Y, Wang S, et al. The morphology of graphene on a non-developable concave substrate[J]. Applied Physics Letters, 2016, 108(3):031905. [3] Wang S, Chen Y, Wu J, et al. A mode-independent energy-based buckling analysis method and its application on substrate-supported graphene[J]. International Journal of Solids and Structures, 2017, 124: 73-88. Acknowledgments National Natural Science Foundation of China (nos. 11622214, 11472027 and 11202012).

## An Architecture of Flexible Host Platform for Multi-Physics Numerical Computation

Zhaosong Ma<sup>\*</sup>, Chun Feng<sup>\*\*</sup>

<sup>\*</sup>Institute of Mechanics, Chinese Academy of Sciences, <sup>\*\*</sup>Institute of Mechanics, Chinese Academy of Sciences

### ABSTRACT

A host platform has been designed for numerical computation, including FEM, FVM, DEM, as well as particle simulation. The platform supports any number of user-defined multi-physics variables, which are optionally shown via OpenGL. The solving flow can be driven by JavaScript, written by developer or end user. In addition, a result cache server has been developed to support high performance calculation and real-time post processing. The Platform is written in C++ language, with complete post-processing and limited pre-processing functionality, which can host user-written kernel solvers, user-written GUI modules. Users can define their own multi-physics problem description, problem associated parameters, DOFs, and any number of result variables. These variables can be of any data types. To define a variable, a C++ class should be filled to describe the variable's hierarchy, the variable's name and other information, with a self-defined sample variable to tell the host about the data type and data size. To improve post-processing performance, a cache mechanism has been designed by setting up an embedded result server to run in another worker thread. The server maintains a result queue with an adaptive size limit determined by system available memory. A kernel solver submits result asynchronously. When a solver module received a set of results, the server records the step number, the time stamp, and push the result data into the back of result queue, which is instantly rendered on the screen. If the queue size exceeds the limit, the front of the queue is popped up. Whatever the queue size exceeds the limit, the step result is written to disc. This process runs in background while the kernel solver is proceeding. A JavaScript host has also been implemented in the platform by means of windows script hosting technique which provides syntax checking, interpreting, and debugging functionality. The script engine supports ActiveX and COM Technology, which makes the platform able to call most third-party functionalities like CAD, CAE, GIS, word processing and database. The script can be from a source file or from a command input, either of them can take full control of the solving flow. Unlike Python and Java, JavaScript supports "Just in Time Operation" (JIT), which is very important to interactive computation. For example, users can change the solving flow whenever needed. The architecture of the platform is introduced and various results are shown.

## Design of an Endovascular Chemofilter Device with CFD Modeling

Nazanin Maani<sup>\*</sup>, Daryl Yee<sup>\*\*</sup>, Julia Greer<sup>\*\*\*</sup>, Steven Hetts<sup>\*\*\*\*</sup>, Vitaliy Rayz<sup>\*\*\*\*\*</sup>

<sup>\*</sup>Purdue, <sup>\*\*</sup>Caltech, <sup>\*\*\*</sup>Caltech, <sup>\*\*\*\*</sup>UCSF, <sup>\*\*\*\*\*</sup>Purdue

### ABSTRACT

Purpose: Intra-Arterial Chemotherapy (IAC) used for treating Hepatocellular Carcinoma by local injection of Doxorubicin (Dox) into the tumor, causes systemic toxicity due to 50-70% of the drug passing to the systemic circulation [1]. A catheter-based Chemofilter device can be deployed in the veins downstream of the tumor to filter the excessive Dox from blood during the IAC procedure. The optimal design of the Chemofilter will minimize pressure drop and flow disturbance, while providing sufficient binding sites for Dox chemical adsorption on the filter's surface. In this study, the effect of the Chemofilter's configuration, microstructure, and surface texture on hemodynamic performance of the device is investigated with CFD simulations. Methods: The chemofilter's membrane consists of 3D-printed micro-trusses that form an interconnected porous lattice of symmetric micro-units. The micro-units provide adequate porosity for the passage of blood cells, and large contact area for the Dox binding. To study the flow through the individual micro-units (100-200  $\mu$ m) as well as the whole device (about 10 mm), a multi-scale approach is used for CFD modeling of the Chemofilter. The general configuration of the membrane resembles an umbrella which is installed on a supporting structure, inspired by the RX AccUNET embolic protection device. The design parameters include 1) the leading angle, 2) the number of membrane sectors, 3) the thickness of membrane, and 4) the size of gap between the membrane and the vessel wall. The shark skin effect, i.e. surface texturing, is investigated to examine the shear stress reduction and platelet activation on the surface. The numerical results are obtained with the finite-volume solver Fluent (ANSYS). Results: The simulations of hemodynamic performance for different Chemofilter configurations indicate that the pressure drop across the membrane increases with the leading angle, the number of umbrella sectors, and the membrane thickness. However, an acute leading angle of the device can result in increased area of flow recirculation and stagnation. The fewer number of the sectors results in the larger gap near the wall, thus allowing a large fraction of the flow to bypass the filter. Therefore, the membrane sectors should be curved and extended to the wall in order to prevent escaping jets. The application of the shark-skin texture on the surface results in reduction of the shear stress, by shifting the regions of high velocity and vorticity away from the surface. Reference: M.S. Aboian et al., Biomed microdevices. 2016;18(6):98.

## A Geometrically Exact Euler-Bernoulli Beam Formulation with an Interface to Arbitrary Nonlinear Material Laws

Sascha Maassen<sup>\*</sup>, Cátia da Costa e Silva<sup>\*\*</sup>, Paulo de Mattos Pimenta<sup>\*\*\*</sup>, Jörg Schröder<sup>\*\*\*\*</sup>

<sup>\*</sup>Universität Duisburg-Essen, <sup>\*\*</sup>University of São Paulo, <sup>\*\*\*</sup>University of São Paulo, <sup>\*\*\*\*</sup>Universität Duisburg-Essen

### ABSTRACT

In this work a geometrically exact Euler-Bernoulli beam finite element is presented, which is based on [1] and subject to [3]. The beam formulation is embedded into the three-dimensional space and obeys the Euler-Bernoulli hypothesis of remaining plain cross-sections and of shear rigidity when subjected to bending deformation. The rotational group is parametrized using Rodrigues formula with an efficient update scheme for the parameter set. In hand with out of plane warping, this allows for arbitrary large rotations and deformation within this model. For the implementation of arbitrary material laws, as shown in [2], the resulting deformation measure needs to result in stress states at each material point, that obeys the special stress condition of beams. This is enforced by a local iteration which allows application of arbitrary material laws. Throughout this presentation the restrictions of hyperelastic materials and rectangular cross-sections is made. On the element level a straight reference configuration is considered where the displacements are interpolated using C1 continuous Hermite polynomials which a priori leads to satisfaction of the shear rigidity constraint. In many engineering applications, non-straight connections of structural members with variable cross section geometries and/or materials have to be analyzed. We address this modelling challenge with a unique rotational continuity extension which allows for the modeling of material- and geometrical- discontinuities. The necessity of the continuous rotational group is enforced using Lagrange multipliers and a penalty method. The capabilities of the formulation will be displayed through numerical examples. 1.Pimenta P. M. and Yoho T., "Geometrically-exact analysis of spatial frames", Applied Mechanics Reviews, ASME, New York, v.46, 11, 118-128, 1993. 2.Klinkel, S. &&& Govindjee, S. "Using finite strain 3D-material models in beam and shell elements", Engineering Computations, v.19, 3,254-271, 2002. 3.Silva, C.C., Maassen, S., Pimenta, P.M. &&& Schröder, J. "Geometrically exact analysis of Bernoulli-Euler rods", in preparation for Computer Methods In Applied Mechanics and Engineering, 2017.

## **INVERSE METHOD FOR DETERMINATION OF HARDENING PARAMETERS OF DUCTILE MATERIALS BY A MULTI-IMAGE ANALYSIS OF INDENTATION PROFILES FROM HARDNESS TESTS: NUMERICAL AND EXPERIMENTAL ASPECTS**

L.Q. MACHADO<sup>1</sup> AND L. MALCHER<sup>2</sup>

<sup>1,2</sup> University of Brasília, Faculty of Technology, Department of Mechanical Engineering, Campus Darcy Ribeiro, Brasília – Distrito Federal – Brazil.

<sup>1</sup> [lucasqmachado@gmail.com](mailto:lucasqmachado@gmail.com)

<sup>2</sup> [malcher@unb.br](mailto:malcher@unb.br)

**Abstract:** The plastic behavior of a material is resultant of non-linearities which leads to complex stress-strain fields, making it difficult to devise analytical relationships beyond the elastic domain. Traditionally, the material's stress-strain relationship has been acquired from uniaxial testing, which is widely used to describe its behavior under plastic deformation. However, the hardness test is more versatile, operative, cheaper and faster than the uniaxial test. Therefore, over the past years new techniques have been devised to obtain the stress-strain relationship of bulk metallic materials from the reaction curve of an indentation test with the formulation of an inverse method for parametrical identification, which is possible thanks to the development of numerical methods and instruments able to provide the load-displacement data by continuously measuring the depth of indentation. When it comes to traditional hardness tests, such as in the Brinell, Knoop, Rockwell and Vickers, they have been mostly used as a way to assess the capability a material has to resist plastic deformation by relating the applied load to the resultant area or depth of indentation. From the Brinell hardness test, due to its simplicity and versatility, a newer approach was devised to correlate this test to the material's full plastic characterization by finding its hardening parameters. The methodology consists of performing four Brinell hardness tests to have a representative material's response and from it do a multi-image comparison of the resultant indentation profiles obtained from a confocal laser microscope with the predicted output of repeated FEM modelling. The parametric identification is conducted by an optimization technique using the Trust-Region-Reflective Least Square Algorithm available in the MATLAB's Optimization Toolbox. In this process several trial stress-strain curves are provided to minimize the discrepancy between numerical and experimental data in an iterative FEM modeling of the indentation process until reaching the established tolerance and thus providing the hardening parameters that best fit the experimental data. The new method then numerically replicates the same indentation impression left in the specimen by the indenter in a real experiment. The methodology for characterizing the elastic-plastic properties from the indentation's reaction curve is also presented in parallel to the multi-image analysis to compare its performance, since both were developed seeking to replace the traditional uniaxial test. Finally, the hardening curves obtained from uniaxial and indentation tests are compared to corroborate the new methodology.

**Keywords:** parametric identification, indentation multi-image analysis, hardening curve, optimization process.

## 1 INTRODUCTION

Indentation hardness tests have been traditionally understood as a way to assess the capability a material has to resist plastic deformation by relating the applied load to the resultant area or depth of indentation, such as in Brinell, Knoop, Rockwell and Vickers hardness tests <sup>1</sup>. Over the past years, new techniques have been devised for probing the mechanical properties of materials by an indentation test. This is mainly due to the development of instruments able to provide the indentation load-displacement data by continuously measuring the depth of indentation while a normal load is being applied on the material and thanks to numerical methods, such as the Finite Element Method, that makes possible to analyze complex stress-strain fields in contact mechanics <sup>2-5</sup>.

The plastic behavior of a material is resultant of non-linearities which leads to complex stress and strain fields, making it difficult to devise analytical relationships beyond the elastic domain. Traditionally, the material's stress-strain relationship acquired from uniaxial testing has been widely used to describe its behavior under plastic deformation. However, the hardness test is more versatile, operative, cheaper and faster than the uniaxial test. Therefore, efforts have been made in using the indentation hardness test to obtain the stress-strain relationship of a material under plastic deformation with the formulation of an inverse method for parametric identification aided by numerical methods.

While the uniaxial test is the forward method to obtain the plastic parameters of a material, the indentation test needs to be aided by numerical methods such as the FEM and other optimization methods in order to characterize the material's plastic behavior and then yielding the hardening parameters that describe the stress-strain relationship of it. The most popular way of evaluating the material response to an indentation load is by analyzing the material's indentation reaction curve<sup>3,4</sup>. However, this work addresses the material response in a newer way by analyzing the resultant indentation impression profile. Basically, the process is the same, the difference is the data being analyzed. Since there are some other effects related to the indentation profile, such as pile-up and sink-in phenomena, this work seeks to provide a more precise assessment of the indentation process and thus a more accurate determination of the material's hardening parameters.

## 2 EXPERIMENTAL PROCEDURES

Both traditional tensile tests and indentation hardness tests are carried out for a marine grade steel. The tensile test is the direct way to determine the hardening parameters of the material, while the indentation hardness test is part of an inverse method of parametric identification aided by numerical methods. In this contribution, the hardening curve is approximated by an exponential function according Ludwick (1909), and represented as:

$$\sigma_y(\bar{\epsilon}^p) = \sigma_{y0} + H\bar{\epsilon}^p{}^n, \quad (1)$$

where  $\sigma_{y0}$  is the material's initial yield stress,  $H$  is the isotropic hardening modulus,  $\bar{\epsilon}^p$  represents the accumulated plastic strain, and lastly,  $n$  is the so-called hardening exponent. Therefore, to have a way of comparison and to validate the new methodology, a uniaxial tensile test is performed. In the sequence, uniaxial and indentation hardness testes are addressed.

### 2.1 Uniaxial Tensile Test

The tensile test was conducted in an MTS machine (Figure 1) with a 100 kN load capacity, where the specimen was elongated until collapsing. The deformation was measured aided by a clip gauge of 25 mm of length gauge (+ 5 / -2.5 mm).



**Figure 1: MTS with Clip Gauge Used for Tensile Test.**

The hardening stress-plastic strain relationship is shown in Figure 2, which is later used to evaluate the proposed inverse method for parameter identification.

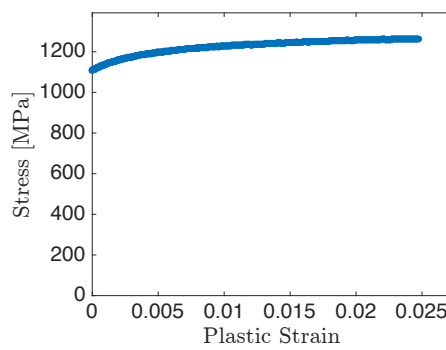


**Figure 2. Stress-Strain Curve from Uniaxial Test and Nonlinear Regression.**

## 2.2 Brinell Hardness Test

The Brinell indentation tests were realized in the Zwick/Roell ZHU250 universal hardness machine using a carbide tungsten indenter of 2.5 mm diameter, as shown in Figure 3.

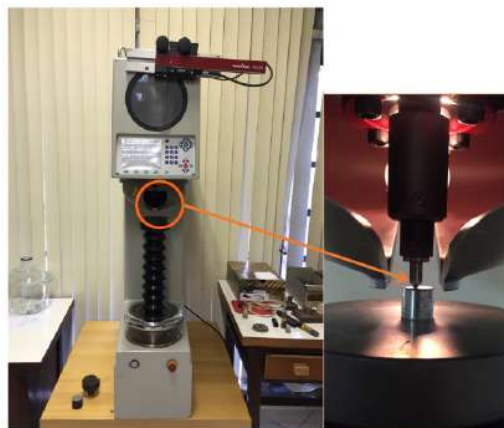


**Figure 3. Zwick/Roell ZHU250 Universal Hardness Machine.**

The specimen is then submitted to three different load configurations of the Brinell hardness test: HBW 31.25/2.5, HBW 62.5/2.5 and HBW 187.5/2.5. The indentation profiles (Figure 4) are assessed with a *LEXT OLS4100* laser confocal microscope

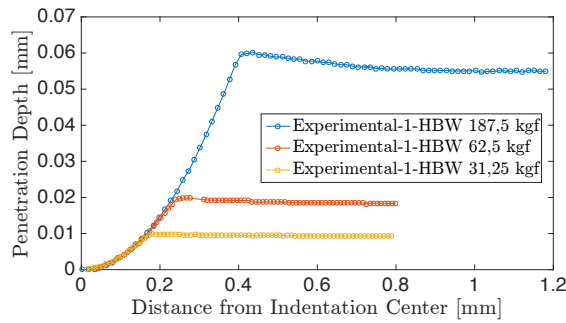


Figure 4. Indentation Profile

### 3 NUMERICAL APPROACH

The numerical analysis was carried out in a Finite Element Environment using Abaqus. This software is licensed by Dassault Systèmes, 2012 and is widely used by engineers to solve diverse problems encompassing a wide range of industrial applications. This section presents a discussion on contact formulation and mesh convergence to decide the most suitable model configuration. Therefore, comparisons are made in terms of contact pressure, penetration depth and simulation time for procedures comprising the elastic and the elastic-plastic formulations. For simulations purely elastic, the predicted output is compared to the analytical solution provided by Hertz's<sup>6</sup> theory while the elastic-plastic numerical response is used for mesh convergence purposes. The elastic analyses are performed for a rigid indenter while the elastic-plastic assumes a deformable indenter with Elastic Modulus of 645 GPa and Poisson Ratio of 0.22. The specimen is a marine grade steel with Elastic Modulus of 200 GPa and Poisson Ratio of 0.3.

#### 3.1 Part Module

The sphere-plane contact is modeled in a 2D axisymmetric configuration. Both bodies are defined as deformable shells, however, when necessary to grant a rigid characteristic to the sphere, its elastic modulus is assigned a value four orders greater than the specimen's elastic modulus.

In Figure 5, it can be seen that both, specimen and indenter, were partitioned into different regions. It was done to facilitate meshing, making it possible to have suitable refinement in the contact region and, at the same time, to avoid unnecessary elements in other regions less affected by the stress field due to the contact.

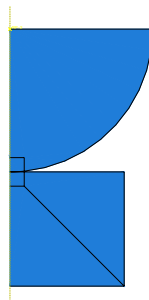


Figure 5. Contact Configuration

#### 3.2 Property Module

Each defined part indenter and specimen is made of a different material, both isotropic. To define the indenter's material property is enough to consider it has only a linear elastic

behavior, which is done by informing its elastic modulus and Poisson ratio. The specimen may or may not behave elastically depending on the applied load it bears; therefore, it is necessary to perform an elastic-plastic analysis. The elastic-plastic analysis requires different fields depending on the plasticity model. For this case, besides the elastic definition, the classical metal plasticity model was adopted, which requires the knowledge of the stress-plastic strain data representing the material hardening behavior.

To every part must be assigned material property. Once the materials are defined, sections are created to attend the parts' specifications. Since each part is made of one material kind, one section is created to each part and the correct material property is associated to its respective section. Respecting the pre-established conditions, the section is defined as homogeneous solid with thickness of 1 *mm*.

### 3.3 Assembly Module

In the assembly, the part instances are created and positioned relatively to each other in a global coordinate system, as shown in Figure 5, in a way where the lowest point of the indenter is in contact with the leftmost upper point of the specimen.

### 3.4 Step Module

The simulation was carried out in three steps, defining in this manner the indentation test. In the initial step the contact interaction between indenter and specimen is defined, the boundary conditions establish that the specimen is fully restrained at its base and that there is a symmetry about a plane  $X = \text{constant}$ . A first step, called Penetration, defines that the indenter can only move vertically relatively to the specimen, deforming it. This vertical displacement is caused by a load applied to the indenter. Thereafter, the step two establishes that the indenter returns to its initial position, which allows the materials to spring back so that the impression's maximum depth is not the final depth. The conditions of each step are propagated to the following step, with exception of the load established on the Penetration step that is not propagated to the next step.

During Penetration, instabilities in the model may arise causing local velocities to increase due mainly to mesh size and material behavior. If that happen, part of the strain energy needs to be dissipated, which can be achieved by adding a viscous force to the global equilibrium equations. This viscous force is proportional to a damping factor that in turn is proportional to the nodal velocities. Therefore, an automatic stabilization method with a constant damping factor is considered. However, defining the appropriate damping factor is not an easy task and depends on results from previous runs. An optimal damping factor is found when converged solution is obtained and the dissipated stabilization energy is sufficiently small.

### 3.5 Interaction Module

The interaction module is used to define contact interactions, tie constraints and coupling constraints in the model. Addressing firstly the contact interactions, Abaqus makes it possible to define contact in three main ways: general contact, contact pairs and contact elements.

The model analyzed here counts with the contact of two bodies defined as deformable in a two-dimensional configuration. The physical proximity of these two bodies in the assembly does not indicate interaction, therefore it is necessary to specify what kind of interaction exists between their surfaces and its properties. The contact pair is the most suitable type of interaction for this case because there are only two surfaces that may interact with each other and having a pairwise specification of the contact results in a more robust analysis. Thus, in the Part Module the indenter and the specimen were divided in regions for contact definition

and efficiency purposes, so that the extension of its contact surfaces is appropriate for the contact.

**Contact Formulation.** Once the contact interaction type is determined, the contact formulation defined subsequently will have a considerable impact on how the surfaces interact. It is based on master and slave definitions, contact discretization and tracking approaching. Since the indenter is stiffer and may have coarser mesh, its contact surface is defined as master while the contact surface from the specimen acts as the slave surface. The contact discretization is defined as surface-to-surface and accounts for the way that conditional constraints are applied to interacting surfaces. For a given mesh refinement, the surface-to-surface discretization tends to provide more accurate stress and pressure results than the node-to-surface discretization. It happens because the surface-to-surface discretization resists penetrations in an average perspective over finite regions of the slave surface while the node-to-surface allows master nodes to penetrate the slave surface causing forces to concentrate at the slave nodes. This results in an uneven distribution of pressure over the surface. Figure 6 shows the contact pressure response for both contact discretization methods: surface-to-surface (a) and node-to-surface (b) for the same mesh refinement.

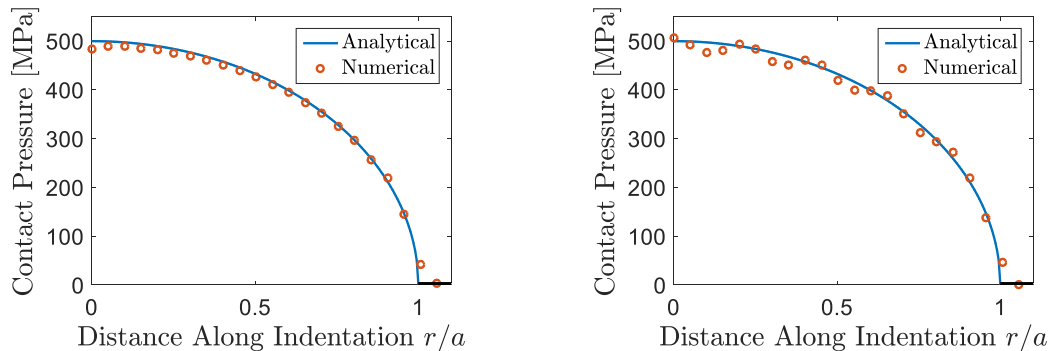


**Figure 6. Contact Pressure Response from Surface-to-Surface (a) and Node-to-Surface (b) Contact Discretization Methods.**

Along the numerical responses for contact pressure, the chart shows also the analytical result, as described by Hertz<sup>6</sup>. While the surface-to-surface method provides contact pressure values uniformly distributed along the analytical solution, the node-to-surface method provides values fluctuating up and down near the analytical values.

To have a better idea of which discretization method is more appropriate, a point to point scalar relative error is calculated comparing the exact and numerical results, which is shown in the Figure 7:

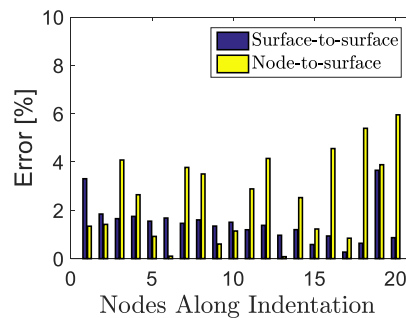


**Figure 7. Contact Pressure Error for Each Node Along Indentation.**

Figure 7 gives a clear understanding of the nodal pressure error distribution along indentation for the surface-to-surface and node-to-surface discretization methods. As it can be seen, the node-to-surface nodal errors oscillates from 0.08% to almost 6 % in the contact pressure prediction, while the surface-to-surface nodal errors does not oscillate as much. Thus, to decide which model is more appropriate, a second error calculation is performed measuring the Frobenius norm of the error and exact vectors, as shown in Equation 3:

$$Error = \frac{\|R_i^{FEM} - R_i^{Exact}\|_F}{\|R_i^{Exact}\|_F} \quad (2)$$

where  $R_i^{FEM}$  and  $R_i^{Exact}$  are the numerical and the analytical responses for each analysed node  $i$ . Equation 23 evaluates the numerical responses as a whole and yields a relative error of 1.69 % for the surface-to surface and 2.67 % for the node-to-surface contact discretization models. Since the computational time is not an issue for these analyses, the surface-to-surface contact discretization is the one that provides better results.

The tracking approach can be defined as finite-sliding or small sliding, being responsible for dictating the relative motion relationships between the interacting surfaces. For the case where the relative motion of the contact surfaces is small, the assumption of a contact pair defined from the undeformed body configuration is acceptable and the small-sliding tracking approach can be used. However, when facing significative relative motion, the finite-sliding is preferable since the contact pair is determined upon the relative tangential motion of the contact surfaces. Using the small-sliding tracking approach represents computational savings, but also means less accuracy. For the same model in analyses, the small sliding tracking approach yielded a pressure error of 1,58 % and 1:14 of computational time while the finite sliding tracking approach yielded 1.47 % pressure error and 1:17 of computational time.

For either cases, when using the node-to-surface discretization method or the small sliding tracking approach, it was necessary to apply a damping factor to force convergence, otherwise the simulation would fatally abort due to excessive node/element penetration. For all cases analyzed so far, the small sliding tracking approach was ignored. However, when the material being assessed is too soft and a high load is applied, convergence is more easily reached if a damping factor is considered and the node-to-surface contact discretization method is applied.

**Contact Constraint Enforcement Methods.** One of the issues that arises when dealing with computational contact mechanics has to do with defining a relationship that establishes a rule for surface's motion. The chosen contact constraint enforcement method establishes how contact constraints are resolved in the analysis. Two main approaches are the Penalty and the Lagrange Multiplier methods.

The penalty method in its formulation allows penetration whose amount depends on the stiffness that the penalty term grants to the system. Its kinematical constraint equation is fulfilled when the stiffness  $\epsilon \rightarrow \infty$ , yielding the same solution given by the Lagrange multiplier method<sup>7</sup>. For this reason, the Lagrange multiplier method usually add more degrees of freedom to the model and requires more iterations to achieve the solution, hence the computational costs increase.

For protection and efficiency against numerical errors related to ill-conditioning, that can occur if a high contact stiffness is in effect, the Augmented Lagrange Multiplier method is adopted, which uses the same kind of stiff approximation as the penalty method but with augmented iterations to improve the accuracy of the approximation.

**Constraints** Tie and coupling constraints are used in the model to define the relationships among part instances and references points. The tie constraint is used from the necessity to fuse two-part instances that belong to the same body but with dissimilar meshes, as can be seen in Figure 8 for the indenter (a) and the specimen (b):

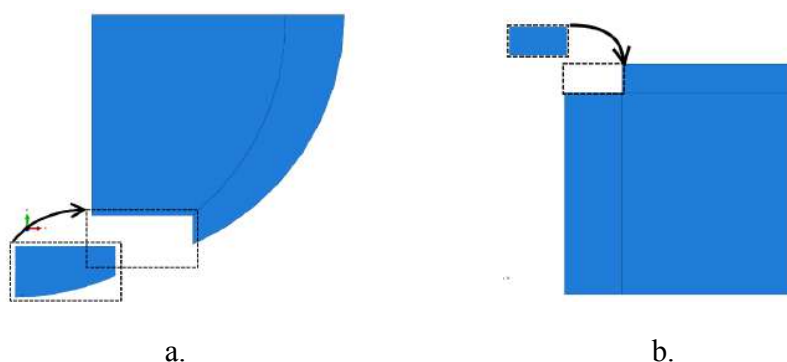


**Figure 8. Tie Constraints Applied to the Indenter (a) and the Specimen (b)**

There are two reference points whose motion constrains the motion of two surfaces, thus the necessity to use the coupling constraint to perform this task. The first reference point is used to transfer a concentrated force to the whole model by applying it to a reference point that has a coupling constraint relationship with the indenter's upper surface, as shown in Figure 9.a. Second, the bottom of the specimen is totally constrained with an encastre, However, for output readings purposes, this condition is applied to the reference point and a coupling constraint between this point and the specimen's bottom surface is applied, as shown in Figure 9.b.

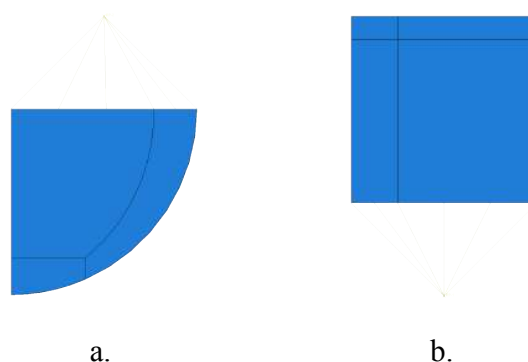


**Figure 9. Coupling Constraints Applied to the Indenter (a) and to the Specimen (b).**

### 3.6 Load Module

Load and boundary conditions are applied to the model, and since they are step-dependent objects it is necessary to specify in which steps they are active, as it has been described in the Step Module section. At the initial step, the encastre boundary condition is applied to a reference point that is coupled to the specimen's bottom surface (Figure 9.b). The axisymmetry boundary condition is applied to the specimen's and indenter's surfaces lying on the symmetry line. The indenter's initial position is defined by allowing its motion in the vertical direction only, by constraining the motion of the reference point that is coupled to the indenter's upper surface (Figure 9.a) in the horizontal direction and from rotating about the z-axis. In the subsequent step a concentrated force is applied to the reference point coupled to the indenter's upper surface so that the load is transmitted to the whole model. The last step consists in bringing the indenter back to its initial position allowing the specimen to spring back having an elastic recovery after unloading.

### 3.7 Mesh Module

The process of generating meshes requires a convergence study to guarantee the needs of the analysis. First, for efficiency purposes, a region of contact was defined in the indenter and in the specimen to make it possible to assign dissimilar meshes to the same body without the need of a zone of transition between them, as shown in Figure 10.

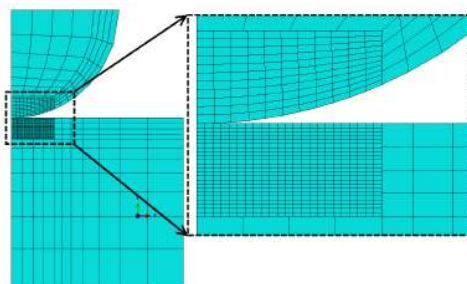


**Figure 10. Meshing Assignment.**

As it can be seen in Figure 10, the contact zone has a finer mesh than the other regions for efficiency purposes and the indenter's mesh is slightly coarser than the specimen's due to its greater stiffness and also to minimize the penetration of the master surface nodes in case of choosing the node-to-surface contact. The number of nodes and elements varies depending on the contact length, which in turn depends on the load applied, material definitions and if the analysis is purely elastic or elastic-plastic. In general, the contact length is estimated analytically, when dealing with elastic analysis, or experimentally, when for the elastic-plastic analysis. However, despite the length of contact, the coarser mesh is programmed in a way where the elements in the vicinity of the contact zone have five times the size of the finer mesh with a bias applied making it to increase in size until reaching an element size five times greater than the first one defined for the coarser mesh.

Using the surface-to-surface contact discretization method, a mesh converge assessment is carried out for two element types (Table 1) and five mesh refinement levels of the contact zone. The two element types are:

**Table 1. Element Types Description.**

Element Type	Description
CAX4R	A 4-node bilinear axisymmetric quadrilateral, reduced integration, hourglass control.
CAX4	A 4-node bilinear axisymmetric quadrilateral.

The refinement level takes into consideration the experimental contact length obtained from a Brinell Hardness test HBW 187.5/2.5 that yielded an indentation diameter of 1.03 mm. The number of nodes in the contact zone depends of two definitions: the length of the contact region and the mesh element size. For a better analysis, the length of the contact region is not defined as being of the same as the experimental one but assumes a size two times longer than the experimental indentation radius. Once the length of the contact region is defined, the number of nodes in the contact region depends only of the mesh element size. The equivalent plastic strain and the von Mises equivalent stress convergence are the assessed variables used to define the best refinement level. To capture its distribution along the contact, the mesh is initially built with an element size ten times smaller than the adopted contact length, then fifteen, twenty, twenty-five, and thirty.

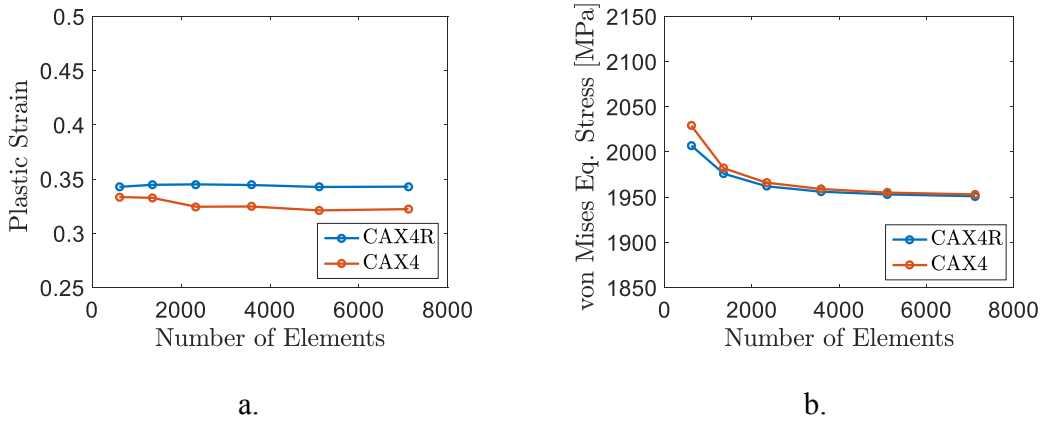


**Figure 11. Mesh Convergence Analysis.**

Figure 11 shows that, even though the full integration is more expensive than the reduced integration, both converge to the same amount of von Mises equivalent stress and keep approximately amount of equivalent plastic strain for different refinement levels. On the other hand, when going from reduced to full integration, the discrepancy between them is not significant enough to pay back the computational cost when using full integration. Therefore, the mesh configuration that yields the appropriate response in a suitable amount of time is composed of 2335 4-node bilinear axisymmetric quadrilateral elements with reduced integration.

#### 4 RESULTS

The optimization procedure is a curve fitting process. New parameters are suggested until the numerical indentation impression (Figure 12.a) matches the experimental data (Figure 12.b).

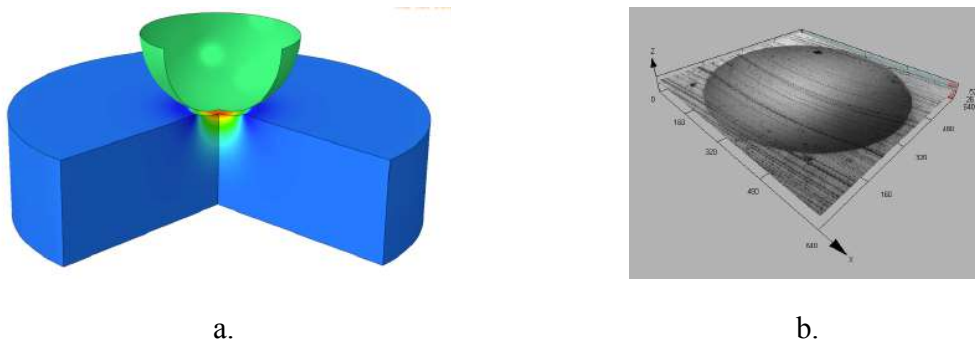


**Figure 12. Simulation Configuration**

The parametric identification is conducted by an optimization technique using the Trust-Region-Reflective Least Square Algorithm available in the MATLAB's Optimization Toolbox. After 27 global iterations, the objective function was satisfied, and the optimization process yielded the best fitting profile shown in Figure 13.

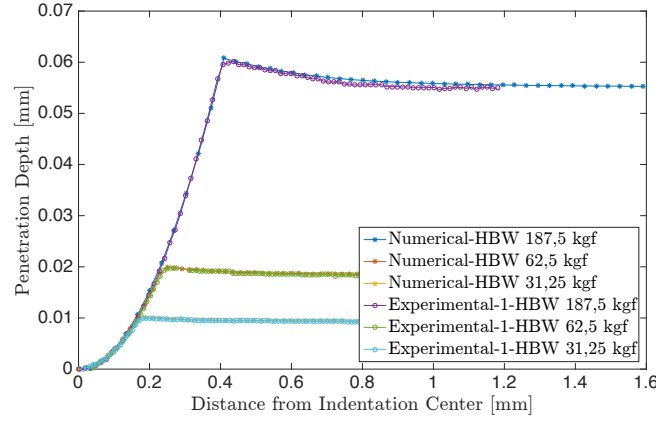


**Figure 13. Profile Best Fitting.**

The optimum hardening parameters that generated this best fitting are  $\sigma_{y0} = 1081.3 \text{ MPa}$  for the initial the yield stress,  $H = 769.9$  for the hardening modulus and  $n = 0.43$  for the hardening exponent (Equation 1).

#### 4.1 Comparative Analysis

The optimization routine generated the optimum parameters used to describe the hardening curve for the marine grade steel. The hardening curve obtained from the indentation test is presented in Figure 14 in comparison with that obtained from uniaxial test.

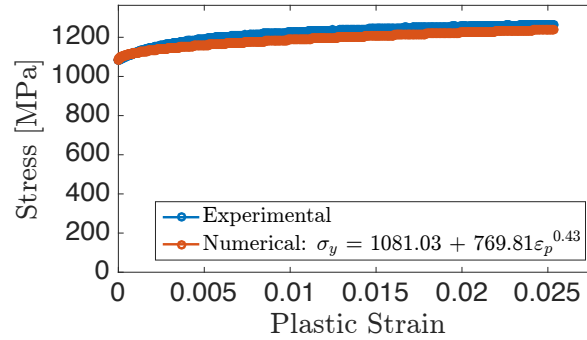


**Figure 14. Comparison Between Hardening Curves Obtained by Tensile and Indentation Tests**

From Figure 14, the error between numerical and experimental data is 2.5 %, calculated according to Equation (3).

$$Error = \frac{\|R_i^{FEM} - R_i^{Exact}\|_F}{\|R_i^{Exact}\|_F}, \quad (3)$$

where  $R_i^{FEM}$  and  $R_i^{Exact}$  are the numerical and the analytical responses for each analysed point  $i$  and  $\|\cdot\|_F$  is the Frobenius norm.

Considering that the Brinell indentation test causes the material to plastic deform beyond the amount acquired from uniaxial test, Figure 15 shows the hardening curve used in the numerical simulation to generate the results shown in Figure 13. The Brinell hardness test in the configuration HBW 187.5/2.5 provides information for 25.2 % of plastic strain.

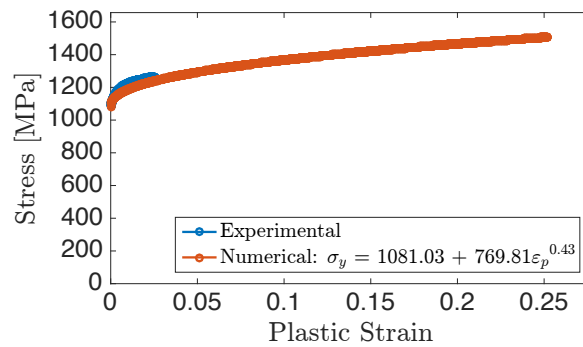


**Figure 15. Hardening Curve Used for the Brinell Indentation Test Simulation Considering a Maximum Plastic Strain of 25.2 % in Comparison with the Experimental Hardening Curve Obtained from Tensile Test.**

## 5 CONCLUSION

To determine the hardening parameters by an indentation test, a new approach was proposed considering the Brinell Hardness test to generate the experimental data set. This data set is then used to extract the mechanical properties of ductile materials through an inverse parametric identification method. Brinell hardness tests are performed and the indentation profile data, which is the indentation depth  $h$  and the impression diameter  $d$ , is extracted assisted by the *LEXT OLS4100* laser confocal microscope.

Since the goal is to provide hardening parameters that will describe the material's plastic behavior, the model was validated considering the case purely elastic whose solution is provided by Hertz<sup>6</sup>. The methodology consists of repeating FEM simulations of the indentation model and continuously comparing numerical and experimental data. In this way, the appropriate results are determined when the objective function reaches a minimum, yielding the parameters that leads to the best fitting.

Traditional and new approaches are compared by calculating the discrepancy in the stress-strain data yielded by the two methods. Taking the uniaxial test as a reference, the parameters resultant from the indentation multi-profile analysis present an error of 2.5 %.

## REFERENCES

1. Chandler H. Introduction to Hardness Testing. *Hardness Test*. 1999;14. doi:10.1126/scisignal.2001965.
2. Oliver WC, Pharr GM. An improved technique for determining hardness and elastic modulus using load and displacement sensing indentation experiments. *J Mater Res*. 1992;7(06):1564-1583. doi:10.1557/JMR.1992.1564.
3. Dean J, Clyne TW. Extraction of plasticity parameters from a single test using a spherical indenter and FEM modelling. *Mech Mater*. 2017;105:112-122. doi:10.1016/j.mechmat.2016.11.014.
4. Kang J. Determination of elastic-plastic and visco-plastic material properties from instrumented indentation curves. 2013.
5. Guillonneau G, Kermouche G, Bec S, Loubet J-L. Determination of mechanical properties by nanoindentation independently of indentation depth measurement. *J Mater Res*. 2012;27(19):2551-2560. doi:10.1557/jmr.2012.261.
6. Johnson KL. Contact Mechanics. *J Am Chem Soc*. 1985;37(22):1-17. doi:10.1115/1.3261297.
7. Wriggers P. *Computational Contact Mechanics*;2006. doi:10.1007/978-3-540-32609-0.

## Multiscale Enrichment Method with Automatic Detection of Critical Regions for Modeling Composite Materials

Michael Macri\*, Andrew Littlefield\*\*

\*Benet Labs, \*\*Benet Labs

### ABSTRACT

This presentation reviews a methodology for solving an FEA simulation that uses the homogenization method [1] throughout the model and the multiscale enrichment method within critical regions. An algorithm has been developed that implements a partition of unity multiscale enrichment approach [2, 3] when an element exceeds a threshold criteria. The multiscale enrichment approach has been shown to capture the micro phenomena with improved accuracy compared to using the homogenization method [2, 3]. Thus, in critical regions of the model, the multiscale enrichment approach is implemented to accurately capture the material response, while the rest of the model is solved for using the more computationally efficient homogenization method. The elements surrounding the critical region are adapted to act as a transition from the multiscale region to the homogenization region. To avoid numerical errors, careful consideration was performed in the derivation of the enrichment functions for these transition or blended elements. Calculating the integrands in these elements and the material properties used is also discussed in this presentation. Within this discussion we present several examples, including the validation of the multiscale enrichment method with experimental data from testing. Additional results show that using the automatic detection algorithm can significantly reduce the computational cost. In the examples presented, the runtime of the simulation was reduced by up to 70% when compared to simulations performed using the multiscale enrichment method throughout the entire model. REFERENCES 1. Bakhlov, N. & Panasenko, G. Homogenization: Averaging process in periodic media. Dordrecht: Kluwer Academic Publishers, 1989. 2. Fish, J. & Yuan, Z. "Multiscale enrichment based on partition of unity." International Journal for Numerical Methods in Engineering 24 (2005): 1341–1359. 3. Macri, M. & Littlefield A. "Enrichment Based Multi-scale Modeling of Composite Materials undergoing Thermo-Stress", International Journal for Numerical Methods in Engineering 93 (2013): 1147-1169.

## Recent Applications in Multiobjective Optimization with Direct Search

Jose Madeira\*

\*IDMEC-IST and ADM-ISEL

### ABSTRACT

In practical applications it is common to have to optimise problems with several conflicting objective functions in multi-objective optimization. Frequently, these functions are nondifferentiable or discontinuous, could be subject to numerical noise and, or be of black-box type, preventing the use of derivative-based techniques. An overview of some recent developments in derivative-free optimisation with direct search will be presented. The basic concepts and ideas commonly considered in multiobjective optimization will be given. Direct MultiSearch (DMS) [1] is a solver for multiobjective optimization problems, without the use of derivatives and does not aggregate any components of the objective function. It essentially generalizes all direct-search methods of directional type from single to multiobjective optimization. DMS maintains a list of feasible nondominated points. At each iteration, the new feasible evaluated points are added to this list and the dominated ones are removed. Successful iterations correspond then to an iterate list changes, meaning that a new feasible nondominated point was found. Otherwise, the iteration is declared as unsuccessful. MULTIGLODS [2] (global and local multiobjective optimization using direct search) is a well-established derivative-free optimization algorithm, based in directional direct search, which extends the concept of GLODS [3] to multiobjective optimization. In GLODS, for single-objective directional direct search, a strategy was proposed aiming at identifying several local minimizers. In MULTIGLODS we attempt to identify global and local Pareto fronts. Applications of these direct search algorithm to real problems will be presented. REFERENCES [1] A. L. Custódio, J. F. A. Madeira, A. I. F. Vaz, and L. N. Vicente. Direct multisearch for multiobjective optimization. *SIAM J. Optim.*, 21:1109–1140, 2011. [2] A.L. Custodio, J. F. A. Madeira, MULTIGLODS: global and local multiobjective optimization using direct search. Submitted, 2017. [3] A.L. Custodio, J. F. A. Madeira, GLODS: Global and Local Optimization using Direct Search. *Journal of Global Optimization*, 62(1):1-28,2015.

## Direct Coupling of Peridynamics with Finite Elements Without a Transition Zone

Erdogan Madenci<sup>\*</sup>, Mehmet Dorduncu<sup>\*\*</sup>, Atila Barut<sup>\*\*\*</sup>, Nam Phan<sup>\*\*\*\*</sup>

<sup>\*</sup>University of Arizona, <sup>\*\*</sup>University of Arizona, <sup>\*\*\*</sup>University of Arizona, <sup>\*\*\*\*</sup>Naval Air Systems Command (NAVAIR)

### ABSTRACT

This study presents a variational approach to couple PeriDynamic (PD) and Finite Element (FE) analyses to take advantage of their salient features. The region of PD can be completely or partially surrounded by a region of traditional finite elements. There exists no transition region along the interface of these regions unlike the previous coupling techniques. Therefore, this approach does not require a morphing or a blending function that facilitates coupling over a transition zone. The PD region with an arbitrary geometry is interfaced with traditional local (conventional) elements while satisfying the displacement continuity through Lagrange multipliers. The resulting global system of equations includes the contributions arising from the PD points and the FE nodes. These equations are solved simultaneously without requiring an iterative procedure. Therefore, it is a direct coupling approach. This coupling approach is demonstrated by considering an isotropic plate under tensile loading. Part of the plate is modeled with PD points, and the remaining region with linear triangular elements. The PD region can share a boundary with FEM region or completely embedded in the FE region. The results from the coupled PD/FE approach agree well with those of PD and FE analyses.

## Shared-Memory Parallel Implementation of High-Order Asynchronous Spacetime Discontinuous Galerkin Methods

Amit Madhukar<sup>\*</sup>, Robert Haber<sup>\*\*</sup>, Volodymyr Kindratenko<sup>\*\*\*</sup>, Reza Abedi<sup>\*\*\*\*</sup>

<sup>\*</sup>University of Illinois at Urbana-Champaign, <sup>\*\*</sup>University of Illinois at Urbana-Champaign, <sup>\*\*\*</sup>University of Illinois at Urbana-Champaign, <sup>\*\*\*\*</sup>University of Tennessee Knoxville (UTK) / Space Institute (UTSI)

### ABSTRACT

We present a new parallel-adaptive shared-memory implementation of high-order asynchronous spacetime discontinuous Galerkin methods for hyperbolic problems; see for example [1] for a serial implementation. We use the Tent Pitcher algorithm [2] to generate fully unstructured spacetime meshes that satisfy a causality constraint to enable locally implicit aSDG solutions. These involve local Galerkin projections on a sequence of spacetime patches (small clusters of spacetime finite elements) that inherit the stability of implicit solvers while the overall solution exhibits the linear computational complexity reminiscent of explicit methods. The duration of each patch is determined independently and is not restricted by the order of the local basis. The processes of constructing and solving patches are interleaved, asynchronous and share the same granularity, so most of the algorithm is embarrassingly parallel. Advancing a conforming space-like front mesh through the spacetime analysis domain subject to the causality constraint is the heart of the Tent Pitcher algorithm. This front mesh is the only global data structure. We copy fragments of the front mesh into private data structures called footprints that render the generation and solution of each new patch embarrassingly parallel. Gather and scatter operations between the front and footprint meshes are not embarrassingly parallel, but they represent a tiny fraction of the overall computational expense. In this presentation, we focus on the architectural details of our parallel implementation. These include coarse-grained, patch-level parallelization across multiple cores; strict separation of shared front-mesh and private patch-level data; task queues and use of hardware threads for asynchronous execution of major operations, such as footprint construction, patch generation, patch solution, and front updates; and NUMA-aware data storage. We present numerical performance results to demonstrate near perfect scaling for high-order models of varying order and the effects of various software optimizations. References: [1] R. Abedi, B. Petracovici, and R. B. Haber. "A spacetime discontinuous Galerkin method for linearized elastodynamics with element-wise momentum balance. *Comp. Methods Appl. Mech. Engrng.* 195(25-28), 3247–3273 (2006). [2] Shripad Thite. *Spacetime Meshing for Discontinuous Galerkin Methods*. Ph.D. thesis, Dept. Computer Science, Univ. Illinois Urbana-Champaign, August (2005).

## **A Diffuse Manifold Approach to the Exploration of Geometry of Damage in Composites**

Anna Madra<sup>\*</sup>, Piotr Breitkopf<sup>\*\*</sup>

<sup>\*</sup>Massachusetts Institute of Technology, <sup>\*\*</sup>UTC CNRS Roberval

### **ABSTRACT**

The characterization of the geometry of damage in fiber-reinforced composites is a crucial element towards understanding failure mechanisms. Given that the geometry of damage varies from relatively simple to highly sophisticated, it is imperative to identify the main characteristics that would enable its characterization across different length scales. We propose a data-driven model of damage geometry based on 2D optical photos and 3D X-ray microtomographic scans of carbon fiber and epoxy laminates subject to different loading paths. High-dimensional snapshots of damage geometry are taken, and Singular Value Decomposition (SVD) of the centered observation matrix is performed providing basis vectors of affine feature space. Projection of the data points into the feature space allows to study the intrinsic dimensionality of the embedded low-dimensional manifold, providing consequently for a minimal parameterization of the damage geometry enabling thus to compare the efficiency of 2D and 3D characterization methods.

## Explicit Computational Wave Propagation in Micro-Heterogeneous Media

Roland Maier\*, Daniel Peterseim\*\*

\*University of Augsburg, \*\*University of Augsburg

### ABSTRACT

Explicit time stepping schemes are popular for linear acoustic and elastic wave propagation due to their simple nature. However, explicit schemes are only stable if the time step size is bounded by the mesh size in space subject to the so-called CFL condition. In micro-heterogeneous media, this condition is typically prohibitively restrictive because spatial oscillations of the medium need to be resolved by the discretization in space. This talk presents a way to reduce the spatial complexity in such a setting and, hence, also enable a relaxation of the CFL condition. This is done using the Localized Orthogonal Decomposition method as a tool for numerical homogenization. References: [1] Daniel Peterseim and Mira Schedensack. Relaxing the CFL condition for the wave equation on adaptive meshes. *Journal of Scientific Computing*, 72(3):1196-1213, 2017. [2] Axel Målqvist and Daniel Peterseim. Localization of elliptic multiscale problems. *Mathematics of Computation*, 83(290):2583-2603, 2014.

## On the Treatment of Body Forces in a Two-scale FE2 Scheme

Simon Maike\*, Jörg Schröder\*\*

\*Institute of Mechanics, University of Duisburg-Essen, \*\*Institute of Mechanics, University of Duisburg-Essen

### ABSTRACT

Many materials in engineering applications exhibit complex heterogeneous micro-structures. Even today, the simulation of such materials with respect to a full resolution of the microstructure is almost impossible due to tremendous computational costs. One possibility to tackle this problem is the incorporation of a homogenization procedure within a multiscale approach. Assuming a scale separation between the two appearing scales, the micro- and macroscale, and applying a FE2 scheme allows for the resolution of representative volume elements which are attached to each macroscopic point, see e.g. [1]. This method is well proven in various fields where the body forces in the balance of momentum or comparable quantities in other balance laws are neglected on the micro-scale. In contrast to that there are only a few works where these quantities are included as in [2]. Motivated by similar effects for the modeling of multiphase porous media, e.g. within the framework of the Theory of Porous Media (TPM) [3], in a multiscale approach, this contribution deals with the treatment of body forces within the FE2 method. The influence on the macro-homogeneity condition and therefore the boundary conditions on the micro-scale is investigated. The goal is to compute the stresses on the micro-scale as accurate as possible since these are crucial for the design of engineering structures, especially when irreversible material behavior is taken into account. Concluding, the results will be discussed with respect to the applicability within the TPM. References [1] J. Schröder: A numerical two-scale homogenization scheme: the FE 2-method, in J. Schröder, K. Hackl (editors) *Plasticity and Beyond*, CISM Vol. 550, Springer, 1–64, 2014. [2] E.A. de Souza Neto and P.J. Blanco and P.J. Sanchez and R.A. Feijoo, An RVE-based multiscale theory of solids with micro-scale inertia and body force effects. *MM*, 80, 136–144, 2015. [3] R. de Boer: *Theory of Porous Media*, Springer, 2000.

## **Integrating In Vivo Mechanics and Multi-scale Computational Models to Address Questions in Bone Cell and Tissue Mechanobiology**

Russell Main<sup>\*</sup>, Kari Verner<sup>\*\*</sup>, Melanie Venderley<sup>\*\*\*</sup>, Eric Nauman<sup>\*\*\*\*</sup>

<sup>\*</sup>Purdue University, <sup>\*\*</sup>Purdue University, <sup>\*\*\*</sup>Purdue University, <sup>\*\*\*\*</sup>Purdue University

### **ABSTRACT**

The vertebrate skeleton is sensitive to externally applied mechanical stimuli and alters bone mass and shape in response to loading regimes different from those typically encountered during daily life. At the tissue level, there is evidence that new bone is formed in regions where the difference between habitual and increased applied tissue stresses and strains are greatest. However, the physical and biological mechanisms by which tissue-level stimuli are sensed and alter the biology of bone cells, such as osteoblasts and osteocytes, are still largely unknown. Through an ongoing series of complementary studies, we are using experimental biomechanics approaches to measure habitual loading environments in the limb bones of running animals. Using these in vivo characterizations, we are able to base the stimuli used in our in vivo applied loading studies relative to functional locomotor biomechanics. In order to isolate the in vivo skeletal response to load from age-, species-, or disease-related differences in systemic physiology, we have developed an ex vivo loading bone organ culture system. Here, we have characterized tissue deformation in relation to our in vivo loading model while maintaining living cells in a highly controlled environment to study interactions between chemical, physical, or thermal stimuli on bone cell and tissue mechanobiology. Ultimately, we believe that the bone cells, and very likely the matrix-embedded osteocytes, play a key role in governing the tissue response to organ-level mechanical stimuli. Therefore, assessing the mechanical environment at the cellular level becomes important for understanding how changes in tissue-level stimuli are perceived at the cell. To this end, we are developing lacunar-canalicular models of osteocytes using processed confocal microscopy images and application of mixture theory to characterize the effects of tissue-level deformation on fluid mechanics in the osteocyte peri-cellular space. Integration of these complementary approaches will ultimately allow us to base the results of both controlled in vivo and ex vivo adaptation studies relative to everyday mechanical stimuli and provide a cellular basis for the tissue-level bone adaptation.

# ALTERNATIVE TO RETURN -MAPPING ALGORITHM FOR GEOMATERIALS WITH NON LINEAR INFLUENCE OF MEAN STRESS. APPLICATION TO CLAY MODELS REVISED BY THE SMP CRITERION

**Siegfried Maiolino**

Cerema/DTerCE/Department Laboratory of Lyon  
25, avenue Mitterrand  
69674 Bron cedex France  
e-mail: siegfried.maiolino@cerema.fr

**Keywords:** Computing Methods, Elastoplasticity, Finite Element Methods, Numerical Methods, Geomechanics, Return Mapping

**Abstract.** *Computing plastic strain is a crucial issue in finite element methods. This problem is also known as closest point projection. The radial return used for circular models reduces the computations to literal expressions. But in geomechanics, the deviatoric shape of yield functions is generally non circular, so that return mapping algorithm becomes cumbersome and time consuming.*

*Works that will be presented rather focus on a geometric based methods. It will be demonstrated that the numerical problem of closest point projection of the trial stress on the yield surface is equivalent to a geometrical bounded problem. Whereas this property is intuitive, the tools ensuring a straightforward equivalence between the two problems were to be developed.*

*We identify the geometric problem associated to the problem of the closest point projection in the deviatoric plane. The geometric problem is independent from the mechanical one, and can be solved with trigonometric and geometric laws. Those laws are integrated in a general algorithm to compute plastic strain, taking account of associated and non associated dilatancy for the computation of volumic plastic strains.*

*We adapted this method to models specific to clay : a Cam Clay model, modified to take into account the SMP*

## 1 INTRODUCTION

The Mohr' envelope of many porous media - soils, rocks, bones, compacted powder, show their dependence to mean stress, and also differences in strength between triaxial extension and triaxial compression. Criteria like Coulomb or Høek-Brown [3] take into account this dependence but present corners, whereas circular yield functions like Drucker-Prager don't. Experimental results using true triaxial tests prove that geomaterials present a triangular deviatoric shape with rounded corners [12]. Taking into account this particular shape in a smooth criterion involves using the third invariant. Various yield functions had been proposed, for soils [6, 10], concrete [15] or rocks [7].

The radial return [14] used for circular models reduces the computations to literal expressions [5]. The main drawback of non circular models is that return mapping algorithm becomes complex, expensive [13] and time consuming, even if the efficiency is increased with spectral decomposition techniques [1, 2]. Works that will be presented rather focus on a geometric based methods : in order to bypass the computational costs of return mapping algorithm, we will focus on simpler equivalent geometric problem.

## 2 POLAR DECOMPOSITION OF THE YIELD SURFACE

Traction stresses are positive, and the principal stresses ordered as follow :  $\sigma_I \geq \sigma_{II} \geq \sigma_{III}$

### 2.1 Geometric parametrage

For a given mean stress ( $\sigma_m = \text{Tr}\underline{\underline{\sigma}}/3$ ), the yield surface can be reduced to its cross-sectional shape on the deviatoric plane, or  $\pi$  plane. A yield surface ( $f(\underline{\underline{\sigma}}) = 0$ ) can be represented in a unique manner by the mean stress and the deviatoric invariants ( $J_2 = \frac{1}{2}\text{Tr}(\underline{\underline{s}}^2)$ ,  $J_3 = \frac{1}{3}\text{Tr}(\underline{\underline{s}}^3)$ , with  $\underline{\underline{s}} = \underline{\underline{\sigma}} - \sigma_m \underline{\underline{1}}$ ), but it is more practical to replace the third invariant by the Lode angle  $\theta$ , to work in the  $\pi$  plane (deviatoric plane).

$$-\frac{\pi}{6} \leq \theta = \frac{1}{3} \arcsin \left( \frac{-3\sqrt{3}}{2} \frac{J_3}{\sqrt{J_2^3}} \right) \leq \frac{\pi}{6} \quad (1)$$

The set  $(\sqrt{J_2}, \theta)$  define polar coordinates on one sixth of the deviatoric plane, which is sufficient for an isotropic criterion. Zienkiewicz and Pande [16], using the fact that a yield surface can be reduced to its polar expression, provided tools to study the regularity, the sensitivity to the extension and the convexity of a criterion starting from the shape function  $g_p(\theta)$

$$\sqrt{J_2} = \sigma^+ g_p(\theta) \quad (2)$$

The deviatoric radius :  $\sigma^+(\sigma_m) = \sqrt{J_2/\theta=\frac{\pi}{6}}$ , gives the yield function in the meridional plane  $(\sigma_m, \sqrt{J_2})$ , for  $\theta = \frac{\pi}{6}$ . This value of the Lode angle corresponds to a classical triaxial test, or compression triaxial test ( $\sigma_I = \sigma_{II} > \sigma_{III}$ ). The function  $g_p(\theta)$  is the shape function of the yield surface in the deviatoric plane. It is normalized ( $g_p(\frac{\pi}{6}) = 1$ ) and gives directly the value of the extension ratio  $g_p(-\frac{\pi}{6}) = L_S$  which is more detailed in the following section.

### 2.2 Characteristic function of a material

The deviatoric radius  $\sigma^+$  can be easily deduced from triaxial compression tests. Whether the shape is straight or parabolic, the deviatoric radius used can be the Coulomb or Høek-Brown.

The extension ratio  $L_S$  has a physical meaning and can be determined from experiment. The condition  $\theta = -\frac{\pi}{6}$  corresponds to extension triaxial tests ( $\sigma_I > \sigma_{II} = \sigma_{III}$ ), which can be performed with the same triaxial cell as compression triaxial test.

$$L_S = \frac{\sqrt{J_2}(\theta = -\frac{\pi}{6})}{\sqrt{J_2}(\theta = \frac{\pi}{6})} = \frac{(\sigma_I - \sigma_{III}) (extension)}{(\sigma_I - \sigma_{III}) (compression)} \quad (3)$$

Physically, this means that for the same mean stress, the yield value of  $\sqrt{J_2}$  would be lower in extension than in compression. The value of  $L_S$  is directly linked to the deviatoric shape of a yield surface. While this value can be independent from the mean stress (Coulomb), some rocks present a shape of their yield surface changing from triangular (low confinement) to circular (high confinement) [4], i.e,  $L_S$  increases from 0.5 to 1.

### 2.3 Introduction of the orthoradial tensor

We consider for stresses and strains (i.e. symmetric second order tensors) the following scalar product. For two tensors,  $\underline{\underline{T}}_1$  and  $\underline{\underline{T}}_2$  :

$$\underline{\underline{T}}_1 \cdot \underline{\underline{T}}_2 = \underline{\underline{T}}_1 : \underline{\underline{T}}_2 = \text{Tr} \underline{\underline{T}}_1 \underline{\underline{T}}_2 \quad (4)$$

Hence defining the following norm (Frobenius norm) for a symmetric second order tensor  $\underline{\underline{T}}$  :

$$\| \underline{\underline{T}} \| = \sqrt{\underline{\underline{T}} : \underline{\underline{T}}} \quad (5)$$

We introduce the orthoradial tensor,  $\underline{\underline{v}}$  :

$$\underline{\underline{v}} = 3 \frac{\sqrt{3}}{2} \frac{1}{J_2} \underline{\underline{s}}^2 - \sqrt{3} \underline{\underline{1}} - \frac{9\sqrt{3}J_3}{4J_2^2} \underline{\underline{s}} \quad (6)$$

This tensor is orthoradial as  $\underline{\underline{v}} \cdot \underline{\underline{1}} = \underline{\underline{v}} \cdot \underline{\underline{s}} = 0$ , hence those three tensors,  $\underline{\underline{1}}$ ,  $\underline{\underline{s}}$ ,  $\underline{\underline{v}}$  constitute an orthogonal basis of the space of symmetric second order tensors, for the Frobenius scalar product.

We can then easily decompose the derivatives of the yield function along this orthogonal basis, as the expression of the gradient of invariants can easily be expressed. It is necessary to introduce the orthogonal tensor, as the gradient of the third invariant cannot be expressed using only the hydrostatic tensor or the deviatoric tensor. Expressions of the three gradients of invariants are the following :

$$\frac{\partial I_1}{\partial \underline{\underline{\sigma}}} = \underline{\underline{1}} \quad (7)$$

$$\frac{\partial J_2}{\partial \underline{\underline{\sigma}}} = \underline{\underline{s}} \quad (8)$$

$$\frac{\partial J_3}{\partial \underline{\underline{\sigma}}} = \underline{\underline{s}}^2 - \frac{2J_2}{3} \underline{\underline{1}} = \frac{3J_3}{2J_2} \underline{\underline{s}} + \frac{2J_2}{3\sqrt{3}} \underline{\underline{v}} \quad (9)$$

Hence the gradient of any yield surface can be orthogonally decomposed.

$$\frac{\partial f}{\partial \underline{\underline{\sigma}}} = f_u \underline{\underline{1}} + f_s \underline{\underline{s}} + f_v \underline{\underline{v}} \quad (10)$$

We can observe that the deviatoric part of the gradient,  $\text{dev} \frac{\partial f}{\partial \underline{\underline{\sigma}}}$  can be split in two orthogonal component, a radial  $f_s \underline{\underline{s}}$ , and a orthoradial,  $f_v \underline{\underline{v}}$ . This later part is null for criteria independent from the third invariant.

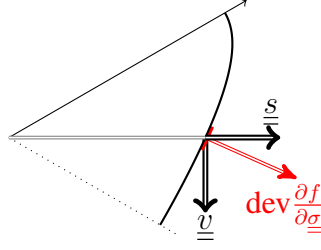


Figure 1: Orthogonal decomposition of the deviatoric part of the gradient

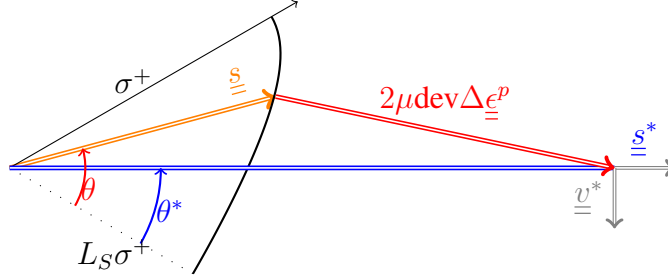


Figure 2: Physical problem in the deviatoric plane

## 2.4 Consequences for return mapping algorithm

Let us consider at an integration point, the increment from step  $n$  to  $n + 1$ . We want to calculate the plastic strain, if the trial stress  $\underline{\underline{\sigma}}^*$  doesn't satisfy the yield condition. We want to implicitly solve the relation that gives the stress.

$$\underline{\underline{\sigma}}_{n+1} = \underline{\underline{\sigma}} = \underline{\underline{\sigma}}^* - \underline{\underline{L}} \Delta \underline{\underline{\epsilon}}^p \quad (11)$$

Where  $\underline{\underline{L}}$  is the elasticity tensor. We can split this relation between two orthogonal components: an hydrostatic and a deviatoric.

$$\sigma_m - \sigma_m^* = -K \text{Tr} \Delta \underline{\underline{\epsilon}}^p \quad (12)$$

$$\underline{\underline{s}} - \underline{\underline{s}}^* = -2\mu \text{dev} \Delta \underline{\underline{\epsilon}}^p \quad (13)$$

Where  $K$  is the bulk modulus and  $\mu$  the shear modulus.

We can notice that the hydrostatic part (12) is purely scalar and that the main difficulties come from the deviatoric part(13).

## 3 GEOMETRIC EQUIVALENCE OF CLOSEST POINT PROJECTION

We introduce the following quantity [8, 9]:

$$\rho = \frac{\sqrt{J_2^*}}{\sigma^+(\sigma_m^* + \Delta \sigma_m)} \quad (14)$$

The closest point projection of  $\underline{\underline{s}}^*$  on the trace of yield surface (Figure 2) is equivalent to the following geometric problem(Figure 3): find the closest point projection (polar coordinates:

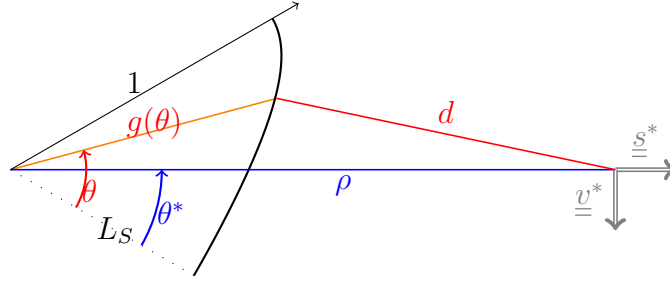


Figure 3: Geometric problem in polar coordinates

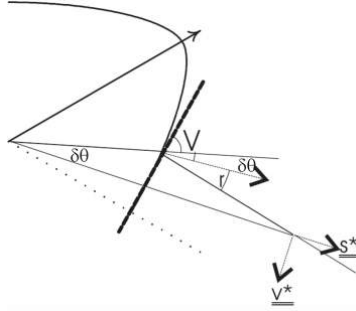


Figure 4: Angular relations:  $V + r + \delta\theta = \frac{\pi}{2}$ ,  $(\delta\theta = \theta - \theta^*)$

$(\theta, g_p(\theta))$  of the point  $(\rho, \theta^*)$  on the curve defined by the shape function  $g_p(\theta)$ . The function  $d(\theta)$  reaches its minimum at this point.

$$d(\theta)^2 = g_p^2(\theta) + \rho^2 - 2g_p(\theta)\rho \cos(\theta - \theta^*) \quad (15)$$

Expression of the norm of the deviatoric plastic strain is straightforward:

$$\|\text{dev}\Delta\underline{\underline{\epsilon}}^p\| = \frac{d(\theta)\sigma^+}{\sqrt{2}\mu} \quad (16)$$

Now,  $\text{dev}\Delta\underline{\underline{\epsilon}}^p$  can be expressed in the local base associated to the trial stress

$$\text{dev}\Delta\underline{\underline{\epsilon}}^p = \|\text{dev}\Delta\underline{\underline{\epsilon}}^p\| \left( \frac{\cos r}{\sqrt{2}\sqrt{J_2^*}} \underline{s}^* + \frac{\sin r}{\|\underline{v}^*\|} \underline{v}^* \right) \quad (17)$$

The value of the  $r$  angle can be deduced from trigonometric considerations (figure 4),  $V$  being the angle between the tangent to a polar curve and the radial axis :

$$\tan V = \frac{g}{g'} \quad (18)$$

## 4 COMPUTATION OF DEVIATORIC AND HYDROSTATIC PLASTIC STRAIN

### 4.1 General algorithm

The geometric equivalence allows to get the plastic strain if  $\Delta\sigma_m$  is known. This quantity is calculated using an iterative method. Initially,  $\Delta\sigma_m^0 = 0$ , and the stopping condition  $c$  is satisfied when the ratio between hydrostatic and deviatoric parts is equal to the dilatancy angle  $\delta$ .

$$c(\Delta\sigma_m, \|\text{dev}\Delta\underline{\underline{\epsilon}}^p\|, \tan \delta) = \|\text{dev}\Delta\underline{\underline{\epsilon}}^p\| \sqrt{3}K \tan \delta + \Delta\sigma_m < \varepsilon \quad (19)$$

We use the following definition of the dilatancy angle :

$$\tan \delta = \frac{g_u \sqrt{3}}{\sqrt{g_s^2 \|\underline{s}\|^2 + g_v^2 \|\underline{v}\|^2}} \quad (20)$$

With  $g_u$ ,  $g_s$  and  $g_v$  are the components of the normal to the plastic potential :

$$\frac{\partial g}{\partial \underline{\sigma}} = g_u \underline{\mathbb{1}} + g_s \underline{s} + g_v \underline{v} \quad (21)$$

The dilatancy angle can be deduced from the expression of the yield function (associated potential) or from a non associated potential. Whereas it is not easy to identify the potential, without extensive true triaxial tests, the dilatancy angle can be easily identified using classical triaxial compression tests.

If  $\delta > 0$  material is said to be dilatant. The alternative return mapping algorithm can be expressed as follow, at a given integration point, for a dilatant material

1. Compute  $\underline{\sigma}^* = \underline{\sigma}^0 + \underline{L} \left( \underline{\epsilon}_{n+1} - \underline{\epsilon}_n^p \right)$
2. Check  $f(\underline{\sigma}^*) > 0$ ? No set  $\underline{\sigma}_{n+1} = \underline{\sigma}^*$  and exit.
3. Yes : set  $i = 0$  and  $\Delta \sigma_m^0 = 0$
4. Set  $\rho^i = \frac{\sqrt{J_2^*}}{\sigma^+(\sigma_m^* + \Delta \sigma_m^i)}$  and if  $L_S$  depends of mean stress :  $L_S^i = L_S(\sigma_m^* + \Delta \sigma_m^i)$
5. Compute  $\theta^i$ ,  $d(\theta^i)$ ,  $\sqrt{J_2^i}$  and  $\|\text{dev} \Delta \underline{\epsilon}^p\|^i$
6. Evaluate  $\tan \delta^i = \tan \delta(\sigma_m^* + \Delta \sigma_m^i, J_2^i, J_3^i)$
7. Evaluate stopping criterion  $|c(\sigma_m^* + \Delta \sigma_m^i, \|\text{dev} \Delta \underline{\epsilon}^p\|^i, \tan \delta^i)| < \epsilon$ . If Yes compute angle  $r$  and tensor  $\Delta \underline{\epsilon}^p$ . Update  $\underline{\sigma}_{n+1} = \underline{\sigma}^* - \underline{L} \Delta \underline{\epsilon}^p$  and exit.
8. If No, set  $i = i + 1$  and  $\Delta \sigma_m^i = \Delta \sigma_m^{i-1} + \Delta^2 \sigma_m$ , then loop to step 4.

The evaluation of  $\Delta^2 \sigma_m$  depends of the nature of yield function  $f$  and  $\delta$

## 4.2 Evaluation of mean stress increment

One natural way to compute  $\Delta^2 \sigma_m$  is to apply a Newton-Rhapson like iterative function to (19), but it can be not so straightforward and be costly, even for circular criteria, as the Cam Clay model, because of the presence derivative of the deviatoric radius. So

$$\Delta^2 \sigma_m = -c(\Delta \sigma_m^{i-1}) \frac{\Delta \sigma_m^{i-1} - \Delta \sigma_m^{i-2}}{c(\Delta \sigma_m^{i-1}) - c(\Delta \sigma_m^{i-2})} \quad (22)$$

Where  $c$  can be directly expressed :

$$c(\Delta \sigma_m) = \sqrt{\frac{2}{3}} \frac{K}{\mu} \tan \delta(\sigma_m^* + \Delta \sigma_m) \left( \sqrt{J_2^*} - g_p(\theta(\Delta \sigma_m)) \sigma^+(\sigma_m^* + \Delta \sigma_m) \right) + \Delta \sigma_m \quad (23)$$

With the following expression for the first increment :

$$\Delta \sigma_m^1 = -\sqrt{\frac{2}{3}} \frac{K}{\mu} \left( \sqrt{J_2^*} - g_p(\theta^0) \sigma^+(\sigma_m^*) \right) \tan \delta(\sigma_m^*) \quad (24)$$

## 5 Cam Clay model revised by the SMP criterion

Cam Clay models and modified Cam Clay models don't take into account the influence of the third invariant. This influence can be taken into account through a transformation of the stress tensor [11], so that the deviatoric shape is the one of Matsuoka-Nakai.

Another solution is to use the Maiolino general yield function [7] :

$$f(\underline{\sigma}) = \frac{3}{2}\sqrt{3}(1 - L_S)J_3 + (L_S^2 + 1 - L_S)\sigma^+J_2 - \sigma^{+3}L_S^2 \quad (25)$$

When fitted with Coulomb deviatoric radius and extension ratio, this criterion is equal to standard Matsuoka-Nakai.

We can also use the deviatoric radius of Cam Clay (with  $p = -\sigma_m$  and  $q = \sqrt{3}\sqrt{J_2}$ ), so that :

$$\sigma^+ = -\sigma_m M \sqrt{\frac{1}{\sqrt{3}} \left(1 + \frac{p_0}{\sigma_m}\right)} \quad (26)$$

To integrate the SMP, we have to determinate the extension ratio. We can adopt the following value :

$$L_S = \frac{3 - \sin \phi_i}{3 + \sin \phi_i} \quad (27)$$

With  $\phi_i$  an instantaneous friction angle :

$$\sin \phi_i = \frac{3 \frac{\partial \sigma^+}{\partial \sigma_m}}{\frac{\partial \sigma^+}{\partial \sigma_m} + 2\sqrt{3}} \quad (28)$$

## 6 CONCLUSIONS

We have shown that for  $J_3$  dependant yield function, the problem of closest point projection is equivalent to a pure geometric problem in polar coordinates. For different values of  $(\rho, \theta^*)$ , solutions can be computed and values of  $d(\theta) \sin 3\theta$  and  $g_p(\theta)$  are saved, allowing to shortcut computational costs of return mapping in the deviatoric plane. For the hydrostatic part, we propose a general algorithm that allows to take account of the dilatancy in the computation of plastic strain.

This general algorithm can be applied to Cam Clay models revised by the SMP criterion. Further work will be done to take into account non associate deviatoric plastic flow, and adapt the framework to pressure dependent elasticity.

## 7 Acknowledgment

The work presented and this communication are part of the project Anticipation and mitigation of slow landslides in the Alps (MLA3) that benefits of the support of the European Union and Provence-Alpes-Côte d'Azur (PACA) Region through the European Regional Development Fund (ERDF) interregional operational program "Massif des Alpes" (POIA).

## References

- [1] R. Borja, K. Sama, and P. Sanz. On the numerical integration of three invariant elasto-plastic constitutive models. *Comput. Methods Appl. Mech. Engrg*, 192(9-10):1227–1258, 2003.

- [2] C. Foster, R. Regueiro, A. Fossum, and R. Borja. Implicit numerical integration of a three-invariant, isotropic/kinematic hardening cap plasticity model for geomaterials. *Comput. Methods Appl. Mech. Engrg.*, 194(50-52):5109–5138, 2005.
- [3] E. Hoek and E. Brown. Empirical strength criterion for rock masses. *J. Geotech. Engng DIV., ASCE*, 106(GT9):1013–1035, 1980.
- [4] M. Kim and P. Lade. Modelling rock strength in three dimensions. *Int. Journ. Rock Mech. Min. Sci. Abstracts*, 21(1):21–33, 1984.
- [5] R. D. Krieg and S. M. Key. Implementation of a Time Dependant Plasticity Theory into Structural Computer Programs. *Constitutive Equations in Viscoplasticity : Computational and Engineering Aspects*, 20:125–137, 1976.
- [6] P. V. Lade. Elasto-plastic stress-strain theory for cohesionless soil with curved yield surfaces. *Int. Journ. Solids Structures*, 13:1019–1035, 1977.
- [7] S. Maiolino. Proposition of a general yield function in geomechanics. *Comptes Rendus Mécanique*, 333:279–284, 2005.
- [8] S. Maiolino. *Fonction de charge générale en géomécanique : application aux travaux souterrains*. PhD thesis, École Polytechnique, 2006. General yield function in geomechanics : application to tunneling (in French).
- [9] S. Maiolino. Numerical abacuses method based on the equivalence between the closest point projection and a bounded geometric problem. In *8th. World Congress on Computational Mechanics (WCCM8) , 5th European Congress on Computational Methods in Applied Sciences and Engineering (ECCOMAS 2008), Venice*, July 2008.
- [10] H. Matsuoka and T. Nakai. Stress-deformation and strength characteristics of soil under three different principal stresses. In *Proc. JSCE*, volume 232, pages 59–70, 1974.
- [11] H. Matsuoka, Y. Yao, and D. Sun. The cam–clay models revised by the smp criterion. *SOILS AND FOUNDATIONS*, 39(1):81–95, 1999. doi: 10.3208/sandf.39.81.
- [12] P. Michelis. True triaxial yielding and hardening of rock. *J. Geotech. Engng DIV., ASCE*, 113(6):616–635, 1987.
- [13] J. Simo and T. Hughes. *Computational Inelasticity*. 1998.
- [14] J. L. Wilkins. Calculation of Elastic-plastic Flow. *Methods of Computational Physics*, 8, 1964.
- [15] K. William and E. Warnke. Constitutive models for the triaxial behavior of concrete. In *International Association of Bridge and Structural Engineering (IABSE) Seminar on "Concrete Structures Subjected to Triaxial Stresses"*, Bergamo, volume 19, pages 1–30, 1975.
- [16] O. C. Zienkiewicz and G. N. Pande. Some useful forms of isotropic yield surfaces for soil and rock mechanics. In *Numerical methods in soil and rock mechanics, Karlsruhe*, pages 3–16, september 1975.

## Numerical Study on Nonlinear Electrophoresis of a Charged Dielectric Droplet

Partha Sarathi Majee\*, Somanth Bhattacharyya\*\*

\*Indian Institute of Technology Kharagpur, \*\*Indian Institute of Technology Kharagpur

### ABSTRACT

The study of electrophoresis of a charged spherical droplet is important for its wide applications in atmospheric physics, inkjet printers, pharmaceutical, lab-on-a-chip, and electrospray applications. The dielectric polarization of the droplet under an external electric field creates a nonlinear dependence of the electrophoretic velocity on the applied electric field. The surface of the droplet is not stationary and a lower droplet viscosity increases the fluid convection in the Debye layer, which in turn enhances the double layer polarization and surface conduction. The polarization effect of double layer due to fluid convection is analyzed extensively in the present work. The electrophoresis of a charged spherical droplet of an immiscible dielectric liquid in an electrolyte in response to an applied electric field is studied. Fluid inside and outside the droplet is governed by the Navier-Stokes equations, ion transport in electrolyte is described by Nernst-Planck equation, the electric potential within and outside the droplet is governed by the Laplace and Poisson equations, respectively. Governing equations along with proper boundary conditions are solved numerically through a control volume approach over a staggered grid arrangement. Discretized equations are solved through the pressure correction based iterative SIMPLE (Semi-Implicit Method for Pressure-Linked Equations) algorithm. Electrophoretic velocity of the droplet is determined by balancing the electric and drag forces experienced by the droplet. The present numerical model successfully accounts the double layer polarization and relaxation effects. Solutions are obtained without invoking weak field condition or thin Debye layer assumption unlike the analytic solutions of Ohshima et al.(1984) or thin layer analysis of Schnitzer et al.(2013). The electrophoretic velocity is presented to analyze its dependency on droplet-to-electrolyte viscosity ratio, Debye length, droplet-to-electrolyte permittivity ratio. Electrophoretic velocity diminishes with the increase of droplet-to-electrolyte viscosity ratio and it also decreases with the rise of droplet-to-electrolyte permittivity ratio. The present solutions over-estimate the results of Ohshima et al.(1984) for thinner Debye layer. At a fixed surface potential the mobility shows a non-linear variation with the droplet size. The enhancement rate of mobility with the decrease of droplet-to-electrolyte viscosity ratio is higher for a thinner Debye length compares to a thick one. Surface conduction effect slows down the increment rate of mobility with droplet charge at thinner Debye layer. References [1] H. Ohshima, T. W. Healy, and L. R. White, J. Chem. Soc. Faraday Trans. 80(12), 1643–1667 (1984). [2] O. Schnitzer, I. Frankel, and E. Yariv, J. Fluid Mech. 722, 394–423 (2013).

## Field-Controlled Soft-Matter Electronics with Ferromagnetic Elastomers and Liquid Metal

Carmel Majidi\*

\*Carnegie Mellon University

### ABSTRACT

There has been extraordinary progress in recent decades in the development of electronics that are mechanically soft and stretchable. These range from conductive elastomer composites and fabrics to circuits with wavy metal electrodes or liquid metal (LM) traces. Most of this work has focused on wiring and electrical interconnects, although there has also been progress in soft electronics that have active properties for electrical switches, diodes, and tunable radio transmission. The ultimate goal is to produce “field-controlled” soft electronics that, like conventional semiconductor-based field effect transistors (FETs) or electromagnetic relays, change their state in response to an applied electrical or magnetic field. Such elements would help broaden the electronic functionality of soft materials within emerging applications like wearable computing, soft robotics, inflatable structures, and shape-programmable matter. In this talk, I will present recent efforts by my research group (CMU Soft Machines Lab) to introduce field-controlled soft electronics using soft elastomers (silicone rubber), ferromagnetic microparticles (Fe, Ag-coated Ni), and Ga-based LM alloy (eutectic gallium indium; EGaIn). I will primarily focus on elastomers embedded with LM droplets[1] or LM-coated ferromagnetic microparticles[2]. These composites can be engineered to exhibit a broad range of electrical and thermal properties, from electrical conductors that maintain fixed electrical conductivity when stretched or damaged (e.g. tearing, puncture) to high-k dielectric insulators with metal-like thermal conductivity. They can also be integrated into an electrical switches that reversibly open and close in response to an electrical or magnetic field. In addition to experimental implementations, I will present analytic models that combine theories of elasticity and Maxwell’s equations to predict electromagnetic responses that are in strong agreement with measurements. I will close the talk by discussing potential applications of LM-elastomer and LM-ferroelastomer composites to the emerging field of soft robotics. If time permits, I will also present recent efforts with an electrochemical LM switch that responds to low voltage activation.[3] This switch exhibits some features of a traditional FET – e.g. source/drain/gate layout, ~1V response, high on/off switching ratio – and can be extended to other active functionalities. References: [1] M. D. Bartlett, N. Kazem, M. J. Powell-Palm, X. Huang, W. Sun, J. A. Malen, and C. Majidi, “High thermal conductivity in soft elastomers with elongated liquid metal inclusions,” *Proceedings of the National Academy of Sciences* 114 2143–2148 (2017). [2] V. Ramachandran, M. D. Bartlett, J. Wissman, C. Majidi, “Elastic instabilities of a ferroelastomer beam for soft reconfigurable electronics,” *Extreme Mechanics Letters* 9 282-290 (2016). [3] J. Wissman, M. D. Dickey, C. Majidi, “Field-Controlled Electrical Switch with Liquid Metal,” *Advanced Science* 4 1700169 (2017).

## **Towards the Tensegrity Beam Structural Element**

Manoranjan Majji<sup>\*</sup>, Edwin Peraza Hernandez<sup>\*\*</sup>, Robert Skelton<sup>\*\*\*</sup>

<sup>\*</sup>Dept. of Aerospace Engineering, Texas A&M; University, <sup>\*\*</sup>Dept. of Aerospace Engineering, Texas A&M; University, <sup>\*\*\*</sup>Dept. of Aerospace Engineering, Texas A&M; University

### **ABSTRACT**

A novel paradigm that is the basis for an innovating multibody dynamics approach to model flexible structures is presented in this work. We particularly focus on modeling flexible beams. As opposed to the traditional approximations based on the superposition principle, the new approach decomposes the continuum into discrete tensegrity structures (denoted as tensegrity elements). A matrix approach for modeling tensegrity systems is employed to model the individual elements and the Newton-Euler and Lagrangian approaches for multibody dynamics are used to assemble the individual tensegrity elements to realize the beam structure. The goal of this multibody tensegrity discretization process is to match the dynamic characteristics of the flexible structure. To this end, we perform topology optimization studies pertaining to the natural frequency and mode shape matching as a function of the number and topology of the tensegrity elements involved in the discretization process. To baseline our proposed approach, we use finite element approximations using cubic spline elements and the assumed modes methods employing eigenfunctions for Euler-Bernoulli beams subjected to a variety of loading and boundary conditions. Since nonlinear tensegrity elements are used to furnish constituent approximations, new tools are developed to solve the resulting nonlinear eigenvalue problems for the mode shapes of the structure and the calculation of the natural frequencies. Theoretic concepts of dynamic response of the nonlinear structure will be employed to identify natural frequencies.

## **Modeling of Work Hardening and Strain-rate Sensitivity of Precipitation Strengthened Ultrafine-grained and Nanostructured Materials**

Janusz Majta<sup>\*</sup>, Remigiusz Bloniarz<sup>\*\*</sup>, Krzysztof Muszka<sup>\*\*\*</sup>

<sup>\*</sup>AGH University of Science and Technology, Krakow, Poland, <sup>\*\*</sup>AGH University of Science and Technology, Krakow, Poland, <sup>\*\*\*</sup>AGH University of Science and Technology, Krakow, Poland

### **ABSTRACT**

This study aims at understanding the work hardening ability of precipitation strengthened ultrafine-grained (UFG) and nanostructured (NS) materials at different strain rates. The investigations were performed for two materials: high strength Nb microalloyed ferrite (b.c.c.) and austenite (f.c.c.). A range of different grain sizes was developed using multi-axial compression tests (MaxStrain). As a result different nanostructures were observed in the investigated alloys characterized by different grain size and dislocation density. From a microscopic viewpoint, plastic deformation and work-hardening of a crystal are caused by dislocation motions and dislocation accumulations. In order to model mechanical behavior of UFG and NS precipitation strengthened materials, there is a need, first of all, to understand the deformation and strengthening mechanisms governing the plastic deformation of such material. To capture these phenomena in a sufficient way, multiscale modelling approach was applied in the present study, since the conventional material models are not amendable to bridge the gap arising from different scales at which those phenomena are taking place. Multiscale modeling was based on the combination of discrete techniques such as continuous finite element (FE) models as well as on the combination of traditional differential equations describing material behavior in the micro scale with FE models. Stochastic processes, such as new grains nucleation on the grain boundaries, development of the shear bands and its influence on the nucleation process, as well as influence of defects or inclusions on nucleation process, have been taken into account. Analysis was performed in the nano- and micro- scale with respect to the dislocation structures evolution during processing. The data needed for a successful and complete interpretation of all mechanical tests, performed to define the correlation between microstructure and mechanical properties was possible due to the results of the transmission electron microscopy (TEM) and scanning electron microscopy (SEM) with EBSD analysis. The Taylor test and Split Hopkinson Pressure Bar (SHPB) tests were applied in the analysis of the mechanical response of the UFG and NS materials under dynamic loading conditions. Based on the study of the precipitation and substructure strengthening a modification of the Khan-Huang-Liang flow stress model was proposed, so it relates the strain hardening with strain, strain rate and precipitates as well as dislocation cell sizes. Our approach was tailored to the unique aspects of UFG and NS microalloyed steels, with the thrust being and understanding of the key physical mechanisms that govern plastic deformation behavior under dynamic loading.

## Strain Hardening and Crack Growth in '2.5D' Discrete Dislocation Dynamics

Eleanor Mak\*, William Curtin\*\*

\*École Polytechnique Fédérale de Lausanne, \*\*École Polytechnique Fédérale de Lausanne

### ABSTRACT

Discrete dislocation dynamics (DD) methods have been widely used to investigate plasticity-related phenomena at the sub-continuum scale. Although 3D models can capture the realistic generation, motion, and interaction of dislocation loops, they are often prohibitively expensive in computational cost for the non-homogeneous loading, complex boundaries, and explicit interfaces in crack growth problems. Thus, 2D models are commonly used as a computationally tractable framework to provide insight to plastic flow and fracture. Strain hardening from forest dislocations, which emerges due to the entanglement of loops on intersecting slip planes, is inherently a 3D effect which cannot be captured by conventional 2D models. A new '2.5D' DD framework addresses this major shortcoming by projecting 3D effects onto a 2D problem [1]. The '2.5D' parameters are physically motivated and are obtained from 3D DD, and hardening behavior then emerges naturally. Here, a cohesive zone (CZ) model with realistic cohesive parameters is combined with the '2.5D' DD framework using the O'Day and Curtin [2] superposition method. Crack growth, near-crack dislocation structuring and hardening, and Mode I fracture toughness are then studied as a function of material yield strength, strain hardening, and internal material length scales. [1] Keralavarma, S. M., & Curtin, W. A. (2016). Strain hardening in 2D discrete dislocation dynamics simulations: A new '2.5 D' algorithm. *Journal of the Mechanics and Physics of Solids*, 95, 132-146. [2] O'Day, M. P., & Curtin, W. A. (2004). A superposition framework for discrete dislocation plasticity. *Transactions of the ASME-E-Journal of Applied Mechanics*, 71(6), 805-815.

## **Effect of the Stress Triaxiality on the Mechanical Behavior of Ductile Materials**

Lucival Malcher<sup>\*</sup>, LEONEL LEONARDO DELGADO MORALES<sup>\*\*</sup>, André Trajano<sup>\*\*\*</sup>

<sup>\*</sup>Group of Fatigue, Fracture and Materials - GFFM University of Brasília, <sup>\*\*</sup>Group of Fatigue, Fracture and Materials - GFFM University of Brasília, <sup>\*\*\*</sup>Group of Fatigue, Fracture and Materials - GFFM University of Brasília

### **ABSTRACT**

The correct determination of the mechanical behavior of materials is one of the main challenges faced by researchers and an important step for the design of mechanical components. Stress triaxiality is one of the elastoplastic parameters with the greatest influence on the behavior of ductile materials and is determined as a function of the ratio between the hydrostatic stress and the equivalent stress. In this context, this contribution contemplates the study of this parameter on the mechanical behavior of the SAE 4340 alloy, annealed and normalized. In order to achieve the desired objective, experimental tests are carried out for smooth and notched cylindrical specimens, as well as, specimens subjected to pure shear. Furthermore, it is also proposed the implementation of Gao's elastoplastic model, with nonlinear isotropic hardening, in an academic finite element framework, through an implicit integration strategy. The experimental and numerical reaction curves for the specimens are analyzed and fracture curve, showing the influence of the stress triaxiality on the behavior of the material. At the end, it is proposed a correction in the reaction curve, assuming the calibration of the Gao's model, and an equation that characterizes the fracture curve for the material 4340 alloy, regarding wide range of stress triaxiality.

## A Hybridized Discontinuous Galerkin Framework for High-Order Conservative Particle-Mesh Methods

Jakob Maljaars<sup>\*</sup>, Robert Jan Labeur<sup>\*\*</sup>, Nathaniel Trask<sup>\*\*\*</sup>, Deborah Sulsky<sup>\*\*\*\*</sup>, Matthias Möller<sup>\*\*\*\*\*</sup>

<sup>\*</sup>Delft University of Technology, <sup>\*\*</sup>Delft University of Technology, <sup>\*\*\*</sup>Sandia National Laboratories, <sup>\*\*\*\*</sup>The University of New Mexico, <sup>\*\*\*\*\*</sup>Delft University of Technology

### ABSTRACT

Despite successful applications, since its introduction in the late 1950s [1], the particle-in-cell (PIC) method still faces some unresolved issues. In particular, PIC-methods have difficulty unifying accuracy and exact, local conservation. More specific to incompressible flows, maintaining local volume conservation remains a daunting task for PIC-based methods. These are not exclusively issues with PIC, but of particle methods in general (eg. [2]). Whereas various grid-based methods, hybridized Discontinuous Galerkin (HDG) (eg. [3]) among them, can achieve high accuracy with exact conservation, there are still difficulties associated with discretization of nonlinear advection terms and choices of numerical fluxes. This contribution presents a novel particle-mesh operator-splitting framework, utilizing particles and HDG, to resolve these challenges. More precisely, the particle-mesh interactions are interpreted in terms of a PDE-constrained minimization problem in order to reconcile accuracy and exact conservation. The key idea in formulating the constraint equations is that from a mesh-perspective the particle motion must satisfy an advection operator. Derivation of the corresponding optimality conditions reveals that the HDG-method is indispensable in providing the required optimality control. Consistency and rigorous conservation of the resulting scheme are derived. By means of various numerical examples for the linear advection-diffusion equation and the non-linear Navier-Stokes equations the accuracy of the method is further unveiled. High Reynolds-number tests give further evidence for the robustness of the scheme. Given its crucial importance, specific attention is paid to the uniformity of the particle distribution when simulating transient, incompressible fluid flows. Apart from using an accurate particle advection scheme, it will be demonstrated that another important criterion for maintaining a correct particle distribution is to transport the particles in velocity fields being H(div)-conforming. We will show how this criterion can be met in the scope of the HDG-framework [3]. Practical impediments of not satisfying the H(div)-criterion are extensively discussed by comparing the particle distributions obtained for a numerical test using Taylor-Hood elements, and using a HDG-based method both with and without H(div)-conforming velocity fields. [1] M. Evans, F. Harlow, E. Bromberg. The particle-in-cell method for hydrodynamic calculations. Technical report, Los Alamos Scientific Laboratory, 1957. [2] G. Dilts, A. Haque, J. Wallin. Tuned local regression estimators for the numerical solution of differential equations, volume 26 of Lecture Notes in Computational Science and Engineering, pages 87–104. Springer-Verlag, Berlin, 2003. [3] S. Rhebergen, G.N. Wells. A hybridizable discontinuous Galerkin method for the Navier–Stokes equations with pointwise divergence-free velocity field. 2017.

## **In-silico Assisted Evaluation of the Airflow Resistance in Canine Upper Airways Comparing Different Dog Breeds**

Mauro Malvè\*, Rocío Fernández-Parra\*\*, Pascaline Pey\*\*\*, Luca Zilberstein\*\*\*\*

\*Public University of Navarra, \*\*Western College of Veterinary Medicine, University of Saskatchewan, \*\*\*Antech Imaging Services, \*\*\*\*École Nationale Vétérinaire d'Alfort

### **ABSTRACT**

Brachycephalic breeds are prone to breathing difficulties due to their upper airways anatomy that includes stenotic nares, intranasal turbinates swelling, reduced tracheal lumen and elongated soft palate [1]. Several surgical techniques exist to correct these anatomical pathologies that focus on widening the nasal apertures and/or reducing tissue of the soft palate. Since many problems still remains after surgery, further knowledge is necessary for improving clinical outcomes. In this study we have developed high-performance computational fluid dynamics models of different canine breeds with aim of comparing pressure-based airflow resistances. Larger grids were required in order to capture in details the canine nasal airways structure that has been reconstructed from computerized tomography. The numerical simulations modeled the respiratory flow as turbulent and performed steady inspiration imposing breed-specific physiological airflow rates. The mesh independent study performed to one selected dog skull anatomy pushed the grid refinements up to 50x106 cells. While the results suggest that the computed pressure drop is moderately grid independent as found by other authors [2,3], the rigorous finite volume-based computational study performed to nine non-pathological healthy dogs allowed a comprehensive fluid dynamics comparison between different canine morphologies. The latter revealed higher resistance regions in healthy brachycephalic dogs with respect to meso- and dolichocephalic breeds. Additionally, different brachycephalic dogs presented different airways resistances at different locations. The proposed methodology represents a novel non-invasive approach for quantifying the upper airways flow structure, pressure and resistance that can be used as a surgical planning in veterinary medicine as widely proposed for humans in biomechanics and in the biomedical engineering. [1] Hostnik et al. 2017, Quantification of nasal airflow resistance in English bulldogs using computed tomography and computational fluid dynamics, *Veterinary Radiology Ultrasound, American College of Veterinary Radiology*, 58:542-551. [2] Craven et al., 2009, Development and Verification of a High-Fidelity Computational Fluid Dynamics Model of Canine Nasal Airflow, *Journal of Biomechanical Engineering*, 131:091002-1/11. [3] Craven et al., 2009, The fluid dynamics of canine olfaction: unique nasal airflow patterns as an explanation of macrosmia, *Journal of Royal Society Interface*, doi:10.1098/rsif.2009.0490.

## TENSOR-VALUED RANDOM FIELDS DESCRIBING THE PIEZOELECTRIC EFFECT

ANATOLIY MALYARENKO\* AND MARTIN OSTOJA-STARZEWSKI†

\*Professor, Mälardalen University  
Västerås, Sweden  
anatoliy.malyarenko@mdh.se, <http://www.mdh.se/ukk/personal/maa/amo01>

†Professor, University of Illinois at Urbana-Champaign  
Urbana, IL, USA  
martinos@illinois.edu, <http://martinos.mechanical.illinois.edu>

**Key words:** Piezoelectricity, Symmetry Class, Representation, Random Field.

**Abstract.** The 18-dimensional space of piezoelectric tensors carries a natural action of the group  $O(3)$  of the orthogonal matrices. By the result of Geymonat and Weller (C. R. Math. Acad. Sci. **335** (10), 847–852, 2002), this action has 16 symmetry classes. For each class, consider the corresponding fixed point set  $V$ . It carries an orthogonal representation  $\rho$  of a symmetry group  $G$ . Our task is to describe the one- and two-points correlation tensors of a  $V$ -valued homogeneous and isotropic random field as well as the spectral expansion of the field in the form of stochastic integrals with respect to scattered orthogonal random measures.

We give an affirmative answer for the typical cases: a) the representation  $\rho$  is trivial; b) the group  $G$  is a subgroup of the group  $SO(3)$  and  $\rho$  is nontrivial; c) the group  $G$  is of type III and  $\rho$  is nontrivial; d) the most complicated case when  $G = O(3)$  and  $\rho = 2\rho_1 \oplus \rho_2 \oplus \rho_3$ . We describe and use a general method of obtaining such spectral expansions.

### 1 INTRODUCTION

Let  $B$  be a subset of the three-dimensional affine Euclidean space  $E^3$  occupied by a body. Let  $\mathbf{D}(\mathbf{x}): B \rightarrow \mathbb{R}^3$  (resp.  $\mathbf{E}(\mathbf{x}): B \rightarrow \mathbb{R}^3$ , resp.  $\varepsilon(\mathbf{x}): B \rightarrow \mathbf{S}^2(\mathbb{R}^3)$ , resp.  $\mathbf{e}(\mathbf{x}): B \rightarrow \mathbf{S}^2(\mathbb{R}^3) \otimes \mathbb{R}^3$ ) be the induction vector field (resp. the electric vector field, resp. the dielectric permeability tensor field, resp. the piezoelectric tensor field). The symbol  $\mathbf{S}^2(\mathbb{R}^3)$  denotes the set of rank 2 *symmetric* tensors over  $\mathbb{R}^3$ . The above fields are connected by the constitutive equation

$$D_i = e_{ijk}\varepsilon_{jk} + \varepsilon_{ik}E_k,$$

that describes the piezoelectric effect. Here, the Einstein summation convention is in use.

In the presence of spatially random material microstructure, we have to consider the body  $B$  as a *random medium*. Then, the piezoelectric tensor field  $\mathbf{e}(\mathbf{x})$  becomes random. That is, there is a probability space  $(\Omega, \mathfrak{F}, \mathbf{P})$  and a function of two variables  $\mathbf{e}(\mathbf{x}, \omega): B \times \Omega \rightarrow \mathbf{S}^2(\mathbb{R}^3) \otimes \mathbb{R}^3$  such that for any point  $\mathbf{x}_0 \in B$  the map  $\omega \mapsto \mathbf{e}(\mathbf{x}_0, \omega)$  is a  $\mathbf{S}^2(\mathbb{R}^3) \otimes \mathbb{R}^3$ -valued random tensor.

Assume that the random field  $\mathbf{e}(\mathbf{x})$  is *second-order*, that is,  $\mathbf{E}[\|\mathbf{e}(\mathbf{x})\|^2] < \infty$  for all  $\mathbf{x} \in B$ , and *mean-square continuous*, that is,

$$\lim_{\|\mathbf{x}-\mathbf{x}_0\| \rightarrow 0} \mathbf{E}[\|\mathbf{e}(\mathbf{x}) - \mathbf{e}(\mathbf{x}_0)\|^2] = 0, \quad \mathbf{x}_0 \in B.$$

Assume that the random field  $\mathbf{e}(\mathbf{x})$  is a restriction to  $B$  of a random field defined on all of  $E^3$ . Introduce a Cartesian coordinate system in  $E^3$  and identify the resulting space with the *space domain*  $\mathbb{R}^3$ . When one shifts the origin of the introduced system, the random field  $\mathbf{e}(\mathbf{x})$  is not changing. In particular, the *one-point correlation tensor*  $\langle \mathbf{e}(\mathbf{x}) \rangle = \mathbf{E}[\mathbf{e}(\mathbf{x})]$  does not depend on  $\mathbf{x} \in \mathbb{R}^3$ , while its *two-point correlation tensor*  $\langle \mathbf{e}(\mathbf{x}), \mathbf{e}(\mathbf{y}) \rangle = \mathbf{E}[(\mathbf{e}(\mathbf{x}) - \langle \mathbf{e}(\mathbf{x}) \rangle) \otimes (\mathbf{e}(\mathbf{y}) - \langle \mathbf{e}(\mathbf{y}) \rangle)]$  depends only on the difference  $\mathbf{z} = \mathbf{y} - \mathbf{x}$ . Such a field is called *wide-sense homogeneous*. In what follows we omit the words “wide-sense”.

The *orthogonal group*  $\mathbf{O}(3)$  of  $3 \times 3$  orthogonal matrices naturally acts in the space  $\mathbf{S}^2(\mathbb{R}^3) \otimes \mathbb{R}^3$ . For any point  $\mathbf{x} \in \mathbf{S}^2(\mathbb{R}^3) \otimes \mathbb{R}^3$ , let  $G_{\mathbf{x}} = \{g \in \mathbf{O}(3): g \cdot \mathbf{x} = \mathbf{x}\}$  be the *stationary subgroup* of the point  $\mathbf{x}$ . Call two stationary subgroups  $G_{\mathbf{x}}$  and  $G_{\mathbf{y}}$  *conjugate*, if there is  $h \in \mathbf{O}(3)$  such that  $G_{\mathbf{y}} = \{hgh^{-1}: g \in G_{\mathbf{x}}\}$ . The equivalence classes of this relation are called *piezoelectricity classes*.

Geymonat and Weller [1] proved that there are 16 piezoelectricity classes. For a representative  $G_0$  of a fixed piezoelectricity class, let  $V$  be the linear subspace of the space  $\mathbf{S}^2(\mathbb{R}^3) \otimes \mathbb{R}^3$  defined as is the maximal linear subspace where the group  $G_0$  acts *trivially*:

$$V = \{\mathbf{x} \in \mathbf{S}^2(\mathbb{R}^3) \otimes \mathbb{R}^3: g \cdot \mathbf{x} = \mathbf{x} \quad \text{for all } g \in G_0\}.$$

The space  $V$  is the space of all piezoelectric tensors of a fixed symmetry defined by the group  $G_0$ . There may exist a group  $G$  such that  $G_0$  is a proper closed subgroup of  $G$  but the space  $V$  is *invariant* under the action of  $G$ , that is,  $g \cdot \mathbf{x} \in V$  for all  $\mathbf{x} \in V$  and for all  $g \in G$ . It turns out that a group  $G$  has the above property if and only if it is a closed subgroup of the *normaliser*  $N(G_0) = \{h \in \mathbf{O}(3): hG_0h^{-1} = G_0\}$ . The group  $G$  acts in  $V$  by an *orthogonal representation*  $\rho$ , that is, the functions  $\rho(g): V \rightarrow V$  acting by  $\rho(g)\mathbf{x} = g \cdot \mathbf{x}$  is an orthogonal linear operator in  $V$  satisfying  $\rho(g_1g_2) = \rho(g_1)\rho(g_2)$ .

Assume that the random field  $\mathbf{e}(\mathbf{x})$  takes values in  $V$ . What happens when one rotates or reflects the Cartesian coordinate system by means of a matrix  $g \in G$ ? After the transformation  $g$  the point  $\mathbf{x}$  becomes the point  $g\mathbf{x}$ . Evidently, the tensor  $\mathbf{e}(\mathbf{x})$  is transformed into  $\rho(g)\mathbf{e}(\mathbf{x})$ . It is easy to see that the one- and two-point correlation tensors of the initial and transformed fields are equal if and only if

$$\begin{aligned} \langle \mathbf{e}(g\mathbf{x}) \rangle &= \rho(g)\langle \mathbf{e}(\mathbf{x}) \rangle, \\ \langle \mathbf{e}(g\mathbf{x}), \mathbf{e}(g\mathbf{y}) \rangle &= (\rho \otimes \rho)(g)\langle \mathbf{e}(\mathbf{x}), \mathbf{e}(\mathbf{y}) \rangle. \end{aligned} \tag{1}$$

The fields satisfying (1) are called *wide-sense isotropic*. As before, we will omit the words “wide-sense” in what follows.

We would like to find the general form of one- and two-point correlation tensors of a homogeneous and isotropic random field describing the piezoelectric effect and the spectral expansion of the field with respect to orthogonal random scattered measures.

The rest of the extended abstract is organised as follows. In Section 2, we describe the idea of solution and find the spectral expansion of the two-point correlation tensor of a homogeneous and isotropic random field taking its values in a fixed piezoelectricity class. In Section 3, we show how the methods of Section 2 work in practice by giving examples of spectral expansions of random fields for several typical cases.

## 2 AN IDEA OF SOLUTION

First, note that the answer to our question depends on the choice of a coordinate system in  $V$ . We try to write as many formulae as possible in the coordinate-free form and choose an appropriate coordinate system as late as possible.

Second, the solution can be naturally divided into two stage. At the first stage, we describe all homogeneous random fields. Then, we choose those fields that are isotropic.

Unfortunately, there exist no complete description of homogeneous random fields taking values in a finite-dimensional *real* linear space. Such a description exists for the case of a *complex* linear space and has been found by Cramér [2]. Equation

$$\langle \mathbf{e}(\mathbf{x}), \mathbf{e}(\mathbf{y}) \rangle = \int_{\hat{\mathbb{R}}^3} e^{i(\mathbf{p}, \mathbf{y} - \mathbf{x})} dF(\mathbf{p}), \quad (2)$$

where  $\hat{\mathbb{R}}^3$  is the *wavenumber domain*, establishes a one-to-one correspondence between the set of two-point correlation tensors of second-order mean-square continuous  $W$ -valued homogeneous random fields and the set of measures defined on the Borel  $\sigma$ -field  $\mathfrak{B}(\hat{\mathbb{R}}^3)$  and taking its values in the set of Hermitian nonnegative-definite linear operators on a finite-dimensional *complex* linear space  $W$ .

Recall that a *real structure* on  $W$  is an operator  $J: W \rightarrow W$  satisfying the following conditions:

$$J(\alpha \mathbf{x} + \beta \mathbf{y}) = \bar{\alpha} J(\mathbf{x}) + \bar{\beta} J(\mathbf{y}), \quad J^2 = I$$

for all  $\alpha, \beta \in \mathbb{C}$ ,  $\mathbf{x}, \mathbf{y} \in W$ , where  $I$  is the identity operator in  $W$ . The set of all eigenvectors of  $J$  corresponding to the eigenvalue 1 is a *real* linear space, call it  $V$ . Let  $(\cdot, \cdot)$  be an inner product in  $W$ . We adopt the *physical* convention: an inner product is linear in its second argument and anti-linear in the first one. For a linear operator  $L$  in  $W$ , let  $L^\top$  be the linear operator defined by

$$(LJ\mathbf{x}, \mathbf{y}) = (J\mathbf{x}, L^\top \mathbf{y}), \quad \mathbf{x}, \mathbf{y} \in W$$

(it’s just the coordinate-free definition of the transposed matrix).

We do not know *necessary and sufficient conditions* under which the  $W$ -valued random field  $\mathbf{e}(\mathbf{x})$  takes values in  $V$ . However, we know a *necessary condition*: if  $\mathbf{e}(\mathbf{x})$  takes values in  $V$ , then

$$F(-A) = F(A)^\top, \quad A \in \mathfrak{B}(\hat{\mathbb{R}}^3), \quad (3)$$

where  $-A = \{-\mathbf{p}: \mathbf{p} \in A\}$ .

Let  $\mathbf{e}_0 \in V$  be the one-point correlation tensor of the homogeneous random field  $\mathbf{e}(\mathbf{x})$ . The first line in Equation (1) means that  $\mathbf{e}_0 \in V_0$ , where

$$V_0 = \{x \in V: \rho(g)x = x \text{ for all } g \in G\}.$$

In the language of representation theory,  $V_0$  is the maximal subspace of  $V$  where the multiple of the trivial representation acts.

Similarly, the second line in Equation (1) means that

$$F(gA) = (\rho \otimes \rho)(g)F(A), \quad g \in G, \quad A \in \mathfrak{B}(\hat{\mathbb{R}}^3), \quad (4)$$

where we used Equation (2). The next idea is as follows: we would like to replace Equations (3) and (4) by *one* equation. To do this, we need more notation.

The conjugacy classes of closed subgroups of the group  $O(3)$  fall into three types.

**Type I** The subgroups of the group  $SO(3)$ .

**Type II** The subgroups containing  $-I$ .

**Type III** The remaining subgroups.

Let  $Z_2^c$  be the subgroup of the group  $O(3)$  defined by  $Z_2^c = \{I, -I\}$ . This group has two irreducible orthogonal representations:  $A_g(h) = 1$  and  $A_u(h) = \det h$ ,  $h \in Z_2^c$ . Let  $\pi: O(3) \rightarrow SO(3)$  be the projection of the Cartesian product  $O(3) = SO(3) \times Z_2^c$  to the first term. The space  $S^2(V)$  is an invariant subspace of the representation  $\rho \otimes \rho$ . Denote by  $S^2(\rho)$  the restriction of the representation  $\rho \otimes \rho$  to the above subspace. Similarly, the space  $\Lambda^2(V)$  of rank 2 skew-symmetric tensors over  $V$  is an invariant subspace, and the restriction of the representation  $\rho \otimes \rho$  to this subspace is denoted by  $\Lambda^2(\rho)$ . Finally, let  $\rho$  be a representation of a group  $G$  of type III, let  $\rho^\pi$  be the representation of the group  $\pi(G)$  defined by  $\rho^\pi(g) = \rho(\pi^{-1}(g))$ , and let  $\widehat{\Lambda^2(\rho^\pi)}$  be the representation of  $\pi(G)$  given by

$$\widehat{\Lambda^2(\rho^\pi)} = \begin{cases} \Lambda^2(\rho^\pi), & \text{if } g \in G \cap \pi(G), \\ -\Lambda^2(\rho^\pi), & \text{otherwise.} \end{cases}$$

**Lemma 1.** *There exists a group  $\tilde{G}$  and its orthogonal representation  $\tilde{\rho}$  in a real finite-dimensional space  $\tilde{V}$  such that the measure  $F$  takes values in  $\tilde{V}$  and Equations (3) and (4) are equivalent to the equation*

$$F(\tilde{g}A) = \tilde{\rho}(\tilde{g})F(A), \quad \tilde{g} \in \tilde{G}, \quad A \in \mathfrak{B}(\hat{\mathbb{R}}^3). \quad (5)$$

Moreover:

- If  $G$  is of type I, then  $\tilde{G} = G \times Z_2^c$ ,  $\tilde{V} = V \otimes V$ , and

$$\tilde{\rho} = S^2(\rho) \hat{\otimes} \dim S^2(\rho) A_g \oplus \widehat{\Lambda^2(\rho^\pi)} \hat{\otimes} \dim \widehat{\Lambda^2(\rho^\pi)} A_u.$$

- If  $G$  is of type II, then  $\tilde{G} = G$ ,  $\tilde{V} = S^2(V)$ , and  $\tilde{\rho} = S^2(\rho)$ .
- If  $G$  is of type III, then  $\tilde{G} = \pi(G) \times Z_2^c$ ,  $\tilde{V} = V \otimes V$ , and

$$\tilde{\rho} = S^2(\rho^\pi) \hat{\otimes} \dim S^2(\rho^\pi) A_g \oplus \widehat{\Lambda^2(\rho^\pi)} \hat{\otimes} \dim \widehat{\Lambda^2(\rho^\pi)} A_u.$$

*Remark 1.* Malyarenko and Ostoja-Starzewski [3] considered the case of *elasticity classes*. In this case, all groups  $G$  are of type II, and the second part of Lemma 1 have been formulated and proved there. The complete proof may be found in the forthcoming book by Malyarenko and Ostoja-Starzewski [4].

Consider the measure  $\mu$  defined by  $\mu(A) = \text{tr } F(A)$ , the trace of the operator  $F(A)$ . It is well-known that the measure  $F$  is absolutely continuous with respect to  $\mu$ , and the Radon–Nykodym derivative  $f(\mathbf{p})$  is a measurable function taking values in the set of nonnegative-definite operators with unit trace. Equation (2) takes the form

$$\langle \mathbf{e}(\mathbf{x}), \mathbf{e}(\mathbf{y}) \rangle = \int_{\hat{\mathbb{R}}^3} e^{i(\mathbf{p}, \mathbf{y} - \mathbf{x})} f(\mathbf{p}) d\mu(\mathbf{p}),$$

while condition (5) becomes

$$f(\tilde{g}\mathbf{p}) = \tilde{\rho}(\tilde{g})f(\mathbf{p}), \quad \mu(\tilde{g}A) = \mu(A), \quad \tilde{g} \in \tilde{G}, \quad A \in \mathfrak{B}(\hat{\mathbb{R}}^3). \quad (6)$$

The description of all measures  $\mu$  satisfying the second condition is well-known, see Bourbaki [5]. Consider the action of the group  $\tilde{G}$  on  $\hat{\mathbb{R}}^3$  by matrix-vector multiplication. This action is an orthogonal representation of a compact group  $\tilde{G}$  and has finitely many symmetry classes, see Duistermaat and Kolk [6]. Introduce a partial ordering on the set of symmetry classes:  $[G_1] \leq [G_2]$  if and only if any representative of the class  $[G_1]$  is conjugate to a subgroup of  $G_2$ . The maximal element of the introduced partial ordering is  $[G_0] = [G]$ . Enumerate the remaining elements in such an order that  $[G_i] \leq [G_j]$  if  $i \leq j$ . There is also the minimal element  $[G_{M-1}]$ , where  $M$  is the number of symmetry classes. Any chain of this ordering has at most  $1 + \dim \hat{\mathbb{R}}^3 / \tilde{G}$  many elements, where  $\hat{\mathbb{R}}^3 / \tilde{G}$  is the orbit space of the action. Denote by  $(\hat{\mathbb{R}}^3 / \tilde{G})_m$  the set of all orbits whose stationary subgroups are representatives of the class  $[G_m]$ ,  $0 \leq m \leq M-1$ . The sets  $(\hat{\mathbb{R}}^3 / \tilde{G})_m$  are manifolds. We have  $[G_i] \leq [G_j]$  if and only if  $(\hat{\mathbb{R}}^3 / \tilde{G})_j$  is a subset of the closure of  $(\hat{\mathbb{R}}^3 / \tilde{G})_i$ . In particular, the set  $(\hat{\mathbb{R}}^3 / \tilde{G})_{M-1}$  is open and dense in  $\hat{\mathbb{R}}^3 / \tilde{G}$ , it is called the *principal orbit type*, while  $(\hat{\mathbb{R}}^3 / \tilde{G})_0 = \{\mathbf{0}\}$ .

Denote by  $\nu_m$  the probabilistic  $G_m$ -invariant measure on the orbit  $\tilde{G} / G_m$ . The measure  $\mu$  has the form

$$\mu = \sum_{m=0}^{M-1} \int_{(\hat{\mathbb{R}}^3 / \tilde{G})_m} \nu_m d\mu_m,$$

where  $\mu_m$  are arbitrary finite measures on the Borel  $\sigma$ -fields  $\mathfrak{B}((\hat{\mathbb{R}}^3/\tilde{G})_m)$ . For simplicity, assume that there exists a chart  $\varphi^m$  of the manifold  $\tilde{G}/G_m$  and a chart  $\lambda^m$  of the manifold  $(\hat{\mathbb{R}}^3/\tilde{G})_m$  with dense domains. The two-point correlation tensor of the random field  $\mathbf{e}(\mathbf{x})$  takes the form

$$\langle \mathbf{e}(\mathbf{x}), \mathbf{e}(\mathbf{y}) \rangle = \sum_{m=0}^{M-1} \int_{(\hat{\mathbb{R}}^3/\tilde{G})_m} \int_{\tilde{G}/G_m} e^{i((\lambda^m, \varphi^m), \mathbf{y}-\mathbf{x})} f(\lambda^m, \varphi^m) dv_m(\varphi^m) d\mu_m(\lambda^m).$$

It remains to analyse the first condition in Equation (6). Denote

$$V_m = \{ \mathbf{x} \in \tilde{V} : \tilde{\rho}(\tilde{g})\mathbf{x} = \mathbf{x} \text{ for all } \tilde{g} \in G_m \}.$$

The subspace  $V_m$  has positive dimension, because the representation  $\tilde{\rho}$  contains at least one trivial irreducible component. The intersection of  $V_m$  with the convex compact set of Hermitian nonnegative-definite linear operators with unit trace is a convex compact set, call it  $C_m$ . Let  $\varphi_0^m$  be the coordinate of the point of  $\tilde{G}/G_m$  with stationary subgroup  $G_m$ . The function  $f(\lambda^m, \varphi^m)$  is an arbitrary measurable function on  $(\hat{\mathbb{R}}^3/\tilde{G})_m$  taking values in  $C_m$ . By the first condition in Equation (6), the function  $f(\lambda_m, \varphi_m)$  becomes

$$f(\lambda^m, \varphi^m) = \tilde{\rho}(\varphi^m) f(\lambda^m, \varphi_0^m),$$

and the two-point correlation tensor of the random field  $\mathbf{e}(\mathbf{x})$  takes the form

$$\langle \mathbf{e}(\mathbf{x}), \mathbf{e}(\mathbf{y}) \rangle = \sum_{m=0}^{M-1} \int_{(\hat{\mathbb{R}}^3/\tilde{G})_m} \int_{\tilde{G}/G_m} e^{i((\lambda^m, \varphi^m), \mathbf{y}-\mathbf{x})} \tilde{\rho}(\varphi^m) f(\lambda^m, \varphi_0^m) dv_m(\varphi^m) d\mu_m(\lambda^m).$$

To calculate the inner integral, choose a basis  $\mathbf{e}^1, \dots, \mathbf{e}^{\dim V}$  in the space  $V$ . The tensor square  $V \otimes V$  has several different bases. The *coupled basis* is the set of tensor products  $\mathbf{e}^i \otimes \mathbf{e}^j$ ,  $1 \leq i, j \leq \dim V$ . The  *$m$ th uncoupled basis* is constructed as follows. The space  $\tilde{V} \subseteq V \otimes V$  falls into the direct sum of several subspaces, where the irreducible components of the representation  $\tilde{\rho}$  act. Let  $H^{m11}, \dots, H^{m1k_1}, \dots, H^{mL_m1}, \dots, H^{mL_mk_{L_m}}$  be the set of all subspaces that satisfy the following conditions.

- The irreducible component  $\rho^l$  acts in the spaces  $H^{m11}, \dots, H^{mlk_l}$ ,  $0 \leq m \leq M$ ,  $1 \leq l \leq L_m$ .
- $H^{mlk} \cap V_m \neq \{0\}$ ,  $0 \leq m \leq M$ ,  $1 \leq l \leq L_m$ ,  $1 \leq k \leq k_l$ .

Choose a basis  $\{\mathbf{e}^{mlkn} : 1 \leq n \leq \dim H^{mlk} \cap V_m\}$  in the intersection  $H^{mlk} \cap V_m$  and complement the chosen basis to a basis of the space  $V \otimes V$  arbitrarily. The tensors of the coupled basis are linear combinations of the tensors of the  $m$ th uncoupled basis:

$$\mathbf{e}^i \otimes \mathbf{e}^j = \sum_{l=1}^{L_m} \sum_{k=1}^{k_l} \sum_{n=1}^{\dim H^{mlk} \cap V_m} c_{ijmlkn} \mathbf{e}^{mlkn} + \dots,$$

where the dots denote non-essential terms. One needs to choose bases in such a way that the *Clebsch–Gordan coefficients*  $c_{ijmlkn}$  are calculating as easy as possible. Let  $f^{mlkn}(\boldsymbol{\lambda}^m, \boldsymbol{\varphi}_0^m)$  be the components of the tensor  $f(\boldsymbol{\lambda}^m, \boldsymbol{\varphi}_0^m)$  in the  $m$ th uncoupled basis. Then we have

$$\begin{aligned} \langle \mathbf{e}(\mathbf{x}), \mathbf{e}(\mathbf{y}) \rangle_{ij} &= \sum_{m=0}^{M-1} \sum_{l=1}^{L_m} \sum_{k=1}^{k_l} \sum_{q=1}^{\dim \rho^l} \sum_{n=1}^{\dim \mathbb{H}^{mlk}} \int_{(\hat{\mathbb{R}}^3/\tilde{G})_m} \int_{\tilde{G}/G_m} e^{i((\boldsymbol{\lambda}^m, \boldsymbol{\varphi}^m), \mathbf{y}-\mathbf{x})} \\ &\times \rho_{qn}^l(\boldsymbol{\varphi}^m) f^{mlkn}(\boldsymbol{\lambda}^m, \boldsymbol{\varphi}_0^m) d\nu_m(\boldsymbol{\varphi}^m) d\mu_m(\boldsymbol{\lambda}^m). \end{aligned}$$

By the Fine Structure Theorem [7], there is a subset  $N_{ml}$  of the set  $\{1, 2, \dots, \dim \mathbb{H}^{mlk}\}$  such that the functions  $\sqrt{\dim \rho^l} \rho_{qn}^l(\boldsymbol{\varphi}^m)$ ,  $1 \leq q \leq \dim \rho^l$ ,  $n \in N_{ml}$ , form an orthonormal basis in the space of square-integrable functions on the orbit  $\tilde{G}/G_m$  with respect to the measure  $\mu_m$ . Denote

$$j_{qn}^{ml}(\boldsymbol{\lambda}^m, \mathbf{y} - \mathbf{x}) = \int_{\tilde{G}/G_m} e^{i((\boldsymbol{\lambda}^m, \boldsymbol{\varphi}^m), \mathbf{y}-\mathbf{x})} \rho_{qn}^l(\boldsymbol{\varphi}^m) d\mu_m(\boldsymbol{\lambda}^m).$$

Then we obtain the spectral expansion of the two-point correlation tensor of the field:

$$\langle \mathbf{e}(\mathbf{x}), \mathbf{e}(\mathbf{y}) \rangle_{ij} = \sum_{m=0}^{M-1} \sum_{l=1}^{L_m} \sum_{k=1}^{k_l} \sum_{q=1}^{\dim \rho^l} \sum_{n \in N_{ml}} \int_{(\hat{\mathbb{R}}^3/\tilde{G})_m} j_{qn}^{ml}(\boldsymbol{\lambda}^m, \mathbf{y} - \mathbf{x}) f^{mlkn}(\boldsymbol{\lambda}^m, \boldsymbol{\varphi}_0^m) d\mu_m(\boldsymbol{\lambda}^m).$$

To obtain the spectral expansion of the field  $\mathbf{e}(\mathbf{x})$ , write down the complex exponent as

$$e^{i((\boldsymbol{\lambda}^m, \boldsymbol{\varphi}^m), \mathbf{y}-\mathbf{x})} = e^{i((\boldsymbol{\lambda}^m, \boldsymbol{\varphi}^m), \mathbf{y})} \overline{e^{i((\boldsymbol{\lambda}^m, \boldsymbol{\varphi}^m), \mathbf{x})}},$$

and apply the Fine Structure Theorem to each term *separately*. Then, apply Karhunen's Theorem [8]. We perform this in the following examples in each case separately.

### 3 EXAMPLES

**Example 1.** The *dihedral group*  $D_2$  generated by the rotation about the  $z$ -axis with angle  $\pi$  and the rotation about the  $x$ -axis with the same angle, is a piezoelectric class. Its symmetry class  $\mathbb{V}$  has dimension 3, and the group  $D_2$  acts in  $\mathbb{V}$  trivially. The basis of  $\mathbb{V}$  is

$$\mathbb{T}^1 = \frac{1}{\sqrt{2}} \begin{pmatrix} 0 & 1 & 0 \\ 1 & 0 & 0 \\ 0 & 0 & 0 \end{pmatrix} \otimes \begin{pmatrix} 0 \\ 0 \\ 1 \end{pmatrix}, \mathbb{T}^2 = \frac{1}{\sqrt{2}} \begin{pmatrix} 0 & 0 & 1 \\ 0 & 0 & 0 \\ 1 & 0 & 0 \end{pmatrix} \otimes \begin{pmatrix} 0 \\ 1 \\ 0 \end{pmatrix}, \mathbb{T}^3 = \frac{1}{\sqrt{2}} \begin{pmatrix} 0 & 0 & 0 \\ 0 & 0 & 1 \\ 0 & 1 & 0 \end{pmatrix} \otimes \begin{pmatrix} 1 \\ 0 \\ 0 \end{pmatrix}.$$

The group  $\tilde{G}$  is  $\tilde{G} = D_2 \times Z_2^c$ . The orbit type stratification is

$$\begin{aligned} (\hat{\mathbb{R}}^3/D_2 \times Z_2^c)_1 &= \{(0, 0, p_3): p_3 > 0\}, \\ (\hat{\mathbb{R}}^3/D_2 \times Z_2^c)_2 &= \{(0, p_2, 0): p_2 > 0\}, \\ (\hat{\mathbb{R}}^3/D_2 \times Z_2^c)_3 &= \{(p_1, 0, 0): p_1 > 0\}, \\ (\hat{\mathbb{R}}^3/D_2 \times Z_2^c)_4 &= \{(p_1, p_2, 0): p_1 > 0, p_2 > 0\}, \\ (\hat{\mathbb{R}}^3/D_2 \times Z_2^c)_5 &= \{(p_1, 0, p_3): p_1 > 0, p_3 > 0\}, \\ (\hat{\mathbb{R}}^3/D_2 \times Z_2^c)_6 &= \{(0, p_2, p_3): p_2 > 0, p_3 > 0\}, \\ (\hat{\mathbb{R}}^3/D_2 \times Z_2^c)_7 &= \{(p_1, p_2, p_3): p_1 > 0, p_2 > 0, p_3 > 0\}. \end{aligned}$$

Let  $\Phi$  be a finite measure on  $\hat{\mathbb{R}}^3/D_2 \times Z_2^c$ , and let  $f(\mathbf{p})$  be a  $\Phi$ -equivalence class of measurable functions acting from  $\hat{\mathbb{R}}^3/D_2 \times Z_2^c$  to the set of nonnegative-definite Hermitian linear operators on  $V_{\mathbb{C}}$  with unit trace. Let  $u_n(\mathbf{p}, \mathbf{x})$  be 8 different products of cosines and sines of  $p_i x_i$ :

$$\begin{aligned} u_1(\mathbf{p}, \mathbf{x}) &= \sin(p_1 x_1) \sin(p_2 x_2) \sin(p_3 x_3), & u_2(\mathbf{p}, \mathbf{x}) &= \cos(p_1 x_1) \cos(p_2 x_2) \sin(p_3 x_3), \\ u_3(\mathbf{p}, \mathbf{x}) &= \cos(p_1 x_1) \sin(p_2 x_2) \cos(p_3 x_3), & u_4(\mathbf{p}, \mathbf{x}) &= \sin(p_1 x_1) \cos(p_2 x_2) \cos(p_3 x_3), \\ u_5(\mathbf{p}, \mathbf{x}) &= \cos(p_1 x_1) \cos(p_2 x_2) \cos(p_3 x_3), & u_6(\mathbf{p}, \mathbf{x}) &= \sin(p_1 x_1) \sin(p_2 x_2) \cos(p_3 x_3), \\ u_7(\mathbf{p}, \mathbf{x}) &= \sin(p_1 x_1) \cos(p_2 x_2) \sin(p_3 x_3), & u_8(\mathbf{p}, \mathbf{x}) &= \cos(p_1 x_1) \sin(p_2 x_2) \sin(p_3 x_3). \end{aligned}$$

The one-point correlation tensor of a homogeneous and  $(D_2, 3A)$ -isotropic random field  $\mathbf{e}(\mathbf{x})$  is

$$\langle \mathbf{e}(\mathbf{x}) \rangle_{ijk} = \sum_{m=1}^3 C_m \mathbb{T}_{ijk}^m,$$

where  $C_m \in \mathbb{R}$ . Its two-point correlation tensor has the form

$$\begin{aligned} \langle \mathbf{e}(\mathbf{x}), \mathbf{e}(\mathbf{y}) \rangle &= \int_{\hat{\mathbb{R}}^3/D_2 \times Z_2^c} \cos(p_1 z_1) \cos(p_2 z_2) \cos(p_3 z_3) f_S(\mathbf{p}) \, d\Phi(\mathbf{p}) \\ &+ \int_{(\hat{\mathbb{R}}^3/Z_2 \times Z_2^c)_7} \sin(p_1 z_1) \sin(p_2 z_2) \sin(p_3 z_3) f_A(\mathbf{p}) \, d\Phi(\mathbf{p}), \end{aligned}$$

The field has the form

$$\begin{aligned} \mathbf{e}_{ijk}(\mathbf{x}) &= \sum_{m=1}^3 C_m \mathbb{T}_{ijk}^m + \sum_{m=1}^3 \sum_{n=1}^4 \int_{\hat{\mathbb{R}}^3/D_2 \times Z_2^c} u_n(\mathbf{p}, \mathbf{x}) \, dZ_{mn}^1(\mathbf{p}) \mathbb{T}_{ijk}^m \\ &+ \sum_{m=1}^3 \sum_{n=5}^8 \int_{(\hat{\mathbb{R}}^3/Z_2 \times Z_2^c)_7} u_n(\mathbf{p}, \mathbf{x}) \, dZ_{mn}^2(\mathbf{p}) \mathbb{T}_{ijk}^m, \end{aligned}$$

where  $\mathbf{Z}^{1n}(\mathbf{p}) = (Z_{1n}^1(\mathbf{p}), \dots, Z_{3n}^1(\mathbf{p}))^\top$  (resp.  $\mathbf{Z}^{2n}(\mathbf{p}) = (Z_{1n}^2(\mathbf{p}), \dots, Z_{3n}^2(\mathbf{p}))^\top$ ) are centred  $\mathbb{V}$ -valued random measures on  $\hat{\mathbb{R}}^3/D_2 \times Z_2^c$  (resp. on  $(\hat{\mathbb{R}}^3/D_2 \times Z_2^c)_7$ ) with control measure  $f_S(\mathbf{p})$  and cross-correlation

$$\mathbb{E}[\mathbf{Z}_n^S(A) \otimes \mathbf{Z}_{n+4}^A(B)] = -\mathbb{E}[\mathbf{Z}_n^A(A) \otimes \mathbf{Z}_{n+4}^S(B)] = \int_{A \cap B} f_A(\mathbf{p}) \, d\Phi(\mathbf{p}).$$

**Example 2.** The dihedral group  $D_4$  acts in the space  $\mathbb{V}$  of Example 1 by the nontrivial representation  $\rho = A_1 \oplus 2B_1$  (for the notation used, see [9]). The basis of  $\mathbb{V}$  is

$$\mathbb{T}^{1,3} = \frac{1}{\sqrt{2}} \left[ \begin{pmatrix} 0 & 1 & 0 \\ 1 & 0 & 0 \\ 0 & 0 & 0 \end{pmatrix} \otimes \begin{pmatrix} 1 \\ 0 \\ 0 \end{pmatrix} \pm \begin{pmatrix} 0 & 0 & 0 \\ 0 & 0 & 1 \\ 0 & 1 & 0 \end{pmatrix} \otimes \begin{pmatrix} 0 \\ 0 \\ 1 \end{pmatrix} \right]$$

and the same  $\mathbb{T}^2$  as the one in Example 1.

The group  $\tilde{G}$  is  $\tilde{G} = D_4 \times Z_2^c$ . The orbit type stratification is

$$\begin{aligned} (\hat{\mathbb{R}}^3/D_4 \times Z_2^c)_1 &= \{ (0, 0, p_3) : p_3 > 0 \}, \\ (\hat{\mathbb{R}}^3/D_4 \times Z_2^c)_2 &= \{ (p_1, p_2, 0) : p_1 = p_2 > 0 \}, \\ (\hat{\mathbb{R}}^3/D_4 \times Z_2^c)_3 &= \{ (p_1, 0, 0) : p_1 > 0 \}, \\ (\hat{\mathbb{R}}^3/D_4 \times Z_2^c)_4 &= \{ (p_1, p_2, 0) : 0 < p_2 < p_1 \}, \\ (\hat{\mathbb{R}}^3/D_4 \times Z_2^c)_5 &= \{ (p_1, p_2, p_3) : p_1 = p_2 > 0, p_3 > 0 \}, \\ (\hat{\mathbb{R}}^3/D_4 \times Z_2^c)_6 &= \{ (p_1, 0, p_3) : p_1 > 0, p_3 > 0 \}, \\ (\hat{\mathbb{R}}^3/D_2 \times Z_2^c)_7 &= \{ (p_1, p_2, p_3) : 0 < p_2 < p_1, p_3 > 0 \}. \end{aligned}$$

Let  $\Phi$  be a finite measure on  $\hat{\mathbb{R}}^3/D_4 \times Z_2^c$ , and let  $f^{3,7}(\mathbf{p})$  be a  $\Phi$ -equivalence class of measurable functions acting from  $\hat{\mathbb{R}}^3/D_4 \times Z_2^c$  to the set of nonnegative-definite Hermitian operators on  $\mathbb{V}$  with unit trace. Let an equivalence class  $f^{0,1}(\mathbf{p})$  acts to the set of diagonal matrices,  $f^2(\mathbf{p})$  acts to the set of matrices satisfying  $f_{12}^2(\mathbf{p}) = f_{13}^2(\mathbf{p}) = 0$ , and  $f^{4,6}(\mathbf{p})$  acts to the set of matrices with real-valued entries. Finally, define  $\sigma f$  as follows:

$$(\sigma f)_{12} = f_{21}, \quad (\sigma f)_{13} = f_{31},$$

and  $(\sigma f)_{ij} = f_{ij}$  otherwise. Denote

$$\begin{aligned} u_1(\mathbf{p}, \mathbf{x}) &= \cos(p_1 x_1) \cos(p_2 x_2) \cos(p_3 x_3), \\ u_2(\mathbf{p}, \mathbf{x}) &= \sin(p_1 x_1) \sin(p_2 x_2) \sin(p_3 x_3), \\ u_3(\mathbf{p}, \mathbf{x}) &= \cos(p_1 x_2) \cos(p_2 x_1) \cos(p_3 x_3), \\ u_4(\mathbf{p}, \mathbf{x}) &= \sin(p_1 x_2) \sin(p_2 x_1) \sin(p_3 x_3). \end{aligned}$$

The one-point correlation tensor of a homogeneous and  $(D_4, A_1 \oplus 2B_1)$ -isotropic random field  $\mathbf{e}(\mathbf{x})$  is

$$\langle \mathbf{e}(\mathbf{x}) \rangle_{ijk} = C \mathbb{T}_{ijk}^1,$$

where  $C \in \mathbb{R}$ . Its two-point correlation tensor has the form

$$\begin{aligned} \mathbf{e}_{ijk}(\mathbf{x}) = & \int_{(\hat{\mathbb{R}}^3/D_4 \times Z_2^c)_{0,1}} [u_1(\mathbf{p}, \mathbf{x}) f_S^{0,1}(\mathbf{p}) + u_2(\mathbf{p}, \mathbf{x}) f_\Lambda^{0,1}(\mathbf{p}) \\ & + u_3(\mathbf{p}, \mathbf{x}) (\sigma f)_S^{0,1}(\mathbf{p}) + u_4(\mathbf{p}, \mathbf{x}) (\sigma f)_\Lambda^{0,1}(\mathbf{p})] d\Phi(\mathbf{p}) \\ & + \int_{(\hat{\mathbb{R}}^3/D_4 \times Z_2^c)_2} [u_1(\mathbf{p}, \mathbf{x}) f_S^2(\mathbf{p}) + u_2(\mathbf{p}, \mathbf{x}) f_\Lambda^2(\mathbf{p}) \\ & + u_3(\mathbf{p}, \mathbf{x}) (\sigma f)_S^2(\mathbf{p}) + u_4(\mathbf{p}, \mathbf{x}) (\sigma f)_\Lambda^2(\mathbf{p})] d\Phi(\mathbf{p}) \\ & + \int_{(\hat{\mathbb{R}}^3/D_4 \times Z_2^c)_{3,7}} [u_1(\mathbf{p}, \mathbf{x}) f_S^{3,7}(\mathbf{p}) + u_2(\mathbf{p}, \mathbf{x}) f_\Lambda^{3,7}(\mathbf{p}) \\ & + u_3(\mathbf{p}, \mathbf{x}) (\sigma f)_S^{3,7}(\mathbf{p}) + u_4(\mathbf{p}, \mathbf{x}) (\sigma f)_\Lambda^{3,7}(\mathbf{p})] d\Phi(\mathbf{p}) \\ & + \int_{(\hat{\mathbb{R}}^3/D_4 \times Z_2^c)_{4,6}} [u_1(\mathbf{p}, \mathbf{x}) f_S^{4,6}(\mathbf{p}) + u_2(\mathbf{p}, \mathbf{x}) f_\Lambda^{4,6}(\mathbf{p}) \\ & + u_3(\mathbf{p}, \mathbf{x}) (\sigma f)_S^{4,6}(\mathbf{p}) + u_4(\mathbf{p}, \mathbf{x}) (\sigma f)_\Lambda^{4,6}(\mathbf{p})] d\Phi(\mathbf{p}). \end{aligned}$$

**Example 3.** The *prismatic group*  $D_4^h$  of order 8 is generated by the product of the rotation about the  $z$ -axis with angle  $\pi/2$  and the reflection through the plane normal to the same axis, and the rotation about the  $x$ -axis with angle  $\pi$ . It acts in the space  $V$  of Example 1 by the nontrivial representation  $\rho = 2A_1 \oplus B_1$ . The basis of  $V$  and the group  $\tilde{G}$  are the same as in Example 2.

Let  $\Phi$  be a finite measure on  $\hat{\mathbb{R}}^3/D_4 \times Z_2^c$ , and let  $f(\mathbf{p})$  be a  $\Phi$ -equivalence class of measurable functions acting from  $\hat{\mathbb{R}}^3/D_4 \times Z_2^c$  to the set of nonnegative-definite Hermitian linear operators on  $V$  with unit trace. Let  $f^S(\mathbf{p})$  be its symmetric part, and let  $if^A(\mathbf{p})$  be its skew-symmetric part. Let  $f^{S,B}(\mathbf{p})$  be the same class with  $f_{13}^{S,B}(\mathbf{p}) = f_{23}^{S,B}(\mathbf{p}) = 0$ . Let  $f^{A,B}(\mathbf{p})$  be the same class with  $f_{12}^{A,B}(\mathbf{p}) = 0$ , and let  $f^{A,A}(\mathbf{p})$  be the same class with  $f_{13}^{A,A}(\mathbf{p}) = f_{23}^{A,A}(\mathbf{p}) = 0$ .

The one-point correlation tensor of a homogeneous and  $(D_4^h, 2A_1 \oplus B_1)$ -isotropic random field  $\mathbf{e}(\mathbf{x})$  is

$$\langle \mathbf{e}(\mathbf{x}) \rangle = C_1 \mathbb{T}_{ijk}^1 + C_2 \mathbb{T}_{ijk}^3.$$

Its two-point correlation tensor is

$$\begin{aligned}
 \langle \mathbf{e}(\mathbf{x}), \mathbf{e}(\mathbf{y}) \rangle &= \frac{1}{2} \int_{(\hat{\mathbb{R}}^3/D_4 \times Z_2^c)_{3,4,6,7}} \cos(p_1 z_1) \cos(p_2 z_2) \cos(p_3 z_3) f^S(\mathbf{p}) \, d\Phi(\mathbf{p}) \\
 &+ \frac{1}{2} \int_{(\hat{\mathbb{R}}^3/D_4 \times Z_2^c)_{0,1,2,5}} \cos(p_1 z_1) \cos(p_2 z_2) \cos(p_3 z_3) f^{S,B}(\mathbf{p}) \, d\Phi(\mathbf{p}) \\
 &+ \frac{1}{2} \int_{(\hat{\mathbb{R}}^3/D_4 \times Z_2^c)_{3,7}} \cos(p_1 z_1) \sin(p_2 z_2) \cos(p_3 z_3) f^A(\mathbf{p}) \, d\Phi(\mathbf{p}) \\
 &+ \frac{1}{2} \int_{(\hat{\mathbb{R}}^3/D_4 \times Z_2^c)_2} \cos(p_1 z_1) \sin(p_2 z_2) \cos(p_3 z_3) f^{\Delta,B}(\mathbf{p}) \, d\Phi(\mathbf{p}) \\
 &+ \frac{1}{2} \int_{(\hat{\mathbb{R}}^3/D_4 \times Z_2^c)_5} \cos(p_1 z_1) \sin(p_2 z_2) \cos(p_3 z_3) f^{\Delta,A}(\mathbf{p}) \, d\Phi(\mathbf{p}).
 \end{aligned}$$

The field has the form

$$\begin{aligned}
 \mathbf{e}_{ijk}(\mathbf{x}) &= C_1 \mathbb{T}_{ijk}^1 + C_2 \mathbb{T}_{ijk}^3 + \frac{1}{\sqrt{2}} \sum_{m=1}^3 \sum_{n=1}^8 \int_{(\hat{\mathbb{R}}^3/D_4 \times Z_2^c)_{3,4,6,7}} g_n(\mathbf{p}, \mathbf{x}) \, dZ_{mn}^S(\mathbf{p}) \mathbb{T}_{ijk}^m \\
 &+ \frac{1}{\sqrt{2}} \sum_{m=1}^3 \sum_{n=1}^8 \int_{(\hat{\mathbb{R}}^3/D_4 \times Z_2^c)_{0,1,2,5}} g_n(\mathbf{p}, \mathbf{x}) \, dZ_{mn}^{S,B}(\mathbf{p}) \mathbb{T}_{ijk}^m \\
 &+ \frac{1}{\sqrt{2}} \sum_{m=1}^3 \sum_{n=1}^8 \int_{(\hat{\mathbb{R}}^3/D_4 \times Z_2^c)_{3,7}} g_n(\mathbf{p}, \mathbf{x}) \, dZ_{mn}^A(\mathbf{p}) \mathbb{T}_{ijk}^m \\
 &+ \frac{1}{\sqrt{2}} \sum_{m=1}^3 \sum_{n=1}^8 \int_{(\hat{\mathbb{R}}^3/D_4 \times Z_2^c)_5} g_n(\mathbf{p}, \mathbf{x}) \, dZ_{mn}^{\Delta,B}(\mathbf{p}) \mathbb{T}_{ijk}^m \\
 &+ \frac{1}{\sqrt{2}} \sum_{m=1}^3 \sum_{n=1}^8 \int_{(\hat{\mathbb{R}}^3/D_4 \times Z_2^c)_2} g_n(\mathbf{p}, \mathbf{x}) \, dZ_{mn}^{\Delta,A}(\mathbf{p}) \mathbb{T}_{ijk}^m,
 \end{aligned}$$

where  $\mathbf{Z}_n^S(\mathbf{p}) = (Z_{1n}^S(\mathbf{p}), \dots, Z_{3n}^S(\mathbf{p}))^\top$  (resp.  $\mathbf{Z}_n^{S,B}(\mathbf{p})$ , resp.  $\mathbf{Z}_n^A(\mathbf{p})$ , resp.  $\mathbf{Z}_n^{\Delta,B}(\mathbf{p})$ , resp.  $\mathbf{Z}_n^{\Delta,A}(\mathbf{p})$ ) are uncorrelated centred  $\mathbb{V}^{D_4^h}$ -valued random measures on  $\hat{\mathbb{R}}^3/D_4 \times Z_2^c$  with control measure  $f^S(\mathbf{p})$  (resp.  $f^{S,B}(\mathbf{p})$ , resp.  $f^A(\mathbf{p})$ , resp.  $f^{\Delta,B}(\mathbf{p})$ , resp.  $f^{\Delta,A}(\mathbf{p})$ ) and cross-correlations

$$\begin{aligned}
 \mathbb{E}[\mathbf{Z}_1^S(A) \otimes \mathbf{Z}_3^A(B)] &= \mathbb{E}[\mathbf{Z}_2^S(A) \otimes \mathbf{Z}_4^A(B)] = \int_{A \cap B} f_A(\mathbf{p}) \, d\Phi(\mathbf{p}), \\
 \mathbb{E}[\mathbf{Z}_1^A(A) \otimes \mathbf{Z}_3^S(B)] &= \mathbb{E}[\mathbf{Z}_2^A(A) \otimes \mathbf{Z}_4^S(B)] = - \int_{A \cap B} f_A(\mathbf{p}) \, d\Phi(\mathbf{p}),
 \end{aligned}$$

and where  $g_n(\mathbf{p}, \mathbf{x})$  are 8 different products of cosines and sines of  $p_i x_i$ .

**Example 4.** Let  $G = O(3)$  and let  $\rho$  be the natural orthogonal representation of  $G$  in the space  $V = S^2(\mathbb{R}^3) \otimes \mathbb{R}^3$ .

The one-point correlation tensor of a homogeneous and  $(O(3), \rho)$ -isotropic random field  $C(\mathbf{x})$  is equal to 0. Its two-point correlation tensor has the spectral expansion

$$\langle \mathbf{e}(\mathbf{x}), \mathbf{e}(\mathbf{y}) \rangle_{ijk'i'j'k'} = \sum_{n=1}^3 \int_0^\infty \sum_{q=1}^{21} N_{nq}(\lambda, \rho) L_{iik'i'j'k'}^q(\mathbf{y} - \mathbf{x}) d\Phi_n(\lambda),$$

The measures  $\Phi_n(\lambda)$  satisfy the condition

$$\Phi_1(\{0\}) = 2\Phi_2(\{0\}).$$

The spectral expansion of the field has the form

$$\begin{aligned} \mathbf{e}_{ijk}(\rho, \theta, \varphi) = & 2\sqrt{\pi} \sum_{n=1}^3 \sum_{\ell=0}^{\infty} \sum_{m=-\ell}^{\ell} \int_0^\infty j_\ell(\lambda\rho) \sum_{(\ell', m', i', j', k') \leq (\ell, m, i, j, k)} L_{\ell m i j k, n}^{\ell' m' i' j' k'}(\lambda) \\ & \times dZ_{ijk\ell m}^n(\lambda) S_\ell^m(\theta, \varphi), \end{aligned}$$

where  $S_\ell^m(\theta, \varphi)$  are real-valued spherical harmonics,  $j_\ell(\lambda\rho)$  are the spherical Bessel functions, and where  $Z_{ijk\ell m}^n$  are centred uncorrelated real-valued random measures on  $[0, \infty)$  with control measures  $\Phi_n$ . The functions  $N_{nq}(\lambda, \rho)$  and  $L_{iik'i'j'k'}^q(\lambda)$  are given in [4].

## REFERENCES

- [1] Geymonat, G. and Weller, T. Classes de symétrie des solides piézoélectriques. C. R. Math. Acad. Sci. Paris (2002) 335:847–852.
- [2] Cramér, H. On the theory of stationary random processes. Ann. of Math. (1940) 41:215–230.
- [3] Malyarenko, A. and Ostoja-Starzewski, M. A random field formulation of Hooke’s law in all elasticity classes. J. Elasticity (2017) 127:269–302.
- [4] Malyarenko, A. and Ostoja-Starzewski, M. Tensor-valued random fields for continuum physics. Cambridge University Press (2019), Cambridge.
- [5] Bourbaki, N. Integration. II. Chapters 7–9. Springer (2004), Berlin.
- [6] Duistermaat, J.J., and Kolk, J.A.C. Lie groups. Springer (2000), Berlin.
- [7] Hofmann, K.H., and Morris, S.A. The structure of compact groups. De Gruyter (2013), Berlin.
- [8] Karhunen, K. Über lineare Methoden in der Wahrscheinlichkeitsrechnung. Ann. Acad. Sci. Fennicae. Ser. A. I. Math.-Phys. (1947) 37:1–79.
- [9] Altmann, S.L., and Herzog, P. Point-group theory tables. Clarendon Press (1994), Oxford.

## Detection and Selection System of Healthily Growth Seedlings for a Plant Factory

Yasuhiko Manabe<sup>\*</sup>, Hitohide Usami<sup>\*\*</sup>, Taiyo Maeda<sup>\*\*\*</sup>, Shigeo Kawata<sup>\*\*\*\*</sup>

<sup>\*</sup>National Institute of Technology, Numazu College, <sup>\*\*</sup>Tamagawa University, <sup>\*\*\*</sup>Saitama Institute of Technology, <sup>\*\*\*\*</sup>Utsunomiya University

### ABSTRACT

We study about an automatic detection and selection of healthily growing seedlings and an automatic robot planting in a plant factory. The plant factory has various problems that should be solved. For example, the healthily growing seedlings are almost selected manually by experienced staffs of the plant factory. The detection speed has a limit. The employment cost of the staffs cannot also be ignored. If this process is automated, the production efficiency of the plant factory would be improved. Our PSE (Problem Solving Environment) system for the automatic detection, selection and planting in plant factory aims to automate these processes. This automation will contribute to reduce the total cost of the plant factory. In addition, the production efficiency will be improved at the plant factory. At first we describe about the automatic detection of the healthily growth seedlings. The PSE system takes pictures of the seedlings on a tray. Each seedling is labeled with markers. The system determines that where the seedlings exist on the tray by using markers. The pictures are analyzed by the image processing: the pictures are divided into each seedling area. Then the area of leaves of each seedling is calculated by the divided seedling pictures. Before the analysis, the pictures must be converted into grayscale color spaces. Because the pictures taken is in the RGB color spaces. However, if the pictures of RGB color spaces are converted into the grayscale, the color information of the pictures has been lost. Therefore, it becomes difficult to obtain the form of the leaves from the grayscale pictures. We use the HSV color spaces instead of RGB. The HSV color space has an advantage of the extracting particular colors. Thus, the HSV color spaces is suitable to obtain the shapes of the leaves. We obtain the clear shapes of the leaves by using the HSV color spaces. We can also obtain the area of the leaves by counting the white pixels of the pictures. The system determines healthily good seedlings from the area of the leaves. In addition, when the robot grips the healthy seedlings, the roots of the seedling hang by the gravity. The system also measures the length of the roots. The requirement of the healthy seedling includes the length. The robot transfers the really healthy seedlings to the next tray, which is transferred into the inside of the plant factory.

## **Atomic-scale Simulations of High Velocity Impact of Nanocrystalline Nanoparticles: Effect of Surface Roughness**

Poshit Nag Mandali<sup>\*</sup>, Moneesh Upmanyu<sup>\*\*</sup>, Alireza Shahabi<sup>\*\*\*</sup>, Sinan Muftu<sup>\*\*\*\*</sup>

<sup>\*</sup>Northeastern University, <sup>\*\*</sup>Northeastern University, <sup>\*\*\*</sup>Northeastern University, <sup>\*\*\*\*</sup>Northeastern University

### **ABSTRACT**

High velocity impact of nanoparticles onto growing substrates has the potential for a range of next-generation additive manufacturing techniques. Nanoparticle synthesis techniques such as gas atomization usually result in rough surfaces, and the effect of the roughness on the impact dynamics remains poorly understood. In this talk, we focus aspects related to surface roughness of both the impacting nanoparticle, as well as the substrate. Molecular dynamics simulations of high velocity (500-2000 m/s) impact of Al nanocrystalline particles on single and polycrystalline substrates show that the dissipation of the kinetic energy is dramatically altered by the roughness. In addition to deformation of the substrate, the amorphization and flow of the roughness related asperities becomes an important aspect that determines the nature and extent of particle impingement. We present a simple theoretical model that captures the modified dissipation mechanism. The implications on additive techniques such as cold spray and laser-shock processing are discussed.

## Scalable, Multi-Scale Methods for Coastal Modeling

Kyle Mandli\*, Jiao Li\*\*

\*Columbia University, \*\*Columbia University

### ABSTRACT

Coastal flooding due to severe storms is one of the most wide-spread and damaging hazards faced around the world. The threat of these events has grown not only due to increased population and economic reliance on coastal regions but also due to climate change impacts such as sea-level rise. Computational predictive capabilities are critical to addressing this threat but require the ability to handle multiple, disparate scales, handle the physics relevant at each of these scales, and remain tractable under the necessity of large ensembles to handle uncertainty in the input. In this context we present a novel Riemann solver based method developed to handle coastal barriers that are not required to align with a computational grid while not needing to be restricted by arbitrary CFL time-step restrictions made problematic by such approaches. Importantly the properties of the original Riemann solver, such as conservation and correct wet-dry interfaces, are maintained while allowing for the application of adaptive mesh refinement.

## Dimensional Reduction of FEM-based Eigenvector Functions

Herbert A. Mang\*

\*Vienna University of Technology & College of Civil Engineering, Tongji University

### ABSTRACT

Historically, stability limits on nonlinear prebuckling paths were often determined by means of so-called accompanying linear eigenvalue analysis in the framework of the Finite Element Method (FEM). One of the two coefficient matrices of the underlying linear eigenvalue problems was the tangent stiffness matrix, whereas the other one was an arbitrary real symmetric matrix. The aim of the present work is to support the hypotheses that (a) the absolute value of the initial vector velocity and (b) the ratio of the absolute value of the vector acceleration to its initial value are invariants with respect to the second coefficient matrix. By “vector velocity” and “vector acceleration” the first and the second derivative of the “fundamental eigenvector” of the linear eigenvalue problem concerned, with respect to a pseudo time, is meant. It must be equal to the arc length of the load-displacement path. At the stability limit, the “fundamental eigenvector” corresponds to the null eigenvalue. The mechanical background of the aforementioned hypotheses is the assumption that the product of the two asserted invariants is equal to one half of the non-membrane percentage of the strain energy. The nucleus of this work is computation of curves on the unit sphere, described by the vertex of the non-uniformly moving “fundamental eigenvector” of the linear eigenvalue problem concerned. To determine these curves, the N-dimensional “fundamental eigenvector” must be “reduced” to a vector, the vertex of which is defined by the two spherical coordinates. This “dimensional reduction” is based on the split of a relation for the rate of change of the radius of curvature of the surface curves to be determined. It allows for computation of the rate of change of the zenith angle, which is a prerequisite for determination of the azimuth angle. The practical added value of this work is the possibility to choose a particularly simple form of the underlying linear eigenvalue problem, with the unit matrix as one of the two coefficient matrices, to compute the non-membrane percentage of the strain energy. This quantity provides insight into the load-carrying mechanism of structures, subjected to proportional loading [1]. References: [1] H.A. Mang, Evolution and verification of a kinematic hypothesis for splitting of the strain energy. *Comput. Methods Appl. Engrg.*, Vol. 324, pp. 74-109, 2017.

## Mechanical Positioning of Multiple Myonuclei in Muscle Cells

Angelika Manhart\*, Alex Mogilner\*\*

\*Courant Institute, New York University, \*\*Courant Institute, New York University

### ABSTRACT

Many types of large cells have multiple nuclei. In long muscle cells, the nuclei are distributed almost uniformly along their length. This nuclear positioning is crucial for cell function. Mechanisms of the nuclear positioning remain unclear. We examine computationally the hypothesis that a force balance generated by microtubules positions the nuclei. Rather than assuming what the forces are, we allow various types of forces between the pairs of nuclei and between the nuclei and cell boundary to position the nuclei according to the laws of mechanics. Mathematically, this means that we start with a great number of potential models. We use the reverse engineering approach by screening the models and requiring their predictions to fit imaging data on nuclei positions and shapes from hundreds of muscle cells of *Drosophila* larva. Computational screens result in a small number of feasible models, the most adequate of which suggests that the nuclei repel from each other and cell boundary with forces that decrease with distance. This suggests a hypothesis that microtubules growing from nuclear envelopes push on neighbouring nuclei and cell boundary, which is sufficient for the nearly-uniform nuclear spreading. We support this hypothesis with simulations of an agent-based mechanical model. The model makes nontrivial predictions about the increased nuclear density near the cell poles, zigzag patterns of the nuclei positions in wider cells, and about correlations between the cell width and elongated nuclear shapes, which we confirm by image analysis of the experimental data.

## Simulation and Learning for Process Modeling and Control of Powder-Bed Metal Additive Manufacturing

Antoinette Maniatty<sup>\*</sup>, Souvik Roy<sup>\*\*</sup>, James Dolan<sup>\*\*\*</sup>, Sandipan Mishra<sup>\*\*\*\*</sup>, Alexander Shkoruta<sup>\*\*\*\*\*</sup>

<sup>\*</sup>Rensselaer Polytechnic Institute, <sup>\*\*</sup>Rensselaer Polytechnic Institute, <sup>\*\*\*</sup>Rensselaer Polytechnic Institute, <sup>\*\*\*\*</sup>Rensselaer Polytechnic Institute, <sup>\*\*\*\*\*</sup>Rensselaer Polytechnic Institute

### ABSTRACT

A finite element simulation tool for modeling metal powder-bed additive manufacturing is developed and used to study the effect of processing parameters on metrics associated with part quality. An efficient finite element formulation is derived that predicts temperature, phase (melt/solid), and porosity for given processing parameters – power, beam diameter, and path history. In the formulation, we introduce two state variables into the first law of thermodynamics, a phase parameter to characterize the transition between solid and melt, and a consolidation parameter to characterize the degree of consolidation from powder to dense material, which naturally predict local porosity. The model is fully implicit, and is expressed in a total Lagrangian framework that accounts for the changing geometry as the powder consolidates. The formulation is implemented in a parallel simulation framework allowing for scalable computations on high performance computing platforms. From the temperature and phase history, the evolution of the grain structure at key locations in the part are predicted using a novel Monte Carlo algorithm for predicting grain growth in the presence of time varying temperature gradients. Input and output data from the simulations is analyzed to develop control-oriented low order models. Such control-oriented models can be used for designing and certifying feedback and feedforward control algorithms that can regulate, for example, melt pool geometry or temperature fields inside the melt pool itself. As an example, an iterative learning control algorithm is designed based on this lower order model to update processing parameters for improved part performance. The algorithm is then validated on the simulation tool to certify its performance. Test cases for a single layer process and for a multi-layer partial part build are used to demonstrate the simulation capabilities and quality improvement through process control applied to the simulation tool.

## On Modeling Cyclic Mobility of Sand

Majid Manzari\*

\*The George Washington University

### ABSTRACT

Cyclic mobility of medium dense saturated sands subjected to cyclic shearing is the cause of significant deformations in civil infrastructure systems that are subjected to severe ground shaking. While several existing elastoplastic constitutive models are shown to capture the observed responses of sands in monotonic shearing, these models are rarely able to produce realistic simulations of sand behavior in cyclic shearing, particularly when cyclic mobility is involved. In this work, the capabilities of a critical state two-surface plasticity model of sand (Manzari and Dafalias, 1997; Dafalias and Manzari, 2004, Manzari and Yonten, 2010) are evaluated against a range of stress and strain paths that are caused by earthquakes. In particular, the model performance is evaluated in simulation of cyclic direct simple shear tests on medium dense soils that exhibit cyclic mobility. The key similarities and differences between the numerical simulations and the experimentally observed responses are noted and analyzed. Specific enhancements are then proposed to improve the capabilities of the model in simulation of cyclic mobility. The proposed enhancements are implemented in a fully-coupled stress-flow finite element platform for analysis of seismic response of saturated soil structures. Two boundary value problems that involve cyclic mobility of medium dense sands are then simulated and the role of model enhancement in the improvement of the simulation results are identified. It will be shown that a more accurate simulation of plastic shear strains in the calibration phase of the constitutive model will lead to noticeable improvement of the ability of the model and the numerical simulation platform to simulate permanent deformations of saturated sand deposits that are subjected to significant shaking levels.

1. Manzari, M.T. and Dafalias, Y. F. (1997). A critical state two-surface plasticity model for sands. *Geotechnique*, Volume 47 Issue 2, April 1997, pp. 255-272. <https://doi.org/10.1680/geot.1997.47.2.255>
2. Dafalias, Y.F. and Manzari, M.T. (2004). Simple Plasticity Sand Model Accounting for Fabric Change Effects. *Journal of Engineering Mechanics*, Vol. 130, Issue 6, [https://doi.org/10.1061/\(ASCE\)0733-9399\(2004\)130:6\(622\)](https://doi.org/10.1061/(ASCE)0733-9399(2004)130:6(622)).
3. Manzari, M. T. and Yonten, K. (2011). Analysis of post-failure response of sands using a critical state micropolar plasticity model, *Interaction and Multiscale Mechanics*, Vol. 4, No. 3, <http://dx.doi.org/10.12989/imm.2011.4.3.187>.

## **Adaptive Stopping Criterion for Iterative Linear Solvers in an Anisotropic Stabilized AFEM Framework, with Applications to Convection-dominated Problems**

Gabriel Manzinali<sup>\*</sup>, Youssef Mesri<sup>\*\*</sup>, Elie Hachem<sup>\*\*\*</sup>

<sup>\*</sup>MINES ParisTech, PSL - Research University, CEMEF - Centre for material forming, <sup>\*\*</sup>MINES ParisTech, PSL - Research University, CEMEF - Centre for material forming, <sup>\*\*\*</sup>MINES ParisTech, PSL - Research University, CEMEF - Centre for material forming

### **ABSTRACT**

Adaptive finite elements methods (AFEM) are nowadays well known to be a reliable approach to achieve better accuracy in the solution of PDEs, at a reduced computational cost. A typical adaptation procedure starts from a solution on an initial discretization of the computational domain, computes the estimated error distribution on that mesh, and using this information defines the topology of the new spatial discretization. The solving step implies the solution of the linear system that stems from the discretization of the continuous problem. Usually the solution of this system is assumed to be exact. In real-world application however, this kind of system can be solved efficiently only with an iterative procedure, which provides an approximation to the exact solution. The accuracy of this approximation is controlled by the stopping criteria used to drive the convergence of the iterative procedure. As remarked by Becker, Johnson, and Rennacher in their seminal work [1], ad hoc stopping criteria are commonly used. These criteria are straightforward to implement, but have no direct link to the actual error in the approximate solution. This could possibly affect efficiency and accuracy. On one hand, a highly accurate approximation is inefficient and most likely unnecessary, on the other hand, a poor approximation affects the accuracy of the solution and the convergence of the adaptation procedure. In this work we propose an adaptive stopping criterion that follows the approach proposed in [2], integrated with the anisotropic mesh adaptation procedure. Using information from this procedure we provide an adaptive control for the linear solver that proves to be effective to considerably reduce the number of iteration needed by the solver, without spoiling the accuracy of the solution. We apply this framework to convection-diffusion problems in 2D and 3D, relying on a stabilized finite element method. References: [1] Roland Becker, Claes Johnson, and Rolf Rannacher. Adaptive error control for multigrid finite element. *Computing*, 55(4):271–288, 1995. [2] Marco Picasso. A stopping criterion for the conjugate gradient algorithm in the framework of anisotropic adaptive finite elements. *International Journal for Numerical Methods in Biomedical Engineering*, 25(4):339–355, 2009.

## Three-dimensional multiscale modeling of concrete based on the use of finite element with high aspect ratio and coupling finite elements

Oswaldo L. Manzoli<sup>\*</sup>, Eduardo A. Rodrigues<sup>\*\*</sup>, Luís A. G. Bitencourt Jr.<sup>\*\*\*</sup>, Pedro R. Cleto<sup>\*\*\*\*</sup>, Heber A. A. Fabbri<sup>\*\*\*\*\*</sup>

<sup>\*</sup>Sao Paulo State University (UNESP), <sup>\*\*</sup>Sao Paulo State University (UNESP), <sup>\*\*\*</sup>Polytechnic School at the University of Sao Paulo, <sup>\*\*\*\*</sup>Sao Paulo State University (UNESP), <sup>\*\*\*\*\*</sup>Sao Paulo State University (UNESP)

### ABSTRACT

The mechanical properties and arrangement of the constituents of concrete in mesoscale determine its mechanical behavior and failure process. Modeling a representative distribution of the coarse aggregates into the mortar matrix constitutes a typical situation that requires a three-dimensional arrangement representation. This work proposes a three-dimensional concurrent multiscale model for plain concrete, consisting of two well-separated macro and mesoscale. In the macroscale the concrete is treated as an elastic material with homogenized elastic parameters. To construct the concrete in mesoscale, coarse aggregates with regular and irregular shaped are generated from a grading curve and placed into the mortar matrix randomly, using the 'take-and-place' method. To represent the interfacial transition zone (ITZ) and simulate the crack propagation process the mesh fragmentation procedure is used [1]. This technique is based on the use of standard finite elements with high aspect ratio, which are inserted in between all regular finite elements of the mortar matrix and in between the mortar matrix and aggregate elements, representing the ITZ [2]. A tension damage constitutive relation between stresses and strains consistent with the Continuum Strong Discontinuity Approach (CSDA) is used to describe crack formation and propagation. The use of coupling finite elements (CFEs) [3] is proposed to enforce the continuity of displacements between the non-matching meshes corresponding to the two different finer and coarser scales. These CFEs can ensure the correct connection between these scales without increasing the total number of degrees of freedom of the problem. Numerical examples are performed to show the ability of the proposed method to predict the behavior of cracks initiation and propagation in the tensile region of the material. The numerical results are compared with the experimental ones. Keywords: 3D numerical analysis, multiscale analysis, finite element, damage model, interface finite element, coupling finite element, plain concrete, cracks propagation. References: [1] Manzoli OL, Maedo MA, Bitencourt Jr. LAG, Rodrigues EA. On the use of finite elements with a high aspect ratio for modeling cracks in quasi-brittle materials. *Engineering Fracture Mechanics*, 153: 151-170, 2016 [2] Rodrigues EA, Manzoli OL, Bitencourt Jr LAG, Bittencourt TN. 2D mesoscale model for concrete based on the use of interface element with a high aspect ratio. *International Journal of Solids and Structures*, 94–95: 112–124, 2016. [3] Bitencourt Jr. LAG, Manzoli OL, Prazeres PGC, Rodrigues EA, Bittencourt TN. A coupling technique for non-matching finite element meshes. *Comput. Methods Appl. Mech. Engrg.*, 290: 19–44, 2015.

## Data-driven Computing with Deep Neural Networks for Inverse Modeling of Two-phase Flows

Xiaoyu Mao<sup>\*</sup>, Vaibhav Joshi<sup>\*\*</sup>, Tharindu Pradeeptha Miyanawala<sup>\*\*\*</sup>, Rajeev Kumar Jaiman<sup>\*\*\*\*</sup>

<sup>\*</sup>National University of Singapore, <sup>\*\*</sup>National University of Singapore, <sup>\*\*\*</sup>National University of Singapore,  
<sup>\*\*\*\*</sup>Natioanl University of Singapore

### ABSTRACT

Efficient prediction of fluctuating wave force on a floating or a submerged body is of great significance in many offshore and marine engineering applications. While a tremendous amount of wave-body interaction data is generated in offshore engineering via both CFD simulations and experiments, the results are generally underutilized. Design space exploration and motion control of such practical scenarios are still time-consuming using high-fidelity physical data. In this talk, we present a Convolutional Neural Network (CNN) based data-driven computing to predict the unsteady wave forces on submerged bodies due to the free-surface wave motion. The wave forces are investigated by the stabilized finite element method solver based on the Navier-Stokes equations and the Allen-Cahn phase-field approach. For the interface capturing, the Allen-Cahn equation is solved in the mass-conservative form by imposing a Lagrange multiplier technique [1]. An alternative to semi-analytical modeling, CNN is a class of deep neural network for solving inverse problems which are efficient in parametric data-driven computation and can use the domain knowledge [2]. In this study, CNN-based data-driven computing is utilized to predict the wave forces on bluff bodies with different geometries and distances to free surface. The predictions are made after the CNN is trained by a constructed input function based on input parameters and the target data generated by the full-order model. The proposed CNN-based model reduction procedure has a profound impact on the parametric design of bluff bodies experiencing wave loads. Following this, we next propose a deep neural network procedure, which combines Convolutional Neural Network (CNN) and Recurrent Neural Network (RNN) to construct the reduced-order model for two-phase modeling. While the CNN is responsible for processing the spatial information in the flow field, the RNN performs the predictions for the temporal evolution based on the training flow field data from the full-order model. After training for several initial time steps, the neural network is utilized for the fast prediction with a reduced computational cost in the following time steps. We demonstrate the accuracy and validation of the proposed data-driven technique for increasing complexity of problems. References [1] Joshi, V., and Jaiman, R. K., 2017. "A positivity preserving and conservative variational scheme for phase-field modeling of two-phase flows". *Journal of Computational Physics*, <http://arxiv.org/abs/1710.09831> [2] Miyanawala, T. P., and Jaiman, R. K., 2017. "An efficient deep learning technique for the Navier-Stokes equations: Application to unsteady wake flow dynamics". arXiv preprint arXiv:1710.09099

## Fracture of Elastomeric Materials by Crosslink Failure

Yunwei Mao\*, Lallit Anand\*\*

\*Department of Mechanical Engineering, MIT, \*\*Department of Mechanical Engineering, MIT

### ABSTRACT

If an elastomeric material is subjected to sufficiently large deformations it eventually fractures. There are two typical micromechanisms of failure in such materials: chain scission and crosslink failure. The chain scission failure mode is mainly observed in polymers with strong covalent crosslinks, while the crosslink failure mode is observed in polymers with weak crosslinks. In two recent papers we have proposed a theory for progressive damage and rupture of polymers with strong covalent crosslinks. In this talk we extend our previous framework and formulate a phase field damage theory for modeling failure of elastomeric materials with weak crosslinks. We first introduce a model for the deformation of a single chain with weak crosslinks at each of its two ends using statistical mechanics arguments, and then upscale the model from a single chain to the continuum-level for a polymer network. Finally, we introduce a damage variable to describe the progressive damage and failure of polymer networks. A central feature of our theory is the recognition that the free energy of elastomers is not entirely entropic in nature, there is also an energetic contribution from the deformation of the backbone bonds in a chain and/or the crosslinks. For polymers with weak crosslinks this energetic contribution is mainly from the deformation of the crosslinks. It is this energetic part of the free energy which is the driving force for progressive damage and fracture of elastomeric materials. We have numerically implemented this theory in an open-source finite element code MOOSE by writing our own application. Using this simulation capability we have presented results from simulations of: (i) fracture of single-edge-notched specimens; (ii) fracture of an asymmetric double-edge-notched specimen; and (iii) fracture of a sheet specimen with multiple circular and elliptical holes, under our plane stress conditions. These examples show the powerful capability of our gradient damage theory and its numerical implementation to simulate the complicated fracture process of nucleation, propagation, branching and merging of cracks in elastomeric materials in arbitrary geometries undergoing large deformations. We expect that our theory and numerical simulation capability will be useful in studying various interesting phenomena such as crazing and cavitation in soft materials.

## Dynamic Elasto-Plasticity in Metals Computed by a Discrete Element Method

Frédéric Marazzato\*, Alexandre Ern\*\*, Christian Mariotti\*\*\*, Karam Sab\*\*\*\*

\*Université Paris-Est, Cermics (ENPC), F-77455 Marne-la-Vallée cedex 2 and Inria Paris, EPC SERENA, F-75589 Paris, France and CEA, DAM, DIF, F-91297 Arpajon, France, \*\*Université Paris-Est, Cermics (ENPC), F-77455 Marne-la-Vallée cedex 2 and Inria Paris, EPC SERENA, F-75589 Paris, France, \*\*\*CEA, DAM, DIF, F-91297 Arpajon, France, \*\*\*\*Université Paris-Est, Laboratoire Navier (UMR 8205), CNV, ENPC, IFSTTAR, F-77455 Marne-la-Vallée, France

### ABSTRACT

Since their first use by Hoover et al (1974) in models for crystalline materials and Cundall & Strack (1979) in geotechnical problems, Discrete Elements methods (DEM) have found a large field of application in granular materials, soil and rock mechanics. The handling of a set of particles interacting by means of forces and torques allows a variety of models for the expression of these bonds and for the material's behavior. L. Monasse and C. Mariotti (2012), have been able to simulate the deformation and fragmentation of a three-dimensional linear elastic brittle material. The discretisation is achieved through rigid convex polyhedral particles. The forces and torques are computed directly through macroscopic quantities like the distance and relative rotation between two particles. The aim of this presentation is to introduce an extension of this formalism with the goal to compute anisothermal dynamic plasticity with strain rate dependence in metals. The behaviors considered are for instance the Johnson-Cook model (1983). Elements of proof for the well-posedness and convergence of the discretisation will also be given. A special attention has been given to the correct approximation of the elastic inequality constraint. In addition, since energy dissipation is crucial for cracking phenomena, a special energy-conserving time-integration scheme has been developed in (F. Marazzato et al, 2017) to compute the solid dynamics.

## Note on Initiation of Turbulence, a Systemic View

Pedro Marcal\*

\*Mpact Corp.

### ABSTRACT

Turbulence is a much studied subject in Fluid Flow. Though we are able to predict some of its behavior numerically, other features remain somewhat obscure. In particular, at what point does a laminar flow transition into turbulence? Launder and Spalding used a two equation transport model [1] for turbulence. This model requires an initial seeding of turbulence. In this note we will make some assumptions as to the nature of the phenomenon and then using a Least Squares Finite Element Method (LSFEM, Jiang [2]) implemented in the MPACT code, we carry out a simulation to gain some further insight. Here we follow methods similar to those used in linear fracture mechanics [3], where we use a balance of energy for pre and post fracture conditions. Because of the nature of the viscous flow, we consider a balance of the rate of work prior to turbulence and post turbulence. This balance gives the initiation conditions which include the transition of one or more elements (volume) to turbulent flow. The transition elements are assumed to transform into elements with a large number of frequencies and as such contribute nearly nothing to the laminar flow. The balance of rate of work is established by numerical analysis of the flow system. When we increase the velocity of flow, the equivalent stress increases to a point where the fluid system can no longer support any further increase in stress so that the laminar flow morphs into a turbulent flow. We assume it turns into local eddies of random and high frequencies that are subsequently dissipated. We assume that turbulence initiation takes place in the elements in the regions of max equiv\_stress. One for each region to maintain symmetry of flow. The chosen elements are assumed to have reduced flow with no memory of the applied stress caused by the flow. Its assumed to have a reduced shear rate modulus that is a tenth or less of its original value, in order to keep up the mean flow. References [1] B.E. Launder; D.B. Spalding, D.B., The numerical computation of turbulent flows,. Computer Methods in Applied Mechanics and Engineering. 3 (2): 269–289, 1974 [2] Bo-Nan Jiang, Louis A. Povinelli, Least-squares Finite Element Method for Fluid Dynamics, NASA Technical Memorandum 102352, ICOMP-89-23, 1989 [3] J.R. Rice, A path independent integral and the approximate analysis of strain concentrations by notches and cracks, J. Appl. Mechanics, 35, 379-386, 1968

## **Influence of Meso-Structure on the Mechanical Response of FDM 3D Printed Material**

Sonia Marfia<sup>\*</sup>, Gianluca Alaimo<sup>\*\*</sup>, Ferdinando Auricchio<sup>\*\*\*</sup>, Elio Sacco<sup>\*\*\*\*</sup>

<sup>\*</sup>Department of Civil and Mechanical Engineering, University of Cassino and Southern Lazio, Italy, <sup>\*\*</sup>Department of Civil Engineering and Architecture, University of Pavia, Italy, <sup>\*\*\*</sup>Department of Civil Engineering and Architecture, University of Pavia, Italy, <sup>\*\*\*\*</sup>Department of Structures for Engineering and Architecture, University of Naples Federico II, Italy

### **ABSTRACT**

Lately, Additive Manufacturing (AM) processes via 3D printers have made several progress with the aim of becoming rapid manufacturing methods to produce finished components. A crucial point in the use of AM solutions for direct production is the satisfactory evaluation of the mechanical properties of the printed components, so that they can be correctly accounted for in the design phase [1]. The present study focuses on the determination of the mechanical properties of Fused Deposition Modeling (FDM) 3D-printed objects. In FDM processes a thermoplastic filament is heated and extruded: the material is deposited layer by layer on a printing surface. Each printed layer is made of filaments, called fibers and deposited in a plane parallel to the printing surface, and of voids, since the deposited material is not able to full the space due to geometrical and process constraints. Thus, the obtained material can be considered as a composite with two phases, i.e. fibers and voids. Process parameters, such as fiber thickness, width and orientation and fiber-to-fiber overlap significantly influences the printed material overall mechanical response. Some studies have been proposed in literature to investigate the response of FDM 3D-printed materials [2]. Accordingly, the aim of the present study is to develop a meso-macro analysis for studying the mechanical response of FDM 3D-printed material. To this end a representative volume element (RVE) of the heterogeneous material made by the filament and the voids is analyzed. Initially, a micromechanical approach based on nonlinear finite element analyses is developed. Finite elements characterized by 3D displacement fields that do not vary along the fiber axis are proposed. Then, a homogenization technique, based on Transformation Field Analysis [3], is implemented. The homogenization approach is able to model the nonlinear phenomena occurring at the mesoscale level, introducing an approximation for the inelastic strain field. Thus, a proper constitutive model for the filament, able to describe all the non-linear phenomena occurring in the material, is proposed. The RVE is divided in subsets, and in each subset the inelastic strain is considered uniform. A numerical procedure is developed to study the evolution of the subset inelastic strains that represent the internal variables of the problem. Several types of RVEs characterized by different distribution of filaments and by the presence of voids of different shapes are studied. In order to assess the efficiency of the proposed micromechanical approach and homogenization technique comparisons with experimental data are performed.

## Computational Strategies for Chemo-Mechano-Biological Response to Arterial Injury

Michele Marino<sup>\*</sup>, Meike Gierig<sup>\*\*</sup>, Malte Rolf-Pissarczyk<sup>\*\*\*</sup>, Peter Wriggers<sup>\*\*\*\*</sup>

<sup>\*</sup>Institute of Continuum Mechanics, Leibniz Universität Hannover, <sup>\*\*</sup>Institute of Continuum Mechanics, Leibniz Universität Hannover, <sup>\*\*\*</sup>Institute of Continuum Mechanics, Leibniz Universität Hannover, <sup>\*\*\*\*</sup>Institute of Continuum Mechanics, Leibniz Universität Hannover

### ABSTRACT

A common approach for modeling stress-induced growth and remodeling on a continuum level is the introduction of a multiplicative split of the deformation gradient into an elastic and inelastic part. The evolution of the inelastic part is described by physically motivated growth and remodeling laws governed by a target function based on a homeostatic stress value. These laws allow to govern the effects related to changes in the stress-free configuration induced by mass variations of tissue constituents that are optimal for the maintenance of a physiological stress [1]. On the other hand, in living systems, the injury of a tissue activates a cascade of cell-cell interactions, involving biologically active molecular species (e.g., growth factors, proteinases and cytokines) that induce changes in the composition and the histology of extracellular matrix, as well as growth of specific cell species [2]. Although these mechanisms can be implicitly incorporated in classical approaches for growth and remodeling, a mechanistic insight on these chemo-mechano-biological mechanisms provide a special insight on non-functional responses to tissue injury, such as the ones occurring during in-stent restenosis. Accordingly, this work presents computational strategies for incorporating the explicit description of chemo-mechano-biological effects in the context of tissue growth and remodeling following arterial tissue injury. From the theoretical and computational point of view, the aim of present work inherits significant challenges: the deformation gradient is decomposed into an elastic and an inelastic part to consider elastoplastic effects [3]; an ad hoc invariant-based Helmholtz free energy is formulated in order to include the anisotropic tissue mechanical response [2,3]; a transport problem modeling cell-cell signaling pathways is defined and regulated by the internal variable associated with plastic mechanisms [3]; growth and remodeling laws are defined on the basis of the resulting molecular concentrations. The computational models are firstly implemented in a staggered way. Then, by exploiting the separation of the characteristic time scales, strategies for coupling these multiphysics simulations are traced. Parametric simulations will be conducted, considering both idealised and patient-specific geometries, as well as variations in the diffusivity properties of a tissue, in loading conditions associated with different physio-pathological conditions, or in mechanobiological relationships between transport and growth and remodeling. [1] Cyron, C.J., Aydin, R.C., Humphrey, J.D. *Biomechanics and Modeling in Mechanobiology*, 15(6):1389-1403 (2016). [2] Marino, M., Pontrelli, G., Vairo, G., Wriggers, P. *Journal of the Royal Society Interface* 14:20170615 (2017). [3] Gasser, T.C., Holzapfel, G.A. *Computational Mechanics* 40:47-60 (2007).

## **A Meshless Method for Quasi-static Crack Propagation in 3D Heterogeneous Elastic Media**

Anatoly Markov<sup>\*</sup>, Sergei Kanaun<sup>\*\*</sup>

<sup>\*</sup>Tecnologico de Monterrey, <sup>\*\*</sup>Tecnologico de Monterrey

### **ABSTRACT**

An efficient mesh-free numerical method for the solution of the problem of slow crack growth in an infinite 3D-homogeneous medium containing inhomogeneities (cracks and inclusions) is developed. A finite region of the medium containing the inhomogeneities is subjected to arbitrary external forces. The problem is reduced to a system of surface integral equations for crack opening vectors and volume integral equations for stress tensors inside the inclusions. Stress fields inside inclusions and crack opening vectors are approximated by Gaussian functions centered at a system of nodes. The elements of this matrix are calculated in closed analytical forms (for inclusions) or expressed in terms of five standard 1D-integrals (for cracks). For regular node grids, the matrix of discretized system has Toeplitz's structure, and Fast Fourier Transform technique can be used for calculation of matrix-vector products with such matrices. An iterative process is proposed for the construction of the crack shape in the process of crack growth. At every iteration of this process, calculation of so-called equilibrium crack is required. For such a crack, the stress intensity factors (SIFs) on the crack edge are equal to the corresponding material fracture toughness. Examples of crack evolution for various properties of medium and types of loading are presented.

## Thrust Membrane Analysis of Masonry Vaults

Francesco Marmo<sup>\*</sup>, Luciano Rosati<sup>\*\*</sup>

<sup>\*</sup>Università di Napoli Federico II, <sup>\*\*</sup>Università di Napoli Federico II

### ABSTRACT

Based on Heyman's principles of limit analysis of no tension structures, the Thrust Network Analysis (TNA) was firstly contributed by O'Dwyer [Funicular analysis of masonry vaults. *Computers and Structures*, 73:187-197, (1999)] who proposed a technique for modelling the principal stresses in a masonry vault as a discrete network of forces in equilibrium with the applied loads. Using projective geometry and linear optimization algorithms, Block [Thrust Network Analysis. PhD thesis, Massachusetts Institute of Technology, (2009)] provided a graphical and intuitive interpretation of O'Dwyer's method. O'Dwyer's and Block's versions of the method have been recently reformulated by Marmo and Rosati [Reformulation and extension of the thrust network analysis. *Computers and Structures*, 182:104-118, (2017)] where the methodology is extended to include the effects of horizontal forces and the presence of holes or free edges. The generality and efficiency of this recent improved approach has been witnessed by his application to masonry stairs of very complicated geometry. All versions of the TNA model membrane stresses as concentrated thrust forces lying along the branches of the network. Hence, although the method is very general and applicable to the limit analysis as well as to the form finding of structures having a very complicated geometry, the evaluation of the membrane stresses starting from the value of branch thrust is still an issue. Here we present the preliminary results of the application of an alternative strategy in which the membrane thrusts within the structure are modeled by triangular stress elements. These elements substitute the classical network branches so that the correspondence between thrust stresses and the equilibrium condition of the membrane nodes is straightforward. The method is applied to the limit analysis of a cross vault in which membrane elements, representing the membrane stresses within the vault, and branch elements, representing thrust forces within the groins, are both used within the same model.

## EULER-EULER MODELLING OF THE INTERACTION OF A GAS-PARTICLE MIXTURE WITH A DETACHED SHOCK

G. MAROIS\*<sup>†</sup>, P. VILLEDIEU<sup>#†</sup>, J. MATHIAUD\*

gentien.marois@cea.fr  
philippe.villedieu@onera.fr  
julien.mathiaud@cea.fr

\*CEA CESTA, 14 Avenue des Sablières, Le Barp, France

<sup>†</sup>INSA-TOULOUSE, 135 Avenue de Rangueil, Toulouse, France

<sup>#</sup>ONERA/DMPE, Université de Toulouse, F-31055 Toulouse (France)

**Key words:** Multiphase flows, Gas-particle mixtures, Shock Disturbance.

**Abstract.** This work deals with the interaction of a mist of solid particles and a stationary detached shock wave. Experiments over a 3 inches sphere were done in the 70's at the Boeing Hypersonic Wind Tunnel<sup>[1]</sup>. A very strong modification of the detached shock was observed. The aim of the present work was to check the capability of numerical simulations based on an Euler-Euler approach to reproduce this behavior. Comparisons with Hulin and Znaty<sup>[2]</sup> simulations (performed with an Eulerian-Lagrangian approach) have been carried out and the results are discussed.

### 1 INTRODUCTION

Studies of gas-particle two-phase flows (both subsonic and supersonic) are fairly recent and complex since they involve a lot of additional physical phenomena compared to single-phase flows. The work presented here deals with the interaction of a stationary detached shock wave with a mist of spherical particles (that are solid particles in the scope of the present study). Such interactions are encountered in a large range of scientific and engineering applications, from planetary explorations to motors design.

During last decades, several studies have been devoted to this problem. Analytical works were done for example by Carrier<sup>[3]</sup> or Marble<sup>[4]</sup>. Experimental investigations were performed, for example in Boeing laboratories<sup>[1,5]</sup> and were completed by numerical simulations (Papadopoulos<sup>[6]</sup>, Palmer<sup>[7]</sup>). These numerical studies were all based on the so-called Eulerian-Lagrangian method which consists in an Eulerian treatment of the gas phase and a Lagrangian treatment of the particulate phase. This approach is very popular since it can be quickly implemented and allows to easily take into account complex physical phenomena like particle breakup, complex wall-particle interactions, etc. However, when one is interested in the rate of particle impact on a surface or the density of particles in the vicinity of an obstacle, this approach requires the use of a very large number of numerical particles to get accurate results. In addition, due to load balancing issues, this approach is very difficult to implement efficiently on a massively parallel computer.

To overcome this limitation, in the present work, the Eulerian-Eulerian approach has been preferred even if it is more complex both from a numerical and a physical point of view. A finite volume method has been used to solve the equations of both phases. The particulate phase being very diluted in all targeted applications, its volume fraction (but not its mass density) is assumed to be negligible and its influence on the gas flow is taken into account via source terms in the right-hand side of the gas equations.

The paper is divided into four parts. First, the model is presented. We then detail the numerical method used as well as some results of validation tests carried out to ensure that the method has been correctly implemented and gives the expected results in simple but representative cases of application. The last part is devoted to attempts to replicate the Boeing experiment of the 70's concerning the interaction of a shock wave with a mist of particles.

## 2 PROBLEM FORMULATION

### 2.1 Eulerian model for the gas

The gas phase is modeled by the Navier-Stokes equations adapted for reacting gases (including vibrational energy effects, chemical reactions of dissociation, etc.). More details can be found in <sup>[8]</sup>. These equations can be schematically written as:

$$\partial_t \mathbf{U}_g + \partial_x \mathbf{G}(\mathbf{U}_g, \nabla \mathbf{U}_g) = \mathbf{S}_{\text{ext}} + \mathbf{S}_{\text{ch}} + \mathbf{S}_p \quad (1)$$

where  $\mathbf{U}_g$  denotes the vector of the gas phase conservative variables,  $\mathbf{G}$  corresponds to the flux terms,  $\mathbf{S}_{\text{ch}}$  corresponds to the chemical reaction source terms,  $\mathbf{S}_p$  denotes the source terms that takes into account the influence of the particles on the gas flow, and  $\mathbf{S}_{\text{ext}}$  is a source term that takes into account other effects like external forces, etc.

### 2.2 Eulerian model for the particles

In this paper, we limit ourselves to the case where the dispersed phase is composed of solid spherical particles whose only interactions with the gas phase are the exchange of momentum (via the drag force) and heat (by forced convection). However, the model presented below as well as its numerical treatment can be adapted to deal with more general cases (in particular the case of liquid particles), for which other phenomena must be taken into account like particle evaporation, sublimation, break-up, etc. <sup>[18]</sup>

There are several variants of the Eulerian approach for the treatment of the particulate phase (see for example <sup>[6, 7]</sup>). Here, we have chosen the sampling method <sup>[9]</sup> which has the advantage of being the simplest to implement. It consists of dividing the particulate phase into  $N$  classes, each characterized by its number density field  $n_i(t, \mathbf{x})$ , its mass density field  $m_i(t, \mathbf{x})$ , its velocity field  $\mathbf{v}_i(t, \mathbf{x})$  and its temperature field  $T_i(t, \mathbf{x})$ . Assuming that all the particles belonging to the same class and located at the same point have the same velocity, same diameter and same temperature, the following set of conservation equation can be easily derived:

$$\begin{cases} \partial_t n_i + \nabla_x(n_i \mathbf{v}_i) = 0 \\ \partial_t m_i + \nabla_x(m_i \mathbf{v}_i) = 0 \\ \partial_t m_i \mathbf{v}_i + \nabla_x(m_i \mathbf{v}_i \otimes \mathbf{v}_i) = n_i \mathbf{F}_i \\ \partial_t m_i h_i + \nabla_x(m_i \mathbf{v}_i h_i) = n_i H_i \end{cases} \quad (2)$$

where  $h_i = h_p(T_i)$  denotes the specific enthalpy of the particles of class  $i$  (supposed to be very close to their specific internal energy  $e_p(T_i)$ ),  $\mathbf{F}_i$  denotes the drag force acting on the particles of class  $i$  and  $H_i$  correspond the convective heat flux for the particles of class  $i$ . The drag force is given by:

$$\mathbf{F}_i = -\frac{\pi}{8} d_i^2 \rho_f C_D \|\mathbf{v}_i - \mathbf{u}_g\| (\mathbf{v}_i - \mathbf{u}_g) \quad (3)$$

where  $C_D$  is the drag coefficient. The particle mass density  $m_i$ , the particle number density  $n_i$ , the particle diameter  $d_i$  and the particle temperature  $T_i$  are linked by the following relationship:

$$m_i = \frac{\pi}{6} n_i \rho_p(T_i) d_i^3 \quad (4)$$

where  $\rho_p$  denotes the particulate phase bulk density (supposed to depend only on the temperature). The drag coefficient  $C_D$  depends on the particle Reynolds number  $Re_i$  and particle Mach number  $M_i$ . It can be calculated by combining Swain<sup>[10]</sup> with Clift and Gauvin<sup>[11]</sup> empirical formula:

$$\begin{cases} C_D^1(M_i, Re_i) & \text{for } M_i < 0.6 \\ C_D^2(M_i, Re_i) & \text{for } M_i > 1.3 \\ C_D^1(0.6, Re_i) + \frac{M_i - 0.6}{0.7} (C_D^2(1.3, Re_\infty) - C_D^1(0.6, Re_i)) & \text{elsewhere} \end{cases} \quad (5)$$

with:

$$\begin{aligned} C_D^1(M_i, Re_i) &= \frac{24}{Re_i} (1 + 0.15 Re_i^{0.687}) + \frac{0.42}{1 + 42500 Re_i^{-1.16}} \\ C_D^2(M_i, Re_i) &= 1 + 4.66 Re_i^{-0.5} \end{aligned} \quad (6)$$

Introducing the Nusselt number,  $Nu_i$ , the heat flux  $H_i$  can be defined as:

$$H_i = \lambda_g \pi Nu_i d_i (T_g - T_i) \quad (7)$$

with the Nusselt number being calculated thanks to Fox formula<sup>[12]</sup> which is an extension of classical subsonic fits<sup>[13]</sup> to supersonic flows:

$$Nu_i = \frac{2 \exp(-M_i)}{1 + 17 M_i / Re_i} + 0.459 Pr^{0.33} Re_i^{0.55} \frac{1 + 0.5 \exp(-17 M_i / Re_i)}{1.5} \quad (8)$$

The particulate source term in the r.h.s. on the gas phase balance equations can be easily deduced from the conservation of momentum and energy. It writes:

$$\mathbf{S}_p = - \begin{pmatrix} 0 \\ \sum_{i=1}^N n_i \mathbf{F}_i \\ \sum_{i=1}^N n_i \mathbf{F}_i \cdot \mathbf{v}_i + n_i H_i \end{pmatrix} \quad (9)$$

where  $n_i \mathbf{F}_i \cdot \mathbf{v}_i$  corresponds to the power of the drag force. This term does not appear in the particles' equations (2) because the last equation involves the particle specific enthalpy (or  $G$ . internal energy) instead of the particle total energy. It is worth mentioning that this formulation is adapted even in the case of supersonic flows because the fields associated with the particulate phase is not discontinuous through shocks (due to the finite relaxation time scales of the particles). If the gas equations are coupled with a turbulence model, it is also necessary, at least from a theoretical point of view and for consistency reasons, to take into account the influence of the particulate phase on turbulence production and dissipation by adding source terms in the turbulence model equations. We will come back to this question in section 5.3.

In most applications, particle interactions with solid walls play a fundamental role. In the Eulerian approach, since all the particles of a given class and located at the same point are supposed to have the same velocity (no pressure term in the momentum equation contrary to the gas phase), it is mandatory to introduce additional classes to deal with the secondary particles created during the impact of particles onto a wall (due to rebound, fragmentation and erosion). The number of additional classes will depend on the complexity of the impact model. In the present work, for the sake of simplicity, we have only considered the simplest model which consists of allocating only one secondary class to each primary class.

Let's denote by  $i_r$  the index of the class of secondary particles corresponding to the class  $i_p$  of primary particles. At the beginning of the calculation, there is no particle in class  $i_r$  (which means that  $m_{i_r} = 0$  in all mesh cells). When particles of class  $i_p$  impinge the wall, new particles are created in the corresponding class  $i_r$ . In the present work, the following model was used to compute the mass flux of the reemitted particles, their velocity, their diameter and their temperature:

$$\begin{cases} \mathbf{v}_{i_r} \cdot \mathbf{n} = \epsilon_n \mathbf{v}_{i_p} \cdot \mathbf{n} \\ \mathbf{v}_{i_r} \cdot \mathbf{t} = \epsilon_t \mathbf{v}_{i_p} \cdot \mathbf{n} \\ \epsilon_n m_{i_r} = G m_{i_p} \\ \epsilon_n n_{i_r} = F n_{i_p} \\ T_{i_r} = H T_{i_p} \end{cases} \quad (10)$$

$G$  is a mass gain parameter which allows to take into account the creation of new particles by erosion effects ( $G = 1$  corresponds to mass conservation during impact).  $F$  is a parameter which accounts for the combined effect of erosion and fragmentation (which both lead to the creation of new particles and thus to  $F > 1$ ). The parameter  $H$  allows to take into account the energy transfer during the particle impact.  $\epsilon_n$  and  $\epsilon_t$  correspond to the normal and tangential restitution coefficients. Naturally a model has to be prescribed for  $G$ ,  $F$ ,  $H$ ,  $\epsilon_n$  and  $\epsilon_t$ .

### 3 NUMERICAL TREATMENT OF THE PARTICLE PHASE EQUATIONS

The generalized Navier-Stokes equations for the gas phase are solved using a classical finite volume scheme on structured meshes that will not be described here. Details can be found for example in <sup>[14,15,16]</sup>.

Regarding the spatial discretization of (2), the following finite volume method has been used. For each class, let's first introduce the vector  $\mathbf{V}_i$  of specific variables defined as follows:

$$\mathbf{V}_i = (n_i/m_i, 1, \mathbf{v}_i, h_i)^t \quad (11)$$

Using this notation, system (2) can be rewritten under the following generic form:

$$\partial_t m_i \mathbf{V}_i + \nabla_x (m_i \mathbf{v}_i \mathbf{V}_i) = \mathbf{S}_i \quad (12)$$

which is more suited for the numerical discretization. Introducing  $|K|$  the volume (or area) of a given control volume  $K$  and  $|e|$  the area (or length) of the cell edge  $e$ , and integrating (12) on  $K$  leads to the semi-discretized equation:

$$|K| d_t (m_i \mathbf{V}_i) + \sum_{e \in \partial K} \Phi_{ie,K} |e| = |K| \mathbf{S}_i \quad (13)$$

where  $\Phi_{ie,K}$  denotes the flux through the edge  $e$ . Let's define the edge mean particle velocity (for the class of particles  $i$ ) by:

$$\mathbf{v}_{ie} = \frac{m_{i,K} \mathbf{v}_{i,K} + m_{i,Ke} \mathbf{v}_{i,Ke}}{m_{i,K} + m_{i,Ke}} \quad (14)$$

Applying an upwind scheme based on the sign of  $\mathbf{v}_{ie} \cdot \mathbf{n}_{e,K}$  the expression of the flux  $\Phi_{ie,K}$  reads:

$$\Phi_{ie,K} = v_{ie,K}^+ \mathbf{V}_{i,K} + v_{ie,K}^- \mathbf{V}_{i,Ke} \quad (15)$$

where  $v_{ie,K}^+$  and  $v_{ie,K}^-$  denote the positive (respectively negative) part of  $\mathbf{v}_{ie} \cdot \mathbf{n}_{e,K}$ . In addition, this space discretization scheme can be combined with the MUSCL approach <sup>[15,17]</sup> to get a second order accurate scheme.

As far as the time discretization is concerned, a first order semi-implicit scheme has been used which consists of using an explicit scheme for the flux terms and a partially implicit scheme for the treatment of the source terms. An advantage of this method is that, under a CFL-like condition, it can be shown to insure the positivity of the number density and to satisfy a maximum principle on the components of  $\mathbf{V}_i$  (which are directly related to the particle velocity, temperature and diameter).

Regarding the treatment of the particle source term in the gas phase equations,  $\mathbf{S}_p$ , a relaxation method has been implemented to enforce the stability of the coupling in dense zones.

## 4 BASIC VALIDATION TESTS

Several test cases were carried out in order to check the correct implementation of the above described numerical model and to assess its capability to accurately reproduce basic interactions between a gas flow and a cloud of particles. Here, for the sake of concision, we only present a one-dimensional test case (but performed using a 2D mesh).

The test consists of injecting gas and particles in a tube in non-equilibrium conditions. The gas flow at the inlet being supersonic, the whole gas and particle states are prescribed at the inlet. No boundary condition is imposed at the outlet. The gas is supposed to be perfect and inviscid and heat conduction effects are neglected. The objective of the test case is to assess the capability of the code to calculate the relaxation towards the equilibrium between the two phases along the tube.

In the first variant of the test, we only focus on the solution at the outlet of the tube which is assumed to be long enough for the particles and the gas to be at equilibrium at the output. By using the conservation of particle mass, particle number, gas mass, global momentum and global energy, it is possible to compute analytically the expression of the equilibrium velocity, pressure and temperature at the tube outlet for any inlet conditions. This calculation was done and numerical tests were performed for several inlet conditions. For all cases, the numerical results were in perfect agreement with the theoretical solution, showing that the global conservation properties are correctly ensured by the code. Due to the lack of room, the results of these tests will not be shown here.

The second variant of the test consists in computing the steady state solution according to the abscissa  $x$  along the tube. Solving analytically the full non-linear system is not possible. However, it is possible to compute the analytical solution of the linearized system around an equilibrium state. Each quantity  $q$  can be written as the sum of its equilibrium value  $\bar{q}$  and a small perturbation  $\hat{q}$ . In the simplest case when it is possible to neglect the heat transfer between the gas and the particles, the solution of the linearized system reads:

$$\left\{ \begin{array}{l} \hat{\rho}_g = -\frac{\bar{m}_p}{\bar{u}} \frac{M^2}{M^2 - 1 + \epsilon M^2} [\hat{u}_p(0) - \hat{u}_g(0)] \left\{ 1 - \exp \left[ \frac{-x}{\tau_{\mathcal{F}} \bar{u}} \left( 1 + \epsilon \frac{M^2}{M^2 - 1} \right) \right] \right\} \\ \hat{m}_p = \frac{\bar{m}_p}{\bar{u}} \frac{M^2 - 1}{M^2 - 1 + \epsilon M^2} [\hat{u}_p(0) - \hat{u}_g(0)] \left\{ 1 - \exp \left[ \frac{-x}{\tau_{\mathcal{F}} \bar{u}} \left( 1 + \epsilon \frac{M^2}{M^2 - 1} \right) \right] \right\} \\ \hat{u}_g = \hat{u}_g(0) + \frac{\epsilon M^2}{M^2 - 1 + \epsilon M^2} [\hat{u}_p(0) - \hat{u}_g(0)] \left\{ 1 - \exp \left[ \frac{-x}{\tau_{\mathcal{F}} \bar{u}} \left( 1 + \epsilon \frac{M^2}{M^2 - 1} \right) \right] \right\} \\ \hat{u}_p = \hat{u}_p(0) - \frac{M^2 - 1}{M^2 - 1 + \epsilon M^2} [\hat{u}_p(0) - \hat{u}_g(0)] \left\{ 1 - \exp \left[ \frac{-x}{\tau_{\mathcal{F}} \bar{u}} \left( 1 + \epsilon \frac{M^2}{M^2 - 1} \right) \right] \right\} \\ \hat{p}_g = -\frac{\gamma \bar{p}_g \epsilon}{\bar{u}} \frac{M^2}{M^2 - 1 + \epsilon M^2} \left\{ 1 - \exp \left[ \frac{-x}{\tau_{\mathcal{F}} \bar{u}} \left( 1 + \epsilon \frac{M^2}{M^2 - 1} \right) \right] \right\} \end{array} \right. \quad (16)$$

where  $\bar{m}_p$  is the equilibrium particle mass density,  $\bar{p}_g$  is the equilibrium pressure,  $\bar{u}$  is the equilibrium velocity of both phases,  $M = \frac{\bar{u}}{\sqrt{\frac{\gamma \bar{p}_g}{\bar{\rho}_g}}}$  is the corresponding Mach number,  $\gamma$  is the classical heat capacity

ratio,  $\epsilon = \frac{\bar{m}_p}{\bar{\rho}_g}$  is the equilibrium mass loading ratio and  $\tau_{\mathcal{F}} = \frac{\bar{\rho}_p d^2}{18 \mu_g}$  is the dynamic relaxation time of the particles (Stokes regime) and  $\mu_g$  is the viscosity.

Figures 1 show the density and velocity profiles for the two phases. The dashed line corresponds to the asymptotic solution given by the global conservation equations. It can be seen that the numerical results (full line) agree very well with the two analytical profiles.

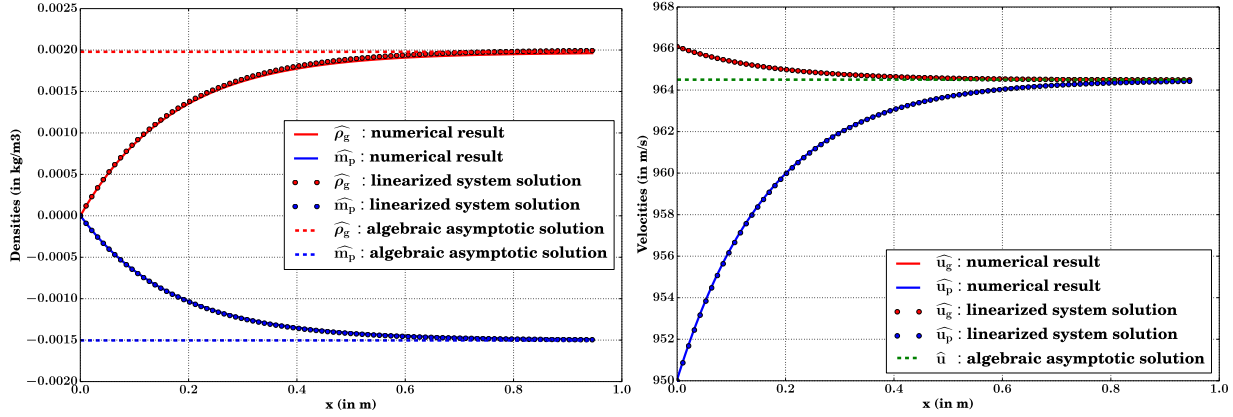


**Figure 1:** Left: evolution of the gas density and particle mass density along the tube at the steady state. Right: evolution of the gas and particle velocity along the tube at the steady state. Solid lines: numerical results - Dotted lines: theoretical solution - Green dashed line: equilibrium theoretical solution.

## 5 SIMULATION OF BOEING HYPERSONIC WIND TUNNEL EXPERIMENT

### 5.1 Experimental conditions

In the 70's experiments were carried out at the Boeing Hypersonic Wind Tunnel (BHWT) <sup>[1]</sup>. In these experiments, a solid metallic sphere was plunged into a Mach 6.1 free stream flow containing silica particles. In table 1, the flow stagnation conditions (at the input of the tunnel) and the infinity flow conditions (inlet of our computational domain) of the considered test run are summarized:

	Stagnation flow conditions	Infinity flow conditions
Pressure	44.8 $10^5$ Pa	2564 Pa
Temperature	633.1 K	75 K
Density	24.6 $\text{kg.m}^{-3}$	0.12 $\text{kg.m}^{-3}$
Sound speed	504.4 $\text{m.s}^{-1}$	173.6 $\text{m.s}^{-1}$

Table 1: Stagnations and infinity flow conditions

The silica particles injected in the flow were of 100  $\mu\text{m}$  diameter. In the following,  $c_\infty$  will denote the ratio between the particles mass flow rate and the gas mass flow rate. Its value was:

$$c_\infty = \frac{\dot{m}_{part}}{\dot{m}_{gas}} = 7.3 \cdot 10^{-4} \quad (17)$$

A strong shock disturbance was observed due to the presence of the particles, especially in the vicinity of the symmetry axis. The objective of the numerical simulations presented hereafter was to check the ability

of model (1)-(2)-(10) to capture this phenomenon and, as far as possible, to use the results to better understand its physical origin.

## 5.2 Modeling choices of HULIN and ZNATY<sup>[2]</sup>

Numerical simulations of BHWT experiments have already been successfully performed by Hulin and Znaty <sup>[2]</sup> but using a Lagrangian approach for the particulate phase. These researchers performed two types of simulation. In the first case, each numerical particle was associated with a real particle so as to account for the discrete nature of the solid phase and the fact that in the experiment the average distance between two neighboring particles is in the order of a few mm which is far from being negligible in the considered application. In the second case, the number of numerical particles that they used was much larger than the number of real particles. Each numerical particle was therefore assigned a weight that could be associated with a probability of presence. This second method, for which the concentration field of the particulate phase is quasi-continuous is therefore very close to an Eulerian approach. As Hulin and Znaty say in their paper that they get the same results in both cases, we expected to obtain comparable results with the Eulerian approach.

Hulin and Znaty have proposed a set of hypotheses to take into account the influence of fragmentation and erosion phenomena due to particle impacts. According to their model, after an impact,

- each incident particle is supposed to fragment into 5 smaller particles ;
- erosion leads to the creation of new particles with the same characteristics as the particles created by fragmentation of the incident particles ; the total mass of the eroded particles is supposed to be four times the mass of the incident particles ;
- the total kinetic energy of the reemitted particles (initial particle fragments + eroded particles) is supposed to represent 30% of the incident kinetic energy ;
- the restitution parameters,  $\varepsilon_n$  and  $\varepsilon_t$  are supposed to have the same value.

These assumptions lead to the following values for the impact model parameters (see equation (10)):  $G = 5$ ,  $F = 25$ ,  $\varepsilon_n = \varepsilon_t = 0.24$ . Since no assumption was mentioned in [2] regarding thermal effects, we simply assumed that  $H=1$  for the sake of simplicity, even if it is not realistic from a physical point of view.

## 5.3 Results

The classical  $k-\omega$  model[20] was used to account for the effect of turbulence on the gas flow mean properties. We performed two different numerical simulations with the particles. In the first simulation, we did not take into account any influence of the particles on the turbulence production and dissipation. In the second simulation, the turbulence source term model proposed by Hulin and Znaty <sup>[2]</sup> was used. As far as the turbulent kinetic energy source term is concerned, their model reads:

$$S_p^k = \sum_{i=1}^N n_i \mathbf{F}_i \cdot (\mathbf{v}_g - \mathbf{v}_i) \quad (18)$$

It is worth noticing that this model is not correct as it involves the mean slip velocity between the gas and the particles instead of the gas fluctuating velocity as it should be the case from a theoretical point of view. The correct expression should be:

$$S_p^k = \sum_{i=1}^N n_i \overline{\mathbf{F}'_i \cdot \mathbf{v}'_g} \quad (19)$$

Since the mean slip velocity is very high behind the shock, model (18) necessarily leads to a very high production rate of turbulent kinetic energy. It is thus not surprising that the presence of particles has a strong influence on the turbulence level, as noticed by Hulin and Znaty.

We point out that the calculations made in this paper do not reach a steady state. Indeed, the particles indefinitely accumulate along the shock. This phenomenon will be discussed later. This accumulation makes difficult the establishment of a steady state. This is why the results presented below are snapshots taken during the calculation.

Figures 2 show a comparison of the obtained numerical results for the gas phase density field without particles (left), with particles but without any turbulence production by the particle (middle), with particles and turbulence production by the particles using model (18) (right). Figures 3 and figures 4 show a similar comparison but for the gas Mach number field and for the turbulent kinetic energy field respectively.

We can see that without any influence of the particles on the turbulence production rate, no shock disturbance is observed whereas a clear modification of the shock appears if model (18) is applied. According to these results, the shock disturbances that have been observed in BHWT experiments seem to result from the strong production of turbulence by the particles in the vicinity of the shock. We recover similar conclusions as in <sup>[2]</sup> even if our numerical results do not exactly coincide with theirs. However, as already mentioned above, model (18) is not correct and is expected to strongly overestimate the turbulence production due to the presence of particles. We can therefore question the truth of this conclusion. To investigate this question, this will need at least to replace model (18) by a more correct one derived from (19) using closure assumptions. This will be the subject of future work.

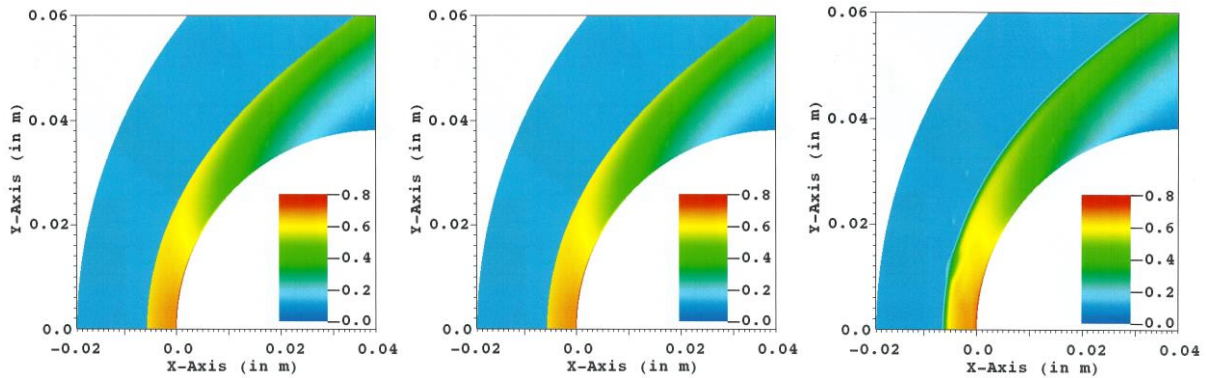


Figure 2: Gas phase density field (in  $\text{kg}\cdot\text{m}^{-3}$ ). Without particles (left) – With particles but without turbulence production by the particles (middle) – With particles and model (18) for turbulence production by the particles (right)

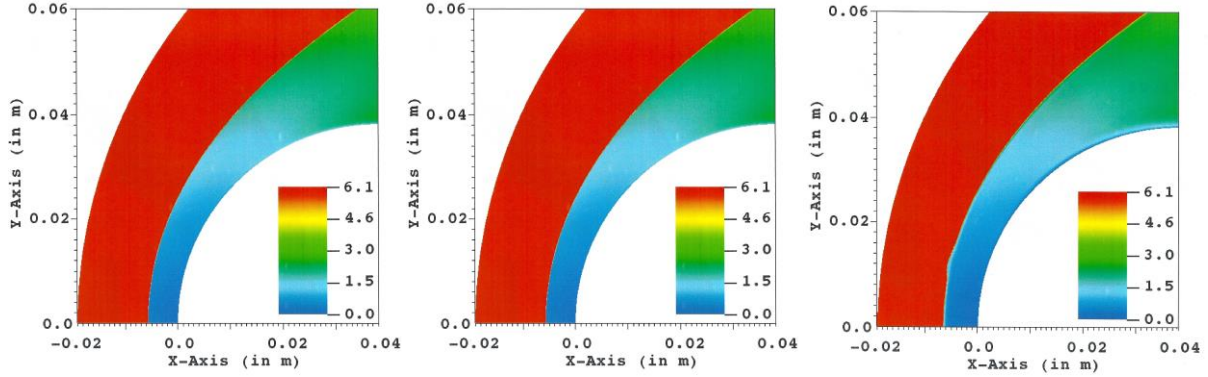
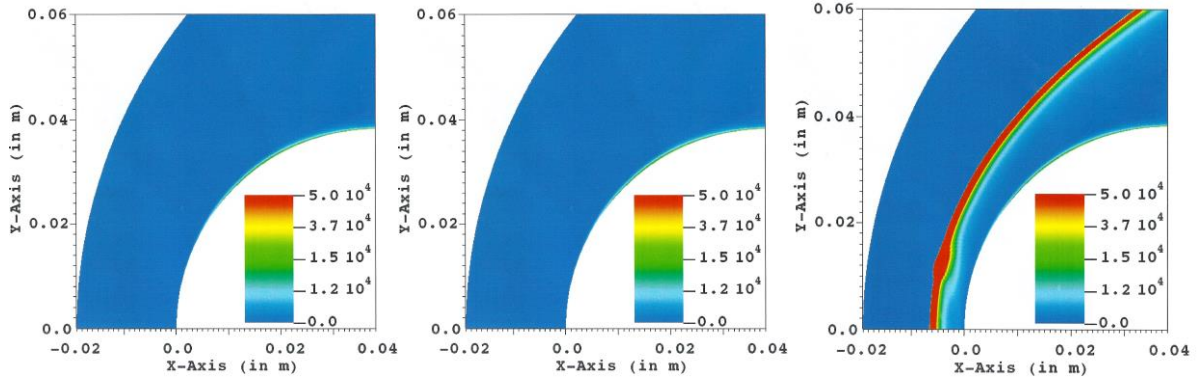


Figure 3: Gas Mach number field. Same legend as for Figure 2.

Figure 4: Turbulent kinetic energy field (in  $\text{kg}\cdot\text{m}^2\cdot\text{s}^{-2}$ ). Same legend as for Figure 2.

Another interesting consequence of the interaction of the particles with the detached shock can be observed in Figures 5 on the particle mass density fields. The secondary particles that are reemitted from the wall due to fragmentation and erosion phenomena are strongly decelerated by the gas flow and tend to accumulate in the vicinity of the shock, leading to very high density of particles compared to the far field. Even if this phenomenon is certainly overestimated by the Eulerian treatment of the particle phase (well-known effect of single-velocity Eulerian model <sup>[19]</sup>), it is physically plausible and could also play a role in the shock disturbance mechanism.

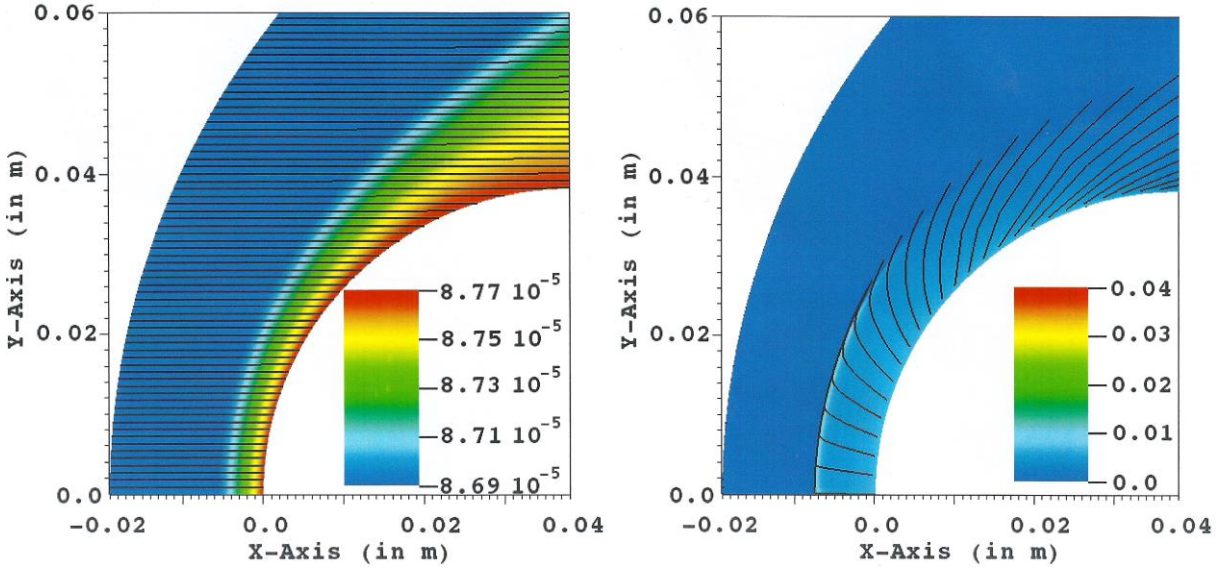


Figure 5: Particle mass density field (in  $\text{kg}\cdot\text{m}^{-3}$ ) and particle velocity streamlines. – Left : primary particle class –  
Right : secondary particle class

## CONCLUSION

In this work, an Eulerian-Eulerian approach has been proposed to simulate particle laden hypersonic flows. It has been applied to the simulation of the BHWT experiment with the aim to reproduce the particle induced shock disturbances that were experimentally observed. We have obtained similar results as Hulin and Znaty<sup>[2]</sup> who already performed the same simulations in the past but using an Euler-Lagrange approach. In the numerical simulations, the influence of the particles on the turbulent kinetic energy production rate in the vicinity of the shock seems to play a determinant role for shock disturbances to appear. However the model used by Hulin and Znaty<sup>[2]</sup> (and that was used as well in the present study for the sake of comparison) is not correct from a theoretical point of view and tends to strongly overestimate the turbulence generation by the particles. The validity of the simulation results obtained with this model are thus strongly questionable. Further investigations are necessary to better understand the physical phenomena at the origin of the shock displacement and to ensure that Euler-Euler, and as well Euler-Lagrange models, are able to reproduce the experimental results.

**REFERENCES**

- [1] W.FLEENER and R.WATSON. Convective heating in dust-laden hypersonic flows. In 8th Thermophysics Conference, page 761, 1973.
- [2] A.HULIN and E.ZNATY. Aerodynamic modelling of hypersonic erosive reentry flows. In *Aerothermodynamics for space vehicles*, volume 367, page 391, 1995
- [3] G.F.CARRIER. Shock waves in a dusty gas. *Journal of Fluid Mechanics*, 4(4):376–382, 1958.
- [4] F.E.MARBLE. Dynamics of dusty gases. *Annual Review of Fluid Mechanics*, 2(1):397–446, 1970.
- [5] L.DUNBAR, J.COURTNEY, and L.MCMILLEN. Heating augmentation in particle erosion environments. In 8th Aerodynamic Testing Conference, page 607, 1974.
- [6] P.PAPADOPOULOS, M.E.TAUBER, and I.D.CHANG. Heatshield erosion in a dusty martian atmosphere. *Journal of Spacecraft and Rockets*, 1993.
- [7] G.PALMER, Y.K.CHEN, P.PAPADOPOULOS, and M.TAUBER. Reassessment of effect of dust erosion on heatshield of mars entry vehicle. *Journal of Spacecraft and Rockets*, 37(6):747–752, 2000.
- [8] J.D.ANDERSON Jr. *Hypersonic and High Temperature Gas Dynamics*. AIAA Publications, AIAA, Reston, VA, 2000.
- [9] F.LAURENT and M.MASSOT. Multi-fluid modelling of laminar polydisperse spray flames: origin, assumptions and comparison of sectional and sampling methods, 2001.
- [10] C.E.SWAIN. The effect of particle/shock layer interaction on reentry vehicle performance. 1975.
- [11] R.CLIFT, J.R.GRACE, and M.WEBER. *Bubbles, drops and particles*. Academic, New York, 1978.
- [12] TW FOX, CW RACKETT, and JA NICHOLLS. Shock wave ignition of magnesium powders. 1978.
- [13] R.M.DRAKE, Discussion: “Forced Convection Heat Transfer From an Isothermal Sphere to Water” (Vliet, GC, and Leppert, G., 1961, *ASME J. Heat Transfer*, 83, pp. 163–170). *Journal of Heat Transfer*, 83(2), 170-172, 1961
- [14] W.K.ANDERSON, J.L.THOMAS, and B.VAN LEER. Comparison of finite volume flux vector splittings for the Euler equations. *AIAA journal*, 24(9):1453–1460, 1986.
- [15] E. F.TORO. *Riemann solvers and numerical methods for fluid dynamics: a practical introduction*. Springer Science & Business Media, 2013.
- [16] B.VAN LEER, J.L.THOMAS, P.L.ROE, and R.W.NEWSOME. A comparison of numerical flux formulas for the Euler and Navier-Stokes equations. 1987.
- [17] B.VAN LEER. Towards the ultimate conservative difference scheme V: a second-order sequel to godunov’s method. *Journal of computational Physics*, 32(1):101–136, 1979.
- [18] G.MAROIS, PhD Thesis, Toulouse University, in preparation, 2018
- [19] O.Desjardin, R.Fox, Ph.Villedieu. A quadrature-based moment method for dilute fluid-particle flows. *Journal of Computational Physics*, 227(4), 2514-2539, 2008
- [20] D.C. WILCOX, *Turbulence models for CFD*. DCW Industries, La Cañada, CA, EUA, 1998

## An Accurate and Robust Immersed Method for Flow Problems

Alexandre Marques<sup>\*</sup>, Jean-Christophe Nave<sup>\*\*</sup>, Rodolfo Rosales<sup>\*\*\*</sup>

<sup>\*</sup>Massachusetts Institute of Technology, <sup>\*\*</sup>McGill University, <sup>\*\*\*</sup>Massachusetts Institute of Technology

### ABSTRACT

We present an immersed method that solves flow problems to high order of accuracy using compact discretization stencils. High order of accuracy is especially important for computing derivatives of flow variables adjacent to the immersed boundaries. For instance, derivatives of the velocity are needed to compute stresses acting on the boundaries, which is required in fluid-structure interaction applications. This method, named the Correction Function Method (CFM), is based on three main concepts: (i) defining smooth extensions of the flow variables across the immersed boundaries as solutions to a Cauchy problem, (ii) solving the Cauchy problem locally for each discretization stencil that crosses the immersed boundaries, and (iii) solving the Cauchy problem via a least squares minimization. The result is a general framework to compute smooth extensions of the flow variables across immersed boundaries to high order of accuracy, and that are independent of the underlying computational grid. These smooth extensions can then be applied with standard discretizations that may straddle the boundaries, maintaining their original order of accuracy and compactness. Furthermore, because the CFM is independent of the underlying computational grid, it is very robust with respect to the arbitrary shape the boundaries can assume under deformation. Similarly, the CFM seamlessly solves problems where multiple interfaces are arbitrarily close. The CFM also facilitates the implementation of complex boundary conditions that arise in the context of high-order methods to solve the incompressible Navier-Stokes equations, such as boundary conditions that involve the divergence or the curl of the velocity. In this talk we will present results of a fourth order implementation of the CFM.

## **Computational Modeling of the Cardiovascular System: Origins, Recent Advances, and Contributions of TJR Hughes**

Alison Marsden\*

\*Stanford University

### **ABSTRACT**

In this talk, I will aim to highlight the early contributions of Thomas JR Hughes to the development of cardiovascular modeling, starting with his early work on 1D blood flow solvers and progressing to his pioneering work on development of patient-specific modeling and finite element blood flow simulations. I'll then highlight how these contributions are continuing to impact current work in the field of cardiovascular simulation and treatment planning. In particular, I will discuss recent advances in computational methodology for cardiovascular modeling, including large-deformation fluid structure interaction simulations, physiologic coupled boundary conditions, uncertainty quantification, optimization, and high-throughput image segmentation. I will then highlight recent applications to clinical problems in pediatric and adult cardiovascular disease, including single ventricle physiology, coronary artery bypass graft surgery, and cardiac development.

## Improvements in the Accuracy of the Theta Method for the Calculation of the Stress Intensity Factors in 3D

Alexandre Martin<sup>\*</sup>, Matthieu Le Cren<sup>\*\*</sup>, Claude Stolz<sup>\*\*\*</sup>, Patrick Massin<sup>\*\*\*\*</sup>, Nicolas Moes<sup>\*\*\*\*\*</sup>

<sup>\*</sup>IMSIA, UMR EDF-CNRS-CEA-ENSTA ParisTech 9219, <sup>\*\*</sup>IMSIA, UMR EDF-CNRS-CEA-ENSTA ParisTech 9219,

<sup>\*\*\*</sup>IMSIA, UMR EDF-CNRS-CEA-ENSTA ParisTech 9219, <sup>\*\*\*\*</sup>IMSIA, UMR EDF-CNRS-CEA-ENSTA ParisTech 9219, <sup>\*\*\*\*\*</sup>Ecole Centrale de Nantes, UMR CNRS 6183

### ABSTRACT

The theta method was proposed by Destuynder et al. [1] to compute the energy release rate and stress intensity factors. This method is based on domain integrals and Lagrangian derivation of the potential energy with respect to a virtual crack extension velocity field. Currently, the method allows obtaining very good results in 2D but has several drawbacks for three-dimensional cracks that will be addressed. To better understand the problems encountered, we propose to study two 3D cases: -- a 3D case that is an extrusion of a 2D case so that the solution is the same for the 2D case and the 3D case along the extrusion direction. -- a Penny-shaped crack which has also an analytical solution [2]. In each case, the results of the calculation for the energy release rate and stress intensity factors will be obtained with the extended finite element method [3] and the finite element method in order to compare both. First, we propose an improvement of the theta field discretization and secondly, an extension of the asymptotic fields for the computation of the stress intensity factors in order to obtain more accurate results with the curved cracks. [1] P. Destuynder, M. Djaoua, S. Lescure. Some remarks on elastic fracture mechanics J. Méca. Théo. Appl. Vol. 2, N° 1, 113-135, 1983. [2] H. Tada, P. Paris, G. Irwin, The stress analysis of cracks handbook, 3ème éd., 2000 [3] N. Moes, J. Dolbow et T. Belytschko, «A finite element method for crack growth without remeshing», International Journal for Numerical Methods in Engineering, pp. 135-150, 1999.

## Risk Average Optimal Control Problem for Elliptic PDEs with Uncertain Coefficients

Matthieu Martin<sup>\*</sup>, Fabio Nobile<sup>\*\*</sup>, Sebastian Krumscheid<sup>\*\*\*</sup>

<sup>\*</sup>CSQI, Institute of Mathematics, Ecole Polytechnique Federale de Lausanne, 1015 Lausanne, Switzerland, <sup>\*\*</sup>CSQI, Institute of Mathematics, Ecole Polytechnique Federale de Lausanne, 1015 Lausanne, Switzerland, <sup>\*\*\*</sup>CSQI, Institute of Mathematics, Ecole Polytechnique Federale de Lausanne, 1015 Lausanne, Switzerland

### ABSTRACT

We consider a risk averse optimal control problem for an elliptic PDE with uncertain coefficients. The control is a deterministic distributed forcing term and is determined by minimizing the expected  $L^2$ -distance between the state (solution of the PDE) and a target deterministic function. An  $L^2$ -regularization term is added to the cost functional. We consider a finite element discretization of the underlying PDE and derive an error estimate on the optimal control. Concerning the approximation of the expectation in the cost functional and the practical computation of the optimal control, we analyze and compare two strategies. In the first one, the expectation is approximated by either a Monte Carlo estimator, and a steepest descent algorithm is used to find the discrete optimal control. The second strategy, named Stochastic Gradient is again based on a steepest-descent type algorithm. However the expectation in the computation of the steepest descent is approximated with independent Monte Carlo estimators at each iteration using possibly a very small sample size. The sample size and possibly the mesh size in the finite element approximation could vary during the iterations. We present error estimates and complexity analysis for both strategies and compare them on few numerical test cases.

## **Finite Element Analysis of Steel-Concrete Composite Floor Systems under Traveling Fire Exposures**

Jason Martinez\*, Ann Jeffers\*\*

\*University of Michigan - Ann Arbor, \*\*University of Michigan - Ann Arbor

### **ABSTRACT**

Preliminary research has shown that the structural response of a building can be significantly influenced by the size and spread rate of a traveling fire. However, prior works have only focused on 2D structural frames, without taking into account the floor system. To address this limitation, this presentation highlights a computational investigation that was undertaken to better understand the global behavior of a 3D steel-concrete composite (SCC) floor system under a traveling fire exposure. Using the Traveling Fires Methodology, a range of spatially and time-varying fire exposures were applied to a 3D finite element model of a SCC floor system. The sequentially coupled thermal-mechanical simulations were carried out using ABAQUS, where the modeling approach was verified against existing test data on full-scale fire test. Essential factors influencing the fire resistance of SCC floor systems, namely the passive fire protection scheme, and the burning size of the fire, were varied to investigate the global structural response. Simulation results indicate that structural response during a traveling fire is not only dominated by material stiffness and strength reduction during heating, but also by large axial forces in the beam-to-column connections during the heating and cooling phase of the fire, structurally-significant displacements of the floor slab, and load redistribution between columns occurring as the fire progresses across the floor plan. Additionally, useful trends were observed, in particular the dependency of the slab displacement rate and the maximum displacement to both the distance from the fire origin and fire burning size.

## Numerical Modelling of the Combined Effect of Mechanical Deployment and Drug Delivery in Endovascular Devices

Miguel A. Martinez\*, Javier Escuer\*\*, Martina Cebollero\*\*\*, Estefania Peña\*\*\*\*

\*Aragón Institute of Engineering Research, University of Zaragoza, Spain. Centro de Investigación Biomédica en Red en Bioingeniería, Biomateriales y Nanomedicina (CIBER-BBN), Spain, \*\*Aragón Institute of Engineering Research, University of Zaragoza, Spain, \*\*\*Aragón Institute of Engineering Research, University of Zaragoza, Spain, \*\*\*\*Aragón Institute of Engineering Research, University of Zaragoza, Spain. Centro de Investigación Biomédica en Red en Bioingeniería, Biomateriales y Nanomedicina (CIBER-BBN), Spain

### ABSTRACT

Cardiovascular diseases are the first cause of death and disability in developed countries. Specifically, atherosclerotic disease results in millions of sudden deaths annually. Endovascular devices such as stents and balloons have become very successful devices to treat advanced atherosclerotic lesions. However, one of the main issues with these interventions is the development of restenosis that is related with the migration of SMCs from the media to the intima causing intima hyperplasia and possible lumen obstruction. An important advance in the treatment of this postsurgical effect is the development drug eluting devices. The controlled delivery of anti-proliferative drugs limits this restenosis phenomenon avoiding the migration and proliferation of SMC, however an excessive drug concentration can have a toxic consequence delaying re-endothelialization of the intima. Many mathematical models describing the drug elution from the device and transport in arteries have been developed. However, most of them do not consider how the mechanical expansion of the endovascular device compresses the porous arterial wall and the transport properties are modified by the mechanical deformation. Therefore the main objective of this work is to study the influence of the mechanical expansion of the device in the diffusion properties of the vessel and on the spatial concentration of the drug. To simulate the mechanical expansion, a fibre-reinforced hyperelastic constitutive model is used to describe arterial wall behaviour and a linear elastic model for the device. Blood flow is modeled by Navier-Stokes equations in the arterial lumen domain. Concerning to drug diffusions properties, the arterial wall is modelled as a multilayer anisotropic porous structure distinguishing intima, media and adventitia. Darcy's law is used to calculate filtration velocity through porous layers and convection-diffusion equations are used to model drug transport through blood, intima, media and adventitia, incorporating a reaction term for the media layer. Endothelium, internal and external elastic laminae are treated as semipermeable membranes and the flux across them is described by Kedem-Katchalsky equations<sup>1</sup>. A non-linear saturable reversible binding model describes binding of drug to specific and non-specific sites. The transport properties of the arterial wall are modified by the local deformation caused by the device deployment. The inclusion of the mechanical expansion of the device modifies the peak concentration on points of the media layer with maximum compressive deformation. The long-time drug average concentration is unaffected by the consideration of device expansion. [1] Bozsak, F., Chomaz, J.M., Barakat, A.I. (2014). Biomech. Model. Mechanobiol. 13(2), 327–347.

## 3D Reconstruction of Histological Sections with Constituent and Morphological Analyses

Pedro Martins\*, Carolina Rocha\*\*, Rita Rynkevic\*\*\*, Marco Parente\*\*\*\*, António Fernandes\*\*\*\*\*

\*INEGI, University of Porto, Faculty of Engineering, \*\*University of Porto, Faculty of Engineering, \*\*\*INEGI, University of Porto, Faculty of Engineering, \*\*\*\*INEGI, University of Porto, Faculty of Engineering, \*\*\*\*\*INEGI, University of Porto, Faculty of Engineering

### ABSTRACT

The microstructure of soft biological tissues has a significant influence on the mechanical properties at a macroscopic level. Using the ovine animal model, a good agreement between tissue contents (collagen, elastin, smooth muscle and myofibroblasts) and biomechanical properties [1] has been established. Despite the importance of constituents' quantity on the overall mechanical behavior of a given biological soft tissue, their three-dimensional arrangement will ultimately dictate the macroscopic mechanical response. In this work, tissue from ovine ewes was collected, and consecutive histology samples were prepared. A 3D reconstruction of the multiple sections of the vagina (full-thickness) was carried out using Mimics software. From this analysis it was possible to study the 3D arrangement of tissue constituents through the tissue thickness. The volumetric estimation of tissue constituents was also a direct result of the current work. References: [1] R. Rynkevic, P. Martins, L. Hympanova, H. Almeida, A. A. Fernandes, and J. Deprest, "Biomechanical and morphological properties of the multiparous ovine vagina and effect of subsequent pregnancy," *Journal of Biomechanics*, vol. 57, pp. 94–102, 2017.

## **Design and Numerical Analysis of a Gasket Based on Auxetic Structures**

Arturo A. Martínez\*, Fernando Velázquez\*\*

\*Universidad Nacional Autónoma de México, \*\*Universidad Nacional Autónoma de México

### **ABSTRACT**

In the present article the design and analysis of a bell and spigot joint gasket based on an auxetic materials is proposed to solve leaks produced by severe misalignment. With current gaskets, misalignments in the joints can produce separations between his elements, which can represent a major environmental, health or economic problem. The auxetic structure design is analyzed and evaluated by finite element (FE) analysis to simulate the auxetic behavior of the proposed structure. The auxetic structure used is based on a simple geometry in periodical arrangements. The proposed gasket modifies its volume, maintaining contact with the surfaces to be sealed even with large joint deflection.

## A Machine Learning Tool for the Mechanical Characterization of Cardiovascular Tissues

Javier Martínez\*, Myriam Cilla\*\*, Ignacio Pérez-Rey\*\*\*, Miguel Ángel Martínez\*\*\*\*, Estefanía Peña\*\*\*\*\*

\*4.-Department of Natural Resources and Environmental Engineering, University of Vigo, Vigo, Spain. 5.-Centro Universitario de la Defensa (CUD), Marín, Spain, \*\*1.-Centro Universitario de la Defensa (CUD), Zaragoza, Spain. 2.-Aragon Institute of Engineering Research (I3A), University of Zaragoza, Zaragoza, Spain. 3.-3CIBER's Bioengineering, Biomaterials and Nanomedicine (CIBER-BBN), Spain, \*\*\*4.-Department of Natural Resources and Environmental Engineering, University of Vigo, Vigo, Spain, \*\*\*\*2.-Aragon Institute of Engineering Research (I3A), University of Zaragoza, Zaragoza, Spain. 3.-3CIBER's Bioengineering, Biomaterials and Nanomedicine (CIBER-BBN), Spain, \*\*\*\*\*2.-Aragon Institute of Engineering Research (I3A), University of Zaragoza, Zaragoza, Spain. 3.-3CIBER's Bioengineering, Biomaterials and Nanomedicine (CIBER-BBN), Spain

### ABSTRACT

**Introduction** The research of the mechanical response of biological tissues is the basis for the creation of computational models which can accurately reproduce their mechanical behaviour. The experimental data are used to estimate the material model parameters through a Strain Energy Function (SEF) within the framework of the continuum theory of large deformation hyperelasticity. Traditionally, material parameters associated with the material model have been fitted by means of a Levenberg-Marquardt type minimization algorithm and/or inverse models combined with finite element models. However, motivated by the well-known problem of these numerical methods based on gradients, that is, their limitation to find local optimization, and therefore, their instability and dependence of the selected initial seed, a new approach is explored in the presented study. The use of Artificial Neural Networks (ANNs) is proposed to solve the parameter identification of constitutive laws for soft biological tissues. **Methods** Data is collected from circumferential and longitudinal uniaxial tests carried out on cardiovascular tissues. 1080 analytical curves, which cover a range of response from highly anisotropic to quasi-isotropic, were used. From uniaxial tests, it is possible to recover stress-strain pairs for each longitudinal and circumferential cases. The input of the ANN was defined by extracting three customized parameters (initial slope, middle point and final slope) from test results. The ANN was trained with these inputs providing the parameters which define the behavior of the tissue by means of the SEF defined by Gasser et al. [1]. The tool was trained repetitively until convergence and it was carried out by considering a different number of neurons in the hidden layers. A validation with new observations of analytical curves (previously unseen observations by the ANN) and with eight kinds of cardiovascular experimental data was performed. **Results** The train and test errors show a great efficiency during the training process to find correlations between inputs and outputs; besides the correlation coefficients were very close to 1. In addition, the results show an excellent agreement between the prediction of the material parameters of the SEF and the analytical curves. **Discussion** We found that the method was able to consistently identify model parameters, and we believe that the use of this numerical tool could imply an improvement in the characterization of cardiovascular tissues. **References** [1] C.T. Gasser, R.W. Ogden and G.A. Holzapfel. Hyperelastic modelling of arterial layers with distributed collagen fibre orientations. *Journal of The Royal Society of Interface*- 3:15:35. 2006.

# ADVANCES IN THE TREATMENT OF TRIMMED CAD MODELS DUE TO ISOGOMETRIC ANALYSIS

BENJAMIN MARUSSIG<sup>\*,†</sup>

<sup>\*</sup>Graz University of Technology  
Graz Center of Computational Engineering (GCCE)  
Krenngasse 37/I, 8010 Graz, Austria  
marussig@tugraz.at; www.gcce.tugraz.at

<sup>†</sup>Graz University of Technology  
Institute of Mechanics  
Kopernikusgasse 24/IV, 8010 Graz, Austria

**Key words:** Isogeometric Analysis, Trimming, SSI operation, CAGD

**Abstract.** Trimming is a core technique in geometric modeling. Unfortunately, the resulting objects do not take the requirements of numerical simulations into account and yield various problems. This paper outlines principal issues of trimmed models and highlights different analysis-suitable strategies to address them. It is discussed that these concepts not only provide important computational tools for isogeometric analysis, but can also improve the treatment of trimmed models in a design context.

## 1 INTRODUCTION

Isogeometric analysis (IGA) aims to bridge the gap between computer aided geometric design (CAGD) and analysis by using CAGD technologies for numerical simulations. Since the introduction of IGA in 2005, it has been demonstrated that the synthesis of these disciplines allows not only an improved interaction, but yields many computational advantages<sup>1-3</sup>. Nowadays, IGA is widely recognized as a powerful alternative to the conventional analysis methodology. In the following, the attention is drawn to a somewhat different aspect, namely (potential) benefits for CAGD due to developments made in IGA. It is focused on challenges concerning robustness and interoperability. In particular, the treatment of trimmed models is addressed, because these representations play a central role in engineering design and the integration of design and analysis<sup>4</sup>. First, the evolution of trimmed CAD models is presented in order to outline the related problems. Based on that, corresponding advances of IGA are discussed.

## 2 A BRIEF HISTORY OF TRIMMED SOLID MODELS

The problem of computing surface-to-surface intersections (SSI) is closely related to trimming and thus, it is discussed at the beginning of this section. Then, the formulation of solid models defined by trimmed surfaces is presented and finally related robustness issues and the role of trimmed models with respect to the exchange of CAD data are discussed.

### 2.1 SSI operations

Computing intersections of surfaces is a crucial task in various types of modeling processes. First of all, it is the core ingredient for Boolean operations which are the most important functions in creating CAD objects<sup>5</sup>. In general, the intersection of two parametric surfaces

$$\mathcal{S}_1(u, v) = (x_1(u, v), y_1(u, v), z_1(u, v)) \quad (1)$$

$$\mathcal{S}_2(s, t) = (x_2(s, t), y_2(s, t), z_2(s, t)) \quad (2)$$

leads to a system of three nonlinear equations<sup>6</sup>. These equations represent the three coordinate differences of the surfaces,  $\mathcal{S}_1$  and  $\mathcal{S}_2$ , with the four unknown surface parameters  $u, v, s, t$ . In most cases, the solution describes a curve, but intersection points, subsurfaces, or empty sets may occur as well.

Efficiently providing *all* features of these solutions is the purpose of SSI operations<sup>7</sup>. The development of a good SSI procedure is a very challenging task due to the fact that the operation has to be *accurate, efficient, and robust*. These attributes are indeed quite contradictory and the definition of an adequate balance between them depends strongly on the application context. Early solid modeling systems employed analytic methods to compute exact parametric descriptions of intersections between linear and quadratic surfaces<sup>8</sup>. Unfortunately, the algebraic complexity of an intersection increases rapidly with the degree of  $\mathcal{S}_1$  and  $\mathcal{S}_2$ , which has been thoroughly discussed by Sederberg and co-workers<sup>9-11</sup> in the 1980s. This makes analytic approaches impractical; a fact often illustrated by the algebraic degree of an intersection of two general bicubic surfaces which is 324.

Hence, alternative SSI schemes are needed. These concepts can be broadly classified as lattice evaluation schemes<sup>12,13</sup>, subdivision methods<sup>14</sup>, and marching methods<sup>15,16</sup>. The former reduces the dimensionality of the problem by computing intersections of a number of isocurves of  $\mathcal{S}_1$  with  $\mathcal{S}_2$  and vice versa. The second strategy uses approximations of the actual surfaces, often defined by a set of piecewise linear elements, and computes the related intersections with respect to the simplified objects. Finally, marching methods define an intersection curve by stepping piecewise along the curve. This requires detection of appropriate starting points, determination of point sequences along the intersection that emit from the starting points, and proper sorting and merging of these individual sequences. Marching methods are by far the most widely used schemes due to their generality and ease of implementation<sup>17</sup>. However, each intersection strategy has its advantages and drawbacks, hence SSI algorithms usually use hybrid concepts that combine different features of these approaches<sup>17-19</sup>.

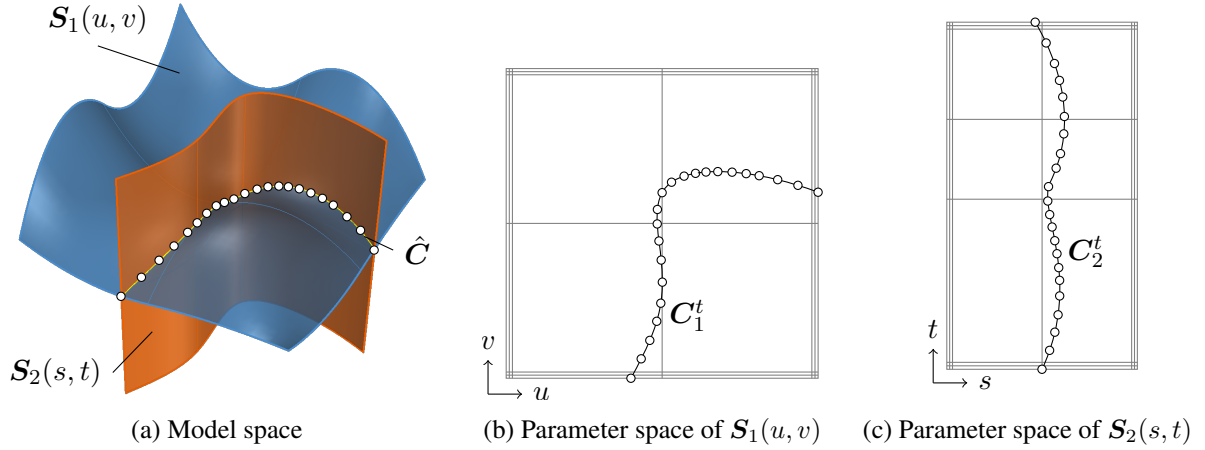


Figure 1: Independent curve interpolation of an ordered point set to obtain approximations of the intersection of two patches  $S_1(u, v)$  and  $S_2(s, t)$ . The set of sampling points depends on the SSI algorithm applied. The subsequent interpolation of these points is performed in (a) the model space and the parameter space of (b)  $S_1(u, v)$  and (c)  $S_2(s, t)$  leading to independent curves  $\hat{C}$ ,  $C_1^t$ , and  $C_2^t$ .

Irrespective of the scheme applied, the initial result of a SSI operation is usually a set of sampling points that represent the intersection<sup>20</sup>. An *approximate* intersection curve in model space  $\hat{C}$  is subsequently obtained by some curve-fitting technique such as point interpolation or least-squares approximation. Thus,  $\hat{C}$  does not lie on either of the intersecting surfaces in general. Furthermore, the sampling points are mapped into the parameter spaces of  $S_1$  and  $S_2$ , where they are again used as input for a curve-fitting procedure. This yields the main result of the SSI process, namely *trimming curves*  $C^t$  in the two-dimensional parametric domains. These  $C^t$  are usually represented by spline curves. They are essential because they allow the definition of arbitrarily shaped partitions within a tensor product surface, which enables proper visualization of intersecting surfaces and the application of Boolean operations. Every  $C^t$  can be mapped into model space, but the resulting image  $\tilde{C}^t$  will not coincide with  $\hat{C}$ . In short, SSI operations yield various independent approximations of the actual intersection (see Figure 1), rather than an unambiguous solution. It is emphasized that there is no direct mapping between these different approximations and that the sampling point data for their construction is usually discarded once the curves are computed.

## 2.2 Trimmed solid models

There are various approaches for representing geometric objects<sup>20–22</sup>. The most popular one in engineering design is the boundary representation (B-Rep) and the benefits of storing an object's shape by means of its boundary were already elaborated in the seminal work of Braid<sup>23</sup>. B-Rep solid modeling utilizes SSI schemes to create arbitrarily defined free-form geometric entities. The corresponding algorithms, however, require more than the computation

of intersection curves. Essential attributes of geometric modeling operators are<sup>24</sup>:

- the determination of the geometric surface descriptions,
- the determination of the topological descriptions, and
- the guarantee that the geometry corresponds unambiguously to the topology.

Topological data is not metrical, but addresses connectivity and dimensional continuity of a model<sup>20</sup>. Its determination requires the classification of the neighborhood of various entities (faces, edges, and vertices) involved in the intersections<sup>21</sup>. In CAGD, the term *solid* model emphasizes that a representation contains the descriptions of an object's shape, i.e., the geometry, as well as its structure, i.e., the topology; it does not refer to the dimension of the object defined.

The idea of a trimmed model appeared already in 1974 and was proposed by Pierre Bézier<sup>25</sup>. However, the approach was presented with little theoretical support and it took some time to develop a rigorous way to represent trimmed free-form solid models. The first formulation supporting Boolean operations and free-form geometry was presented by Farouki<sup>26</sup> as well as Casale and Bobrow<sup>27,28</sup> in the late 1980s. In general, the connectivity between intersecting surfaces is established by assigning the approximate intersection curves (which do not coincide) to a single topological entity. Further, Boolean operations define the relation of the faces, edges, and vertices of a model. Various data structures for B-Reps have been proposed to find a compromise between storage requirements and response to topological questions. The crucial discrepancy, which still exists, is that solid modeling is concerned with the use of *unambiguous* representations, but SSI schemes introduce approximations and do not provide a unique representation of an intersection. In other words, all these modeling approaches have to deal with imprecise data and thus, fail to guaranty exact topological consistency<sup>29</sup>. Thus, the robustness of a trimmed B-Rep becomes a crucial factor.

### 2.3 Robustness issues of trimmed models

Several robustness issues arise in case of imprecise geometric operations. As a matter of fact, numerical output from simple geometric operations can already be quite inaccurate - even for linear elements<sup>21</sup>. For SSI schemes, ill-conditioned intersection problems are particularly troublesome. Such cases occur when intersections are tangential or surfaces overlap, for instance. Since geometrical decisions are based on *approximate* data and arithmetic operations of *limited* precision, there is an interval of uncertainty in which the numerical data cannot yield further information<sup>30</sup> and the fact that SSI operations do not provide a unique intersection curve makes the situation even more delicate.

The most common strategy to address robustness issues is the use of tolerances<sup>14</sup>. They shall assess the quality of geometrical operations and may be adaptively defined<sup>31,32</sup> or dynamically updated<sup>33</sup>. Alternative approaches employ interval arithmetic<sup>34</sup> or exact arithmetic<sup>35</sup>, but

these concepts have certain drawbacks (especially with respect to efficiency) and hence, tolerance based approaches are usually preferred. Unfortunately, tolerances cannot guarantee robust algorithms since they do not deal with the inherent problem of limited-precision arithmetic.

Overall, the formulation of *robust* solid models with trimmed patches is still an open issue. This is particularly true when a model shall be transferred from a CAD system to another software tool. Since there is no canonical representation of trimmed solid models, different systems may employ different data structures and robustness checks. Consequently, data exchange involves a translation process which can lead to misinterpretation. This makes the treatment of trimmed solid models a key aspect for the interoperability of design and analysis.

### 3 DEVELOPMENTS IN ISOGOMETRIC ANALYSIS

Since the introduction of IGA, more and more scientists in the field of computational mechanics have become aware of the advantages and deficiencies of design models and various analysis-suitable approaches dealing with CAD-related challenges have been proposed. Here, we highlight advances made in the context of local refinement of multivariate splines, which are important to derive watertight models, and the treatment of trimmed geometries.

#### 3.1 Local refinement

The lack of local refinement of conventional tensor product splines was one of the first issues tackled by the IGA community. The topic emerged to an active area of research and several techniques have been developed, such as T-splines<sup>36,37</sup>, LR-B-splines<sup>38,39</sup>, hierarchical B-splines<sup>40-42</sup>, and truncated hierarchical B-splines<sup>43</sup>. Some of these concepts were first presented in the context of CAGD (e.g., T-splines and hierarchical B-splines). However, their application in an analysis setting has provided a huge impetus to their further enhancement. In fact, these concepts have become so technically mature that the question is no longer if local refinement of multivariate spline is feasible, but what technique do you prefer.

Besides the apparent computational benefits, these advances in local refinement techniques also offer new possibilities for the design community. Admittedly, these local refinement concepts are usually not incorporated in current CAD systems (yet), but a strong indicator for the impact of IGA is a novel capability of the next version of the Standard for the Exchange of Product Model Data (STEP) – the most involved neutral exchange standard. That is, it will include entities that facilitate a canonical representation of locally refined tensor product splines<sup>44</sup>. To be precise, this feature affects the part “geometric and topological representations,” which focuses on the definition of geometric models and represents a core component of STEP. Regarding trimmed models, the ability of local refinement can be a powerful tool as well. For instance, effects of trimming may be localized<sup>45</sup> or trimmed surfaces may even be joined as it is done during the conversion of trimmed B-Reps to watertight T-spline models<sup>46</sup>.

## 3.2 Dealing with non-watertight representations

The term "non-watertight" is commonly used to stress that trimmed models have small gaps and overlaps between their intersecting surfaces. They occur due to the inevitable approximations introduced by SSI operations as discussed in Section 2.1. Watertight representations, on the other hand, possess unambiguously-defined edges and a direct link between adjacent elements. This link is missing in case of trimmed models and has to be established (or at least taken into account) in order to make them analysis-suitable. Current attempts for the integration of trimmed geometries into IGA can be divided into global and local approaches<sup>4</sup>. The former aims to convert trimmed solid models to watertight ones in a pre-processing step (or even already during the design stage), whereas the latter intends to enhance the simulation tool so that it is able to cope with the models' flaws.

### 3.2.1 Local approaches

The basic idea of local approaches is that trimmed parameter spaces are used as background parameterization for the simulation. Hence, there is a close relation to fictitious domain methods and the corresponding challenges are indeed similar: First, the elements needed for the analysis have to be detected<sup>47-49</sup>. Second, special integration techniques for elements cut by a trimming curve<sup>47-54</sup> have to be employed. Third, weak enforcement of boundary conditions or weak coupling of adjacent surfaces has to be addressed<sup>50,53,55,56</sup>. Finally, stability issues of cut elements with small support should be taken into account<sup>45,57</sup>. The main difference to fictitious domain methods is that an additional effort is required to associate the degrees of freedom of adjacent patches, keeping in mind that their intersections have non-matching parameterizations, gaps, and overlaps. Usually, point inversion algorithms<sup>58,59</sup> are utilized to establish a link between adjacent surfaces. Alternatively, simulation methods that allow discontinuities between elements<sup>57,60</sup> can be applied.

The majority of the publications on IGA with trimmed geometries employs such local concepts. A possible reason could be that these approaches focus on analysis aspects and thus, may seem more feasible for researchers in the field of computational mechanics. On the other hand, this also means that the number of subjects that may affect CAGD is relatively small. The essential common ground is the problem of finding robust procedures and the use of tolerances to achieve a proper model treatment. However, this does not mean that the task is trivial. As outlined in Section 2.3, the robust treatment of trimmed models is a really challenging issue in CAGD. Regarding IGA, an additional obstacle complicates the situation, that is, analysis software has to deal with extracted data. In other words, the input data provides only a reduced portion of the information that would be available in the initial CAD tool. Furthermore, this portion may be altered due to the translation process that might be required for the exchange. This aspect could be improved when the exchange procedure is tailored to a specific CAD system using its native data format. Yet, this would require vendor interaction and the restriction to a single software. Most importantly, this option is not very sustainable since a native format

of a CAD system may become obsolete after a new software version is released.

### 3.2.2 Global approaches

Global approaches decompose trimmed model components into a set of regular surfaces or replace them by other spline representations such as subdivision surfaces or T-splines. Similar to the developments regarding local refinement, some strategies may originate from CAGD. For instance, isogeometric analysis with subdivision surfaces<sup>61,62</sup> and T-splines<sup>36,63</sup> can be included into the class of global techniques. Reconstruction concepts proposed in the context of analysis usually aim to replace trimmed surfaces by a set of regular ones. This is done by means of ruled surfaces<sup>64</sup>, Coons patches<sup>65</sup>, triangular Bézier patches<sup>66</sup>, or a reconstruction based on isocurves<sup>67</sup>.

Global approaches seek to resolve the core problem of trimmed solid models and hence, they are more related to CAGD than their local counterpart. Consequently, advances in this research area are more likely to have an impact in the design community. T-splines are a prime example in this regard. The introduction of T-splines in IGA has led to various enhancements such as analysis-suitable T-spline spaces that guarantee linear independent basis functions and it would be no exaggeration to say that IGA has been a driving force for the development T-splines in the past years. Approaches emerging from an analysis perspective can also be very useful for design applications. For instance, the reconstruction scheme introduced by Urick<sup>67</sup> could be utilized to create watertight Boolean operations. This possibility is currently under investigation and a preliminary example is illustrated in Figure 2. Note that Figure 2(c) shows a single surface with a matching parameterization across the computed intersection.

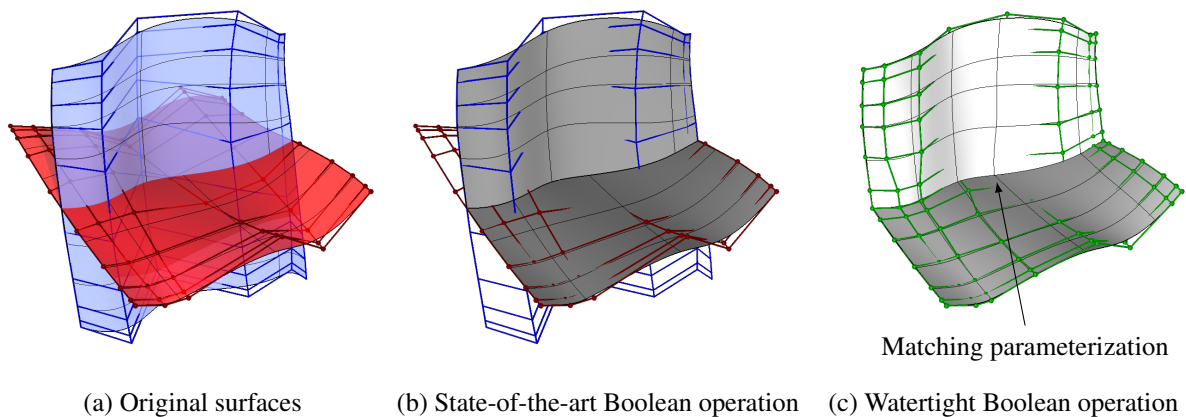


Figure 2: Comparison of conventional and watertight Boolean operations: (a) initial surfaces and their control grids colored in blue and red, respectively, (b) the outcome based on a conventional Boolean operation, and (c) the result of the watertight counterpart. The control grids in (a) and (b) are identical, whereas in (c) the control points are updated to reflect the intersection which is defined as an isocurve of the watertight surface.

In contrast to local approaches, it is hard to identify general ingredients associated to global reconstruction procedures. Each global strategy requires a self-contained concept which becomes more and more sophisticated with its capabilities. This is indeed a potential drawback, especially when new features are added later on. Once a global scheme can be successfully applied, that is, it leads to a watertight model, two fundamental questions have to be addressed: (i) the representation of unstructured meshes and (ii) the treatment of extraordinary points (EPs). These topics are indeed of great interest for CAGD. Current model data is usually based on a structured mesh setting, where all control points of a surface are arranged in a regular grid. When local refinement of tensor product surfaces is considered as well, a structured mesh admits only interior points of valence 4 and T-junctions. But in case of smooth watertight models points with any valence (e.g., 3, 4, 5, ...) can occur and the arising non-regular points are referred to as EPs. These EPs also affect analysis properties and hence, their proper treatment is important for IGA<sup>68</sup>. It is worth noting that IGA researchers are also included in recent attempts seeking to include the capability of representing unstructured meshes in STEP.

Looking at the overall scope of global schemes, it is fair to say that they do address core issues of trimmed models. A compelling analysis-suitable approach could eventually resolve the robustness and interoperability of trimmed models not only for analysis, but all downstream applications. On the other hand, they are more complex and their success will also depend on their acceptance in CAGD.

#### 4 CONCLUSION AND OUTLOOK

A brief overview of the development of surface-to-surface intersection operations and the formulation of trimmed solid models is provided to indicate the potential problems related to these popular computer aided geometric design (CAGD) representations. Strategies for isogeometric analysis (IGA) with trimmed geometries are listed and divided into two categories: (i) local approaches aim to enhance the analysis process and (ii) global approaches try to convert trimmed objects to regular models before the simulation. It is argued that these advances also bring new insights for CAGD, indicating the mutual benefits due to the interaction of the design and analysis communities. That IGA solutions lead to improvements for analysis as well as design has already been demonstrated by the evolution of local refinement concepts for multivariate splines and the recent developments regarding the treatment of trimmed models are indeed on a similar trajectory.

#### REFERENCES

- [1] J. A. Cottrell, A. Reali, Y. Bazilevs, T. J. R. Hughes, Isogeometric analysis of structural vibrations. *Computer Methods in Applied Mechanics and Engineering*, 195(41–43), 5257–5296, 2006.
- [2] J. Cottrell, T. Hughes, A. Reali, Studies of refinement and continuity in isogeometric

- structural analysis. *Computer Methods in Applied Mechanics and Engineering*, 196(41–44), 4160–4183, 2007.
- [3] S. Lipton, J. A. Evans, Y. Bazilevs, T. Elguedj, T. J. R. Hughes, Robustness of isogeometric structural discretizations under severe mesh distortion. *Computer Methods in Applied Mechanics and Engineering*, 199(5–8), 357–373, 2010.
- [4] B. Marussig, T. J. R. Hughes, A review of trimming in isogeometric analysis: Challenges, data exchange and simulation aspects. *Archives of Computational Methods in Engineering*, 1–69, 2017.
- [5] J. Corney, T. Lim, *3D modeling with ACIS*. Saxe-Coburg, 2001.
- [6] E. Cohen, R. F. Riesenfeld, G. Elber, *Geometric modeling with splines: An introduction*. A K Peters, 2001.
- [7] N. M. Patrikalakis, T. Maekawa, *Shape interrogation for computer aided design and manufacturing*. Springer Science & Business Media, 2009.
- [8] C. M. Brown, PADL-2: A technical summary. *IEEE Computer Graphics and Applications*, 2(2), 69–84, 1982.
- [9] T. W. Sederberg. *Implicit and parametric curves and surfaces for computer aided geometric design*. PhD thesis, Purdue University, 1983.
- [10] T. W. Sederberg, D. C. Anderson, R. N. Goldman, Implicit representation of parametric curves and surfaces. *Computer Vision, Graphics, and Image Processing*, 28(1), 72–84, 1984.
- [11] S. Katz, T. W. Sederberg, Genus of the intersection curve of two rational surface patches. *Computer Aided Geometric Design*, 5(3), 253–258, 1988.
- [12] A. Limaiem, F. Trochu, Geometric algorithms for the intersection of curves and surfaces. *Computers & Graphics*, 19(3), 391–403, 1995.
- [13] J. R. Rossignac, A. A. G. Requicha, Piecewise-circular curves for geometric modeling. *IBM Journal of Research and Development*, 31(3), 296–313, 1987.
- [14] J. Hoschek, D. Lasser, *Grundlagen der geometrischen Datenverarbeitung*. Vieweg+Teubner, 1992.
- [15] C. L. Bajaj, C. M. Hoffmann, R. E. Lynch, J. E. H. Hopcroft, Tracing surface intersections. *Computer Aided Geometric Design*, 5(4), 285–307, 1988.
- [16] R. T. Farouki, The characterization of parametric surface sections. *Computer Vision, Graphics, and Image Processing*, 33(2), 209–236, 1986.
- [17] S. Krishnan, D. Manocha, An efficient surface intersection algorithm based on lower-dimensional formulation. *ACM Transactions on Graphics*, 16(1), 74–106, 1997.
- [18] E. G. Houghton, R. F. Emmett, J. D. Factor, C. L. Sabharwal, Implementation of a divide-and-conquer method for intersection of parametric surfaces. *Computer Aided Geometric Design*, 2(1), 173–183, 1985.
- [19] R. E. Barnhill, S. Kersey, A marching method for parametric surface/surface intersection. *Computer Aided Geometric Design*, 7(1–4), 257–280, 1990.

- [20] M. E. Mortenson, *Geometric modeling*. Wiley, 2nd edition, 1997.
- [21] C. M. Hoffmann, *Geometric and solid modeling*. Morgan Kaufmann, 1989.
- [22] M. Mäntylä, *An introduction to solid modeling*. Computer Science Press, 1988.
- [23] I. C. Braid, *Designing with volumes*. Cantab Press, Cambridge University, England, 2 edition, 1974.
- [24] K. J. Weiler. *Topological structures for geometric modeling*. PhD thesis, Rensselaer Polytechnic Institute, 1986.
- [25] P. Bézier, Mathematical and practical possibilities of UNISURF. In R. E. Barnhill, R. F. Riesenfeld, editors, *Computer Aided Geometric Design*, 127–152. Academic Press, 1974.
- [26] R. T. Farouki, Trimmed-surface algorithms for the evaluation and interrogation of solid boundary representations. *IBM Journal of Research and Development*, 31(3), 314–334, 1987.
- [27] M. S. Casale, Free-form solid modeling with trimmed surface patches. *IEEE Computer Graphics and Applications*, 7(1), 33–43, 1987.
- [28] M. S. Casale, J. E. Bobrow, A set operation algorithm for sculptured solids modeled with trimmed patches. *Computer Aided Geometric Design*, 6(3), 235–247, 1989.
- [29] R. T. Farouki, C. Y. Han, J. Hass, T. W. Sederberg, Topologically consistent trimmed surface approximations based on triangular patches. *Computer Aided Geometric Design*, 21(5), 459–478, 2004.
- [30] C. M. Hoffmann, J. E. Hopcroft, M. S. Karasick. Towards implementing robust geometric computations. In *Proceedings of the Symposium on Computational Geometry*, 106–117. ACM, 1988.
- [31] D. J. Jackson. Boundary representation modelling with local tolerances. In *Proceedings of the Symposium on Solid Modeling and Applications*, 247–254. ACM, 1995.
- [32] M. Segal, Using tolerances to guarantee valid polyhedral modeling results. *SIGGRAPH Computer Graphics*, 1990.
- [33] S. F. Fang, B. Bruderlin, X. H. Zhu, Robustness in solid modeling: A tolerance-based intuitionistic approach. *Computer-Aided Design*, 1993.
- [34] C.-Y. Hu, N. M. Patrikalakis, X. Ye, Robust interval solid modelling part I: representations. *Computer-Aided Design*, 28(10), 807–817, 1996.
- [35] S. Krishnan, D. Manocha, M. Gopi, T. Culver, J. Keyser, BOOLE: A boundary evaluation system for boolean combinations of sculptured solids. *International Journal of Computational Geometry & Applications*, 11(1), 105–144, 2001.
- [36] Y. Bazilevs, V. M. Calo, J. A. Cottrell, J. A. Evans, T. J. R. Hughes, S. Lipton, M. A. Scott, T. W. Sederberg, Isogeometric analysis using T-splines. *Computer Methods in Applied Mechanics and Engineering*, 199(5–8), 229–263, 2010.
- [37] T. W. Sederberg, J. Zheng, A. Bakenov, A. Nasri, T-splines and T-NURCCs. *ACM Trans. Graph.*, 2003.
- [38] T. Dokken, T. Lyche, K. F. Pettersen, Polynomial splines over locally refined box-

- partitions. *Computer Aided Geometric Design*, 30(3), 331–356, 2013.
- [39] K. A. Johannessen, T. Kvamsdal, T. Dokken, Isogeometric analysis using LR B-splines. *Computer Methods in Applied Mechanics and Engineering*, 269, 471–514, 2014.
- [40] P. B. Bornemann, F. Cirak, A subdivision-based implementation of the hierarchical b-spline finite element method. *Computer Methods in Applied Mechanics and Engineering*, 253, 584–598, 2013.
- [41] R. Kraft, *Adaptive and linearly independent multilevel B-splines*. SFB 404, 1997.
- [42] A. V. Vuong, C. Giannelli, B. Jüttler, B. Simeon, A hierarchical approach to adaptive local refinement in isogeometric analysis. *Computer Methods in Applied Mechanics and Engineering*, 2011.
- [43] C. Giannelli, B. Jüttler, H. Speleers, THB-splines: The truncated basis for hierarchical splines. *Computer Aided Geometric Design*, 2012.
- [44] V. Skytt, J. Haenisch. Extension of ISO 10303 with isogeometric model capabilities. ISO TC 184/SC 4/WG 12, *ISO*, 2013.
- [45] B. Marussig, R. Hiemstra, T. J. R. Hughes, Improved conditioning of isogeometric analysis matrices for trimmed geometries. *Computer Methods in Applied Mechanics and Engineering*, 334, 79–110, 2018.
- [46] T. W. Sederberg, X. Li, H. W. Lin, H. Ipson, G. T. Finnigan, Watertight trimmed NURBS. *ACM Transactions on Graphics*, 2008.
- [47] R. Schmidt, R. Wüchner, K.-U. Bletzinger, Isogeometric analysis of trimmed NURBS geometries. *Computer Methods in Applied Mechanics and Engineering*, 241–244, 93–111, 2012.
- [48] H.-J. Kim, Y.-D. Seo, S.-K. Youn, Isogeometric analysis for trimmed CAD surfaces. *Computer Methods in Applied Mechanics and Engineering*, 198(37–40), 2982–2995, 2009.
- [49] H.-J. Kim, Y.-D. Seo, S.-K. Youn, Isogeometric analysis with trimming technique for problems of arbitrary complex topology. *Computer Methods in Applied Mechanics and Engineering*, 199(45–48), 2796–2812, 2010.
- [50] M. Ruess, D. Schillinger, A. I. Özcan, E. Rank, Weak coupling for isogeometric analysis of non-matching and trimmed multi-patch geometries. *Computer Methods in Applied Mechanics and Engineering*, 269, 46–71, 2014.
- [51] B. Marussig. *Seamless integration of design and analysis through boundary integral equations*. PhD thesis, Graz University of Technology, 2015.
- [52] Y.-W. Wang, Z.-D. Huang, Y. Zheng, S.-G. Zhang, Isogeometric analysis for compound B-spline surfaces. *Computer Methods in Applied Mechanics and Engineering*, 261–262, 1–15, 2013.
- [53] M. Breitenberger, A. Apostolatos, B. Philipp, R. Wüchner, K.-U. Bletzinger, Analysis in computer aided design: Nonlinear isogeometric B-Rep analysis of shell structures. *Computer Methods in Applied Mechanics and Engineering*, 284, 401–457, 2015.
- [54] B. Philipp, M. Breitenberger, I. D’Auria, R. Wüchner, K.-U. Bletzinger, Integrated design

- and analysis of structural membranes using the isogeometric B-Rep analysis. *Computer Methods in Applied Mechanics and Engineering*, 303, 312–340, 2016.
- [55] M. Breitenberger. *CAD-integrated design and analysis of shell structures*. PhD thesis, Technische Universität München, 2016.
- [56] Y. Guo, J. Heller, T. J. R. Hughes, M. Ruess, D. Schillinger, Variationally consistent isogeometric analysis of trimmed thin shells at finite deformations, based on the STEP exchange format. *Computer Methods in Applied Mechanics and Engineering*, 336, 39–79, 2018.
- [57] B. Marussig, J. Zechner, G. Beer, T.-P. Fries, Stable isogeometric analysis of trimmed geometries. *Computer Methods in Applied Mechanics and Engineering*, 316, 497–521, 2016.
- [58] Y. L. Ma, W. T. Hewitt, Point inversion and projection for NURBS curve and surface: Control polygon approach. *Computer Aided Geometric Design*, 2003.
- [59] L. A. Piegl, W. Tiller, *The NURBS book*. Springer, 2nd edition, 1997.
- [60] J. Zechner, B. Marussig, G. Beer, T.-P. Fries, The isogeometric Nyström method. *Computer Methods in Applied Mechanics and Engineering*, 306, 212–237, 2015.
- [61] F. Cirak, Q. Long, Subdivision shells with exact boundary control and non-manifold geometry. *International Journal for Numerical Methods in Engineering*, 88(9), 897–923, 2011.
- [62] A. Riffnaller-Schiefer, U. H. Augsdörfer, D. W. Fellner, Isogeometric shell analysis with NURBS compatible subdivision surfaces. *Applied Mathematics and Computation*, 272, Part 1, 139–147, 2016.
- [63] M. A. Scott. *T-splines as a design-through-analysis technology*. PhD thesis, 2011.
- [64] G. Beer, B. Marussig, J. Zechner, A simple approach to the numerical simulation with trimmed CAD surfaces. *Computer Methods in Applied Mechanics and Engineering*, 285, 776–790, 2015.
- [65] H. Harbrecht, M. Randrianarivony, From Computer Aided Design to wavelet BEM. *Computing and Visualization in Science*, 13(2), 69–82, 2010.
- [66] S. Xia, X. Qian, Isogeometric analysis with Bézier tetrahedra. *Computer Methods in Applied Mechanics and Engineering*, 316, 782–816, 2016.
- [67] B. Urick. *Reconstruction of tensor product spline surfaces to integrate surface-surface intersection geometry and topology while maintaining inter-surface continuity*. PhD thesis, The University of Texas at Austin, 2016.
- [68] D. Toshniwal, H. Speleers, T. J. R. Hughes, Smooth cubic spline spaces on unstructured quadrilateral meshes with particular emphasis on extraordinary points: Geometric design and isogeometric analysis considerations. *Computer Methods in Applied Mechanics and Engineering*, 327, 411–458, 2017.

## Computational Design of Lattice Models of Next-generation Structural Materials under Testing

Ida Mascolo<sup>\*</sup>, Mariano Modano<sup>\*\*</sup>, Francesco Fabbrocino<sup>\*\*\*</sup>, Francesco Colangelo<sup>\*\*\*\*</sup>, Ilenia Farina<sup>\*\*\*\*\*</sup>

<sup>\*</sup>University of Salerno, Italy, <sup>\*\*</sup>University of Naples Federico II, Italy, <sup>\*\*\*</sup>Pegaso Telematic University, Italy,  
<sup>\*\*\*\*</sup>University of Naples Parthenope, Italy, <sup>\*\*\*\*\*</sup>University of Naples Parthenope, Italy

### ABSTRACT

Keywords: Tensegrity, prestress, frequency bandgaps. Recent studies have explored the use of additively manufactured reinforcing elements of innovative construction materials, which consist of fibers with structural hierarchy manufactured from computer-aided design (CAD) data, employing additive manufacturing techniques based either on photopolymers (SLA) and the electron beam melting (EBM) of a metallic powder [1][2]. The present study employs strut-and-tie lattice models [3][4] to capture the experimental response of such materials under short-beam shear tests, which are aimed at determining the first-crack strength and toughness of the material. A comparative theory vs. experiment study shows that the employed lattice models accurately describe the actual response of prismatic elements in correspondence with the cracked regime. Their use to predict the mechanical properties of nextgeneration composite materials, such as, e.g., the overall strength and fracture toughness of totally or partially additively manufactured composites, awaits attention.

## Automated Conformal Discretization Of Complex Heterogeneous Microstructures

Thierry J. Massart<sup>\*</sup>, Karim Ehab Moustafa Kamel<sup>\*\*</sup>, Bernard Sonon<sup>\*\*\*</sup>

<sup>\*</sup>Université libre de Bruxelles (ULB), <sup>\*\*</sup>Université libre de Bruxelles (ULB), <sup>\*\*\*</sup>Université libre de Bruxelles (ULB)

### ABSTRACT

The response of heterogeneous materials is highly dependent on their micro-morphology. Fine scale constitutive models are therefore developed to establish a link between experimental observations and the physical underlying mechanisms, coupled to information on the morphology of microstructures of interest. Such ingredients are nowadays routinely upscaled using computational homogenization techniques. However, this requires the availability of some Representative Volume Elements (RVEs) of the microstructure, which can be obtained either experimentally (e.g. CT scans) or numerically by using algorithms aiming to reproduce the main micro-morphological features [1]. The complexity of discretizing complex geometries motivated the development of XFEM approaches based on the concept of partition of unity over the last decade. The use of available conventional finite packages is however still of interest for multi-scale analyses as it allows using existing formulations and constitutive models, especially when large strains and/or coupled processes are considered. This motivated the development of a hierarchical Delaunay mesh generator based on an extended Persson-Strang truss analogy optimization [2], and using an input level set function in order to produce conformal tetrahedral meshes. A local control of element sizes is enforced using an analogy with the equilibrium of a truss system made of the element edges. Desired bar lengths evaluated from a constructed element size function are used in combination with distances from material interfaces to compute nodal forces acting on the truss nodes to converge to an equilibrated truss situation when the targeted element size is reached. A mesh of material interfaces is first obtained starting from an initial Delaunay surface mesh. An optimized shape of these surface elements is reached by controlling their size with a tension/compression force field in the bars to reach the targeted lengths. This is achieved while preventing nodal displacements away from interfaces based on a level set (distance) function. A 3D mesh is subsequently obtained based on same optimization principles, using a constrained Delaunay generation based on the material interfaces discretization. The versatility of the approach will be illustrated based on computationally generated RVEs for 3D woven composites and porous materials; as well as for experimentally obtained images of metallic materials. [1] B. Sonon, B. François, T.J. Massart (2012). A unified level set based methodology for fast generation of complex microstructural multi-phase RVEs. *Comp. Meth. Appl. Mech. Engng.*, 223–224, 103-122. [2] P.O. Persson and G. Strang (2004). A simple mesh generator in MATLAB, *SIAM Review*, 46(2), 329-345.

## Cut Discontinuous Galerkin Methods for Surface and Multi-dimensional Coupled Problems

Andre Massing\*, Ceren Gürkan\*\*

\*Umeå University, \*\*Umeå University

### ABSTRACT

In this talk, we present novel stabilized cut discontinuous Galerkin methods (cutDGM) for the numerical treatment of surface and multi-dimensional problems coupling partial differential equations on domain of different topological dimensionality. The domains of interest such the surface or the bulk domain can be embedded arbitrarily into a background mesh and are generally not fitted to it. To remedy the numerical challenges caused by small cut cells, we combine stabilization techniques from the cut finite element method [1] with the interior penalty discontinuous Galerkin methods (DG) for elliptic [2] and hyperbolic problems [3]. Using only a few abstract assumptions on the employed cutDG stabilization, we can establish geometrically robust optimal a priori error and condition number estimates irrespective of how the embedded geometry cuts the background mesh. Motivated by flow and transport problems in fractured porous media, the theoretical properties are corroborated by a number of numerical experiments for surface problems, interface problems on surfaces and coupled surface/interface-bulk problems. REFERENCES [1] E. Burman, S. Claus, P. Hansbo, M. G. Larson, and A. Massing. CutFEM: discretizing geometry and partial differential equations. *Internat. J. Numer. Meth. Engrg.*, 104(7):472- 501, November 2015. [2] D.N. Arnold. An interior penalty finite element method with discontinuous elements. *SIAM J. Num. Anal.* , 19(4):742-760, 1982. [3] F. Brezzi, L. D. Marini, and E. Süli, *Math. Models Methods Appl. Sci.* 14(12):1893-1903, 2004.

## A Discontinuous Galerkin Method for Thermoelasticity at Finite Strains

Arif Masud\*, Pinlei Chen\*\*

\*University of Illinois at Urbana-Champaign, \*\*University of Illinois at Urbana-Champaign

### ABSTRACT

This talk presents a stabilized Discontinuous Galerkin (DG) method at finite strains for thermomechanical problems that have embedded weak and strong discontinuities in the mechanical and thermal fields. The new method is designed to address technical issues that present themselves in the emerging field of additive manufacturing. Starting from a thermomechanically coupled formulation, a Lagrange multiplier method is developed that couples fields across the embedded interfaces. Employing ideas from VMS based stabilization that are applied to internal interfaces arising across discontinuities, an interfacial fine scale problem is derived. The interfacial fine scales are expanded via edge bubbles and are resolved locally to extract analytical models for Lagrange multipliers in terms of the jumps in the fields and their fluxes. Since the derived expressions are a function of the mechanical and thermal fields, the resulting stabilized formulation contains numerical flux and stability tensors that provide an avenue to variationally embed interfacial kinetic and kinematic models for a robust representation of interfacial physics. A significant contribution of the method is that it is free of any ad hoc or user defined parameters. Several benchmark problems are presented to show stability and variational consistency of the method. References: [1] A. Masud and T. Truster, A Framework for Residual-Based Stabilization of Incompressible Finite Elasticity: Stabilized Formulations and F-bar Methods for Linear Triangles and Tetrahedra. *Computer Methods in Applied Mechanics and Engineering*, vol. 267, 359-399, 2013. [2] P. Chen, T.J. Truster, and A. Masud, Interfacial Stabilization at Finite Strains for Weak and Strong Discontinuities in Multi-Constituent Materials. *Computer Methods in Applied Mechanics and Engineering*. 328, 717–751, 2018.

## Prediction of Numerical Analysis Results using Machine Learning

Masato Masuda\*, Yasushi Nakabayashi<sup>†</sup>, AND Yoshiaki Tamura<sup>††</sup>

\*Center for Computational Mechanics Research, Toyo University  
1-1-1, Yayoi, Bunkyo, Tokyo, Japan  
masuda.masato@mail.u-tokyo.ac.jp

<sup>†</sup>Toyo University  
2100, Kujirai, Kawagoe, Saitama, Japan  
nakabayashi@toyo.jp

<sup>††</sup>Toyo University  
2100, Kujirai, Kawagoe, Saitama, Japan  
tamura@toyo.jp

**Key words:** CFD, Convolutional Neural Network(CNN), Long Short-Term Memory(LSTM), Convolutional LSTM

**Abstract.** This study is to predict the solution of the nonlinear problem of computational fluid dynamics (CFD) using machine learning. We predict the results of CFD analysis using Convolutional LSTM(Long Short-Term Memory) which expanded to handle time series data based on Convolutional Neural Network. In this paper, we did not use physical quantities of CFD results. For simplicity, we used visualized images of CFD results. A visualized image of a vorticity field (1-channel) was used for learning. The training image and the untrained image were input using the model after learning and the learning accuracy was verified by Mean Squared Error and Structural Similarity Index Measure. In addition, assuming that physical quantities are to be input, learning is performed by increasing the number of channels of the image to 2-channels. It was confirmed that learning accuracy was the same as in the case of 1-channel.

### 1 Introduction

In recent years, an artificial intelligence boom is coming back by the image recognition competition<sup>[1]</sup> and Google's cat<sup>[2]</sup>. In this artificial intelligence boom, research and development using deep learning is mainstream. In image recognition, it is known that CNN (Convolutional Neural Network) can obtain better results than conventional feature extraction techniques<sup>[1]</sup>, and is widely used not only in images but also in many fields such as speech recognition<sup>[3]</sup>. In deep learning, LSTM (Long Short-Term Memory) which extends Recurrent Neural Network (RNN) is used to realize learning that adds temporal state information<sup>[4]</sup>.

On the other hand, in the field of numerical analysis, highly accurate analysis using computer power is very active <sup>[5]</sup> <sup>[6]</sup>, such as ultra-large-scale analysis, coupled analysis, multiscale analysis, complex shape analysis, etc. However, it takes a lot of time for ultra-large-scale analysis or complicated analysis, and calculation may take time from several days to several weeks in one case. Therefore, if we could know the approximate analysis result in advance, we can obtain clues for detailed analysis. Therefore, it is thought that reduction of the number of trials of analysis leads to shortening of total analysis time. Besides, convergence of the calculation could be improved by predicting the initial value in the internal iterations of an implicit solution.

The final goal of this research is prediction of numerical analysis results using deep learning. We construct a network that predicts the state at the next time from the state of arbitrary analysis time. Since the analysis results of numerical analysis have physical quantities on nodes, the spatial information is very important. CNN is capable of feature extraction maintaining spatial information. However, although CNN can hold spatial information, it is not good to hold time information. On the other hand, LSTM is good at handling time information, but it cannot handle spatial information. So, we use Convolutional LSTM (ConvLSTM)<sup>[7]</sup> which combines the advantages of the two methods. It combines features that can keep spatial information holding of CNN and handling time series of LSTM. Originally, ConvLSTM is a network developed to predict future images from moving images. By giving the physical quantity of the node as the input channel of the convolution layer, it is possible to predict the numerical analysis result by treating the node information as spatial information. In this paper, we propose to use ConvLSTM for prediction of numerical analysis result. In this paper, in order to investigate whether it is possible to predict the analysis result, learning was performed using images visualizing the vorticity of the analysis result. By using the visualized image, it is possible to represent part of the physical quantity of the analysis result, simplifying the coding and speeding up the learning. We use the trained ConvLSTM to predict the analysis result and compare it with the correct image. And we demonstrate the usefulness of the proposed method. MSE and SSIM are used as quantitative evaluation. In addition, we added images of pressure field to the network input. This is 2-channels learning. This is an experiment to increase the number of channels for the physical quantities as input in future. It confirms that there is no problem in prediction accuracy even when the number of channels increases.

## 2 Convolutional LSTM<sup>[7]</sup>

LSTM is one type of method for estimating the future state based on temporal state information. LSTM conventionally calls 1-dimensional feature quantity information recursively. When predicted, input vector of the current step and feature quantity vector of the previous step are merged and treated as input information for learning. Convolutional LSTM (ConvLSTM) can extend the 1-dimensional feature information to 2-dimensional Convolutional layer and store past input information. Therefore, it is possible to track spatial information temporally. Equation 1 shows each gate and activation function of ConvLSTM.

$$\begin{aligned}
 i_t &= \sigma\left(W_{xi} * X_t + W_{hi} * \mathcal{H}_{t-1} + W_{ci} \circ C_{t-1} + b_i\right) \\
 f_t &= \sigma\left(W_{xf} * X_t + W_{hf} * \mathcal{H}_{t-1} + W_{cf} \circ C_{t-1} + b_f\right) \\
 C_t &= f_t \circ C_{t-1} + i_t \circ \tanh\left(W_{xc} * X_t + W_{hc} * \mathcal{H}_{t-1} + b_c\right) \\
 o_t &= \sigma\left(W_{xo} * X_t + W_{ho} * \mathcal{H}_{t-1} + W_{co} \circ C_t + b_o\right) \\
 \mathcal{H}_t &= o_t \circ \tanh\left(C_t\right)
 \end{aligned} \tag{1}$$

Here,  $X$  represents the input group,  $\mathcal{H}$  is the state of the hidden layer, and  $C$  is the output of the cell.  $i, f, o$  represent the gates of input, forget, and output, respectively.

These variables have a 3rd-order tensor, which time  $t$  and 2-dimensional spatial information (row, column). The calculation symbol "\*" is the convolution product, and "o" is the Hadamard product.

## 3 Analysis data for learning

Deep learning and neural networks require a lot of training data. Training data must be correct combination data of input vector and output vector. ConvLSTM generally uses image data for both input and output. The input and output vector used in this research are visualized images of analysis results. By replacing this image data with the physical quantity of the numerical analysis result, it is possible to predict the physical quantity of the numerical analysis result. For simplicity, this time visualized image data is assumed.

The analysis model is an incompressible flow around a two-dimensional cylinder, and the computational domain was discretized with  $1250 \times 800$  equidistant Cartesian grid. The pseudo compressibility method was used for analysis method, and the third order upwind difference was used for the convective terms. The analysis conditions are shown in Table 1.

Table 1 Analysis conditions

Cylinder Diameter	40
Reynolds number	1,000
Courant number	0.25

The training data is image data visualizing the vorticity distribution of the numerical analysis result. One image is generated every 100 steps and 300 images are collected. The image size is  $512 \times 476$  pixels, and by expressing it in gray scale of 256 gradations, the channel of the Convolutional layer is taken as 1-channel of vorticity distribution. The image was trimmed with a size of  $200 \times 100$ , that the flow field of the cylinder and the cylinder wake was captured. In this paper, we created the learning data to predict the input of the past 4 frames and an image of the future vorticity fields 1 frame later. Also, training data was created from the pressure field likewise. The training data of the pressure field is learned together with the vorticity field at the time of learning of two channels.

#### 4 Construction of learning device

The input to the network is the image size (200, 100), the input image is a visualized grayscale image of the vorticity distribution, and the number of channels is (1). When the pressure field is also used, the number of channels is (2). Therefore, the input vector is (200, 100, 1 or 2). In this network, 4-layers of ConvLSTM are laminated from the input layer, and in the uppermost layer, 3-dimensional Convolutional layer is arranged. We built a total of 6-layers of networks. Figure 1 shows the network structure for 1-channel. The kernel size of ConvLSTM was set to  $(3 \times 3)$  for all layers. The inputs of the three dimensional Convolutional layer(the uppermost layer) are (20, 4, 200, 100) and the kernel size is  $(3 \times 3 \times 3)$ . The stride was (1, 1) and (1, 1, 1) in all layers. The loss function cross entropy was adopted for the loss function, optimization used Adadelta, weights were modified by back propagation method.

## 5 Results of Learning

The data of 250 images (frame number  $t = 0$  to 249) were used as the input data for training. The number of epochs is 10,000. First, using the learned model, the image used for learning was given to the input, and the predicted image was generated. The predicted image is shown in Fig.2. In Fig.2, "Actual" is a visualized image of numerical analysis result. "Predicted" is an image predicted by input data of 4 visualized images of the numerical analysis results from 4 frames before. For example, images of time  $t-3$ ,  $t-2$ ,  $t-1$ ,  $t$  are given to input data, and an image of time  $t+1$  is predicted. Although the prediction results of training data are shown in this paper, similar results were obtained for untrained input data. The prediction result in the case of 2-channels is shown in Fig.3. And the output images were evaluated by MES (Mean Square Error) and SSIM (Structural Similarity Index Measure) (Table 2). Each calculation formula is shown below. MES is an indicator of how much difference is between the images. When the value is small, the error of the image is small. SSIM is an image similarity index. Similarity is high if the value is close to 1.

$$MES = \frac{1}{row \cdot col} \sum_{i=0}^{row-1} \sum_{j=0}^{col-1} (Actual - Predicted) \quad (2)$$

$$SSIM(x, y) = \frac{(2\mu_x\mu_y + C_1)(2\sigma_{xy} + C_2)}{(\mu_x^2 + \mu_y^2 + C_1)(\sigma_x^2 + \sigma_y^2 + C_2)} \quad (3)$$

Here, row and col represent image sizes, and Actual and Predicted are correct images and predicted images. Taking the square root of MES gives the difference in gradation of the pixel. It is the average of pixel differences across the images. SSIM is calculated for each small area (window) in the image, and the average value of the entire an image is calculated. Equation 3 indicates a process on window.  $x, y$  are index having each pixel in the window as an element.  $\mu$  is the average value of pixels in each window.  $\sigma_x, \sigma_y$  are standard deviations of pixel values within the window.  $\sigma_{xy}$  is the covariance of  $x$  and  $y$ .  $C$  is a constant, here  $C_1 = (0.01 \times 255)^2$ ,  $C_2 = (0.03 \times 255)^2$  were used.

From Fig.2, we can see that predictive images similar to "Actual" are obtained by learning. The vortices in the wake are slightly blurry, but it seems to be maintaining a qualitatively correct structure. In addition, the SSIM of the quantitative evaluation result of Table 2 shows prediction accuracy about 70%. From the results, it was confirmed that structurally similar images were output. Since MES also shows a relatively low value, it was confirmed that ConvLSTM can be predicted to some extent. Even when the number of input channels is increased, the results are the same as for single channel.

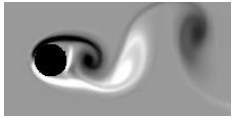
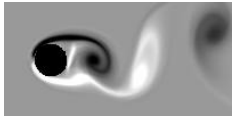
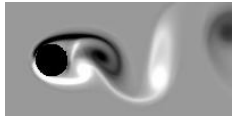
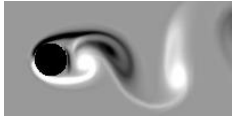
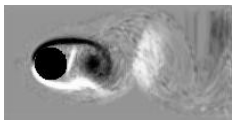
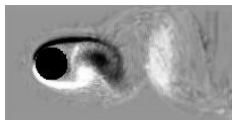
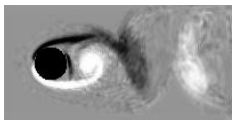
	t-1	t	t+1	t+2
Actual (Vorticity)				
Predicted (Vorticity)				

Fig.2 Prediction of analysis results using Convolutional LSTM (t is frame of figure, t=31.)

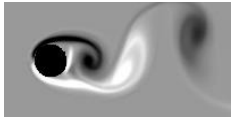
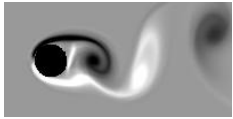
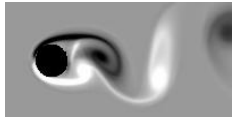
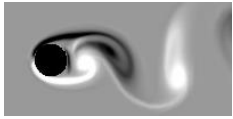
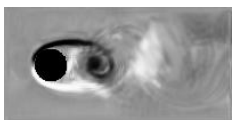
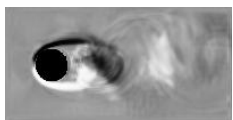
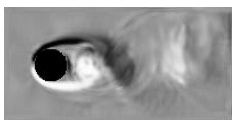
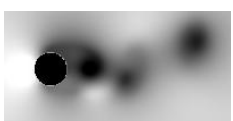
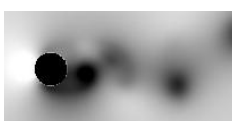
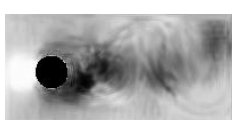
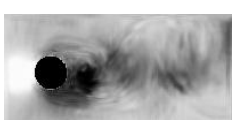
	t-1	t	t+1	t+2
Actual (Vorticity)				
Predicted (Vorticity)				
Actual (Pressure)				
Predicted (Pressure)				

Fig.3 Prediction of analysis results by 2-channels (t is frame of figure, t=31.)

Table 2 Result of MES & SSIM  
(1ch is only vorticity field, 2ch is both fields of vorticity and pressure)

		t	t+1	t+2
1ch	MES (Vorticity)	248.862	257.929	127.669
	SSIM (Vorticity)	0.7196	0.750	0.759
2ch	MES (Vorticity)	357.922	361.254	322.959
	MES (Pressure)	501.031	381.589	327.583
	SSIM (Vorticity)	0.728	0.722	0.723
	SSIM (Pressure)	0.702	0.719	0.724

## 6 Conclusions

In this research, we proposed to use ConvLSTM for prediction of numerical analysis results. Numerical analysis results of 1 or 2 channels were predicted using training data. The obtained results are as follows.

- (i) We succeeded in generating the visualized image of the next frame by giving the visualized image of the analysis result of the past 4 frames to the input.
- (ii) It was confirmed that prediction images can be generated even when 2 images of vorticity and pressure are given to the input, and increasing the number of channels does not affect the prediction accuracy.
- (iii) We evaluated output images by MES and SSIM. The SSIM results showed about 70% similarity. Moreover, it was found that the error per pixel in the MES result is relatively small.

It was confirmed that ConvLSTM is useful for predicting numerical analysis results. In the future, we implement the following two things. First, we will change the input vector from image to physical quantity. Next, we will implement algorithms to learn the whole calculation area.

## Acknowledgements

This research was partly supported by grants from the Project of the NARO Bio-oriented Technology Research Advancement Institution(R&D matching funds on the field for Knowledge Integration and innovation).

## REFERENCES

- [1] Alex Krizhevsky, Ilya Sutskever, Geoffrey E. Hinton, ImageNet Classification with Deep Convolutional Neural Networks, NIPS2012, 2012.
- [2] Quoc V. Le, Marc’Aurelio Ranzato, Rajat Monga, Matthieu Devin, Kai Chen, Greg S. Corrado, Jeff Dean, Andrew Y. Ng, Building High-level Features Using Large Scale Unsupervised Learning, International Conference on Machine Learning, 2012.

- [3] Alex Graves, Abdel-rahman Mohamed, Geoffrey Hinton, Speech recognition with deep recurrent neural networks, IEEE International Conference on Acoustics, Speech and Signal Processing, pp.6645-6649, 2013.
- [4] Klaus Greff, Rupesh Kumar Srivastava, Jan Koutník, Bas R. Steunebrink, Jürgen Schmidhuber, LSTM: A Space Odyssey, arXiv:1503.04069, 2015.
- [5] Masao OGINO, Kaworu YODO, Ryuji SHIOYA, Hiroshi KAWAI, Two-level extension of the hierarchical domain decomposition method, Mechanical Engineering Letters, vol.4(No.18-00088) 1-8, 2018.
- [6] Yuri Bazilevs, Kenji Takizawa, Tayfun E. Tezduyar, Computational Fluid-Structure Interaction: Methods and Applications, Wiley, 2013.
- [7] Xingjian Shi, Zhourong Chen, Hao Wang, Dit-Yan Yeung, Wai-kin Wong, Wang-chun Woo, Convolutional LSTM Network: A Machine Learning Approach for Precipitation Nowcasting, arXiv:1506.04214v2, 2015.

## Integrated Computational Materials Engineering

Karel Matous\*

\*University of Notre Dame

### ABSTRACT

With concentrated efforts from the material science community to develop new multifunctional materials using unique processing conditions, the need for modeling tools that accurately describe the physical phenomena at each length scale has only further been emphasized. For example, additive manufacturing and shock synthesis lead to unique material morphologies that need to be understood for reliable engineering analysis and product safety assessments. Considering these material complexities, Direct Numerical Modeling (DNM) is accessible only for moderate system sizes. Thus, a multiscale strategy must recognize that just a relatively small part of the material will typically be instantaneously exposed to rapid material transformations. Macroscopic constitutive models obtained from homogenization, of the complex but slowly varying microstructure, may adequately describe the rest of the material. Nonlinear model reduction, pattern recognition and data-mining are a key to future on-the-fly modeling and rapid decision making. To address these challenges, we present an image-based (data-driven) multiscale framework for modeling the chemo-thermo-mechanical behavior of heterogeneous materials while capturing the large range of spatial and temporal scales. This integrated computational approach for predicting the behavior of complex heterogeneous systems combines macro- and micro-continuum representations with statistical techniques, nonlinear model reduction and high-performance computing. Our approach exploits the instantaneous localization knowledge to decide where more advanced computations are required. Simulations involving this wide range of scales,  $O(10^6)$  from nm to mm, and billions of computational cells are inherently expensive, requiring use of high-performance computing. Therefore, we have developed a hierarchically parallel high-performance computational framework that executes on hundreds of thousands of processing cores with exceptional scaling performance. Any serious attempt to model a heterogeneous system must also include a strategy for constructing a complex computational domain. This work follows the concept of data-driven (image-based) modeling. We will delineate a procedure based on topology optimization and machine learning to construct a Representative Unit Cell (RUC) with the same statistics (n-point probability functions) to that of the original material. Our imaging sources come from micro-computed-tomography (micro-CT), focused ion beam (FIB) sectioning, and advanced photon source nano-tomography at the Argonne National Laboratory. We show that high-performance DNM of these statistically meaningful RUCs coupled on-the-fly to a macroscopic domain is possible. Therefore, well-resolved microstructure-statistics-property (MSP) relationships can be obtained. Finally, the integrated V&V/UQ program with co-designed simulations and experiments provides a platform for computational model verification, validation and propagation of uncertainties.

## Space-time Characterization of Macroscopic Thermo-Mechanical Behavior Reflecting Microscopic Unsteady Heat Conduction

Seishiro Matsubara<sup>\*</sup>, Kenjiro Terada<sup>\*\*</sup>

<sup>\*</sup>Tohoku University, <sup>\*\*</sup>Tohoku University

### ABSTRACT

The present study proposes a method of space-time characterization of the macroscopic thermo-mechanically coupled behavior in consideration of the microscopic unsteady heat conduction. An emphasis is placed on how the unsteadiness of microscopic temperature distribution affects the macroscopic thermo-mechanical behavior. The incremental variational formulation (IVF) [1] is employed to define the global and local saddle point problems for thermo-mechanically coupled phenomena within a certain time interval. The unsteadiness of heat conduction arises from the time rate of entropy change, which is determined by not only the thermal expansion and specific heat in the case of thermo-elastic solids, but also the inelastic part of free energies in general dissipative solids. In fact, the heat sources due to self-generated heat are formulated as the gradients of the inelastic dual dissipation potential with respect to the rates of both the deformation and state variables, and in turn affect the unsteadiness of heat conduction involving for general dissipative solids. To this end, the relationship between time rates of micro- and macroscopic entropies must be determined through appropriate numerical material testing within the standard computational homogenization framework that enables us to characterize the macroscopic heat conduction under the assumption that both the geometry of microstructures of composites under consideration and the time evolution are periodic. Nonetheless, since the temporal scale need not be periodic in the present problem setting, the standard space-time homogenization scheme cannot be applied. Instead, we introduce the concept of time-homogenization that defines the macroscopic time increment by the time spent to attain the microscopic steady state. We begin with formulating two-scale problem under the assumption of periodicities of state variables in space and time along the line of the two-scale spatial discretization approach [2] and then the integration factor in the IVF is utilized to define the micro- and macroscopic time scales. Several numerical examples are presented to demonstrate the idea and concept of our new space-time homogenization for thermo-mechanical coupled problems. A series of numerical material testing are performed to illustrate the capability in characterizing the macroscopic thermo-mechanical behavior reflecting the microscopic unsteady heat conduction. [1] Q. Yang and L. Stainier and M. Ortiz: A variational formulation of the coupled thermomechanical boundary-value problem for general dissipative solids, *J. Mech. Phys. Solids*, Vol.54 (2006), No.2, pp.401-424. [2] I. Temizer and P. Wriggers: Homogenization in finite thermoelasticity, *J. Mech. Phys. Solids*, Vol.59 (2011), No.2, pp.344-372.

## **Development of Homeschooling Support Framework Using Desktop Robotic Arm with Computer Vision**

Masami Matsumoto\*

\*National Institute of Technology, Yonago College

### **ABSTRACT**

In this research, we propose a Problem Solving Environment (PSE) for education that supports homeschooling using robotic arm with computer vision. A useful system is necessary for science, technology, engineering, mathematics (STEM) education. The purpose of this research is to develop self-study support system using information communication (ICT) environment. The developed system consists of four hardware elements: a system control unit, a robotic arm, a smart pad, and a camera. The framework developed for operating the system interactively controls the robotic arm by using the image analysis result photographed by the two cameras. This system is built by Linux system on a small single board computer developed to promote the basic computer science lecture. The robotic arm is controlled by the G-code sent from the control unit via the serial line. G-code is used for head control of numerical control (NC) machines and 3D printers, and porting to other systems is also easy. Users can interactively use the basic actions registered in the library. Images from two cameras attached to the overhead view camera and robotic arm are analyzed by the computer. By exchanging data with the GPU server on the Internet via wireless LAN, various processing becomes possible. Since, this system can be expected to increase the visual effect by using the robot arm with motion as the user interface. This system provides scoring, searching, and task management functions. Problems imposed on users are semi-automatically generated from Web pages provided in Wikipedia format. The answers solved on a paper basis can also be scored by the robotic arm. Users create their own drill type problems and learn by scoring interactively. Simultaneously, handwritten characters are recognized by Artificial Intelligence (AI) system, and information is digitized and stored. In addition, a problem management system using the Web is provided. The management system provides guidance that makes task deadlines important. Give the user a badge to accomplish the task within the deadline and admire it. It is also expected to expand the voice operation function by introducing the smart speaker. Practice of science and technology education is an important issue in modern society. The user extends the framework provided in this research and pushes forward homeschooling.

## Boundary Integral Based Method for Treatment of Solid Wall in a Particle Method

Takuya Matsunaga<sup>\*</sup>, Kazuya Shibata<sup>\*\*</sup>, Seiichi Koshizuka<sup>\*\*\*</sup>

<sup>\*</sup>Department of Systems Innovation, The University of Tokyo, <sup>\*\*</sup>Department of Systems Innovation, The University of Tokyo, <sup>\*\*\*</sup>Department of Systems Innovation, The University of Tokyo

### ABSTRACT

Many important applications in engineering involve an incompressible fluid flow with moving boundaries. For such background, particle methods in computational fluid dynamics have been becoming more important. One representative particle method for incompressible fluid dynamics is the moving particle semi-implicit (MPS) method. When it first emerged, a solid wall was represented by a set of spatially-fixed particles called wall particles [1]. While the representation by wall particles has high numerical stability and thus reliable, difficulties are encountered when it is used for complicated geometry, especially in three dimensions. On the other hand, the polygon wall boundary model proposed by Harada et al. (2008) [2] is known suited for such cases. It represents solid wall by surface mesh (a set of polygons). Thus, even in three dimensions it can be handled easily using CAD tools. Today, this technique has been used widely in engineering applications. However, it is known that unphysical behaviors of particles are often observed, and improvement of accuracy is desired. In these circumstances, this study has been done to propose a novel numerical treatment for solid wall boundary. In our approach, wall geometry is represented by a surface mesh and thus suited for problems with three-dimensional complicated boundaries. The wall contribution is derived using the integration over boundary surface. Since present method considers boundary shape more precisely, computational accuracy is expected to be improved compared to the polygon wall boundary model. Main differences between other boundary integral based approaches such as by Feldman and Bonet (2007) [3] and ours are related to derivation of the wall contribution term in discrete equation. In the present scheme, not only the particle number density but also the spatial derivatives are evaluated considering the volume integration over truncated domain. The volume integrations are mathematically transformed into the surface integral form using the divergence theorem. The proposed method was applied to several test problems. As a result, it was clarified that the present boundary integral based scheme has an accuracy comparable with the wall particle method and much better than the polygon wall boundary model. [1] S. Koshizuka et al., *Int. J. Numer. Methods Fluids* 26, 751-769 (1998). [2] T. Harada et al., *Transactions of JSCES*, 20080006 (2008). (in Japanese) [3] J. Feldman and J. Bonet, *Int. J. Numer. Meth. Engng.* 72, 295-324 (2007).

## Uncertainty Quantification in Drug-induced Arrhythmias

Kristen Matsuno<sup>\*</sup>, Franciso Sahli<sup>\*\*</sup>, Paris Perdikaris<sup>\*\*\*</sup>, Jiang Yao<sup>\*\*\*\*</sup>, Ellen Kuhl<sup>\*\*\*\*\*</sup>

<sup>\*</sup>Stanford University, <sup>\*\*</sup>Stanford University, <sup>\*\*\*</sup>Massachusetts Institute of Technology, <sup>\*\*\*\*</sup>Dassault Systemes,  
<sup>\*\*\*\*\*</sup>Stanford University

### ABSTRACT

The QT interval of an electrocardiogram signal, which begins with the activation of the ventricles and ends with their recovery, is a function of both heart rate and ventricular repolarization time. A prolonged QT interval is typically indicative of a patient's vulnerability to Torsade de Pointes, a potentially fatal arrhythmia characterized by rapid depolarization and repolarization of the ventricles. Various drugs have undesired side effects associated with a prolongation of the QT interval and an increased pro-arrhythmic risk. Two landmark parameters that quantify the effect of drug are the drug concentration IC<sub>50</sub> at 50% blockage of an ion channel, and the slope,  $h$  of the dose-response curve at this point. Here we present a novel high resolution, multi-scale, multi-fidelity computational model to predict the QT interval for a wide ranges of IC<sub>50</sub> and  $h$  values [0]. The experimental variability of these two parameters is the origin of uncertainty in the model. Using previously developed hierarchical Bayesian inference methods [2], we sample a set of 500 IC<sub>50</sub> and  $h$  parameter pairs from the experimental dose-response data for 30 common drugs [1]. For each pair of parameters and a chosen drug concentration, we calculate the conductance block of a specific ion channel. Using these ion channel blocks, we adopt a multi-fidelity model to predict a set of QT intervals via Gaussian process regression. We use Gaussian kernel density estimations to produce the probability density function of the QT interval at each concentration. Our uncertainty quantification reveals that, for a compound with three dose-response experiments, the QT interval has up to 76% variability at the maximum concentration compared to a baseline case of zero concentration and zero ion channel blockage. Our results contribute to predict the pro-arrhythmic risk of common drugs and assess their effect on cardiovascular performance. [0] F. Sahli, J. Yao, E. Kuhl. Predicting drug-induced arrhythmias by multiscale modeling. 2017; submitted. [1] Johnstone RH, Bardenet R, Gavaghan DJ and Mirams GR. "Hierarchical Bayesian inference for ion channel screening dose-response data" [version 2; referees: 2 approved] Wellcome Open Research 2017, 1:6 (doi: 10.12688/wellcomeopenres.9945.2) Copyright: © 2017 Johnstone RH et al. [2] Crumb, William J., et al. "An evaluation of 30 clinical drugs against the comprehensive in vitro proarrhythmia assay (CiPA) proposed ion channel panel." Journal of pharmacological and toxicological methods 81 (2016): 251-262.

## A Padé-localized Absorbing Boundary Condition for 2D Time-harmonic Elastodynamic Scattering Problems

Vanessa Mattesi<sup>\*</sup>, Marion Darbas<sup>\*\*</sup>, Christophe Geuzaine<sup>\*\*\*</sup>

<sup>\*</sup>University of Liège, Belgium, <sup>\*\*</sup>University of Picardie Jules Verne, Amiens, France, <sup>\*\*\*</sup>University of Liège, Belgium

### ABSTRACT

We focus on the construction of an absorbing boundary condition (ABC) for 2D isotropic elastic waves in high frequency regime. Problem statement We consider a spherical obstacle of radius  $r_{int}$ , the propagation domain is its complementary into the plane. Considering a time-harmonic incident wave, the scattering problem is formulated as follows: find the displacement in domain solution to the Navier equation with a Dirichlet boundary condition on the boundary of the obstacle and satisfying the Kupradze radiation conditions at infinity. The stress tensor is isotropic. In view of a finite element discretization, the infinite media is truncated by an artificial boundary, which delimits the bounded domain under study. On the fictitious boundary, we put an ABC involving an absorbing operator. Comparisons of two ABCs Multiple choices are possible for the absorbing operator  $\mathcal{B}$ , the optimal operator being the exact exterior Dirichlet-to-Neumann map. We investigate two approximations: \*The Lysmer and Kuhlemeyer condition: We point out the limitations of this low-order condition in high-frequency regime and/or with incident S-waves. It motivates the investigation of a high-order condition. \*A Padé-localized condition: it involves the tangential Günter derivative [1] and two operators using Padé local representations of the inverse of the square-root operator with rotating branch-cut [2]. We detail the choice of the different parameters and the construction of this high-order condition which is an adaptation of Chaillat et al. [1] to the 2D case. Numerical simulations in low and high frequency regime attest the efficiency of this ABC. [1] S. Chaillat, M. Darbas and F. Le Louër, Approximate local Dirichlet-to-Neumann map for three-dimensional time-harmonic elastic waves, in Computer Methods in Applied Mechanics and Engineering, 297 (2015), pp. 62-83. [2] S. Chaillat, M. Darbas and F. Le Louër, Fast iterative boundary element methods for high-frequency scattering problems in 3D elastodynamics, in J. Comput. Phys. 341 (2017), pp. 429-446.

## Bayesian Inverse Problems and Low-Rank Approximations

Hermann Matthies\*

\*Technische Universitaet Braunschweig, Institute of Scientific Computing

### ABSTRACT

We look at Bayesian updating in the frame work of updating a random variable (RV) whose distribution is the prior distribution. It is assumed that this RV is a function of many more elementary random variables. Furthermore it is assumed that computationally the RV is represented in either a sampling format or in a functional or spectral representation like the the polynomila chaos expansion. The samples resp. the coefficients may be viewed as a high degree tensor, and hence it is natural to assume a low-rank approximation for this. Conditioning, the central element of Bayesian updating, is theoretically based on the notion of conditional expectation. Here we use this construct also as the computational basis, namely the ability to compute conditional expectations. With this in hand, we formulate an updating process, which produces a new RV through successively finer approximations, whose law resp. distribution is the sought posterior distribution. This is in effect a kind of filter. It will be shown that it the filter can be computed using low-rank tensor approximations, and that it directly operates on the low-rank representation of the RV representing the prior, to produce a low-rank represenatation of the posterior RV.

## Calibration and Propagation of Model Discrepancy Across Experiments

Kathryn Maupin\*, Laura Swiler\*\*

\*Sandia National Laboratories, \*\*Sandia National Laboratories

### ABSTRACT

Model inadequacy due to model form error remains a concern in all areas of mathematical modeling, despite continuing advances in statistical inversion and the availability of cost-effective high-performance computing infrastructure. The Bayesian paradigm naturally integrates uncertainties from both experimental data and model formulation, including initial or boundary conditions, model form and parameters, and numerical approximation. However, model error is unavoidable in many situations due to incomplete understanding of the underlying physics, likely in addition to large and possibly poorly characterized uncertainties in calibration and validation data. Put simply, infinite amounts of data may still result in inadequate models. Model correction techniques have the potential to increase the range of applicability and enhance the predictive power of models that suffer from model-form error. It has been argued that some approaches preserve the physical meaning and improve the transferability of parameters of physics-based models. Calibrating a discrepancy model requires careful consideration regarding problem-specific formulation, parameter estimation, and uncertainty quantification. In the presence of large data sets, it may be necessary to select only those points which are the most informative of the discrepancy model. Furthermore, the validity of the original physical model, the inadequacy model, and the combined model for the prediction of quantities of interest remains in question. A generalized approach and implementation of model discrepancy detection, construction, and propagation into a predictive setting is presented in the context of Bayesian model calibration.

## The Variational Phase-field Models of Brittle Fracture with Anisotropic Surface Energy

Corrado Maurini\*, Bin LI\*\*

\*Sorbonne Universit'es, \*\*Sorbonne Universit'es

### ABSTRACT

Combining Griffith's theory and a suitable crack path selection criterion, one can successfully predict the crack path for the fracture of brittle materials with isotropic surface energy and quasi-static conditions. However, many materials have anisotropic surface energy because of their inherent microstructure or the manufacturing process, which can strongly influence the crack path. The understanding of the crack path selection criterion is under question for this case [2,3]. Experimental results [3,4] show that even a relatively small anisotropy in the surface energy always present in common materials, can cause the real crack paths to significantly deviate from those predicted with the assumption of an isotropic surface energy. The great success of the variational approach to fracture suggests that the variational model for fracture could provide a unifying and general framework capable of addressing fracture with anisotropic surface energy. A recent work [1] within the framework of variational approach to fracture had reproduced the key features of strongly anisotropic fracture and strikingly well recent experimental observations [2]. However, there are still a lot of fundamental questions that are open and need to be addressed, e.g. it is not clear that the energetic penalty for crack bending is intrinsic or extrinsic in real materials with strongly anisotropic surface energy, and what is the physical meaning of such energetic penalty; what crack path criterion in three dimensional and anisotropic surface energy setting. In this contribution, we formulate a phase-field model depending on the Hessian of phase-field, which can capture both weakly and strongly anisotropic surface energy with orthorhombic and cubic symmetry. The variational nature of the model suggests that the underlying crack-path selection principle is related to the maximum energy release rate (MERR) criterion. We verify this point by comparing the crack propagation directions observed from simulations under various loading and strength of anisotropy with MERR criterion predictions. We also analyze the energetic penalty for crack bending implicit in the model and highlight the difference of quenched crack behaviors between isotropic and anisotropic fracture surface energy. [1] B. Li, C. Peco, D. Millán, I. Arias, M. Arroyo, 2015. INT J NUMER METH ENG 102 (3-4), 711-727. [2] A. Takei, B. Roman, J. Bico, E. Hamm, F. Melo, 2013. Phys. Rev. Lett 110 (14), 144301. [3] A. Ibarra, B. Roman, F. Melo, 2016. Soft Matter 12, 5979-5985. [4] P. Judt, A. Ricoeur, G. Linek, 2015. ENG FRACT MECH 138, 33-48.

## Meshless Solution of Thermomechanical Slice Model of Continuous Casting of Steel

Boštjan Mavri?\*, Tadej Dobravec\*\*, Robert Vertnik\*\*\*, Božidar Šarler\*\*\*\*

\*Institute of Metals and Technology, Ljubljana, and University of Ljubljana, \*\*Institute of Metals and Technology, Ljubljana, \*\*\*Store Steel and Institute of Metals and Technology, Ljubljana, \*\*\*\*University of Ljubljana and Institute of Metals and Technology, Ljubljana

### ABSTRACT

The continuous casting of steel is well established process for producing steel billets, blooms and slabs used as semi-products for further downstream processing. The demand of the various steel consumers for ever higher quality products influences the steel producers to continuously improve the casting process. To achieve this, the producers increasingly rely on computer models. The traveling slice model [1] is particularly useful to model continuous casting. The model assumes that diffusion and deformation processes occur only perpendicular to the casting process and that the advection is the principal process in the direction of the casting. These assumptions, valid for most of the involved fields, allow the slice model to be computationally very effective. It can thus serve as a standard off-line tool for multiobjective optimization of the process parameters with respect to the quality and productivity as well as in on-line mode for regulation. In this work we develop a solid mechanics model to complement the existing traveling slice model of heat transport, solidification and grain growth [2]. The solid mechanics model is stated in plane stress formulation and a two-phase model is used to determine stress equilibrium of the inhomogeneous material. The governing equations are discretized by a local RBF collocation method augmented by first order monomials [3]. The shape parameter is determined automatically by adjusting the condition number of the interpolation matrix. The implicit Euler method is used to perform the time stepping to facilitate the coupling of the solid shell to the liquid through the mushy zone. The results from the mechanical model are integrated into a hot-tearing criterion and used to predict the occurrence of cracks in the material. We compare the results for the shape of the billet and the prediction of crack nucleation points with the experience from the industry. [1] A. Z. Lorbiecka et al., "Numerical modeling of grain structure in continuous casting of steel," *Comput. Mater. Contin.*, vol. 8, no. 3, pp. 195–208, 2009. [2] T. Dobravec, B. Mavri?, R. Vertnik, and B. Šarler, "Meshless modelling of microstructure evolution in the continuous casting of steel," in *Coupled problems VII?: proceedings of the VII International Conference on Coupled Problems in Science and Engineering*, Rhodes Island, 2017, pp. 156–166. [3] B. Mavri? and B. Šarler, "Local radial basis function collocation method for linear thermoelasticity in two dimensions," *Int. J. Numer. Methods Heat Fluid Flow*, vol. 25, no. 6, pp. 1488–1510, 2015.

## Continuous and Discrete Energy Based Methods for Accurate Force Computations on Shells in the Immersed Boundary Method

Ondrej Maxian<sup>\*</sup>, Andrew Kassen<sup>\*\*</sup>, Wanda Strychalski<sup>\*\*\*</sup>

<sup>\*</sup>Case Western Reserve University, <sup>\*\*</sup>University of Utah, <sup>\*\*\*</sup>Case Western Reserve University

### ABSTRACT

The immersed boundary method is a mathematical formulation and numerical method for solving fluid-structure interaction problems. For many biological problems, such as models that include the cell membrane, the immersed structure is a two-dimensional infinitely thin elastic shell immersed in an incompressible viscous fluid. When the shell is modeled as a hyperelastic material, forces can be computed by taking the variational derivative of an energy density functional. A new method for computing a continuous force functional on the entire surface of a hyperelastic elastic shell is presented. The method extends work from [1], where forces on a hyperelastic solid were computed without using stress tensors. The new method is compared to a previous formulation from [2] where the surface and energy functional are discretized before forces are computed. For the case of Stokes flow, a method for computing quadrature weights is provided to ensure the integral of the elastic spread force density remains zero throughout a dynamic simulation. Tests on the method are conducted when the shell is represented using spherical harmonics. Results show that it yields more accurate force computations than previous formulations as well as more accurate geometric information including mean curvature. The method is then applied to a new 3D model of cellular blebbing. [1] D. Devendran, C. S. Peskin, An immersed boundary energy-based method for incompressible viscoelasticity, *J. Comput. Phys.* 231 (14) (2012) 4613–4642. [2] T. G. Fai, B. E. Griffith, Y. Mori, C. S. Peskin, Immersed boundary method for variable viscosity and variable density problems using fast constant-coefficient linear solvers I: Numerical method and results, *SIAM J. Sci. Comput.* 35 (5) (2013) B1132–B1161.

## **A Multiscale Approach to Determine Permeability Tensor for Simulation of Composites Manufacturing Using RTM**

Ravisankar Mayavaram<sup>\*</sup>, Wentao Xu<sup>\*\*</sup>, Mohit Tyagi<sup>\*\*\*</sup>, Jacob Fish<sup>\*\*\*\*</sup>

<sup>\*</sup>Altair Engineering, Inc., <sup>\*\*</sup>Columbia University, <sup>\*\*\*</sup>Altair Engineering India Pvt. Ltd., <sup>\*\*\*\*</sup>Columbia University

### **ABSTRACT**

Composite materials are of great importance to aerospace and auto industry owing to the high strength to weight ratio exhibited by these materials. Resin Transfer Molding (RTM) and its variants such as VARTM are used to manufacture composite parts. Fundamentally, these processes involve infusing a preform with a thermosetting resin. In the numerical simulation of an RTM process, one of the major challenges is to have an accurate characterization of the material preform data. This is an expensive procedure and not offered as part material characterization services by most laboratories. We aim to address this challenge by numerically determining the permeability tensor of the preform using multiscale modeling. This numerical determination is performed using Altair's commercial CFD solver AcuSolve® and the subsequent RTM simulation is done using HyperXtrude®-RTM solver. We first determine the permeability tensor by taking into account the periodic microstructures in the preform and the Darcy's law. Using the microscale permeability, we then perform the mesoscale modeling. Finally, we upscale mesoscale permeability to perform macroscale RTM simulation at an optimal cost and increased accuracy. We demonstrate this approach by performing RTM simulation of a cylindrical pressure vessel with hemispherical ends. This simulation involves the use of multiple local coordinate systems. Results demonstrate an innovative approach to perform a complete simulation of the RTM process starting with material characterization.

## Parameter Estimation and Uncertainty Quantification in Hurricane Storm Surge Modeling

Talea Mayo\*

\*University of Central Florida

### ABSTRACT

Storm surges pose a significant threat to coastal regions. They are the primary cause of life and property loss during a hurricane. Real-time forecasting as well as long-term risk analysis are both critical to protecting coastal environments and their inhabitants. Due to the sparsity of hurricanes and storm surge events, hydrodynamic storm surge models have become increasingly important to the preservation of life and property, particularly as the climate and storm climatology change, and coastal populations increase. The effectiveness of both real-time forecasting and long-term risk analysis is largely dependent on the accuracy of the storm surge models employed. In recent decades, storm surge models have become increasingly accurate due to improvements in numerical methods and advancements in high performance computing. However, these models remain dependent on parameters which are often uncertain or unknown. For example, uncertainties in storm surge models largely result from uncertainties in the winds that are used to drive them, and specifically from uncertainties in how the winds are represented. Uncertainties in other model parameters such as bottom friction are also common sources of error. Parameter estimation methods can be implemented to reduce these types of model uncertainties using observed data. However, traditional inverse modeling techniques are often computationally intensive and can generally only be implemented offline, i.e. they are not feasible for the timely prediction of hurricane storm surges. Alternatively, statistical data assimilation techniques are non-intrusive methods that have been developed to estimate model parameters in real-time. In addition to parameter estimates, they provide estimates of associated uncertainties. In this talk, such approaches to parameter estimation and uncertainty quantification are discussed.

## Automated Composite Material Model Development with Multiscale Designer

Colin McAuliffe<sup>\*</sup>, Robert Crouch<sup>\*\*</sup>, Jeff Wollschlager<sup>\*\*\*</sup>, Jacob Fish<sup>\*\*\*\*</sup>, Venkat Aitharaju<sup>\*\*\*\*\*</sup>,  
Roger Ghanem<sup>\*\*\*\*\*</sup>

<sup>\*</sup>Altair Engineering Inc, <sup>\*\*</sup>Altair Engineering Inv, <sup>\*\*\*</sup>Altair Engineering Inc, <sup>\*\*\*\*</sup>Columbia University, <sup>\*\*\*\*\*</sup>General Motors, <sup>\*\*\*\*\*</sup>University of Southern California

### ABSTRACT

Development of accurate computational models for composite materials presents a challenge for industry practitioners. The input parameters to a multiscale model of a composite are the properties of the constituent materials, e.g. carbon fiber and epoxy. It is often not possible to fully characterize a complex constituent material like carbon fiber from performing experiments on them individually. Even if it were, manufacturing processes may result in different in situ properties. Model development therefore must be accomplished through inverse identification, where experimental observations on the composite are used with a model to infer the constituent properties. This presents its own set of challenges, since inverse problems are notoriously difficult to solve correctly. Additionally, the success of the inverse solution requires that each of the constitutive properties be constrained by at least one experimental observation. Due to the expense associated with testing of composites, there is strong motivation to minimize the number of tests. Multiscale Designer employs both deterministic and stochastic approaches to the model development problem for linear and nonlinear property identification. These approaches are automated and highly accessible to practicing engineers. The stochastic approaches provide crucial insight into the reliability of the inverse solution, and can inform the analyst when the lack of a particular experimental observation negatively impacts this solution. In this case, a purely deterministic approach may give the false impression of a good solution. In this presentation, the technical details of these approaches are presented, and their ability to successfully identify composite properties is demonstrated.

## **A Low-Mach Number Preconditioner for the 10-Moment Closure with Application to Non-Equilibrium Gas Flows**

James McDonald\*, Fabien Giroux\*\*

\*University of Ottawa, \*\*University of Ottawa

### **ABSTRACT**

The ten-moment, Gaussian closure of gas dynamics is an accurate mesoscopic model for low-Mach-number laminar gas flows in which heat transfer does not play a significant role. This is true in the traditional continuum regime, as well as for higher-Knudsen-number transition-regime flows. Unfortunately, for exactly these low-speed applications, the partial differential equations governing the model can be numerically difficult to solve. This is due to the fact that there is a large discrepancy between the magnitude of the wave speeds present in the system. In such ill-conditioned hyperbolic systems, computational time-steps are limited by fast-moving acoustic-like waves, while processes of interest are related to slower-moving waves. The result is long run times and excessive numerical dissipation. There are several preconditioners available for traditional continuum models that alleviate this issue for classical low-speed flows. These local preconditioners alter the eigenstructure of the system such that all wave speeds are of the same order, even at low Mach numbers. The subject of this talk is the derivation and application of a similar low-Mach-number preconditioner for the Gaussian closure with the BGK collision operator. Preconditioning of the Gaussian closure brings an added difficulty as compared to traditional models. This is because of the interplay between the hyperbolic wave nature of the model and the effects of the collision operator. The apparent waves display a dispersive nature with wave speeds that depend on the timescale of gas-particle collisions. The preconditioner must, therefore, be constructed to effectively control the condition number across all possible flow regimes, from continuum to free molecular. The current preconditioner is inspired by the traditional Weiss-Smith preconditioner for the Euler equations, but extended for the ten equations of the Gaussian model and adapted to work effectively from the continuum to the free-molecular regime. This presentation demonstrates the construction of the preconditioner as well as a dispersion analysis that demonstrates its effectiveness across all levels of rarefaction. A numerical implementation is briefly reviewed and the ability of the preconditioner to effectively control run times and numerical dissipation for canonical low-speed transition-regime flows is demonstrated.

## **Free Energy Analysis of Cell Spreading on Collagen Coated Elastic Substrates**

Eoin McEvoy\*, Patrick McGarry\*\*

\*National University of Ireland Galway, \*\*National University of Ireland Galway

### **ABSTRACT**

Cell behaviour has been shown to depend on substrate stiffness and surface collagen density. In this study we provide new insights into the processes underlying cell mechano-sensitivity by developing a novel modelling framework. Beginning with a thermodynamic description of sub-cellular actin-myosin interactions, we demonstrate that spreading of cells is driven by a competition between passive and active cytoskeletal free energy. The cell explores its physical environment as it attempts to achieve a homeostatic free energy. This dynamic process is simulated on substrates of differing stiffness and surface collagen density using a Markov chain Monte-Carlo(MCMC) scheme. This entails the simulation of 2.5 million spread states and the associated distributions of stress fibres and focal adhesions. Our MCMC simulations predict an ensemble of cell spread states on compliant and rigid substrates. For cells on a rigid substrate, both the mean and standard deviation of the spread area are predicted to increase as the collagen density increases. As substrate stiffness decreases, lower spread areas are computed. These predictions are extremely similar to experimentally observed cell behaviour.

## Modelling Transient Active Force Generation in Cell Stress Fibres

Patrick McGarry\*, Eoin McEvoy\*\*

\*National University of Ireland Galway, \*\*National University of Ireland Galway

### ABSTRACT

Mechanical priming strategies have been developed in an ongoing drive to engineer tissues with increased functional viability. As cells actively respond to loading in the 3D microenvironment, the development of a fundamental mechanistic understanding of the effects of mechanical conditioning on cell biomechanics is critical. In this study we develop a novel framework for active cell contractility when subjected to uniaxial and biaxial dynamic loading conditions. Uniaxial and biaxial experiments are simulated using an active thermodynamically motivated model for cell contractility. The modelling framework includes a novel cross-bridge cycling formulation for transient force generation and an anisotropic constitutive law for collagen realignment and compaction. The active model predicts that highly aligned high concentration sarcomeres are formed when the stress state is uniaxial, whereas a biaxial stress state leads to the computation of unaligned low concentration sarcomeres. The model also accurately predicts measured tissue forces. Model results confirm that the small experimentally measured difference (36%) in uniaxial and biaxial force for contractile tissue (compared to the large difference (100%) for a passive hydrogel) is due to stronger sarcomere formation and alignment induced by a uniaxial stress state.

## Shape Morphing of Non-periodic Metamaterial Sheets

Connor McMahan<sup>\*</sup>, Paolo Celli<sup>\*\*</sup>, Chiara Daraio<sup>\*\*\*</sup>, Brian Ramirez<sup>\*\*\*\*</sup>, Basile Audoly<sup>\*\*\*\*\*</sup>

<sup>\*</sup>California Institute of Technology, <sup>\*\*</sup>California Institute of Technology, <sup>\*\*\*</sup>California Institute of Technology,  
<sup>\*\*\*\*</sup>California Institute of Technology, <sup>\*\*\*\*\*</sup>LMS, École Polytechnique, CNRS, Université Paris-Saclay

### ABSTRACT

The dominant approach in the design of mechanical metamaterials revolves around ordered arrangements of mesoscale constituents. In this work, we demonstrate that the shape morphing abilities of two-dimensional architected sheets can be enhanced by resorting to non-periodic (graded, or fully aperiodic) geometries. Through theoretical considerations, numerical simulations and desktop-scale experiments, we demonstrate that rectangular sheets can morph shape, in-plane and out-of-plane, when subjected to carefully-engineered load patterns. Leveraging modes of inextensional deformation, the systems are designed to display large deformations for small input energies.

## **An Evaluation of Mesh-free Hydrodynamic Methods for Blast Wave Modeling and Blast-Structure Interaction**

Casey Meakin<sup>\*</sup>, Dominic Wilmes<sup>\*\*</sup>, Fabien Teulieres<sup>\*\*\*</sup>

<sup>\*</sup>Karagozian & Case, Inc., <sup>\*\*</sup>Karagozian & Case, Inc., <sup>\*\*\*</sup>Karagozian & Case, Inc.

### **ABSTRACT**

The advantages provided by mesh-free numerical methods for modeling solids and fluids are becoming more attractive as simulation models become more complex. The ability to rapidly develop models by side-stepping the often time consuming process of mesh generation is of particular interest. Mesh-free algorithms can also provide elegant solutions to several notable limitations associated with grid based methods including large deformation in solids and contact tracking at fluid interfaces. Despite growing interest in mesh-free methods for fluids dynamics, however, their performance for treating shock waves and shock-structure interactions remain poorly characterized. In order to address this issue, the effectiveness of using a recently developed class of fully conservative, consistent, mesh-free hydrodynamic methods for these types of problems is investigated. Key performance metrics considered include computational efficiency, accuracy, and ease of model development compared to more traditional grid-based hydrodynamic solvers.

## Fully Explicit Three-Dimensional Lagrangian Simulation of Fluid-Structure-Interaction Problems

Simone Meduri<sup>\*</sup>, Umberto Perego<sup>\*\*</sup>, Massimiliano Cremonesi<sup>\*\*\*</sup>

<sup>\*</sup>Politecnico di Milano (Italy), <sup>\*\*</sup>Politecnico di Milano (Italy), <sup>\*\*\*</sup>Politecnico di Milano (Italy)

### ABSTRACT

A partitioned fully Lagrangian and fully explicit approach for the simulation of FSI problems is presented. Partitioned approaches are particularly interesting for the application to real engineering problems because of the possibility to make use of existing software. Moreover, explicit methods can be advantageous in many large scale applications characterized by fast dynamics and/or a high degree of nonlinearity. In this work, we propose an explicit version of the Particle Finite Element Method (PFEM) [1] for the weakly compressible fluid domain, coupled with the commercial software Abaqus/Explicit for the structural one. The Gravouil and Combescure approach [2] has been chosen to enforce a strong coupling together with a global system of fully decoupled (explicit) equations [3]. Nonconforming meshes and time increments in the fluid and solid subdomains can be used to optimize the discretization for the overall efficiency of the coupled solver. The use of a commercial software as structural solver allows including in the model its advanced functionalities, such as the libraries of material constitutive models and finite elements and other advanced features. Furthermore, the fully Lagrangian framework of the coupled PFEM-FEM approach makes this method particularly suitable for applications with free-surface fluid flows and large displacements of the solid partition. In 3D problems, a frequent remeshing of the fluid domain is required by the PFEM. The resulting new mesh is often of a bad quality, with many slivers (tetrahedra with almost zero volume), leading to a vanishing critical time step size. A novel efficient mesh smoothing technique has been developed to produce a regular mesh, with a reasonably large stable time increment for the explicit solver. This smoothing algorithm is fully explicit and parallelizable, because it exploits the same architecture of the fluid solver thanks to an elastic analogy. Several three-dimensional examples have been considered to validate the approach against available analytical, experimental and numerical solutions, confirming the robustness and effectiveness of the proposed method. [1] E. Onate, S. Idelsohn, "The particle finite element method: an overview." *Int J Comput Meth*, 2004;2:267-307. [2] A. Gravouil, A. Combescure, "Multi-time-step explicit-implicit method for non-linear structural dynamics." *Int J Numer Meth Engng*. 2001;50:199-225. [3] S. Meduri et al. "A partitioned fully explicit Lagrangian finite element method for highly nonlinear fluid-structure interaction problems." *Int J Numer Meth Engng*. 2018;113:43-64.

## EVALUATION OF THE PERFORMANCE OF BUND WALL SYSTEMS UNDER THE EFFECT OF CATASTROPHIC FAILURE OF STORAGE TANKS VIA NUMERICAL MODELLING

ISLEM MEGDICHE WILLIAM ATHERTON CLARE HARRIS GLYNN  
ROTHWELL<sup>4</sup> AND DAVID ALLANSON

<sup>1</sup> Department of Civil Engineering, Liverpool John Moores University  
15-21 Webster St, Liverpool L3 2ET  
[I.Megdiche@2015.ljmu.ac.uk](mailto:I.Megdiche@2015.ljmu.ac.uk)

<sup>2</sup> Department of Civil Engineering, Liverpool John Moores University  
Peter Jost Enterprise Centre, 3 Byrom St, Liverpool L3 3AF  
[W.Atherton@ljmu.ac.uk](mailto:W.Atherton@ljmu.ac.uk), <https://www.ljmu.ac.uk/about-us/staff-profiles/faculty-of-engineering-and-technology/department-of-civil-engineering/bill-atherton>

<sup>3</sup> Department of Civil Engineering, Liverpool John Moores University  
Peter Jost Enterprise Centre, 3 Byrom St, Liverpool L3 3AF  
[C.B.Harris@ljmu.ac.uk](mailto:C.B.Harris@ljmu.ac.uk), <https://www.ljmu.ac.uk/about-us/staff-profiles/faculty-of-engineering-and-technology/department-of-civil-engineering/clare-harris>

<sup>4</sup> Department of Maritime and Mechanical Engineering, Liverpool John Moores University  
James Parsons Building, 3 Byrom St, Liverpool L3 3AF  
[G.Rothwell@ljmu.ac.uk](mailto:G.Rothwell@ljmu.ac.uk), <https://www.ljmu.ac.uk/about-us/staff-profiles/faculty-of-engineering-and-technology/department-of-maritime-and-mechanical-engineering/glynn-rothwell>

<sup>5</sup> Department of Maritime and Mechanical Engineering, Liverpool John Moores University  
James Parsons Building, 3 Byrom St, Liverpool L3 3AF  
[D.R.Allanson@ljmu.ac.uk](mailto:D.R.Allanson@ljmu.ac.uk), <https://www.ljmu.ac.uk/about-us/staff-profiles/faculty-of-engineering-and-technology/department-of-maritime-and-mechanical-engineering/david-allanson>

**Key words:** bund wall, Fluid Structure Interaction, storage tank, impact load.

**Abstract.** The failure of storage tanks is a very serious problem that has occurred in many countries around the world due to natural disasters and accidental releases. The consequences of such failures recorded in the literature have impacts on the environment, the immediate community and the economy. The United States (US) is one of the countries that has suffered most from this kind of problem and lately many above-ground storage tanks have ruptured in the Houston area due to Hurricane Harvey. Usually, refineries, chemical plants and oil depots are required to provide safety measures to mitigate the effects of the rupture of storage tanks where the collapse is unavoidable due to extreme natural disasters or because of the use of decades-old technology already in place. These safety measures imply the use of a secondary containment surrounding the storage tanks where the intention is to contain any spilled materials. The secondary containment is referred to as a bund wall. In the UK, bund walls are designed according to BS EN 1992-3:2006, where only static pressure is accounted for due to

slow leaks. However, in the wake of the catastrophic failure of storage tanks, the bund wall is subjected to the impact of the rapidly escaping fluid. Such scenarios require accounting for the dynamic pressure in addition to the traditional approach, especially since previous failures proved that bund walls designed for static pressure only, were ineffective and collapsed under the impact of surging fluids. In this study, it is proposed to investigate the performance of a bund wall system under the effect of fluid impact via the use of numerical modelling. The analysis involves the interaction between the structure and the fluid domains. The fluid problem is modelled as a multiphase flow and solved using OpenFoam software, while the structural problem is solved with the dynamic explicit solver of Abaqus. The coupling between the two computational fluid dynamics (CFD) and finite element modelling (FEM) packages was carried out using MpCCI software. Numerous load configurations and bund shapes have been analysed. The numerical analysis indicates that the bund walls constructed from plain concrete (block) are not able to withstand the impact of the fluid and ruptured providing no secondary containment.

## 1 INTRODUCTION

Throughout many years, numerous incidents related to the storage of hazardous substances have occurred in many countries <sup>[1]</sup>. The most affected country is the United States of America (USA) as it is subjected to many natural disasters apart from the accidental releases that pose further risk for the sudden failure of the primary storage (tank) facility. Recently, an explosion took place at the Husky Energy oil refinery on April 2018 in Superior, Wisconsin. It was reported that a tank of asphalt exploded at 10 a.m. on 26<sup>th</sup> April. Later on, on the following day, at 3.15 p.m. another tank caught the fire <sup>[2]</sup>. The root cause of the explosion is still unclear, however the blast occurred while the workers were preparing to shut down the facility, which is considered one the most sensitive times, where the risk of failure increases. It was also reported that at the time of the explosion, staff were carrying out construction work, which might have contributed to the failure <sup>[3]</sup>. The consequences were deemed very disastrous, resulting in the shaking of buildings up to one mile away from the scene. The ignition of a huge fire and the spread of thick smoke across a wide area around the refinery was evident. This resulted in the evacuation of the residents living in a three miles radius around the plant, together with the evacuation of schools and a hospital in the affected region. A state of emergency was also declared in Douglas County. The smoke was very harmful as it contained mixes of hydrocarbons and other chemical mixtures and was extremely dense, as people living 30 miles away for the incident could see the smoke spreading. In terms of casualties, the number of injured persons is not exact, but at least 11 persons were injured with one person being seriously affected <sup>[4]</sup>.

Natural disasters are considered potential factors that trigger the failure of storage tanks. Texas is an area subjected to hurricanes, and during Hurricane Harvey, that swept Houston on August 2017, many failures were subsequently reported. Houston is a hub of oil refineries, chemical plants and storage facilities. The capacity of the crude storage of the region has increased from 21 million barrels to 56 million in the last six years. Many companies use floating roof storage tanks, about 400 out of more than 1000 storage tanks in Houston itself.

The design proved to be inadequate, as many companies reported failures of these tanks due to the huge weight of accumulated water on the roofs that reached 50 inches, while the roofs are only designed to hold up to 10 inches of rain. The storm caused the roofs to flip, releasing toxic materials into the atmosphere. The technology of floating roofs was deemed responsible for spills as well. It was reported that 500,000 gallons of gasoline escaped from two storage tanks located in the Galena Park storage complex, which belongs to Magellan Midstream Partners [5]. Additionally, many large companies reported leaks and spillages at their facilities, such as BASF, which is the second largest producer of chemical products in North America. Tanks overflowed leaving chemicals to spill in a diked area which itself then overflowed to the surrounding area [6]. At Exxon Mobil's Beaumont Oil Refinery, storage tanks leaked, resulting in the oil escaping to the nearby county road. The spills were considered small enough compared to those recorded in the aftermath of Hurricane Katrina, where millions of gallons were released into the residual areas [7].

Safety measures are essential to reduce the extent of any failure. In many parts of the world such as the UK and the USA, companies that perform any activity associated with hazardous materials are required to provide secondary containment in the form of a wall that surrounds a single or multiple storage tanks to contain spillage caused by the rupture of the tanks. The secondary containment is known as bund wall and can be constructed from concrete, bricks or earth [1]. In the UK, it is designed according to BS EN 1992-3:2006, where it is only required to withstand the static pressure of the released material. During catastrophic failures and major events, a number of facilities failed to withstand the torrential waves of the escaping materials, which is a subsequent mode of failure [8].

In this study, it is proposed to investigate the performance of the bund walls under the effect of the catastrophic failure of storage tanks that gives rise to a surge of fluid. Three different shapes of bund walls were investigated namely, circular, square and rectangular bund walls with a centered and off-centered storage vessel. Results indicated that a better performance is obtained when using a circular wall, while the square and rectangular bund walls behaved almost the same manner, with a slightly better performance for the square bund wall.

## 2 METHODOLOGY

At the moment of complete failure of storage tank, a column of fluid falls under the effect of gravity until it hits the bund wall. Then, depending on the shape and the height of the wall, part of the fluid will be diverted back in the banded area and the rest of the fluid overtops and escapes to the surrounding area. The bund wall might exhibit damage, depending on the severity of the surging wave. A numerical modelling approach involving fluid/structure interaction was used to model this problem. The fluid part was solved following a multiphase flow modelling approach using OpenFoam software. For the structural part, the bund wall was modelled using Abaqus software and the coupling between the fluid and the structural codes was performed using the MpCCI coupling environment.

For the OpenFoam side, InterDyFoam was used to solve the Navier Stokes equation (1) and a specie transport equation (2) derived from the conservation of mass equation, based on the Volume of Fluid (VoF) method, with  $\alpha$  being the phase fraction. The Navier Stokes equation

contains an additional term to model the surface tension between the considered fluids which are oil and air <sup>[9]</sup>.

$$\frac{\partial \rho U}{\partial t} + \nabla \cdot (\rho U U) = -\nabla p + [\nabla \cdot \mu \nabla U + \nabla U \cdot \nabla \mu] + \rho g + \int_{S(t)} \sigma k' n' \delta(x - x') dS \quad (1)$$

$$\frac{\partial \alpha}{\partial t} + \nabla \cdot (U \alpha) = 0 \quad (2)$$

The turbulence was modelled using the low Reynolds version of the shear stress Transport (SST) -  $k$ - $\omega$  model, as it can accurately model the behaviour of fluid flow exhibiting droplet formation and separation that occurs at the moment of the impact.

InterDyMFoam solves the multiphase flow using a dynamic mesh. Although, InterFoam was able to predict the flow behaviour and yields accurate results for certain configurations of tank and bund wall arrangements, the dynamic solver was used because MpCCI requires the dynamic solver to move the interface between the structural and fluid domains.

The InterDyMFoam solver uses the Multidimensional Universal Limiter for Explicit Solution (MULES) method that allows maintenance of the boundedness of the phase fraction <sup>[9]</sup>. The discretization schemes are not therefore restricted to those, which are bounded. The discretization schemes used are: The Euler scheme for the temporal term, which is first order, implicit and bounded allowing the determination of a stable solution, the Gauss linear upwind scheme for the convective term, utilized to obtain improved accuracy, the Gauss linear scheme for the gradient term and the Gauss VanLeer scheme for the compression flux in the specie transport equations ensuring boundedness.

The total time for the simulation is 2s which is believed (on the basis of experimental and numerical results) to be a sufficient time for the wave to settle. The time step is equal to 0.001s and the maximum Courant number was allowed to reach unity because of the use of the semi-implicit version of the MULES algorithm. Regarding the convergence control, tolerances were specified for each physical quantity. They are  $10^{-7}$  for pressure,  $10^{-5}$  for all of velocity, kinetic energy and specific dissipation rate and  $10^{-8}$  for phase fraction,  $\alpha$ .

In regards to boundary conditions, it is assumed that the fluid is not able to penetrate through the surrounding walls of the computational domain and the ground, walls are not slippery and, that the domain is free to atmosphere (a reasonable assumption given the ratio of the mass densities involved and the open domain). The boundary conditions that permit modelling in OpenFoam are: fixed flux pressure equal to zero for pressure and fixed value equal to zero for velocity, zero fixed flux pressure and zero velocity (no-slip) is applied to all surrounding walls and the ground. Total pressure, pressure inlet outlet velocity and inlet outlet boundary conditions for the pressure, velocity and phase fraction respectively to model the free surface.

For Abaqus, an explicit approach was adopted using the explicit solver, which is the appropriate solver for problems involving impacts. The geometric model was discretized using hexahedral, first order and reduced integration elements with an aspect ratio equal to unity. These types of elements are efficient in modelling contact impact or large distortions problems <sup>[10]</sup>. For the material modelling, the Concrete Damage Plasticity (CDP) was used for its suitability for problems involving dynamic loading <sup>[11]</sup>. The model requires the density of the concrete, the Poisson Ratio and Young's Modulus parameters, to model the elastic behaviour of the concrete. For the plastic behaviour modelling, the stress- strain and stress-displacement

relationships for the compressive and tensile curves need to be defined. In order to account for the damage of the concrete, additional tabular data representing the damage-displacement has to be provided. The tensile damage is modelled because of the weakness of concrete under tensile loading. The material parameters were taken from [11] and summarized in Table 1.

**Table 1:** Material properties for the CDP model for plain concrete finite element modelling

Density	2643		
<b><u>Concrete Elasticity</u></b>			
Elastic modulus (GPa)	31		
Poisson's ratio	0.15		
<b><u>The parameters for CDP model</u></b>			
Dilation angle (degrees)	36.31		
Eccentricity	0.1		
$f_{b0} / f_{c0}$	1.16		
$K_c$	0.667		
$\mu$	0		
<b><u>Compressive behaviour of the concrete</u></b>			
Yield stress (Pa)	Inelastic strain		
13000000	0		
24000000	0.001		
<b><u>Concrete tension stiffening</u></b>			
Yield stress (Pa)	Displacement (m)	Damage variable	Displacement (m)
2900000	0	0	0
1943930	6.6185E-05	0.381217	6.6185E-05
1303050	0.00012286	0.617107	0.00012286
873463	0.000173427	0.763072	0.000173427
585500	0.00022019	0.853393	0.00022019
392472	0.000264718	0.909282	0.000264718
263082	0.000308088	0.943865	0.000308088
176349	0.00035105	0.965265	0.00035105
118210	0.000394138	0.978506	0.000394138
79238.8	0.000437744	0.9867	0.000437744
53115.4	0.000482165	0.99177	0.000482165

For MpCCI, the coupling procedure consists of 5 steps: Models step, Coupling step, Monitors step, Edit step and the Go step [12]. The Models, coupling and Monitors steps are mandatory to couple OpenFoam and Abaqus. The Models step consists of defining the coupled software and the input files for OpenFoam and Abaqus models. The Coupling step consists of defining the global variables, creating and configuring the coupling regions. For this problem, the global variable represents the time step that is sent from OpenFoam to Abaqus, and the coupling region represents the surface of the bund wall as represented in Fig.1. During the computation, OpenFoam solves the governing equations of the fluid domain and sends the

pressure to Abaqus denoted in MpCCI by RelWallForce. Abaqus uses those values to solve the governing equations of the structure and then sends the deformations back to OpenFoam. The final step in the coupling process is the Go step in which the coupling scheme, the initial quantities transfer and other parameters need to be defined. Here, the explicit-transient coupling scheme was used, which is the only possible coupling scheme to solve for the transient problem when using the Abaqus explicit solver. The initial quantities transfer determines whether the coupling is serial or parallel. For this problem, the initial quantities transfer are receive and exchange modes for Abaqus and OpenFoam respectively which yields a serial coupling.

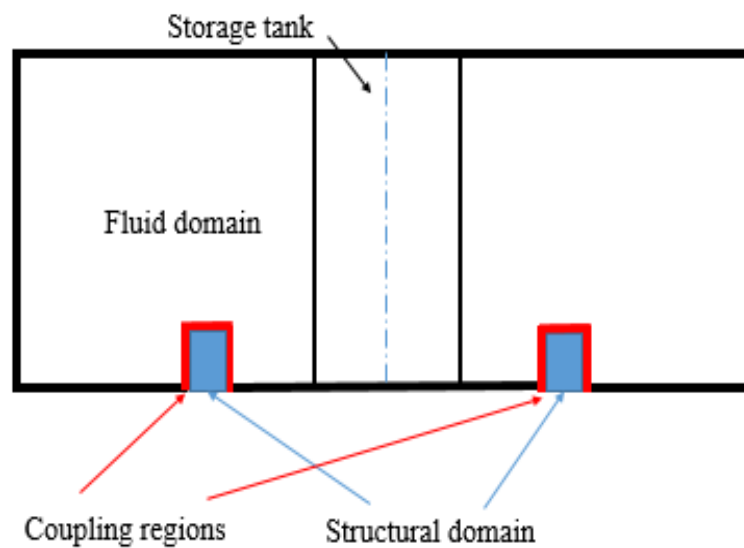


Fig.1: Fluid-Structure domain

The dimensions of the bund walls were calculated based on a scale factor of 30. Three shapes of bund walls were tested which were the circular, square and rectangular. The bund walls have the same volume for the banded region, the height of the circular bund wall is 0.24m while the height of the square and rectangular bund walls are 0.12m. The thickness of all walls is 0.007m. The bund walls were subjected to the impact of a column of oil with an initial height of 6m, which was determined by increasing the height of the fluid until damage appeared in the concrete when using a circular wall. The effect of the asymmetric load modelled by an off-centred tank has been investigated by moving the column of fluid by 0.05m from the central position along x or y-axes. Such a situation is considered in case the fluid escapes the tank in a non-symmetric fashion. In total, seven simulations were run, three simulations when the load is centred with the three different bund shapes, and four simulations when the load is off-centred. For the rectangular bund wall, the load is off-centred in the x and y directions with the same magnitude. Fig. 2 represents a nomenclature of the three different bund walls.

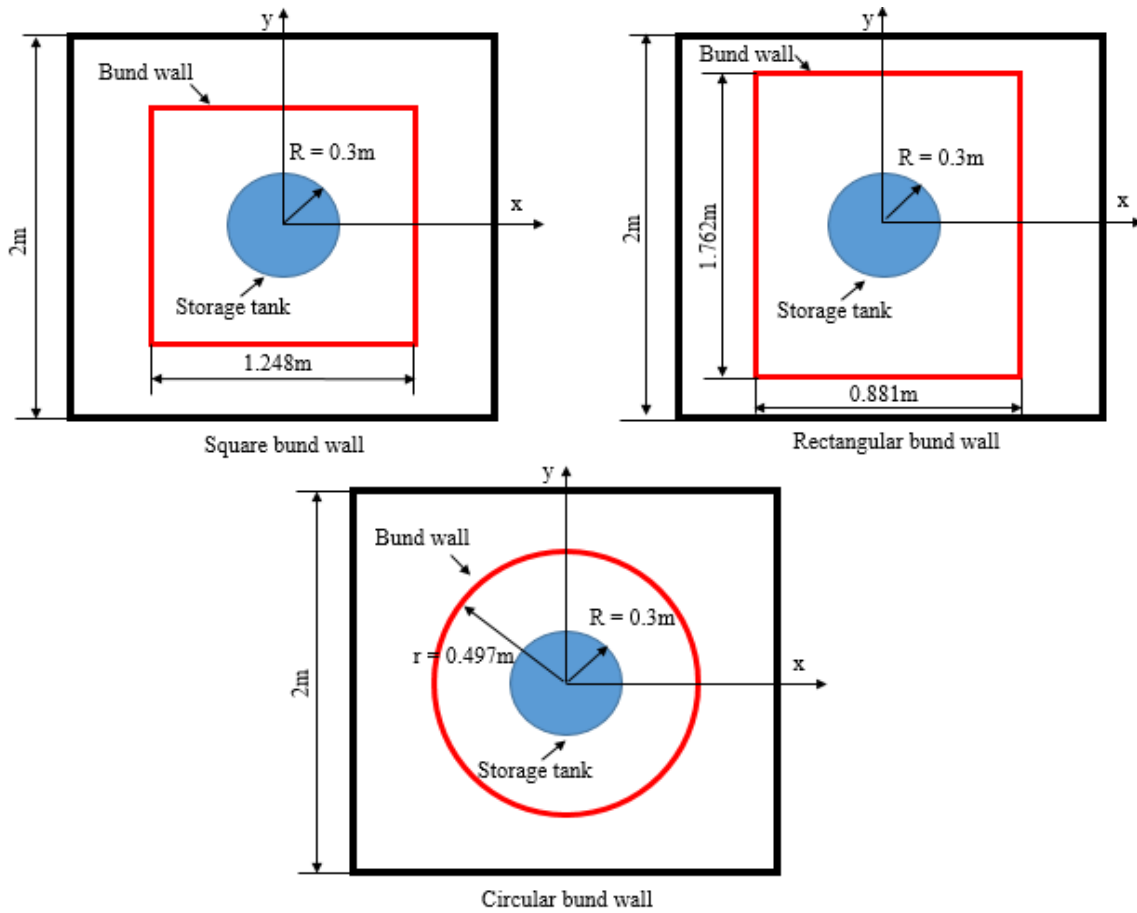


Fig. 2: Nomenclature for bund walls

### 3 RESULTS AND DISCUSSIONS

Figs.3, 4 and 5 show the flow structure and the bund wall behaviour in terms of tensile damage corresponding to the circular, square and rectangular bund walls with centred releases. Due to the page limit of this paper, figures of the behaviour of the structures under an off-centred release are not included, but results of dynamic pressure, VonMises stress and tensile damage denoted  $\text{damage}_T$  are presented in Tables 2, 3, 4 and 5 as a function of time until the failure occurs. A comparison between the three shape configurations shows that a circular bund outweighs square and rectangular bund walls in terms of the maximum pressure that it can take and the magnitude of damage incurred. A circular bund wall withstands 40kPa with only minor damage of the order of 0.3%. In contrast, square and a rectangular bund walls are structurally weaker. The performance of the square bund wall is slightly better than a rectangular bund wall, i.e. a square bund wall fails slightly after the rectangular bund wall (0.653s for the square wall versus 0.6074s for the rectangular wall). A temporal comparison between the magnitude of the damage indicates that the square bund wall exhibits less damage compared to a rectangular bund; for example at  $t = 0.5\text{s}$ , the tensile damage of a square bund wall is 40.48% versus 69.71%

for a rectangular bund wall.

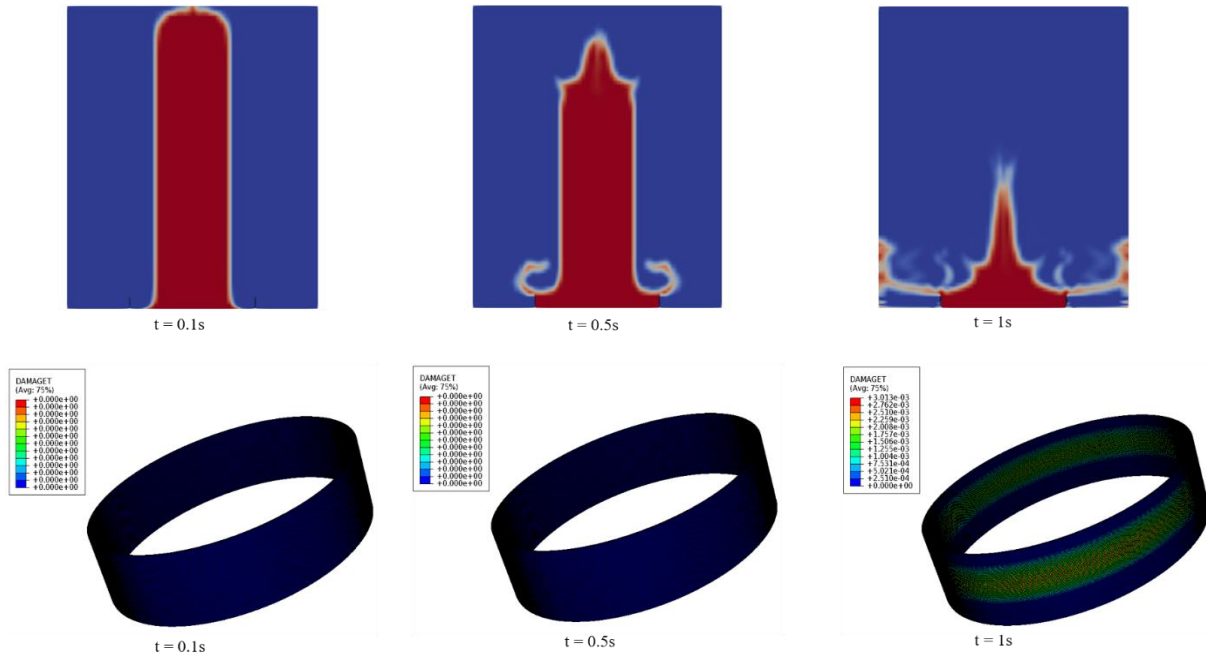


Fig.3: Flow and structural behaviour for a circular bund wall

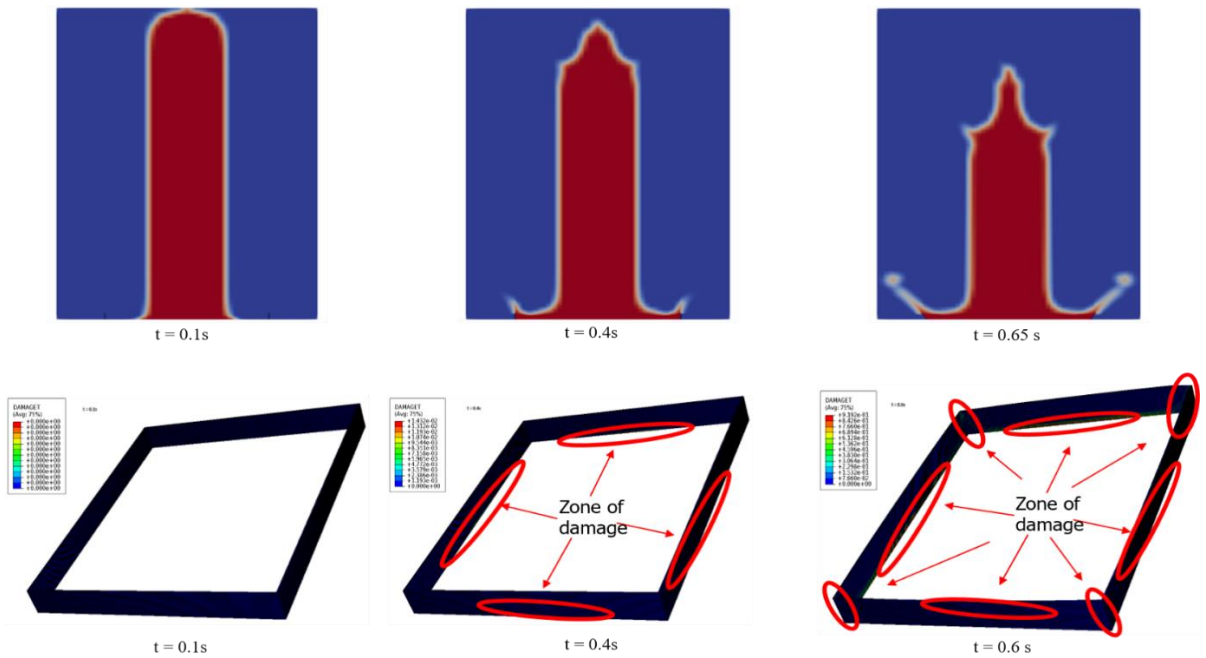


Fig.4: Flow and structural behaviour for a square bund wall

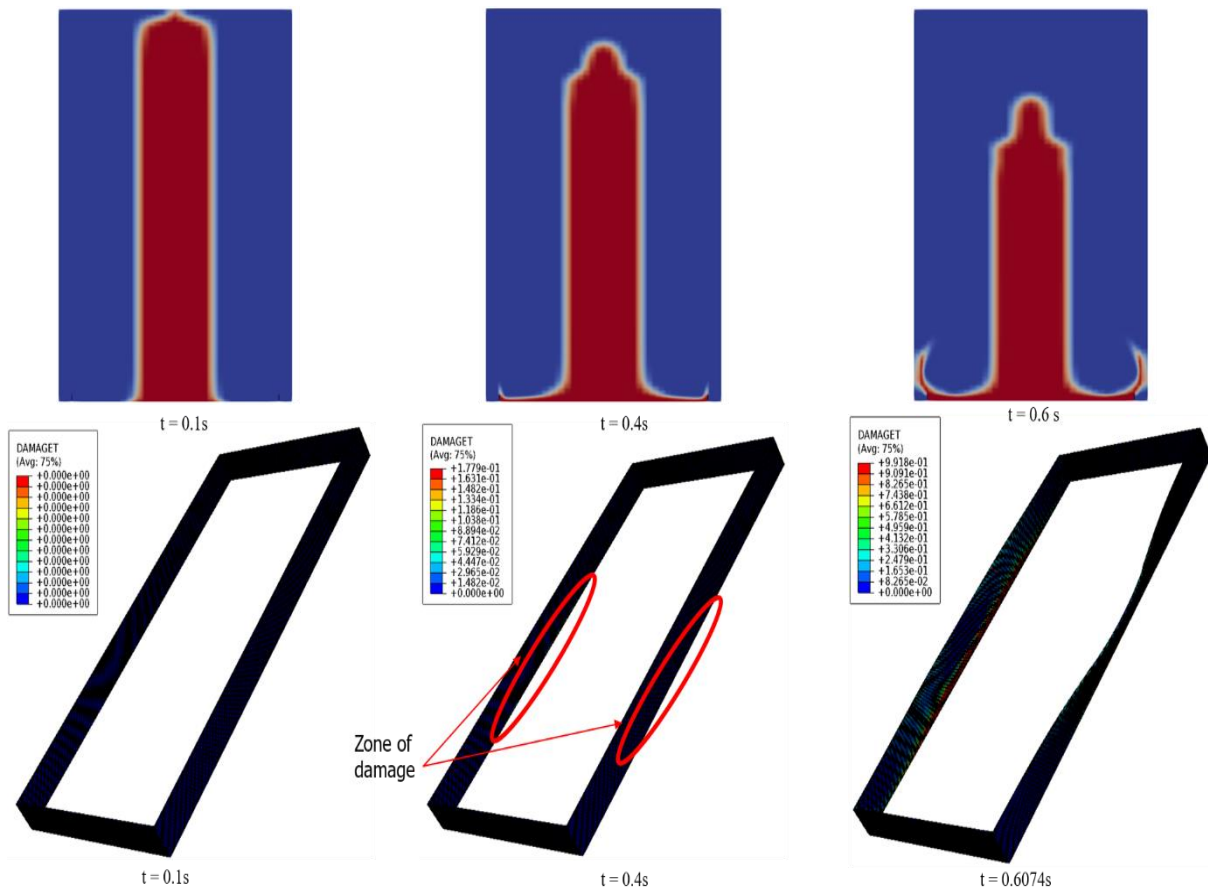


Fig.5: Flow and structural behaviour for a rectangular bund wall

The assumption of a centred release is ideal, as during the failure, the fluid flow moves in a different fashion with respect to the direction. This asymmetry of the load is due to the fluid flow as it hits an obstacle in the banded region. To take this into consideration, the fluid column was shifted by 0.05m from the centre along x or y-axes. From Tables 2, 3, 4 and 5 a comparison between the performance of the banded configurations of the same shape, under a centred and an off-centred load shows that generally, the bund wall exhibits a higher magnitude of damage with an off-centred load. As an example, the damage to a circular bund wall is 0.34% with an off-centred load compared to 0.30% with a centred load at  $t = 1.1s$ . This increase in damage is minor for the circular bund wall, while for a square bund wall the increase in the tensile damage is more significant. For example at  $t = 0.5s$ , the damage increases from 40.48% with a centred load to 47.01% with off-centred load. This behaviour is due that the fluid flow hits one side of the bund before hitting the other sides, which triggers an earlier damage and higher magnitude of damage, as only one side will be initially subjected to the load. The only exception of this behaviour is with a rectangular bund wall, when the load is moved along the y axis which is in the direction of the longest side of the rectangular bund wall.

A comparison between the shape of bund walls under an off-centred load leads to the same conclusion as when using a centred load. The circular bund wall withstands a higher level of dynamic pressure without significant damage, while the performance of square and rectangular bund walls is almost the same.

**Table 2:** Results of dynamic pressure, tensile damage and stress for a circular bund wall

Time (s)	centred load			Time (s)	off centred load		
	Dynamic pressure near the bund wall (Pa)	damage (%)	Maximum VonMises stress (MPa)		Dynamic pressure near the bund wall (Pa)	damageT	Maximum VonMises stress (MPa)
0	2500	0	0	0	2500	0	0
0.1	2800	0	0.18	0.1	2800	0	0.18
0.2	4200	0	0.25	0.2	5400	0	0.36
0.3	8300	0	0.55	0.3	8900	0	0.63
0.4	13000	0	0.90	0.4	13000	0	0.91
0.5	14000	0	1.01	0.5	15000	0	1.05
0.6	19000	0	1.41	0.6	20000	0	1.45
0.7	26000	0	1.92	0.7	24000	0	1.79
0.8	32000	0	2.29	0.8	32000	0	2.39
0.9	39000	0	2.79	0.9	38000	0	2.74
1	42000	0.3	2.75	1	43000	0.33	3.13
1.1	17000	0.3	1.17	1.1	18000	0.34	1.85
1.2	16000	0.3	0.62	1.2	36000	0.34	1.15
1.3	17000	0.3	0.53	1.3	9900	0.34	1.13
1.4	18000	0.3	0.51	1.4	5700	0.34	0.78
1.5	18000	0.3	0.55	1.5	4500	0.34	0.55
1.6	23000	0.3	0.48	1.6	5400	0.34	0.56
1.7	16000	0.3	0.49	1.7	5600	0.34	0.53
1.8	13000	0.3	0.6	1.8	9300	0.34	0.69
1.9	12000	0.3	0.73	1.9	13000	0.34	0.95
2	19000	0.3	0.81	2	14000	0.34	0.91

**Table 3:** Results of dynamic pressure, tensile damage and stress for a square bund wall

Time (s)	centred load			Time (s)	off centred load		
	Dynamic pressure near the bund wall (Pa)	damageT	Maximum VonMises stress (MPa)		Dynamic pressure near the bund wall (Pa)	damageT	Maximum VonMises stress (MPa)
0	1900	0	0	0	1900	0	0
0.1	2300	0	0.46	0.1	2300	0	0.46
0.2	3800	0	0.46	0.2	3800	0	0.46
0.3	6000	0	1.07	0.3	6000	0	1.64
0.4	9000	1.43	2.91	0.4	9000	4.12	3.02
0.5	13000	40.48	4.38	0.5	13000	47.01	4.56
0.6	17000	91.92	6.02	0.6	17000	98.88	6.6
0.65	20000	-	-	0.6393	-	99.18	-
0.6536	-	99.18	-	-	-	-	-

**Table 4:** Results of dynamic pressure, tensile damage and stress for a rectangular bund wall

Time (s)	Centred load			Time (s)	Off centred load		
	Dynamic pressure near the bund wall (Pa)	damageT	Maximum VonMises stress (MPa)		Dynamic pressure near the bund wall (Pa)	damageT	Maximum VonMises stress (MPa)
0	1900	0	0	0	1900	0	0
0.1	2300	0	0.29	0.1	2300	0	0.295
0.2	4600	0	1.11	0.2	4700	0	1.81
0.3	6300	0	2.58	0.3	6500	0.14	2.61
0.4	9200	17.79	2.97	0.4	9200	20	3.03
0.5	13000	69.71	5.28	0.5	13000	77.12	5.88
0.6	17000	99.18	8.96	0.55	15000	99.18	-
0.6074	-	99.18	-	0.5946	-	-	-

**Table** : Results of dynamic pressure, tensile damage and stress for a rectangular bund wall with off-centred load

Time (s)	Off centred load y		
	Dynamic pressure near the bund wall (Pa)	damageT	Maximum VonMises stress (MPa)
0	1900	0	0
0.1	2300	0	0.29
0.2	4500	0	1.08
0.3	6200	0	2.58
0.4	9200	17.06	2.97
0.5	13000	69.17	5.31
0.6	17000	99.18	6.72
0.619	-	99.18	-

#### 4 CONCLUSIONS

In this paper, the performance of bund walls, which are structures that surround storage tanks to retain any spillage of hazardous materials in the event of failure were investigated. A numerical approach was followed, which involved the fluid/structure interaction using OpenFoam, Abaqus and MpCCI packages. In total, three configurations of bund walls were analysed, which were circular, square and rectangular bund walls under a centred and off-centred load. The simulations showed that a circular bund wall is superior in terms of structural performance. The square and rectangular bund walls behave almost in the same manner. When the load is off-centred, the bund wall exhibits more extensive damage. For future work, the performance of the square and rectangular bund walls need to be enhanced, as they are used most commonly within the industry.

#### Ac knowledgements

The first author would like to thank Liverpool John Moores University for the financial support provided for this project.

#### REFERENCES

- [1] Atherton, W. *n Empirical investigation of catastrophic and partial failures of bul storage vessels and subse uent bund wall overtopping and dynamic pressure*. PhD thesis, Liverpool John Moores University, 2008.
- [2] Forliti, A. and Baenen, J. Police: Evacuation order lifted following Wisconsin refinery blast injured 11 [Internet]. Chicago Tribune. 2018 [cited 10 May 2018]. Available from: <http://www.chicagotribune.com/news/nationworld/midwest/ct-wisconsin-refinery->

- [explosion-20180426-story.html](#)
- [3] Millar, J. Wisconsin explosion: Dozens hurt after ‘Sonic Boom’ in US city – Evacuation underway [Internet]. Express UK. 2018 [cited 10 May 2018]. Available from: <https://www.express.co.uk/news/world/951698/wisconsin-explosion-Husky-oil-refinery-injuries-police>
  - [4] Dellinger, A.D. City Evacuated, State of emergency declared in Wisconsin country following oil refinery explosion [Internet]. Gizmodo UK. 2018 [cited 10 May 2018]. Available from: <https://gizmodo.com/city-evacuated-state-of-emergency-declared-in-wisconsin-1825583765>
  - [5] Blum, J. Failures of floating-roof oil tanks during Harvey raise concerns [Internet]. Houston Chronicle. 2017 [cited 10 May 2018]. Available from: <https://www.houstonchronicle.com/business/energy/article/Failures-of-floating-roof-tanks-during-Harvey-12269513.php#photo-14326482z>
  - [6] Mufson, S. Chemical companies have already released 1 million pounds of extra air pollutants, thanks to Harvey [Internet]. The Washington post. 2017 [cited 10 May 2018]. Available from: [https://washingtonpost.com/news/energy-environment/wp/2017/09/04/chemical-companies-have-already-released-1-million-pounds-of-extra-air-pollutants-thanks-to-harvey/?noredirect=on&utm\\_term=.0770b2c3c6df](https://washingtonpost.com/news/energy-environment/wp/2017/09/04/chemical-companies-have-already-released-1-million-pounds-of-extra-air-pollutants-thanks-to-harvey/?noredirect=on&utm_term=.0770b2c3c6df)
  - [7] Associated Press. Tank failures in Harvey reveal vulnerabilities in storm [internet]. Wtop. 2017 [cited 10 May 2018]. Available from: <https://wtop.com/business-finance/2017/09/tank-failures-in-harvey-reveal-vulnerabilities-in-storm/>
  - [8] BS EN 1992-3:2006, *Design of concrete structures. Part 3: Design of retaining and containing structures*. BSI, ISBN:0 580 48267 7, 2006.
  - [9] Greenshields, C.J. (2017). OpenFOAM: User guide. Retrieved from <http://foam.sourceforge.net/docs/Guides-a4/OpenFOAMUserGuide-A4.pdf>
  - [10] Othman, H. A. B. *Performance of ultra high performance fibre reinforced concrete plates under impact loads*. . PhD thesis, Ryerson University, 2016.
  - [11] ABAQUS (2016), ABAQUS Documentation, Dassault Systèmes Simulia Corp, Providence, RI, USA.
  - [12] MpCCI 4. 5.2 (2018), MpCCI coupling environment, Fraunhofer Institute for Algorithms and Scientific Computing SCAI, Germany.

## Integrated Stochastic Prediction for Composites

Loujaine Mehrez<sup>\*</sup>, Roger Ghanem<sup>\*\*</sup>, Ziad Ghauch<sup>\*\*\*</sup>, Venkat Aitharaju<sup>\*\*\*\*</sup>, William  
Rodgers<sup>\*\*\*\*\*</sup>, Arnaud Dereims<sup>\*\*\*\*\*</sup>, Praveen Pasupuleti<sup>\*\*\*\*\*</sup>

<sup>\*</sup>University of Southern California, <sup>\*\*</sup>University of Southern California, <sup>\*\*\*</sup>University of Southern California,  
<sup>\*\*\*\*</sup>General Motors Research Center, <sup>\*\*\*\*\*</sup>General Motors Research Center, <sup>\*\*\*\*\*</sup>ESI Group, <sup>\*\*\*\*\*</sup>ESI Group

### ABSTRACT

Mechanical properties of NCF composites are the byproduct of a manufacturing process that involves a sequence of steps where multiple physical processes, operating at distinct time and spatial scales. Mathematical and computational models of these processes are necessarily incomplete, resulting in both modeling and parametric uncertainties. Predicted performance of these composites, in the elastic and inelastic regimes, as well as near instabilities, is thus dependent on the details of their manufacturing process, and inherit uncertainties accumulated throughout the modeling of that process. Further, as the details of the manufacturing process predict the morphology of the composite on a fine scale and its constituents properties, methods for upscaling to large-scale performance must be relied upon. The challenge in predicting device-scale performance is further exacerbated by the need to account for uncertainties in the manufacturing process in addition to uncertainties in the upscaling process. A key challenge is computational, requiring multi-physics/multiscale simulations in a high-dimensional parameter space. A second challenge is conceptual (as well as numerical, and deals with modeling errors. We present an integrated procedure for tackling both of these challenges. Our procedure relies on adapted and doubly stochastic polynomial chaos expansions that permit highly-accurate approximations in high-dimensional stochastic spaces. By treating the coefficients of the polynomial chaos expansions as random, modeling errors becomes an integral part of the modeling and computational process. The methodology is demonstrated on the validation of a stochastic model for a composite component.

## Efficient Stochastic Analysis and Prediction for Infrastructure Networks Using Compressive Sampling

Hadi Meidani\*, Negin Alemazkoor\*\*

\*University of Illinois at Urbana-Champaign, \*\*University of Illinois at Urbana-Champaign

### ABSTRACT

In order to efficiently quantify the uncertainties in the behaviors of high dimensional infrastructure networks, fast analytical surrogates can be used to replace full-scale simulation models. Polynomial chaos expansion (PCE) is one of the widely adopted surrogates. To build PCEs, non-intrusive stochastic techniques such as regression can be used. These techniques in spite of their increasing use still suffer from the curse of dimensionality. This is because the number of required samples for accurate surrogate estimation rapidly increases with the number of random inputs. This is while the PCE surrogates for infrastructure networks are typically sparsely represented in terms of input uncertainties. Therefore, compressive sampling can be used to build these PCE with a significantly small number of sampled simulations. In this work, we apply novel compressive sampling approaches on the analysis of transportation and power systems. Specifically, we consider uncertain travel demands in the transportation network, and random power consumptions and generations in a power system with renewable energy sources are uncertain. Reliable short-term control of these systems require fast stochastic computation of system's response, e.g. travel time in transportation system and voltage levels in power system. To bypass the need to run a prohibitively large number of expensive simulations and facilitate fast, and almost real time analysis and prediction, we use polynomial surrogates using compressive sampling. In particular, we employ an incremental algorithm to identify the influential parameters, e.g. origin-and-destination pairs that their demand significantly impacts a given link's travel time and network nodes at which power consumption/generation substantially affect the voltage at another given node. Identifying important random inputs and removing unimportant ones not only results in more accurate analysis, but also since our algorithm ranks random inputs based on their influence, it can be readily used for control purposes. We show the applicability and efficiency of our algorithm using benchmark problems in transportation and power systems, namely the Sioux Falls road network and the IEEE 33 bus test system.

## **Metal Additive Manufacturing by Selective Laser Melting: Modeling and Simulation Approaches Across Length Scales**

Christoph Meier\*, A. John Hart\*\*, Wolfgang A. Wall\*\*\*

\*Mechanosynthesis Group, Massachusetts Institute of Technology, 77 Massachusetts Ave, Cambridge, MA 02139, USA / Institute for Computational Mechanics, Technical University of Munich, Boltzmannstraße 15, D-85748 Garching, Germany, \*\*Mechanosynthesis Group, Massachusetts Institute of Technology, 77 Massachusetts Ave, Cambridge, MA 02139, USA, \*\*\*Institute for Computational Mechanics, Technical University of Munich, Boltzmannstraße 15, D-85748 Garching, Germany

### **ABSTRACT**

Among the manifold of existing additive manufacturing (AM) processes, selective laser melting (SLM) of metals has attracted much scientific attention because it offers near-net-shape production of near-limitless geometries, and eventual potential for pointwise control of microstructure and mechanical properties. However, the overall SLM process is complex and governed by a variety of (competing) physical mechanism, motivating the development of elaborate modeling and simulation approaches in order to gain further understanding. The existing modeling approaches in the context of SLM processes can typically be classified in three categories: macroscopic, mesoscopic and microscopic models [1]. Macroscopic models typically treat the powder phase as a homogenized continuum resulting in efficient numerical tools capable of simulating entire SLM-manufactured parts. These models commonly aim to determine spatial distributions of temperature, residual stresses as well as dimensional warping within SLM parts, without explicitly resolving the fluid dynamics within the melt pool. On the contrary, mesoscopic models resolve individual powder grains and account for the melt pool thermo-hydrodynamics in an explicit manner. Mesoscopic models commonly predict resulting melt pool and part properties such as melt track stability, surface quality and layer-to-layer adhesion as well as creation mechanism of defects such as pores and inclusions. Last, microscopic models consider the evolution of the metallurgical microstructure involving the resulting grain sizes, shapes and orientations as well as the development of thermodynamically stable or unstable phases. The presentation will review existing modeling and simulation approaches on different length scales. In this context, also the first steps of the authors' ongoing research work in developing a mesoscopic simulation model for the SLM processes will be presented. Our approach especially focuses on the particle-to-particle interaction between individual powder grains, both, during the actual selective laser melting process but also in the initial powder coating process. The latter, which has rarely been studied so far, is crucially governed by adhesive forces prevalent at this length scale and essentially determines powder bed properties such as packing density, surface roughness or particle coordination number and, thus, also the properties of the final metal part after the rapid melting and solidification process in SLM. References: [1] C. Meier, R. Penny, Y. Zou, J.S. Gibbs, A.J. Hart. Thermophysical phenomena in metal additive manufacturing by selective laser melting: Fundamentals, modeling, simulation and experimentation. Annual Review of Heat Transfer, accepted for publication.

## Photosynthesis and Its Biomedical Applications: NMR Properties of FMO Light-harvesting Complexes

Roderick Melnik\*, Shyam Badu\*\*

\*MS2Discovery Institute, Wilfrid Laurier University, \*\*MS2Discovery Institute, Wilfrid Laurier University

### ABSTRACT

The bacteriochlorophyll is one of the most important molecular systems found in the light-harvesting complex in which the photosynthesis event occurs. Most recently, bacteriochlorophylls, found in the light-harvesting complexes, have been used for the photodynamic therapy for treatment of some forms of cancer. In order to understand the application of these photosynthetic materials in biomedicine, as well as in the plant cycle and other life science applications, it is very important to understand the structure of these molecules. Therefore, in this contribution, we study the structural properties of the bacteriochlorophyll taken from the Fenna-Matthew-Olsen light-harvesting complex found in the green sulfur bacteria. Specifically, in our current study, we present the nuclear magnetic resonance (NMR) spectrum of the bacteriochlorophyll that is directly taken from the FMO complex, as well as the spectrum for this system for its optimized geometry. We use density functional theory to calculate the optimized geometry and the NMR spectra of the bacteriochlorophyll. From our calculations, we found that the chemical shift values are slightly lower for the optimized geometry of the bacteriochlorophyll than the values obtained for the unoptimized bacteriochlorophyll. The differences observed between these two spectra are due to the fact that the unoptimized structure of the bacteriochlorophyll possesses the influence of the protein environment of FMO complex.

## Investigation on Generation Method of Meso-scale Simulation Model for W-Cu Shaped Charge Liner and its Dynamic Response under Explosive Loading

Jianbing Men<sup>\*</sup>, Fang Wang<sup>\*\*</sup>, Jianwei Jiang<sup>\*\*\*</sup>, Shuyou Wang<sup>\*\*\*\*</sup>, Mei Li<sup>\*\*\*\*\*</sup>

<sup>\*</sup>Beijing Institute of Technology, <sup>\*\*</sup>Beijing Institute of Technology, <sup>\*\*\*</sup>Beijing Institute of Technology, <sup>\*\*\*\*</sup>Beijing Institute of Technology, <sup>\*\*\*\*\*</sup>Beijing Institute of Technology

### ABSTRACT

Tungsten-copper(W-Cu) is a kind of composites constituted of two immiscible phases which are mechanically mixed without interfacial reaction. It is always regarded as homogeneous material in conventional simulations. However, the dynamic response of W-Cu under explosive loading is still unclear especially in the meso-scale scope due to the significant difference between the chemical and physical properties of tungsten and copper. In order to investigate the mesoscopic mechanism of W-Cu shaped charge jet formation, the generation program of W-Cu meso-discrete model was developed based on the random particles principle. The discrete models of W-Cu liner with different ratios of two phases and various diameters of tungsten particles were successfully established by the program. The multi-scale finite element numerical simulations were carried out on the particle-matrix materials and the referenced equivalent homogeneous material by using Autodyn-2D Euler solver. The results show that the average velocity of Cu phase is much higher than W phase, leading to a phase segregation and composition gradient in W-Cu jet during its forming process. The content of Cu is higher in the jet tip compared with the liner material while the W particles mainly concentrate in the slug. A novel recovery experiment was designed to verify the microstructural change of W-Cu composite during the jet formation process. The W-Cu jet residue recovered from the target surface was observed by scanning electron microscopy. The experiment results also indicate that composition gradient exists in the W-Cu jet, which was in good agreement with the simulation results. Reference: [1]D. Eakins, N.N. Thadhani. Discrete Particle Simulation of Shock Wave Propagation in a Binary Ni+Al Powder Mixture [J]. Journal of Applied Physics, 2007, 101, 043508 [2]Liu Jintao, Cai Hongnian, Wang Fuchi etc. Multiscale Numerical Simulation of the Shaped Charge Jet Generated from Tungsten-copper Powder Liner [J]. Journal of Physics: Conference Series, 2013, 419: 1-8 [3]Seong Lee, Moon-hee Hong, Joon-wong Noh etc. Microstructural Evolution of a Shaped-charge Liner and Target Materials during Ballistic Tests [J]. Metallurgical and Materials Transactions A, 2002, 33A: 1069-1074

## **Analysing the Relationship between the Hopper Angle and the Mass Flow Rate in Conical Hoppers**

David Mendez<sup>\*</sup>, Raul Cruz Hidalgo<sup>\*\*</sup>, Diego Maza<sup>\*\*\*</sup>

<sup>\*</sup>University of Navarra, <sup>\*\*</sup>University of Navarra, <sup>\*\*\*</sup>University of Navarra

### **ABSTRACT**

The accurate prediction of the mass flow rate in silos and bins is obviously important in many industries. In past decades, accurate correlations predicting the mass flow rate in granular hoppers were introduced [1,2]. However, there is a lack of a generalized formulation connecting the mass flow rate with the grains properties, the hopper geometry, and the macroscopic stress field. On the other hand, examining industrial silos by R&D factories and technical offices, continuous models are the most commonly used numerical tools. Those algorithms are usually very sophisticated and have many tuning parameters, so they require an extensive experimental calibration. In this work, we use a continuous description [3] to analyze the relationship between the hopper angle and the mass flow rate in conical hoppers. Adjusting the parameters of the simulation and feedbacking the code with experimental results, we develop an accurate calibration procedure, which can be employed in both simplified lab conditions and industrially relevant systems. Furthermore, executing a systematic study, changing the hopper angle and the size of the aperture, we find that the used numerical implementation captures the main features of the granular flux through the orifice, such as the velocity and density profiles. Moreover, the results suggest that the hopper angle controls the system's dynamics near the exit, determining the discharge rate at the outlet. [1] W. A. Beverloo, H. A. Leniger, and J. J. Van de Velde, Chem. Eng. Sci. 15, 260 (1961) [2] C. Mankoc, A. Janda, R. Arévalo, M. Pastor, I. Zuriguel, A. Garcimartin, and D. Maza, Granular Matter 9, 407 (2007) [3] A. Janda, I. Zuriguel, and D. Maza, Phys. Rev. Lett. 108, 248001 (2012) [4] ANSYS Fluent <http://www.ansys.com/Products/Fluids/ANSYS-Fluent>

## Study on Pull-out Failure of Headed Inserts in Concrete Based on Peridynamic Theories

Xianhong Meng<sup>\*</sup>, Jianan Bi<sup>\*\*</sup>, bo Jiang<sup>\*\*\*</sup>, Xiaofeng Wang<sup>\*\*\*\*</sup>

<sup>\*</sup>Shenyang Jianzhu University?Shenyang?China?110168, <sup>\*\*</sup>Shenyang Jianzhu University?Shenyang?China?110168, <sup>\*\*\*</sup>China Academy of Building Research?Beijing?China?100013, <sup>\*\*\*\*</sup>China Academy of Building Research?Beijing?China?100013

### ABSTRACT

The metal inserts are widely used in lifting and handling of concrete components. The concrete cone capacity of headed inserts subjected to axial tension load was studied by many researchers, However, the research on the numerical simulation method is still insufficient. The finite element simulation results are far from the actual situation, and the reason is that the continuum mechanics is difficult to describe the discontinuous problem of concrete cracking. The peridynamic(PD) method is more advantageous in solving the problem about the concrete crack expansion and material damage, etc. A peridynamic(PD) model based on PMB was established, two kinds of critical stretch of the bond in concrete and the lifting inserts were applied to distinguish the different tensile strength, and the bond of linkage between the concrete and the lifting inserts took the mean value of the above two kinds of critical stretch. Through this model and the continuous medium finite element model, the failure process of the embedded headed inserts was simulated. The comparison between the simulation results and the experimental results indicated that the PD model was closer to the actual situation than the finite element method in solving the crack propagation of the concrete cone failure. It was proved that PD method can be used to analyze the pull-out damage of the lifting inserts in the concrete, provided a theoretical basis for the engineering application of the lifting inserts. [1]Karin Lundgren,Kent Gylltoft.A model for the bond between concrete and reinforcement[J].Magazine of Concrete Research,2000,52(1):53-63 [2]HUANG Dan,ZHANG Qing,QIAO Pi-zhong,et al.A review on peridynamics method and its applications[J].Advances in Mechanics,2010,40(4):448-459. [3]SHI Hongshun?QIAN Songrong?XU Ting?YUAN Qunsheng?ZHANG Guo-hao.Study on reinforced concrete structure failure based on peridynamic theories[J].Guizhou Science,2016,34(06):64-68.

## SCRAMJET Design Optimization Using SNOWPAC in Dakota

Friedrich Menhorn<sup>\*</sup>, Youssef Marzouk<sup>\*\*</sup>, Florian Augustin<sup>\*\*\*</sup>, Michael Eldred<sup>\*\*\*\*</sup>, Gianluca Geraci<sup>\*\*\*\*\*</sup>

<sup>\*</sup>Technical University of Munich, <sup>\*\*</sup>Massachusetts Institute of Technology, <sup>\*\*\*</sup>MathWorks/ Massachusetts Institute of Technology, <sup>\*\*\*\*</sup>Sandia National Laboratories, <sup>\*\*\*\*\*</sup>Sandia National Laboratories

### ABSTRACT

SNOWPAC (Stochastic Nonlinear Optimization With Path-Augmented Constraints) [Augustin & Marzouk 17] is a method for stochastic derivative-free optimization, developed to treat nonlinear constrained optimization problems with uncertain parameters. These uncertain parameters represent, for example, a lack of knowledge about the system under consideration, or other errors in the models entering the objective and constraints. Optimization in these settings employs measures of robustness and risk in order to describe a suitable solution—for instance, to identify solutions that are relatively insensitive to parameter uncertainties. SNOWPAC extends the path-augmented constraint framework introduced by NOWPAC [Augustin & Marzouk 14], via a noise-adapted trust region approach and Gaussian process approximations. It solves optimization problems where Monte Carlo sampling is used to estimate robustness or risk measures comprising the objective function and/or constraints. We consider problems where expensive black box model evaluations are needed to construct these estimates, and thus we focus on a small sample size regime. This regime involves significant noise in the estimators, which slows the optimization process. To mitigate the impact of noise, SNOWPAC employs Gaussian process regression to smooth models of the objective and constraints in the trust region. In a recent development, SNOWPAC has been integrated with the Dakota framework, which offers a highly flexible interface to couple the optimizer with different sampling strategies and surrogate models. In this presentation, we showcase the combined SNOWPAC-Dakota capability by performing design optimization under uncertainty in two challenging problems: a bump in a 2D supersonic duct and supersonic turbulent spray combustion in a SCRAMJET engine. The SCRAMJET follows the HIFiRE design and is modeled by an LES simulation code developed by Sandia National Laboratories. We compare deterministic optimization results with results obtained by introducing uncertainty in the inflow parameters. As a sampling strategy, we contrast simple Monte Carlo sampling with more sophisticated multilevel Monte Carlo approaches. Here, Dakota serves as the driver of the optimization process, employing SNOWPAC as optimization method on the black box problem. We show that all approaches provide reasonable optimization over the design while seeking/maintaining feasibility in the final minimized objective. Furthermore, we see significant improvements in the computational cost when employing multilevel approaches that combine solutions from different grid resolutions.

## Impact Modelling of Bioinspired Pseudo-ductile Composite Laminates with Hierarchical Energy Absorption Mechanism

Michele Meo<sup>\*</sup>, F. Rizzo<sup>\*\*</sup>, F. Pinto<sup>\*\*\*</sup>

<sup>\*</sup>University of Bath, <sup>\*\*</sup>University of Bath, <sup>\*\*\*</sup>University of Bath

### ABSTRACT

The intrinsic layered nature of carbon fiber and their weak resistance to out-of-plane loads leads to overdesigned composite structural parts, preventing the full exploitation of their unique characteristics and limiting their use in harsh environments. Therefore, composite laminates able to respond with a pseudo-ductile behaviour when subjected to an out-of-plane load is of crucial importance as it would eliminate the need of overdesigned parts and extend the range of applications available to composite structures. This paper presents the design, manufacturing and characterisation of a bioinspired CFRP laminate in which the pseudo-ductility arises from an ordered pattern of discontinuities which are created over the surface of the different layers before the curing reaction, called platelets. The presence of this carved pattern creates a hierarchical interplay of high-strength carbon fibre segments and elastic soft matrix-rich areas which resembles the interaction between the  $\beta$ -sheets crystalline domains and amorphous helical and  $\beta$ -spiral structures typical of spider silk and other biological structures (e.g. cellulose, hair) which enables a combination of high mechanical strength and elasticity. The effect of different geometrical parameters of the carved pattern such as critical length, shape and dimensions, on the mechanical properties of the laminate were modelled via Finite Element Analyses in order to identify the optimal configuration of the discontinuities, finding the best trade-off between in-plane and out-of-plane mechanical properties. Samples with different carved patterns were then manufactured and their properties were assessed by subjecting them to Low Velocity Impacts (LVIs). An optimisation process was carried out to optimise critical fiber length of the platelets. The predicted internal distribution of damaged areas was compared to experimentally measured damage using different Non Destructive Techniques. The energy absorption improvement was assessed by comparing it to the behaviour of traditional CFRP. Results showed that the presence of the artificial discontinuities is able to induce pseudo-ductile behaviour into the CFRP, improving the energy absorption mechanism during out-of-plane solicitations without severely affecting the in-plane properties. 1. Pinto, F., A. White, and M. Meo, Characterisation of ductile prepregs. *Applied Composite Materials*, 2013. 20(2): p. 195-211. 2. Keten, S., et al., Nanoconfinement controls stiffness, strength and mechanical toughness of  $\beta$ -sheet crystals in silk. *Nature materials*, 2010. 9(4): p. 359. 3. Mirkhalaf, M. and F. Barthelat, Nacre-like materials using a simple doctor blading technique: Fabrication, testing and modeling. *Journal of the mechanical behavior of biomedical materials*, 2016. 56: p. 23-33.

## Variational Model for Solid and Hydraulic Fracturing Problems Using Interface Elements

Günther Meschke\*, Ildar Khisamitov\*\*

\*Ruhr University Bochum, \*\*Ruhr University Bochum

### ABSTRACT

In this presentation, we propose a variational formulation for fracture in brittle materials, which is inspired by the class of phase-field models [1, 2] but which is incorporated into a zero-thickness interface modeling framework instead of a continuum damage framework [3]. The fractured structure is variationally formulated as the sum of bulk elastic and fracture surface energies. With the help of a damage variable used as an additional degree of freedom, the fracture propagates according to a minimization principle of the total potential energy. As a criterion for the crack propagation, an energy criterion, checking, if the elastic energy within the interface surface exceeds the critical energy release rate is used. Equilibrium of the discretized structural boundary value problem is found using a staggered scheme, solving first the mechanical problem and then searching for the solution for the updated damage variable. The model is first presented in the context of crack propagation simulations in structures made of quasi-brittle materials. In a second step, the computational model is formulated in a coupled poromechanics framework to enable the numerical simulation of hydraulic fracturing problems. This type of analysis finds applications in hydraulic stimulation of deep geothermal reservoirs, which is characterized by the creation of hydraulically driven fractures, which eventually interact with pre-existing fractures and natural faults. Besides selected benchmark tests, also various laboratory tests fluid induced fracture propagation are analyzed numerically and compared with experimentally obtained fracture paths. [1] Bourdin, B., Francfort, G.A. and Marigo, J.J., The variational approach to fracture , *Journal of elasticity*, 91, 5–148 (2008). [2] Miehe, C., Welschinger, F. and Hofacker, M., Thermodynamically consistent phase-field models of fracture: Variational principles and multi-field FE implementations , *International Journal for Numerical Methods in Engineering*, 83, 1273–1311 (2010). [3] Khisamitov, I. and Meschke, G., Variational approach to interface element modeling fracture propagation, *Computer Methods in Applied Mechanics and Engineering*, 328, 452-476 (2018).

## **Phase-field Modeling of Anisotropic Phase-change and Fracture in Silicon Anodes in Li-ion Batteries**

Ataollah Mesgarnejad\*, Alain Karma\*\*

\*Northeastern University, \*\*Northeastern University

### **ABSTRACT**

The chemo-mechanical modes of failure in Li-ion battery remain poorly understood. In this talk, motivated by new experimental observations, we will present the results of our simulations of complex finite elasto-plastic model for Si/Ge-anode structures. Due to their high theoretical capacity, Silicon and Germanium as anode material for Li-ion batteries has attracted wide interest in the research community. However, the intercalation of Li ions in crystalline Si (or Ge) results in phase change and amorphization of Si to  $\text{Li}_x\text{Si}$  accompanied by  $\sim 300\%$  volume expansion. Amorphization, in turn, results in an inelastic deformation flow and fracture. Furthermore, the intercalation occurs as a reaction-controlled invasion of Li where the sharp amorphous-crystalline interface between Li-rich amorphous phase and crystalline phase moves anisotropically due to the crystallographic directions. Over the past two decades, the phase-field models have emerged as exceptional computational tools for modeling a spectrum of physical phenomena from phase change to fracture. The variational nature of these models allows for coupling between a range of physical phenomena. To model intercalation of Si structures, we combine formulations of finite neo-Hookean elasticity and finite J-2 plasticity with a modified Allen-Cahn model of the amorphous-crystalline phase change and a phase-field fracture. We show how our numerical simulations reproduce the experimentally observation where the crystalline directions significantly modify the onset of fracture and its propagation direction.

## Anisotropic Mesh Adaptation on Emerging Architectures

Youssef Mesri<sup>\*</sup>, Philippe Meliga<sup>\*\*</sup>, Franck Pigeonneau<sup>\*\*\*</sup>, Rudy Valette<sup>\*\*\*\*</sup>, Elie Hachem<sup>\*\*\*\*\*</sup>

<sup>\*</sup>Mines Paristech, <sup>\*\*</sup>CNRS, <sup>\*\*\*</sup>Mines Paristech, <sup>\*\*\*\*</sup>Mines Paristech, <sup>\*\*\*\*\*</sup>Mines Paristech

### ABSTRACT

This work is motivated by the success of the anisotropic adaptive finite element methods in accurately simulating complex physical systems in science and engineering. The parallel implementation of anisotropic adaptive finite element methods is a challenging task for which efficiency continues to be a significant issue due to its dynamic data structure modification along the simulation. We have developed and optimized in the last years, mesh adaptation tools and algorithms to manage efficiently the dynamic load balancing in the context of SPMD based parallelism [1, 4]. However, the performance of these algorithms is deteriorated with the advent of new architectures such as Intel Xeon Phi Knights Landing processors or GPUs. Indeed, the heterogeneity of the hardware resources and the memory hierarchy require the adaptation of the existing algorithms according to these characteristics. The effort should then goes back to focus only on the efficiency of a single computing node. The leading question that arises from this analysis is then as follows: Which effort is the most rewarding: code optimization, algorithmic adaptation or both? In this paper, we present the recent improvements brought to the anisotropic mesh adaptation tools to meet the efficiency challenges imposed by the heterogeneity of the emerging architectures. Indeed, we developed algorithms and techniques to efficiently use CPU and memory. The main data arrays are vectorized with Intel AVX-512 intrinsics, the data locality is improved by considering a suitable renumbering algorithm for unstructured meshes, and the mesh is efficiently mapped into the threads. We conduct performance analysis over different CFD benchmarks to highlight effectiveness of the proposed approach.

REFERENCES [1] Y. Mesri, H. Dignonnet, T. Coupez. Advanced parallel computing in material forming with CIMLib. E. J. of Computational Mechanics, 18(7-8):669-694, 2009. [2] Mesri Y., Dignonnet H., Guillard H. Mesh Partitioning for Parallel Computational Fluid Dynamics Applications On a Grid. Finite Volumes for complex applications IV. Hermes Science Publisher, pp. 631—642, 2005 [3] Y. Mesri, H. Dignonnet, T. Coupez, Hierarchical adaptive multi-mesh partitioning algorithm on heterogeneous systems. Parallel Computational Fluid Dynamics 2008, 299-306 [4] Mesri Y., Gratien J.-M., Ricois O., Gayno R. Parallel Adaptive Mesh Refinement for Capturing Front Displacements: Application to Thermal EOR Processes. SPE paper, 2013

## Optimization of Periodic Structures with Convolutional Neural Network Surrogate Models

Mark Messner\*

\*Argonne National Laboratory

### ABSTRACT

The development of additive manufacturing methods has spurred interest in the optimization of periodic, mesoscale structural unit cells. These unit cells can be printed to fill a component shape, forming an effective material on the macroscale with optimized material properties. This presentation describes a method for optimizing the effective, homogenized material properties of such periodic mesostructures using neural network surrogate models. Convolutional neural networks are a machine learning tool that has been successfully applied to a variety of image recognition problems. The convolutional network structure is also ideally suited for solid mechanics homogenization: the homogenization of a particular periodic mesostructure can be viewed as an image recognition problem. This presentation describes the development and training of a convolutional neural network surrogate model that can accurately predict the effective elastic and inelastic properties of 2D periodic mesostructure. A forward evaluation of the model is six orders of magnitude faster than a corresponding finite element simulation. Such fast surrogate models can be used to find globally optimal material mesostructures through genetic algorithm optimization. This presentation details the results of several example optimization problems. For the simplest, elastic optimization problems the surrogate model approach finds similar structures to those found through conventional, gradient based topology optimization methods. The surrogate modeling approach can also optimize for inelastic effective material properties like energy dissipation. These kinds of optimization problems are harder to solve with conventional methods and are relevant to finding optimally dissipative structures for armor and ballistic protection applications.

## Variability Response Function of Axial Characteristic

Mladen Mestrovic\*

\*University of Zagreb

### ABSTRACT

The axial characteristic of beam used in second order theory of beam bending is taken for stochastic analysis. The flexural rigidity of the beam is assumed to be random variable with given expectation, variance and coefficient of variation. That assumption leads to variability of axial characteristic. Variability response function of axial characteristic is defined to determinate its expectation, variance and coefficient of variation. The coefficient of variation of axial characteristic is expressed as function of coefficient of variation of flexural rigidity. The variation of axial characteristic is needed for further investigation of variability of the beam stiffness matrix defined according the second order theory of elasticity.

## Modeling Strategies for Magnetosensitive Elastomers on Different Scales: A Link between Microscopic and Macroscopic Models

Philipp Metsch<sup>\*</sup>, Karl Alexander Kalina<sup>\*\*</sup>, Jörg Brummund<sup>\*\*\*</sup>, Markus Kästner<sup>\*\*\*\*</sup>

<sup>\*</sup>Institute of Solid Mechanics, TU Dresden, <sup>\*\*</sup>Institute of Solid Mechanics, TU Dresden, <sup>\*\*\*</sup>Institute of Solid Mechanics, TU Dresden, <sup>\*\*\*\*</sup>Institute of Solid Mechanics, TU Dresden

### ABSTRACT

Magnetosensitive elastomers (MSEs) represent a class of active materials which typically consist of micron-sized magnetizable particles embedded in a cross-linked elastomer matrix. Due to mutual interactions of the particles, MSEs are able to alter their effective material behavior reversibly if subjected to an external magnetic field. Moreover, they show a large magnetostrictive response: compared to pure ferromagnetic materials, their field-induced deformation is increased by orders of magnitude. This strong coupling of magnetic and mechanical fields facilitates a variety of applications in the fields of actuators and sensors. Within this contribution, a modeling strategy for MSEs is presented: starting from the properties of the magnetizable particles and the elastomer matrix, a continuum formulation of the problem is applied on the microscale in order to determine the macroscopic material behavior by means of a computational homogenization [1]. The governing equations are solved using the finite element method. For these calculations, an efficient monolithic solution scheme is developed in order to account for the strong nonlinear coupling of magnetic and mechanical fields [2]. Initially, the modeling approach is applied to investigate the influence of microstructural geometric as well as constitutive properties of MSEs on their behaviour. A comparison between our simulations and experiments is used to identify deformation mechanisms which can be observed in both simplified and complex MSE samples [3]. Moreover, the discrepancy between widely used two-dimensional approaches and a full three-dimensional solution of the problem is investigated qualitatively and quantitatively. Based on these findings, the macroscopic behavior of MSEs is predicted by performing a statistical evaluation of different random microstructures. The results of our approach are used to identify parameters of available macroscopic models from the literature - an optimization procedure for the parameter identification allows for the link between microscopic and macroscopic models. This strategy allows for an efficient prediction of the effective behavior of realistic MSE samples. References: [1] Metsch, P., Kalina, K. A., Spieler, C., Kästner, M., A numerical study on magnetostrictive phenomena in magnetorheological elastomers, *Computational Materials Science*, 124, pp. 364-374 (2016) [2] Kalina, K. A., Metsch, P., Kästner, M., Microscale modeling and simulation of magnetorheological elastomers at finite strains: A study on the influence of mechanical preloads, *International Journal of Solids and Structures*, 102-103, pp. 286-296 (2016) [3] Puljiz, M., Huang, S., Auernhammer, G. K., Menzel, A. M., Forces on Rigid Inclusions in Elastic Media and Resulting Matrix-Mediated Interactions, *Physical Review Letters*, 117, pp. 238003 (2017)

## Surface Mechanics Improved Solutions to an Elastic Half-space Subjected to Nanoscale Surface Traction

Changwen Mi<sup>\*</sup>, Xiaobao Li<sup>\*\*</sup>

<sup>\*</sup>Southeast University, China, <sup>\*\*</sup>Hefei University of Technology, China

### ABSTRACT

To better understand the impact of surface stress effects on fundamental solutions of elasticity, a three-dimensional stress analysis is performed for an elastic half-space subjected to surface tractions applied within a nanoscale circular portion of its plane boundary. The method of Boussinesq displacement functions is used to address the problem, where local elastic field including displacements and stresses in the vicinity of the loading area is semi-analytically determined by solving a set of improper integral equations. Numerical results are presented to examine effects and the stress disturbances caused by the coupling of surface loads and surface mechanics. The results show that a metallic layer with properly designed mechanical behavior coated on the free surface of a half-space substrate of even the same material can function as a stiffener and stress reliever. The results suggest a means of optimizing the local displacements, strains and stresses by controlling the material properties of the half-space boundary. Keywords: Surface mechanics; Half-space; Surface loads; Stress disturbance

## CFD and FFD Method for Lines Optimization Design of Twin-skeg Ship

Aiqin Miao\*, Decheng Wan\*\*

\*Shanghai Jiao Tong University, \*\*Shanghai Jiao Tong University

### ABSTRACT

The optimization design method for a twin-skeg ship's stern shape is presented here. The stern shape of a twin-skeg ship greatly affects its resistance, propulsion and maneuverability. Therefore, to improve hydrodynamic performance, the local hull lines of a twin-skeg ship's stern can be optimized in the preliminary design stage according to some scientific transformation method. This paper intends to optimize the stern of a twin-skeg ship based on OPTShip-SJTU, a solver for ship optimization design developed independently by Computational Marine Hydrodynamics Laboratory (CMHL). Free-form Deformation (FFD) method is introduced and developed to transform twin skegs locally. The total resistance and the wake fraction in the stern are considered as two objective functions, calculated by our in-house CFD solver, naoe-FOAM-SJTU based on the viscous flow theory. Finally, NSGA-II algorithm is called for the multi-objective optimization solution to obtain optimal hulls with the best resistance and propulsion performance in the design space. Notably, in order to reduce the numerical computational cost, the relationship between ship transformation parameters (design variables) and hydrodynamic performance (objective functions) is expressed as two surrogate models by design of experiment and Kriging method. These two models are directly applied to evaluate the objective functions of any new individual in the optimization process, instead of direct numerical simulations. The selected optimal ship is compared with the parent ship in terms of the wave elevation, pressure distribution, vorticity field and wake field. It turns out that the research provides an effective guide to the stern shape design of the twin-skeg ship and the solver OPTShip-SJTU is practical for ship optimization design.

## **The Importance of Geometry and Mesh Association in Adaptive Meshing**

Todd Michal\*

\*Boeing Research and Technology

### **ABSTRACT**

The last decade has seen an increased use of adaptive meshing in computational analysis. Adaptive meshes are continuously changing throughout the analysis requiring a close association between the mesh and geometry model. In this talk the importance of associating the geometry and mesh and tracking that association throughout the analysis will be explored. Examples from the context of anisotropic adaptive meshing on complex aerospace applications will be presented.

## **Multi-Scale simulation for Part-Level Metal AM**

Pan Michaleris<sup>\*</sup>, Jeff Irwin<sup>\*\*</sup>, Erik Denlinger<sup>\*\*\*</sup>, Michael Gouge<sup>\*\*\*\*</sup>, Serge Sidorov<sup>\*\*\*\*\*</sup>

<sup>\*</sup>Autodesk, <sup>\*\*</sup>Autodesk, <sup>\*\*\*</sup>Autodesk, <sup>\*\*\*\*</sup>Autodesk, <sup>\*\*\*\*\*</sup>Autodesk

### **ABSTRACT**

A primary challenge for Laser Powder Bed Fusion (LPBF) to become a reliable and economically feasible method of component production is the warping of parts during production. This distortion adds expense of the process, can take weeks or months of experimentation to minimize, and may prematurely end the businesses case for implementing AM into production. Autodesk offers a software, Netfabb Simulation, which can predict and mitigate build failure prior to manufacture, by using a multi-scale modeling approach. This study shows through simulation-experimental comparisons that this software can be used to make timely and useful predictions of distortion for common AM metals. It will also document the successful modeling of the secondary failure mechanisms of support structure delamination and recoater blade interference. Simulation based distortion mitigation will be demonstrated by simulating a part and compensating the build geometry to reduce deformation. Finally, the concept of multi-scale modeling will be extended to the prediction of hot-spots and lack of fusion related defects on Part-Level AM builds.

## Modeling of Masonry Walls under Blast Loads

Georgios Michaloudis\*, Norbert Gebbeken\*\*

\*University of the Bundeswehr Munich, \*\*University of the Bundeswehr Munich

### ABSTRACT

Masonry walls represent one of the most common applied constructions in civil engineering and architecture. The inhomogeneous nature of masonry imposes a challenge in the development of robust modeling techniques especially under high dynamic loads. Under extreme loading conditions the numerical model must take into account failure mechanisms which do not occur under static loads. In this contribution some modeling strategies are discussed which are suitable for the simulation of unreinforced masonry walls under detonation loads. The damage formation in the wall under loads resulting from far-field as well as contact detonations is investigated. Firstly the issue of an appropriate material model for bricks under high strain rates is discussed. Through a proper adaptation of a material model initially developed for concrete under blast loads we derive all the necessary parameters for the bricks. In this way we develop a suitable strength model as well as an equation of state for the simulation of the material behavior under high strain rates. We apply the simplified micro-model as the general strategy for the modeling of the walls. The numerical results resulting from the simulation of the walls under far-field detonation loads are validated with experiments. Subsequently we refine these models in order to be able to capture the local damage formation and the resulting debris due to a contact detonation. Small parts of the wall in the proximity of the explosion separate from the main body of the wall and travel at high velocities. They can establish an additional danger for persons and infrastructure which theoretically lie in a secure distance from the target of the explosion. This failure mechanism is dominant in contact detonation but negligible in far-field blast scenarios. We propose a numerical algorithm in order to alter the numerical model in the regions where formation of debris is expected due to a contact detonation. The algorithm is based in Lagrangian finite elements so that the general formulation of the model (Lagrangian) does not need to be changed. The numerical results also of the contact detonation scenarios are validated with appropriate experiments.

## State-of-the-art of Analysis Techniques for Masonry Arches and Shells Subjected to Seismic Loading and Their Applicability to Conceptual Design

Tim Michiels\*, Sigrid Adriaenssens\*\*

\*Princeton University, \*\*Princeton University

### ABSTRACT

The design of new masonry shells is attracting renewed attention because the embodied energy of masonry structures is exceptionally low, making them environmentally friendly construction solutions [1]. Extensive research has led to a wide array of analysis methods for masonry arches and shells, but only few of these methods have been translated into tools for their conceptual design. While most of these conceptual design tools focus on gravitational loading, earthquakes can be the design-guiding stressors for masonry shells. And while also for seismic loads, analysis methods for masonry are well established, tools for shape-finding in seismic areas are nearly non-existent. Therefore, this presentation provides an overview of the available analysis techniques to evaluate the seismic response of masonry arches and shells and evaluates the usefulness of each technique to perform conceptual design for shells in earthquake areas. The considered methods include upper-and lower-bound equilibrium approaches – such as thrust line and network analysis, kinematic limit state analysis and membrane analysis and explain while these are the most promising tools for form-finding. Furthermore, while analytic solution methods have been developed for arches, the application of these analytic solutions to 3D-geometries has not yet been accomplished. Instead, researchers typically resort to macro-modelling, such as non-linear finite element modeling (FEM) techniques assuming homogeneous material behavior. It is shown how these methods are more suitable for validation, than to perform conceptual design due to their high computational demand. Similarly, it is shown that distinct element methods can be an excellent analysis technique for shells or arches which can be discretized into realistic discrete blocks. Additionally, a set of recently published, lesser-known methods, such as the reformulated thrust-network analysis and the relaxed-funicularity method are discussed because of their potential for form-finding [2]. Finally, examples are provided that show how simplified equilibrium methods can be used to find new shapes for masonry shells in seismic areas, while their seismic capacity is validated using non-linear FEM [3].

1. De Wolf, C., M. Ramage, and J. Ochsendorf, Low Carbon Vaulted Masonry Structures. *Journal of the International Association for Shell and Spatial Structures*, 2016 (Vol. 57 (2016) No. 4 December n. 190): p. 275-284.
2. Gabriele, S., V. Varano, G. Tomasello, and D. Alfonsi, R-Funicularity of form found shell structures. *Engineering Structures*, 2018. 157: p. 157-169.
3. Michiels, T. and S. Adriaenssens, Form-finding algorithm for masonry arches subjected to in-plane earthquake loading. *Computers & Structures*, 2018. 195: p. 85-98.

## **Multiscale and Multiphysics Integrated Computational Materials Engineering Framework for Linking Additive Manufacturing Process Parameters with Part Performance**

John Michopoulos<sup>\*</sup>, Athanasios Iliopoulos<sup>\*\*</sup>, John Steuben<sup>\*\*\*</sup>, Andrew Birnbaum<sup>\*\*\*\*</sup>

<sup>\*</sup>US Naval Research Laboratory, <sup>\*\*</sup>US Naval Research Laboratory, <sup>\*\*\*</sup>US Naval Research Laboratory, <sup>\*\*\*\*</sup>US Naval Research Laboratory

### **ABSTRACT**

Additive manufacturing (AM) has become an important technology for the fabrication of a wide variety of components and structures. Interest in AM has been primarily driven by the potential for object fabrication relatively free of geometric constraints as well as the introduction of features across multiple length scales. Despite these advantages, currently implemented AM processes continue to be highly non-uniform in terms of undesirable, process-induced features both from material and geometry perspectives. Experimental studies have shown that these non-uniformities lead to AM-induced micro/meso structures and morphologies that differ drastically from those produced by conventional methods. Consequently, additively manufactured products suffer from issues including geometric errors, residual stresses and strains that may be very large, layer delamination, as well as porosity and poor or indeterminate material properties. These issues lead to further uncertainty in functional performance that often preclude the use of AM technology in performance-critical applications. To address these issues our team has embarked on the development of a Multiscale and Multiphysics Integrated Computational Materials Engineering (MMICME) framework for AM. Our description will be the topic of this talk. This framework incorporates multiscale multiphysics modeling and experimentation in order to fully encapsulate the important roles that micro- and meso-structures play in tailoring material properties and responses in engineering applications. The immediate goals of this effort is to enable on-demand control of AM processes for tailoring meso- and micro-structures to endow desirable properties and eliminate undesirable ones. This talk describes an overview of the multiscale and multiphysics modeling and simulation elements, which have been developed in order to implement our MMICME framework for AM.

## APPLICATION OF THE MESHLESS METHOD TO THE FILTRATION EQUATION

MAGDALENA MIERZWICZAK\*

\*Poznan University of Technology, Institute of Applied Mechanics  
Jana Pawła II 24,  
60-965 Poznan, POLAND  
magdalena.mierzwiczak@wp.pl

**Key words:** Beavers-Joseph boundary condition, permeability, slip constant, fibrous porous media, meshless methods.

**Abstract.** In this paper the permeability and the slip constant on the boundary of the considered fibrous porous region are determined by numerical simulation of the imaginary physical experiment. The porous medium is modeled by a parallel bundle of straight fibers arranged in a regular triangular, square, or hexagonal array. In order to determine the permeability, the flow driven by the pressure gradient in an unbounded porous medium is considered. To determine the slip constant, the shear flow between a flat immovable wall containing both the porous and free flow layers is considered. In both numerical simulations, the meshless procedure is applied. The influence of the volume fraction of the fibres on the value of the permeability and the slip constant is investigated. In all considered cases the value of the slip constant is lower than one. The slip constant decreases with increasing the volume fraction of fibers for a high porosity. For a square and hexagonal array the value of slip constant starts increasing for small porosity. For the same volume fraction of the fibers, both the permeability and the slip constant for the triangular array is smaller than for the square and the hexagonal array. Proposed algorithm is easy to implementation, accurate and is mesh free.

### 1 INTRODUCTION

The viscous fluid flow in a channel coupled with the flow through an adjacent porous region is often found in several engineering applications. In order to solve this type of problem numerically, a set of proper governing equations for the flow through two distinct, neighboring and interconnected domains has to be established. The incompressible flow in the fluid region is well represented by Navier-Stokes equations, while Darcy equation is used to describe the flow in the adjoining porous medium. For these governing equations problem is with the boundary condition. Beavers and Joseph [1] proposed that the interfacial velocity of the freely flowing fluid and the fluid velocity in the porous matrix could be related by

$$\frac{du}{dx} = \frac{\alpha}{\sqrt{k}}(u - q) \quad (1)$$

where  $u$  is a velocity of the fluid flow calculated at boundary (slip velocity),  $k$  is a permeability of porous medium, and  $q$  is a seepage velocity measured at small distance outside the interface, suggesting the existence of a thin layer just inside the porous medium over which the velocity transition occurs. The dimensionless slip coefficient  $\alpha$  is an independent of the fluid viscosity and apart from permeability depends on the structural parameters of the porous medium and is specific to the geometric features of the interface.

For determination the slip coefficient, Beavers and Joseph described experiments performed in a parallel-plate channel, one of the bounding walls was made of the porous material while the other one was impermeable. Identical axial pressure gradients were imposed on the channel and the porous medium, thereby giving rise to parallel axial flows.

This paper presents a numerical simulation of the Beavers-Joseph's experiment for the fibrous porous media. The longitudinal laminar flow in a parallel-plate conduit is considered. The first half of the considered region is a porous medium and the second one is a free fluid region. The porous medium is modelled as a bundle of parallel fibres. The purpose of the present consideration is determination of the slip constant in the Beavers-Joseph boundary condition for Newtonian fluid. But for do this the permeability of the porous medium is required. For to determine the last one the flow with the pressure gradient in unbounded porous medium was considered. Numerical simulations are conducted using the Trefftz method [2]. Essential novelty of this paper is numerical simulation of the Beavers-Joseph experiment for the Newtonian fluid. The influence of the volume fraction of the fibres on the value of the slip constant is investigated.

## 2 DETERMINATION OF THE SLIP CONSTANT

It is convenient in numerical simulations to use directly the Beavers-Joseph boundary condition to determined the slip coefficient. Let us consider a plane infinite channel adjoining with a plane infinite porous region in which flow is governed by the Darcy law in the following form

$$\frac{du}{dx} = \frac{\alpha}{\sqrt{k}} \left( u - \frac{k}{\mu} \frac{dp}{dz} \right). \quad (2)$$

Let us introduce the following dimensionless variables

$$U = \frac{\mu \cdot u}{-b^2 \cdot \frac{dp}{dz}}, \quad X = \frac{x}{b}, \quad \sigma = \frac{b}{\sqrt{k}}, \quad (3)$$

where  $b$  is the characteristic dimension.

Substituting Eq. (3) into Eq. (2) the following dimensionless condition is obtained

$$\frac{dU}{dX} = \frac{\alpha}{\sigma} (\sigma^2 U - 1). \quad (4)$$

Assuming that values of the dimensionless slip velocity, the derivative of the dimensionless slip velocity on the boundaries  $dU/dX$  and the dimensionless parameter of the permeability are known, the slip coefficient can be determined from the following formula

$$\alpha = \frac{\sigma \frac{dU}{dX}}{\sigma^2 U - 1} \quad (5)$$

In such approach in which the slip constant is determined by means of the numerical simulation the permeability of the porous medium is calculated independently. Thus two independent numerical experiments are needed. In both numerical experiments the porous medium is modeled by a bundle of a regular fibers. The radius of the fibers is equal to  $a$ , and the distance between the fibers is equal to  $2b$ . In the first experiment the considered bundle of fibers is infinite in all directions (Fig. 1). Because of the symmetry that fluid flow can be considered in the repeating part of the region (Fig. 2) and the permeability of the porous medium can be determined. In the second experiment a regular bundle of fibers is located between two parallel walls (Fig. 4). However the porous medium is located only in one half of this channel. Fluid flow is considered only in the repeating element of the considered channel (Fig. 6). The slip velocity  $U$  and the derivative  $dU/dX$  on the boundary can be calculated. Then the slip constant is determined from Eq. (5).

### 3 THE MICRO STRUCTURAL BOUNDARY VALUE PROBLEMS FOR DETERMINATION OF THE PERMEABILITY

In this section a porous medium modeled by a regular array of parallel fibers is considered. Square, triangular and hexagonal arrays of fibers (see Fig. 1) are analyzed.

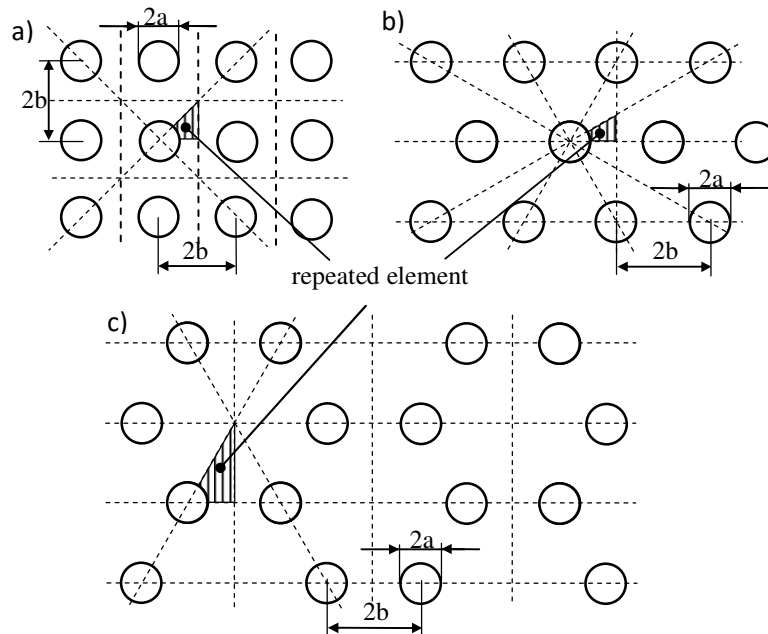


Fig. 1. Unbounded porous medium: (a) square array, (b) triangular array, (b) hexagonal array.

One of the basic method for determination of the permeability of the porous medium is an experiment in which the flow rate is measured. In the present paper the solution is obtained using the special purpose Trefftz functions [3, 4]. This method is semi-analytical. That means, that

application of the method gives analytical form of the dimensionless permeability of the porous medium.

Let us consider steady, fully developed, laminar, isothermal flow of an incompressible viscous fluid driven by a constant pressure in a system of regular parallel fibers. The flow is longitudinal with respect to fibers. In such case the equation of motion is reduced to a single partial differential equation in the polar coordinate system by

$$\frac{\partial^2 w}{\partial r^2} + \frac{1}{r} \frac{\partial w}{\partial r} + \frac{1}{r^2} \frac{\partial^2 w}{\partial \theta^2} = \frac{1}{\mu} \frac{dp}{dz}, \text{ in } \Omega_F \quad (6)$$

where  $w$  is the velocity component in the  $z$ -axis direction [m/s],  $dp/dz$  is the constant pressure gradient [Pa/m],  $\mu$  is the viscosity of the fluid [Pa·s], and  $\Omega_F$  is the fluid domain.

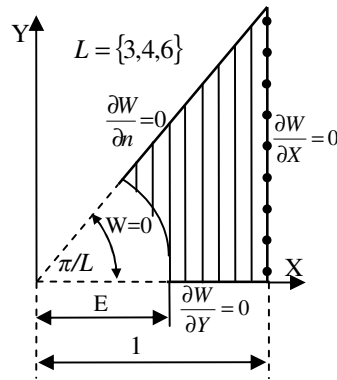


Fig. 2. Repeated element  $\Omega_F$  of unbounded porous medium.

It is convenient to introduce the dimensionless variables

$$W = -\frac{w}{b^2 \frac{dp}{dz}}, \quad R = \frac{r}{b}, \quad E = \frac{a}{b}. \quad (7)$$

Now, the governing Eq. (6) has the form

$$\frac{\partial^2 W}{\partial R^2} + \frac{1}{R} \frac{\partial W}{\partial R} + \frac{1}{R^2} \frac{\partial^2 W}{\partial \theta^2} = -1, \quad (8)$$

and is solved with the boundary conditions

$$W = 0 \text{ for } R = E, \quad (9a)$$

$$\frac{\partial W}{\partial \theta} = 0 \text{ for } \theta = \begin{cases} 0, \\ \pi/L, \end{cases} \quad (9b)$$

$$\frac{\partial W}{\partial X} = 0 \text{ for } X = 1, \quad (9c)$$

The fiber volume fraction is given by

$$\varphi = \frac{\Omega_P}{\Omega_T} = \frac{\pi \cdot E^2}{L \cdot \tan\left(\frac{\pi}{L}\right)}. \quad (10)$$

where  $\Omega_T = 0.5 \tan(\pi/L)$  is the total area of the repeated element (the fluid and the fiber areas together) and  $\Omega_P = 0.5 E^2 \cdot \pi/L$  is the area of the fiber in the repeated element (Fig.2).

The exact solution of Eq. (8) can be expressed using the special purpose Trefftz functions

$$W(R, \theta) = -\frac{1}{4}(R^2 - E^2) + \sum_{k=1}^{N-1} B_k \left( R^{Lk} - \frac{E^{2Lk}}{R^{Lk}} \right) \cos(Lk\theta) + B_N \ln\left(\frac{R}{E}\right), \quad (11)$$

The solution (11) satisfies exactly the boundary conditions (9a)–(9b). The unknown coefficients  $B_k$  ( $k = 1, \dots, N$ ) are determined by solving the system of linear equations resulting from satisfying of the boundary condition (9c) using the boundary collocation technique [5, 6]. Using the definition of the non-dimensional velocity (7) and introducing the fiber volume fraction (10) the longitudinal component of the filtration velocity can be expressed as

$$q_z = -\frac{b^2}{\mu} F(\varphi) \frac{dp}{dz}, \quad (12)$$

where

$$F(\varphi) = \frac{k}{\beta \cdot b^2} = \frac{\iint_{\Omega_F} W(X, Y) dXdY}{\beta \cdot \Omega_T} = \frac{2}{L \tan\left(\frac{\pi}{L}\right)^2} \int_0^{\frac{\pi}{L} \sec(\theta)} \int_E W \cdot R dR d\theta \quad (13)$$

is the non-dimensional component of the permeability tensor in the direction parallel to the fibers,  $\Omega_F = \Omega_T - \Omega_P$  is the region occupied by the fluid in the repeated element (Fig. 2). A dimensionless parameter of the porous medium is calculated as  $\beta = L \tan(\pi/L)$ .

After analytical integration in Eq. (13) the dimensionless permeability is a function of the number of collocation points  $N$  and can be calculated from

$$F = \left( \frac{E^2}{4} - \frac{1}{12} - \frac{1}{24 \cos\left(\frac{\pi}{L}\right)^2} \right) - \frac{\pi E^4}{8L \tan\left(\frac{\pi}{L}\right)} + \frac{2}{\tan\left(\frac{\pi}{L}\right)} \sum_{k=1}^{N-1} B_k \left[ \frac{H_k E^{2Lk}}{Lk - 2} + \frac{G_k}{Lk + 2} \right] + B_N \left[ \ln\left( \frac{1}{E \cos\left(\frac{\pi}{L}\right)} \right) - \frac{3}{2} \right] \quad (14)$$

where

$$H_k = \frac{\sin\left[(1 - Lk)\frac{\pi}{L}\right]}{(1 - Lk) \left[ \cos\left(\frac{\pi}{L}\right) \right]^{1-Lk}}, \quad G_k = \frac{\sin\left[(1 + Lk)\frac{\pi}{L}\right]}{(1 + Lk) \left[ \cos\left(\frac{\pi}{L}\right) \right]^{1+Lk}}. \quad (15)$$

The value of the dimensionless permeability as a function of the fibers volume fraction is presented in Fig. 3. Permeability  $F(\varphi)$  for all types of fiber arrays is similar and substantially different for  $\varphi > 0.3$ . The problem was solved for  $N = 7$  collocation points on the boundary. The

numerical results (marks) are compared with the analytical presented by Drummond and Tahir [7] (line). Compatibility between the results is great.

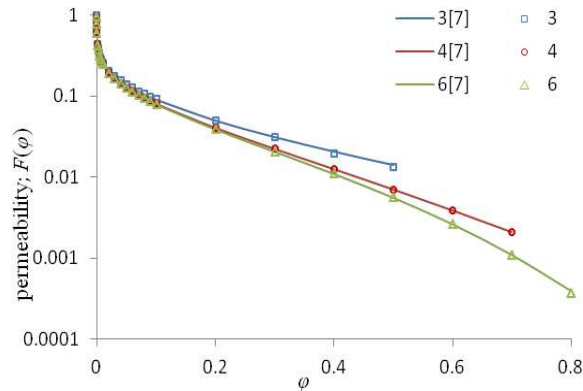


Fig. 3. The non-dimensional component of the permeability tensor in the direction parallel to the fibers. The numerical results (marks) compared with the analytical solution (line).

#### 4. THE MICRO STRUCTURAL BOUNDARY VALUE PROBLEMS FOR DETERMINATION OF THE SLIP CONSTANT

After determination of the permeability, the microstructural flow in the layer of porous medium can be considered (Fig. 4).

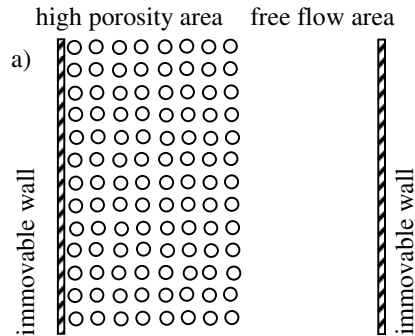


Fig. 4. Porous medium with very high porosity in the presence of free fluid region between two impermeable walls.

Let us consider a layer of the porous medium located between two fixed plates (Fig. 4). The problem is governed by the dimensionless Poisson equation

$$\frac{\partial^2 W}{\partial R^2} + \frac{1}{R} \frac{\partial W}{\partial R} + \frac{1}{R^2} \frac{\partial^2 W}{\partial \theta^2} = -1 \quad (16)$$

with the no-slip boundary conditions:  $W = 0$  on the immovable wall.

Since the array of fibers is streaked and periodic in one direction it is sufficient to consider the problem only in one repeated strip which is depicted in Fig. 5. In all cases the repeated strip is divided into smaller elements associated with each of the fibers which are called large finite elements.

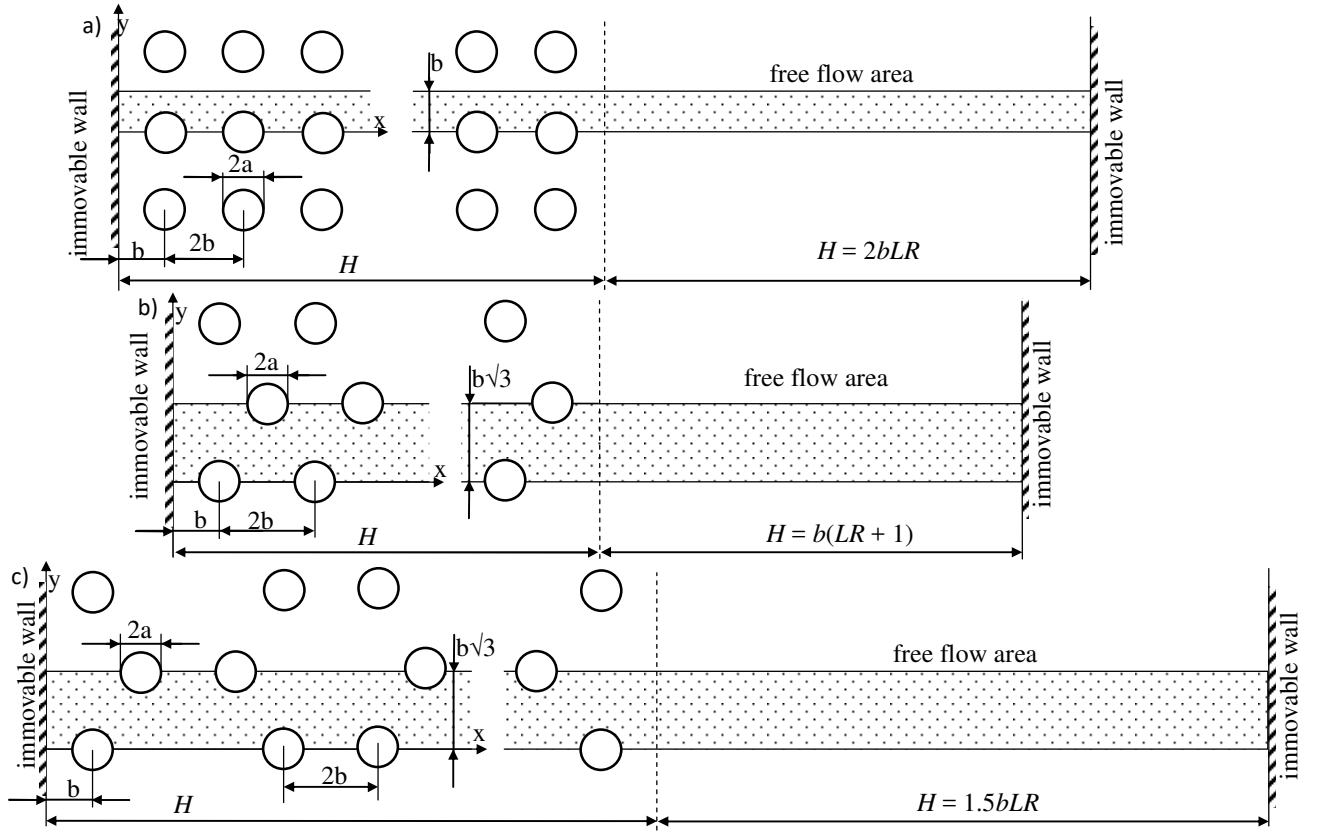


Fig. 5. The repeating part of the considered channel with fibers arranged according (a) square (b) triangular and (c) hexagonal array

In the fibrous porous area the special purpose Trefftz functions are used to express the numerical solution. For each large finite element the approximate solution is express as

$$W(R, \theta) = \sum_{k=1}^{N-1} B_k \left( R^{Lk} - \frac{E^{2Lk}}{R^{Lk}} \right) \cos(Lk\theta) + B_N \ln\left(\frac{R}{E}\right), \quad (17)$$

which satisfies exactly the governing Eq. (16) and some of the boundary conditions

$$W = 0 \text{ for } R = E \quad (18a)$$

$$\frac{\partial W}{\partial \theta} = 0 \text{ for } \theta = \begin{cases} 0 \\ \pi \end{cases} \quad (18b)$$

For the free flow area the approximate solution is express as

$$W^*(X, Y) = -\frac{X^2 + Y^2}{4} + \sum_{n=0}^M c_n F_n(X, Y) + \sum_{n=1}^M d_n G_n(X, Y) \quad (19)$$

where  $F_n(X, Y)$  and  $G_n(X, Y)$  are the trial functions

$$F_n(X, Y) = \sum_{k=0}^{\lfloor \frac{n}{2} \rfloor} (-1)^k \frac{X^{n-2k} Y^{2k}}{(n-2k)!(2k)!}; \quad G_n(X, Y) = \sum_{k=0}^{\lfloor \frac{n-1}{2} \rfloor} (-1)^k \frac{X^{n-2k-1} Y^{2k+1}}{(n-2k-1)!(2k+1)!}. \quad (20)$$

The unknown coefficients  $B_k$  ( $k = 1, 2, \dots, N$ ),  $c_k$ ,  $d_k$  ( $k = 1, 2, \dots, M$ ) and  $c_0$  are determined using the boundary collocation technique [6] by satisfying the boundary conditions as shown on Fig. 6. The boundary between the porous and fluid regions is located for  $X = H$ . The value of slip velocity  $U$  and the derivative  $dU/dX$  at this boundary can be calculated by numerical integration.

The slip constant can be determined from Eq. (5) where  $\sigma = \frac{1}{\sqrt{\beta \cdot F}}$  is the permeability parameter.

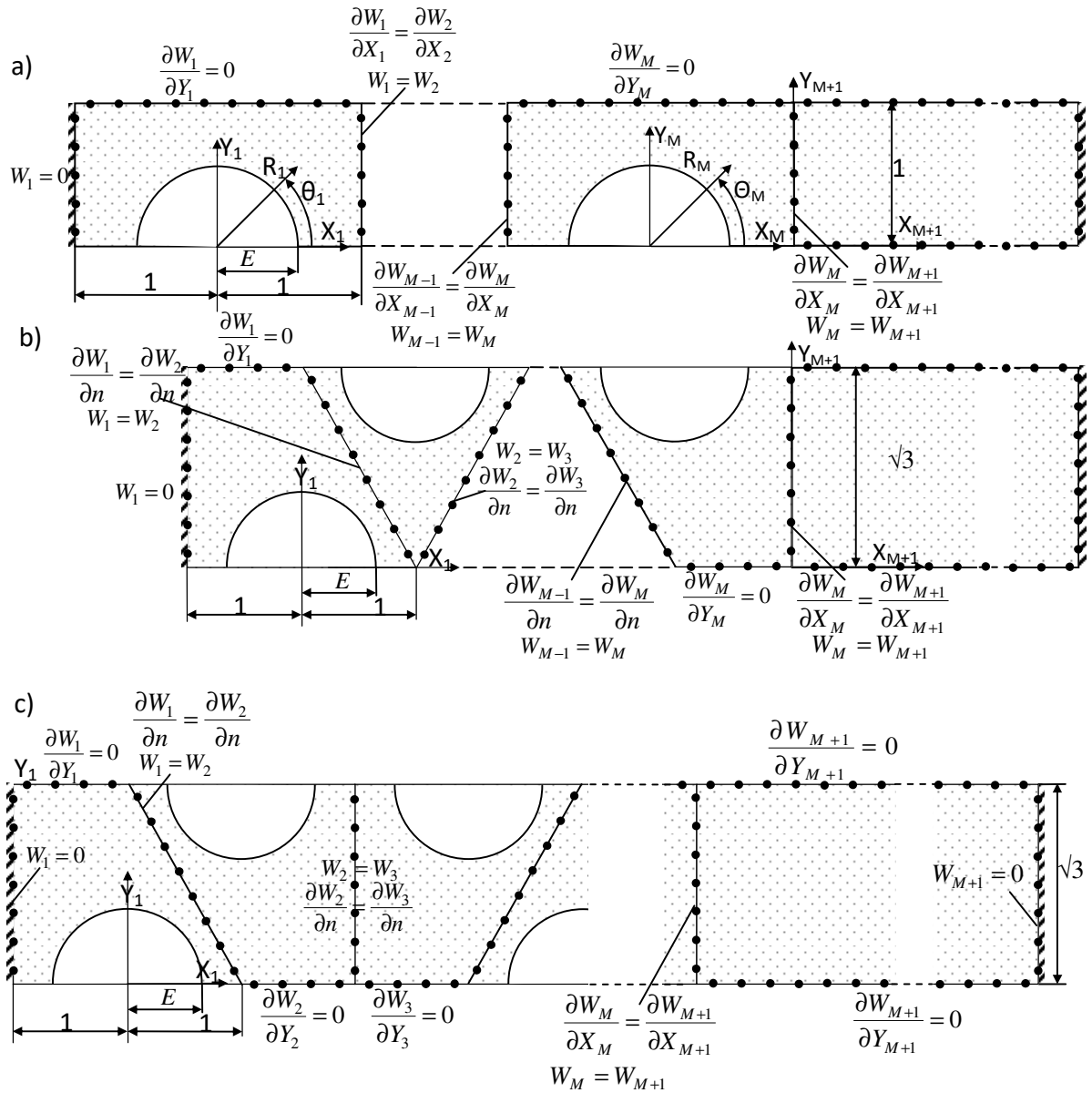


Fig. 6. The repeating part of the considered region with the boundary and contact conditions for square (a), triangular (b) and hexagonal array (c)

## 5. NUMERICAL RESULTS AND DISCUSSION

In the first part of the numerical experiment the value of the dimensionless effective permeability as a function of the fibers volume fraction is calculated. The results are presented in Fig. 3. In that case 7 collocation points and the same number of trial function are used.

In the next part the slip constant on the boundary is determined for 10 rows. The width of the porous and free flow area were the same and equals to  $H = 2 \cdot LR$  for square,  $H = 3 \cdot LR$  for hexagonal and  $H = 1 + LR$  for triangular array, where  $LR$  is the number of rows of fibers. For each single edge of the repeated element we chosen  $Mc = 4$  collocation points. For the upper and lower edge of free flow area the number of collocation points are calculated by the formula  $H \cdot Mc / 4$ . The total number of collocation points for the free flow area was equals  $Nc = 2 \cdot (H \cdot Mc / 4 + 2)$ . The total number of collocation points for the porous area was equals  $Nc = 2 \cdot LR \cdot Mc$  for square,  $Nc = 2 \cdot Mc \cdot (LR + 1)$  for triangular and  $Nc = 6 \cdot Mc \cdot LR$  for hexagonal array.

Figure 7 shows the slip constant,  $\alpha$  as a function of the volume fraction of fibers,  $\phi$ . The value of the slip constant is lower than 1.0 and decreases with increasing the volume fraction of fibers for the high porosity. For the hexagonal and square array of the fibers,  $\alpha$  increases for a large share of fibers  $\phi$ . For the triangular array the  $\alpha$  decreases also for a low porosity.

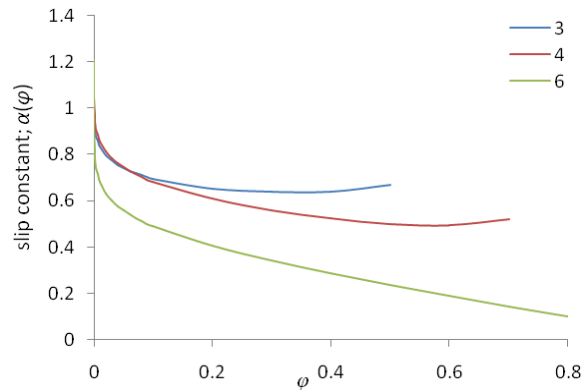


Fig. 7. The slip constant  $\alpha$  as a function of the fiber volume fraction  $\phi$  for square (4), triangular (6) and hexagonal (3) array of fibers for  $LR = 10$ ,  $Mc = 4$

The effect of the number of rows of the fibers  $LR$  on the value of the effective permeability for the triangular, square and hexagonal array was examined. Figure 8 shows the obtained numerical results. The influence of the number of the fibers rows is significant and its effect disappears for  $LR$  equal to 12. The influence of the number of the fibers rows is more significant for the porous medium with high porosity (small  $\phi$ ). For small value of the volume fraction of fibers,  $\phi$  just four rows of the fibers are sufficient for determining the slip constant,  $\alpha$ .

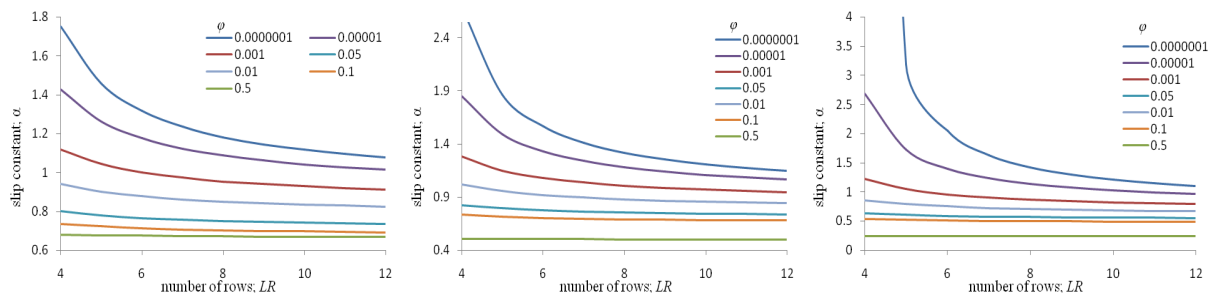


Fig. 8. Influence of the number of rows at a slip constant for a hexagonal, square and triangular array of fibers

## 6. CONCLUSIONS

In this paper the permeability and the slip constant on the boundary of the considered region were determined by numerical simulation of the imaginary physical experiment. The porous medium was modeled by a parallel bundle of straight fibers arranged in a regular triangular or square array. In order to determine the permeability, the flow driven by the pressure gradient in an unbounded porous medium was considered. To determine the slip constant, the shear flow between a flat immovable wall containing both the porous and free flow layers was considered. In both numerical simulations, the Trefftz method with the special purpose Trefftz functions and trial functions was applied. In all considered cases the value of the slip constant is lower than one. The slip constant decreases with increasing the volume fraction of fibers for a high porosity. For a square and hexagonal array the value of slip constant starts increasing for small porosity. For the same volume fraction of the fibers, both the permeability and the slip constant for the triangular array is smaller than for the square and the hexagonal array. The number of collocation points has inconsiderable effect on the simulation results. To determine the permeability a few collocation points are enough to get an accurate result ( $Mc = 4$ ). More visible influence has the number of rows, especially for high porosity. For all the cases 10 rows of fibers is sufficient to determine the slip constant. Proposed algorithm is easy to implementation, accurate and is mesh free.

## ACKNOWLEDGMENTS

This work was supported by the grant 2015/19/D/ST8/02753 from the National Science Center, Poland.

## REFERENCES

- [1] G. S. Beavers and D. D. Joseph, Boundary conditions at a naturally permeable wall, *J. Fluid Mech.*, 30 (1967) 197-207.
- [2] Trefftz E.: Ein Gegenstück zum Ritzschen Verfahren, *Proceedings of the 2nd International Congress of Applied Mechanics (Zurich)*, Orell Fussli Verlag (1926):131-137.
- [3] J.A. Kolodziej and W. Dudziak, The determination of the stationary incompressible laminar viscous flow past a hexagonal lattice parallel cylindrical bars by means of boundary collocation (in Polish), *Archiwum Budowy Maszyn* (1979) 26:101-114.
- [4] J.A. Kolodziej, Influence of the porosity of a porous medium on the effective viscosity in Brinkman's filtration equation, *Acta Mech.* (1988) 75:241-254.
- [5] G. Fairweather and A. Karageorghis, The method of fundamental solutions for elliptic boundary value problems, *Adv. Comput. Math.* (1998) 9:69-95.
- [6] J.A. Kolodziej and A.P. Zieliński, *Boundary Collocation Techniques and their Application in Engineering*, WIT Press, Southampton (2009).
- [7] J.E. Drummond and M.I. Tahir, Laminar viscous flow through arrays of parallel solid cylinders. *Int. J. Multiphase Flow* (1984) 10:515-540.

## Maximum Entropy-based Uncertainty Modeling at the Finite Element Level

Marc Mignolet<sup>\*</sup>, Pengchao Song<sup>\*\*</sup>

<sup>\*</sup>Faculties of Mechanical and Aerospace Engineering, Arizona State University, <sup>\*\*</sup>Faculties of Mechanical and Aerospace Engineering, Arizona State University

### ABSTRACT

A novel approach is proposed for the modeling of uncertainties in finite element models of linear structural or thermal problems. This uncertainty is introduced at the level of each finite element by randomizing the corresponding elemental matrices (e.g., mass, stiffness, conductance) using maximum entropy concepts. In performing this randomization, it is first recognized that elemental matrices corresponding to different elements cannot be simulated independently of each other. Doing so would induce very high spatial frequency variations which are unphysical. Rather, it is proposed here to adopt the matrix field modeling proposed in [1] which views each randomness generating matrix as the transformation of a zero mean, unit variance Gaussian field with a specified, parametrized stationary autocorrelation function. The second requirement is that the correlation between random elemental matrices of neighboring finite elements implied by the above algorithm must be reflected on every component of the assembled matrix. That is, if a strong correlation is expected between two different finite elements, then there must exist a similarly strong correlation between the components of their elemental matrices as they are added together in the construction of the global matrix. Since the elemental matrix is built from independent fields, this condition can be satisfied if: (1) the elemental matrices of the mean and uncertain models are expressed in the same (i.e., global) frame of reference, and (2) each simulated sample of the random global matrix is independent of the ordering of the nodes in each element. The proposed approach is characterized by a limited set of parameters, one expressing the overall level of uncertainty with the rest characterizing the correlation structure underlying the random elemental matrices. It is exemplified on a structural example and the effects of the overall uncertainty level and correlation length of the random elemental matrices are analyzed. [1] C. Soize, Non-Gaussian positive-definite matrix-valued random fields for elliptic stochastic partial differential operators. Computational Methods in Applied Mechanics and Engineering, 195, pp. 26-64, 2006.

## **Analysis of Elliptical and Semi-Elliptical Fatigue Crack Propagation**

Yozo Mikata\*

\*Bechtel

### **ABSTRACT**

The fatigue crack propagation of a 3D crack is investigated under a uniform loading. As for crack geometry, an elliptical crack and a semi-elliptical crack are considered. The focus of this paper is to solve a pair of coupled differential equations derived from Paris law. Stress intensity factors are approximate except for an elliptical crack in an infinite body, for which an exact result is available. The approximate stress intensity factors used for semi-elliptical cracks are based on an empirical equation given in Newman and Raju.

## **Mechanically-evoked ATP Release is Regulated by Facilitated Membrane Resealing in Murine Osteoblasts**

Nicholas Mikolajewicz<sup>\*</sup>, Elizabeth Zimmerman<sup>\*\*</sup>, Bettina Willie<sup>\*\*\*</sup>, Svetlana Komarova<sup>\*\*\*\*</sup>

<sup>\*</sup>McGill University, <sup>\*\*</sup>Shriners Hospital for Children, Canada, <sup>\*\*\*</sup>McGill University, <sup>\*\*\*\*</sup>McGill University

### **ABSTRACT**

Mechanical environment is an important determinant of bone health. ATP release is one of the first events induced by mechanical stimulation of bone-forming osteoblasts and bone-resident osteocytes; however, the dominant pathways of ATP release remain disputed. We examined the mechanism of ATP release from mechanically-stimulated compact bone or bone marrow-derived osteoblasts. We demonstrated that  $70 \pm 24$  amol ATP/cell were released in response to single cell membrane deformation and  $21 \pm 11$  to  $422 \pm 97$  amol ATP/cell in response to turbulent fluid shear stress. Mechanical stimulation induced exocytosis of quinacrine-positive ATP-containing vesicles. Pharmacological activation of protein kinase C (PKC) potentiated vesicular exocytosis, while PKC inhibition reduced exocytosis. Unexpectedly, increase in vesicular release coincided with a significant decrease in released ATP, and vice versa. To examine the contribution of injury to ATP release, we evaluated membrane integrity during and after mechanical stimulation using membrane impermeable markers. We demonstrated that in vitro or in vivo mechanical stimuli induced magnitude-dependent repairable cell membrane injury.  $Ca^{2+}$ /PLC/PKC-dependent vesicular release was critical for successful repair of membrane damage, suggesting that rather than delivering ATP to extracellular space, vesicular exocytosis limits the much larger efflux of intracellular ATP through damaged membranes. Prior activation of PKD/vesicular signaling improved membrane integrity and limited ATP release induced by subsequent mechanical stimulation. Our study suggests a new model of biological adaptation to mechanical forces that combines graded perception of mechanical environment through membrane injury and an ability to effectively counteract the destructive potential of mechanical forces through membrane repair.

## **Computational Investigation of a Blast Loaded Surrogate Head Model with Application Towards Traumatic Brain Injury**

Scott Miller<sup>\*</sup>, Candice Cooper<sup>\*\*</sup>, Paul Tayloer<sup>\*\*\*</sup>, Adam Willis<sup>\*\*\*\*</sup>, Ricardo Mejia-Alvarez<sup>\*\*\*\*\*</sup>

<sup>\*</sup>Sandia National Laboratories, <sup>\*\*</sup>Sandia National Laboratories, <sup>\*\*\*</sup>Sandia National Laboratories, <sup>\*\*\*\*</sup>San Antonio Military Medical Center, <sup>\*\*\*\*\*</sup>Michigan State University

### **ABSTRACT**

Blast-induced Traumatic Brain Injury (bTBI) is a signature wound of modern warfare and can leave victims at risk for persistent neurologic/behavioral symptomatology, including headaches, sleep disorder, cognitive impairment and mood disturbance. Clinical experience and neuropathologic analysis has identified some unique features of this injury: injury to the blood vessels at both large and small length scales manifesting with brain swelling, subarachnoid hemorrhage or pseudoaneurysm, vasospasm, and astroglial scarring at multiple intracranial interfaces. The mechanisms and thresholds of these injuries are not yet understood mechanically. In this talk, we discuss an on-going project whose goal is to build a model which reproduces the human intracranial injury after blast exposure in order to isolate the mechanism(s) of injury. A surrogate head model was developed and tested experimentally. Computational simulations were performed that coupled an Eulerian shock-physics model of the incident blast to a Lagrangian finite element model of the test object. We will present the coupling methodology and our current results. Particular emphasis is placed on cavitation modeling and resolution near fluid-structure interfaces.

## Computational Framework for Assessment of Injection-based Drug Delivery

David Milner<sup>\*</sup>, Prateek Dixit<sup>\*\*</sup>, John Mould<sup>\*\*\*</sup>, Mahesh Kailasam<sup>\*\*\*\*</sup>

<sup>\*</sup>Thornton Tomasetti, <sup>\*\*</sup>Thornton Tomasetti, <sup>\*\*\*</sup>Thornton Tomasetti, <sup>\*\*\*\*</sup>Thornton Tomasetti

### ABSTRACT

Delivery of drugs via injection is a widely and long-used method to administer continuous and low dose drug treatments. With the advent of new types of drugs such as biologics, the increased usage of self-administered injections, and other developments, there is increasing need for a more systematic evaluation of delivery mechanisms. Such evaluations can facilitate more precise specification of drug delivery location and rate, selection of the most appropriate needle type, and reduction of pain. These issues have traditionally been investigated via laboratory experiments, analytical assessments, and clinical trials. Advances in computational modeling, however, now facilitate virtual testing which is rapid, cost-effective, and provides more insights than are available through traditional physical testing. With these benefits, computational modeling is becoming increasingly attractive, especially when used in combination with advances in imaging technologies. In this study, a systematic computational framework is developed to understand various mechanisms involved in drug injection. Using the finite element method, coupled pore pressures and tissue stresses are computed to predict bolus growth, including advancement of the wetting fronts and the corresponding tissue strains, as the drug perfuses through tissue. The computational methodology is first validated by comparing computed bolus growth to experimental data obtained by x-ray/CT imagery of porcine tissue injected with fluids such as saline (Kim, 2017) or insulin; multiple injection rates, needle types, and tissue types are considered. Once validated, various parameters are modified, including the volume, viscosity, and injection rate of the perfusate, and the permeability, porosity, and mechanical properties of the tissue. The effects of these parameters on bolus size, shape, and growth are assessed. Tissue stresses and strains are also computed and compared as a measure of relative pain. (Finocchietti, 2012) Insights provided by this framework will allow both the development and selection of more effective delivery methodologies depending on patient characteristics and other care requirements. References Kim, Hyejeong; Park, Hanwook; Lee, Sang Joon. Effective method for drug injection into subcutaneous tissue. Scientific Reports 7: 9613, 2017 Finocchietti, Sara; Takahashi, Ken; Okada, Kaoru; Watanabe, Yasuharu; Graven-Nielsen, Thomas; Mizumura, Kazue. Deformation and pressure propagation in deep tissue during mechanical painful pressure stimulation. Medical &&& Biological Engineering &&& Computing, Volume 51 (2), 2012

## **Stress-constrained Multi-Material Topology Optimization Considering Thermal Expansion**

Seungjae Min<sup>\*</sup>, Youngsuk Jung<sup>\*\*</sup>

<sup>\*</sup>Department of Automotive Engineering, Hanyang University, Seoul, Korea, <sup>\*\*</sup>Department of Automotive Engineering, Hanyang University, Seoul, Korea

### **ABSTRACT**

This paper presents a stress-based topology optimization method of the multi-material structure by considering thermal expansion. As the use of multiple materials increases with the demand for lightweight structure design, the design with mixed-materials using welding and adhesion is increasing. However, the different thermal expansion between dissimilar materials make the unexpected stress increments in the interface area, and it could lead to the product failure and to decrease performance. Deaton [1] suggest the single material thermal structures with a stress constraint using topology optimization, and Tong [2] suggest the multi-material thermal structure design for the compliance minimization problem. However, the multi-material design and the stress constraints were not considered simultaneously, and only single temperature condition was allowed for each optimum design. In this paper, we perform a multi-material topology optimization with the stress constraints for various temperature conditions. We formulate the optimization problem that minimizes the weight with the stiffness performance and the stress constraints of each material. For the validation of the proposed method, the design example of an automotive component with the operating temperature range -40? to +85? was considered. For the stable optimization of the design-dependent loads, the RAMP (Rational Approximation of Material Properties) model is adopted to interpolate of material properties such as elastic modulus and thermal expansion coefficient. From the design example results, we can find that the optimum result has different layouts depending on the set of temperature conditions, and we can get a robust design against the temperature change by taking into account the multiple temperature conditions. [1] J. D. Deaton and R. V. Grandhi, "Stress-based design of thermal structures via topology optimization", *Struct. Multidisc. Optim.*, 2015 [2] G. Tong et al., "Topology optimization of thermo-elastic structures with multiple materials under mass constraint", *Struct. Multidisc. Optim.*, 2016

## DEM Simulations for the Investigations of the Mechanochemical Activation of Copper Ores

Masaya Minagawa<sup>\*</sup>, Shosei Hisatomi<sup>\*\*</sup>, Tatsuya Kato<sup>\*\*\*</sup>, Giuseppe Granata<sup>\*\*\*\*</sup>, Chiharu Tokoro<sup>\*\*\*\*\*</sup>

<sup>\*</sup>Graduate School of Creative Science and Engineering, Waseda University, <sup>\*\*</sup>Graduate School of Creative Science and Engineering, Waseda University, <sup>\*\*\*</sup>Graduate School of Creative Science and Engineering, Waseda University, <sup>\*\*\*\*</sup>Faculty of Science and Engineering, Waseda University, <sup>\*\*\*\*\*</sup>Faculty of Science and Engineering, Waseda University

### ABSTRACT

The high demand of copper has been pushing the copper industry to process low-grade ores. For this reason, the developments of new technologies able to promote the dissolution of copper from refractory ores are highly anticipated. The mechanochemical activation is a phenomenon resulting in the enhancement of leachability of metal minerals due to the transfer of large amounts of energy through high-intensity grinding operations. The enhancement can be result of a decrease of the particle size and/or the consequence of induced transformation of the crystal structure. Although the occurrence and the effectiveness of this phenomenon towards the enhancement of leaching have been proved, its quantitative relation to provided mechanical energy is not fully elucidated. In this study, we elucidated the mechanism of mechanochemical activation of covellite with two types of dry grinding technologies: vertical stirred ball milling and planetary ball milling. We performed grinding experiments under different operating conditions and then DEM simulations to assess the collision energy involved in the grinding process. Following this step, we carried out leaching experiments by sulfuric acid to determine the leaching rate constant to be related to the collision energy of grinding. DEM simulations were performed with considering both collisions of grinding media and grinded particles. XRD and XAFS results after grinding revealed the partial amorphization of covellite by intensifying the grinding conditions. As a consequence, the leaching of samples grinded under more intense conditions resulted into higher leaching rate constants. In order to understand whether the increase was due to a simple increase of surface area or due to an induced-transformation of the crystal structure of covellite, we performed a correlation between collision energy and leaching rate-constants. The rate constants had a unique correlation to the collision energy calculated by DEM for the two different mills. The correlation between leaching rate constant and collision energy exhibited a sudden increase of the rate constant beyond 0.25 J/mol?sec. This increase can be considered as a consequence of the occurred mechanochemical reaction previously confirmed by XRD results.

## **3D-Printable Soft-Actuator Composites**

Aslan Miriyev\*, Hod Lipson\*\*

\*Columbia University in the City of New York, \*\*Columbia University in the City of New York

### **ABSTRACT**

One of the main gaps in conventional robotics is the lack of compliance, resulting in poor human-robot interface, thus preventing the ability of humans to work side by side with robots. Soft-material robotics is an emerging domain aiming to provide compliant robots, allowing soft-bodied locomotion and soft touch. The main challenge in soft robotics is development of multi-functional materials, combining actuation and sensing with computerized control. I will demonstrate a new-developed compact approach, allowing to replace conventional motors and existing massive soft-actuation devices by self-contained 3D-printable composite materials. Specifically, I will present a silicone/ethanol composite material, capable of exhibiting actuation stress and strain exceeding those of natural muscles. The working mechanism, properties and performance of the soft-actuator composites, as well as their fabrication by 3D-printing, will be discussed.

## Reduced Order Modeling of Coronary Blood Flow

Mehran Mirramezani\*, Shawn Shadden\*\*

\*UC Berkeley, \*\*UC Berkeley

### ABSTRACT

Reduced-order modeling (ROM) of blood flow offers the possibility to study hemodynamics of large cardiovascular networks with negligible computational cost. A basic approach is to use lumped-parameter (LP) models, which describe regional pressure-flow relationships in vascular beds. The accuracy of such models may become questionable for resolving hemodynamics at individual-artery-scale especially when complex flow features are present. The goal of this study is to compare and develop ROM to capture pressure and flow dynamics in the coronary arteries. To model coronary hemodynamics, we developed 3D time-dependent (3D+t) fluid structure interaction (FSI) simulations and 3D+t rigid wall (CFD) simulations as gold standards. Minimal difference was observed between 3D-FSI and 3D-CFD. We then considered ROM starting from 2D “multiring” method and then classical 1D formulations. As an alternative to these PDE models, we developed a novel distributed LP approach, that assigns a net effective resistance to each vascular segment by considering various sources of energy dissipation. We sought two main objectives. The first was a fully LP-type model that could resolve vessel-level hemodynamics throughout the coronaries with minimal computational cost. The second was the specific ability compute transstenotic pressure drop and fractional flow reserve (FFR) in diseased coronaries, since such information is highly relevant to clinical diagnosis of coronary artery disease (CAD) and a major driver of coronary modeling. We considered a series of image-based models that included major coronary arteries. We considered patient-specific models with CAD, without CAD, and synthetically generated lesions to enable systematic exploration. We first considered the ability of ROM to accurately predict FFR by considering ROM of only the stenotic artery, and then we then considered ROM of the entire aortic-coronary complex. For computation of transstenotic pressure drop and FFR, major differences were observed between 3D and 2D and 1D models. Major differences were also observed between algebraic models; however, a particular algebraic model was found to have strong agreement with 3D simulations, including for patient-specific stenoses. We next considered the ability of a fully LP-type framework to accurately predict pressure and flow throughout the coronary tree. We developed a quasi-LP approach that demonstrated strong agreement with fully 3D+t simulations. Average errors in pressure at coronary outlets were  $\leq 3\%$ , including arteries with significant stenosis. The developed framework as made fully automated and requires  $\leq 10$ sec runtime on a desktop computer. These results support the notion that an appropriately-derived LP framework may provide high diagnostic value for coronary modeling.

## Reinforcing and Scattering Reduction for Flexural Vibrations in a Rectangular Lattice

Diego Misseroni<sup>\*</sup>, Davide Bigoni<sup>\*\*</sup>, Alexander B. Movchan<sup>\*\*\*</sup>

<sup>\*</sup>DICAM, University of Trento, Italy, <sup>\*\*</sup>DICAM, University of Trento, Italy, <sup>\*\*\*</sup>University of Liverpool, UK

### ABSTRACT

A novel concept has been introduced and tested for reduction of the scattering by faults in a flexural lattice. The majority of the relevant published works are based on the so-called "cloaking transformation". This approach originally came from electromagnetism and optics, and is linked to the Maxwell system of equations or, in special cases, to the Helmholtz equation. In the present work, we address an elastic system and apply a different principle, concerning a reinforcement of the boundary and a redistribution of mass. We demonstrate that this approach, which is simple in nature, enables one to significantly reduce the coefficients in the multipole expansion of the scattered field. Accurate numerical simulations and a quantitative analysis of the scattered fields for 'cloaked' and uncloaked faults are provided. A constructive simple algorithm has been proposed and verified through numerical simulations in a wide range of frequencies. The results are accurate and supplied with evaluation of the Fourier coefficients on two circular contours enclosing the square hole in the lattice, which shows a significant reduction of the scattered field for the case of a hole, with the appropriately reinforced boundary and redistributed mass. This method can also be considered an 'approximate cloaking', and being simple in nature it is appealing in a range of practical applications involving flexural waves in plates with defects.

## **A Statistical Learning Based Characterization of Lithium-Ion Battery Electrodes**

Aashutosh Mistry<sup>\*</sup>, Chance Norris<sup>\*\*</sup>, Partha Mukherjee<sup>\*\*\*</sup>

<sup>\*</sup>Purdue University, <sup>\*\*</sup>Purdue University, <sup>\*\*\*</sup>Purdue University

### **ABSTRACT**

With recent advances in X-ray tomography based imaging, lithium-ion battery electrode microstructures can be probed with sufficient resolution. Such porous electrode structures, obtained from 3D X-ray imaging, exhibit spatial heterogeneity, which requires appropriate representative volume element (RVE) delineation for analyzing the influence of interface and transport properties, which in turn affect the electrochemical performance. For example, a typical electrode volume imaging based on X-ray tomography, may contain several RVEs, which can be analyzed to build a correlation among structural features and effective properties. This statistical learning map can be used to further analyze microstructural variations. In this work, statistical learning based characterization is presented for tomographed datasets of Li-ion battery electrodes, including a discussion on the microstructural variabilities emanating from processing conditions.

## **SAND2017-13837 A: Upscaling Microstructural Effects by Combining Local/Nonlocal Models**

John Mitchell\*

\*Sandia National Laboratory

### **ABSTRACT**

Shock wave propagation in solids has a long history [1], yet modeling microstructure effects for weak shocks remains elusive. Aggregate effects of grain size and shape, residual stresses, and grain orientations cause shock fronts to spread; non-uniform states of shear stress occur at grain size length scales due to differing grain orientations and residual stresses of adjacent grains. These nonlocal effects inhibit formation of sharp elastic-plastic wave fronts. In this talk, a nonlocal peridynamic inspired yield function [2] is used to incorporate and upscale microstructure features; this function is used in conjunction with a more traditional local plasticity model. In this way, existing local computational frameworks for shock propagation are leveraged while at the same time important microstructural and nonlocal effects are incorporated. This approach is applied to microstructures arising from additive manufacturing and welding [3] where grain sizes approach macroscale (1 mm) and morphologies are non-equiaxed. Mathematical constructs for the model will be introduced and simple demonstration calculations will be presented. Time permitting, key computational aspects will be discussed. [1] Asay, James R. and Chhabildas, Lalit C. and Lawrence, Jeffery R., and Sweeney, Mary Ann. "Impactful Times," Springer, 2017. [2] Mitchell, J.A., "A non-local, ordinary-state-based plasticity model for peridynamics," Sandia National Laboratories Report SAND2011-8064, 2011. [3] Rodgers, Theron M., Mitchell, John A., and Tikare, Veena, "A Monte Carlo model for 3D grain evolution during welding", Modeling and Simulation in Materials Science and Engineering, Volume 25, Number 6, September 2017.

## Parallel Simulation of Thermal Conduction in Coal Gasification Vessel Coupled with Cooling Pipe Model

Naoto Mitsume<sup>\*</sup>, Byungsoo Song<sup>\*\*</sup>, Tomonori Yamada<sup>\*\*\*</sup>, Shinobu Yoshimura<sup>\*\*\*\*</sup>

<sup>\*</sup>The University of Tokyo, <sup>\*\*</sup>The University of Tokyo, <sup>\*\*\*</sup>The University of Tokyo, <sup>\*\*\*\*</sup>The University of Tokyo

### ABSTRACT

Research and development with regard to advanced coal-fired power plants to reduce CO<sub>2</sub> emission have been conducted. Coal gasification is one of the key technologies. In reactor for the coal gasification, coal is crushed into fine particulate matter and then partially burned into gas in a high-pressure environment in the reactor. Our research group has carried out a project to tackle a coupled problem of thermo-fluid-structure interaction for quantification of its efficiency, environmental load, and structural integrity. As one of key components of the project, we present a large-scale parallel simulation of three-dimensional (3D) thermal conduction in a gasification vessel. As a parallel solver for thermal conduction, we adopt ADVENTURE\_Thermal [1], which is based on the hierarchical domain decomposition method and the balancing domain decomposition preconditioner. To simulate effect of cooling pipes in the vessel, we model heat transfer in the pipe as a one-dimensional (1D) convection-diffusion equation, and develop a discontinuous Galerkin-based solver [2]. These 3D and 1D solvers are coupled by a staggered coupling scheme with a subcycling technique [3] to deal with different time increments in the 1D and 3D analyses. We perform a validation test for our proposed system for the coupled analysis and discuss parallel efficiency. [1] Mukaddes, A. M. M., Ogino, M., Kanayama, H., Shioya, R.: A scalable balancing domain decomposition based preconditioner for large scale heat transfer problems. *JSME International Journal Series B Fluids and Thermal Engineering* 49(2), 533-540 (2006) [2] Cockburn, B., Shu, C. W.: The local discontinuous Galerkin method for time-dependent convection-diffusion systems. *SIAM Journal on Numerical Analysis* 35 (6), 2440–2463 (1998) [3] Farhat, C., Lesoinne, M.: Two efficient staggered algorithms for the serial and parallel solution of three-dimensional nonlinear transient aeroelastic problems. *Computer Methods in Applied Mechanics and Engineering* 182(3), 499–515 (2000)

## Polycrystalline Grain Growth Simulations Using the Molecular-Dynamics and Multi-Phase-Field Methods

Eisuke Miyoshi<sup>\*</sup>, Tomohiro Takaki<sup>\*\*</sup>, Yasushi Shibuta<sup>\*\*\*</sup>, Munekazu Ohno<sup>\*\*\*\*</sup>

<sup>\*</sup>Kyoto Institute of Technology, <sup>\*\*</sup>Kyoto Institute of Technology, <sup>\*\*\*</sup>The University of Tokyo, <sup>\*\*\*\*</sup>Hokkaido University

### ABSTRACT

During the heat treatment of a polycrystalline material, grain growth occurs after completion of solidification, allotropic transformation, or recrystallization. The ability to predict and control the microstructural evolution through grain growth is crucial for developing materials with superior mechanical properties. Therefore, in order to predict the microstructural evolution systematically, numerical simulations of grain growth have been frequently performed in recent years. Grain growth simulations are classified into two categories according to their methodologies: one is the atomic level calculations including the molecular dynamics (MD) method or phase-field crystal method. The other is the continuum model-based simulations using the phase-field method, Monte-Carlo method, vertex method, and so forth. The former can express spontaneous nucleation process, enabling successive simulation of grain growth and its preceding phenomena such as solidification. However, owing to the large computational cost, it is difficult to simulate grain growth until the late stage. On the other hand, the continuum-based methods allow for relatively efficient computations. In particular, the multi-phase-field (MPF) method [I. Steinbach and F. Pezzolla, *Physica D*, 134 (1999) 385], which is an extension of the phase-field method to multi-phase and polycrystalline systems, is widely employed as the most powerful tool capable of simulating grain growth with accuracy and efficiency; however, the MPF method requires some assumption to reproduce nucleation process, and the simulated results are strongly dependent upon the used assumption. The purpose of this study is to enable comprehensive prediction of the microstructural evolutions from nucleation to late-stage grain growth by using the MD and MPF methods successively; in this framework, nucleation process is simulated by the MD method, and the obtained microstructure is used as the initial structure for MPF grain growth simulation. To this effect, we propose a novel method to convert MD-generated atomic configurations into phase-field profiles. In addition, MPF and MD grain growth simulations are directly compared using the proposed method, through which the accuracy of the MPF simulation is examined.

## CONSTRUCTION OF DAMAGE OBSERVATION SYSTEM FOR BOTH STRUCTURAL AND NON-STRUCTURAL MEMBERS WITH OVERLAYING

YASUNORI MIZUSHIMA\*, YOICHI MUKAI<sup>†1</sup>, YASUYUKI NAGANO<sup>†2</sup>

\* Takenaka Corporation  
1-5-1, Ohtsuka, Inzai-shi, Chiba, 270-1395, Japan  
E-mail: mizushima.yasunori@takenaka.co.jp

<sup>†1</sup>Kobe University  
1-1, Rokkodai-cho, Nada-ku, Kobe, 657-8501, Japan  
E-mail: ymukai@port.kobe-u.ac.jp

<sup>†2</sup> Graduate School of Simulation Studies, University of Hyogo  
7-1-28, Minatojima-Minamimachi, Chuo-ku, Kobe 650-0047, Japan  
E-mail: nagano@sim.u-hyogo.ac.jp

**Key words:** Structural Analysis, Large-Scale Model, FEM Analysis.

**Abstract.** This study presents the first step in the development of a visualization system that would predict simultaneously the expected entire seismic damage of both structural and non-structural members, such as non-structural walls and ceilings, in building, by superposing seismic analytical results of non-structural members on those of structural members. A large-scale FE structural analysis of a building was conducted to evaluate structural damages and to extract local responses that will be used to evaluate non-structural damages on the building.

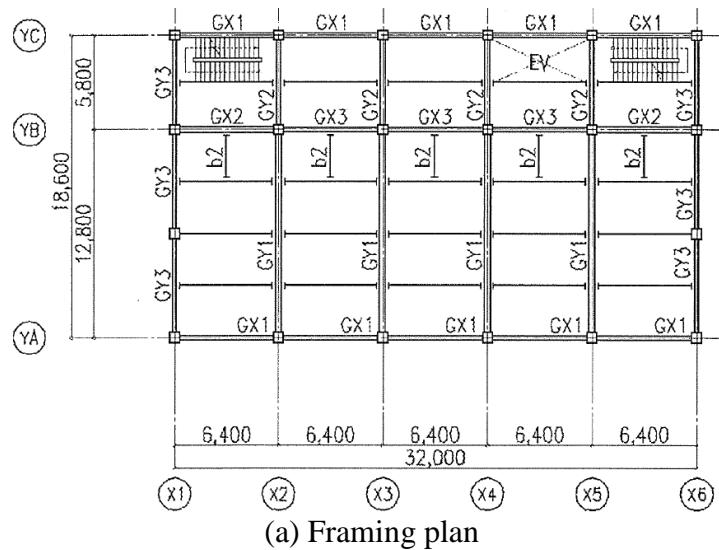
## 1 INTRODUCTION

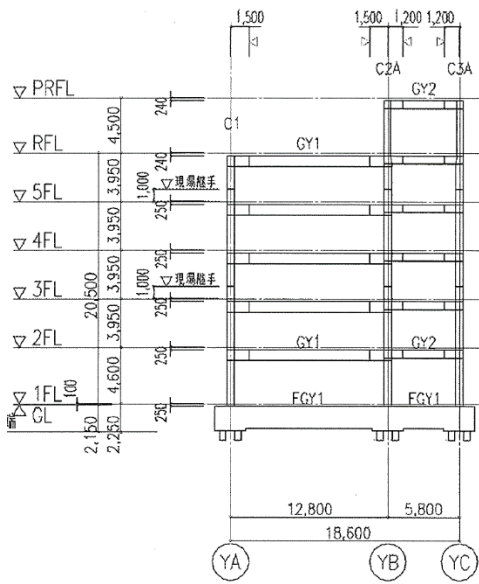
This study aims to develop a system that can show the seismic damage undergone by structural and non-structural members at the same time. Past seismic damage examples showed that harms on humans had been caused by not only structural damages but also by damages of non-structural members. Whereas safety of structural members is constantly confirmed in the structural design process of buildings, there is no detailed process for safety of non-structural members as they are made by specification design without any consideration to their locations. In order to reduce damage to non-structural members that may harm humans, non-structural members should be designed considering local seismic responses. To accurately evaluate local seismic responses of non-structural members, it is necessary to accurately evaluate seismic responses of structural members on which non-structural members are attached.

In this study, the structural damage in a building was evaluated accurately by using detailed finite element (FE) model of all structural members of the building. The authors showed, in a previous study, that a detailed and entire FE model of the building structure simulated accurately the actual seismic behavior of the building<sup>[1]</sup>. By the detailed FE model, local seismic responses of the structural parts on which non-structural members were connected could be extracted because the original shapes of all the structural members were reproduced as precisely as possible in the model. The local responses could be used to evaluate the seismic damage to the non-structural members.

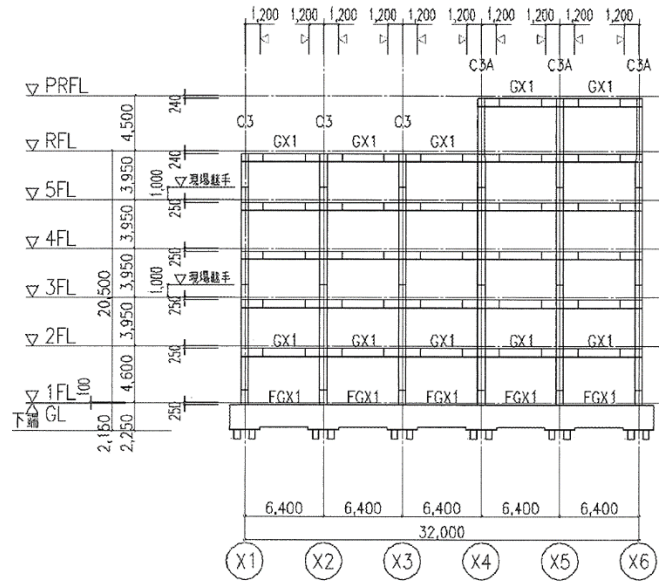
## 2 ANALYTICAL TARGET BUILDING<sup>[2]</sup>

An analytical target is shown in Fig. 1. The building was a 7-story (include Pent house), 5-bay in X-direction and 3-bay in Y-direction. The columns were made of square tube(BCR295) and beams were made of H-shaped steel. The properties of columns are listed in Table 1, and those of beams are listed in Table 2.





(b) Framing elevation 1



(c) Framing elevation 2

Fig.1 Structural drawings of analytical target building

Table 1 Section list of columns

	C1	C2, C2A	C3, C3A	C4
RF		B-460×16	B-460×16	-
5F	B-500×22	B-500×22	B-500×22	B-500×22
4F				
3F				
2F				
1F				

Table 2 Section list of beams

	GX1		GX2		GX3	
	edge	center	edge	center	edge	center
PRF	H-600×250×12×19		H-600×250×12×22		H-600×200 ×12×22	
RF			H-600×200 ×12×25	H-600×200 ×12×22		
5F						
4F	H-600×250 ×12×22	H-600×250 ×12×19	H-600×200 ×12×22	H-600×200 ×12×19	H-600×250 ×12×22	H-600×250 ×12×19
3F						
2F						

	GY1		GY2		GY3	
	edge	center	edge	center	edge	center
PRF	-		H-600×200×12×19		-	
RF	H-800×350×16×25				H-600×200 ×12×22	
5F					H-600×200 ×12×25	H-600×200 ×12×22
4F			H-600×250 ×12×22	H-600×250 ×12×19		
3F						

### 3 ANALYTICAL MODEL

An outline of the analytical model is shown in Fig. 2. In this study all steel members were modeled with 1st order planer elements that have 4-node at a unit length of 40mm. The planer elements had 4 integration points in the thickness direction and 1 integration point in the plane. As the concrete parts, 8-node solid elements were used. In the model, beam elements were used as the reinforcement bar and headed stud. The concrete mesh and reinforcement mesh were generated separately, so that their nodes were not shared in the model. The solid elements which was used for slabs and the beam elements which was used for reinforcement were coupled by constraint methods. The number of elements and nodes was 6,526,889 and 7,381,537, respectively.

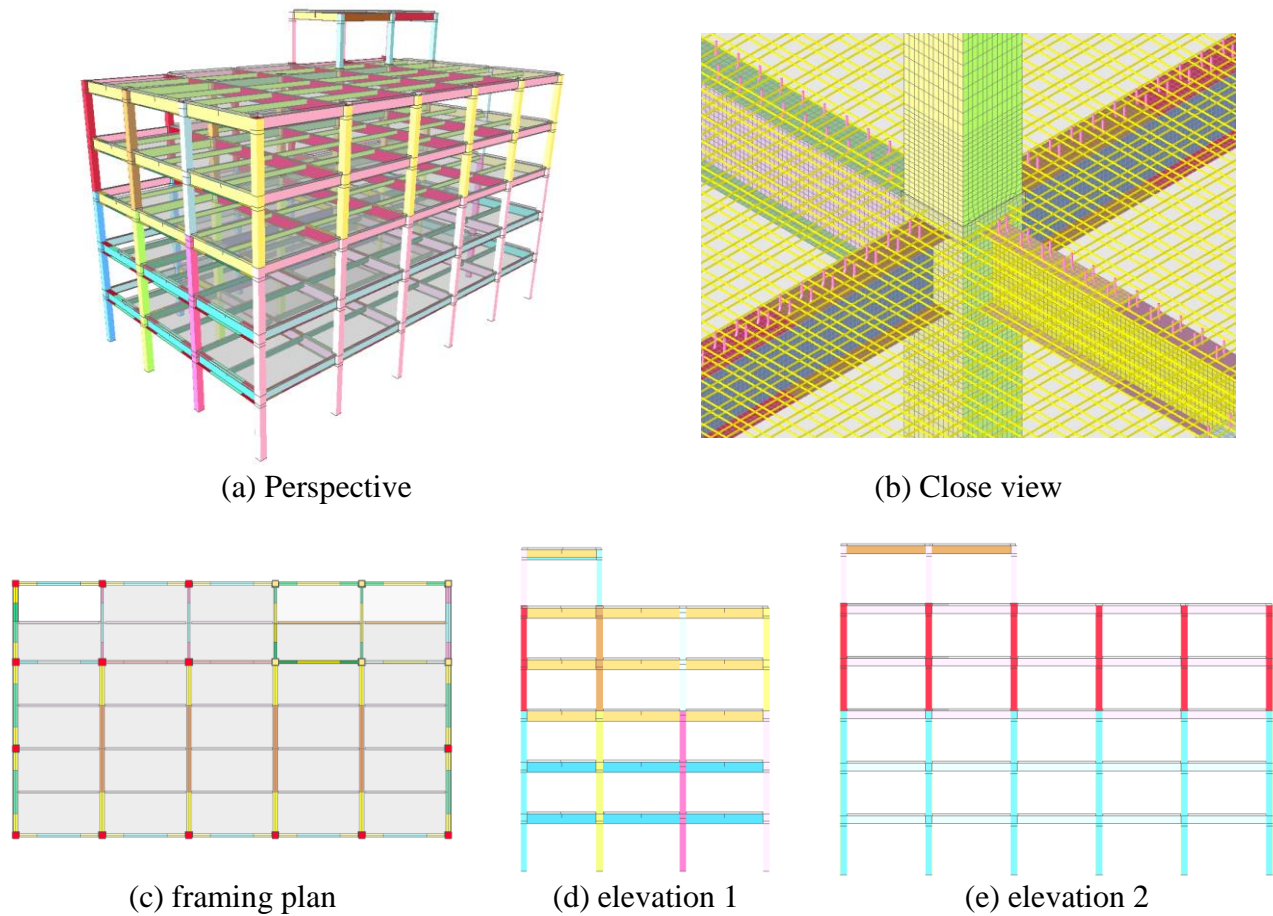


Fig.2 Analytical model

Input motion used in this study was 3-directional JR-Takatori wave, which was recorded at a railway station in Hyogo-ken Nambu earthquake(1995). Time histories of acceleration of the input motion are shown in Fig.3. Input motions that were recorded in north-south, east-west and up-down direction were inputted, respectively, X, Y and Z directions that was defined in the analytical model.

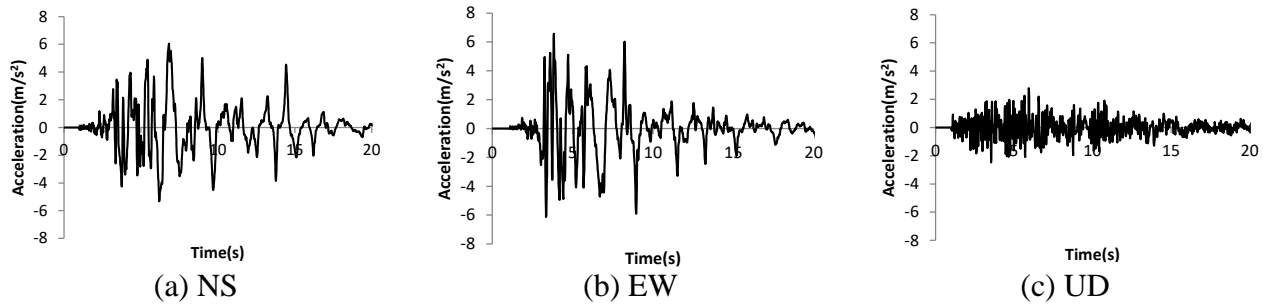


Fig.3 Input motion

### 3 ANALYTICAL RESULT AND CONNECTION TO ANALYSIS FOR NON-STRUCTURAL MEMBERS

Time histories of story drift are shown in Fig.4. Maximum story drift reached 191mm and 90mm in X and Y direction, respectively. Deformation and stress distributions obtained from the analysis are shown in Fig.5. These results were observed at a time when the maximum story drift in X direction occurred. It can be seen that local buckling of bottom of columns occurred at 1st story. Torsional motion was observed because times when the maximum story drift was different between X and Y directions. Local response that will be used to evaluate non-structural damages is shown in Fig.6 The local response is relative displacement between input motion and points that will be connected to suspension rod for ceilings.

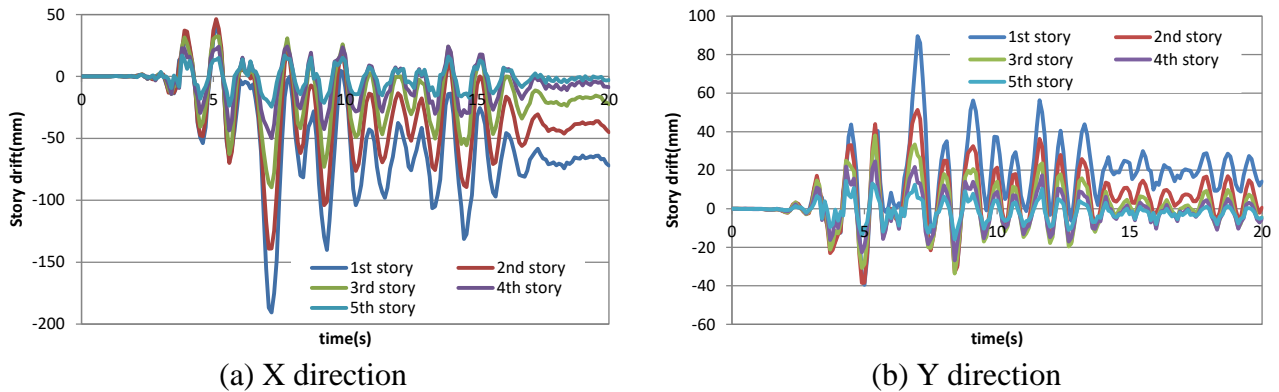
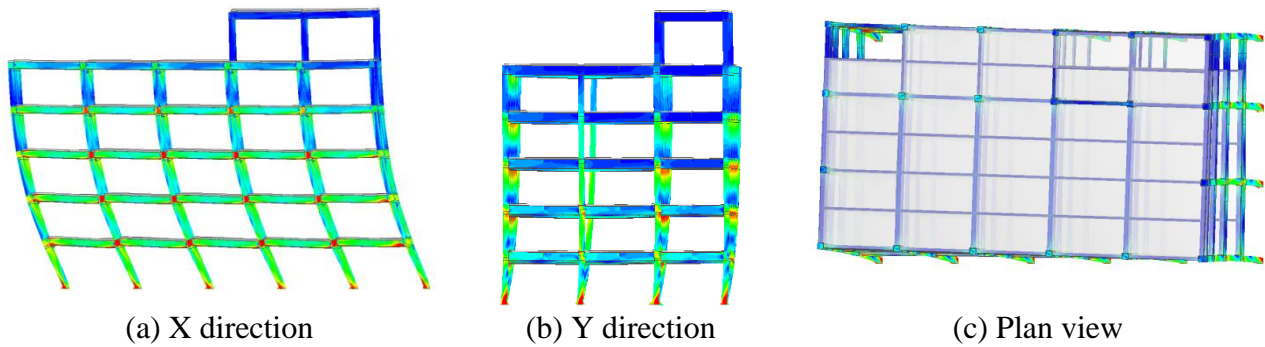


Fig.4 Story drift



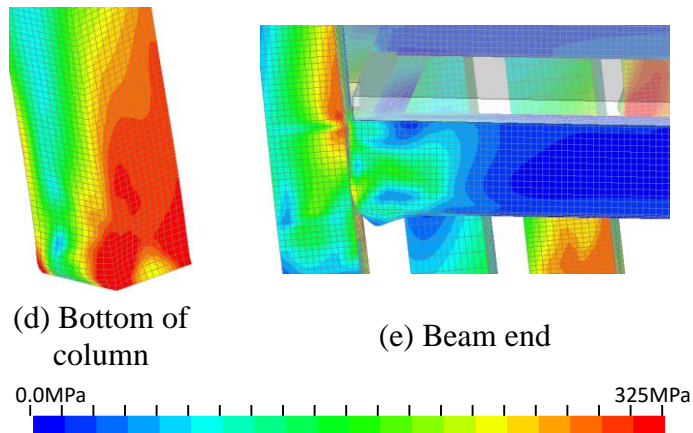


Fig. 5 Deformations and von Mises stress distribution

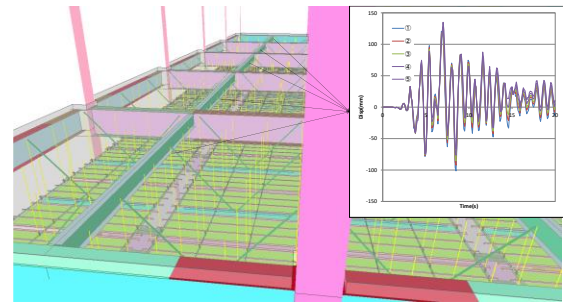


Fig.6 Local response

## 6 CONCLUSIONS

- Structural analysis of the entire building was carried out. Steel structural members in the model were modeled by shell element in order to replicate their original shapes.
- Local responses of the model can be extracted and the result will be used to evaluate non-structural damages on the building.

## ACKNOWLEDGMENTS

This work was supported by JSPS KAKENHI Grant Number JP16H03124.

## REFERENCES

[1] Yasunori Mizushima, Yoichi Mukai, Hisashi Namba, Kenzo Taga and Tomoharu Saruwatari : Super-detailed FEM simulations for full-scale steel structure with fatal rupture at joints between members -Shaking-table test of full-scale steel frame structure to estimate influence of cumulative damage by multiple strong motion: Part 1, *Japan Architectural Review*, AIJ, Vol.1, Issue 1, pp.96-108, Jan., (2018)  
DOI : <https://doi.org/10.1002/2475-8876.10016>

[2] The Japan Building Disaster Prevention Association: Case Examples of Structural Design of Buildings and Their Members, (2007) (in Japanese)

## An Unbiased Nitsche's Formulation of Frictional Contact and Self-contact

Rabii Mlika<sup>\*</sup>, Yves Renard<sup>\*\*</sup>, Franz Chouly<sup>\*\*\*</sup>

<sup>\*</sup>INSA-Lyon, France., <sup>\*\*</sup>INSA-Lyon, France., <sup>\*\*\*</sup>Université Bourgogne Franche-Comté, France

### ABSTRACT

In this work, we present a new formulation of frictional contact between two elastic bodies based on Nitsche's method. Nitsche's method was adapted to unilateral contact in [1]. It aims to treat the interface conditions in a weak sense, thanks to a consistent term stabilized with a Nitsche parameter. At first, we introduce the study carried out in the small strain framework for an unbiased version of the method. The non-distinction between a master surface and a slave one will allow the method to be more generic and directly applicable to the self-contact problem. As in [1], we describe a class of methods through a generalization parameter  $\theta$ . Particular variants have different properties from a numerical point of view, in terms of accuracy and robustness. The restrictive framework of small strain and Tresca friction allowed us to obtain theoretical results on the consistency and convergence of the method (see [2]). The Nitsche's method is then extended to the large strain case more relevant for industrial applications and situations of self-contact. The method is formulated for an hyper-elastic material and declines in the two versions: biased and unbiased. To prove the accuracy of the method for large deformations, we provide several validation tests (Taylor patch test, elastic half ring, cross tubes ...). The description of the method and all the results are detailed in [3]. We provide, finally, a study of the influence of numerical quadrature on the accuracy and convergence of the method. This study covers a comparison of several integration rules (element-based, segment-based, non-symmetric integration) proposed in the literature for other integral methods. References [1] F. Chouly, P. Hild, and Y. Renard. Symmetric and non-symmetric variants of Nitsche's method for contact problems in elasticity: theory and numerical experiments. *Mathematics of Computation*, 84:1089–1112, 2015. [2] F. Chouly, R. Mlika, and Y. Renard. An unbiased Nitsche's approximation of the frictional contact between two elastic structures. To appear in *Numerische Mathematik*, Available on HAL as hal-01240068, 2016. [3] R. Mlika, Y. Renard, and F. Chouly. An unbiased Nitsche's formulation of large deformation frictional contact and self-contact. *Computer Methods in Applied Mechanics and Engineering*, 325(Supplement C):265 – 288, 2017.

## **An Efficient DDM with Cross-points for the Parallel Finite Element Solution of Helmholtz Problems**

Axel Modave<sup>\*</sup>, Xavier Antoine<sup>\*\*</sup>, Christophe Geuzaine<sup>\*\*\*</sup>

<sup>\*</sup>CNRS, POEMS, University of Paris-Saclay, France, <sup>\*\*</sup>Institut Élie Cartan de Lorraine, Université de Lorraine, France, <sup>\*\*\*</sup>University of Liège, Belgium

### **ABSTRACT**

Solving high-frequency time-harmonic scattering problems using finite element techniques is challenging, as such problems lead to very large, complex and possibly indefinite linear systems. Optimized Schwarz domain decomposition methods (DDMs) are currently a very promising approach, where subproblems of smaller sizes are solved using sparse direct solvers, and are combined with iterative Krylov subspace techniques. It is well-known that the convergence rate of these methods strongly depends on the transmission condition enforced on the interfaces between the subdomains. Local transmission conditions based on high-order approximations of the free-space Dirichlet-to-Neumann (DtN) operator have proved well suited. They represent a good compromise between basic impedance conditions (which lead to suboptimal convergence) and the exact DtN map related to the complementary of the subdomain (which is very expensive to compute). However, a direct application of this approach for domain decomposition configurations with cross-points, where more than two subdomains meet, leads to disappointing convergence results. In this talk, we will present novel strategies to efficiently address configurations with cross-points. These strategies are based on corner treatments developed for high-order absorbing boundary conditions. Computational results obtained with the GetDP and GetDDM environments will be presented.

## Sampling Full Extreme Event Statistics for Nonlinear Dynamical Systems through Sequential Surrogate Models

Mustafa Mohamad\*, Themistoklis Sapsis\*\*

\*Courant Institute of Mathematical Sciences, \*\*Massachusetts Institute of Technology

### ABSTRACT

We develop a method for the evaluation of extreme event statistics associated with nonlinear dynamical systems, using a small number of samples. Extreme events in this context are related to intermittent behavior that occur on short-time scales and have large magnitude responses. From an initial dataset of design points, we formulate a sequential strategy that provides the 'next-best' data point (set of parameters) that when evaluated results in improved estimates of the probability density function (pdf) for a scalar quantity of interest. The approach utilizes Gaussian process regression to perform Bayesian inference on the parameter-to-observation map describing the quantity of interest. We then approximate the desired pdf along with uncertainty bounds utilizing the posterior distribution of the inferred map. The 'next-best' design point is sequentially determined through an optimization procedure that selects the point in parameter space that maximally reduces uncertainty between the estimated bounds of the pdf prediction. Since the optimization process utilizes only information from the inferred map it has minimal computational cost. Moreover, the special form of the criterion emphasizes the tails of the pdf. This strategy is unlike traditional failure probability methods in that we determine the full pdf not just the probability of a desired failure level. The method is applied to estimate the extreme event statistics to several examples including a high-dimensional system with millions degrees of freedom: an offshore platform subjected to three-dimensional irregular waves. It is demonstrated that the developed approach can accurately determine the extreme event statistics using orders from a small of samples.

## **Intergranular and Transgranular Fracture Modes in H.C.P. Alloys**

I. Mohamed\*, S. Ziaei\*\*, M. Zikry\*\*\*

\*North Carolina State University, \*\*North Carolina State University, \*\*\*North Carolina State University

### **ABSTRACT**

A dislocation-density based multiple slip crystalline plasticity formulation and a new computational fracture approach have been used to investigate and predict intergranular and transgranular fracture in hexagonal cubic packed (h.c.p.) materials with a focus on h.c.p. alloys subjected to large changes in strains, strain-rates, and temperatures. This validated predictive framework has been used to understand and predict the interrelated effects of dislocation-density interactions, generation, and recovery on the competition between intergranular and transgranular crack nucleation and propagation. The predictions indicate that iodine pits that have diffused into the GB dominate intergranular fracture and that transgranular fracture is dominated by interrelated dislocation-density interactions and threshold fracture stresses along transgranular cleavage planes.

## Wind Reliability Assessment of Power Transmission Lines Using an Error Rate-Based Adaptive Kriging Method

Yousef Mohammadi Darestani<sup>\*</sup>, Kyunghwa Cha<sup>\*\*</sup>, Zeyu Wang<sup>\*\*\*</sup>, Abdollah Shafieezadeh<sup>\*\*\*\*</sup>

<sup>\*</sup>Ohio State University, <sup>\*\*</sup>Ohio State University, <sup>\*\*\*</sup>Ohio State University, <sup>\*\*\*\*</sup>Ohio State University

### ABSTRACT

Estimation of wind reliability of transmission line systems is critical for risk assessment and management of power grids. This is a complex task considering various uncertainties involved in structural properties and wind load parameters. Conventional Monte Carlo simulation techniques can be utilized to analyze the reliability of these structures. However, considering the large number of random variables involved, these methods would require a significantly large number of realizations of uncertain parameters to accurately estimate failure probabilities. On the other hand, the mechanistic behavior of transmission line systems under extreme wind loadings is considerably complex. Given that these structures are composed of a large number of components such as lattice members and connections and considering large uncertainties involved, there exist numerous potential modes of failure. Analysis of numerical models capable of capturing these complex behaviors is considerably time-consuming. In order to efficiently estimate the probability of failure of transmission line systems, the current study adopts an advanced error rate-based adaptive Kriging method proposed by the authors. In this regard, a small set of realizations of uncertain variables are generated using Latin Hypercube sampling method and the limit state function for each realization is estimated subsequently using a high-fidelity nonlinear model of the tower in OpenSEES Finite Element platform. Nonlinear static pushover analyses are employed with failure defined as the event of exceeding the capacity of the system determined via pushover analyses. A Kriging model is constructed to evaluate the established limit state function. The initial surrogate model is refined continually by strategically selecting additional random realizations of uncertain variables from a novel effective sampling region (ESR). The region refers to a set of realizations that have a joint probability density larger than a threshold. The additional training points are chosen from those within ESR based on an Expected Learning Function that prioritizes points that are near the limit state function and/or have high variance. The model is improved adaptively until the maximum error rate associated with the Kriging prediction of probability of failure is less than a desired threshold. The error rate here is estimated using an extension of central limit theorem based on Lindeberg condition. Results indicate that error rate-based adaptive Kriging method can significantly reduce the number of Finite Element simulations in order to accurately estimate the probability of failure of transmission line systems.

## Computational Modeling of Large People Traffic in Building Environments with Fuzzy Logic

Gray Moita<sup>\*</sup>, Henrique Braga<sup>\*\*</sup>, Paulo Eduardo Almeida<sup>\*\*\*</sup>

<sup>\*</sup>Centro Federal de Educação Tecnológica de Minas Gerais (CEFET-MG), Brazil, <sup>\*\*</sup>Centro Federal de Educação Tecnológica de Minas Gerais (CEFET-MG), Brazil, <sup>\*\*\*</sup>Centro Federal de Educação Tecnológica de Minas Gerais (CEFET-MG), Brazil

### ABSTRACT

The traffic of people in building environments is an important issue whose knowledge and implications directly influences the quality of life of everyone, including our own safety. Tragedies, as occurred in Brazil in 2013 [1], where 242 peoples lost their life and hundreds were injured, can be avoided, or at least minimized, if the human flow was correctly considered, both in normal situations and in case of an emergency. Due to the high number of people who can occupy a building at the same time, and therefore are subject to various risks, it can be said that this is a matter of great public and social interest. Thus, there are several prescriptive legal criteria that establish parameters of design and occupation of these highly diverse environments in search of more controllable human movement. Still, these codes are often nonspecific, not being able to promote certain improvements, and even to avoid dangerous situations. In this way, the existence of computational tools that can help in the verification of the conditions of quality, fluidity and safety of an environment becomes very relevant. However, different from the usual granular mechanical modeling, human movement must also consider several qualitative and quantitative aspects related to human behavior, including mental and cognitive features. This is lacking in many of the available models. In this work, a brand new model is introduced. It is called Fuga, Version 2.0, in which the dynamics of people flow is simulated by the association of artificial intelligence techniques and fuzzy logic, to emulate the human decision making process, taking into account several of the ergonomics aspects. The main focus here is to detail the step-by-step of the entire system, with specific examples, and its relation with the ergonomic human aspects. In the sequence, it is shown how this fuzzy system is transformed into a fuzzy table, and how this knowledge is introduced into the modeling program. This is a necessary step in order to improve the model performance in large scale situations, fundamental when it involves hundreds (sometimes thousands) of people moving at the same time. Examples of effective simulations of human movement using the system are presented and discussed, showing the relevance of the model to contribute in the design and maintenance of safer building. [1] H.C. Braga, G.F. Moita. On the Boate Kiss Fire and the Brazilian Safety Legislation - what we can learn. *Collective Dynamics*, v. 2, 2017.

## **A Combined NFEM - Conservative Level-Set Method for Interface Propagation**

Jorge Molina-Moya<sup>\*</sup>, Pablo Ortiz<sup>\*\*</sup>, Alejandro Martínez-Castro<sup>\*\*\*</sup>

<sup>\*</sup>University of Granada, <sup>\*\*</sup>University of Granada, <sup>\*\*\*</sup>University of Granada

### **ABSTRACT**

The conservative Level-Set (CLS) [1] is one of the most successful interface-capturing methods [2]. Frequently, the CLS is composed of very high order schemes for the transport, and of fast marching methods (FMM) to reconstruct the signed distance function. Although this kind of procedures gives proper results for interfaces propagation problems, they are computationally expensive, even for structured meshes. We propose a methodology consisting of a second order non-oscillatory finite element method (NFEM) [3] applied to the phase function transport step and of a reinitialization step formulated as a non-linear diffusion equation. Reinitialization is completed by the use of the NFEM sign-preserving correction to obtain the final solution. Calculation of interface normals in the CLS leads recurrently to oscillations in the phase function. In this work we propose a simplified local computation of normals with substantial savings on computational cost. Concerning hydrodynamics solution, we employ an improved NFEM for incompressible flows. Numerical model is tested for typical stringent experiments as the Zalesak disk, and dam-break problem. Numerical experiments are also focused on the propagation of air cavities in ducts during pressurized stages. Results are satisfactory both in terms of error norms and in terms of enclosed volume conservation, and are competitive with those obtained from very high order schemes. Acknowledgements: This research is supported by MICIIN Grant #BIA-2015-64994-P (MINECO/FEDER). REFERENCES [1] Olsson, Elin and Kreiss, Gunilla, A conservative level set method for two phase flow. *J. Comput. Phys.*, Vol. 210, pp. 225–246, 2005. [2] Cruchaga, Marcela et al., Numerical Modeling and Experimental Validation of Free Surface Flow Problems. *Arch. Computat. Methods Eng.*, Vol. 23, pp. 139–169, 2016. [3] Ortiz, Pablo, Non-oscillatory continuous FEM for transport and shallow water flows. *Comput. Methods Appl. Mech. Engrg.*, Vol. 223, pp. 55–69, 2012.

## Three-dimensional Fluid Structure Interaction between a Compressible Fluid and a Fragmenting Structure with a Conservative Immersed Boundary Method

Laurent Monasse\*

\*Inria Sophia Antipolis

### ABSTRACT

In this work, we present a conservative method for three-dimensional inviscid fluid-structure interaction problems. On the fluid side, we consider an inviscid Euler fluid in conservative form, discretized with a Finite Volume method on a Cartesian grid. On the solid side, we consider an elastic deformable solid with possible fragmentation. We use a Discrete Element method (particles connected with springs) for the discretization of the solid. Body-fitted methods are not well-suited for large displacements or fragmentation of the structure, since they involve possibly costly remeshing of the fluid domain. We use instead an immersed boundary technique through the modification of the finite volume fluxes in the vicinity of the solid, in the spirit of cut-cell methods. The method is tailored to yield the exact conservation of mass, momentum and energy of the system and exhibits consistency properties [1, 2]. In the event of fragmentation, void can appear due to the velocity of crack opening. Since the numerical flux used is not stable in the presence of void, we resort locally to the Lax-Friedrichs flux near cracks [3]. Since both fluid and solid methods are explicit, the coupling scheme is designed to be explicit too. The computational cost of the fluid and solid methods lies mainly in the evaluation of fluxes on the fluid side and of forces and torques on the solid side. It should be noted that the coupling algorithm evaluates these only once every time step, ensuring the computational efficiency of the coupling. We will present numerical results showing the robustness of the method in the case of a fragmenting solid coupled with a compressible fluid flow. [1] M. A. Puscas, L. Monasse, A three-dimensional conservative coupling method between an inviscid compressible flow and a moving rigid solid body, *SIAM Journal on Scientific Computing* 37, pp. 884-909, 2015 [2] M. A. Puscas, L. Monasse, A. Ern, C. Tenaud, C. Mariotti, V. Daru, A time semi-implicit scheme for the energy-balanced coupling of a shocked fluid flow with a deformable structure, *Journal of Computational Physics* 296, pp. 241-262, 2015 [3] M. A. Puscas, L. Monasse, A. Ern, C. Tenaud, C. Mariotti, A conservative embedded boundary method for an inviscid compressible flow coupled with a fragmenting structure, *International Journal for Numerical methods in Engineering* 103(13), pp. 970-995, 2015

## Modeling Fracture in BCC-Fe Using Cohesive Zone Model Coupled with Crack-tip Plasticity in Multiphysics Object Oriented Simulation Environment (MOOSE)

Geeta Monpara<sup>\*</sup>, Ray Fertig<sup>\*\*</sup>, Wen Jiang<sup>\*\*\*</sup>

<sup>\*</sup>University of Wyoming, <sup>\*\*</sup>University of Wyoming, <sup>\*\*\*</sup>Idaho National Laboratory

### ABSTRACT

Ferritic steels with 9-12%Cr are a candidate material for Gen-IV nuclear fission reactors due to their improved creep resistance with respect to current generation of steels. Fission process releases high energy particles, which interact with the structural components surrounding the nuclear fuel rods, such as cladding, pressure vessel etc. Such interactions lead to large displacement of atoms in the bulk of a material, resulting in many microstructural defects. Such defects could cause radiation-induced segregation and embrittlement of the grain boundaries. This leads to a change in cohesive energy of a grain boundary, which can affect fracture of the material. The Multiphysics Object-Oriented Simulation Environment (MOOSE) is used to model fracture in our study. MOOSE is a finite-element, multiphysics framework primarily developed by Idaho National Laboratory. In this study, we use cohesive zone model for grain boundary fracture in pure body-centered cubic (BCC) Fe. The cohesive law is implemented in MOOSE framework using Extended Finite Element Method module. All commercial finite element packages use viscous regularization to improve convergence issues. A study by Kuhn and Fertig show that use of energy conserving trilinear cohesive law obsoletes viscous regularization, resulting load-displacement curve matches well with the experimental data [1]. Such trilinear cohesive law is implemented for mode-I fracture in MOOSE. We simulate a micro-cantilever beam to model fracture along a grain boundary. Fracture is set to initiate at a notch on the grain boundary. The cantilever beam is loaded to propagate the crack from notch according to a cohesive law. The tip of the crack sees significant plastic deformation. The plastic zone ahead of the crack tip is modeled with a crystal plasticity model. Here, Crystal plasticity model is based on modified Schmid's law. This is derived from atomistic studies to incorporate nonplanar nature of a screw dislocation core in BCC materials [2]. Results of load-displacement curves are compared with the experimental data from our collaborators. References: 1. Kuhn, K. and R. Fertig III. A Physics-Based Fatigue Life Prediction for Composite Delamination Subject to Mode I Loading. in Proceedings of the American Society for Composites: Thirty-First Technical Conference. 2016. 2. Koester, A., A. Ma, and A. Hartmaier, Atomistically informed crystal plasticity model for body-centered cubic iron. Acta Materialia, 2012. 60(9): p. 3894-3901.

## Spline Parameterization of 2D and 3D Geometries for its Application in Isogeometric Analysis

Rafael Montenegro\*, Marina Brovka\*\*, José Iván López\*\*\*, José María Escobar\*\*\*\*

\*University Institute for Intelligent Systems and Numerical Applications in Engineering (SIANI), University of Las Palmas de Gran Canaria, Spain, \*\*University Institute for Intelligent Systems and Numerical Applications in Engineering (SIANI), University of Las Palmas de Gran Canaria, Spain, \*\*\*University Institute for Intelligent Systems and Numerical Applications in Engineering (SIANI), University of Las Palmas de Gran Canaria, Spain, \*\*\*\*University Institute for Intelligent Systems and Numerical Applications in Engineering (SIANI), University of Las Palmas de Gran Canaria, Spain

### ABSTRACT

We present an optimization based method for parameterization of 2D and 3D geometries for its application in isogeometric analysis. This method is a continuation of our previous works [1, 2, 3]. The proposed technique allows to obtain a good quality global spline parameterization from the boundary representation of the domain. The key of strategy lies in the simultaneous untangling and smoothing procedure used for the relocation of the interior control points in order to obtain optimal quality spline parametric mapping. Optimization is based on the mean ratio shape quality measure which attains its maximum when the mapping is conformal. Another important feature of the technique is the use of the regularized distortion measure which allows to perform unconstrained smooth optimization pursuing two goals at the same time: a valid parametric mapping (positive Jacobian) and a mapping as conformal as possible. We give a detailed description of the proposed method and show some examples. Also, we present some examples of the application of isogeometric analysis in geometries parameterized with our method. REFERENCES [1] Brovka M., López J.I., Escobar J.M., Cascón J.M., Montenegro R. (2014) A new method for T-spline parameterization of complex 2D geometries. *Engineering with Computers* 30: 457-473. [2] López J.I., Brovka M., Escobar J.M., Montenegro R., Socorro G.V. (2016) Strategies for optimization of hexahedral meshes and their comparative study. *Engineering with Computers* 33: 33-43. [3] López J.I., Brovka M., Escobar J.M., Montenegro R., Socorro G.V. (2017) Spline parameterization method for 2D and 3D geometries based on T-mesh optimization. *Computer Methods in Applied Mechanics and Engineering* 322: 460-482.

## **A Complex Variable Finite Element-Based Approach for Rapid Estimates of Residual Stress Variance**

Arturo Montoya<sup>\*</sup>, Harry Millwater<sup>\*\*</sup>, Randal Fielder<sup>\*\*\*</sup>, Patrick Golden<sup>\*\*\*\*</sup>

<sup>\*</sup>University of Texas at San Antonio, <sup>\*\*</sup>University of Texas at San Antonio, <sup>\*\*\*</sup>University of Texas at San Antonio,  
<sup>\*\*\*\*</sup>Air Force Research Laboratory

### **ABSTRACT**

Residual stresses can be introduced intentionally to structural components as a means to improve their fatigue performance. Methods for introducing beneficial residual stresses include autofrettage, cold working, low plasticity burnishing and laser shot peening. However, there is frequently significant uncertainty regarding the magnitude of the induced residual stresses due to variation in material properties, loading, geometry, variables of the thermo/mechanical processes, and measurement uncertainty. The residual stress variation must be quantified in order to have confidence that the behavior of a structure, during its entire operation time, will be within safety limits. The traditional approach to estimate this variance is the Monte Carlo simulation (MCS). However, MCS requires a large number of simulations to accurately predict the variance, and becomes prohibitively time consuming for large-scale models and nonlinear analyses. This paper presents a unique, efficient approach to quantifying the uncertainty associated with residual stresses induced during manufacturing processes. The variance in the residual stresses is approximated using a few nonlinear complex-variable finite element analyses. The key ingredient for this method is to compute the sensitivities of the residual stress field with respect to each random variable using the complex variable finite element method, ZFEM. This sensitivity information are fed to a first order Taylor series approximation in order to provide a first-order estimate of the residual stress variance. The method was verified using the autofrettage process of a sphere subject to random stress-strain properties, internal pressure, and geometry. Four ZFEM nonlinear analyses were conducted to obtain the sensitivities of the residual stress field with respect to the four random variables of interest. The CPU time required for the four ZFEM analyses was about 2% of the total CPU time required to generate the MCS results from 1000 realizations. In addition, the approximate method provided a sensitivity analysis that allowed the most critical random variables to be identified quickly. Although demonstrated using the autofrettage process, the ZFEM-based methodology is general and can be applied to other residual stress inducing processes.

## Multiscale Analysis of Photomechanics of Liquid Crystalline Polymer via Coarse-grained Molecular Dynamics Simulation

Junghwan Moon<sup>\*</sup>, Byungjo Kim<sup>\*\*</sup>, Joonmyung Choi<sup>\*\*\*</sup>, Maenghyo Cho<sup>\*\*\*\*</sup>

<sup>\*</sup>Seoul National University, <sup>\*\*</sup>Seoul National University, <sup>\*\*\*</sup>Samsung Electronics Co., <sup>\*\*\*\*</sup>Seoul National University

### ABSTRACT

Crosslinked liquid crystalline polymer (LCP) containing azo-based photochromic mesogens is a kind of photo-responsive polymers (PRPs), which can realize reversible mechanical deformation under irradiation of ultraviolet (UV) and visible lights. The difficulty in precise prediction of the photo-actuated deformation originates from the multiscale and multiphysics nature of the phenomenon. Even though some finite element method (FEM)-based computational models have been established [1,2], those cannot reflect the dependence of the molecular architecture on the macroscopic deformation. Also, full-atomistic molecular dynamics (MD) simulations have limitations of massive computational costs for describing diverse liquid crystalline phases. Therefore, we developed a multiscale computational framework, which combines the information at different scales to establish a relation between microscopic photochemical reaction and corresponding mechanical actuation. First, a photo-switching potential, which can be derived by a density functional theory (DFT) calculation, was utilized to describe the trans -to cis- isomerization of the azobenzene moieties in the MD simulation [3]. Then, light-induced liquid crystalline structural changes are reflected to the mesoscale simulation by deriving the coarse-grained (CG) potentials. Especially, we used a structure-based iterative Boltzmann inversion (IBI) method to derive the non-bonded energy of the CG MD simulation. As a result, our multiscale computational model efficiently described thermal and light response of the azo-LCP. The smectic-nematic-isotropic phase transition temperature and photo-strain had a good accordance with those of the experimental findings. Furthermore, a relationship between microscopic LC order parameters and shape parameter of the polymer networks was characterized with various molecular architectures, which is useful to precisely predict the macroscopic photo-mechanical deformation in continuum scale analysis. We expect our multiscale simulation scheme can broaden the applicability of the computational mechanics in research fields of the photo-responsive soft actuators. Acknowledgements This work was supported by a grant from the National Research Foundation of Korea (NRF) funded by the Korea government (MSIP) (Grant No. 2012R1A3A20488 41). References [1] Y. Lin, L. Jin, Y. Huo, Int. J. Solids. Struct. 2012, 49, 2668-2680. [2] H. Chung, J. Park, M. Cho, Phys. Rev. E 2016, 94, 042707. [3] J. Choi, H. Chung, J.-H. Yun, Appl. Phys. Lett. 2014, 105, 221906.

## Recent Developments in Polygonal and Polyhedral Discontinuous Petrov-Galerkin Methods (PolyDPG)

Jaime Mora<sup>\*</sup>, Federico Fuentes<sup>\*\*</sup>, Leszek Demkowicz<sup>\*\*\*</sup>, Ali Vaziri Astaneh<sup>\*\*\*\*</sup>

<sup>\*</sup>University of Texas at Austin, <sup>\*\*</sup>University of Texas at Austin, <sup>\*\*\*</sup>University of Texas at Austin, <sup>\*\*\*\*</sup>MSC Software Corporation

### ABSTRACT

After the birth of PolyDPG methods, that is, the introduction of the discontinuous Petrov-Galerkin methodology (DPG) into the flourishing family of polytopal discretization techniques, these have kept maturing as a suitable set of finite element methods for general polytopes. This ongoing development of PolyDPG methods has involved both their mathematical foundations and their applications, and new extensions that may be of great interest to this community are currently in progress. In [1], the initial stage of 2D PolyDPG was consolidated, therein delivering: (1) a clear procedure for the discretization using the broken ultraweak formulation in meshes of arbitrary polygonal elements; (2) a complete proof of convergence as a conforming method for the mentioned variational formulation; and (3) a few practical examples where PolyDPG successfully satisfied the expectations arisen from the theory. Now, a new set of results of PolyDPG for two-dimensional problems is provided, where our methodology shows how competitive it is with respect to other polygonal technologies. Additionally, PolyDPG has been extended to the three-dimensional realm. Given the limitations of some of the ideas that work in 2D when extrapolated to polyhedra, three possibilities for the 3D problem can be explored: (i) considering polyhedral elements of triangular and quadrilateral faces only; (ii) using alternative shape functions for the polygonal faces (which require some degree of continuity across edges); or (iii) implementing a non-conforming DPG methodology. To conclude, the first sample of results of PolyDPG in 3D is presented and discussed. [1] A. Vaziri Astaneh, F. Fuentes, J. Mora, L. Demkowicz, High-order polygonal discontinuous Petrov–Galerkin (PolyDPG) methods using ultraweak formulations, *Comput. Methods Appl. Mech. Engrg.* (2017), <https://doi.org/10.1016/j.cma.2017.12.011>

## Constrained Relative Entropy for Coarse-Grained Force Field Development of Room Temperature Ionic Liquids

Alireza Moradzadeh<sup>\*</sup>, Hossein Motevaselian<sup>\*\*</sup>, Sikandar Mashayak<sup>\*\*\*</sup>, Narayana Aluru<sup>\*\*\*\*</sup>

<sup>\*</sup>Department of Mechanical Science and Engineering Beckman Institute for Advanced Science and Technology University of Illinois at Urbana-Champaign, <sup>\*\*</sup>Department of Mechanical Science and Engineering Beckman Institute for Advanced Science and Technology University of Illinois at Urbana-Champaign, <sup>\*\*\*</sup>Department of Mechanical Science and Engineering Beckman Institute for Advanced Science and Technology University of Illinois at Urbana-Champaign, <sup>\*\*\*\*</sup>Department of Mechanical Science and Engineering Beckman Institute for Advanced Science and Technology University of Illinois at Urbana-Champaign

### ABSTRACT

Room temperature ionic liquids (RTILs) are an emerging class of solvents with many potential applications in energy-storage, biochemistry, etc. Molecular dynamics (MD) simulation is a powerful tool to study RTILs behavior in order to connect their microscopic behavior with their macroscopic properties. However, the high computational cost hinders the all-atom MD (AAMD) simulations of RTILs for large time- (~ $\mu$ s) and length-scales (~ $\mu$ m). During the past decade, coarse-grained (CG) simulations have become popular to study systems on larger time- and length-scales. In this study, we extend the relative entropy method with the addition of a constraint to reproduce the thermodynamics properties such as pressure in addition to the structure. In this study, the constrained relative entropy (CRE) method is applied for (CG) force field development of imidazolium-based ionic liquids. In addition to Lagrange multiplier for CRE minimization, we treat Coulombic interaction in a more systematic manner, which is of significant importance in RTILs behavior. To do so, we consider a global charge scalar for CG force field and obtain its optimal value within the CRE framework. Finally, we demonstrate that our CG force-field can accurately predict the structural, thermodynamic, and dynamical properties of imidazolium-based ionic liquids. The coarse-graining method presented in this study is also applicable for other classes of RTILs, such as Pyridinium-based and di-cationic ILs.

## Finite Element Simulations of Two-phase Flow and Floating Bodies Using FEniCS-HPC

Margarida Moragues Ginard<sup>\*</sup>, Daniel Castañón Quiroz<sup>\*\*</sup>, Niyazi Cem Degirmenci<sup>\*\*\*</sup>, Johan Jansson<sup>\*\*\*\*</sup>, Vincenzo Nava<sup>\*\*\*\*\*</sup>, Ezhilmathi Krishnasamy<sup>\*\*\*\*\*</sup>, Johan Hoffman<sup>\*\*\*\*\*</sup>

<sup>\*</sup>Basque Center for Applied Mathematics (BCAM), <sup>\*\*</sup>University of Montpellier, <sup>\*\*\*</sup>Basque Center for Applied Mathematics (BCAM), <sup>\*\*\*\*</sup>KTH Computational Technology Laboratory and Basque Center for Applied Mathematics (BCAM), <sup>\*\*\*\*\*</sup>Tecnalia R&I; and Basque Center for Applied Mathematics (BCAM), <sup>\*\*\*\*\*</sup>Basque Center for Applied Mathematics (BCAM), <sup>\*\*\*\*\*</sup>KTH Computational Technology Laboratory

### ABSTRACT

We present a variational multiscale stabilized finite element method to solve the variable density incompressible Navier-Stokes equations for the simulation of two-phase flow. We introduce a level-set method based on the compression technique similar to [1]. For the simulation of floating devices we make use of a simplified rigid body motion scheme and a deforming mesh approach [2]. The mesh deforms elastically following the movement of the body. An implicit turbulence model is used where turbulence is modelled by the numerical stabilization. The described methods are implemented in the open source software framework FEniCS-HPC [3] provided with an automated methodology for discretization and error control. We are working in a project for marine energy generation together with Tecnalia R&I. In this context we simulate floating platforms that will be used for marine energy generation or device experimentation in the ocean. The aim is to study the dynamics of this kind of off-shore devices. Our simulation results are compared against the experimental data obtained by Tecnalia R&I company in the experimental tank of CEHIPAR in Spain. We also participate in the IEA-OES Task 10 project where different simulations of floating bodies are carried out. The results are compared against other groups simulations that use different methodologies. [1] E. Olsson, G. Kreiss, A conservative level set method for two phase flow, *Journal of Computational Physics* 210 (1) (2005) 225-246. [2] A.A. Johnson and T.E. Tezduyar, Mesh update strategies in parallel finite element computations of flow problems with moving boundaries and interfaces, *Computer Methods in Applied Mechanics and Engineering* 119 (1) (1994) 73-94 [3] Hoffman J., Jansson J., Jansson N., FEniCS-HPC: Automated Predictive High-Performance Finite Element Computing with Applications in Aerodynamics, PPAM 2015. *Lecture Notes in Computer Science*, vol 9573 (2016). Springer, Cham

## Three-Dimensional Model for Smooth Muscle Contraction: Urinary Bladder Wall Application

Enrique Morales Orcajo<sup>\*</sup>, Robert Seydewitz<sup>\*\*</sup>, Tobias Siebert<sup>\*\*\*</sup>, Markus Böl<sup>\*\*\*\*</sup>

<sup>\*</sup>Institute of Solid Mechanics, Braunschweig, Germany, <sup>\*\*</sup>Institute of Solid Mechanics, Braunschweig, Germany,  
<sup>\*\*\*</sup>Institute of Sport and Motion Science, Stuttgart, Germany, <sup>\*\*\*\*</sup>Institute of Solid Mechanics, Braunschweig,  
Germany

### ABSTRACT

The urinary bladder wall is a soft tissue that constitute the bladder organ and control all its functions. Such a functionality is achieved due to a specific hierarchical layered structure which featured non-linear hyperelastic mechanical response with hysteresis and softening effects as well as regional variability across the organ. Therefore, a detailed constitutive model of urinary bladder wall that account for its singularities will provide a useful tool for medicine and biomedical engineering applications. To work in that direction, a recently developed model for smooth muscle contraction of the urinary bladder [Seydewitz et al. 2017] is improved with new region-specific mechanical and histological data. The model features the urinary bladder wall in two layers: One layer with passive mechanical properties, the tunica mucosa, and another layer with passive and active response, the tunica muscularis. For the passive response, location-specific biaxial tests of the intact bladder wall as well as the mucosa and muscularis layers independently were use to identify the parameters. At the same positions, the smooth muscle orientation was histologically measured catching the in-plane and transmural fibre distribution. For the active response, layer-specific orientation-dependent uniaxial test were use. As a result, the temporal progression of four variables namely, electrical potential, calcium concentration, degree of activation and von Mises stress are simulated in a three-dimensional urinary bladder model. References R. Seydewitz, R. Menzel, T. Siebert, M. Böl, Three-dimensional mechano-electrochemical model for smooth muscle contraction of the urinary bladder, Journal of the Mechanical Behavior of Biomedical Materials, 75, 128-146, 2017.

## **A New Shell Formulation for Composite Delamination Modelling under Transient Dynamic Loading**

Lionel Morancay<sup>\*</sup>, Said Mamouri<sup>\*\*</sup>, Jean-Baptiste Mouillet<sup>\*\*\*</sup>, Juan Pedro Berro Ramirez<sup>\*\*\*\*</sup>

<sup>\*</sup>ALTAIR Engineering, <sup>\*\*</sup>ALTAIR Engineering, <sup>\*\*\*</sup>ALTAIR Engineering, <sup>\*\*\*\*</sup>ALTAIR Engineering

### **ABSTRACT**

When composite structures are subject to highly dynamic loading such as crash or impact, it may be necessary to take into account delamination, especially if it is necessary to estimate energy absorption and failure modes. A first approach consists in either a full solid elements (in which all layers are modelled with solid element) or modelling each layer with one element connected by cohesive elements to take into account the delamination properties. With the ever increasing size of models in term of element size and number of plies, those approach are becoming very expensive in terms of computation time especially for “full vehicle models”. In addition, solid CAD are sometimes difficult to handle within the industrial processes for modelling full components, the shell approach being often preferred for instance in automotive industry. To reduce computational time and model design time, a new shell element was developed and implemented in the RADIOSS transient non-linear explicit code. Based on the MICT4 shell [1], the model is enriched by introducing additional degrees of freedom for representing the relative motion of the plies wrt actual positions of the - through the thickness - integration points. These additional degrees of freedom are calculated according to the interlayer properties, which are based on the transverse material properties of the laminate. A delamination criterion such as Ladevèze [2] can be associated. Full element delamination in mode I or II is modelled by relaxation of the corresponding interlayer stiffness. This approach results in a shell modelling approach, giving CPU times comparable to shell models and significantly faster than “full3D models”, while the transverse behaviour is significantly better represented and it allows to identify delamination phenomenon in crash or impact situation on thin structures. The so-called PLY-XFEM shell formulation will be first presented. To assess the capacities of modelling delamination, the PLY-XFEM formulation is next compared to solid elements on an ENF test. Another application of a bird strike onto a Kevlar plate at 45 degrees incidence is presented. References [1] E. Dvorkin and K. J. Bathe, “A Continuum Mechanics Based Four-Node Shell Element for General Nonlinear Analysis”, *Engineering Computations*, 1, 77-88, 1984. [2] O. Allix and P. Ladevèze, “Interlaminar interface modeling for the prediction of delamination”, *Composite Structures*, 22, 235-242, 1992.

## Mesh Refinement for T-Splines in Any Dimension

Philipp Morgenstern\*

\*Leibniz University Hannover, Germany

### ABSTRACT

T-splines are a generalization of tensor-product B-splines to non-uniform meshes. They have been introduced as a free-form geometric technology in the Computer-Aided Design community and have therefore caught much attention in Isogeometric Analysis, particularly with regard to constructing a mesh-adaptive Galerkin Method that uses the data structures from CAD applications. We present a generalized adaptive refinement procedure for n-dimensional axis-parallel box meshes with user-defined grading, i.e., the user chooses the number of children in a single elements' refinement. We prove linear independence of the T-spline functions that correspond to the generated meshes, nestedness of the generated T-spline spaces and linear computational complexity of the refinement procedure in terms of the number of marked and generated mesh elements. REFERENCES [1] P. Morgenstern, Globally structured three-dimensional analysis-suitable T-splines: Definition, linear independence and m-graded local refinement, SIAM Journal on Numerical Analysis 54 (2016), no. 4, 2163–2186. [2] P. Morgenstern, Mesh refinement strategies for the adaptive isogeometric method, Ph.D. thesis, Institut für Numerische Simulation, Universität Bonn, 2017.

## DEM-based Optimal Design of Rockfall Protection Walls

Shuji Moriguchi<sup>\*</sup>, Hasuka Kanno<sup>\*\*</sup>, Kenjiro Terada<sup>\*\*\*</sup>

<sup>\*</sup>International Research Institute of Disaster Science, Tohoku University, <sup>\*\*</sup>Department of Civil and Environmental Engineering, Tohoku University, <sup>\*\*\*</sup>International Research Institute of Disaster Science, Tohoku University

### ABSTRACT

Strong variability is generally involved in rockfalls. Although the variability comes from both the epistemic and aleatory uncertainties, the latter uncertainty that originates in complex movements of rockfalls is focused in this study. When we predict the behavior of rockfalls, there should be different rockfall paths to be considered. Because this variability is an irreducible uncertainty, it must be one of the important aleatory uncertainties in the prediction of rockfall movement. This study presents an optimal design of rockfall protection retaining walls in consideration of the variability of rockfall paths and kinetic energies. Although a retaining wall is generally designed to resist the energies of rockfalls, the determination of optimal position and width of retaining walls is also demanded in practice. In particular, it is difficult to evaluate an effect of the horizontal distance between toe of slopes and retaining walls, while this parameter is quite important for designing retaining walls. The proposed framework enables us to determine optimal horizontal distance and width of retaining walls based on results of DEM [1] simulations. A cost function is selected as an objective function with these design parameters along with a safety indicator as a constraint condition. A number of DEM simulations are conducted to obtain appropriate sets of rockfall paths and kinetic energies so that a response surface of the objective function can be formed. The response surface is approximately constructed by a polynomial function with the help of multiple linear regression analyses. Then, the optimization becomes possible to determine the optimal parameters under the employed constraint condition. Selecting a virtual site with a simple slope condition, a numerical example is presented to demonstrate the capability of the suggested optimal design approach. During the course of the demonstration, the appropriateness of each element of the suggested method is also examined; the selection of design parameters, the definition of a cost function and constraint conditions and the accuracy of a response surface as a surrogate model of the cost must be subjects of study.

## Improvements on Highly Viscous Fluid Simulation Using a Particle Method and Its Application to Landslide Problems

Daniel Morikawa<sup>\*</sup>, Mitsuteru Asai<sup>\*\*</sup>

<sup>\*</sup>Kyushu University, <sup>\*\*</sup>Kyushu University

### ABSTRACT

The objective of this work is to show some improvements on highly viscous fluid simulation using the Smoothed Particle Hydrodynamics (SPH). SPH is one of the Lagrangian particle methods, and it is used on fluid dynamics problems [1]. It is already well recognized for dealing with problems of low viscosity fluids (eg., water). However, SPH needs some modifications in order to accurately simulate for highly viscous fluids, which need to model the landslide problems as a macroscopic continuum model. The main improvement is related to the free-surface treatment. In the original SPH method, there is no transition between inner particles and the void space outside the fluid domain which causes some instability on the free-surface particles. Here, we propose the concept of Space Potential Particles (SPP) in order to overcome this problem. Although the original SPP formulation introduced by Tsuruta et al [2] was used to avoid gaps inside the fluid domain, the present work promotes its usage to create fictitious mass around the free-surface. This implementation increases the free-surface stability. In addition, most of highly viscous simulations with the SPH method do not account for an accurate pressure distribution of the fluid particles. To overcome this problem, we applied a relaxation of the density invariance condition together with a semi-implicit time integration scheme proposed by Asai et al [1]. Validation of these improvements includes the hydrostatic problem for pressure distribution calculation and free-surface verification. Combining these improvements, we are able to calculate accurately both the particle movement and the pressure distribution throughout the fluid domain. To demonstrate it, we will present the viscous fluid coiling effect validation problem, which requires highly accurate modelling in the viscous term. Results of this problem agree with some of the experiments on Ribe et al. [3]. At last, we will show some examples of landslide simulations using the proposed solution with the aim of improving disaster prevention measures. References [1] Asai, M., Aly, A. M., Sonoda, Y., Sakai, Y. (2012). A Stabilized Incompressible SPH Method by Relaxing the Density Invariance Condition. International Journal for Applied Mathematics No. 20130011. [2] Tsuruta, N., Khayyer, A., Gotoh, H. (2015). Space Potential Particles to Enhance the Stability of Projection-based Particle Methods. International Journal of Computation Fluid Dynamics. DOI: 10.1080/10618562.2015.1006130. [3] Ribe, N. M., Habibi, M., Bonn, D. (2012). Liquid Rope Coiling. The Annual Review of Fluid Mechanics. DOI: 10.1146/annurev-fluid-120710-101244.

## Rail Pad Super-Elements for Track Decay Rate Computation

Benjamin Morin<sup>\*</sup>, Bart Van Damme<sup>\*\*</sup>, Gwenael Hannema<sup>\*\*\*</sup>, Armin Zemp<sup>\*\*\*\*</sup>

<sup>\*</sup>Empa, <sup>\*\*</sup>Empa, <sup>\*\*\*</sup>Empa, <sup>\*\*\*\*</sup>Empa

### ABSTRACT

The state of art mechanical model for the superstructure of railway tracks, rail pads, sleepers and ballast is to represent the whole assembly as a parallel array of mass and springs [1]. This kind of model is used to compute the Track Decay Rate (TDR) which is considered to be a key parameter in limiting the radiated rail noise. As a result of the spring representation, only the stiffness of the rail pads has an influence on the TDR. Neither the frequency-(pre)load-temperature dependent properties of material nor the pads geometry are described. Ageing, which is of primary importance for maintenance purpose is also missing. The proposed approach is to use the finite element method to obtain a more complete representation of the rail pads. As a first step, the present work focuses on adding visco-thermo-elasticity [2] to the pads model and also on high preloads affects the pads behaviour. The resulting model is able to (i) access the behavior of pads under finite strain preloads, (ii) exhibit stiffness/damping related to frequency and temperature, (iii) represent the possibly complex geometry of the pads. To achieve practical computation time, a Craig-Bampton type reduction method is used to obtain a super-element of pads based on the finite element model. Following [3], the frequency dependence of pads is implemented in the super-element and similar features can be achieved for thermo-elasticity and preload. Thanks to the reduction method, interfaces between the pads and the rails or sleepers can still be modeled and for instance introduce contact/friction in the model. To validate the proposed approach, TDR computed by using super-elements will be compared to in-situ measured TDR. The material parameters of the pads are characterized experimentally. This work is part of the "Novel Rail Pads for Improved Noise Reduction and Reduced Track Maintenance" project, funded by the Swiss Federal Office for the Environment. [1] D. Thompson. (2008). *Railway Noise and Vibration: Mechanisms, Modelling and Means of Control.*, Elsevier Science. ISBN: 978-0-08-045147-3 [2] Lion, A. (1997). A physically based method to represent the thermo-mechanical behaviour of elastomers. *Acta Mechanica*, 123(1–4), 1–25. DOI: 10.1007/BF01178397 [3] B. Morin et al. (2016). Reduced Order Models for Dynamic Behavior of Elastomer Damping Devices. *J. Phys. Conf. Ser.* DOI: 10.1088/1742-6596/744/1/012134

## Implementation of Higher-order Vertical Finite Elements in ISSM for Improved Ice Sheet Flow Modeling over Paleoclimate Timescales

Mathieu Morlighem<sup>\*</sup>, Joshua Cuzzone<sup>\*\*</sup>

<sup>\*</sup>University of California Irvine, <sup>\*\*</sup>University of California Irvine

### ABSTRACT

Ice sheet models are being used in conjunction with paleoclimate proxies to determine how the Greenland ice sheet responded to past changes, particularly during the last deglaciation. Although these comparisons have been a critical component in our understanding of the Greenland ice sheet's sensitivity to past warming, they rely on modeling experiments that favor minimizing computational expense over increased model physics. Over Paleoclimate timescales, simulating the thermal field within an ice sheet has large implications on the modeled ice viscosity, which can feedback onto the basal sliding and ice flow. To accurately capture the thermal field, models often require a high number of vertical layers. This is not the case for the stress balance computation, however, where a high vertical resolution is not necessary. Accordingly, since both computations are generally performed on the same model mesh, more time is spent on the stress balance computation than is otherwise necessary. For these reasons, running a higher-order ice sheet model (e.g. Blatter-Pattyn) over timescales equivalent to the paleoclimate record has not been possible without incurring a large computational expense. To mitigate this issue, we propose a method that can be implemented within ice sheet models, whereby the vertical interpolation along the z-axis relies on higher-order polynomials, rather than the traditional linear interpolation. This method is tested within the Ice Sheet System Model (ISSM) using quadratic and cubic finite elements for the vertical interpolation on an idealized case and a realistic Greenland configuration. A transient experiment for the ice thickness evolution of a single dome ice sheet demonstrates improved accuracy using the higher-order vertical interpolation compared to models using the linear vertical interpolation, despite having fewer degrees of freedom. This method is also shown to improve a model's ability to capture sharp thermal gradients in an ice sheet particularly close to the bed, when compared to those models using a linear vertical interpolation. This is corroborated in a thermal steady-state simulation of the Greenland ice sheet using a higher-order model. In general, we find that using a higher-order vertical interpolation decreases the need for a high number of vertical layers in a model, while dramatically decreasing model runtime for transient simulations. The findings suggest that this method will allow higher-order models to be used in studies investigating ice sheet behavior over paleoclimate timescales at a fraction of the computational cost than would otherwise be needed for a model using a linear vertical interpolation.

## Linking High-Throughput Binary Calculations to Phase Evolution in Multicomponent Alloys

James R. Morris<sup>\*</sup>, Louis Santodonato<sup>\*\*</sup>, M. Claudia Troparevsky<sup>\*\*\*</sup>, Raymond R. Unocic<sup>\*\*\*\*</sup>,  
Peter K. Liaw<sup>\*\*\*\*\*</sup>

<sup>\*</sup>Oak Ridge National Lab, <sup>\*\*</sup>Oak Ridge National Lab, <sup>\*\*\*</sup>Oak Ridge National Lab, <sup>\*\*\*\*</sup>Oak Ridge National Lab,  
<sup>\*\*\*\*\*</sup>University of Tennessee

### ABSTRACT

The development of high-throughput calculations provides significant data available for materials discovery. In this work, we demonstrate how the large amount of data associated with high-throughput first-principles calculations may be directly utilized for studying high entropy and related alloys, which have many components in near equal composition. These alloys are quite far from the binaries, and from traditional alloys that are based on one- or two-component systems, with minor alloying additions. We have demonstrated [Troparevsky 2015] that these calculations may be used to predict high entropy alloys with single-phase compositions. We have also examined the Al(x)CrFeCoNi materials as a function of Al content, utilizing a Monte Carlo model derived from high-throughput calculations, and demonstrate that the predicted phase evolution is remarkably close to results from neutron scattering and in situ microscopy experiments. This work demonstrates that the development of materials databases may be utilized for discovery and elucidation of materials. [Troparevsky 2015] M. C. Troparevsky, J. R. Morris, P. R. C. Kent, A. R. Lupini, and G. M. Stocks, Criteria for predicting the formation of single-phase high-entropy alloys, *Phys. Rev. X* 5, 011041 (2015); M. C. Troparevsky, J. R. Morris, M. Daene, Y. Wang, A. R. Lupini, and G. Malcolm Stocks, Beyond atomic sizes and Hume-Rothery Rules: Understanding and predicting high entropy alloys, *JOM* 67, 2350 (2015). This work has been supported by the USDOE BES MSED program, by the High Flux Isotope Reactor and Spallation Neutron Source, and through a user proposal at the Center for Nanophase Materials Sciences, a USDOE Office of Science User Facility. PKL acknowledges support from the USDOE Office of Fossil Energy.

## Representing Model Inadequacy in Interacting Systems, Using Physics-Constrained Data-Driven Stochastic Operators

Rebecca Morrison\*, Youssef Marzouk\*\*

\*Massachusetts Institute of Technology, \*\*Massachusetts Institute of Technology

### ABSTRACT

An emerging area in computational modeling is the effective combination of physics-based and data-driven models. This combination is well-suited to address problems of model error and, in particular, model inadequacy for desired prediction goals. Often we cannot improve a model purely through physics-based approaches, either because we do not have better descriptions of the physics or because doing so would be computationally infeasible. An alternative is to develop a data-driven representation of the model inadequacy. Yet there is often rich physical information that can and should be used to constrain such a representation. This work explores how to represent model inadequacy via physics-constrained stochastic operators in the context of interacting systems, exemplified here by the generalized Lotka-Volterra (LV) equations. These equations are a generalization of predator-prey models to an arbitrary number of species  $N$ , and consist of a set of  $N$  ordinary differential equations (ODEs). The dynamics of this system are governed by a random intrinsic growth rate vector and a random interaction matrix. Given: (i) a reduced model representing the dynamics of  $n$  species, where  $n < N$ ; (ii) limited observations of the original  $N$ -species system; and (iii) information about the species growth rates and interactions, we construct a stochastic operator to capture the error in the reduced model. Rather than simply correcting the model output to the data, this operator is embedded within the reduced set of ODEs. The latter approach---capturing the model error where it occurs---is critical when using the augmented model to make predictions beyond the regime of available observations.

## Computed Binding of Peptides to Proteins with Information-Accelerated Molecular Dynamics Simulation

Joseph Morrone\*

\*IBM T.J. Watson Research Center

### ABSTRACT

The in silico prediction of binding modes and affinities for peptide-protein complexes is a challenging problem, particularly as peptides may undergo large conformational changes upon binding. Significant strides have been made by developing a method that combines molecular dynamics simulation with sparse, ambiguous external information that restricts sampling to regions of interest. This technique, known as MELD (Modeling Employing Limited Data), was developed for protein structure prediction and fully accounts for peptide flexibility. Only weak information about the binding motif is employed and not knowledge of the detailed binding mode that is typically required by other free-energy-based methods. MELD is implemented on large-scale, parallel GPU clusters and is illustrated by studying the association of peptide inhibitors with the P53-regulator-proteins MDM2 and MDMX. It is found that binding induces the peptide into the correct helical conformation, resulting in binding modes that are in excellent agreement with experiment. In addition, relative binding affinities may also be estimated. Reference: (1) Morrone, J. A.; Pérez, A.; MacCallum, J.; Dill, K. A. Computed Binding of Peptides to Proteins with MELD-Accelerated Molecular Dynamics. *J. Chem. Theory Comput.* 2017, 13 (2), 870–876. (2) Morrone, J. A.; Pérez, A.; Deng, Q.; Ha, S. N.; Holloway, M. K.; Sawyer, T. K.; Sherborne, B. S.; Brown, F. K.; Dill, K. A. Molecular Simulations Identify Binding Poses and Approximate Affinities of Stapled  $\alpha$ -Helical Peptides to MDM2 and MDMX. *J. Chem. Theory Comput.* 2017, 13 (2), 863–869.

## Simulation of Fracture and Fragmentation of Glass Lites under Blast Loading Using the Applied Element Method with Comparison to the Finite Element Method

Jonathan Moss<sup>\*</sup>, Adam Howe<sup>\*\*</sup>, Matthew Whelan<sup>\*\*\*</sup>, David Weggel<sup>\*\*\*\*</sup>

<sup>\*</sup>The University of North Carolina at Charlotte, <sup>\*\*</sup>The University of North Carolina at Charlotte, <sup>\*\*\*</sup>The University of North Carolina at Charlotte, <sup>\*\*\*\*</sup>The University of North Carolina at Charlotte

### ABSTRACT

The Applied Element Method (Meguro and Tagel-Din, 2000), which has been developed into an effective alternative to the Finite Element Method, features distinct advantages compared to other methods of analysis when applied to blast simulation problems featuring fracture and fragmentation. The advantages of the Applied Element Method render the method especially well-suited for predictive simulations involving element separation, which is an important aspect in the simulation of blast events that could potentially result in material fracturing or debris field formation. In this study, the Applied Element Method is explored as a tool for post-blast forensics investigation through comparison of predicted fracture, fragmentation, and debris field formation under blast loading against field observations and measurements. An overview of the Applied Element Method will be presented with specific details on the development of a model for simulating fracture and fragmentation of a glass fenestration system under blast loading. Experimental data from a set of six open arena blast tests performed on a façade structure consisting of six glass lites supported by aluminum mullions on a steel reaction frame will be used for assessment of the predictive fidelity of the simulations. Measurement of incident and reflected blast pressures, high-speed videography, 3D scanning and scene reconstruction, and a vertical witness panel to capture hazardous glass fragments were employed across each test to provide an experimental reference. Results obtained using the Applied Element Method will be compared to results obtained from similar analytical models developed using commercial Finite Element Method software. Specifically, the comparisons will focus on the predicted dynamic response of the lites under blast loading, fracture patterns, and fragmentation. Meguro, K. and Tagel-Din, H. (2000) "Applied Element Method for Structural Analysis: Theory and Applications for Linear Material," Structural Engineering/Earthquake Engineering JSCE, 17(1). 21-35.

## The Schwarz Alternating Method for Quasistatic Multiscale Coupling in Solid Mechanics

Alejandro Mota<sup>\*</sup>, Coleman Alleman<sup>\*\*</sup>, Irina Tezaur<sup>\*\*\*</sup>

<sup>\*</sup>Sandia National Laboratories, <sup>\*\*</sup>Sandia National Laboratories, <sup>\*\*\*</sup>Sandia National Laboratories

### ABSTRACT

We advance the Schwarz alternating method as a means for concurrent multiscale coupling in finite deformation solid mechanics. We prove that the Schwarz alternating method converges to the solution of the problem on the entire domain and that the convergence rate is geometric provided that each of the subdomain problems is well-posed, i.e. their corresponding energy density functions are quasi-convex. It is shown that the use of a Newton-type method for the solution of the resultant nonlinear system leads to two kinds of block linearized systems, depending on the treatment of the Dirichlet boundary conditions. The first kind is a symmetric block-diagonal linear system in which each diagonal block is the tangent stiffness of each subdomain, i.e. the off-diagonal blocks are all zero and the coupling terms appear only on the right-hand side. The second kind is a nonsymmetric block system with off-diagonal coupling terms. Several variants of the Schwarz alternating method are proposed for the first kind of linear system, including one in which the Schwarz alternating iterations and the Newton iterations are combined into a single scheme. This version of the method is particularly attractive, as it lends itself to a minimally intrusive implementation into existing finite element codes. Finally, we demonstrate the performance of the proposed variants of the Schwarz alternating method on several one-dimensional and three-dimensional examples. Support for this work was received through the U.S. Department of Energy's (DOE) Advanced Simulation and Computing (ASC) Program at Sandia National Laboratories. Sandia National Laboratories is a multimission laboratory managed and operated by National Technology and Engineering Solutions of Sandia, LLC., a wholly owned subsidiary of Honeywell International, Inc., for the U.S. Department of Energy's National Nuclear Security Administration under contract DE-NA-0003525.

## Generation of Training Data for Scene Labeling Using Neural Network

Yuichiro Motegi<sup>\*</sup>, Takahiro Suzuki<sup>\*\*</sup>, Yuta Matsuda<sup>\*\*\*</sup>, Makoto Murakami<sup>\*\*\*\*</sup>

<sup>\*</sup>Toyo University, <sup>\*\*</sup>Toyo University, <sup>\*\*\*</sup>Toyo University, <sup>\*\*\*\*</sup>Toyo University

### ABSTRACT

Some researchers have proposed neural networks for scene labeling which assigns class label to each pixel of an image. The class accuracy for objects included enough in a training set such as sky or road is high, but the accuracy for objects included less in the training set tends to be low. To improve the average per-class accuracy, we need to increase variations of training images in each class, and reduce the difference in the number of training images/pixels in each class. But it takes time to annotate a lot of images at the pixel level manually to make training set. There are some researches to generate many pixel-level annotated images using computer graphics. We propose the method to generate large training set for scene labeling. In our system users register 3D models and the corresponding class labels. And the users input some constraints of the object positions such as &quot;tables must be on the floor&quot; or &quot;cups must be on tables or desks&quot;. And the users input some hyper parameters for training neural network, such as the structure of the network, loss function, etc. The system put some objects in the virtual space based on the constraints, and generates a large set of images labeled at each pixel, to increase the variations of images in each class and to flatten the number of pixels in each class. The neural network is trained using the large set of generated labeled images. And the system repeats training and evaluating while increasing the variations of training images, and output the network parameters which minimize the generalization error measured with the average per-class accuracy. We captured some real images of indoor environment, and labeled each pixel of them using the neural network trained with our system. To evaluate our system we changed some settings of the system and compared the obtained results.

## A Point Dipole CG Model and Quasi-Continuum Treatment of Confined Water

Mohammad Motevaselian\*, Sikandar Mashayak\*\*, Narayana Aluru\*\*\*

\*University of Illinois, \*\*University of Illinois, \*\*\*University of Illinois

### ABSTRACT

In this study, we have developed a systematic, point dipole-based coarse-grained (CG) model using the relative entropy method to reproduce the radial distribution function (RDF) and bulk dielectric permittivity of water in an all-atom (AA) molecular dynamics description of water. The bulk CG potentials may not adequately describe the structure and dielectric permittivity variation of water inside confined slit graphene channels. To overcome this, we introduce a modified/corrected wall-fluid potential to accurately predict the structural variations close to the interface. Next, we employ the CG water potential and the water-fluid potential in the empirical potential-based quasi-continuum theory to predict the water density profiles inside the graphene slit-like channels of various widths, and the results are in good agreement with both AA and CG representations. Furthermore, we have also simulated water close to positively and negatively charged walls. We show that although the dipole-dipole correlations are treated using the mean field approximation (MFA) in the EQT framework, EQT can accurately predict the density and polarization variations of the point dipole CG model close to the charged walls. Our results also reveal that, in addition to the dipolar interactions, the secondary effects such as hydrogen bonding, can also play an important role in determining the water structure and polarization at these interfaces. Hence, to quantitatively reproduce water interfacial properties these effects should be included in the CG models.

## Simulation of Blast Load Effects Using the Duke Human Population XCAT Phantom Data Set

John Mould<sup>\*</sup>, Kerim Genc<sup>\*\*</sup>, Patrick Tompsett<sup>\*\*\*</sup>, Andrew Nicholson<sup>\*\*\*\*</sup>, Mahesh Kailasam,<sup>\*\*\*\*\*</sup>

<sup>\*</sup>Thornton Tomasetti, Inc., <sup>\*\*</sup>Synopsys Inc., <sup>\*\*\*</sup>Synopsys Inc., <sup>\*\*\*\*</sup>Thornton Tomasetti, Inc., <sup>\*\*\*\*\*</sup>Thornton Tomasetti, Inc.

### ABSTRACT

Computational modeling and simulations have proven effective in predicting the effects of blast loads of different intensities and types. This includes effects of airblast due to various reasons, such as terrorist attack, vapor-cloud explosions or other mishaps, on structures and facilities and even underwater explosions on ships and submarines[a]. Simultaneously, computational modeling and simulations of the human body have made significant advances to the point where the behavior of organs, such as the heart or brain, under impact loads can be assessed fairly accurately[b]. In this study, we use the Duke Human Population XCAT Phantom Data Set to develop a framework for efficient assessment of blast effects on reference human bodies at different distances and orientations relative to the blast source. The XCAT models were created[c] using clinical CT images as the source data for the human body along with sophisticated morphing methods to create 150+ highly detailed phantoms of varying body-mass indices (BMIs). These methods reduce manual segmentation and model generation time for a virtual population and capture interior variability from person-to-person resulting in a population representation. We demonstrate the XCAT models, with initially reduced levels of interior details for rapid, assessment of blast effects on a gathering. This can then be followed by more thorough assessments by restoring the details of the human body as needed. The ability to scale the detail level of the models provides an efficient mechanism to tailor the simulations based on the level of accuracy desired. Furthermore, the XCAT models allow the ability to model different sized bodies thereby more accurately representing groups of people, which could prove useful in threat reduction assessments. References a Vaughan, D.; Mould, J.; Levine, H.; Tennant, D. Simulating Explosive Detonations Within Multiroom Buildings. ASME Pressure Vessels and Piping Conference, 2013 b Cotton, R.; Pearce, C.; Young P.; Kota, N.; Leung, A.; Bagchi, A.; Qidwai, S. Development of a geometrically accurate and adaptable finite element head model for impact simulation: The Naval Research Laboratory–Simpleware Head Model. *Comput Methods Biomech Biomed Engin.* 19(1), 2016; c Genc, K.; Segars, P.; Cockram, S.; Thompson, D.; Horner, M.; Cotton R.; Young, P. Workflow For Creating a Simulation Ready Virtual Population For Finite Element Modeling. *J. Med. Devices* 7(4), 2013

## Three-dimensional Simulation of Obstacle-mediated Chemotaxis

Adrian Moure<sup>\*</sup>, Hector Gomez<sup>\*\*</sup>

<sup>\*</sup>Purdue University, <sup>\*\*</sup>Purdue University

### ABSTRACT

Amoeboid cells exhibit a highly dynamic motion based on the extension and retraction of actin-rich protrusions called "pseudopods". Amoeboid cell motility can be directed by external chemical signals, through the process of chemotaxis. Here, we extend the model of amoeboid motion presented in [1,2], which focus on the spontaneous migration of Dictyostelium Discoideum, and propose a three-dimensional model for chemotactic motion of amoeboid cells. By using the diffuse domain (or phase-field) method, we account for the interactions between the extracellular substances, the membrane-bound proteins, and the cytosolic components involved in the signaling pathway that originates cell motility. The motion of the cell is driven by the actin filament network, which is assumed to be a Newtonian fluid subject to the forces caused by the cell motion machinery (membrane surface tension, cell-substrate adhesion, actin-driven protrusion, myosin contraction, and a repulsive force accounting for the interaction with obstacles or fibers). The use of the diffuse domain method permits to solve equations posed on deformable domains (i.e., the cytosol, the membrane, and the extracellular medium) by using a fixed mesh only. We show two- and three-dimensional simulations of cell migration on planar substrates, flat surfaces with obstacles, and fibrous networks. The results show that our model reproduces the main features of chemotactic amoeboid motion. Our simulations unveil a complicated interplay between the geometry of the cell's environment and the chemoattractant dynamics that tightly regulates cell motion. [1] Moure, A. and Gomez, H. 2016. Computational model for amoeboid motion: Coupling membrane and cytosol dynamics. *Physical Review E*, 94(4), 042423. [2] Moure, A. and Gomez, H. 2017. Phase-field model of cellular migration: Three-dimensional simulations in fibrous networks. *Comp. Methods in App. Mech. Eng.*, 320, 162-197.

## Time-variant Reliability Based Risk Optimization Using Surrogate Modeling

Maliki Moustapha<sup>\*</sup>, Henrique Kroetz<sup>\*\*</sup>, André Téofilo Beck<sup>\*\*\*</sup>, Bruno Sudret<sup>\*\*\*\*</sup>

<sup>\*</sup>ETH Zurich, Chair of Risk, Safety and Uncertainty Quantification, <sup>\*\*</sup>São Carlos School of Engineering, University of São Paulo, <sup>\*\*\*</sup>São Carlos School of Engineering, University of São Paulo, <sup>\*\*\*\*</sup>ETH Zurich, Chair of Risk, Safety and Uncertainty Quantification

### ABSTRACT

Structural design optimization is an important part of designing structures that allows one to select among alternate concepts or configurations the one with the best compromise between the conflicting goals of economy, performance and safety. Deterministic design optimization may only partially achieve this as uncertainties, which are ubiquitous to all engineering applications, need to be taken into account. Reliability-based design optimization has been widely used in the literature in an attempt to trade the cost with the probability of failure. However, it is often argued that the solution of the latter is largely dependent on the target failure probability set as constraints of the problem (Beck and Gomes, 2012). Risk optimization addresses this issue by introducing a more global framework where the failure is directly integrated by quantifying and minimizing its associated cost. This framework may also include the cost of construction, operation and/or maintenance. This contribution focuses on a basic formulation of the risk optimization problem where the cost of failure is computed throughout the expected lifetime of the structure using time-variant reliability. For the latter, approaches based on the so-called out-crossing rate are considered. Such approaches may rely on either approximation (FORM) or crude Monte-Carlo simulation. In any case, the computational cost of this procedure is extremely high because of the integration along the time dimension. This is even more so when accounting for the repeated computations associated to different design configurations. To address this issue and allow for efficient solution when expensive computational models are considered, adaptive surrogate modeling is considered. The efficiency and validity of the approach is demonstrated on two application examples. REFERENCES Beck, A. T. and W. J. S. Gomes (2012). A comparison of deterministic, reliability-based and risk-based structural optimization under uncertainty. Prob. Eng. Mech. 28, 18–29.

## **A New Immersed IGA-RKPM Phase Field Framework for Brittle Fracture under Blast Loading**

Georgios Moutsanidis\*, David Kamensky\*\*, Yuri Bazilevs\*\*\*

\*University of California, San Diego, \*\*University of California, San Diego, \*\*\*University of California, San Diego

### **ABSTRACT**

We present a newly developed hyperbolic phase field model for brittle fracture coupled with an immersed formulation for air-blast-structure interaction [1]. A fixed background discretization provides the basis functions used to approximate the unknowns of the coupled fluid-structure interaction problem, while foreground lagrangian particles are used to track the position of the solid, store the history dependent variables, and perform numerical quadrature on the solid terms. In addition, the foreground particles provide the basis functions to approximate the governing equation of the damage field. Isogeometric basis functions are used for the background discretization, while reproducing kernel shape functions are assigned to the particles and approximate the damage field. The presented air-blast-structure interaction problems show the methodology's ability to handle brittle fracture under blast loading. References: [1] Bazilevs, Y., Moutsanidis, G., Bueno, J., Kamran, K., Kamensky, D., Hillman, M.C., Gomez, H. and Chen, J.S., 2017. A new formulation for air-blast fluid-structure interaction using an immersed approach: part II—coupling of IGA and meshfree discretizations. Computational Mechanics, pp.1-16.

## **Practical Multiscale Approach for Analysis of Reinforced and Prestressed Concrete Structures**

Arturo Moyeda\*, Jacob Fish\*\*

\*Columbia University, \*\*Columbia University

### **ABSTRACT**

We present a multiscale approach for analysis of reinforced and prestressed concrete structures, that overcomes two major hurdles in utilization of multiscale technologies in practice: (1) coupling between material and structural scales due to consideration of large representative volume elements, and (2) computational complexity of solving complex nonlinear multiscale problems. The former is accomplished using a variant of computational continua framework that accounts for sizeable reinforced concrete RVEs by adjusting the location of the quadrature points. The latter is accomplished by means of reduced order homogenization customized for structural elements.

## Optimal Design of a Smart Wind Turbine Based on Neural Network, Evolutionary Optimization Technique and CFD

Javier Luis Mroginski\*, Juan Manuel Podesta\*\*, Hugo Guillermo Castro\*\*\*

\*Applied Mechanical Dept., Universidad Nacional del Nordeste, Argentina, \*\*Universidad Nacional del Nordeste, Argentina, \*\*\*CONICET and Applied Mechanical Dept., Universidad Nacional del Nordeste, Argentina

### ABSTRACT

It is well known that one of the global priorities is to implement new technologies that allow us to use in a more efficient manner alternative and renewable energy sources, in order to reduce the consumption of conventional energy sources. Wind is one of the most promising renewable energy and, for a number of years, several different types of wind turbines were used, mainly classified as horizontal axis wind turbines (HAWT's) and vertical axis wind turbines (VAWT's). Nevertheless, there are still many issues to explore or improve in this subject. Regarding its type, some researches support the fact that VAWT's perform better in urban environments than HAWT's [1]. In this work a new model of VAWT is proposed, designed as a combination of the Savonius and Darrieus VAWT's, where the simplest model is the so-called "H" turbine. The optimization of the proposed model is made by coupling computational fluid dynamics (CFD) and neural networks, leading to a "smart" wind turbine with the capability to switch between Savonius and Darrieus types according to the velocity and direction of the incident wind. Furthermore, it is shown how changing length and angle of attack of the blades modify its performance for different wind speeds. The prototype consists of three blades of NACA 0018 profile, initially vertical, with 2 meters high (H) and radius (R) of 1 meter. By means of an opening mechanical device, the operational principle can be interchanged, allowing to start the turbine at relatively low wind speeds. For the CFD simulation, the open-source toolbox OpenFOAM is used with sliding mesh on the rotational domain and SST k-w turbulence model [2]. Considering the wind incidence angle together with the angle of attack of the blades and the average radius of the turbine as optimization variables, the optimal performance of the wind turbine is obtained associated to the maximum energy production and equipment regularity. [1] Li, Q; Maeda, T.; Kamada, Y.; Hiromori, Y.; Nakai, A.; Kasuya, T.; "Study on stall behavior of a straight-bladed vertical axis wind turbine with numerical and experimental investigations" Journal of Wind Engineering and Industrial Aerodynamics, 164 pp.1-12, 2017. [2] H.G. Castro, R.R. Paz, J.L. Mroginski, M.A. Storti &quot;Evaluation of the proper coherence representation in random flow generation based methods&quot; Journal of Wind Engineering and Industrial Aerodynamics, 168, pp 211–227 (2017)

## Evolutionary Topology Optimization of Lightweight Structures with Fatigue Constraints

Mirosław Mrzygłód\*

\*Opole University of Technology

### ABSTRACT

The necessity to carry out research in the field of fatigue design of lightweight structure is mainly related to the needs of the industry - the getting lighter structures, which maintain a high level of fatigue durability is very important for aviation and automotive. Answers to these needs can only be found in the combination of the implementation of the latest research in the field of material fatigue with modern design optimization algorithms. Available commercial tools have great limitations, both in terms of obtaining solutions for light structures as well as the application of modern fatigue constraints. The paper presents a proposal of a new methodology of topological optimization with the use of evolutionary methods dedicated for use in the optimization of lightweight structures with fatigue constraints. The research includes the use of modern hypotheses of multi-axis fatigue of materials and methods of damage accumulation for complex load regime. It can be mentioned criteria based on the critical plane approach, criteria based on stress invariants and criteria based on stress averages in elementary volume [1]. As a part of the research, selected fatigue hypotheses and the procedure of cumulative damage summation were numerically implemented. In addition, new methods have been developed to improve the efficiency of searching for low-mass solutions for the evolutionary algorithm of topological optimization. The Constant Criterion Surface Algorithm (CCSA) was used for research in this area, which was enriched with new procedures [2]. To illustrate the proposed design methodology, several examples of optimization of benchmark structural problems have been presented [3]. In addition to obtaining optimal numerical solutions, they were verified using virtual prototyping methods. The effect of the conducted research is new numerical procedures for rapid estimation of fatigue damages of several multiaxial fatigue criteria and the effective evolutionary topology optimization algorithm dedicated to the design of lightweight structure with fatigue constraints. References [1] Papadopoulos I.V., Davoli P., Gorla C., Filippini M., Bernasconi A., A comparative study of multiaxial high-cycle fatigue criteria for metals, *International Journal of Fatigue*, 19, 1997, 219-235. [2] Mrzygłód M., Multi-constrained topology optimization using constant criterion surface algorithm, *Bulletin of the Polish Academy of Sciences – Technical Sciences*, 60(2), 2012, 229-236. [3] Rozvany G.I.N., Exact analytical solutions for some popular benchmark problems in topology optimization, *Structural Optimization*, 15, 1998, 42-48.

# QUANTITATIVE OBSERVATION AND COMPUTER SIMULATION OF WINDOW GLASS FRAGMENT INTO PIECES AND THEIR SCATTERING DUE TO COLLISION OF FLYING OBJECT

YOICHI MUKAI\*, HIROTO KOHARA\*, YASUFUMI KANNO†,  
MASAKI MATSUMOTO†, YOSHIRO HORI†, AND FUMIHIKO CHIBA†

\*Kobe University  
1-1 Rokkodai-cho, Nada-ku, Kobe, Hyogo 657-8501, Japan  
ymukai@port.kobe-u.ac.jp

†YKK AP Inc.  
3-22-1 Kamezawa, Sumida-ku, Tokyo 130-8521, Japan  
mas\_matsumoto@ykkap.co.jp

**Key words:** Collision Action, Window Glass Fragment, Non-structural Member, Flying Object, Impact load, FEM Analysis.

**Abstract.** In this study, destruction moment of glass window due to flying object is observed with high-speed cameras at the impact-loading experiments, and the behavior of scattering broken glass pieces is estimated through the motion-capturing and the position-data-extracting process. Various types of the projectile objects were shot on the front surface of the plate glass window. Different weight and impacting speed of the flying objects, and thickness of the plate glasses are tested. Each test specimen and test situation is also simulated in the FEM analysis. Numerical results are compared with the actual motions recorded by the high-speed camera. This study clarifies that numerical simulations can adequately reproduce window glass behavior broken into pieces and their scattering motion as observing in the experimental tests. The variation of the material parameters of the projectile object or the plate glass are evaluated to make assure these parameters sensitivity on the numerical simulation results. Through these case studies, the validity of the FEM modeling and the FEM analyses to reproduce the scattering behaviors of broken glass pieces is also discussed.

## 1 INTRODUCTION

A window glass destruction due to impact objects must cause serious human injury, thus, consideration of window glass property placed on a building facade is important for shock-resistant building design against impact actions [1,2]. However, there are few studies to observe and to analyze quantitatively the behavior of scattering pieces of broken glass caused by the impact action of flying or colliding objects.

This study focuses on the destruction moment of plate glass windows due to flying objects and the scattering behavior of broken glass pieces [3]. For this aim, impact-loading experiments are carried out and colliding actions caused by the projectile object are observed using high-speed cameras. The behavior of scattering glass pieces is estimated through the motion-capturing and the position-data-extracting procedures by using recorded video photography in the tests. A launching apparatus with compressive air was used for the experimental tests and various types of the projectile objects were shot on the front surface of the plate glass window. Different weight and impact speed of the projectile object, and thickness of the plate glass are tested. Through the experimental tests, the relationship between the impact action of the projectile object and the scattering motions of the broken glass pieces are quantified and investigated.

Test specimen and test situation are also simulated in the FEM analyses. Numerical results are compared with the actual motion recorded by the high-speed camera. Reproducibility of the actual fracture behavior of plate glass in the numerical simulation is considered in this study. The variation of the material parameters of the projectile object and the impacted plate glass are investigated parametrically to make assure the sensitivity of these parameters on the numerical simulation results. Adequate model condition and parameters are considered for the validity of the FEM analyses to reproduce the scattering behaviors of broken glass pieces.

## 2 EXPERIMENTAL TESTS

To observe the fracture behavior of float plate glass for building windows, the impact tests using the projectile object shot by launching apparatus were carried out. This experimental test focuses on quantifying the scattering motion of broken glass pieces, thus the high-speed cameras were used to record the behavior the impact action of the projectile object and the fracture behavior of the plate glass specimen.



(a) Launching apparatus and test specimen



(b) High-speed camera setting

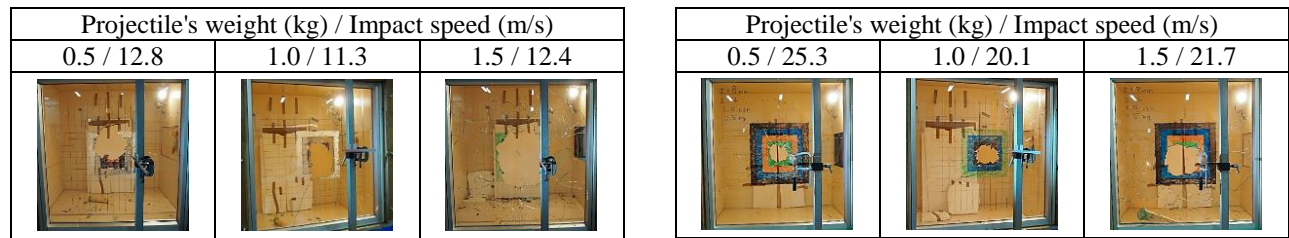
Figure 1 View of experimental test configuration

### 2.1 Outline of experimental test equipment and specimens

The experimental test configurations are displayed in Figure 1. The launching apparatus is set in front of the test specimen of window plate glass where is placed at 2 m of the front from the muzzle of the gun barrel of the launching apparatus. The plate glass specimen is equipped to the aluminum

sash frame, which is 1120 mm width and 1160 mm height, with 8 mm margins to suspend its whole periphery glass edge by placing rubber cushioning. Two kinds of specimens of plate glass which are 6 mm and 8 mm thickness are provided for this test. Both wooden and stainless projectiles are used as the impact objects and these are shot from the launching apparatus for the center of the plate glass window specimen. Wooden projectiles are the two kinds which have circular (94.2 mm diameter) and elliptic (78 mm x 37 mm in major/minor axis) sections. A stainless projectile is a hollow cylinder (95 mm diameter) whose ends are capped stainless plate. Weights of the wooden projectiles are adjusted by their length and three kinds of weights, 0.5 kg, 1.0 kg, and 1.5 kg, are tested. Weights of the stainless projectile are adjusted by the inserting weight into the cylinder and two kinds of weights, 0.5 kg and 1.0 kg, are tested. Impact speed of the projectile object is controlled by the compression air pressures, and the impact tests are operated under three kinds impact speeds, about 15 m/s, 25 m/s and 35 m/s.

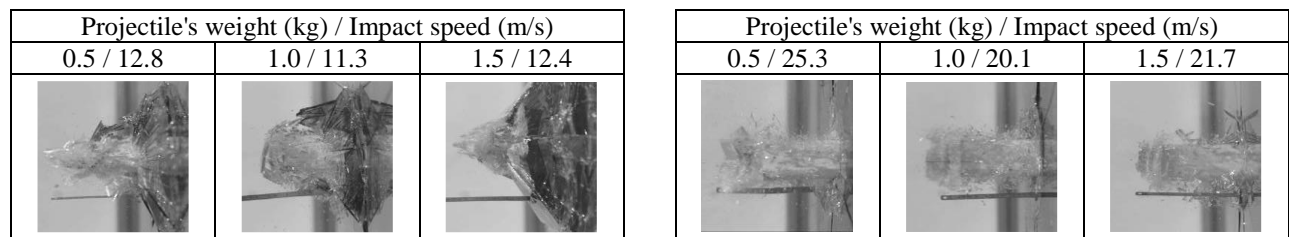
Fracture behavior of window plate glass is photographed by using high-speed video cameras, and then, the recorded motions of scattering broken glass pieces are analyzed to extract their trajectory on the photo screen. Two high-speed video cameras are used; one is placed over the test specimen (as seen in Figure 1(b)) to pick up an image from above of the window plate glass to downward, and the other is placed in the front-side of the test specimen to image from the just beside of the projectile object toward the window surface and to measure its impact speed.



(a) Launching pressure : 0.6 bar

(b) Launching pressure : 1.0 bar

Figure 2 Damage state after penetration of ellipse-section wooden projectile (Glass thickness : 8 mm)



(a) Launching pressure : 0.6 bar

(b) Launching pressure : 1.0 bar

Figure 3 Scattering fragments by collision of ellipse-section wooden projectile (Glass thickness : 8 mm)

## 2.2 Observation of window glass fracture behavior

The front view photographs of the broken plate glass window which remains in the aluminum sash frame are displayed in Figure 2. These are at the case that the ellipse-section wooden projectile is used for shooting to the plate glass of 8 mm. Figure 3 displays scattering glass pieces and penetrating

projectile which are captured by the high-speed camera. As seen in Figures 2 and 3, different fracture modes can be observed depending on the impact speed of the projectile object. When the impact speed is fast (in this study, it is around 20 m/s or more), the projectile object goes through a narrow part and loss of area in broken plate glass is limited to small part. On the other hand, when the impact speed is slow (in this study, it is around 10 m/s), the projectile object breaks a wide part of the plate glass and the plate glass surface are broken with out-of-plane deformation.

### 2.3 Motion capture analysis of scattering glass pieces

Scattering motion of the broken glass pieces caused by collision of the projectile object is extracted using the two-dimensional motion analysis software (DIIP-Motion V/2D, DITECT Co.) for the video movies photographed by the high-speed camera. Displacements of some flying pieces of broken glass on the screen are evaluated by tracking the positions of "markers", which are the designated image areas included on the glass pieces, by every image frame. These markers are chosen from the leading fragments pushed in front of the projectile object, and the scattering speed of the window glass pieces are estimated as the average speed of these designated pieces. Every markers are designated on the photographed video frame after the tests through the software and displacing pixel number of each markers between frames is measured, and then time series of these pixels are decoded to the glass pieces motions. To convert pixels to length for this motion data extraction, a ruler of 150 mm which is equipped by protruding from the glass window is used as the referential length. Photographing frame resolution is  $1280 \times 800$  pixels and frame rate is 1000 fps.

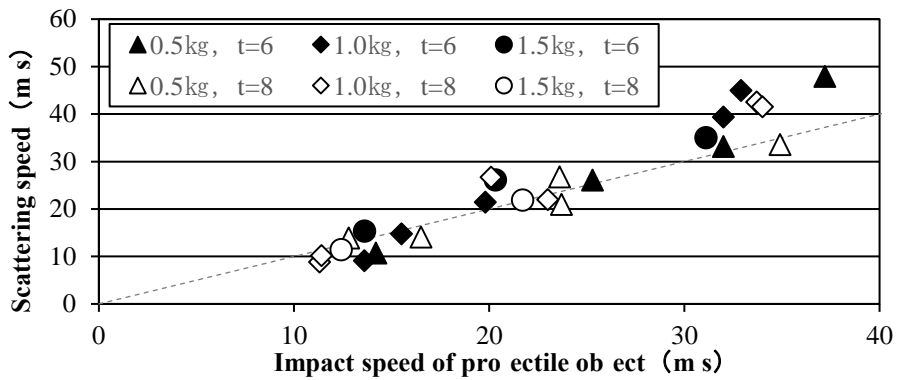


Figure 4 Scattering glass pieces speed vs. collision speed of projectile object (Experimental results)

Relations between scattering glass piece speed and collision object speed for the tests under different projectile objects, impact speeds and plate glass specimens are depicted in Figure 4. Collision speed of projectile object is determined as the just before moment to collide for the plate glass and it is evaluated by using the high-speed camera placed in the front-side of the test specimen. Under this test condition, it is assured that the scattering glass piece speed is proportionally increased depending on the collision object speed and that the scattering glass piece speed has similar value of the collision object speed. However, when the collision object speed becomes large (in this study, it is around 30 m/s or more), the scattering glass piece speeds seem to increase and the variance of these are observed enlarging. While the obvious dependence to the collision object speed is observed

for the scattering glass piece speeds, it is assured that the difference of material or weight of the projectile object influence less to the scattering glass piece speeds within the test condition operating in this study.

### 3 FEM SIMULATIONS

To reproduce the actual behavior of scattering glass pieces caused by collision of projectile objects in the numerical simulations, FEM analyses are carried out. The finite element models are composed by considering the test specimen's features and configurations using in the impact experimental tests. LS-DYNA is used for calculating fracture of plate glass model caused by the projectile object collision. Reproducibility of the analyses is investigated through the comparison with the experimental results.

#### 3.1 Numerical modelling and its parameters

For the FEM analyses, both the projectile object and the plate glass window are composed by the solid element model. As depicted in Figure 5, the center area of the plate glass window, where seem to be broken by the impact of the projectile object, has dense mesh division, and the single element size is 14 mm width x 14 mm height x 2 mm depth, while the single element at the surrounding area is 56 mm width x 56 mm height x 2 mm depth. Three or four layers are given in the thickness direction for the plate glasses of 6 mm or 8 mm. The number of the entire elements and the entire nodes are 3026 elements and 19996 nodes for the plate glass of 6 mm thickness and 4218 elements and 26236 nodes for the plate glass of 8 mm thickness, respectively.

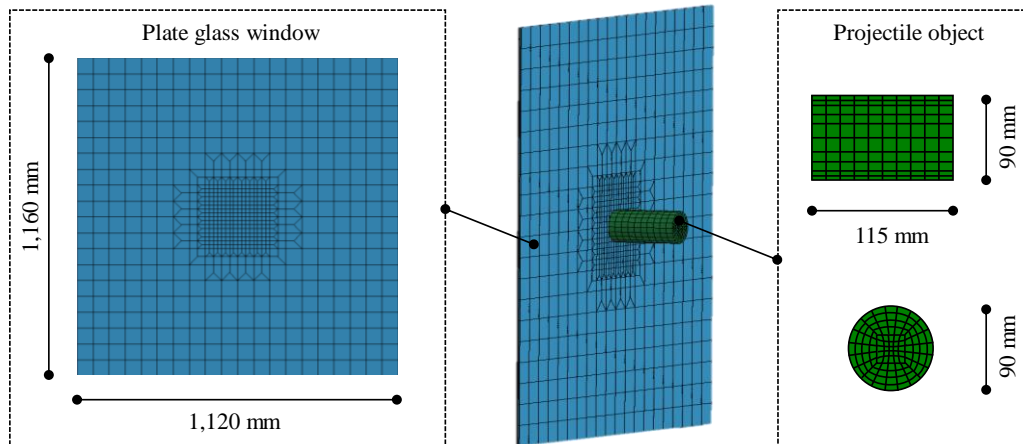


Figure 5 FEM analysis model

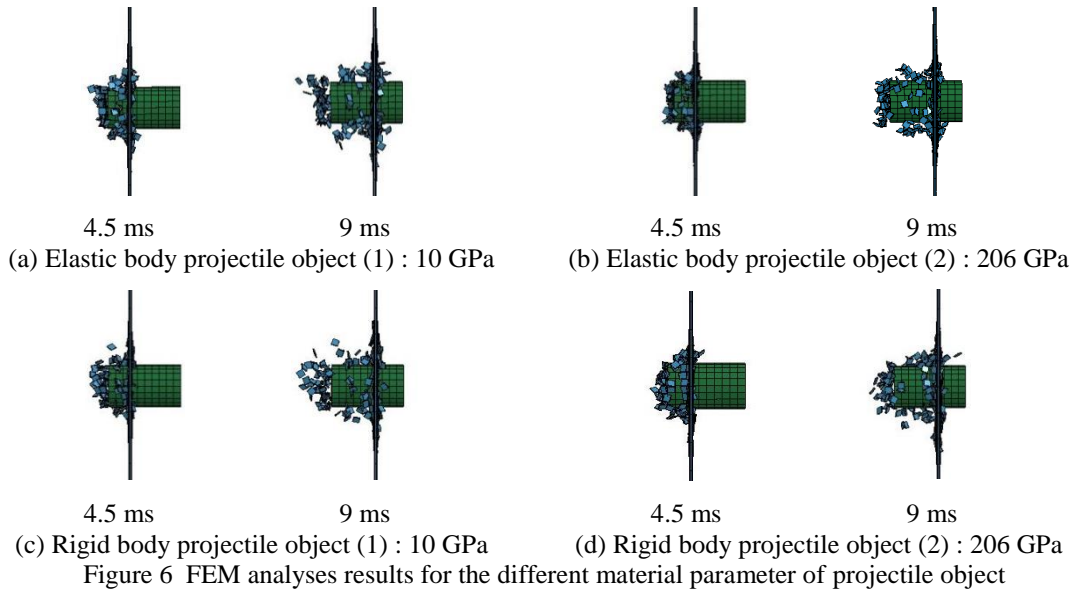
In this numerical study, all surrounding glass edge are assumed to be fixed rigidly. The projectile object part is applied to be contacted automatically to the plate glass part. Numerical calculations are started from the initial situation that the projectile object is placed at the initial position just coming into contact to the plate glass surface, and the impact action is simulated by applying the initial impact speed to the projectile object. To reproduce the scattering behavior of the broken glass

pieces in the simulations, all elements of the plate glass part are provided the condition that any element is restricted to all adjacent ones at its all nodes until reaching their rupture limitation, thus elements of the plate glass are separated at the nodes beyond the rupture limitation, and then the fracture behavior is simulated. In this study, the rupture limitation is considered at the situations when exceeding 0.24% for the equivalent plastic strain or exceeding 60 MPa for the tensile strength, and the node restriction is released [4].

Material model parameters of window plate glass and impact object are listed in Table 1. Material model for the plate glass is applied to the JOHNSON-HOLMQUIST-CERAMICS (MAT110) [5] which is adequate to represent the behavior of the brittle material and the real constants for the material parameter for this model are employed from the values indicated in Hidallana-Gamage's literature [4]. Material model for the projectile object is applied to the normal elastic material model (MAT001) [5], and the normal rigid body material model (MAT20) [4] is also used for comparative investigations with the elastic material model.

Table 1 Material model constants of plate glass and projectile object

Material	Mass density (kg/m <sup>3</sup> )	Young's modulus (GPa)	Poisson's ratio
Plate glass	2530	72	0.22
Projectile object (1)	507	10	0.3
Projectile object (2)	507	206	0.3



### 3.2 Sensitivity analysis for material parameters : Projectile object

At first, parameter sensitivity in FEM analyses is evaluated for the material constants about the projectile object model. In this study, two kinds of the material constant about Young's modulus of the projectile object material as seen in Table 1 are considered for the two kinds of material model types which are the elastic body and the rigid body. Figure 6 displays the fracture behaviors of the

plate glass of 6 mm thickness while colliding 0.5 kg projectile object which has 14.2 m/s of the impact speed. Each case displays the fracture situation images at 4.5 ms and 9 ms after the impact moment. Figure 6 (a) and (b) are corresponding to the cases using the elastic material model for the projectile object with Young's modulus of 10 GPa and 206 GPa, respectively. Figure 6 (c) and (d) are corresponding to the cases using the rigid body material model for the projectile object with Young's modulus of 10 GPa and 206 GPa, respectively. By comparing Figure 6 (a) and (b), or by comparing Figure 6 (c) and (d), it is assured that the difference of the speed and displacement of scattering broken glass pieces are quite small even if the different Young's modulus is considered but the same material model type is applied. This result is consistent to the experimental observation that the scattering speeds of broken glass pieces had less dependence to the difference of projectile object material. By comparing Figure 6 (a) and (c), or by comparing Figure 6 (b) and (d), the speed and displacement of scattering broken glass pieces are reduced in the case using the elastic material model, because of consideration of the local deformation of the projectile object in calculations.

### 3.3 Sensitivity analysis for material parameters : Plate glass

Parameter sensitivity in FEM analyses for the material fracture parameters about the plate glass model are also evaluated. In this study, the equivalent plastic strain and the tensile strength are considered as the fracture index of the plate glass. As the referential case, the rupture limitation of plate glass material is considered 0.24% for the equivalent plastic strain and 60 MPa for the tensile strength. By using the elastic material model with Young's modulus of 10 GPa for the projectile object, the case study about the fracture behavior of the plate glass of 6 mm thickness while colliding the projectile object of 0.5 kg under the impact speed of 14.2 m/s.

Three different parameters of the plate glass fracture limitation for the equivalent plastic strain, which are 0.12%, 0.24% and 0.48%, are investigated under the same fracture limitation of 60 MPa for the tensile strength. And then, three different parameters of the plate glass fracture limitation for the tensile strength, which are 30 MPa, 60 MPa and 120 MPa, are investigated under the same fracture limitation of 0.24% for the equivalent plastic strain.

Figure 7 displays the numerical results of the fracture situation images at 4.5 ms and 9 ms after the impact moment for five cases. Figure 7 (a), (b) and (c) are corresponding to the cases using the plate glass fracture limitation of the equivalent plastic strain of 0.12%, 0.48% and 0.24%, respectively. The same limitation of the tensile strength of 30 MPa are assumed in these 3 cases. By comparing these figures, it is assured that the fracture parameter dependence on the equivalent plastic strain of the plate glass is comparatively small, thus the remarkable difference of the scattering speed of broken glass pieces and the penetration length of the projectile objects are not observed.

Figure 7 (c), (d) and (e) are corresponding to the cases using the plate glass fracture limitation of the tensile strength of 60 MPa, 30 MPa and 120 MPa, respectively. The same limitation of the equivalent plastic strain of 0.24% are assumed in these 3 cases. By comparing these figures, it is assured that the fracture parameter dependence on the tensile strength of plate glass is comparatively small for the the scattering speed of broken glass pieces and the penetration length of the projectile objects. On the other hand, it is observed that loss of area in broken plate glass becomes narrow in the case of the weak strength (30 MPa), and that loss of area in broken plate glass becomes wide in the case of the strong strength (120 MPa).

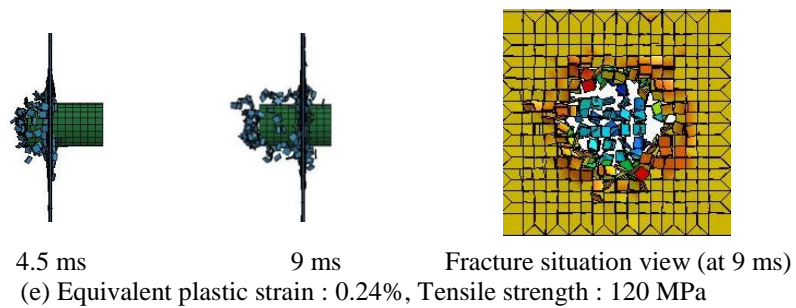
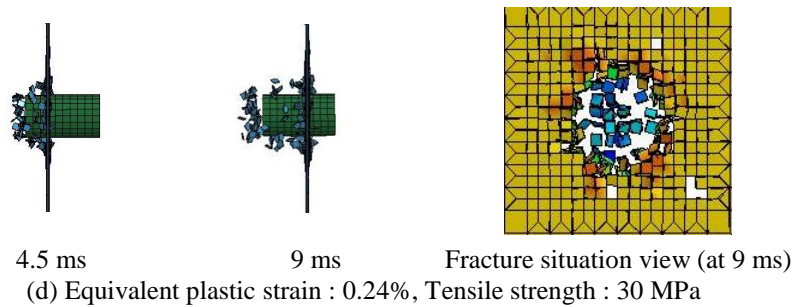
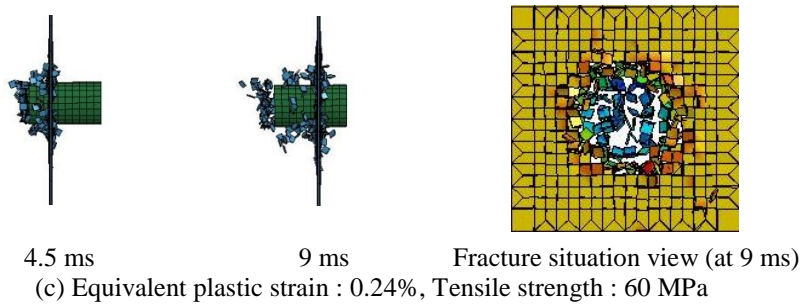
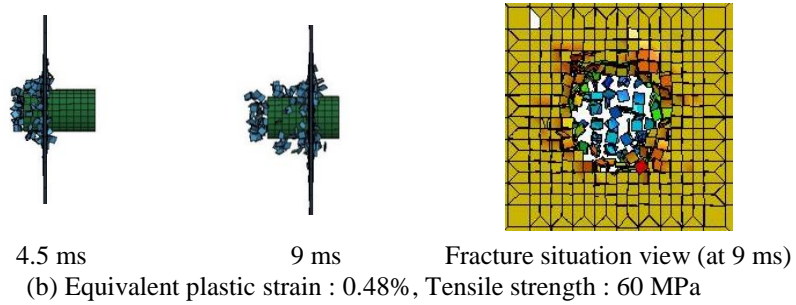
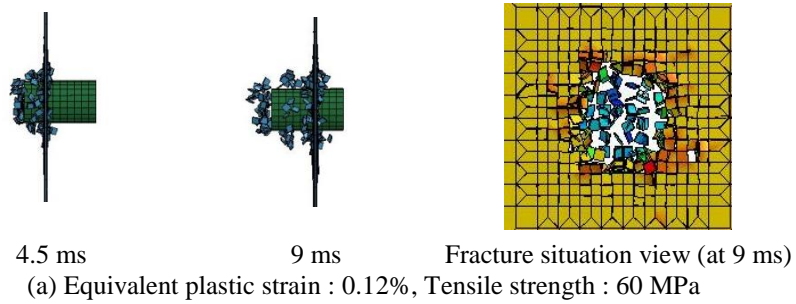


Figure 7 FEM analyses results for the different material parameters of plate glass fracture

### 3.4 Comparative study between FEM analyses and experimental tests

FEM analyses corresponding to every cases of the different test parameters carried out in the experimental tests are executed. The collision speeds of the projectile objects in the simulations are adjusted to each speed observed in the experiment. In this simulation study, FEM model of the projectile object is applied as the elastic material with Young's modulus of 206 GPa, and the rupture limitations of the plate glass are considered to 0.24% for the equivalent plastic strain and 60 MPa for the tensile strength. Relations between scattering glass pieces speed and collision object speed for the different projectiles weight, impact speed and plate glass thickness are depicted in Figure 8.

Under the FEM analyses, it is assured that the scattering glass pieces speed is proportionally increased depending on the collision object speed, and that the scattering glass pieces speed has similar value of the collision object speed. By comparing this numerical result with the experimental result as seen in Figure 4, it is confirmed that the fracture behavior of plate glass can be reproduced capably. When the collision object speed becomes large (around 30 m/s or more), the scattering glass pieces speeds become to increase and the variance of these are observed enlarging in FEM analyses likewise. The dependence on the collision object speed is also observed for the scattering glass pieces speeds, and the weight of the projectile object has also less influence to the scattering glass pieces speeds in the simulation results.

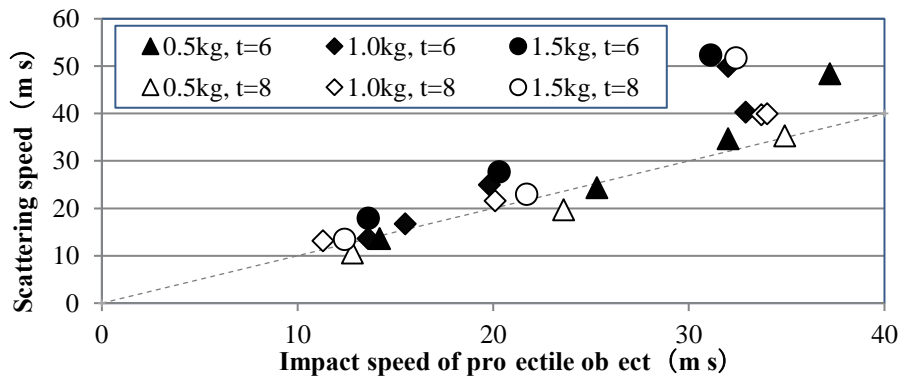
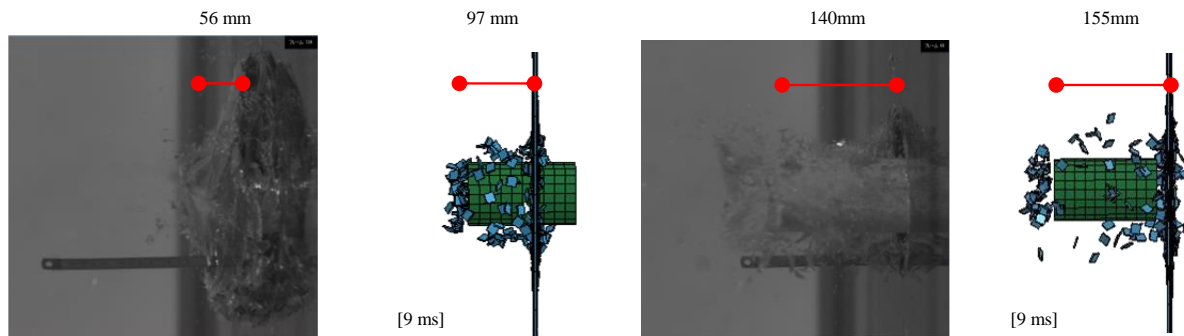


Figure 8 Scattering glass pieces speed vs. collision speed of projectile object (Numerical results)



(a) Collision speed : 14.2 m/s

(b) Collision speed : 25.3 m/s

Figure 9 Comparison between FEM analyses and experimental tests results about penetrating length

Figure 9 displays comparison between the experiment and the FEM analysis results about penetrating length of the projectile object after collision on the plate glass. Figure 9 (a) and (b) are corresponding to the low speed collision (14.2 m/s) and the high speed collision (25.3 m/s), respectively. Both of these cases are the collision of the ellipse-section wooden projectile of 0.5 kg to 6 mm thickness plate glass and both images are corresponding to the instance at 9 ms after impact. FEM analyses are operated using the elastic material model with Young's modulus of 206 GPa, and the rupture limitation of plate glass material is considered 0.24% for the equivalent plastic strain and 60 MPa for the tensile strength.

By comparing the experimental and the numerical results about penetrating length of the projectile object, larger length in the FEM analyses are observed than the experimental results. More difference between the simulation and the test appears in the low speed collision case (as seen in Figure 9 (a)), while difference between them is not much in the high speed collision case. As a reason for this, it is considered that less energy loss of the projectile object is evaluated at the FEM analyses than an actually obtained experimental result. This seems to be the issue to have further consideration about the rupture limitations parameters of the plate glass in the FEM analyses, or the estimation about element mesh size of the plate glass part is also thought about as a new issue.

#### 4 CONCLUSIONS

This study executed the experimental test to observe and photograph the fracture behavior caused by collision of the projectile object. High-speed cameras are used to record the scattering motion of broken glass pieces and the quantitative evaluation of the fracture behavior of plate glass are performed through 2D motion analyses procedures. FEM analyses to reproduce the actual fracture situation of the plate glass are also carried out and the sensitivity of the material model parameters for the FEM models are investigated. By comparing the FEM simulation results with the experimental results, adequateness of the FEM analyses to evaluate the fracture behavior of the plate glass is also discussed. The findings through this study are summarized in the followings.

- Different fracture modes were observed depending on the impact speed of the projectile object. When the impact speed is fast (around 20 m/s or more), the projectile object goes through a narrow part and loss of area in broken plate glass is limited small part. When the impact speed is slow (around 10 m/s), the projectile object breaks a wide part of the plate glass and its surface are broken with out-of-plane deformation.
- Relations between scattering glass pieces speeds and collision object speed for the tests under different projectile objects, impact speeds and the plate glass thicknesses are investigated. It was observed that the scattering glass pieces speed is proportionally increased depending on the collision object speed and it has similar value of the collision object speed, while the difference of material or weight of the projectile object influence less to the scattering glass pieces speeds.
- Numerical simulations can adequately reproduce window glass behavior broken into pieces and their scattering as observing in the experimental tests. While the tendency that influences the results, which are related by the difference of weight or impact speed of the projectile object, or the thickness of the plate glass, could be reappeared in FEM

analyses.

- The penetrating length of the projectile object is observed larger in the FEM analyses than the experimental results. More difference between the simulation and the test appears in the low speed collision case, while difference between them is not much in the high speed collision case. This seems to be depending on evaluation of less energy loss of the projectile object in the FEM analyses than an actually obtained experimental tests.
- The difference of the speed and displacement of scattering broken pieces are quite small even if the different Young's modulus are considered but the same material model type is applied. The speed and displacement of scattering broken glass pieces are reduced in the case using the elastic material model, because of consideration of the local deformation of the projectile object in calculations.
- The fracture parameter dependence on the equivalent plastic strain of plate glass is comparatively small, thus the remarkable difference of the scattering speed of broken glass and the penetration length of the projectile object are not observed in the simulations with the different rupture limitation of the equivalent plastic strain.
- The fracture parameter dependence on the tensile strength of plate glass is comparatively small for the the scattering speed of broken glass and the penetration length of the projectile object. On the other hand, it is observed that loss of area in broken plate glass becomes narrow in the case of the weak strength, and that loss of area in broken plate glass becomes wide in the case of the strong strength.

## ACKNOWLEDGMENTS

The part of this work were supported by JSPS grant No.R2904 in the program for Advancing Strategic International Networks to Accelerate the Circulation of Talented Researchers and JSPS KAKENHI Grant Number 26420552, 16H03124 and 17K18924. Authors also acknowledge Mr. Tsubasa Hattori who graduated the master course of Kobe University for his contribution to the experimental tests and the numerical simulations in this study.

## REFERENCES

- [1] Architectural Institute of Japan. Recommendations for Loads on Buildings, AIJ Design Guideline. AIJ, (2015). (in Japanese)
- [2] Architectural Institute of Japan. Introduction to Shock-Resistant Design of Buildings, AIJ Design Concept. AIJ, (2015). (in Japanese)
- [3] Matsumoto, M. Study on Destructive Behavior of Window Glass by Collision due to Flying Object. Summaries of technical papers of Annual Meeting, Architectural Institute of Japan. Structures I. (2017) 285-288. (in Japanese)
- [4] Hidallana-Gamage, H.D. et al. Numerical modelling and analysis of the blast

Yoichi Mukai, Hiroto Kohara, Yasufumi Kanno, Masaki Matsumoto, Yoshiro Hori and Fumihiko Chiba

performance of laminated glass panels and the influence of material parameters. *Engrg. Failure Analysis*. (2014) 45: 65-84.

[5] JSOL. LS-DYNA Version 971, User's Manual Volume II. (2016) 461-463.

## Hybrid Particle-continuum Computational Models for Thrombus Biomechanics

Debanjan Mukherjee\*, Shawn C. Shadden\*\*

\*University of California, Berkeley, \*\*University of California, Berkeley

### ABSTRACT

Thrombosis and embolisms comprise the primary cause of major cardiovascular diseases like heart attack and stroke, which amount to significant morbidity and mortality worldwide. Additionally, thrombotic and embolic events during surgical procedures or medical device deployment can cause serious complications. Computational tools have rapidly advanced to become a valuable non-invasive technique for investigating cardiovascular phenomena, complementing experimental and clinical investigations. However, developing computational models for thrombus biomechanics within large artery hemodynamics remains a key challenge. Resolving the interaction of a realistic thrombus, comprising arbitrary shape and heterogeneous microstructure, with pulsatile viscous flow is critical. Additionally, robust modeling of the deformation and embolization of these heterogeneous thrombi often requires specialized techniques. Here, we present our recent advancements towards addressing these challenges by devising a mesoscale particle-continuum framework. A thrombus is reconstructed as a heterogeneous aggregate of discrete particles based on medical or experimental image-data. Arterial hemodynamics around this aggregate is resolved by coupling the particle reconstruction to blood flow using a fictitious domain finite element method. Thrombus deformation mechanics is modeled based on the particle reconstruction using a discrete element approach, wherein individual particles interact via effective forces and potentials, and via a network of force-chains interspersing the particles (mimicking the intrinsic fibrin network of thrombi). Each element of the force chain comprises a combination of springs, dashpots, and sliders. The collective dynamics emerging from the particle interactions effectively describe thrombus deformation. Rupture and embolization is recovered by removing particles from the aggregate based on particle-network connectivity and inter-particle forces. We present numerical experiments using model thrombus geometries reconstructed from experimental data reported in the literature. We demonstrate that our methods can resolve not only the complex unsteady flow around large-arterial thrombi, but also estimate the intra-thrombus perfusion flow. Simulations performed on mechanically deforming thrombus aggregates embedded in plasma demonstrated the efficacy of our methods in capturing aggregate thrombus deformation biomechanics. Additionally, we establish that our approach can capture the initiation of thrombus rupture and rupture propagation until complete embolization. Micro-mechanical properties like microstructural order parameters can also be directly computed and compared with experiments. These results, thus, demonstrate the utility of our hybrid particle-continuum treatment in addressing current challenges in thrombus biomechanics modeling. [Acknowledgements: AHA Award: 16POST27500023, NSF Award: 1354541, BWF-CRTG Award: 1016360]

## Stochastic Time Domain Spectral Element Analysis of Timoshenko Beam with Non-Gaussian Properties

Shuvajit Mukherjee\*, Ranjan Ganguli\*\*, S. Gopalakrishnan\*\*\*

\*Department of Aerospace Engineering, Indian Institute of Science, Bangalore-560012, India., \*\*Department of Aerospace Engineering, Indian Institute of Science, Bangalore-560012, India., \*\*\*Department of Aerospace Engineering, Indian Institute of Science, Bangalore-560012, India.

### ABSTRACT

Material uncertainty effects are studied for static, free vibration and dynamic analysis of Timoshenko beam. Uncertainty is inevitable in engineering structures. So, for reliable design of engineering structures, it should be incorporated into the modeling. In this work, random field based modeling is used to account the spatial variability of the material properties. A stochastic time domain spectral element method (STSEM) is proposed for Timoshenko beam. The material properties are considered as 1-D non-Gaussian random fields and optimal linear estimation (OLE) [1] is used for the discretization of the random fields. The OLE-based discretization of a random field allows simulating the random fields digitally followed by the simulation of realizations of stiffness, mass matrix, and dynamic stiffness matrix. Recently, Sasikumar et al. [2] proposed a framework which suggests different independent meshing for random field and finite element discretization resulting in the saving of CPU time. In this current work, computationally efficient time domain spectral element method (TSEM) [3] is used instead of finite element method (FEM) to develop the STSEM formulation. The STSEM reduces the CPU time significantly as the number of degrees of freedom (DOF) is very less than that of FEM. TSEM also provides a consistent diagonal mass matrix and Gauss–Lobatto–Legendre (GLL) quadrature requires less computational cost than the Gauss–Legendre quadrature which lessens the CPU time. Unlike Monte Carlo, the computation time follows almost linear relationship with the number of simulations. In this work, STSEM of Timoshenko beam is proposed and as well as the effect of correlation length on the response statistics is also studied. The deflection statistics of the beam for both static and dynamic cases are investigated considering various boundary conditions. The computational efficiency of the proposed method and effect of material variability on response statistics are discussed. This STSEM formulation can also be applied for complex structural and computationally demanding wave propagation problems. 1. C.-C. Li, A. Der Kiureghian, Optimal discretization of random fields, *Journal of Engineering Mechanics* 119 (6) (1993) 1136–1154. 2. P. Sasikumar, R. Suresh, S. Gupta, Stochastic finite element analysis of layered composite beams with spatially varying non-gaussian inhomogeneities, *Acta Mechanica* 225 (6) (2014) 1503–1522. 3. A. T. Patera, A spectral element method for fluid dynamics: laminar flow in a channel expansion, *Journal of Computational Physics* 54 (3) (1984) 468–488.

# **A CLOSED-FORM FUNCTIONAL DIFFERENTIAL QUADRATURE METHOD (f-DQM) WITH APPLICATIONS IN COMPUTATIONAL MECHANICS**

**FAISAL M. MUKHTAR\***

\* Department of Civil & Environmental Engineering,  
King Fahd University of Petroleum & Minerals,  
31261, Dhahran, Saudi Arabia.

Email; faisalmu@kfupm.edu.sa

**Key words:** Differential Quadrature Method, Closed-form Solution, Symbolic Computation, Radial Basis Functions.

**Abstract.** As a popular numerical technique, the differential quadrature method (DQM) expresses each derivative and/or integral, in the differential or integro-differential equations, as a weighted sum of the solution values at some selected nodes. This allows discrete values of the primary solution variable(s) to be obtained with only few grid points. The method has gained wide acceptance in the area of computational mechanics. Despite its advantages, DQM requires extra efforts for additional quadrature formulations each time any other secondary variable is needed. Moreover, result at few discrete points hinders sufficient visual representation of the overall solution pattern, and results of the non-sampled points may not be obvious in some cases. Also, some terms in nonlinear problems necessitates inconvenient use of intermixed summation indices. In order to increase the flexibility of the method while maintaining its accuracy, this paper proposes the functional differential quadrature method (f-DQM) that yields a symbolic/functional form of the solution valid throughout the domain under consideration. Some of the advantages of the proposed method include (1) ease in post-processing, as any other secondary variable of interest can be obtained by directly operating on the closed-form solution, (2) means for better visual pattern/description of the solution while utilizing quadrature-based formulation to achieve high accuracy with only few nodes, and (3) possibility for direct analytical computation of differentials and/or integrals during the solution process for terms that require inconvenient use of nested quadrature formulations. The convenience and power of symbolic software programs can be harnessed both during the pre and post-processing stages. Problems of bending of a thin plate and linear and nonlinear elastoplastic torsion of a bar are analyzed to illustrate the features of the proposed method.

## **1 INTRODUCTION**

Interest in the use of differential quadrature method (DQM) and/or its variants results, largely, due to their efficiency. Origin of the method can be traced back to Bellman and Casti [1] with full

details later given by Bellman et al. [2]. DQM requires relatively few grid points to achieve accurate results. It has been popularly applied to many works in computational mechanics as well as developing its variances aiming at addressing some of its associated short comings and challenges.

The basis of the method stems from the derivative approximation, rather than the solution approximation. Any  $n^{\text{th}}$  derivative of a function with respect to a space variable (say,  $x$  or  $y$ ) is written as a linear combination of some weighting coefficients multiplied by the discrete values of the function itself at selected sampling points. The weighted sum requires the use of some suitably selected shape functions whose choice, in addition to the number and distribution of points, dictates the accuracy of the final solution. Since the invention of the method, the impetus of research on the subject mainly focuses on the selection of the shape functions and algorithm for the method's implementations. Example of commonly used shape functions includes the polynomial basis function proposed by Shu and Richards [3], the Fourier expansion by Shu and Chew [4], the radial basis function by Wu and Shu [5], etc. With slight modification, a local DQM can be used to tackle problems with irregular boundaries (for example, see [6]).

Suitable selection of the shape functions apriori allows the solution of the weighting coefficients, first, which are then used to obtain the solution for the problem at hand. A tasking exercise in DQM is the need for having to always cast the expression for any secondary variable (such as the stresses) using the quadrature rules, thereby requiring extra efforts in post-processing. In addition, the discrete nature of the solution implies that results for those locations that have not been initially selected as sampling points will be missing. If such results need to be captured, it becomes necessary to use many sampling points before the solution behavior becomes representative of the whole domain. However, the use of unnecessarily more points than is required for accuracy neutralizes the major advantage of the method: few grid points that provides good accuracy. Last, but not the least, is the fact that the formulation of some highly nonlinear derivative terms becomes more involved due to the need for many nested quadrature formulations. This could be inconvenient with a more likelihood of human error resulting from many intermixed summation indices.

This paper proposes and develops a new version of DQM, the functional differential quadrature method (f-DQM), which addresses the aforementioned concerns. The method warrants a chance to increase the flexibility of traditional DQM by (i) presenting its results in symbolic/functional form of the solution valid throughout the domain under consideration which results in the ease in post-processing so that any other secondary variable of interest can be obtained by directly operating on the closed-form function for the solution, (ii) preserving the main advantage of DQM in using fewer points while providing a means for better visual pattern/description of the solution, and (iii) making it possible for direct analytical computation of differentials and/or integrals during the solution process for terms that require inconvenient use of nested quadrature formulations. In addition to the number and distribution of points and shape functions in the conventional DQM, there exists a possibility of choosing different candidate solutions that provide the means to refine the accuracy to different extents in f-DQM. Another secondary advantage of the proposed method is the convenience in utilizing symbolic computational tools capabilities. Overall, the proposed f-DQM provides a means to harness advantages similar to those of the closed-form analytical counterparts and, yet, maintaining high accuracy associated with the conventional DQM.

## 2 TRADITIONAL DQM FORMULATION

The most basic form of DQM is explained here, where for a two-dimensional domain consisting of the spatial variables  $x$  and  $y$ , the derivatives of any given function are, first, sought. For example, consider the rectangular domain of dimensions  $L_x$  by  $L_y$  where the derivative approximation at a typical point  $(x_i, y_j)$ , shown with the symbol  $\bullet$  in Fig. 1(a) will be determined. The  $m^{\text{th}}$  derivative with respect to  $x$  requires the weighted sum of the linear combination of the function values at the grid points represented with the symbol  $\circ$  in the same figure. This derivative is given by Eq. (1). Similarly, the  $n^{\text{th}}$  derivative with respect to  $y$ , given by Eq. (2), requires the weighted sum of linear combination of the function values at the grid points represented with the symbol  $\oplus$  in Fig. 1(a). It can be shown that mixed derivative can be written in the form given by Eq. (3).

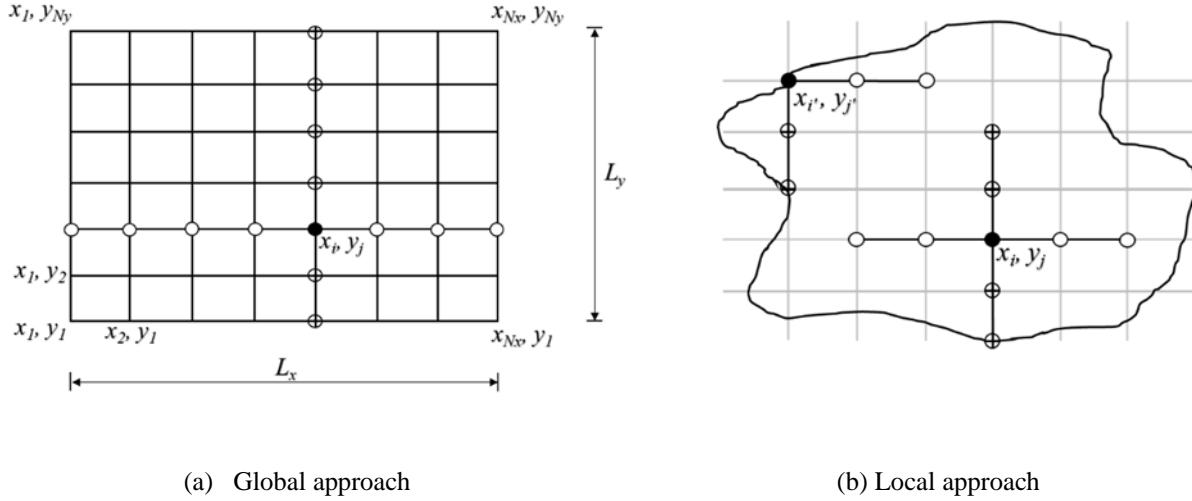


Figure 1: Idea of problem discretization in DQM

$$\frac{\partial^m \psi(x_i, y_j)}{\partial x^m} = \sum_{k=1}^{N_x} \alpha_{ik}^{(m)} \psi(x_k, y_j), \quad i = 1, 2, \dots, N_x \quad \text{at any point } y = y_j \quad (1)$$

$$\frac{\partial^n \psi(x_i, y_j)}{\partial y^n} = \sum_{l=1}^{N_y} \beta_{jl}^{(n)} \psi(x_i, y_l), \quad j = 1, 2, \dots, N_y \quad \text{at any point } x = x_i \quad (2)$$

$$\frac{\partial^{(m+n)} \psi(x_i, y_j)}{\partial x^m \partial y^n} = \sum_{k=1}^{N_x} \alpha_{ik}^{(m)} \sum_{l=1}^{N_y} \beta_{jl}^{(n)} \psi(x_k, y_l), \quad i = 1, 2, \dots, N_x \quad \text{and } j = 1, 2, \dots, N_y \quad (3)$$

The unknown coefficients  $\alpha$  and  $\beta$  are determined by selecting appropriate test function  $\psi(x, y)$  and forcing it to satisfy Eq. (1) at  $N_x$  sampling points and Eq. (2) at  $N_y$  sampling points, respectively. An alternative discretization to the global approach is the use of local DQM discretization, as typically depicted in Fig. 1(b). This becomes particularly useful in cases of irregular geometries where both the internal and boundary points such as  $(x_i, y_j)$  and  $(x_i', y_j')$  can be treated comfortably.

After determining  $\alpha$  and  $\beta$  as described above, any problem of interest such as that described by the general linear (**L**) or nonlinear (**NL**) governing differential equation subject to some boundary condition (**BC**) given by Eq. (4) can be solved. Where,  $f$  and  $g$  are some constants or

functions of the spatial variables. However, while solving Eq. (4), the same domain and its discretization as that used for obtaining  $\alpha$  and  $\beta$  needs to be maintained. This is achieved by substituting Eqs. (1) to (3) into Eq. (4) by using  $u(x_i, y_j)$  instead of  $\psi(x_i, y_j)$  to enable the primary solution variable  $u(x_i, y_j)$  to be obtained at the discrete points  $(x_i, y_j)$  over the domain.

$$\mathbf{NL}(u, \partial_x u, \partial_y u, \dots, \partial_x^m \partial_y^n u) = f \quad \text{in } \Omega \subset \mathfrak{R}^d \quad (4a)$$

$$\mathbf{BC}(u, \partial_x u, \partial_y u, \dots) = g \quad \text{in } \partial\Omega \quad (4b)$$

Where,  $\partial_x^m(\dots) = \frac{\partial^m(\dots)}{\partial x^m}$ ,  $\partial_y^n(\dots) = \frac{\partial^n(\dots)}{\partial y^n}$ , and  $\partial_x^m \partial_y^n(\dots) = \frac{\partial^{(m+n)}(\dots)}{\partial x^m \partial y^n}$

### 3 CLOSED-FORM FUNCTIONAL DIFFERENTIAL QUADRATURE METHOD (f-DQM)

It is obvious that the formulation of the basic DQM presented in the previous section consists of the derivative approximation using quadrature rules and the subsequent solution of the problem of interest at discrete values. As mentioned earlier, in order to obtain other secondary variables, additional quadrature rules must be used for the derivatives. Yet, both the primary and secondary solution variables can only provide results at discrete points. This and the other earlier identified challenges, including the non-representativeness of non-sampled points as well as the issue of nonlinear derivative or integral terms, in DQM can be addressed by the formulations in this section. Instead of only the derivative approximation in traditional DQM, the present work proposes the use of both derivative and the solution approximations as follows.

The solution to Eq. (4) or for a corresponding one dimensional case can be approximated using the linear combination of some function  $\phi(x, y)$  or  $\phi(x)$ , respectively, given by Eq. (5). The coefficients  $\lambda_{ij}$  or  $\lambda_i$  are unknowns that needs to be determined.

$$u(x, y) = \sum_{i=1}^{N_x} \sum_{j=1}^{N_y} \lambda_{ij} \phi_{ij}; \quad u(x) = \sum_{i=1}^{N_x} \lambda_i \phi_i; \quad (5)$$

Depending on their performance, polynomials, radial basis functions (RBFs) or other suitable approximating functions, can be selected as  $\phi$  in Eq. (5). For instance, if a Taylor series expansion around a point  $c$  is selected in a 1D problem, then  $u(x) = \sum_{i=1}^{\infty} \frac{y^i(c)}{i!} (x - c)^i \approx \sum_{i=1}^{N_x} \lambda_i \phi_i$ . Similarly, if a suitably chosen RBF centered at  $x^{ij}$  is used for a 2D case, then  $\phi_{ij} = \phi(\bar{x}, x^{ij})$ . Where,  $\bar{x} = (x, y)$  and  $x^{ij} = (x_i, y_j)$ .

Writing the quadrature analogue of Eq. (4) results in Eq. (6), which is a system of  $N_x \times N_y$  equations that can be solved for the  $N_x \times N_y$  discrete unknowns  $u$  at the sampling points.

$$\mathbf{NL} \left( u(x_i, y_j), \sum_{k=1}^{N_x} \alpha_{ik}^{(m)} u(x_k, y_j), \sum_{l=1}^{N_y} \beta_{jl}^{(n)} u(x_i, y_l), \dots, \sum_{k=1}^{N_x} \alpha_{ik}^{(m)} \sum_{l=1}^{N_y} \beta_{jl}^{(n)} u(x_k, y_l) \right) = f \quad (6a)$$

$$\mathbf{BC} \left( u(x_i, y_j), \sum_{k=1}^{N_x} \alpha_{ik}^{(m)} u(x_k, y_j), \sum_{l=1}^{N_y} \beta_{jl}^{(n)} u(x_i, y_l), \dots \right) = g \quad (6b)$$

However, instead of the direct solution of discrete  $u$  values, the assumed symbolic solution  $u(x, y)$  given by Eq. (5) is substituted in Eq. (6) to obtain Eq. (7), where  $\phi_{pq}^{mn} = \phi(\bar{x}^{pq}, x^{mn})$  and  $\bar{x}^{pq} = (x_p, y_q)$ . Solving Eq. (7) yields the  $N_x \times N_y$  unknowns  $\lambda_{ij}$  which are then substituted back into

Eq. (5) to obtain the final approximate solution in a closed/functional form from which any other secondary variables can be obtained by directly operating on the solution  $u$  rather than having to spend extra effort in using additional quadrature formulations to achieve the same.

$$NL \left[ \sum_{m=1}^{N_x} \sum_{n=1}^{N_y} \lambda_{mn} \phi_{ij}^{mn}, \sum_{k=1}^{N_x} \alpha_{ik}^{(m)} \left( \sum_{m=1}^{N_x} \sum_{n=1}^{N_y} \lambda_{mn} \phi_{kj}^{mn} \right), \sum_{l=1}^{N_y} \beta_{jl}^{(n)} \left( \sum_{m=1}^{N_x} \sum_{n=1}^{N_y} \lambda_{mn} \phi_{il}^{mn} \right), \dots, \sum_{k=1}^{N_x} \alpha_{ik}^{(m)} \sum_{l=1}^{N_y} \beta_{jl}^{(n)} \left( \sum_{m=1}^{N_x} \sum_{n=1}^{N_y} \lambda_{mn} \phi_{kl}^{mn} \right) \right] = f \quad (7a)$$

$$BC \left[ \sum_{m=1}^{N_x} \sum_{n=1}^{N_y} \lambda_{mn} \phi_{ij}^{mn}, \sum_{k=1}^{N_x} \alpha_{ik}^{(m)} \left( \sum_{m=1}^{N_x} \sum_{n=1}^{N_y} \lambda_{mn} \phi_{kj}^{mn} \right), \sum_{l=1}^{N_y} \beta_{jl}^{(n)} \left( \sum_{m=1}^{N_x} \sum_{n=1}^{N_y} \lambda_{mn} \phi_{il}^{mn} \right), \dots \right] = g \quad (7b)$$

It is important to mention that the selection of RBF as the function  $\phi$  in Eq. (5) does not make the f-DQM and Kansa method [7] the same. While Kansa method works by directly operating on the approximated solution in its formulation, the f-DQM utilizes quadrature-based differentials and/or integrals. In fact, the use of  $\phi$  as RBF is just one possibility out of the many choices one may deem fit. The second example in Section 4 illustrates that even if RBF is selected for the function  $\phi$ , there exists a difference in performance between the proposed f-DQM and the Kansa method.

## 4 NUMERICAL IMPLEMENTATION

To illustrate the performance of the proposed f-DQM, two examples are presented. The first, brief, example on bending of thin plates is used to provide a quick overview of the method's application. A more in-depth discussion about the method's many interesting features is provided in the second example; linear elastic and nonlinear elastoplastic torsion of bars. In both the two examples, multiquadric RBF is chosen as the function  $\phi_{pq}^{mn} = \sqrt{\|\bar{x}^{pq} - x^{mn}\|^2 + c^2}$ . Where  $\bar{x}^{pq}$  and  $x^{mn}$  are as earlier defined in Section 3,  $\|\bar{x}^{pq} - x^{ij}\|$  denotes a radial distance between the point  $\bar{x}^{pq}$  and the center  $x^{mn}$  of the RBF.  $c$  is a constant called the shape parameter whose choice is one of the factors that dictate the accuracy of the f-DQM.

### 4.1 Bending of thin plates

Consider a rectangular simply supported thin plate of planar dimensions  $L_x$  by  $L_y$ , thickness  $h$  and loaded with a uniform load  $q$  per unit area. The governing equation and boundary conditions describing the flexural behavior of such plates in terms of the displacement  $w$  can be written as in Eq. (8).

$$D \nabla^2 \nabla^2 w = -q \quad \text{in } \Omega \subset R^2 \quad (8a)$$

$$w = 0; \quad (\partial_{xx} w)n_1 + (\partial_{yy} w)n_2 = 0 \quad \text{on } \partial\Omega \quad (8b)$$

The flexural rigidity is  $D = Eh^3/12(1 - \nu^2)$ .  $\nu$  and  $E$  are, respectively, the Poisson ratio and modulus of elasticity.  $n_1$  and  $n_2$  are the outward unit normal vectors of the boundaries.

The proposed f-DQM is used by, first, approximating the displacement function  $w(x, y) = \sum_{m=1}^{N_x} \sum_{n=1}^{N_y} \lambda_{ij} \phi_{ij}^{mn}$ . The quadrature analogue of Eq. (8a) is then written as Eq. (9a) considering

the definition of the biharmonic operator on the function  $w$  as  $\nabla^2 \nabla^2 w = \frac{d^4 w}{dx^4} + 2 \frac{d^4 w}{dx^2 dy^2} + \frac{d^4 w}{dy^4}$ . Similarly, Eqs. (9b) to (9d) are the quadrature forms of the original boundary conditions (Eq. (8b)).

$$D \left[ \sum_{k=1}^{N_x} \alpha_{ik}^{(4)} \left( \sum_{m=1}^{N_x} \sum_{n=1}^{N_y} \lambda_{mn} \phi_{kj}^{mn} \right) + 2 \sum_{k=1}^{N_x} \alpha_{ik}^{(2)} \sum_{l=1}^{N_y} \beta_{jl}^{(2)} \left( \sum_{m=1}^{N_x} \sum_{n=1}^{N_y} \lambda_{mn} \phi_{kl}^{mn} \right) + \sum_{l=1}^{N_y} \beta_{jl}^{(4)} \left( \sum_{m=1}^{N_x} \sum_{n=1}^{N_y} \lambda_{mn} \phi_{il}^{mn} \right) \right] = -q \quad (9a)$$

$$\sum_{m=1}^{N_x} \sum_{n=1}^{N_y} \lambda_{mn} \phi_{ij}^{mn} = 0 \quad \text{for (I) } i = 1, N_x; \quad j = 1, 2, \dots, N_y, \quad \& \text{ (II) } i = 2, 3, \dots, N_x - 1; \quad j = 1, N_y \quad (9b)$$

$$\sum_{k=1}^{N_x} \alpha_{ik}^{(1)} \left( \sum_{m=1}^{N_x} \sum_{n=1}^{N_y} \lambda_{mn} \phi_{kj}^{mn} \right) = 0 \quad \text{for } i = 1, N_x; \quad j = 2, 3, \dots, N_y - 1 \quad (9c)$$

$$\sum_{l=1}^{N_y} \beta_{jl}^{(1)} \left( \sum_{m=1}^{N_x} \sum_{n=1}^{N_y} \lambda_{mn} \phi_{il}^{mn} \right) = 0 \quad \text{for } i = 2, 3, \dots, N_x - 1; \quad j = 1, N_y \quad (9d)$$

Uniform grid spacing is used in the discretization as shown in Fig. 2, and Eq. (9a) is applied on  $i = 3, 4, \dots, N_x - 2$  and  $j = 3, 4, \dots, N_y - 2$ . Plot of the solution predicted by traditional DQM and the proposed f-DQM (with the parameter  $c = 1$ ) are given in the same figure for a unit square plate with  $q = 1 \text{ kN/m}^2$ ,  $h = 5 \text{ cm}$ ,  $\nu = 0.3$  and  $E = 87,360 \text{ kN/m}^2$ . The solution proves that the continuous nature of the f-DQM provides a better visualization. In addition, there is the ease of directly operating on the functional form of the solution rather than using extra quadrature-based formulations to post-process other desirable secondary variables (such as moment, shear, e.t.c.). Many other important advantages of the method are discussed in the next example.

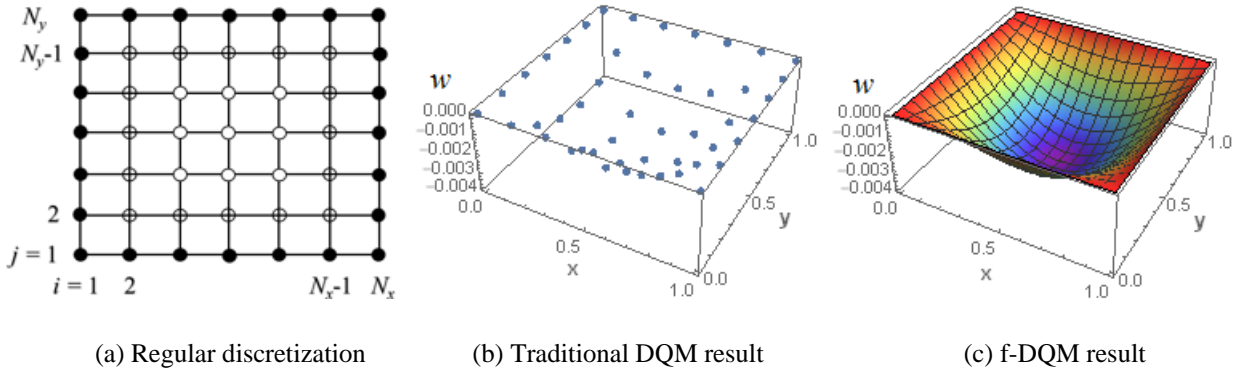


Figure 2: Discretized plate and solution for the displacement  $w$

## 4.2 Linear elastic and nonlinear elastoplastic torsion of bars

For more detailed discussion about the features of the proposed f-DQM, both linear elastic and nonlinear elastoplastic torsion of a bar are analyzed. The governing equation and the boundary condition of the problem, in terms of a non-dimensionalized stress function  $\Psi$ , are given by Eq. (10). Details about the non-dimensionalization of the variables can be found in [8, 9] where similar problem was solved using MFS and pure Kansa approaches, respectively.

$$\nabla^2 \Psi = -\beta - g(x, y) \quad \text{in } \Omega \subset R^2 \quad (10a)$$

$$\Psi = 0 \quad \text{on } \partial\Omega \quad (10b)$$

Where  $\nabla^2(\dots) = \frac{\partial^2(\dots)}{\partial x^2} + \frac{\partial^2(\dots)}{\partial y^2}$  is the Laplacian operator. The effect of the angle of twist  $\theta$  per unit length and the modulus of rigidity  $G$  are contained in the parameter  $\beta = 2G\theta$ . The two stress components can be computed from the solution  $\Psi$  using Eq. (11), and the nonlinear function  $g(x, y)$  that describes the plastic behavior of the section under twisting action is given by Eq. (12).

$$\tau_{xz} = \frac{\partial \Psi}{\partial y}, \quad \tau_{yz} = -\frac{\partial \Psi}{\partial x} \quad (11)$$

$$g(x, y) = 2G \left( \frac{\partial \gamma_{xz}^p}{\partial y} - \frac{\partial \gamma_{yz}^p}{\partial x} \right) \quad (12)$$

$\gamma_{xz}^p$  and  $\gamma_{yz}^p$  are the total plastic strains that need to be added to the elastic strains to obtain the total strains,  $\gamma_{xz}$  and  $\gamma_{yz}$ , using Eq. (13).

$$\gamma_{xz} = \frac{\tau_{xz}}{G} + \gamma_{xz}^p; \quad \gamma_{yz} = \frac{\tau_{yz}}{G} + \gamma_{yz}^p \quad (13)$$

The equivalent total and plastic strains,  $\varepsilon_t$  and  $\varepsilon_p$ , are given by Eq. (14).  $\nu$  is the Poisson ratio and  $m$  is the strain-hardening parameter defined as the ratio between the slope of linear strain-hardening curve to the slope of the elastic curve. Based on deformation theory of plasticity and the Von Mises yield criterion, the plastic strains can be calculated using Eq. (15).

$$\varepsilon_t = \sqrt{(\gamma_{xz}^2 + \gamma_{yz}^2)/3}; \quad \varepsilon_p = \frac{\varepsilon_t^{-(2/3)(1+\nu)}}{1+(2/3)(1+\nu)(m/(1-m))} \quad (14)$$

$$\gamma_{xz}^p = \frac{\varepsilon_p}{\varepsilon_t} \gamma_{xz}; \quad \gamma_{yz}^p = \frac{\varepsilon_p}{\varepsilon_t} \gamma_{yz} \quad \text{for } \varepsilon_p > 0 \quad (15a)$$

$$\gamma_{xz}^p = \gamma_{yz}^p = 0 \quad \text{for } \varepsilon_p \leq 0 \quad (15b)$$

For the case of elastic torsion,  $g(x, y) = 0$  and the problem simplifies to a linear one that can be analyzed in a single step. For the elastoplastic torsion, however, the function  $g(x, y)$  is nonlinear and as can be seen from Eqs. (11) to (15), proper solution can only be obtained using an iterative scheme.

For both the linear elastic and nonlinear elastoplastic torsion problems, the torsional capacity of the section can be computed from the solution  $\Psi$  using Eq. (16).

$$M = 2 \iint_{\Omega} \Psi \, dx dy \quad (16)$$

A traditional DQM formulation of the governing equation and boundary condition (Eq. (10)) is given by Eq. (17), where it is seen that several quadrature derivative formulations are necessary. For example, Eq. (17a) requires the derivatives of both the solution variable  $\Psi$  and the plastic strains on the right hand side to be written in quadrature form. However, the plastic strains themselves contain other nested nonlinear quadrature formulations inside them. This complicates

the iterative solution formulation. Despite such inconvenience, this effort only yields discrete solution results which require a large number of points before the solution behavior becomes obvious. In addition, it will be reiterated that any post-processing using the discrete results to obtain other secondary variables require different quadrature formulations. Sometimes even integral quadrature formulations become necessary for some secondary variables such as the moment in Eq. (16).

$$\sum_{k=1}^{N_x} \alpha_{ik}^{(2)} \Psi(x_k, y_j) + \sum_{l=1}^{N_y} \beta_{jl}^{(2)} \Psi(x_i, y_l) = -\beta - 2G \left( \sum_{l=1}^{N_y} \beta_{jl}^{(1)} \gamma_{xz}^p(x_i, y_l) - \sum_{k=1}^{N_x} \alpha_{ik}^{(1)} \gamma_{yz}^p(x_k, y_j) \right) \quad (17a)$$

$$\Psi(x_1, y_j) = \Psi(x_{N_x}, y_j) = \Psi(x_i, y_1) = \Psi(x_i, y_{N_y}) = 0 \quad \text{for } i = 1, 2, \dots, N_x; j = 1, 2, \dots, N_y \quad (17b)$$

The proposed f-DQM is implemented to analyze the elastic torsion problem described by Eq. (10) on a unit square section  $(x, y) \in (0, 1) \times (0, 1)$ . The power of the method is illustrated by solving and analyzing both the elastic and elastoplastic behavior more conveniently. Firstly, the stress function  $\Psi$  is approximated by Eq. (18) and the quadrature analogues of the original governing equations with the boundary conditions given by Eq. (10) are written as Eq. (19). For convenience, the nonlinear function  $g(x, y)$  is evaluated analytically; thanks to the symbolic form of the proposed f-DQM. This justifies the use of direct analytical computation of differentials and/or integrals during the processing stage in f-DQM for terms that will, otherwise, require inconvenient use of nested quadrature formulations.

$$\Psi(x, y) = \sum_{i=1}^{N_x} \sum_{j=1}^{N_y} \lambda_{ij} \phi_{ij}^{mn} \quad (18)$$

$$\sum_{k=1}^{N_x} \alpha_{ik}^{(2)} \left( \sum_{m=1}^{N_x} \sum_{n=1}^{N_y} \lambda_{mn} \phi_{kj}^{mn} \right) + \sum_{l=1}^{N_y} \beta_{jl}^{(2)} \left( \sum_{m=1}^{N_x} \sum_{n=1}^{N_y} \lambda_{mn} \phi_{il}^{mn} \right) = -\beta - g(x_i, y_j) \quad (19a)$$

$$\sum_{m=1}^{N_x} \sum_{n=1}^{N_y} \lambda_{mn} \phi_{ij}^{mn} = 0 \quad \text{for (I) } i = 1, N_x; j = 1, 2, \dots, N_y, \quad \& \quad \text{(II) } i = 2, 3, \dots, N_x - 1; j = 1, N_y \quad (19b)$$

Elastic behavior for the problem is obtained by solving Eq. (19) while setting  $g(x_i, y_j) = 0$ . The nonlinear elastoplastic solution, however, is obtained in an iterative manner by, first, using the elastic solution for  $\Psi$  as its first iteration. The second iteration starts by using the elastic solution to compute the two stress components in Eq. (11). Next, the total strain components are computed from Eq. (13) while setting the plastic strain components to zero. The equivalent total and plastic strains are then obtained from Eq. (14) after which a check is run for possible onset of plastic zones (i.e.  $\varepsilon_p > 0$ ). The new plastic strain components are obtained using Eq. (15). This completes the second iteration. The procedure is repeated in the subsequent iterations, where the updated values of the variables from previous iterations are used, until convergence.

The parameter  $\beta = 3$  is used in the simulation. Exact solution for the elastic problem exists elsewhere [10], and it is used to calculate the function  $\Psi$  plotted in Fig. 3(a). The elastic solution using the traditional DQM based on Eq. (17) is shown in Fig. 3(b and c). It is obvious that while

the said approach has the power of achieving accurate results with only few grid points, but its inability to provide representative behavior with such a few number of nodes is a setback. It will, thus, be a wasted effort of having to use more nodes in traditional DQM as shown in Fig. 4(c) before the solution depicts the actual behavior similar to that of Fig. 3(a). Interestingly, use of the proposed f-DQM based on Eq. (19) provides a true representative solution with only few nodes as shown in Fig. 4 (a and b). The use of only one domain node in Fig. 4 (a) implies a relatively coarse discretization ( $3 \times 3$  grid) in which neither the DQM nor the f-DQM predicts the solution in exact sense. Yet, it is obvious that despite this relatively coarse discretization, the proposed f-DQM has captured the solution behavior more closely compared to the traditional DQM: An advantage credited to having an interpolated form of the solution (Eq. (18)). More interestingly, however, is the fact that while a grid of  $5 \times 5$  for the traditional DQM (Fig. 3(c)) hardly provides an idea about the solution pattern in the remaining parts (non-sampled points) of the domain, the f-DQM (Fig. 4(b)) is able to achieve that. It should be noticed that the DQM and f-DQM agree with each other at the sampling points. Hence, there is a similar accuracy between the two methods at such points. Therefore, it only remains desirable to illustrate how the f-DQM and the Kansa RBF collocation method compare to each other. This fact is highlighted in following paragraph.

Eq. (16) is used to compute the torsional moment for different discretization density using the proposed f-DQM formulation and the result is shown in Table 1. For performance comparison, the RBF collocation method is formulated and used to solve the same problem. The remarkable performance of f-DQM is obvious in the table.

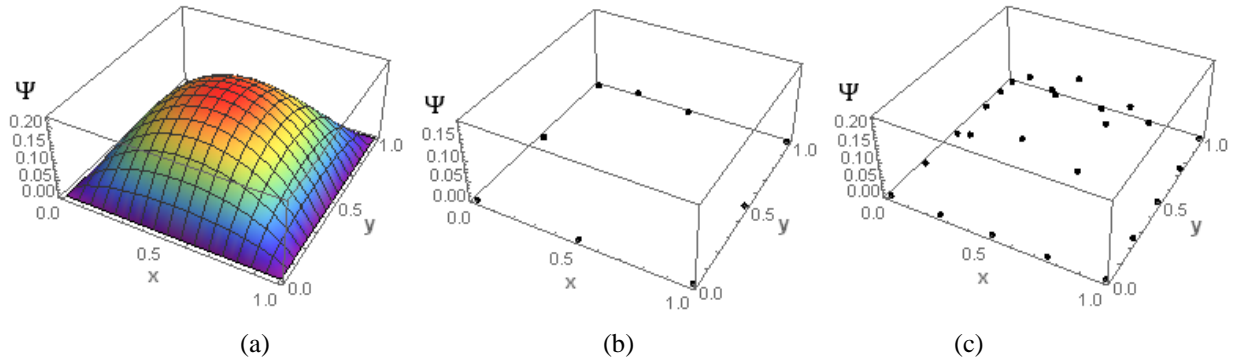


Fig. 3: Elastic solution for the stress function  $\Psi$  (a) Exact [9] (b) Traditional DQM with  $3 \times 3$  grid (c) Traditional DQM with  $5 \times 5$  grid

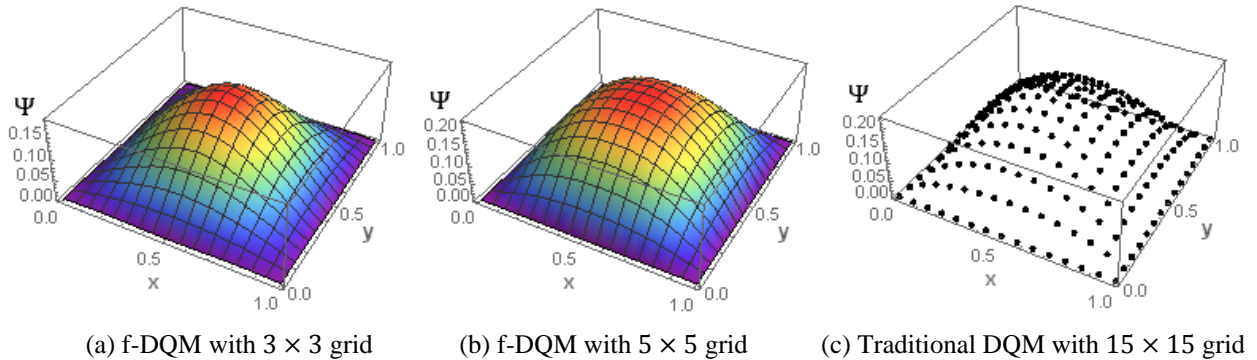


Fig. 4: Ability of the proposed closed-form f-DQM to predict the true elastic solution behavior with fewer nodes compared with traditional DQM

Table 1: Torsional moment (Eq. (16)) for the elastic solution

Discretization	f-DQM ( $c = 0.74$ )	Error (%)	RBF ( $c = 0.84$ )	Error (%)
$3 \times 3$	0.1392	34.0	0.0938	55.5
$4 \times 4$	0.1748	17.1	0.1512	28.3
$5 \times 5$	0.2038	3.4	0.1838	12.9
$6 \times 6$	0.2067	1.9	0.1942	7.9
$7 \times 7$	0.2097	0.6	0.2034	3.6
$8 \times 8$	0.2101	0.4	0.2059	2.4
$9 \times 9$	0.2106	0.1	0.2086	1.1
$10 \times 10$	0.2108	0.0	0.2094	0.7

The elastoplastic solution using the f-DQM (Eq. (19)) is also obtained based on the iterative approach described earlier due to the nonlinearity of the problem. The check in Eq. (15) using  $\varepsilon_p$  determines whether or not a given location in the computational domain undergoes plasticity. The computer code written to solve the problem is programmed in such a way to capture and plot any point at which the behavior becomes plastic. Using a discretization grid of size  $10 \times 10$  and the parameter  $\beta = 3$ , the f-DQM predicts that the whole cross-section remains elastic as seen in Fig. 5. The two stress components,  $\tau_{xz}$  and  $\tau_{yz}$ , corresponding to the mentioned loading parameter are shown in the same figure. Increase in the value of  $\beta$  above 3 results in gradual propagation of the plastic region captured by the f-DQM as shown in Fig. 6.

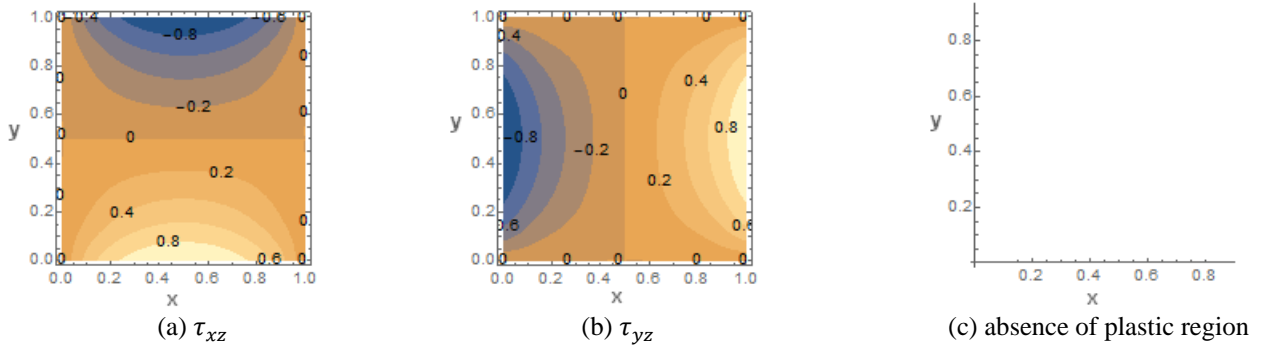


Fig. 5: Computed stresses using f-DQM and a prove of pure elastic behavior at low value of the displacement-controlled loading parameter  $\beta = 3$

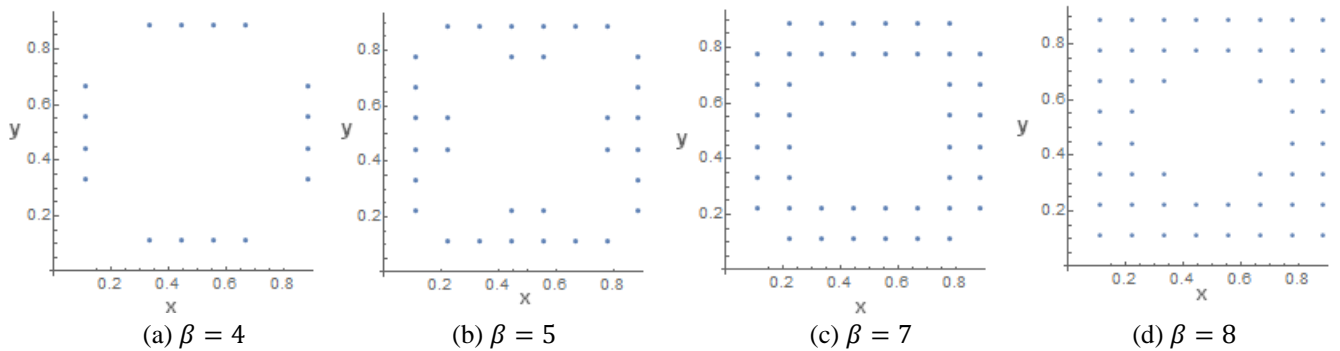


Fig. 6: Plastic region propagation (predicted using f-DQM) as the elastic region diminishes with increase in the displacement-controlled loading parameter  $\beta$

Table 2 summarizes the post-processing formulations in f-DQM compared with those required in the conventional DQM. It is clear that all the secondary variables in the former are obtained using direct analytical differentiation or integration of the symbolic solution for  $\Psi$  against the need for additional differential or integral quadrature formulations required in the latter.

Table 2: Comparison of post-processing formulations between DQM and f-DQM

Secondary variable	DQM	f-DQM
$\tau_{xz} = \frac{\partial \Psi}{\partial y}$	$\sum_{l=1}^{N_y} \beta_{jl}^{(1)} \Psi(x_i, y_l)$	$\frac{\partial \Psi(x, y)}{\partial y}$
$\tau_{yz} = -\frac{\partial \Psi}{\partial x}$	$-\sum_{k=1}^{N_x} \alpha_{ik}^{(1)} \Psi(x_k, y_j)$	$-\frac{\partial \Psi(x, y)}{\partial x}$
$M = 2 \iint_{\Omega} \Psi \, dx dy$	$2 \sum_{k=1}^{N_x} \zeta_k \sum_{l=1}^{N_y} \eta_l \Psi(x_k, y_l)$ *	$2 \iint_{\Omega} \Psi(x, y) \, dx dy$

\*  $\zeta_k$  and  $\eta_l$  are the weighting coefficients for integral quadrature

## 5 CONCLUSIONS

A closed-form functional differential quadrature method (f-DQM) is proposed and applied to analyze two problems, namely, bending behavior of a thin plate as well as an elastic and elastoplastic torsion of a bar. Based on the method's performance, the following conclusions are derived.

1. The proposed f-DQM outperforms the traditional DQM in flexibility and convenience.
2. The symbolic nature of the method makes it possible to harness its advantages similar to those of the analytical counterparts in terms of ease in post-processing.
3. The proposed approach harnesses the convenience and power of a symbolic software package both during preprocessing and post-processing, especially for problems involving terms that require inconvenient use of nested quadrature formulations.
4. The method can be used to yield a truly RBF-DQ approach with a preferable name of RBF-DQ-RBF in cases when the shape functions used in evaluating the weighting coefficients are RBF.
5. Despite some of its common features with RBF collocation (Kansa method) when RBF is chosen as the approximating function, the f-DQM and RBF collocation are not the same; accuracy of the proposed f-DQM is more pronounced, at least, in the torsion problem analyzed in this work.

## ACKNOWLEDGMENT

The author would like to acknowledge the support of King Fahd University of Petroleum & Minerals (KFUPM).

## REFERENCES

- [1] Bellman, R.E. and Casti, J. Differential quadrature and long-term integration. *J. Math. Anal. Appl.* (1971) 34: 235 – 238.
- [2] Bellman, R.E., Kashef, B.G. and Casti, J. Differential quadrature: a technique for the rapid solution of nonlinear partial differential equations. *J. Comput. Phys.* (1972) 10: 40 – 52.
- [3] Shu, C. and Richards. B.E. Application of generalized differential quadrature to solve two-dimension incompressible Navier-Stokes equations. *Int. J. Numer. Methods Fluids.* (1992) 15: 791–798.
- [4] Shu, C. and Chew, Y.T. Fourier expansion-based differential quadrature and its application to Helmholtz eigenvalue problems. *Comm. Numer. Meth. Eng.* (1997) 13: 643–653.
- [5] Wu, Y.L. and Shu, C. Development of RBF-DQ method for derivative approximation and its application to simulate natural convection in concentric annuli, *Comput. Mech.* (2002) 29: 477 – 485.
- [6] Shu, C., Ding, H. and Yeo, K.S. Local radial basis function-based differential quadrature method and its application to solve two-dimensional incompressible Navier-Stokes equations, *Comput. Methods Appl. Mech. Eng.* (2003) 192: 941 – 954.
- [7] Kansa, E.J. Multiquadrics – A scattered data approximation scheme with applications to computational fluid-dynamics–I surface approximations and partial derivative estimates, *Comput. Math. Appl.* (1990) 19: 127 – 145.
- [8] Kolodziej, J.A. and Gorzelanczyk, P. Application of method of fundamental solutions for elasto-plastic torsion of prismatic rods, *Eng. Anal. Boundary Elem.* (2012) 36: 81 – 86.
- [9] Mukhtar, F.M. and Al-Gahtani, H.J. Application of radial basis functions to the problem of elasto-plastic torsion of prismatic bars, *Appl. Math. Model.* (2015) 40: 436 – 450.
- [10] Timoshenko, S. and Goodier, J.N. *Theory of Elasticity.* McGraw Hill Book Company Inc., (1951).

## Chemo-mechanical Regulation of Embryo Development with Time-delay Differential Equations

Jose J Munoz<sup>\*</sup>, Enrique Martín-Blanco<sup>\*\*</sup>, Katerina Karkali<sup>\*\*\*</sup>, Manuel Wenzel<sup>\*\*\*\*</sup>

<sup>\*</sup>Universitat Politècnica de Catalunya, Barcelona, Spain, <sup>\*\*</sup>Institut de Biologia Molecular de Barcelona, Spain,  
<sup>\*\*\*</sup>Alexander Fleming Biomedical Sciences Research Center, <sup>\*\*\*\*</sup>Karlsruhe University, Germany

### ABSTRACT

Time oscillations are ubiquitous during embryo development. Strikingly, these systems have a negligible mass and thus cannot be described through hyperbolic equations. One possible source of these oscillations is the chemo-mechanical coupling between the biological signaling and the active response of the tissue [1]. We here study such interaction for the Central Nervous System during embryo development of *Drosophila* fly. We analyse the strain field and deduce plausible stresses that may generate the observed deformations [2] by solving an inverse problem on the three-dimensional images and assumed field of dipoles at the CNS. We reproduce those results by using a direct problem that is mathematically expressed as differential equation with a delay parameter, i.e. a Delay Differential Equation (DDE). The delay represents the retarded mechanical response of the cells due to a signaling stimulus. The DDE stem from an active rest length change and a linear stress-strain constitutive law. The resulting system of equations can be solved analytically [3] and also numerically. From our results we deduce a critical time delay, below which no oscillations are present. Such critical delay depends on the ability of the cell to adapt the rest length change (remodeling rate) and the tissue stiffness. We are also able to simulate the segmented distribution on space of the oscillations, which can be obtained by using segmented values of the material properties. References [1] Solon J, Kaya-Çopur, Colombelli, Brunne D. Pulsed Forces Timed by a Ratchet-like Mechanism Drive Directed Tissue Movement during Dorsal Closure, *Cell* 137:1331-1342, 2009. [2] JJ Muñoz, D Amat, V Conte. Computation of forces from deformed visco-elastic biological tissues. *Inverse Problems*, Accepted. [3] Kolmanovskii V., Myshkis A. General theory. In: *Applied Theory of Functional Differential Equations. Mathematics and Its Applications (Soviet Series)*, vol 85. Springer, 1992.

## Investigating Blend Morphology of P3HT: PCBM Organic Solar Cells by Coarse-grained Molecular Simulations

Joydeep Munshi<sup>\*</sup>, Ganesh Balasubramanian<sup>\*\*</sup>, Teyu Chien<sup>\*\*\*</sup>, Wei Chen<sup>\*\*\*\*</sup>

<sup>\*</sup>Lehigh University, Bethlehem, PA, <sup>\*\*</sup>Lehigh University, Bethlehem, PA, <sup>\*\*\*</sup>University of Wyoming, Laramie, Wyoming, <sup>\*\*\*\*</sup>Northwestern University, Evanston, IL

### ABSTRACT

Organic photovoltaic bulk heterojunctions (BHJ) typically contain interpenetrating phases of semiconducting polymer acceptors along with fullerene donor materials. Morphology and dynamics of the BHJ active layers significantly affect the power conversion efficiency of solar cells. Mixtures of poly-(3-hexyl-thiophene) (P3HT) and phenyl-C61-butyric acid methyl ester (PCBM) have been widely employed over the past decade as acceptor-donor materials, respectively, for the active layer of the BHJ. The material selection has been driven by the simple and inexpensive synthesis of the flexible semiconducting polymer P3HT, and the high thermal and mechanical stability of both acceptor and donor materials in the BHJ morphology. Atomistic simulations are able to provide insights into the dynamics of blend morphology of organic materials and overcome the experimental challenges in extracting microstructural characterization due to poor contrast in electron microscopy. In addition, coarse-grained molecular dynamics (CGMD) modeling is able to simulate structures approaching the experimental length scales and processing conditions. We present results from CGMD simulations describing the morphological evolution of P3HT:PCBM active layer while solution processing in chlorobenzene. A decrease in the P3HT-PCBM contact areas with increasing solvent temperature reveals an enhanced phase separation of the two materials, and hence an improved crystal growth of the P3HT phase at a solvent temperature of 373K. Thermal annealing of the solvent-free morphology increases the ordering of the P3HT phase, and the predicted microstructures are compared against the as-cast morphologies to determine the changes in the molecular arrangements. We discuss the advantages of thermal annealing for BHJ active layer fabrication in the context of complementary experimental findings.

## **Phase-field Simulation and Neural Network Analysis of the Relationship between Material Parameters and Martensite Microstructure in Low-carbon Steels**

Yoshihiro Murai<sup>\*</sup>, Yuhki Tsukada<sup>\*\*</sup>, Toshiyuki Koyama<sup>\*\*\*</sup>

<sup>\*</sup>Nagoya University, <sup>\*\*</sup>Nagoya University, <sup>\*\*\*</sup>Nagoya University

### **ABSTRACT**

The lath martensite appears in most heat-treatable commercial steels. The size and morphology of martensite phase and dislocation density influence the mechanical properties of steels. The martensite microstructure varies depending on the alloy composition and heat treatment condition. On the other hand, various material parameters such as lattice constants and elastic constants are composition- and temperature-dependent. The relationship between the martensite microstructure and material parameters has not yet been clarified. In this study, phase-field simulation and neural network analysis are used for elucidating the influence of material parameters on the martensite microstructure. Most recently, a phase-field model was developed which considered the fcc-to-bct lattice deformation and slip deformation during the martensitic transformation (MT) in low-carbon steels [1]. Using the developed phase-field model, we performed three-dimensional simulations of the MTs near the martensite finish temperatures in Fe-0.1~0.4mass%C alloys. The composition and temperature dependences of material parameters were considered in the simulations. The simulation results show that the MT progresses with forming the cluster composed of three tetragonal variants of the martensite phase. By analyzing total of 4200 microstructure data obtained by the simulations, fifteen characteristics of the martensite microstructure were measured. For example, the total number of isolated variant domains on {100} cross-sections of the parent phase was counted and used as a measure of the variant domain size. The dislocation density was estimated from the simulated slip deformation field. A feed-forward neural network was trained in order to express the relationship between twelve material parameters and the fifteen characteristics of the martensite microstructure. The prediction error of the trained neural network was confirmed to be sufficiently small. Using the weight parameters and bias parameters of the trained neural network, sensitivity of material parameters to characteristics of martensite microstructure was calculated. It has been found that the yield stress, cubical dilatation of fcc-to-bct lattice deformation, and lattice parameter of the parent phase have significant influences on the martensite microstructure. Reference: [1] Y. Tsukada et al., Proc. of the 5th International Symposium on Steel Science (ISSS 2017), in press.

## High-Order Hybridized Discontinuous Galerkin (HDG) Method and a Multigrid Solver for MHD Applications

Sriramkrishnan Muralikrishnan<sup>\*</sup>, Tim Wildey<sup>\*\*</sup>, Tan Bui-Thanh<sup>\*\*\*</sup>, John Shadid<sup>\*\*\*\*</sup>

<sup>\*</sup>The University of Texas at Austin, <sup>\*\*</sup>Sandia National Labs, <sup>\*\*\*</sup>The University of Texas at Austin, <sup>\*\*\*\*</sup>Sandia National Labs

### ABSTRACT

In this talk we will present a high-order hybridized discontinuous Galerkin (HDG) method and an efficient solver for MHD systems. The advantages of high-order HDG methods over DG methods is that they have much less globally coupled degrees of freedom when combined with implicit time integration schemes. The coupled unknowns are only the hybrid variables introduced on the skeleton of the mesh, which for high-order is much less compared to the total volume unknowns. Here we will present a multi-grid approach defined entirely on the skeletal system (hence least number of unknowns) and demonstrate its scalability. Multigrid solvers on the skeletal system represent difficulty because of the non-nested nature of the grids i.e. new edges/faces appear on refinement which does not have parents from the previous level. With examples from incompressible and compressible MHD systems we will show the effectiveness and scalability of the multigrid solver.

## A Multiscale Analysis of Formation of Ferroelastic Phase in Metallic Oxide

Mayu Muramatsu<sup>\*</sup>, Tatsuya Kawada<sup>\*\*</sup>, Kenjiro Terada<sup>\*\*\*</sup>

<sup>\*</sup>Department of Mechanical Engineering, Keio University, <sup>\*\*</sup>Graduate School of Environmental Studies, Tohoku University, <sup>\*\*\*</sup>International Research Institute of Disaster Science, Tohoku University

### ABSTRACT

In this study, we discuss the changes of the macroscopic material properties of a metallic oxide  $\text{La}_{0.6}\text{Sr}_{0.4}\text{Co}_{0.2}\text{Fe}_{0.8}\text{O}_{3-\delta}$  (LSCF) in relation to its ferroelastic microstructure formation. LSCF is a material which is often used as a cathode electrode of Solid Oxide Fuel Cell (SOFC), and its crystal structure becomes rhombohedral below 700-1100K and cubic above that temperature level. When the cubic structure of LSCF changes to a rhombohedral one with temperature decrease after a cell is sintered, the single crystal grain in a polycrystalline aggregate accommodates some stable phases due to the lattice misfit between crystal structures. The stable rhombohedral phase, which is called ferroelastic phase, is known to exhibit stress relaxation due to the crystal re-orientation when stress is applied. In this study, emphasizes are placed on the mechanism of ferroelastic phase transformation caused by the change of lattice structure during temperature decrease. In order to incorporate the mechanical behavior of ferroelastic phase [1] into the stress analysis of SOFC in consideration of elastic, creep, thermal and reduction strains [2], we propose a mathematical model to predict the formation of ferroelastic phases in crystal grains of a metallic oxide LSCF [3]. The phase-field model equipped with the elastic energy is introduced to realize the morphology formation of ferroelastic phases in a crystal grain. We conduct a series of three-dimensional numerical simulations to reproduce the deformation-induced nucleation and growth of ferroelastic phases of LSCF. The crystal orientations of matrices are also considered in the simulation so that the ferroelastic phase transformation in the polycrystalline aggregates can be reproduced. Then, the changes of the macroscopic material properties are discussed in relation to the ferroelastic microstructure formation. References [1] M. Muramatsu, K. Terada, T. Kawada, K. Yashiro, K. Takahashi and S. Takase, Characterization of time-varying macroscopic electro-chemo-mechanical behavior of SOFC subjected to Ni-sintering in cermet microstructures, *Computational Mechanics*, Vol. 56, pp. 653-676, 2015. [2] Y. Kimura, J. Tolchard, M.-A. Einarsrud, T. Grande, K. Amezawa, S. Hashimoto and T. Kawada, The Effect of Ferroelasticity of  $\text{La}_{1-x}\text{Sr}_x\text{Co}_{1-y}\text{Fe}_y\text{O}_{3-\delta}$  on the Mechanical Stability of Solid Oxide Fuel Cells, *ECS Transactions*, Vol. 57, pp. 635–642, 2013. [3] M. Muramatsu, K. Yashiro, T. Kawada and K. Terada, Simulation of Ferroelastic Phase Formation Using Phase-field Model, *International Journal of Mechanical Sciences*, (Accepted).

# **A Novel Non-Parametric Optimization Method for Free-Orientation of a Laminated Composite Shell Structure for Tailoring Thermal Deformation**

Yoshiaki Muramatsu\*, Masatoshi Shimoda\*\*

\*Graduate School of Advanced Science and Technology, Toyota Technological Institute, \*\*Department of Advanced Science and Technology, Toyota Technological Institute

## **ABSTRACT**

Abstract: Shell structures with composite materials such as carbon fiber reinforced plastics (CFRP) have been widely utilizing in various structural design of cars, aircrafts and so on. They have higher specific mechanical performances, and especially anisotropic materials can be used for tailoring the elastic tensor of a shell structure. From the practical point of view, most of the industrial products are exposed to a thermal load and needs for controlling the thermal deformation to maintain the mechanical performance. On the other hand, there are other industrial products which use the thermal deformation proactivity such as bimaterial thermal actuators. In this study, we propose a material orientation optimization method for optimum design of laminated composite shell structures consisting of anisotropic materials. We aim at controlling thermal displacements to target values without varying shape or thickness. The square displacement error norm is minimized by varying the material orientation of each layer as the design variable. The optimum design problem is formulated as a distributed-parameter optimization problem, and the sensitivity function with respect to the material orientation variation is theoretically derived based on the variational method. The optimal material orientation variations are determined by using the H1 gradient method [1][2], where the sensitivity functions aforementioned are applied as the Robin condition to vary and optimize the material orientation. In detail, after deriving the sensitivity function, we transfer it to the internal heat generation and determine the material orientation variation by using the Poisson's equation for fictitious-heat transfer analysis to ensure the continuously distribution of the material orientation. The optimum design examples show that the proposed optimization method can effectively obtain the optimum material orientation with the smooth curvilinear distribution and can tailor the thermal deformation, simultaneously. Reference: [1] Shimoda M, Liu Y. A non-parametric free-form optimization method for shell structures. *Structural Multidisciplinary Optimization* 2014;50:409–423. [2] Muramatsu Y, Shimoda M. Optimization approach for designing free-orientation of orthotropic materials of a shell structure. *Transactions of the Japan Society of Mechanical Engineers*. 2017;83(851):1-15 (in Japanese).

## **Interfacial Mixing in High-energy-density Matter with Multiphysics Kinetic and Molecular Dynamics Models**

Michael S. Murillo<sup>\*</sup>, Liam Stanton<sup>\*\*</sup>, Jeff Haack<sup>\*\*\*</sup>

<sup>\*</sup>Michigan State University, <sup>\*\*</sup>Lawrence Livermore National Laboratory, <sup>\*\*\*</sup>Los Alamos National Laboratory

### **ABSTRACT**

At the National Ignition Facility, high-powered laser beams are used to compress a small target to generate fusion reactions. A critical issue in achieving this is the understanding of mix at the ablator/fuel interface. Mixing occurs at various length scales, ranging from atomic inter-species diffusion to hydrodynamic instabilities. Because the interface is preheated by energy from the incoming shock, it is important to understand the dynamics before the shock arrives. The interface is in the warm dense matter phase with a deuterium/tritium fuel mixture on one side and a plastic mixture on the other. We would like to understand various aspects of the evolution, including the state of the interface when the main shock arrives, the role of electric field generation at the interface, the 'kinetic-ness' of the system, and the character and time scales for diffusion. We present a multiscale approach to model these processes, which combines molecular dynamics to simulate the ionic degrees of freedom with orbital-free density functional theory to calculate the electronic structure. Simulation results are presented and compared with a newly developed multispecies BGK model, and connections to hydrodynamic models are discussed.

## THE FGM BEAM FINITE ELEMENT INCLUDING WARPING TORSION

J. MURIN\*, M. AMINBAGHAI\*\*, V. KUTIS\*, J. HRABOVSKY\*, J. PAULECH\*,  
S. KUGLER<sup>†</sup>

\* Department of Applied Mechanics and Mechatronics of IAMT, Faculty of Electrical Engineering and Information Technology, Slovak University of Technology in Bratislava, Ilkovičova 3, 812 19 Bratislava, Slovakia  
[justin.murin@stuba.sk](mailto:justin.murin@stuba.sk)

\*\* Institute of Mechanics of Materials and Structures, Vienna University of Technology, Karlsplatz 13, A-1040 Vienna, Austria  
[mehdi.aminbaghai@ac.at](mailto:mehdi.aminbaghai@ac.at)

<sup>†</sup> Department of Applied and Numerical Mechanics, University of Applied Sciences Wiener Neustadt, Johannes Gutenberg-Straße 3, A-2700 Wiener Neustadt, Austria  
[kugler@fhwn.ac.at](mailto:kugler@fhwn.ac.at) [www.fhwn.ac.at](http://www.fhwn.ac.at)

**Key words:** 3D-FGM beam finite element, Warping torsion, Elastostatic and modal analyses.

### 1 INTRODUCTION

Structures with spatially inhomogeneous material properties are of great practical importance in modern product and system design. Functionally Graded Materials (FGMs) are formed by a continuous gradation of two or more constituents over the physical volume, while composites show a discontinuous variation of constitutive properties. The specific variations can be tailored properly in order to achieve optimized characteristics of the component. The numerical assessment of the mechanical or multiphysical behaviour is a critical issue in the product development process and new and enhanced strategies have to be developed. Accurate and efficient structural finite elements like beams, plates and shells require suitable homogenization procedures to arrive effective stiffness quantities for the membrane, bending, transverse and torsional shear properties accompanied with a suitable warping stiffness regarding non-uniform torsion [1,2,3]. In the literature, a huge amount of papers can be found, which deal with modelling and simulation of static and dynamic problems of FGM beams. In [4, 5], a review of the principal developments in FGM structures is processed. A common feature of the cited articles is that constant material properties of the beams in the longitudinal direction are assumed. According to our knowledge, especially for torsion of the FGM beams with longitudinally varying material properties, the warping effect has not yet been considered.

This contribution is an extension of our previous work dealing with derivation of the FGM beam finite elements (with 12x12 stiffness and mass matrix) with longitudinal varying effective material properties that is suitable for analysis of beam structures made of spatially varying FGM. Effects of axial and shear forces are included as well as the Winkler elastic foundation and the Saint Venant torsion is considered in our previous papers. Homogenization of the spatially varying material properties in the real FGM beam and the calculation of effective parameters are done by extended mixture rules and by the multilayer method (MLM) and the direct integration methods (DIM), e.g. [6]. If only symmetric transversal and lateral variations of material properties are considered in the real FGM beam, longitudinally constant effective material properties arises from the homogenization. For spatially varying material properties, where the transversal and lateral variation is symmetric, a longitudinally variation of effective material properties has been obtained, [6, 7,8,9]. This method can also be used in the homogenization of multilayer beams with discontinuous variation of material properties in transversal and lateral direction.

In the contribution, the 3D FGMs Timoshenko beam finite element with 14x14 stiffness and mass matrices for doubly symmetric open and closed cross-section is presented including warping torsion effect (non-uniform torsion). A longitudinal continuous variation of effective material properties is considered by the finite element equations derivation, which is obtained by homogenization of the spatial varying material properties in real FGM beam. Results of numerical elastostatic analysis of the cantilever beam with rectangular hollow cross-section are presented and the accuracy and effectiveness of the new FGM beam finite element is discussed and evaluated.

## 2 THE FGM BEAM FINITE ELEMENT EQUATIONS

Let us consider a straight Timoshenko beam finite element of doubly symmetric cross-section –

**Figure 1.** The Saint Venant torsion is assumed in the first step of this study. The degrees of freedom at node  $i$  according to transfer matrix method (TMM) notation are: the displacements  $u_i, v_i, w_i$  in the local directions  $x, y, z$ , and the cross-sectional area rotations about the  $x, y, z$  directions -  $\varphi_{x,i}, \varphi_{y,i}, \varphi_{z,i}$ . The degrees of freedom at the node  $j$  are denoted in a similar manner. The internal forces at node  $i$  according to transfer matrix method (TMM) notation are: the axial force  $N_i$ , the transversal forces  $R_{y,i}$  and  $R_{z,i}$ , the bending moments  $M_{y,i}$  and, the torsion moment  $M_{x,i}$ . Furthermore,  $n_x = n_x(x)$  denotes the axial force distribution,  $q_z = q_z(x)$  and  $q_y = q_y(x)$  are the transversal and lateral force distributions,  $m_x = m_x(x)$ ,  $m_y = m_y(x)$  and  $m_z = m_z(x)$  are the distributed moments,  $\mu_x = \rho A = \mu_y = \mu_z = \mu$  denote the mass distribution,  $\bar{\mu}_y = \rho I_y$ ,  $\bar{\mu}_z = \rho I_z$  and  $\bar{\mu}_{xT} = \rho I_p$  refer to the distributions of mass moments of inertia,  $\rho = \rho_L^H(x) \equiv \rho_L^H$  is the homogenized effective mass density distribution,  $A$  is the cross-sectional area,  $I_y$  and  $I_z$  are the second moments of area,  $I_p = I_y + I_z$  denotes the polar moment of area,  $k_x = k_x(x)$ ,  $k_y = k_y(x)$ ,  $k_z = k_z(x)$ ,  $\bar{k}_y = \bar{k}_y(x)$ ,  $\bar{k}_z = \bar{k}_z(x)$  are the elastic foundation modules (the torsional elastic foundation is not considered), and  $\omega$  is the circular frequency. The effective homogenized and longitudinally varying stiffness reads as follows:  $EA = E_L^{NH}(x)A$  is the axial stiffness ( $E_L^{NH}(x) \equiv E_L^{NH}$  is the effective elastic modulus for axial loading),  $EI_y = E_L^{MyH}(x)I_y$  is the flexural stiffness about the  $y$ -axis ( $E_L^{MyH}(x) \equiv E_L^{MyH}$  is the

effective elastic modulus for bending about axis  $y$ ),  $EI_z = E_L^{M_zH}(x)I_z$  is the flexural stiffness in axis  $z$ , ( $E_L^{M_zH}(x) \equiv E_L^{M_zH}$  is the effective elastic modulus for bending about axis  $z$ ),  $\bar{G}A_y = G_{Ly}^H(x)k_y^{sm}A$  is the reduced shear stiffness in  $y$ -direction ( $G_{Ly}^H(x) \equiv G_{Ly}^H$  is the effective shear modulus and  $k_y^{sm}$  is the average shear correction factor in  $y$ -direction),  $\bar{G}A_z = G_{Lz}^H(x)k_z^{sm}A$  is the reduced shear stiffness in  $z$  - direction ( $G_{Lz}^H(x) \equiv G_{Lz}^H$  is the effective shear modulus and  $k_z^{sm}$  is the average shear correction factor in  $z$  - direction),  $G_L^{M_xH}(x)I_T$  is the effective torsional stiffness,  $G_L^{M_xH}(x) = G_L^{M_xH}$  is the torsional elastic modulus and  $I_T$  is the torsion constant –  $I_p = I_T$  for the circular and ring cross-section). The homogenization of spatially varying material properties is described in more detail in [6,7,8,9].

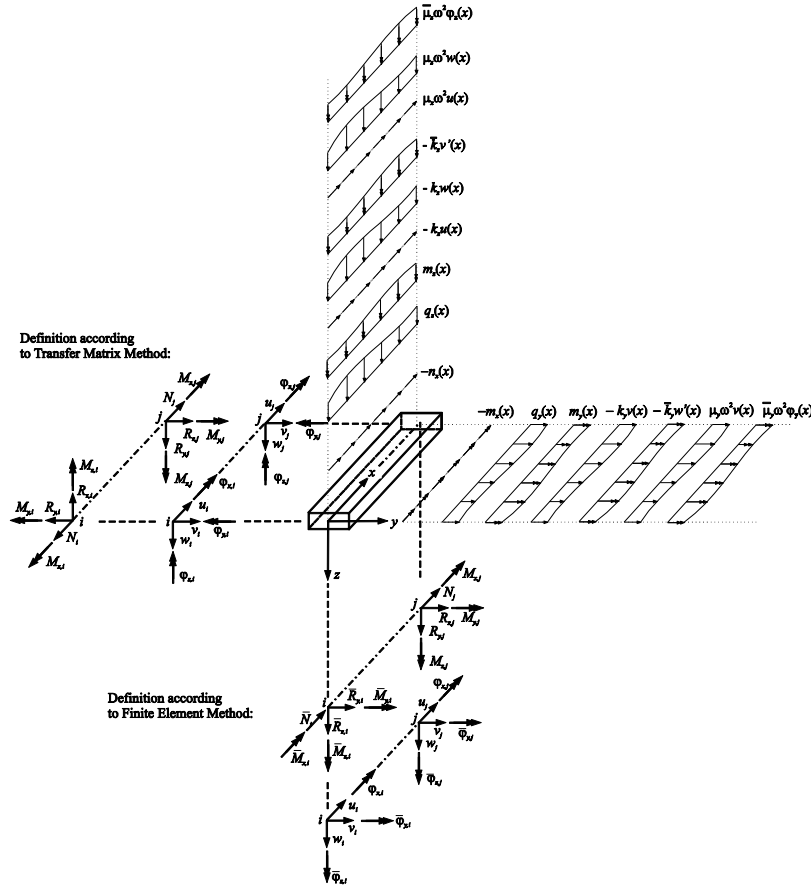


Figure 1: The local internal variables and loads for 12x12 Timoshenko FGM beam finite element.

The derivatives with respect to  $x$  of the relevant variable is denoted with an apostrophe “ ’ ” throughout the article. For establishing the FGM warping torsion beam finite element equations with 14x14 element matrix we use the matrices for axial, transversal lateral loading (according the Figure 1) that were derived and described in our previous papers [6,7,8,9]. The warping torsion equations are described in more detail in the next subchapter.

### 2.1 Non-uniform torsion of the FGM beams with STMDE

Fig. refers to determination of the eigenvibrations due to non-uniform torsion. It shows the torsional moment  $M_T(x)$ , representing the sum of the primary torsional moment  $M_{Tp}(x)$  and

the secondary torsional moment  $M_{Ts}(x)$ , and the bimoment  $M_\omega(x)$  according to the formulation in the framework of the transfer matrix method (TMM).

Fig. 2 also shows the angle of twist  $\psi(x)$ , corresponding to  $M_{Tp}(x)$ . It represents the sum of the angle of twist, resulting from the primary deformation,  $\psi'_M(x)$  and from the secondary deformation,  $\psi'_S(x)$ .

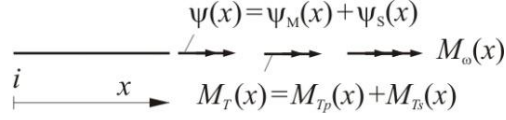


Fig. 2: Non-uniform torsion: torsional moments, bimoment, and angles of twist.

Fig. 3 illustrates the beam element for non-uniform torsion. It is loaded by the equivalent inertial torsional line moment  $\omega^2 I_p \rho(x) \psi(x)$ , the equivalent inertial line bimoment

$\omega^2 I_\omega \rho(x) \psi'_M(x)$ , where  $I_\omega$  stands for the warping constant, and the torsional line moment  $m_T(x)$ , which is equal to zero for modal analysis. These line moments represent the static equivalent of the respective dynamic action. In the following, the equilibrium equations for TMM will be formulated. They are obtained as

$$M'_T(x) = -m_T(x) - \omega^2 I_p \rho(x) \psi(x), \quad (1)$$

where  $m_T(x) = \sum_{k=0}^{\max k} \eta_{m_T,k} x^k$  is the polynomial representation of the torsion moment with the parameters  $\eta_{m_T,k}$ , and

$$\begin{aligned} M'_\omega(x) &= M_T(x) - M_{Tp}(x) + m_\omega(x) + \omega^2 I_\omega \rho(x) \psi'_M(x) = \\ &= M_{Ts}(x) + m_\omega(x) + \omega^2 I_\omega \rho(x) \psi'_M(x), \end{aligned} \quad (2)$$

where  $m_\omega(x) = \sum_{k=0}^{\max k} \eta_{m_\omega,k} x^k$  is the polynomial representation of the warping moment with the parameters  $\eta_{m_\omega,k}$ , and

$$M_T(x) = M_{Tp}(x) + M_{Ts}(x). \quad (3)$$

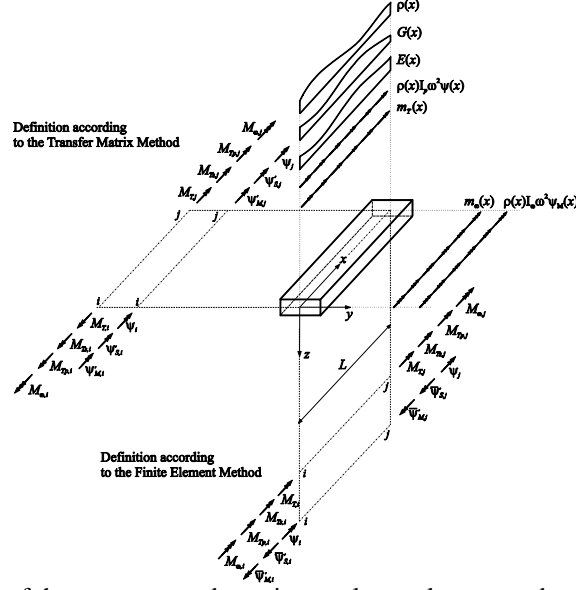


Fig. 3: Positive orientation of the moments and rotation angles at element nodes for the TMM and the FEM.

According to [10,11],

$$\psi''_M(x) = -\frac{M_{\omega}(x)}{E(x)I_{\omega}}, \quad (4)$$

and

$$\psi'(x) = \psi'_M(x) + \psi'_S(x), \quad (5)$$

with

$$\psi'_M(x) = \frac{M_{Tp}(x)}{G(x)I_T}, \quad (6)$$

and

$$\psi'_S(x) = \frac{M_{Ts}(x)}{G(x)I_{Ts}}, \quad (7)$$

where  $I_{Ts}$  denotes the secondary torsion constant and  $E(x)$  and  $G(x)$  stand for the longitudinally varying effective elasticity modulus and shear modulus, respectively. The new polynomial  $G(x)I_{Ts}$  is obtained by multiplication of the secondary torsion constant  $I_{Ts}$  with the polynomial for the effective shear modulus,  $G(x)$ .

The polynomial  $E(x)I_{\omega}$  is obtained by multiplication of the warping constant  $I_{\omega}$  with the polynomial representation of Young's modulus,  $E(x)$ . After mathematical manipulation, [10,11], the following differential equation of fourth order, with the load polynomial  $\eta_L(x)$ , is obtained:

$$\eta_4(x)\psi''''(x) + \eta_3(x)\psi''''(x) + \eta_2(x)\psi''(x) + \eta_1(x)\psi'(x) + \eta_0(x)\psi(x) = \eta_L(x). \quad (8)$$

The variable polynomial coefficients and establishing of the local finite element are given in [10]. The local finite element equations for non-uniform torsion (in particular for free torsional vibrations) read as follows (considering the definitions of positive quantities in the framework of the FEM, resulting in  $\bar{M}_{T,i} = -M_{T,i}$ ,  $\bar{M}_{\omega,i} = -M_{\omega,i}$ ,  $\bar{\psi}'_{M,i} = -\psi'_{M,i}$ , and  $\bar{\psi}'_{M,j} = -\psi'_{M,j}$ ):

$$\begin{bmatrix} \bar{M}_{T,i} \\ \bar{M}_{\omega,i} \\ M_{T,j} \\ M_{\omega,j} \end{bmatrix} = \begin{bmatrix} B_{4,4} & B_{4,7} & B_{4,11} & B_{11,14} \\ B_{7,4} & B_{7,7} & B_{7,11} & B_{7,14} \\ B_{11,4} & B_{11,7} & B_{11,11} & B_{11,14} \\ B_{14,4} & B_{14,7} & B_{14,11} & B_{14,14} \end{bmatrix} \cdot \begin{bmatrix} \psi_i \\ \bar{\psi}'_{M,i} \\ \psi_j \\ \bar{\psi}'_{M,j} \end{bmatrix} + \begin{bmatrix} F_4 \\ F_7 \\ F_{11} \\ F_{14} \end{bmatrix}. \quad (9)$$

In order to include warping, an additional degree of freedom is added to the classical nodal variables at each element nodal point. As mentioned previously, the warping part of the first derivative of the twist angle,  $\mathcal{G}'_M$ , is considered as this degree of freedom [7]. This is advantageous for the formulation of boundary conditions. If the effect of the secondary torsional moment on the deformations is not considered,  $\mathcal{G}'_M(x) \equiv \mathcal{G}'(x)$ . Here,  $\mathcal{G}'(x)$  is the first derivative of the angle of twist (bicurvature) that is very often used as a 7th degree of freedom in the usual non-uniform torsion formulations [12,13,14]. A detailed description of the matrix coefficients in (9) is presented in [10] and [11]. The local finite element matrix  $B$  in (18) is symmetric.

### 3 THE FINITE ELEMENT EQUATIONS OF THE 3D TIMOSHENKO BEAM WITH WARPING

By combination of the equations for axial and bending loads ([6,7,8,9]) and the non-uniform torsion, following system of finite element equations is obtained

$$\begin{bmatrix} F_{int}^e \end{bmatrix} = \begin{bmatrix} B^{le} \end{bmatrix} \begin{bmatrix} u^e \end{bmatrix} + \begin{bmatrix} F^e \end{bmatrix} \quad (10)$$

where  $\begin{bmatrix} u^e \end{bmatrix}^T = \{u_i \ v_i \ w_i \ \psi_i \ \varphi_{y,i} \ \varphi_{z,i} \ \psi'_{M,i} \ u_j \ v_j \ w_j \ \psi_j \ \varphi_{y,j} \ \varphi_{z,j} \ \psi'_{M,j}\}$

is the displacement vector, and

$$\begin{bmatrix} F_{int}^e \end{bmatrix}^T = \{N_i \ R_{y,i} \ R_{z,i} \ M_{x,i} \ M_{y,i} \ M_{z,i} \ M_{\omega,i} \ N_k \ R_{y,j} \ R_{z,j} \ M_{x,j} \ M_{y,j} \ M_{z,j} \ M_{\omega,j}\}$$

is the internal load vector and  $\begin{bmatrix} F^e \end{bmatrix}$  is the external load vector. The local finite element matrix reads

$$\begin{bmatrix} B^{le} \end{bmatrix} = \begin{bmatrix} B_{1,1} & 0 & 0 & 0 & 0 & 0 & 0 & B_{1,8} & 0 & 0 & 0 & 0 & 0 & 0 \\ & B_{2,2} & 0 & 0 & 0 & B_{2,6} & 0 & 0 & B_{2,9} & 0 & 0 & 0 & B_{2,13} & 0 \\ & & B_{3,3} & 0 & B_{3,5} & 0 & 0 & 0 & 0 & B_{3,10} & 0 & B_{3,12} & 0 & 0 \\ & & & B_{4,4} & 0 & 0 & B_{4,7} & 0 & 0 & 0 & B_{4,11} & 0 & 0 & B_{4,14} \\ & & & & B_{5,5} & 0 & 0 & 0 & 0 & B_{5,10} & 0 & B_{5,12} & 0 & 0 \\ S & & & & & B_{6,6} & 0 & 0 & B_{6,9} & 0 & 0 & 0 & B_{6,13} & 0 \\ & Y & & & & & B_{7,7} & 0 & 0 & 0 & B_{7,11} & 0 & 0 & B_{7,14} \\ & & M & & & & & B_{8,8} & 0 & 0 & 0 & 0 & 0 & 0 \\ & & & M & & & & & B_{9,9} & 0 & 0 & 0 & B_{9,13} & 0 \\ & & & & E & & & & & B_{10,10} & 0 & B_{10,12} & 0 & 0 \\ & & & & & T & & & & & B_{11,11} & 0 & 0 & B_{11,14} \\ & & & & & & R & & & & & B_{12,12} & 0 & 0 \\ & & & & & & & I & & & & & B_{13,13} & 0 \\ & & & & & & & & C & & & & & B_{14,14} \end{bmatrix}. \quad (11)$$

The local finite element matrix  $B^{le}$  in (11) consists formally of the linear stiffness matrix  $K_L$  and the linearized geometric stiffness matrix  $K_N$  (containing the terms with second order axial force  $N^{II}$  that has to be known or has to be evaluated by a linear elastic-static calculation)

and the consistent mass matrix  $M$ :

$$[B^{le}] = [K_L + K_N - \omega^2 M]. \quad (12)$$

Solution algorithm for calculation of the matrix  $B^{le}$  and the loads vector  $F^e$  is implemented into the software MATHEMATICA [15]. In the modal analysis, the eigenvalue problem is solved. For given axial forces  $N^I$  and the geometrical parameters and the homogenized material properties and the global boundary conditions, the circular frequency  $\omega$  is increased until the determinant of the global beam structure matrix tends to zero. This circular frequency is the natural circular frequency from which the natural frequency (eigenfrequency) can be calculated. Further, the mode shapes can be calculated by the transfer relations [8]. In elastostatic analysis, the circular frequency is set to zero, and the load vector has to be established.

#### 4 NUMERICAL EXPERIMENTS

Results of numerical experiments on several combined loadings of FGM beams including Saint Venant torsion are presented in articles [8,9,10,11,12]. Issues of modal and elastostatic analyses of thin walled FGM beams with warping consideration is prepared for publication in more detail in papers [10,11]. Due to the limited scope of this paper, only the particular results of numerical experiments on the non-uniform torsion of thin-walled beam with rectangular hollow cross-section will be presented in this contribution. The cantilever FGM beam with a hollow rectangular cross-section of length  $L = 0.1\text{m}$  is considered as shown in Fig. 5. The beam is loaded by the torsional moment  $M_T = 1\text{Nm}$  at point  $k$ . The moment was applied as a distributed load on the whole hollow cross-section. The FGM consists of a mixture of aluminium (denoted with the index  $m$ ) and tungsten (denoted with the index  $f$ ). The material properties are shown in

Table1.

Material properties:		
Young's modulus	$E_f = 4.8 \cdot 10^{11}, E_m = 0.69 \cdot 10^{11}$	Pa
Poisson's ratio	$\nu_f = 0.2, \nu_m = 0.33$	-
Shear modulus	$G_f = 2.0 \cdot 10^{11}, G_m = 0.26 \cdot 10^{11}$	Pa

Table1: Material properties of the FGM constituents.

The longitudinal polynomial variation of the effective Young's modulus and the effective Poisson's ratio (13) is assumed as:

$$E(x) = E_f + (E_m - E_f) \left(\frac{x}{L}\right)^n, \quad \nu(x) = \nu_f + (\nu_m - \nu_f) \left(\frac{x}{L}\right)^n \quad (13)$$

In (13),  $n$  is the order of the polynomial. The effective shear modulus reads as:

$$G(x) = \frac{E(x)}{2(1+\nu(x))}. \quad (14)$$

The longitudinal beam axis  $x$  begins at the clamped end of the cantilever beam

( $x = 0$ ). The axial variations of the material properties are shown in Fig. 4 for  $n \in \langle 1, 5 \rangle$ .

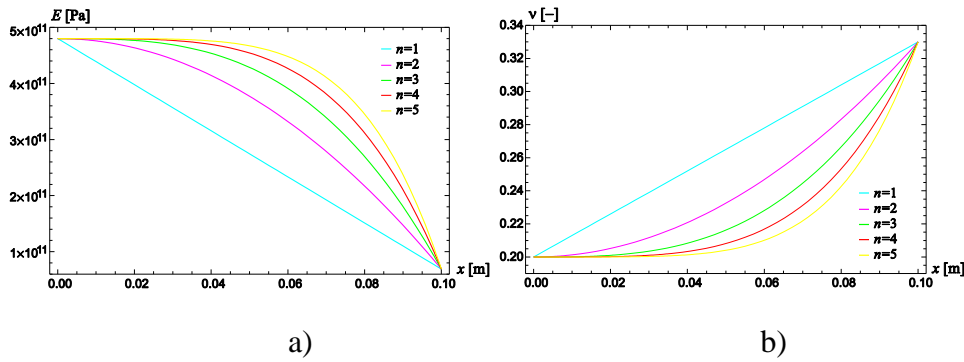


Fig. 4: Variation of the effective Young's modulus and a) and Poisson's ratio b).

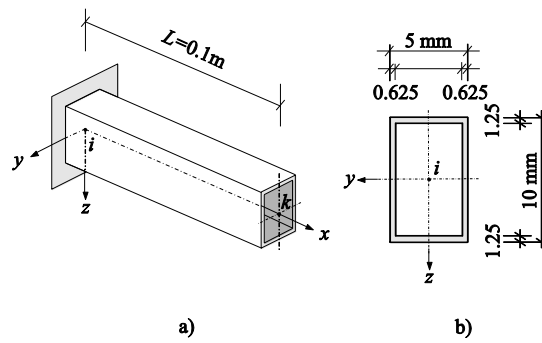


Fig. 5: Cantilever beam with a rectangular hollow cross-section: a) system, b) cross-section.

The cross-sectional parameters of the beam (Figure 5b)) are calculated by ANSYS [16] and by Thin Tube Theory - TTT). They are listed in

Table 2.

Cross-sectional parameters		
Cross-sectional area	$A = 0.21875 \cdot 10^{-4}$	$\text{m}^2$
Second moment of area about the $y$ -axis	$I_z = 0.71208 \cdot 10^{-10}$	$\text{m}^4$
Second moment of area about the $z$ -axis	$I_y = 0.28483 \cdot 10^{-9}$	$\text{m}^4$
Polar moment of area	$I_p = I_y + I_z = 0.31209 \cdot 10^{-9}$	$\text{m}^4$
Torsion constant	$I_T = 0.16748 \cdot 10^{-9}$	$\text{m}^4$
Secondary torsion constant	$I_{Ts} = 0.717773 \cdot 10^{-10}$	$\text{m}^4$
Warping constant	$I_\omega = 0.240426 \cdot 10^{-15}$	$\text{m}^6$

Table 2: Cross-sectional parameters of the hollow cross-section.

The elastostatic torsional analyses were calculated by:

a) only one warping torsion beam finite element (FGM-WT with STMDE); b) a very fine mesh ( number of 500) of our WT BEAM [17] finite elements. Constant material properties of relevant finite element is obtained as an average value, calculated from their values in the element nodes, according the variation in Fig. 4; c) a very fine mesh of 3D SOLID186 finite elements (number of 577000 FE) of the software ANSYS [16].

The results of the analyses, considering the angle of twist and internal moments at the nodes  $i$  and  $k$  for  $n = 1$ , are shown in Table 3.

Variables	FGM-WT with STMDE	WT BEAM [17]
$\psi_k$ [rad]	0.0071	0.0072
$\psi'_{M,k}$ [rad/m]	0.1916	0.1916
$M_{\omega,i}$ [kNm <sup>2</sup> ]	$-1.0352 \times 10^{-6}$	$-1.0351 \times 10^{-6}$
$M_{Tp,i}$ [kNm]	$7.0 \times 10^{-4}$	$7.0 \times 10^{-4}$
$M_{Tp,k}$ [kNm]	$9.497 \times 10^{-4}$	$4.487 \times 10^{-4}$
$M_{Ts,i}$ [kNm]	$3.0 \times 10^{-4}$	$3.0 \times 10^{-4}$
$M_{Ts,k}$ [kNm]	$5.027 \times 10^{-5}$	$5.512 \times 10^{-4}$

Table 3: Twist angel and internal moments for  $n = 1$ .

The longitudinal distribution of the angle of twist and bimoment, due to non-uniform torsion for the cantilever beam of the hollow-cross-section calculated by the FGM-WT with STMDE is shown in Figure 6. Longitudinal distribution of the angle of twist and the bimoment obtained by the WT BEAM is very close to the ones shown in Fig. 6, and therefore is not depicted separately here.

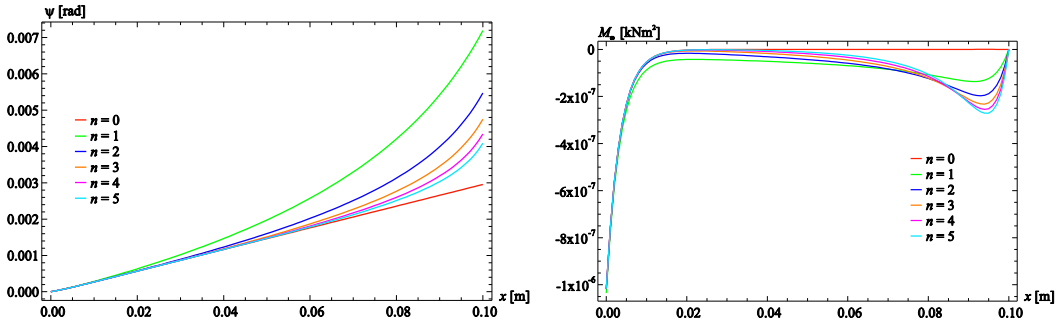


Fig. 6: Angle of the twist,  $\psi$  [rad] and bimoment,  $M_{\omega}$  [kNm<sup>2</sup>].

As presented in Fig. 6, a significant impact of the material properties variation on the twist angle can be observed. On the other hand, the maximal value of the bimoment in the clamped cross-section is not affected significantly by the considered variation of material properties. Some bimoment changes occur at the site of a rapid change in material properties in the beam field. In following, the bimoment normal and torsional shear stress at clamped beam end is calculated (the position of the corners is assumed at the intersection of the center lines of the cross section walls (Fig 7.). The cross-section is loaded by the bimoment

$M_{\omega,i} = -1.0352 \times 10^{-6} \text{ kNm}^2 = -0.0010352 \text{ Nm}^2$  and primary torsional moment  $M_{Tp,i} = 7.0 \times 10^{-4} \text{ kNm} = 0.7 \text{ Nm}$  and secondary torsional moment  $M_{Ts,i} = 3.0 \times 10^{-4} \text{ kNm} = 0.3 \text{ Nm}$ . The bimoment normal stress at the clamped cross-section corners is:  $\sigma_{\omega,i} = \pm \frac{M_{\omega,i}}{I_{\omega}} \omega_R = \pm 24.72 \text{ MPa}$ , where  $|\omega_R| = \frac{hb}{4} \frac{ht - bs}{ht + bs} = 5.74 \text{ mm}^2$  is the warping ordinate at the corners, (Fig. 7a)). The shear stress resulting from the secondary torsional moment is given as:

$$\tau_{s,1} = \frac{M_{Ts}}{t I_{\omega}} S_0 = 3.13 \text{ MPa}, \quad \tau_{s,2} = \frac{M_{Ts}}{s I_{\omega}} S_0 = 6.27 \text{ MPa}, \quad \tau_{s,3} = \frac{M_{Ts}}{t I_{\omega}} S_1 = 10.9 \text{ MPa},$$

$$\tau_{s,4} = \frac{M_{Ts}}{s I_{\omega}} S_2 = -9.40 \text{ MPa}, \quad \text{where } S_0 = \frac{h^2 - b^2}{6\gamma} \omega_R = 3.140258790 \times 10^{(-12)} \text{ m}^4,$$

$$S_1 = S_0 + A_G \frac{\omega_R}{4} = 1.099090576 \times 10^{(-11)} \text{ m}^4, \quad S_2 = S_0 - A_S \frac{\omega_R}{4} = -4.710388182 \times 10^{(-12)} \text{ m}^4,$$

are the auxiliary constants with the web and flange areas

$$A_S = sh = 0.00000546875 \text{ m}^2 \quad \text{and} \quad A_G = tb = 0.00000546875 \text{ m}^2.$$

The shear stress resulting from the primary torsional moment is obtained as:

$$\tau_{p,1} = \frac{M_{Tp} sbh}{I_T (ht + bs)} = 7.31 \text{ MPa}, \quad \tau_{p,2} = \frac{M_{Tp} t bh}{I_T (ht + bs)} = 14.63 \text{ MPa}.$$

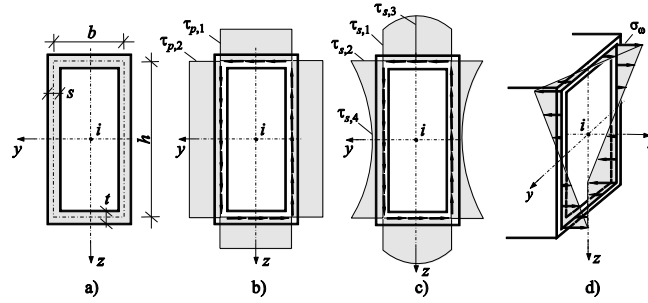


Fig. 7: a) Cross-section, b) primary shear stress, c) secondary shear stress, d) axial stress due to warping.

According to Fig. 7, the total shear stresses are obtained as follow:

$$\tau_1^{total} = \tau_{s,1} + \tau_{p,1} = 10.45 \text{ MPa}, \quad \tau_3^{total} = \tau_{s,3} + \tau_{p,1} = 18.28 \text{ MPa},$$

$$\tau_2^{total} = \tau_{s,2} + \tau_{p,2} = 20.89 \text{ MPa}, \quad \tau_4^{total} = \tau_{s,4} + \tau_{p,2} = 5.22 \text{ MPa}.$$

As can be observed from the above calculations, the magnitude of the normal warping stress in the clamped beam end is comparable to the torsional shear stress magnitude. Distribution of the bimoment normal stress along the beam edges is proportional to the bimoment distribution shown in Fig. 6. To verify the results achieved, numerical analysis of the same beam is done using a very fine mesh of the SOLID186 [16] finite elements. For variation  $n = 1$ , results obtained are shown in Table 4 and Fig. 8. From their comparison, a good match of the achieved results can be found for the angle of twist. By the solid FEM model, the twist angle at the beam free end is calculated from the displacements of the points lying on the hollow cross-section symmetry stress. Some discrepancies occur in both the values and the positions of the maximum normal stress. The SOLID186 solution exhibits maximum normal stresses at points that are offset from the corners of the clamped cross section. This local effect may be caused by an uneven cross sectional wall thickness of the profile and by different base of the beam and solid finite elements modelling. From the detailed stress distribution in Fig. 8 also follows that normal stress in the middle point of the wall thickness at the corners agree well with the results obtained by our FGM-WT beam finite element.

Variables for:	FGM-WT with STMDE	WT BEAM	SOLID186
$\psi_k$ [rad]	0.0072	0.0072	0.0077
$\sigma_{\omega,i}$ [MPa]	24.72	24.71	17.2/20.0

Tab. 4: Results comparison for  $n = 1$ .

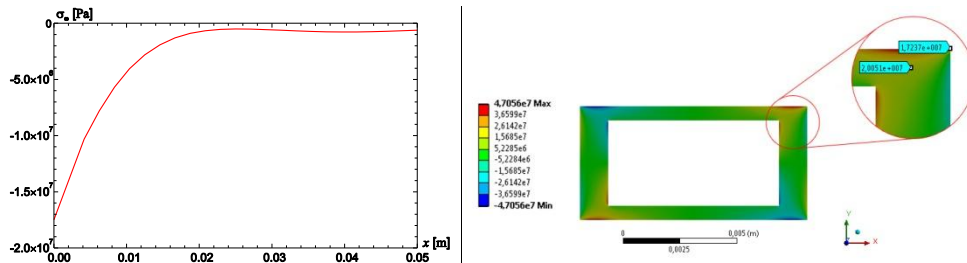


Fig. 8: Distribution of the normal stress along the top edge of the beam and on the clamped cross-sectional area.

## 5 CONCLUSIONS

In the contribution, the 3D FGMs Timoshenko beam finite element with 14x14 stiffness and mass matrices for doubly symmetric open and closed cross-section is presented including warping torsion effect (non-uniform torsion) and the STMDE. A longitudinal continuous variation of effective material properties is considered. This element can be used for modal and elastostatic analysis of FGM beams. The results of the analyzes confirm an acceptable accuracy and very high effectiveness of the new finite element comparing to results obtained by solid FE. FGM beam with continuous spatial variation of material properties can be modelled with only one new FGM-WT beam finite element. This FE is implemented into the 14x14 matrix of the 3D FGM beam finite element that can be used for analysis of the beam structures built of beams with spatially varying material properties.

**Acknowledgement:** The authors gratefully acknowledge financial support by the Slovak Grant Agencies: VEGA No. 1/0102/18 and No. and 1/0081/18.

## REFERENCES

- [1] Murin, J. and Aminbaghai, M. and Hrabovsky, J. and Gogola, R. and Kugler, S. Beam finite element for modal analysis of FGM structures. *Eng. Struct.* (2016) 121: 1 – 18.
- [2] Tsipsis, I.N. and Sapountzakis, and E.J. Generalized warping and distortional analysis of curved beams with isogeometric methods. *Comp. Struct.* (2017) 191: 33 – 50.
- [3] Yoon, K. and Lee, P.S. and Kim, D.N. Geometrically nonlinear finite element analysis of functionally graded 3D beams considering warping effects. *Comp. Struct.* (2015) 132: 1231 – 1247.
- [4] Abrate, S. and Sciuva M. D. Equivalent single theories for composite and sandwich structures: A review. *Comp. Struct.* (2017) 179:482–494.
- [5] Attenshamudin, S.S. and Yuvaraj, M.G. Modeling and analysis of functionally graded sandwich beams: A review. *Mech. of Ad. Mat. and Struct.* (2018) DOI 10.1080/15376494.2018.1447178.
- [6] Murin, J. and Goga, V. and Aminbaghai, M. and Hrabovsky, J. and Sedlar, T. and Mang, H.A. Measurement and modelling of torsional warping free vibrations of beams with rectangular hollow cross-sections. *Eng. Struct.* (2017) 136: 68 – 76.
- [7] Kutis, V. and Murin, J. and Belak, R. and Paulech, J. Beam element with spatial variation of material properties for multiphysics analysis of functionally graded materials. *Comp. and Struct.* (2011) 89: 1192 – 1205.
- [8] Aminbaghai, M and Murin, J. and Balduzzi, G. and Hrabovsky, J. and Hochreiner, G. and Mang, H.A. Second-order torsional warping theory considering the secondary torsion-moment deformation-effect. *Eng. Struct.* (2017) 147: 724 – 739.
- [9] Murin, J. and Goga, V. and Aminbaghai, M. and Hrabovsky, J. and Sedlar, T. and Mang, H.A. Measurement and modelling of torsional warping free vibrations of beams with rectangular hollow cross-sections. *Eng. Struct.* (2017) 136: 68 – 76.
- [10] Murin, J. et all. Torsional warping eigenmodes of FGM beams with longitudinally varying material properties. (2018). Sent for publication.
- [11] Aminbaghai, M. et all. Torsional warping elastostatic analysis of FGM beams with longitudinally varying material properties. (2018). In preparation.
- [12] Aminbaghai M, Murin J, Hrabovsky J, Mang H.A. Torsional warping eigenmodes including the effect of the secondary torsion moment on the deformations. *Eng. Struct.* (2016) 106: 299 – 316.
- [13] ABAQUS/CAE, Version 6.10-1, Dassault Systems Simulia Corp. Providence, RI, USA.
- [14] Przemieniecki, J.S. Theory of matrix structural analysis. McGraw-Hill, NY, 1968.
- [15] Wolfram Mathematica 9.0.1.0, Wolfram Research 2013.
- [16] ANSYS Swanson Analysis System, Inc., 201 Johnson Road, Houston, PA 15342/1300, USA.
- [17] Murin, J. and Aminbaghai, M. and Kutis, V. and Kralovic, V. and Sedlar, T. and Goga, V. and Mang, H.A. A new 3D Timoshenko finite beam element including non-uniform torsion of open and closed cross sections. *Eng. Struct.* (2014) 59: 153 – 160.

## **In Vitro Biaxial Contraction Tests Identify Changes in Arterial Mechanical Properties Not Observed in Isometric Uniaxial Contractions**

Sae-Il Murtada<sup>\*</sup>, Jay Humphrey<sup>\*\*</sup>, Gerhard Holzapfel<sup>\*\*\*</sup>

<sup>\*</sup>Yale University, <sup>\*\*</sup>Yale University, <sup>\*\*\*</sup>Graz University of Technology

### **ABSTRACT**

Multiscale modeling that includes a description of relevant structural components and their interrelations is facilitated to better understand the underlying mechanisms of vascular smooth muscle contractility in intact arteries. Much focus has been given to study the uniaxial length-tension relationship described through changes in the actin and myosin filament overlap for studying characteristics of smooth muscle contractility even though this experimental arrangement does not mimic the in vivo vascular geometry or loading. In contrast, biaxial contraction of an inflated and axially extended vessel provides considerable information, both passive and active, under realistic conditions. Filament lattice spacing has also been reported to have a significant effect in muscle contractility (1), but a clear explanation of its influence has not yet been given. Few investigations have compared these two in vitro approaches directly, namely how their results overlap, how they differ, and if they provide unique complementary information. We present a multiscale mathematical model of arterial contractility accounting for structural and functional constituents at molecular, cellular, and tissue levels. The artery is assumed to be a thick-walled incompressible cylinder described by an anisotropic model of the extracellular matrix and novel model of smooth muscle contractility. The latter includes a three-dimensional structural sensitivity to deformation, including muscle filament overlap and filament lattice spacing. The overall model was able to capture both uniaxial (2) and biaxial (3) experimental contraction data, which was not possible when accounting for filament overlap alone. The model was also used to conduct a parameter sensitivity study that reveals that uniaxial contraction tests are not as efficient as biaxial tests for identifying changes in vascular smooth muscle contractility. References 1. C.D. Williams, M.K. Salcedo, T.C. Irving, M. Regnier, T.L. Daniel, The length-tension curve in muscle depends on lattice spacing, 2013, Proc Biol Sci. 280:20130697. 2. S.-I. Murtada, S. Lewin, A. Arner, J.D. Humphrey. Adaptation of active tone in the mouse descending thoracic aorta under acute changes in loading, 2016, Biomech Model Mechanobiol 15:579–592. 3. S.-I. Murtada, J Ferruzzi, H. Yanagisawa, J.D. Humphrey. Reduced biaxial contractility in the descending thoracic aorta of fibulin-5 deficient mice, 2016, J Biomech Eng 138:051008

## **Modeling Texture Inhomogeneity during Accumulative Angular Drawing Process of Ti-6Al-4V**

Krzysztof Muszka<sup>\*</sup>, Lukasz Madej<sup>\*\*</sup>, Janusz Majta<sup>\*\*\*</sup>, Jakub Kawalko<sup>\*\*\*\*</sup>, Irene Beyerlein<sup>\*\*\*\*\*</sup>,  
Sven Vogel<sup>\*\*\*\*\*</sup>

<sup>\*</sup>AGH University of Science and Technology, <sup>\*\*</sup>AGH University of Science and Technology, <sup>\*\*\*</sup>AGH University of Science and Technology, <sup>\*\*\*\*</sup>AGH University of Science and Technology, <sup>\*\*\*\*\*</sup>University of California Santa Barbara, <sup>\*\*\*\*\*</sup>Los Alamos National Laboratory

### **ABSTRACT**

In the present work, initial results regarding self-consistent computer model for prediction of texture evolution during Accumulative Angular Drawing process of Ti-6Al-4V will be presented. AAD process is recently developed method of Severe Plastic Deformation that allows for production of drawn wires with controlled inhomogeneity of microstructure. It introduces controlled strain path changes that activate additional deformation mechanisms – compared to conventional wire drawing processes. Apart from reduction of the area, bending, torsion and burnishing mechanisms act on the drawn wire. This way, it is possible to accumulate high deformation energy and deform materials that are characterized by low number of possible slip planes and hence limited ductility. Due to a number of process parameters that are characteristic for AAD process, computer modeling offers a robust way to optimize the microstructure and properties of the deformed wires. In the current work, model assumptions and initial results will be presented and compared with microstructural data.

## **Error Representation and Space-Time Goal-Oriented Adaptivity for the Advection-Diffusion Equation Employing Explicit Runge-Kutta Methods**

Judit Muñoz-Matute<sup>\*</sup>, Victor M. Calo<sup>\*\*</sup>, David Pardo<sup>\*\*\*</sup>, Elisabete Alberdi<sup>\*\*\*\*</sup>

<sup>\*</sup>University of the Basque Country (UPV/EHU), Leioa, Spain, <sup>\*\*</sup>Applied Geology, Curtin University, Perth, Australia,  
<sup>\*\*\*</sup>University of the Basque Country (UPV/EHU), Leioa, Spain, <sup>\*\*\*\*</sup>University of the Basque Country (UPV/EHU),  
Leioa, Spain

### **ABSTRACT**

In goal-oriented adaptivity for space-time problems, it is crucial to represent the error in the quantity of interest as an integral over the whole space-time domain. In that way, we can express the error in the quantity of interest as a sum of local element contributions, and perform the adaptive process. A full space-time variational formulation allows such integral representation [2]. Many authors employ implicit methods in time to perform goal-oriented adaptivity [1], like Backward Euler or Crank-Nicholson, as it is well known that these methods present variational structure [3]. However, the variational formulation of explicit methods in time for partial differential equations remains elusive. In this work, we build a Petrov-Galerkin formulation for the advection-diffusion equation that is equivalent to the Forward Euler method in time. Then, we derive an error representation and an explicit goal-oriented adaptive algorithm, enabling dynamic meshes in space. Some numerical results are provided in 1D to illustrate the proposed explicit algorithm. Finally, we provide an overview of how to construct higher order Runge-Kutta methods using a variational formulation and describe a similar goal-oriented procedure. References: [1] W. Bangerth, M. Geiger, and R. Rannacher. Adaptive Galerkin finite element methods for the wave equation. *Computational Methods in Applied Mathematics*, 10(1):3–48, 2010. [2] P. Díez and G. Calderón. Goal-oriented error estimation for transient parabolic problems. *Computational Mechanics*, 39(5):631–646, 2007. [3] D. Estep and A. Stuart. The dynamical behavior of the discontinuous Galerkin method and related difference schemes. *Mathematics of Computation*, 71(239):1075–1103, 2002.

## Patient-specific Finite Element Models of Normal Pregnancy Derived from Time-course Maternal Ultrasound Scans

Kristin Myers<sup>\*</sup>, Andrea Westervelt<sup>\*\*</sup>, Lindsey Carlson<sup>\*\*\*</sup>, Chia-Ling Nhan-Chang<sup>\*\*\*\*</sup>, Joy Vink<sup>\*\*\*\*\*</sup>, Timothy Hall<sup>\*\*\*\*\*</sup>, Helen Feltovich<sup>\*\*\*\*\*</sup>

<sup>\*</sup>Columbia University, <sup>\*\*</sup>Columbia University, <sup>\*\*\*</sup>University of Wisconsin, <sup>\*\*\*\*</sup>Columbia University Medical Center, <sup>\*\*\*\*\*</sup>Columbia University Medical Center, <sup>\*\*\*\*\*</sup>University of Wisconsin, <sup>\*\*\*\*\*</sup>University of Wisconsin

### ABSTRACT

Preterm birth (PTB) is a global health dilemma. It is the leading cause of childhood death worldwide, affecting 1 in 10 babies. In 2016, the PTB rate in the U.S. rose for the second consecutive year. A likely reason for this is misdirected investigation due to combining the multiple phenotypes of PTB into a single diagnosis. Ultrasound measurement of cervical length (CL) is the current standard-of-care for PTB prediction, presumably because it provides information about cervical structural integrity. While this has a strong negative predictive value (0.97), its positive predictive value is weak (0.23) [1]. We hypothesize this is partially because CL provides a 1-dimensional metric for a complex 3-dimensional structure. The overall objective of our research is to develop etiology- and patient-specific models that describe the biomechanical interrelationships of the uterus, cervix, and fetal membranes during pregnancy. In this study, we investigate the patient-specific mechanical environment of a cohort of women at low-risk for PTB to establish normal maternal mechanics. Specifically, we measure maternal anatomy longitudinally throughout pregnancy using multiple ultrasound measurements and characterize tissue stress and stretch using Finite Element Analysis (FEA). For this ongoing study, we recruited 21 multiparous and 9 nulliparous patients. Each has received transabdominal and transvaginal ultrasound exams at four pregnancy timepoints (8-12 weeks, 14-18 weeks, 22-24 weeks, and 32-34 weeks). At each visit, ultrasound images of the uterus and cervix are acquired (Siemens S3000) from both supine and standing orientations. From these, maternal anatomical parameters (uterine diameters, uterine wall thickness, cervical length and diameter, angle between the cervical canal and the anterior lower uterine segment, and the posterior location of the cervix) are measured. 3D computer models of the first timepoint of each patient's anatomy are built and meshed in Trelis 16.1 (csimsoft) using a custom parameterized script. Anatomical boundary conditions and material properties [2] are prescribed and gestation-matched intrauterine pressure [3] applied to the inner fetal membrane surface using FEBio 2.6.4 (febio.org). Material parameters are remodeled so FEA predictions of anatomy shape of later pregnancy timepoints match the experimental data. The uterine, fetal membranes, and cervical tissue stress and stretch is characterized and compared between patients at gestation-matched time points to reveal the common load-bearing and tissue remodeling features of maternal anatomy throughout normal pregnancy. References [1] van Baaren GJ, et al. *ObGyn.* 2014;123:1185–1192. [2] Westervelt AR, et al. *ASME. J Biomech Eng.* 2017;139(5). [3] Fisk, et al. (1992). *BJOG*, 99: 18–22.

## PHASE FIELD BASED MULTIMATERIAL TOPOLOGY OPTIMIZATION

ANDRZEJ M. MYSLINSKI<sup>1,2</sup>

<sup>1</sup> Systems Research Institute,  
ul. Newelska 6, 01-447 Warsaw, Poland,  
e-mail: andrzej.myslinski@ibspan.waw.pl

<sup>2</sup> Warsaw University of Technology,  
Faculty of Manufacturing Engineering, ul. Narbutta 85  
02-524 Warsaw, Poland  
e-mail: a.myslinski@wip.pw.edu.pl

**Key words:** topology optimization, unilateral contact, Tresca friction, phase field regularization, operator splitting method.

**Abstract.** *The paper is concerned with the robust numerical method to solve numerically the multimaterial topology optimization problems for bodies in unilateral contact. This contact phenomenon with Tresca friction is governed by the elliptic boundary value problem with inequality boundary conditions. The body is assumed to consist from more than two distinct isotropic elastic materials. The materials distribution function is chosen as the design variable. The structural optimization problem consists in finding such topology of the domain occupied by the body that the normal contact stress along the boundary of the body is minimized. The original cost functional is regularized using the multiphase volume constrained Ginzburg-Landau energy functional rather than the perimeter functional. The first order necessary optimality condition is recalled and used to formulate the generalized gradient flow equations of Allen-Cahn type. The optimal topology is obtained as the steady state of the phase transition governed by the generalized Allen-Cahn equation. The optimization problem is solved numerically using the operator splitting approach combined with the alternating gradient projection method. Numerical examples are reported to validate the applicability of the proposed approach.*

## 1 INTRODUCTION

The goal of the multimaterial structural topology optimization is to find the optimal distribution of several elastic materials in a given design domain to minimize a functional describing the mechanical or the thermal properties of the structure or its cost [1,2]. The loaded structure is assumed to satisfy the volume or mass constraints imposed on it. In recent years multiple phases topology optimization problems have become subject of the growing interest [3,4,5,6,7]. The use of multiple number of phases during the design of engineering structures opens a new opportunities in the design of smart and advanced structures in material science and/or industry. In contrast to single material design the use of multiple number of materials extends the design space and may lead to better design solutions. Different aspects of the multimaterial structural optimization, including both analytical and numerical, are subject of intensive research (see references in [3,4,5,6,7]). Many methods including the homogenization method [1], the Solid Isotropic Material Penalization (SIMP) method [2], topological derivative method [8] or different methods based on the level set approach [9,10] or phase field approach [11,12,13] successful in single material optimization, have been extended to deal with the multimaterial optimization. The extension of these methods faces several challenges. A crucial issue in the solution of the multimaterial optimization problems is the lack of physically based parametrization of the phases mixture [3,7]. Although in the literature are proposed different material interpolation schemes, in general, they may influence the optimization path in terms of the computational efficiency and the final design. The level set methods can eliminate the need of the material interpolation schemes provided that interfaces are actually tracked explicitly [3]. Among others, in [3] a multimaterial topology optimization problem for the plane elasticity system has been solved using the level set method. The elasticity tensor has been smeared out using the signed distance function. In [7] similar optimization problem has been solved numerically using a generalized Allen–Cahn equation.

The paper is concerned with the structural topology optimization of unilateral contact problems with Tresca friction between the surfaces of the elastic bodies [14] and extends the results from [6]. The optimization problem consists in finding such topology of the domain occupied by the body that the normal contact stress along the boundary of the body is minimized. In literature [10,12] this problem usually is considered as two-phase material optimization problem with voids treated as one of the materials. In the paper the domain occupied by the body is assumed to consist from several elastic materials rather than two materials. Material fraction function is a variable subject to optimization. The regularization of the objective functional by the multiphase volume constrained Ginzburg-Landau energy functional is used. The derivative formula of the cost functional with respect to the material fraction function is calculated and is employed to formulate a necessary optimality condition for the topology optimization problem. The cost functional derivative is also used to formulate a gradient flow equation for this functio-

nal in the form of the generalized Allen–Cahn equation governing the evolution of the material phases. The optimal topology is obtained as a steady state solution to this equation. Two step operator splitting approach [7] is used to solve this gradient flow equation. Finite difference and finite element methods are used as the approximation methods. Numerical examples are reported and discussed.

## 2 PROBLEM FORMULATION

Consider deformations of an elastic body occupying two–dimensional bounded domain  $\Omega$  with the smooth boundary  $\Gamma$  (see Fig. 1). The body is subject to body forces  $f(x) = (f_1(x), f_2(x))$ ,  $x \in \Omega$ . Moreover, the surface tractions  $p(x) = (p_1(x), p_2(x))$ ,  $x \in \Gamma$ , are applied to a portion  $\Gamma_1$  of the boundary  $\Gamma$ . The body is clamped along the portion  $\Gamma_0$  of the boundary  $\Gamma$  and the contact conditions are prescribed on the portion  $\Gamma_2$ . Parts  $\Gamma_0, \Gamma_1, \Gamma_2$  of the boundary  $\Gamma$  satisfy:  $\Gamma_i \cap \Gamma_j = \emptyset$ ,  $i \neq j$ ,  $i, j = 0, 1, 2$ ,  $\Gamma = \bar{\Gamma}_0 \cup \bar{\Gamma}_1 \cup \bar{\Gamma}_2$ .

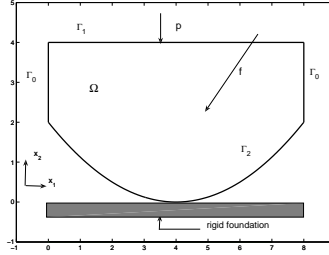


Figure 1: Elastic body occupying domain  $\Omega$  in unilateral contact with the foundation.

The domain  $\Omega$  is assumed to be occupied by  $s \geq 2$  distinct isotropic elastic materials. Each material is characterized by Young modulus. The voids are considered as one of the phases, i.e., as a weak material characterized by low value of Young modulus [1]. The materials distribution is described by a phase field vector  $\rho = \{\rho_m\}_{m=1}^s$  where the local fraction field  $\rho_m = \rho_m(x) : \Omega \rightarrow R$ ,  $m = 1, \dots, s$ , corresponds to the contributing phase. The phase field approach allows for a certain mixing between different materials. This mixing is restricted only to a small interfacial region. In order to ensure that the phase field vector describes the fractions the following pointwise bound constraints called in material science the Gibbs simplex [4,7,8] are imposed on every  $\rho_m$

$$\alpha_m \leq \rho_m \leq \beta_m, \text{ for } m = 1, \dots, s, \text{ and } \sum_{m=1}^s \rho_m = 1, \quad (1)$$

where the constants  $0 \leq \alpha_m \leq \beta_m \leq 1$  are given and the summation operator is understood componentwise. The second condition in (1) ensures that no overlap and gap of fractions are

allowed in the expected optimal domain. Moreover the total spatial amount of material fractions satisfies

$$\int_{\Omega} \rho_m(x) dx = w_m |\Omega|, \quad 0 \leq w_m \leq 1, \quad \text{for } m = 1, \dots, s, \quad \text{and} \quad \sum_{m=1}^s w_m = 1. \quad (2)$$

The parameters  $w_m$  are user defined and  $|\Omega|$  denotes the volume of the domain  $\Omega$ . From the equality (1) it results that  $\rho_s = 1 - \sum_{m=1}^{s-1} \rho_m$  and the fraction  $\rho_s$  may be removed from the set of the design functions. Therefore from now on the unknown phase field vector  $\rho$  is redefined as  $\rho = \{\rho_m\}_{m=1}^{s-1}$ . Due to the simplicity and robustness the SIMP material interpolation model [3,7] is used. Following this model the elastic tensor  $\mathcal{A}(\rho) = \{a_{ijkl}(\rho)\}_{i,j,k,l=1}^2$  of the material body is assumed to be a function depending on the fraction function  $\rho$ :

$$\mathcal{A}(\rho) = \sum_{m=1}^s g(\rho_m) \mathcal{A}_m = \sum_{m=1}^{s-1} g(\rho_m) \mathcal{A}_m + g(1 - \sum_{m=1}^{s-1} \rho_m) \mathcal{A}_s, \quad (3)$$

with  $g(\rho_m) = \rho_m^3$ . The constant stiffness tensor  $\mathcal{A}_m = \{\tilde{a}_{ijkl}^m\}_{i,j,k,l=1}^2$  characterizes the  $m$ -th elastic material of the body. For detailed discussion of the interpolation of the material elasticity tensor see [3,7,16]. It is assumed, that elements  $a_{ijkl}$  and  $\tilde{a}_{ijkl}^m(x)$ ,  $i, j, k, l = 1, 2$ ,  $m = 1, \dots, s$ , of the elasticity tensors  $\mathcal{A}$  and  $\mathcal{A}_m$ , respectively, satisfy [14,15] usual symmetry, boundedness and ellipticity conditions. Denote by  $u = (u_1, u_2)$ ,  $u = u(x)$ ,  $x \in \Omega$ , the displacement of the body and by  $\sigma(x) = \{\sigma_{ij}(u(x))\}$ ,  $i, j = 1, 2$ , the stress field in the body. Consider elastic bodies obeying Hooke's law, i.e., for  $x \in \Omega$  and  $i, j, k, l = 1, 2$ ,

$$\sigma_{ij}(u(x)) = a_{ijkl}(\rho) e_{kl}(u(x)), \quad e_{kl}(u(x)) \stackrel{\text{def}}{=} \frac{1}{2}(u_{k,l}(x) + u_{l,k}(x)), \quad (4)$$

where  $u_{k,l}(x) = \frac{\partial u_k(x)}{\partial x_l}$ . We use here and throughout the paper the summation convention over repeated indices [14]. The stress field  $\sigma$  satisfies the system of equations in the domain  $\Omega$  [14]

$$-\sigma_{ij}(x),_j = f_i(x) \quad \sigma_{ij}(x),_j = \frac{\partial \sigma_{ij}(x)}{\partial x_j}, \quad x \in \Omega, \quad i, j = 1, 2. \quad (5)$$

The following boundary conditions are imposed on the boundary  $\partial\Omega$

$$u_i(x) = 0 \quad \text{on } \Gamma_0, \quad \sigma_{ij}(x)n_j = p_i \quad \text{on } \Gamma_1, \quad i, j = 1, 2, \quad (6)$$

$$(u_N + v) \leq 0, \quad \sigma_N \leq 0, \quad (u_N + v)\sigma_N = 0 \quad \text{on } \Gamma_2, \quad (7)$$

$$|\sigma_T| \leq 1, \quad u_T \sigma_T + |u_T| = 0 \quad \text{on } \Gamma_2, \quad (8)$$

where  $n = (n_1, n_2)$  is the unit outward versor to the boundary  $\Gamma$ . Here  $u_N = u_i n_i$  and  $\sigma_N = \sigma_{ij} n_i n_j$ ,  $i, j = 1, 2$ , represent [14] the normal components of displacement  $u$  and stress  $\sigma$ , respectively. The tangential components of displacement  $u$  and stress  $\sigma$  are given [14] by  $(u_T)_i = u_i - u_N n_i$  and  $(\sigma_T)_i = \sigma_{ij} n_j - \sigma_N n_i$ ,  $i, j = 1, 2$ , respectively.  $|u_T|$  denotes the Euclidean norm in  $R^2$  of the tangent vector  $u_T$ . A gap between the bodies is described by a given function  $v$ .

## 2.1 Phase Field Based Topology Optimization Problem

Before formulating a structural optimization problem for the system (5)-(8) let us introduce a set  $U_{ad}^{\rho}$  of the admissible suitable regular fraction functions:

$$U_{ad}^{\rho} = \left\{ \rho : 1 - \beta_s \leq \sum_{m=1}^{s-1} \rho_m \leq 1 - \alpha_s, \right. \\ \left. \alpha_m \leq \rho_m \leq \beta_m, \int_{\Omega} \rho_m dx = w_m |\Omega| \text{ for } m = 1, \dots, s-1 \right\}. \quad (9)$$

The set  $U_{ad}^{\rho} \subset H^1(\Omega; R^{s-1})$  is assumed to be nonempty. The aim of the structural optimization problem for the bodies in unilateral contact is to reduce the normal contact stress responsible for wear, vibrations, fatigue of the contacting surfaces as well as for a generated noise. The structural optimization problem with normal contact stress functional is difficult to analyze it and to solve it numerically. Therefore following [10] we shall use the cost functional  $J_{\eta} : H^1(\Omega) \rightarrow R$  approximating the normal contact stress on the contact boundary  $\Gamma_2$

$$J_{\eta}(u(\rho)) = \int_{\Gamma_2} \sigma_N(u(\rho)) \eta_N(x) ds, \quad (10)$$

depending on a given auxiliary bounded function  $\eta(x) \in M^{st}$ . The set  $M^{st}$  is given by

$$M^{st} = \{ \eta = (\eta_1, \eta_2) \in H^1(\Omega; R^2) : \eta_i \leq 0 \text{ on } \Omega, i = 1, 2, \|\eta\|_{H^1(\Omega; R^2)} \leq 1 \},$$

where functions  $\sigma_N$  and  $\eta_N$  are the normal components of the stress field  $\sigma$  corresponding to a solution  $u(\rho)$  satisfying the system (5)-(8) and the function  $\eta$ , respectively. The optimization problem consisting in finding such  $\rho \in U_{ad}^{\rho}$  to minimize the functional  $J_{\eta}(u(\rho))$  in general has no solutions [1,4,7,14,16]. In order to ensure the existence of optimal solutions let us regularize the cost functional (10) by adding to it a regularizing term  $E(\rho) : U_{ad}^{\rho} \rightarrow R$  rather than the standard perimeter term [1,16]

$$J(\rho, u(\rho)) = J_{\eta}(u(\rho)) + E(\rho). \quad (11)$$

The Ginzburg-Landau free energy functional  $E(\rho)$  is expressed as [7,16]

$$E(\rho) = \sum_{m=1}^{s-1} \int_{\Omega} \psi(\rho_m) d\Omega, \quad \psi(\rho_m) = \frac{\gamma \varepsilon}{2} |\nabla \rho_m|^2 + \frac{\gamma}{\varepsilon} \psi_B(\rho_m), \quad (12)$$

where  $\varepsilon > 0$  is a real constant governing the width of the interfaces,  $\gamma > 0$  is a real parameter

related to the interfacial energy density. Moreover  $\nabla \rho_m \cdot n = 0$  on  $\Gamma$  for each  $m$ . The function  $\psi_B(\rho_m) = \rho_m^2(1 - \rho_m)^2$  is a double-well potential [22] which characterizes the concentration of the material phases [7]. The structural optimization problem for the system (5)-(8) takes the form: *find*  $\rho^* \in U_{ad}^\rho$  *such that*

$$J(\rho^*, u^*) = \min_{\rho \in U_{ad}^\rho} J(\rho, u(\rho)), \quad (13)$$

where  $u^* = u(\rho^*)$  denotes a solution to the state system (5)-(8) depending on  $\rho^*$  and the set  $U_{ad}^\rho$  is given by (9). The existence of an optimal solution  $\rho^* \in U_{ad}^\rho$  to the problem (13) follows by classical arguments (see [5]). Remark due to (12) the problem (13) is dependent on the interface width parameter  $\varepsilon$ .

### 3 NECESSARY OPTIMALITY CONDITION

The Lagrangian approach combined with adjoint state approach has been applied to compute the derivative of the cost functional (11) with respect to the function  $\rho$ . This derivative is determined for all  $\zeta \in H^1(\Omega; \mathbb{R}^{s-1})$  and  $i, j, k, l = 1, 2$  as

$$\begin{aligned} \int_{\Omega} \frac{\partial J}{\partial \rho}(\rho, u) \zeta dx &= \int_{\Omega} \frac{\partial L}{\partial \rho}(\rho, u, \lambda, p^a, q^a) \zeta dx = \sum_{m=1}^{s-1} \int_{\Omega} [\gamma \varepsilon \nabla \rho_m \cdot \nabla \zeta_m + \\ &\frac{\gamma}{\varepsilon} \psi'_B(\rho_m) \zeta_m] dx + \int_{\Omega} [a'_{ijkl}(\rho_m) e_{ij}(u) e_{kl}(p^a + \eta) - f_i(p_i^a + \eta_i)] \zeta_m dx. \end{aligned} \quad (14)$$

where  $(p^a, q^a)$  denotes the adjoint state. For details see [12]. From (1), (3) and (12) it results the derivatives of the tensor element  $a_{ijkl}(\rho_m)$  and the function  $\psi_B(\rho_m)$  with respect to  $\rho_m$  are equal to  $a'_{ijkl}(\rho) = 3\rho_m^2 \tilde{a}_{ijkl}^m - 3\rho_s^2 \tilde{a}_{ijkl}^s$  and  $\psi'_B(\rho_m) = 4\rho_m^3 - 6\rho_m^2 + 2\rho_m$ , respectively. Using (14) the necessary optimality condition to the optimization problem (13) takes the form [1,15]:

Let  $U_{ad}^\rho$  be a nonempty closed convex subset of  $H^1(\Omega; \mathbb{R}^{s-1})$  and  $\rho^* \in U_{ad}^\rho$  be an optimal solution to the structural optimization problem (13). Then

$$\int_{\Omega} \frac{\partial J}{\partial \rho}(\rho^*, u^*)(\rho - \rho^*) dx \geq 0 \quad \forall \rho \in U_{ad}^\rho. \quad (15)$$

The functions  $(u^*, \lambda^*)$  and  $(p^{a^*}, q^{a^*})$  in the derivative formula (14) denote the solutions to the state system (5)-(8) and the adjoint systems for  $\rho = \rho^*$ , respectively. Using the orthogonal projection operator  $P_{U_{ad}^\rho} : L^2(\Omega; \mathbb{R}^{s-1}) \rightarrow U_{ad}^\rho$  from  $L^2(\Omega; \mathbb{R}^{s-1})$  on the set  $U_{ad}^\rho$  condition (15) can be written [7] in the form:

if  $\rho^* \in U_{ad}^\rho$  is an optimal solution to the structural optimization problem (13), then for  $\mu \in R$  and  $\mu > 0$

$$P_{U_{ad}^\rho}[\rho^* - \mu \frac{\partial J(\rho^*, u^*)}{\partial \rho}] - \rho^* = 0. \quad (16)$$

The parameter  $\varepsilon$  governing the width of the interface zone between the phases in the model (11)-(13) and the optimality systems (15)-(16) is assumed to be fixed. In a case when this parameter tends to zero, i.e.,  $\varepsilon \rightarrow 0$  from (11)-(13) it follows this parameter may be also controlled by the parameter  $\gamma$ . As the interfaces between the material phases subdomains shrink to the subdomain boundaries the phase field model evolves [7] into sharp interface model characterized by boundaries dividing a design domain into subdomains. The sharp interface model corresponds to the level set approach [4,5,6,13]. The transition from phase field model to the sharp interface model is equivalent to the investigation of the convergence of the solutions to the phase field model as the interface width parameter tends to zero. This convergence for the contact problems has been investigated in [5]. Using the theory of bounded variations spaces and the notion of  $\Gamma$  convergence, for the interface width parameter tending to zero the  $\Gamma$ -convergence in the space  $L^1$  of the sequence of phase field regularized functionals to the sharp interface functional regularized using the perimeter term has been shown in [5].

### 3.1 Generalized Allen–Cahn Gradient Flow Equation

Recall [16] the structural optimization problem (13) can be considered as a phase transition setting problem consisting in such evolution of the phases to minimize the cost functional (11) with respect to the initial configuration. In order to describe the evolution of phases in time let us assume that the phase field vector  $\rho$  depends not only on  $x \in \Omega$  but also on time variable  $t \in [0, T]$ ,  $T > 0$  is a given constant, i.e.,  $\rho = \rho(x, t) = \{\rho_m(x, t)\}_{m=1}^{s-1}$ . The variable  $t$  may be interpreted as an artificial time or iteration number in the computational algorithm [7,16]. Using the right hand side of (16) let us formulate the constrained gradient flow equation of Allen–Cahn type [4,7,8,14,22,23] for the cost functional (11): *find function  $\rho \in U_{ad}^\rho$  satisfying the initial boundary value problem:*

$$\frac{\partial \rho}{\partial t} = -P_{U_{ad}^\rho}[\rho - \mu \frac{\partial J(\rho, u)}{\partial \rho}] + \rho \quad \text{in } \Omega, \forall t \in [0, T], \quad (17)$$

$$\nabla \rho \cdot n = 0 \quad \text{on } \partial \Omega, \forall t \in [0, T], \quad (18)$$

$$\rho(0, x) = \rho_0(x) \quad \text{in } \Omega, t = 0, \quad (19)$$

with  $\rho_0(x) = \{\rho_{0m}(x)\}_{m=1}^{s-1}$  denoting a given  $H^1(\Omega; R^{s-1})$  regular function. For such  $\rho_0$  the system (17)-(19) possesses a solution  $\rho$  (see [4,8]). The stationary solutions of (17)-(19) fulfill the first order necessary optimality conditions (15) or (16) for the problem (13) [4,8]. For  $\frac{\partial \rho}{\partial t} = 0$  the right hand side of the equation (17) vanishes and  $\rho(x, t) = \rho^*(x, t)$  is an optimal solution to the problem (13).

For the sake of numerical calculations we reformulate the initial boundary value problem (17)-(19) using the operator splitting approach [7]. Remark, the cost functional (11) may be represented as a sum of two functionals, i.e.,

$$J(\rho, u) = J_1(\rho, u) + J_2(\rho) \quad (20)$$

given by

$$J_1(\rho, u) = J_\eta(u(\rho)) + \sum_{m=1}^{s-1} \int_{\Omega} \frac{\gamma}{\varepsilon} \psi_B(\rho_m) d\Omega, J_2(\rho) = \sum_{m=1}^{s-1} \int_{\Omega} \frac{\gamma \varepsilon}{2} |\nabla \rho_m|^2 d\Omega.$$

The derivatives of these functionals result from formula (14). Assume the time interval  $[0, T]$  is divided into  $N$  subintervals with stepsize  $\Delta t = t_{k+1} - t_k$ ,  $k = 1, \dots, N$  and  $\rho_k = \rho(t_k)$  is known. The design variable  $\rho_{k+1}$  at the next time step  $t_{k+1}$  is calculated in two substeps. First the trial value  $\tilde{\rho}$  is calculated from the gradient flow equation (17) for the functional  $J_1$  only. Next this solution is updated to ensure its  $H^1(\Omega)$  regularity [4] by solving the gradient flow equation (17) for the functional  $J_2$  only with the boundary condition (18), i.e.,

$$\frac{\partial \tilde{\rho}}{\partial t} = -P_{U_{ad}^\rho} \left[ \tilde{\rho} - \frac{\partial J_1(\tilde{\rho}, u)}{\partial \rho} \right] + \tilde{\rho}, \quad \tilde{\rho}(t_k) = \rho_k, \quad t_k < t \leq t_{k+1}. \quad (21)$$

$$\frac{\partial \rho}{\partial t} = -\frac{\partial J_2(\rho)}{\partial \rho}, \quad \rho(t_k) = \tilde{\rho}_{k+1}, \quad t_k < t \leq t_{k+1}. \quad (22)$$

## 4 NUMERICAL RESULTS

The topology optimization problem (13) has been discretized and solved numerically. Time derivatives are approximated by the forward finite difference. Piecewise constant and piecewise linear finite element method is used as discretization method in space variables. The derivative of the double well potential is linearized with respect to  $\rho_m$ . Primal-dual active set method [4,7,12] has been used to solve the state system (5)-(8) and the adjoint system. The initial boundary value problem (17)-(19) has been solved in two steps according to scheme (21)-(22). The algorithms are programmed in Matlab environment. As an example a body occupying 2D domain

$$\Omega = \{(x_1, x_2) \in \mathbb{R}^2 : 0 \leq x_1 \leq 8 \wedge 0 < v(x_1) \leq x_2 \leq 4\}, \quad (23)$$

is considered. The boundary  $\Gamma$  of the domain  $\Omega$  is divided into three disjoint pieces

$\Gamma_0 = \{(x_1, x_2) \in \mathbb{R}^2 : x_1 = 0, 8 \wedge 0 < v(x_1) \leq x_2 \leq 4\}$ ,  $\Gamma_1 = \{(x_1, x_2) \in \mathbb{R}^2 : 0 \leq x_1 \leq 8 \wedge x_2 = 4\}$ ,  $\Gamma_2 = \{(x_1, x_2) \in \mathbb{R}^2 : 0 \leq x_1 \leq 8 \wedge v(x_1) = x_2\}$ . The domain  $\Omega$  and the boundary  $\Gamma_2$  depend on the function  $v(x_1) = 0.125 \cdot (x_1 - 4)^2$ . Domain  $\Omega$  is filled with  $s = 3$  elastic materials. The Poisson's ratio of each material is  $\nu = .3$ . The Young's moduli of materials are:  $E_1 = 6 \cdot E_0$ ,  $E_2 = 3 \cdot E_0$  and  $E_3 = E_0$ ,  $E_0 = 2.1 \cdot 10^{11}$  Pa. The parameters  $w_1, w_2, w_3$  are equal to .25, .5 and .25 respectively. As an initial design  $\rho_0$  a feasible design with the uniform material distribution has been taken. The body is loaded by the boundary traction  $p_1 = 0$ ,  $p_2 = -5.6 \cdot 10^6$  N along the boundary  $\Gamma_1$ , the body forces  $f_i = 0$ ,  $i = 1, 2$ . The auxiliary function  $\eta$  is selected as a piecewise linear on  $\Omega$  and is approximated by a piecewise linear function. The domain  $\Omega$  is divided into  $80 \times 40$  grid. The parameters  $\varepsilon$  and  $\gamma$  are equal to the mesh size and to 0.5, respectively. The total number of iterations  $k_{max}$  in the optimization algorithm has been set to 90. It is approximately equivalent to final time  $T = 125$  s. Fig. 2 presents the optimal topology domain obtained by solving structural optimization problem (13) using the necessary optimality condition (17)-(19). The areas with the weak phases appear in the central part of the body and near the fixed edges. The areas with the strong phases appear close to the contact zone and along the edges.

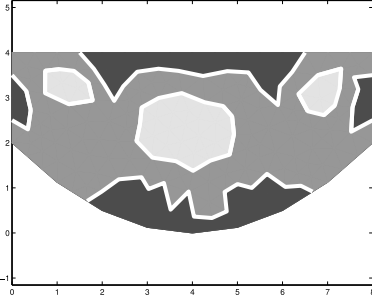


Figure 2: Optimal material distribution in domain  $\Omega^*$ .

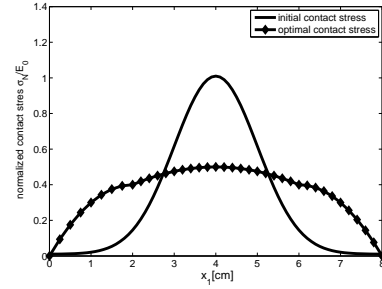


Figure 3: Initial and optimal normal contact stress.

The rest of the domain is covered with the intermediate phase. The obtained normal contact stress for the optimal topology is almost constant along the contact boundary and has been significantly reduced comparing to the initial one (see Fig. 3). The cost functional value decreases almost monotonically when the number of iterations increases. At the beginning this decrease is significant and finally the cost functional value is almost steady. Similarly, after a few initial iterations the gradient of the cost functional also almost monotonically decreases to reach the steady state.

## 5 CONCLUSIONS

- The obtained numerical results indicate that the optimal topologies are qualitatively comparable to the results reported in other phase-field topology optimization methods.
- Since the optimization problem is non-convex it has possibly many local solutions dependent on initial estimate.
- Gradient flow method employed in  $H^1$  space is more regular and efficient than standard Allen-Cahn approach. The obtained solution depends on the interface width parameter. As this parameter tends to zero the optimal solutions to this optimization problem are expected to converge to optimal solution of the perimeter regularized problem.

## REFERENCES

- [1] Allaire, G. Shape optimization by the homogenization method, Springer, New York, (2001).
- [2] Bendsoe, M.P., Sigmund, O. Topology Optimization: Theory, Methods, and Applications, Springer, Berlin, (2004).
- [3] Allaire, G., Dapogny, C., Delgado, G., Michailidis, G. Multi-phase structural optimization via a level set method, ESAIM - Control Optimisation and Calculus of Variations, (2014)20:576–611.
- [4] Blank, L., Garcke, H., Hecht, C., Rupprecht, Ch. Sharp interface limit for a phase field model in structural optimization, SIAM J. Control Optim., (2016)54:1558–1584.
- [5] Myśliński, A. Multimaterial Topology Optimization of Variational Inequalities, in System Modeling and Optimization, eds. L. Bociu, J.P. Desideri, A. Habbal, IFIP AICT 494, 27 th IFIP TC 7 CSMO, Sophia Antipolis, France, June 29 July 3, 2015, Revised Selected Papers, Springer International Publishing, (2016):380 – 389.
- [6] Myśliński, A. Multimaterial Topology Optimization of Contact Problems Using Allen-Cahn Approach, in Advances in Structural and Multidisciplinary Optimization, Eds: A. Schumacher, T. Vietor, S. Fiebig, K.U. Bletzinger, K. Maute, Springer International Publishing, ISBN 978-3-319-67987-7, (2018):1069 - 1082.

- [7] Tavakoli, R. Multimaterial Topology Optimization by Volume Constrained Allen–Cahn System and Regularized Projected Steepest Descent Method, *Comput. Meth. Appl. Mech. Eng.* (2014)276:534–565.
- [8] Kovtunenکو, V.A., Leugering, G. A Shape-Topological Control Problem for Nonlinear Crack-Defect Interaction: The Antiplane Variational Model, *SIAM Journal on Control and Optimization* (2016)54(3):1329–1351.
- [9] van Dijk, N.P., Maute, K., Langlaar, M., van Keulen, F. Level-set methods for structural topology optimization: a review, *Structural and Multidisciplinary Optimization* (2013) 48:437–472.
- [10] Myśliński, A. Piecewise Constant Level Set Method for Topology Optimization of Unilateral Contact Problems, *Advances in Engineering Software* (2015)80:25–32.
- [11] Burger, M., Stainko, R. Phase-field relaxation of topology optimization with local stress constraints, *SIAM J. Control. Optim.*, (2006)45:1447–1466.
- [12] Myśliński, A., Wróblewski, M. Structural optimization of contact problems using Cahn-Hilliard model, *Computers & Structures*, (2017)180:52–59.
- [13] Penzler, P., Rumpf, M. and Wirth, B. A phase-field model for compliance shape optimization in nonlinear elasticity, *ESAIM: COCV*, (2012)18(1):229–258.
- [14] Haslinger, J., Mäkinen, R. *Introduction to Shape Optimization. Theory, Approximation, and Computation*, SIAM Publications, Philadelphia, (2003).
- [15] Tröltzsch, F. *Optimal control of partial differential equations: Theory, methods and applications*, American Mathematical Society, Graduate Studies in Mathematics 112, Providence, Rhode Island, (2010).
- [16] Dede, L., Boroden, M.J., Hughes, T.J.R. Isogeometric analysis for topology optimization with a phase field model, *Archives of Computational Methods in Engineering*, (2012)19(3):427–465.

## Making Use of Symmetries in the Elastic Inverse Homogenization Problem

Carlos Méndez\*, Juan Manuel Podestá\*\*, Sebastián Toro\*\*\*, Alfredo Huespe\*\*\*\*, Javier Oliver\*\*\*\*\*

\*CIMEC – Universidad Nacional del Litoral, Santa Fe, Argentina., \*\*CIMEC – Universidad Nacional del Litoral, Santa Fe, Argentina., \*\*\*CIMEC – Universidad Nacional del Litoral, Santa Fe, Argentina., \*\*\*\*CIMEC – Universidad Nacional del Litoral, Santa Fe, Argentina., \*\*\*\*\*CIMNE - Universitat Politècnica de Catalunya, Barcelona, Spain.

### ABSTRACT

It is a known fact that even the highest symmetry (isotropic) of the elastic tensor can be achieved through topology design using a unit cell with arbitrary shape whose material distribution does not present any symmetry (think about a polycrystal or an amorphous material). However, it is also well known that an adequate choice of the unit cell and the symmetries imposed in the design process can significantly facilitate the finding of certain classes of composites (like Vigdergauz microstructures or new ones proposed by Sigmund [1]). In this work, we make a comprehensive analysis of the connection between the symmetry of the material distribution in the microstructure and the properties of the resulting elastic tensor. Considering periodic structures, we analyze all the possible Bravais lattices and all the plane (wallpaper) groups in order to study the way in which the symmetries of these patterns are reflected in the homogenized elastic tensor. For the unit cell we adopt Wigner-Seitz cells, which are primitive cells that preserve all the symmetries of the subjacent Bravais lattice and simplify the implementation of plane groups. Given an arbitrary elastic tensor, we propose a procedure for the inverse homogenization that allow us to choose the most convenient shape for the unit cell and to select the symmetries to be imposed that guarantee (during the whole optimization process) that the homogenized elastic tensor will have the same symmetry of the tensor to be designed. Concerning the design, several well established tools were used, such as algorithms for the rotation of the tensor to their material axes [2] and topology optimization methods based on SIMP [1] and topological derivative [3]. Some examples regarding the search of new classes of extreme materials are shown, where it can be seen how different composites classes emerge depending on the enforced symmetries. [1] O. Sigmund (2000). A new Class of Extremal Composites. *Journal of the Mechanics and Physics of Solids*, 48(2), 397-428. [2] N. Auffray and P. Ropars (2016). Invariant-based reconstruction of bidimensional elasticity tensors. *International Journal of Solids and Structures*, 87, 183-193. [3] S. Amstutz et al. (2010). Topological derivative for multi-scale linear elasticity models applied to the synthesis of microstructures. *International Journal for Numerical Methods in Engineering*, 84(6), 733-756.

## Theory and Application of Reactive Inelasticity Framework for Modeling Tendon Viscoelasticity, Plastic Deformation, and Damage

Babak N. Safa<sup>\*</sup>, Michael Santare<sup>\*\*</sup>, Dawn Elliott<sup>\*\*\*</sup>

<sup>\*</sup>University of Delaware, <sup>\*\*</sup>University of Delaware, <sup>\*\*\*</sup>University of Delaware

### ABSTRACT

The major inelastic behaviors in tendon are viscoelastic, plastic deformation, and damage. Of these, plastic deformation and damage are particularly significant, because of their potential relation to tissue dysfunction and repair. However, these behaviors have overlapping effects, which hinders their experimental measurement. As a result, a theoretical framework is needed to formulate and characterize them. We have formulated a structurally inspired inelasticity framework for modeling tissue inelasticity, Reactive Inelasticity (RIE), based on the kinetics of molecular bonds [1], and further applied it to experimental data on rat tail tendon fascicles, to determine the role of the inelastic behaviors in the mechanical response of tendon tissue. The RIE framework is based on the kinetics of molecular bonds and assumes different molecular bond types that break and reform when subjected to loading, to model the inelastic behaviors. Three types of bonds are defined: (1) Formative (for viscoelasticity), (2) Permanent (for hyperelasticity), and (3) Sliding (for plastic deformation). The same sets of constitutive equations are used to formulate each of these bonds, with the major difference being the kinetics rate of breakage and reformation of bonds. Further, damage is added to the model by reducing the number of each bond type. To determine the role of each one of the inelastic behaviors in tendon, based on the RIE framework we built two independent models, each specific to plastic deformation or damage, and applied them to a set of experimental stress data on rat tail tendon fascicles [2]. Further, the models were validated against another set of experiments [3]. Overall, both of the models had a similar success in fitting and predicting the mechanical response. Further experimental studies, specifically designed to differentiate between plastic deformation and damage are needed. This study is significant in addressing inelastic behaviors of tendon based on its molecular structure, which can be used to identify structural relationships between its mechanical behavior and external loading. References: [1] B.N. Safa, et al., Summer Biomechanics, Bioengineering, Biotransport Conf., 2017, 434. [2] A.H. Lee, et al., Acta Biomaterialia, 2017, 57, 363. [3] S.E. Szczesny, et al., PloS one, 2014, 9, e99588.

## Macroscopic Models for Crack Propagation in Heterogeneous Lattices based on Phase Field Method

Nhu NGUYEN<sup>\*</sup>, Julien RETHORE<sup>\*\*</sup>, Julien YVONNET<sup>\*\*\*</sup>

<sup>\*</sup>Université Paris-Est Laboratoire MSME UMR CNRS 8208 5 Bd Descartes 77454 Marne-la-Vallée Cedex 2, France., <sup>\*\*</sup>Institute de Recherche en Génie Civil et Mécanique-GeM UMR CNRS 6183, École Centrale de Nantes 1 rue de la Noë 44321, Nantes, France, <sup>\*\*\*</sup>Université Paris-Est Laboratoire MSME UMR CNRS 8208 5 Bd Descartes 77454 Marne-la-Vallée Cedex 2, France.

### ABSTRACT

In heterogeneous quasi-brittle materials like civil engineering materials micro-cracks can propagate and merge to create macro-cracks. Modelling precisely the micro-cracks as well as the heterogeneities in materials and tracking the propagation of micro-cracks is cumbersome and computationally intractable. The phase field approach to fracture has brought appealing advantages in modelling cracks process including the possibility to handle nucleation, propagation, branching and merging of cracks branching and merging of cracks with no predefined path. In heterogeneous materials, propagation of cracks is a multiscale process. Unfortunately, homogenization of damage behavior is associated with many difficulties, including: (i) the intrinsic nonlinearity of the problem; (ii) the difficulty to define an RVE due to localization; (iii) the numerical lack of convergence and of stability at the macroscale; (iv) the definition of the characteristic length scale at both scales. Among many approaches to fracture in a multiscale framework, in the present work, we follow [1] by identifying the different parameters of a damage model at the macroscale but in a direct manner, by fitting the effective parameters of a mechanical test response under crack initiation and propagation in a structure where all heterogeneities are explicitly described. The macroscopic parameters are identified and can then be used without concurrent computations for the macroscale calculations using the phase field method. Specifically, depending on the regularized length, which is considered as a material parameter, the isotropic phase field model [2] is employed to study cracks in the equivalent homogeneous medium or its extensions to anisotropic crack propagation [3] will be used to handle the effects of preferential crack propagation in regular lattices. Within this framework, the scale separation is not required and allows avoiding concurrent (FE2-like) costly computations. Keywords: Phase field method, multiscale modelling, damage, homogenization, crack propagation, quasi-brittle materials. References [1] Hossain M, Hsueh CJ, Bourdin B, Bhattacharya K (2014) Effective toughness of heterogeneous media. *Journal of the Mechanics and Physics of Solids* 71:15–32 [2] Nguyen T, Yvonnet J, Zhu QZ, Bornert M, Chateau C (2015) A phase field method to simulate crack nucleation and propagation in strongly heterogeneous materials from direct imaging of their microstructure. *Engineering Fracture Mechanics* 139:18–39 [3] Nguyen T, Rethore J, Yvonnet J, Baietto M (2017) Multi-phase-field modeling of anisotropic crack propagation for polycrystalline materials. *Comput Mech* 60(2):289–314

## **Tribological Behaviors of Grafted-Nanoparticles on Polymer-Brushed Walls: A Dissipative Particle Dynamics Study**

Vinh Phu NGUYEN\*, Phuoc Quang PHI\*\*, Nghia Trong MAI\*\*\*, Seung Tae CHOI\*\*\*\*

\*Chung-Ang University, \*\*Chung-Ang University, \*\*\*Chung-Ang University, \*\*\*\*Chung-Ang University

### **ABSTRACT**

Synthetic polymer brushes on tribological surfaces have wide potential industrial and medical applications as lubricants, since they are close to biological systems and do not produce any pollute waste like oil lubricants. Understanding the tribological behavior of the polymer brush-coated surfaces under high normal loading can be considered as the first step to enhance their tribological properties and to realize their practical applications. In this study, grafted nanoparticles are proposed as nano bearings on polymer brush-coated surfaces to alleviate the harsh working conditions of polymer brushes and to improve their mechanical stability. As a mesoscale simulation technique, dissipative particle dynamics (DPD) is adapted for the first time to investigate the tribological interaction between grafted nanoparticles and parallel walls with non-charged polymer brushes. DPD simulations are performed to investigate the influences of seven parameters (solvent quality, brush miscibility, grafting density and chain length of nanoparticle brushes, shear rate and hollowness of nanoparticles, and separation distance of parallel walls) on the tribological behavior of the system. Density profile, number of inter-brush interactions and kinetic friction coefficient are analyzed from DPD simulation results to find out the tendencies of structural and tribological responses caused by the variations of the seven parameters. The grafted nanoparticles do obviously act as nano-bearings that partially replace the sliding contact between two walls' brushes with the rolling contact between the grafted nanoparticle itself and two walls' brushes. The solvent quality has a strong effect on kinetic friction coefficient as already known in the literature. The grafting density and chain length of the grafted nanoparticle, which are important to prevent the agglomeration of nanoparticles, also influence the kinetic friction coefficient. However, their effects are relatively weaker than the solvent quality. For some cases, the number of interbrush interactions in the middle of the simulation box is better correlated to the friction coefficient than the total number of interbrush interactions. The DPD simulation results and analysis performed in this study would be beneficial in designing the polymer-brushed surfaces and grafted nanoparticles, predicting their tribological performance, and thus, developing new lubricants, especially water-based lubricants for green technology, both experimentally and computationally.

## **A Multi-phase-field/Polycrystal Plasticity for the Brittle-ductile Transitions of Crystalline Rock with Precipitating Fluid**

SeonHong Na<sup>\*</sup>, WaiChing Sun<sup>\*\*</sup>

<sup>\*</sup>Columbia University, <sup>\*\*</sup>Columbia University

### **ABSTRACT**

A safe and permanent repository for nuclear waste disposal using rock salt has drawn attention due to increasing demand of a sustainable and clean energy. The usage of rock salt for the geological repository is highly related to its desired characteristics, such as high thermal conductivity, low permeability and self-healing mechanism. These complicated physical and chemical mechanisms are closely related to the microscopic properties of rock salt. Previous efforts for investigating rock salt have focused on capturing the phenomenological behaviors. Nevertheless, the induced anisotropy and the rate-dependent behaviors of polycrystalline salt are often originated from the microstructures. In this work, we present an alternative approach in which the crystalline nature and the migration of brine as inclusions and precipitated fluid along the grain boundaries are explicitly modelled. We formulate a phase field framework for rock salt that explicitly model the interactions among crystal grain, grain boundaries and brine inclusions. A multi-phase-field method to capture brine migration due to dissolution and precipitation mechanism of halite under temperature gradient. Meanwhile, the crystal plasticity theory is adopted for modeling each grain to account for the crystallographic properties of rock salt. The texture of the multi-grains of salt is assumed to be random by assigning different sets of orientations to each grain. Numerical examples demonstrate that the proposed model is able to capture the brine migrations, interactions of the brine inclusion inside the halite grain and the fluid precipitating in grain boundaries.

## **A Kriging-PGD Algorithm to Couple Enriched Multifidelity Metamodels and Reduced-order Model to Handle Multiparametric Problem**

Stéphane Nachar<sup>\*</sup>, Pierre-Alain Boucard<sup>\*\*</sup>, David Néron<sup>\*\*\*</sup>

<sup>\*</sup>LMT (ENS-Cachan/CNRS/Université Paris-Saclay), <sup>\*\*</sup>LMT (ENS-Cachan/CNRS/Université Paris-Saclay), <sup>\*\*\*</sup>LMT (ENS-Cachan/CNRS/Université Paris-Saclay)

### **ABSTRACT**

The advent of Virtual Testing and industry's willingness for hyper fine structural optimization impose technical constraints for computational mechanics community. Optimize mechanical criterion for a turbine blade with classical techniques costs around months of CPU computation. To handle this issue, many cost-killer methods have been developed and two major families can be distinguished: surrogate models for an optimal approximation of mechanical criteria in the whole design space or around global optimum; and reduced-order models to approximate mechanical fields and allows evaluation of criteria in real-time. Our contribution is to unify these strategies around a nonlinear solver, well-designed for multiparametric problem: the LATIN-PGD method [Ladevèze, 1999]. It has two key features: each LATIN iteration gives an MOR-approximation of mechanical fields at each time step, known as time-space PGD modes; and it can be (re)started with fields from another solution. With these features, we can consider low-fidelity data from a non-converged LATIN solution, and harness the possibility to create a spatial modes basis for (re)start computation with other parameters set from design space, which drastically cut time computation. Our algorithm relies on building an initial surrogate model of the mechanical criterion with multi-fidelity data observations from a non-converged LATIN solution [Forrester, 2007]. This surrogate model will be enriched with well-chosen points from MSE or EI criterion and spatial modes arising from previous computations will be used to accelerate LATIN convergence. Attention will be focused towards the number of initial points on design space, and the way to choose low-fidelity data. This new algorithm will be presented on an elasto-visco-plastic case, using parallel computing. [Forrester, 2007] Forrester, Alexander I.J., András Sóbester, and Andy J. Keane. "Multi-Fidelity Optimization via Surrogate Modelling." Proceedings of the Royal Society A: Mathematical, Physical and Engineering Sciences 463, no. 2088 (December 8, 2007): 3251–69. [Ladevèze, 1999] Ladeveze, Pierre. Nonlinear Computational Structural Mechanics: New Approaches and Non-Incremental Methods of Calculation. Springer Science & Business Media.

## Image-base Material Homogenization Using Neural Networks under the cgFEM Framework

Enrique Nadal<sup>\*</sup>, Borja Ferrandiz<sup>\*\*</sup>, Manuel Tur<sup>\*\*\*</sup>, Juan José Ródenas<sup>\*\*\*\*</sup>, F. Javier Fuenmayor<sup>\*\*\*\*\*</sup>

<sup>\*</sup>Universitat Politècnica de València. Centro de Investigación en Ingeniería Mecánica, <sup>\*\*</sup>Universitat Politècnica de València. Centro de Investigación en Ingeniería Mecánica, <sup>\*\*\*</sup>Universitat Politècnica de València. Centro de Investigación en Ingeniería Mecánica, <sup>\*\*\*\*</sup>Universitat Politècnica de València. Centro de Investigación en Ingeniería Mecánica, <sup>\*\*\*\*\*</sup>Universitat Politècnica de València. Centro de Investigación en Ingeniería Mecánica

### ABSTRACT

Metal foams, such as aluminium foam, is taking interest due to its acoustic properties, impact energy absorption, etc. However, the structural analysis using the Finite Element Method (FEM) of such structures is complex since the geometry is not available in a CAD file. In fact, the geometry of a metal foam is obtained from a CT-scan. In order to avoid the unneeded step of generating an artificial CAD model from the CT-scan, some new FEM formulations have emerged. Some of them associate one element per pixel, whose elastic properties are related to the pixel color [1], leading to a model with an unaffordable number of elements. In order to avoid this problem, CellFEM [1] and cgFEM [2] methods allow several pixels to be associated with one single element. The latter one uses a special integration quadrature with one integration point per pixel. This methodology is precise, although the high number of integration points used makes it inefficient. In order to speed up the cgFEM, the authors propose in this work to carry out an off-line machine learning (ML) process, based on neural networks, for the homogenization process at each element. The ML process relates the low frequency terms of the Discrete Cosines Transform of the group of pixels falling into one element, which can be extracted from the JPEG compression, with its homogenized material properties. Therefore, a standard quadrature is used speeding up the Finite Element analysis. Results show that the use of 3 DCT coefficients is accurate enough in terms of deformation energy and displacements with respect to the reference solution. References: [1] A. Düster, J. Parvizian, Z. Yang, E. Rank. The finite cell method for three-dimensional problems of solid mechanics. *Computer Methods for Applied Mechanical Engineering*. 198: 3768-3782, 2008 [2] L. Giovannelli, J.J.Rodenas, J. M. Navarro, M. Tur. Direct medical image-based finite element modelling for patient-specific simulation of future implants. *Finite Elements in Analysis and Design*. 136:37-57,2017. [3] E. Nadal. Cartesian grid FEM (cgFEM): High performance h-adaptive FE analysis with efficient error control: application to structural shape optimization. Ph.D. Thesis, Universitat Politècnica de València, 2014. Acknowledgements The financial support to this work of Generalitat Valenciana (PROMETEO/2016/007) and the Spanish Ministerio de Economía, Industria y Competitividad (DPI2017-89816-R) is greatly acknowledged.

## Computational Micromechanics of Defects' Influence and Fiber Kinking on the Response of Fiber-Reinforced Composites

Mehdi Naderi<sup>\*</sup>, Nagaraja Iyyer<sup>\*\*</sup>, Nicole Apetre<sup>\*\*\*</sup>, Kishan Goel<sup>\*\*\*\*</sup>, Nam Phan<sup>\*\*\*\*\*</sup>

<sup>\*</sup>Technical Data Analysis, Inc., <sup>\*\*</sup>Technical Data Analysis, Inc., <sup>\*\*\*</sup>Technical Data Analysis, Inc., <sup>\*\*\*\*</sup>US Naval Air Systems Command, <sup>\*\*\*\*\*</sup>US Naval Air Systems Command

### ABSTRACT

The influence of defects and fiber waviness on the tensile/compressive response of fiber-reinforced composite is studied in this paper via micromechanical approach. Augmented finite element method (AFEM) is used to provide high-fidelity data on damage initiation and propagation along with micromechanical analysis. A python program is written to generate the micromechanical model as the input file for Abaqus model. We also discuss the three dimensional AFEM, developed as Abaqus User Element (UEL). Zero-thickness cohesive elements are inserted on fiber/matrix interface for modelling fiber/matrix interface delamination. Both automatic damage initiation and propagation algorithm is implemented in AFEM to capture discontinuities. Within micromechanical analysis, the effects of fiber volume fractions, fiber shapes are also considered to capture the stochastic behavior of the composite under tensile loading. In order to investigate the effects of voids and defects on ultimate strength of composite, we carry out simulations with random voids and defects. These results strongly show the importance of including defects and voids in the finite element analysis. To study composite response with fiber misalignment under compressive loading, random degree of waviness are considered in different sets of representative volume elements (RVEs). The results show how detrimental is the fiber misalignment to the structural integrity of composite components under compressive loading. It is also seen that the damage initiation and propagation locations are controlled by the degree and location of waviness. [1] M. Naderi, J. Jung, Q. D. Yang, A three dimensional augmented finite element for modeling arbitrary cracking in solids, *International Journal of Fracture*, 2016, 197: 147-168. [2] M Naderi, N Apetre, and N Iyyer. Effect of interface properties on transverse tensile response of fiber-reinforced composites: Three-dimensional micromechanical modeling. *Journal of Composite Materials*, 2017,51: 2963-2977. [3] M Naderi and N Iyyer. 3D modeling of arbitrary cracking in solids using augmented finite element method. *Composite Structures*, 2017, 160: 220–231.

## 6D Response Statistics by Path Integration of a Nonlinear Rotating Shaft Subjected to Colored Noise

Arvid Naess<sup>\*</sup>, Oleg Gaidai<sup>\*\*</sup>, Michael Dimentberg<sup>\*\*\*</sup>

<sup>\*</sup>NTNU, Norway, <sup>\*\*</sup>JUST, China, <sup>\*\*\*</sup>WPI, USA

### ABSTRACT

The paper studies extreme response statistics of random vibrations for a Jeffcott-type rotor with non-linear restoring force, under uniaxial colored noise excitation. The latter type of dynamic system is of wide use in stability studies of rotating machinery. System response statistics are studied by applying the path integration (PI) method. The Jeffcott rotor response statistics are then obtained by solving the Fokker–Planck-Kolmogorov (FPK) equation for a 6D dynamic system. The resulting response probability distributions can serve as an engineering input for a wide range of design issues, e.g. estimates of characteristic values, extreme value statistics and system reliability. Assessment of transverse random vibrations of shafts in rotating machinery may be of practical importance for applications with substantial environmental dynamic loads on supports, particularly in transport/vehicle engineering. Colored noise is a step forward compared to white noise excitation forces, but it raises the mechanical system dimension from 4D to 6D. The major advantage of path integration, relative to direct Monte Carlo simulation, is that path integration yields high accuracy in the probability distribution tail. Improved implementation of the PI algorithm was applied, specifically, the fast Fourier transform (FFT) was used to simulate the additive noise of the dynamic system. PI was accelerated by using a Monte Carlo based estimate of the joint PDF as an initial input. Finally, the key feature of this work is the advance to 6D problems, where very little PI research has been done. The obvious reason is of course the formidable computation load arising from decent 6D mesh. This paper, however, gives a practical solution to the latter challenge, enabling 6D PI calculation on an ordinary desktop within a reasonable amount of time. Using modern computational hardware with a decent GPU (Graphic Processing Unit) will significantly facilitate 6D calculation, making it an easy engineering task.

## Atomistic-Continuum Coupling for Random Alloys

Shankha Nag\*, William Curtin\*\*

\*École polytechnique fédérale de Lausanne, \*\*École polytechnique fédérale de Lausanne

### ABSTRACT

Random alloys are multicomponent systems where occupancy of any lattice site by an atom type is independent of its surrounding. Such systems have statistical fluctuations in local atomic configurations and properties, which prevents accurate application of standard atomistic/continuum coupling methods [1]. Here, two methods for atomistic/continuum coupling that mitigate errors are proposed, studied, and validated. In one method, a fully-relaxed atomistic sample, with atoms displaced from the perfect lattice sites, is carved out of a larger random sample. The outer atoms of the atomistic sample then (i) define nodal positions from which an outer continuum model is constructed and (ii) serve as so-called pad atoms that move with the continuum nodes and transmit forces onto the atoms in the inner atomistic domain. This method ensures no spurious stresses at zero loading, and only small spurious stresses arise under loading. But it requires creation of a much larger initial sample and is specific to that particular atomic distribution. A second method considers an atomistic domain with two outer layers of atoms and then the additional pad region represented as by “average” atoms interatomic potentials [2] that, in principle, match the average bulk lattice and elastic constants of the random alloy. This method separates the random/homogeneous boundary from the atomistic/continuum boundary, avoiding the serious errors that arise when the two boundaries are at the same position. This method creates small spurious stresses under zero load, due to small mismatches in the actual properties of the “average” atoms as compared to the real atoms, and small additional spurious stresses under applied load. The two methods are examined for three different solid solution alloys (dilute Al-5%Mg, Ni-15%Al, and medium entropy FeNiCr, all described by EAM interatomic potentials). Spurious errors for both methods and across all three materials are small ( $<10$  MPa) up to applied strains of  $10^{-3}$ . These methods enable the accurate study of mechanics boundary value problems in random alloys, such as High Entropy Alloys, for problems where it is essential to capture atomistic phenomena in some localized region of the sample. [1] Modelling Simul. Mater. Sci. Eng. 11 (2003) R33–R68 [2] Phys. Rev. B 93, 104201

## KEY ELEMENT BUILDINGS DESIGN METHOD WITH BIDIRECTIONAL EVALUATION BETWEEN STRUCTURAL ANALYSIS AND EVACUATION ANALYSIS

YASUYUKI NAGANO\*, YOICHI MUKAI<sup>†1</sup>, KENSUKE YASUFUKU<sup>†2</sup>,  
YASUNORI MIZUSHIMA<sup>†3</sup> AND TOMOHARU SARUWATARI<sup>†4</sup>

\* Graduate School of Simulation Studies, University of Hyogo  
7-1-28, Minatojima-Minamimachi, Chuo-ku, Kobe 650-0047, Japan  
E-mail: nagano@sim.u-hyogo.ac.jp

<sup>†1</sup>Kobe University  
1-1, Rokkodai-cho, Nada-ku, Kobe, 657-8501, Japan  
E-mail: ymukai@port.kobe-u.ac.jp

<sup>†2</sup> Osaka University  
2-1, Yamadaoka, Suita, Osaka, 565-0871, Japan  
E-mail: yasufuku@cmc.osaka-u.ac.jp

<sup>†3</sup> Takenaka Corporation  
1-5-1, Ohtsuka, Inzai-shi, Chiba, 270-1395, Japan  
E-mail: mizushima.yasunori@takenaka.co.jp

<sup>†4</sup> JSOL Corporation  
Tosabori Daibiru Bldg. 2-2-4, Tosabori, Nishi-ku, Osaka, 550-0001, Japan  
E-mail: saruwatari.tom@jsol.co.jp

**Key words:** Key Element Design, Structural Analysis, Evacuation, FEM Analysis.

**Abstract.** In this study, we aim to construct a ‘Damage Simulator’ which can quantitatively evaluate the damage of nonstructural materials in the building. To avoid human casualties in a large building at the time of big earthquakes, we predict the damage caused by falling furniture inside the building, interior and exterior etc. by using computer simulation. First, we will develop a ‘Damage Assessment Observer’ function that accurately calculates the response of each part of the building using a structural simulator and visualizes and evaluates the degree of damage of nonstructural material. At the same time, the evacuation simulator will develop a ‘Damage Control Operator’ function that creates critical damage sites that cause significant evacuation difficulties, and performs key design elements of nonstructural materials from the importance of

Yasuyuki Nagano, Yoichi Mukai, Kensuke Yasufuku, Harunori Mizushima and Tomoharu Saruwatari

evaluation of nonstructural materials. Subsequently, by integrating the structural simulator and the evacuation simulator, we construct a damage simulator that can comprehensively design necessary specifications and evaluate the performance of nonstructural materials. We propose key elements in the design of a building or a structure by utilizing the damage simulator.

Nonstructural material of buildings is determined by designers in the overall cost plan of the building unlike the structural material. In ordinary building design, quantitative verification of damage created by nonstructural material is not taken into account. On the other hand, if the detailed model structure analysis based on the assumed ground motion during an earthquake is carried out, since the local behavior of the building can be comprehended, it is also possible to determine the damage degree of each nonstructural material. If the degree of damage can be evaluated for each nonstructural material, by assessing the damage resistance of each nonstructural material based on the evacuation simulation results, it is possible to design the nonstructural material to reduce casualties. We propose this new method of evaluating both the structural analysis result of where the building is likely to sustain damage due to an earthquake and the evacuation analysis result by considering the damage caused to the nonstructural material.

## 1 INTRODUCTION

In this study, by combining the incidental functions of the structural simulator and the evacuation simulator, the result of the evacuation simulation is vital to determine the furniture layout of buildings and the specifications of interior and exterior finishing materials. Considering both damage evaluation and damage control, we build a damage simulator. Fig. 1 shows a conceptual diagram of integrated simulation.

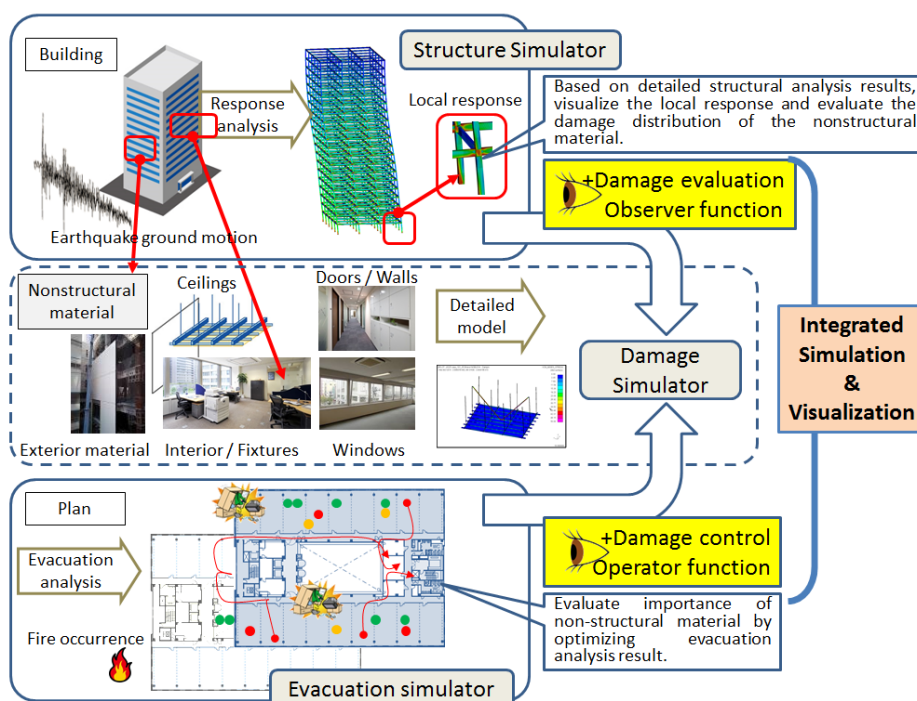


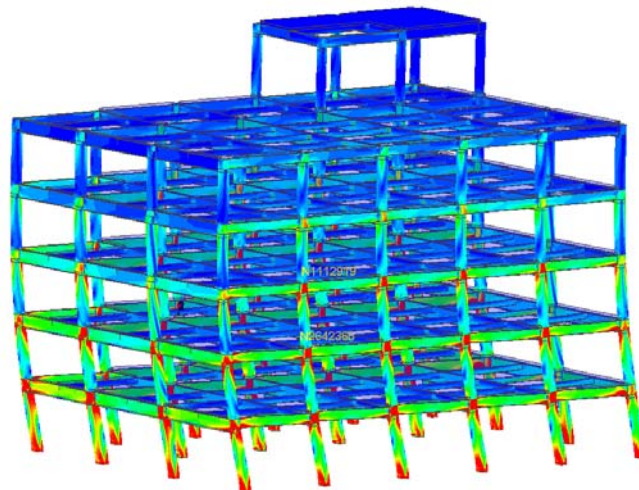
Fig. 1 Conceptual diagram of integrated simulation

## 2 DETAILED STRUCTURAL ANALYSIS WITH FINITE ELEMENT METHOD <sup>[1]</sup>

This study presents the first step in the development of a visualization system that would predict simultaneously the expected seismic damage of both structural and nonstructural members, such as walls and ceilings, by superposing seismic analytical results of nonstructural members on those of structural members.

Past seismic damage examples showed that human casualties had been caused by not only structural damages but also by damages of nonstructural members. Whereas the safety of structural members is constantly confirmed in the structural design process of buildings, there is no detailed process regarding the safety of nonstructural materials as they are made by specification design without any consideration to their locations. In order to reduce damage to nonstructural members that may cause harm to humans, nonstructural members should be designed considering local seismic responses. To accurately evaluate local seismic responses of nonstructural members, it is necessary to accurately evaluate seismic responses of structural members to which nonstructural members are attached. Therefore, it is important to have an overview of the overall responses of structural and nonstructural members.

This study aims to develop a system that can indicate the seismic damage undergone by structural and nonstructural members at the same time. The structural damage in a building was evaluated accurately by using the detailed finite element (FE) model of all structural members of the building (Fig. 2). The authors showed, in a previous study, that a detailed and complete FE model of the building structure simulated accurately the actual seismic behavior of the building. Through the detailed FE model, local seismic responses of the structural parts to which nonstructural members were connected could be extracted because the original shapes of all the structural members were reproduced as precisely as possible in the model. The local responses could be used to evaluate the seismic damage to the nonstructural members. Furthermore, superposing these analytical results enabled the comprehension of the relationship between the damaged members. This may lead to a structural design method that can reduce seismic damage to nonstructural members.



An Example of Stress Distribution

Fig. 2 Detailed finite element model of whole structural members of a building

### 3 ANALYZING THE SEISMIC BEHAVIOR OF NON-STRUCTURAL MEMBERS OF BUILDINGS BY USING THE LARGE-SCALE PARALLEL CALCULATION METHOD [2]

After large-scale earthquake, it is often reported that serious damage was caused to the nonstructural members, for example ceilings and claddings, of buildings with large open spaces such as gymnasiums and assembly halls.

The technical standard for preventive measures against collapsing ceilings is available for buildings, but its application is limited to preventing the damage caused by a middle-scale earthquake for which the behavior of the ceiling can be predicted to some extent. In order to expand this technical standard to the prevention of damage caused by an extremely rare earthquake (large-scale earthquake), it is necessary to have first clarified the behavior of the ceilings that are suspended from the building structure, and then to make the complete structure analysis model. To realize this, the specific analysis methods to evaluate the response of nonstructural members as precisely as possible according to the accurately predicted response of the structural frame of the building against the earthquake.

This study, suspending the ceilings in long-span structures as an example, prepares the detailed structural analysis models made by means of modeling the shape of the structural members so as to reflect the real one as truthfully as possible, and tries to obtain the extremely accurate earthquake response of the structural frame by a large-scale parallel calculation method (Fig. 3).

In the future, the aim will be to evaluate the behavior of a whole building through piling the results of the earthquake response of the ceilings by means of making as the boundary conditions the responses obtained by extremely accurate analysis of the structural frame from which the ceilings are suspended.

1: Max 96200748 : 1.523913E+02, Min 57857 : 1.631545E-13

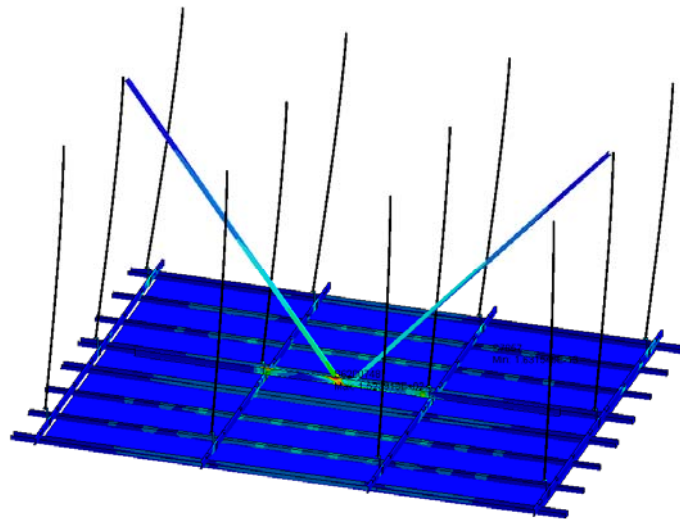


Fig. 3 Suspended ceilings FEM model installed in long-span structures

#### 4 EVACUATION ANALYSIS CONSIDERING MULTIPLE PATH FAILURES WITH MULTI AGENT SYSTEM [3]

When verifying whether all the residents of a building can evacuate safely in the event of a major earthquake, it is necessary to consider various path failures due to earthquakes. For example, evacuation routes may be blocked due to debris such as damaged window panes, walls, ceilings and other exterior and interior (nonstructural) materials, movement of furniture fixtures, falling parts, and the like, which may affect evacuation safety. On the other hand, in recent years, the number of cases where a simulation method based on a multi-agent system that takes individual movements of evacuees into consideration for the evaluation of evacuation safety of buildings is increasing, and it is possible to promptly predict detailed evacuation properties under various conditions.

In this chapter, we propose a method to conduct evacuation analysis by using a multi-agent system, considering multiple path obstacles caused by damage of nonstructural material etc., in order to verify the evacuation safety of the building at the time of a large earthquake occurrence.

##### 4.1 Multi-agent system and route fault setting

The evacuation analysis in this paper is based on the Multi-agent System<sup>[4]</sup>. As an evacuation behavior model, the Social Force model is used. Our model has a feature that the shape of the agent is represented by an ellipse so that it can deal with higher density of crowd flow. In addition, when planning routes of agents and avoiding collisions with obstacles, the plan of the building is divided by a square mesh of 20 cm on each side, and a data structure is held for evacuation route information and obstacle information in each mesh. The evacuation route uses a mesh as a network structure to calculate the shortest route, and the agent refers to the information and selects the shortest route in the real space.

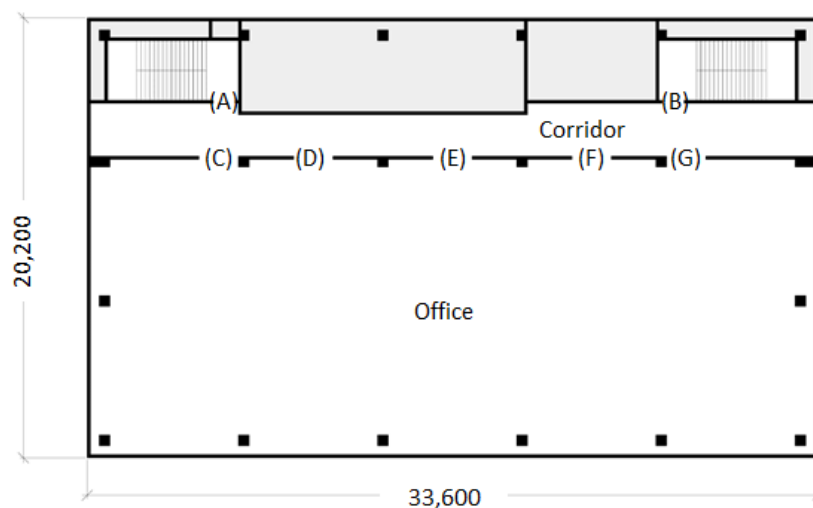


Fig. 4 Case study plan of the reference floor

Table 1 Setting of impassable route

	A	B	C	D	E	F	G
Case 1	✓	✓	✓	✓	✓	✓	✓
Case 2	✓	×	✓	✓	✓	✓	✓
Case 3	✓	×	×	×	✓	✓	✓
Case 4	✓	×	✓	✓	✓	×	×

✓: Passable    ×: Impassable

Fig. 4 shows the standard floor plan of a general office building as a case study. The number of residents is randomly arranged as 57 people (0.125 people /m<sup>2</sup>) and evacuation starts at once. As a route fault setting of the office building, situations where either one of the emergency stairs (A, B) cannot be used, or where one or more of the living room exits (C, D, E, F, G) cannot be used. The case of this route failure is summarized in Table 1. Evacuation routes for each case shall be set as the shortest route avoiding the route fault with the emergency staircase as the destination.

#### 4.1 Results and discussion

Fig. 5 shows the transition of the number of evacuees completed in each case. Case 1 is a setting with no route fault, evacuate to the nearest one of the two emergency stairs A and B. The floor evacuation time is the shortest (41.1 seconds). The changes in the number of evacuees completed slowed to around 30 seconds. It indicates that one emergency staircase is not being used, and there are variations in the number of evacuees. There is a possibility that the evacuation time can be further shortened by appropriate evacuation guidance.

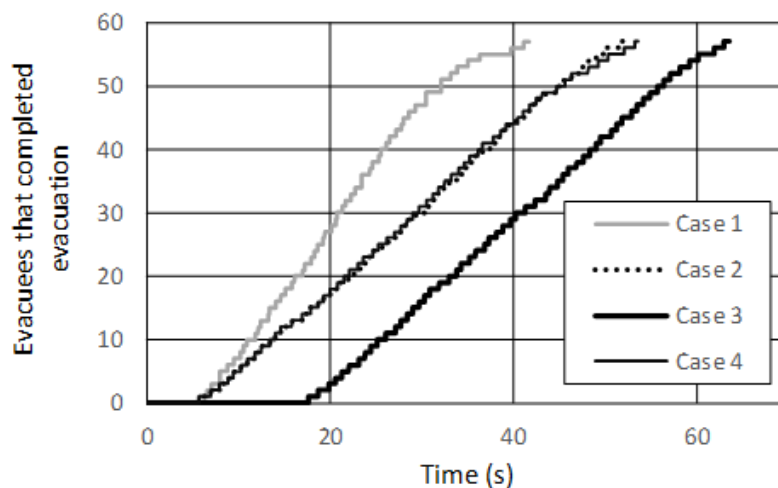


Fig. 5 Changes of number of evacuees that completed evacuation

In Cases 2 to 4, evacuation can take place only from emergency staircase A. Emergency staircase B is set to be unable to be used. Apart from that, the office room exits that can be used are different. Floor evacuation time is 51.8 seconds in Case 2, 63.0 seconds in Case 3, and 53.2 seconds in Case 4. The evacuation time and the evacuation completed number of cases in Case 2 and Case 4 are almost the same. In Case 2, all office room exits can be used, but Case 4 is set to be impassible at two exits F and G. However, since F and G are located far from the emergency staircase that can be used in Case 4, there was almost no influence on the floor evacuation time. On the other hand, in Case 3, it is impossible for two exits of the office room exits C and D close to the emergency staircase A (passable) to pass. It is necessary for the evacuees to take a detour and evacuate, and the floor evacuation time takes longer. However, the flow coefficients from Cases 2 to 4 to the staircase room are almost equal.

Next, the changes in the number of visitors in office rooms and corridors are shown in Fig. 6 and 7. In cases of evacuation of the office room, examples cases 1 and 2, there is no obstacle at the office room exit, so the room evacuation time is as short as 13 seconds. In cases 3 and 4, since 2 of 5 room exits are impossible to pass, it takes 22.5 seconds in Case 3 and 21 seconds in case 4 evacuation time. The reason for this is that there are evacuees whose walking distance in the living room is longer, and evacuees are concentrated in the room exit E. The reason why the evacuation time differs between Cases 3 and 4 is that because Case 3 is unable to pass through exits C and D on the left side and emergency stairs B on the right side, walking on the corridor becomes longer, this is caused by the occurrence of confluence of crowds in the room E and the corridors. From the simulation screen 17 seconds after the start of the simulation in Case 3 shown in Fig. 8, it is also understood that the crowd density is high near the corridor center. Even if there are no changes in the number and width of room exits that can be passed through, it is simulated that the crowd properties and the evacuation time differ due to the confluence of evacuees by the positional relationships and routes with the emergency staircases.

Focusing on the number of people in the corridor, the density of residents in Case 3 is the highest, and that of Case 4 is the lowest. Particularly in Case 4, there are two impassable room exits as compared with Case 2, which takes a long time to evacuate the office room and the number of people staying in the corridor simultaneously decreases. Also, since the distance between the passable room exits and the emergency stairs that can pass through is short, the evacuation time required in the corridor is shortened, and the difference between the final floor evacuation time and Case 2 has disappeared. Fig. 9 shows a simulation screen 10 seconds after the start of simulation in Case 4. As the room exit F and G are unable to pass, more than half of the residents are evacuated from the room exit E. However, because the exit width is suitable, the congestion is small in the office room, you can see that the evacuation is relatively smooth up to the corridor.

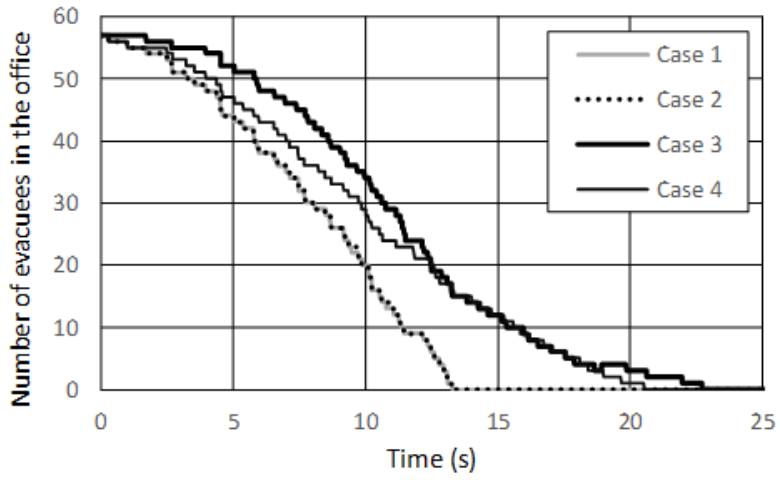


Fig. 6 Changes of number of evacuees in the office

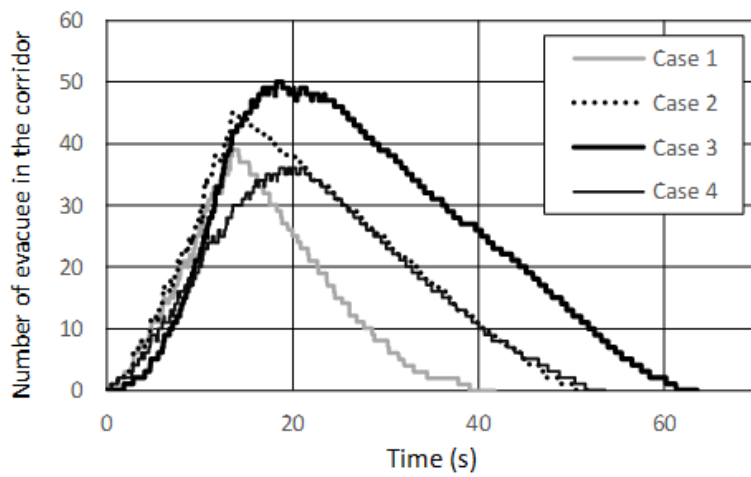


Fig. 7 Changes of number of evacuees in the corridor

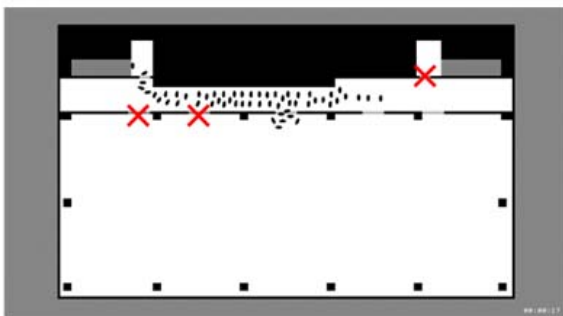


Fig. 8 Evacuation Simulation of Case 3

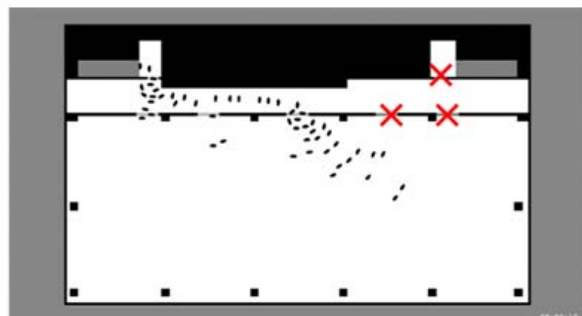


Fig. 9 Evacuation Simulation of Case 4

## 5 INTEGRATED VISUALIZATION

For the mutual link between the structure simulator, the damage simulator, and the evacuation simulator, we have constructed a visualization system that can test each analysis result from an engineering point of view. Fig. 10 shows the overall view, and Fig. 11 shows the detail view.



Fig. 10 Overall view of integrated visualization

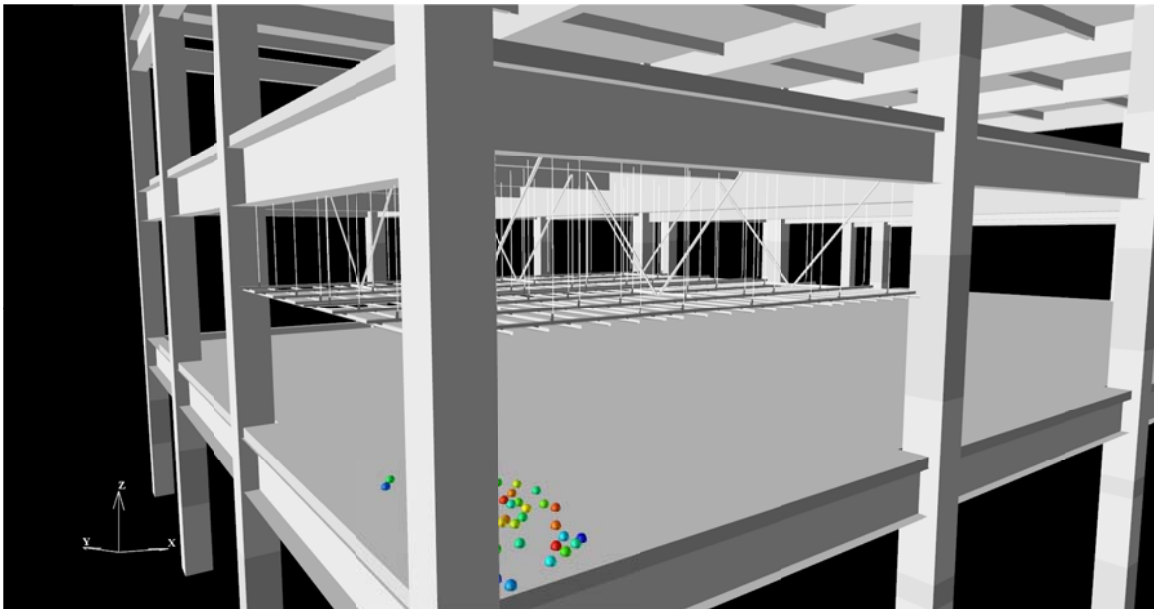


Fig. 11 Detail view of integrated visualization

## 6 CONCLUSIONS

- Structural analysis of the entire building, ceiling material of nonstructural members and evacuation analysis were carried out respectively, and the all results were integrated visualized.
- By looking at the result of the integrated visualization, we developed a function that allows us to judge what the key elements regarding building design are and where in the building they should be implemented.

## ACKNOWLEDGMENTS

This work was supported by JSPS KAKENHI Grant Number JP16H03124.

## REFERENCES

- [1] Yasunori Mizushima, Yasuyuki Nagano and Yoichi Mukai : Construction of damage observation system for both structural and nonstructural members with overlaying, #2019117, *proc. 13<sup>th</sup> WCCM* (2018).
- [2] Tomoharu Saruwatari, Yasuyoshi Umezu, Yoshitaka Ushio, Lyu Zhilun and Yasuyuki Nagano : Earthquake response analysis of nonstructural members of buildings by using the large-scale parallel calculation method, #2020310, *proc. 13<sup>th</sup> WCEE* (2018).
- [3] Kensuke YASUFUKU and Yasuyuki NAGANO : Evacuation Analysis of Several Impassable Routes by Using Multi-agent System, 387-388, *AIJ*, (2017). (in Japanese)
- [4] Kensuke YASUFUKU : REPRODUCTION OF PEDESTRIAN MOVEMENT IN QUEUE BY USING MULTI-AGENT SYSTEM AND ANALYSIS OF CROWD FLOW AFFECTED BY FOLLOWING BEHAVIOR, *J. Archit. Plann., AIJ*, Vol.81 No.722, 821-829, Apr., (2016). (in Japanese)  
DOI : <https://doi.org/10.3130/aija.81.821>

## Aircraft Traffic Model Using Step Back Cellular Automaton

Shinsuke Nagaoka<sup>\*</sup>, Tomoaki Tatsukawa<sup>\*\*</sup>, Kozo Fujii<sup>\*\*\*</sup>, Eri Ito<sup>\*\*\*\*</sup>

<sup>\*</sup>Tokyo University of Science, <sup>\*\*</sup>Tokyo University of Science, <sup>\*\*\*</sup>Tokyo University of Science, <sup>\*\*\*\*</sup>Electronic Navigation Research Institute

### ABSTRACT

In recent years, the number of flights is drastically increasing, and arrival delays are occurring every day worldwide, especially in the Asia-Pacific area. Originally, all of airplanes should fly along the planned routes based on flight plans. However, some airplanes are not able to go through the planned route due to various factors during flight. The most common factor is the over-capacity of the arrival airport. When the arrival airport is already over the capacity, some flights are controlled by "Holding", "Vectoring", "Late departure" or "Flight deck interval management" etc. Airplane delay contributes to various socio-economic problems. Of course, Japanese airport is also no exception. Especially, a great many delay is occurring every day in Tokyo international airport that is the world 5th largest airport. About 70% domestic flights concentrate to the Tokyo International Airport. Moreover, 1.5 times more international and cross over flights are expected in 2015. In addition, number of aircraft for Tokyo international airport is expected to exceed the limit of air traffic capacity of air traffic controllers around 2025. In this kind of situation, there are concerns that is safety aspect too. Based on this situation, we think that more automation support is needed. The objective of this study for socio-economic problems is to develop a computer program for agent model simulation. Specifically, we construct the two-dimension Step Back Cellular Automaton method (SBCA) which is based on Cellular Automaton method. The method is including Base of Aircraft Data (BADA) to calculate behavior of airplane. BADA is preferred by Eurocontrol which has many parameter data, for example velocity, altitude, mass, fuel consumption and so on. Moreover, the method considers multiple routes which is based on actual way point from all airports in Japan to Tokyo international airport as same as actual flight route. By using this method, we compare analysis result with actual flight time table to investigate the effectiveness of the air traffic management model around Tokyo international airport by our proposed method. As a future work, we unravel air traffic congestion around the Tokyo international airport.

## A Virtual Testing Framework for the Analysis of Damage in Composite Structures

Manish Hassan Nagaraj<sup>\*</sup>, Erasmo Carrera<sup>\*\*</sup>, Ibrahim Kaleel<sup>\*\*\*</sup>, Marco Petrolo<sup>\*\*\*\*</sup>

<sup>\*</sup>Department of Mechanical and Aerospace Engineering, Politecnico di Torino, Italy, <sup>\*\*</sup>Department of Mechanical and Aerospace Engineering, Politecnico di Torino, Italy, <sup>\*\*\*</sup>Department of Mechanical and Aerospace Engineering, Politecnico di Torino, Italy, <sup>\*\*\*\*</sup>Department of Mechanical and Aerospace Engineering, Politecnico di Torino, Italy

### ABSTRACT

The present work involves the progressive damage analysis of composite structures using refined beam elements based on advanced structural theories, developed within the framework of the Carrera Unified Formulation (CUF) [1]. The main concept of CUF is the use of expansion functions across the cross-section (for 1D beam elements) and thickness (for 2D shell/plate elements) to enrich the kinematics of the element. Such an approach removes the restrictive assumptions associated with classical 1D and 2D finite elements, resulting in a 3D-like accuracy of the solution at a highly reduced computational cost with respect to standard 3D FEA. It is, therefore, an ideal framework for the virtual testing of failure mechanisms in composite structures, since such a non-linear analysis is extremely computationally expensive. Various computational tools available in CUF are used to predict the progression of damage within the structure. A multi-scale analysis is performed by considering a representative volume element (RVE) at the micro-scale, where the fiber and matrix are independently modeled using Component-Wise (CW) analysis [2]. The CW approach is based on Lagrange-type polynomials leading to a physically based description of the RVE, which results in a high-fidelity model and correspondingly accurate stress fields. Matrix and fiber failure can thus be detected at the microscopic level, where matrix non-linearities are taken into account using an elasto-plastic constitutive model. Interface modeling capabilities are present, via which delamination and debonding effects can be considered. Delamination is modeled using cohesive elements governed by a traction-separation law. Interface modeling can be extended to the domain of contact mechanics by introducing contact elements, thus gaining the ability to solve a new class of structural problems. A combination of the above tools is used to obtain an accurate material response of the structure in the non-linear regime, from the structural level, i.e., macro-scale to the constituent material level, i.e. the micro-scale, in a computationally efficient manner, providing a suitable virtual testing environment for the progressive damage analysis of composite structures. References [1] Carrera E, Cinefra M, Petrolo M, Zappino E. "Finite element analysis of structures through unified formulation", John Wiley & Sons (2014). [2] Kaleel I., Petrolo M., Waas A.M., Carrera E., "Micromechanical Progressive Failure Analysis of Fiber-Reinforced Composite Using Refined Beam Models", Journal of Applied Mechanics (2018), 85.

## **A New Non-Iterative Mesh Generation Algorithm for Modeling Problems with Complex Geometries**

Anand Nagarajan\*, Soheil Soghrati\*\*

\*The Ohio State University, \*\*The Ohio State University

### **ABSTRACT**

We present an integrated computational framework relying on a new non-iterative mesh generation technique, named Conforming to Interface Structured Adaptive Mesh Refinement (CISAMR), for creating high fidelity FE models of composite materials. A NURBS-based reconstruction algorithm is implemented to synthesize the material microstructure by packing arbitrary shaped particles, morphologies of which are extracted from digital data such as micro-computed tomography images. A genetic algorithm (GA) based optimization framework is also employed to simulate the target statistical microstructural descriptors such as the size distribution, volume fraction, and spatial arrangement of particles. CISAMR is then employed to create a FE model of the material by transforming a structured mesh into a high quality conforming mesh with low element aspect ratios and a negligible discretization error. This non-iterative transformation is carried out by combining customized versions of four algorithms: h-adaptivity, r-adaptivity, face-swap, and sub-tetrahedralization. Compared to enriched methods such as extended FEM, CISAMR obviates the additional computational burden associated with evaluating enrichment functions and provides a higher accuracy for recovering the gradient field. Further, unlike conventional mesh generation algorithms such as the Delaunay triangulation, CISAMR can easily handle problems with highly complex geometries without the use of iterative smoothing or relaxation algorithms to improve the elements quality. In this work, we show the application of this integrated reconstruction-meshing framework for simulating the failure response a variety of heterogeneous materials, including particulate and fiber-reinforced composites, as well as non-woven entangled materials such as fiberglass insulation packs. Multiple sources of material and geometrical nonlinearity, including the damage, contact, and cohesive debonding are considered in each simulation.

## Development of Stress Analysis System Using XFEM to Evaluate Strength of Composite Structures

Toshio Nagashima\*

\*Sophia University

### ABSTRACT

Finite Element Analyses (FEAs) are utilized to perform stress analyses for evaluation of structural integrity of CFRP (Carbon Fiber Reinforced Plastics) composite structures. In order to perform such analysis effectively, the extended finite element method (XFEM) in conjunction with the level set method is employed in this study. Two kinds of method based on XFEM have been developed. One is an XFEM code using three-node triangular shell elements enriched with a step function, which can perform stress analyses of thin-walled structures with an open hole. Another is an XFEM code using 6-node pentahedral elements enriched with Heaviside function [1][2], which can perform damage propagation analyses considering both matrix cracks and delamination. In the presentation, both stress analyses of a CFRP stiffened panel with a maintenance hole and damage propagation analyses of an OHT (Open Hole Tension) specimen are demonstrated and validated through comparisons with experimental results. [1] Nagashima, T., Sawada, M. : Development of a damage propagation analysis system based on level set XFEM using the cohesive zone model, *Computers and Structures*. 174(2016) 42-53. [2] R. Higuchi, T. Okabe, T. Nagashima, Numerical simulation of progressive damage and failure in composite laminates using XFEM/CZM coupled approach, *Composites Part A*, 95(2017) 197-207.

## Investigation of Relationship between Copper Liberation and Inner Force of High Pressure Grinding Roll by Applying DEM Simulation

Yu Nagata<sup>\*</sup>, Yukihiro Sawamura<sup>\*\*</sup>, Masaya Minagawa<sup>\*\*\*</sup>, Yuki Tsunazawa<sup>\*\*\*\*</sup>, Giuseppe Granata<sup>\*\*\*\*\*</sup>, Ryo Kawarabuki<sup>\*\*\*\*\*</sup>, Kohei Mitsuhashi<sup>\*\*\*\*\*</sup>, Kouji Tsukada<sup>\*\*\*\*\*</sup>, Takashi Misumi<sup>\*\*\*\*\*</sup>, Chiharu Tokoro<sup>\*\*\*\*\*</sup>

<sup>\*</sup>Graduate School of Creative Science and Engineering, Waseda University, <sup>\*\*</sup>Graduate School of Creative Science and Engineering, Waseda University, <sup>\*\*\*</sup>Graduate School of Creative Science and Engineering, Waseda University, <sup>\*\*\*\*</sup>National Institute of Advanced Industrial Science and Technology, <sup>\*\*\*\*\*</sup>Faculty of Science and Engineering, Waseda University, <sup>\*\*\*\*\*</sup>Research & Development Department, Nittetsu Mining Co., Ltd., <sup>\*\*\*\*\*</sup>Research & Development Department, Nittetsu Mining Co., Ltd., <sup>\*\*\*\*\*</sup>Design Department Industrial Machinery Section, Furukawa Industrial Machinery Systems Co. Ltd., <sup>\*\*\*\*\*</sup>Technology Division, Furukawa Co., Ltd., <sup>\*\*\*\*\*</sup>Faculty of Science and Engineering, Waseda University

### ABSTRACT

Although in the recent years the demand of copper products has been rapidly increasing, the decrease of copper grade in copper ores and the increase of arsenic impurities have become major issues for the copper industry. In this scenario, the development of a new process to efficiently separate and concentrate copper minerals is highly anticipated. Among the available comminution techniques, the high pressure grinding roll (HPGR) was found able to determine an efficient comminution and a high mineral liberation with a relatively low energy consumption. However, a significant barrier to the further develop of this method is determined by the requirement of large amounts of ore samples for pilot-scale tests. In this research, we performed discrete element method (DEM) simulations based on the T10 breakage model to determine the optimum conditions for HPGR pilot-scale tests on copper ore including chalcopyrite and bornite. First, we conducted piston press tests to produce pressing phenomena similar to HPGR. From these tests we determined the model parameters for the ore under investigation. Following this step, we performed DEM simulations by changing four operating variables: pressing force per mm<sup>2</sup>, roll rotational speed, initial roll gap and height of the feed. In order to evaluate the effect of different operating conditions, the liberation of copper was determined by mineral liberation analysis (MLA). Upon determination of the T10 parameters, the DEM simulations could reproduce throughput, roll gap, the energy consumption for all tested conditions. Moreover, the simulation could describe the results of pilot-scale tests, thus confirming the reliability of the method. According to the obtained results, the liberation of copper minerals improved by increasing the roll pressing force from 3 to 7 N/mm<sup>2</sup> and by lowering the initial gap between the rolls from 6 to 3 mm. Under these conditions, the normal direction component of the contact force increased. On the other hand, under the conditions which did not improve the mineral liberation, the normal contact force did not change, thus suggesting that the normal component of the contact force greatly contributes to the liberation of copper minerals.

## **Nanomechanics of Metal Matrix Nanocomposites Embedded with 1D and 2D Materials**

Arun Nair\*

\*University of Arkansas

### **ABSTRACT**

Graphene is a 2-D material with superior mechanical properties. It also possesses an exceptionally high aspect ratio, which makes it highly desirable for use as a fiber in nanocomposites. Previous studies have predicted that the presence of graphene will have a significant impact on the failure mechanisms of metal-graphene nanocomposites. In this talk, we use molecular dynamics to predict how different loading directions and crack orientations will impact the failure mechanisms of metal-graphene nanocomposites. We study both pristine and polycrystalline graphene as part of our nanocomposite model. Different failure mechanisms depending on loading direction, crack orientation, graphene structure (pristine or polycrystalline graphene sheets) will be discussed. Carbyne is a 1-D carbon chain that could be considered the strongest material. Recent experiments have shown that stable chains with lengths of thousands of atoms can be developed. As carbyne manufacture advances, it is important to determine possible applications for use in nanocomposites. We use both using density functional theory and molecular dynamics methods to predict the mechanical properties of metal-carbyne nanocomposites composed of multiple carbyne chains sandwiched within a metal matrix. These studies show that the mechanical properties of metal matrix can be improved with the addition of these 1D and 2D materials and also provide an insight into better design of metal nanocomposites.

## A Tale of Two Velocities

John Nairn\*, Chad Hammerquist\*\*

\*Oregon State University, \*\*FracGeo

### ABSTRACT

The material point method has two velocity fields - the velocities stored on the particles and the velocities of those particles represented on the grid. Each time step involves extrapolation of velocities from the particles to the grid and then back to update both particle velocity and position. The availability of two velocities opens up interesting options for modifications in MPM but new options are prone to errors if not done consistently. For example, two ways to implement damping are to reduce acceleration by velocity on the particle or by velocity on the grid. By implementing both these damping options one can unify standard MPM update methods (called FLIP) with alternative update methods (called PIC or hybrid FLIP/PIC) into a single scheme. The new view reveals that PIC is specific damped form of FLIP and the damping characteristics can be quantified. By re-examining velocity extrapolation back to the particles, we have derived a third MPM update method called XPIC(m). XPIC(1) is identical to PIC, which is a highly damped form of FLIP. As m increases, XPIC(m) optimizing damping performance such that it selectively damps null-space noise resulting a new form of MPM with reduced noise and enhanced stability. The null space arises because typical simulations have more particles than nodes and thus more degrees of freedom on the particles than on the grid. XPIC(m) selectively damps modes on the particles that are invisible to the grid. A potential for error in new MPM options is to focus solely on velocity extrapolations and ignore the role the method has when updating particle positions. Each new MPM update scheme for velocity (FLIP, PIC, or XPIC(m)) also requires modification to the particle position update. The new position methods are non-intuitive but essential for accurate results. This talk will present MPM extrapolations and particle updates in an abstract form and then show how each potential MPM method fits within the abstract scheme. Examples will be given for properties of XPIC(m) and the importance of proper particle position update. For example, MPM modeling with explicit cracks needs to track position of the particle surfaces. By implementing new position update methods for crack surfaces, the surface tracking is significantly improved.

## Design of Nonlinear Materials Using a Multi-scale NURBS-based Shape Optimization Scheme

Ahmad Najafi<sup>\*</sup>, Masoud Safdari<sup>\*\*</sup>, Daniel Tortorelli<sup>\*\*\*</sup>, Philippe Geubelle<sup>\*\*\*\*</sup>

<sup>\*</sup>Department of Mechanical Engineering and Mechanics, Drexel University, <sup>\*\*</sup>Department of Aerospace Engineering, University of Illinois at Urbana-Champaign, <sup>\*\*\*</sup>Department of Mechanical Science and Engineering, University of Illinois at Urbana-Champaign, <sup>\*\*\*\*</sup>Department of Aerospace Engineering, University of Illinois at Urbana-Champaign

### ABSTRACT

Due to recent advances in manufacturing techniques over the past decades, the tailoring of materials with specific macroscopic properties has been the focus of active research in mechanical engineering and materials science over the past decade. The key challenge in this line of work is how to optimize the material microstructure at the mesoscale to achieve a desired macroscopic constitutive response. In this work, we present a method to design the structure of particulate composites at the mesoscale using a shape optimization scheme to minimize or maximize a nonlinear objective function at the macroscale while satisfying a set of constraints (associated, for example, with the volume fraction of inclusions or with the manufacturing technique). Three key elements of the presented technique are i) multiscale nonlinear modeling, ii) sensitivity analysis, and iii) optimization. The multiscale modeling is based on a nonlinear finite element scheme, which combines a classical homogenization scheme with a NURBS-based Interface-enriched Generalized Finite Element Method (NIGFEM) used for accurate and efficient capturing of the displacement field in a heterogeneous material with a finite element discretization that does not conform to the material interfaces. Damage evolution is captured using a three-parameter isotropic damage model, which is applicable to a wide range of failure responses. To perform sensitivity analysis, we formulate a NIGFEM-based analytic nonlinear sensitivity scheme, which is simplified by the fact that only the enrichment control points on material interfaces move, appear or disappear during the shape optimization process. The selected scheme avoids the technical difficulties encountered in the finite difference schemes when the boundary intersects an element very close to a node in a non-conforming mesh. In these situations, the boundary may move to another element during the design perturbation step, resulting in changes of the mesh topology, making the differentiation of the stiffness matrix and load vector problematic. The last part is a gradient-based shape optimization scheme that relies on the stationary nature of the non-conforming meshes used to discretize the periodic unit cell, thereby avoiding mesh distortion issues that plague conventional finite-element-based shape optimization studies. In the current approach, the finite element approximation space used in the NIGFEM is augmented with NURBS to allow for the accurate capture of the weak discontinuity present along complex, curvilinear material interfaces. To demonstrate the performance of the method, we present a set of microstructural shape optimization problems with applications in linear and nonlinear design of heterogeneous particulate composites.

## Application Development Framework for Manycore Architectures -from Exascale to Post Moore Era-

Kengo Nakajima\*

\*The University of Tokyo

### ABSTRACT

"ppOpen-HPC" is an open source infrastructure for development and execution of optimized and reliable simulation code on post-peta-scale (pp) parallel computers based on many-core architectures, and it consists of various types of libraries, which cover general procedures for scientific computation. Source code developed on a PC with a single processor is linked with these libraries, and the parallel code generated is optimized for post-peta-scale systems with manycore architectures, such as the Oakforest-PACS system of Joint Center for Advanced High Performance Computing (JCAHPC). "ppOpen-HPC" is part of a five-year project (FY.2011-2015) spawned by the "Development of System Software Technologies for Post-Peta Scale High Performance Computing" funded by JST-CREST. The framework covers various types of procedures for scientific computations, such as parallel I/O of data-sets, matrix-assembly, linear-solvers with practical and scalable preconditioners, visualization, adaptive mesh refinement and dynamic load-balancing, in various types of computational models, such as FEM, FDM, FVM, BEM and DEM. Automatic tuning (AT) technology enables automatic generation of optimized libraries and applications under various types of environments. We release the most updated version of ppOpen-HPC as open source software every year in November (2012-2015), which is available at <http://ppopenhpc.cc.u-tokyo.ac.jp/ppopenhpc/>. In 2016, the team of ppOpen-HPC joined ESSEX-II (Equipping Sparse Solvers for Exascale) project (Leading P.I. Professor Gerhard Wellein (University of Erlangen-Nuremberg)), which is funded by JST-CREST and the German DFG priority programme 1648 "Software for Exascale Computing" (SPPEXA) under Japan (JST)-Germany (DFG) collaboration until FY.2018. In ESSEX-II, we develop pK-Open-HPC (extended version of ppOpen-HPC, framework for exa-feasible applications), preconditioned iterative solvers for quantum sciences, and a framework for automatic tuning (AT) with performance model. In the presentation, various types of achievements of ppOpen-HPC, ESSEX-II, and pK-OpenHPC project, such as applications using parallel preconditioned iterative solvers will be shown. Finally, future perspectives towards the Post Moore Era will be discussed.

## **Response Analysis of Soil-Foundation-Structure Interaction System of RC Building Using Nonlinear 3-dimensional FEM against Strong Earthquake**

Naohiro Nakamura\*, Takuya Suzuki\*\*

\*Hiroshima University, \*\*Takenaka Corporation

### **ABSTRACT**

It is important to consider the behavior of buildings against earthquakes beyond the current design level because no one can deny the possibility that buildings are attacked by such earthquakes. In this paper, the behavior of middle-rise RC buildings which are not designed by dynamic analysis are studied against the earthquake up to 2 times for the design level using detailed 3-dimensional nonlinear FEM considering soil-foundation-structure interaction. 3 type of soil models (Type1, Type2 and Type3) and 6story building models are used for the analysis. These models are considered with the nonlinear effect of both soil and buildings and the soil structure interaction effect, and analyzed by large scale FEM. The input earthquake level is from 1.0 to 2.0 times of Japanese Level 2 design earthquake. Based on these study, following results are obtained. 1) In the model of the hard soil, as the input increased, the plasticity of the building advanced, but the plasticity of the pile did not proceed. In the soft soil model, as the input increases, the plasticity of the pile progresses but the progress of the plasticity of the building was small. Also, in the model of the second type of general ground, as the input increased, both the plasticity of the building and the pile advanced. These qualitative properties are almost the same as the previous studies. On the other hand, quantitative evaluation is necessary to apply it to real problems. Regarding Level 2 and higher input levels, it is not clear how much accuracy the existing model has. Therefore, it is necessary to compare the accuracy of these models and study to make more suitable model. 2) We compared the models A and B which changed the behaviors of the piles after the ultimate stress. As a result, model A, which loses stiffness after ultimate stress, does not necessarily have the larger response than model B. In the case where the response of model B is large, the subsequent seismic motion is inputted, and the maximum response value is generated there. It is considered that the difference of the vibration characteristics of the coupled system in that state is the cause of the difference of the maximum response value.

## **Application of XFEM Magnetic Field Analysis Using Conformal Mapping to Kinked and Curved Crack Problem**

Shogo Nakasumi\*

\*National Institute of Advanced Industrial Science and Technology (AIST)

### **ABSTRACT**

Extended Finite Element Method (XFEM) is a method that makes the solution more accurate than the conventional FEM due to the effect of the enrichment function. We are researching on XFEM analysis which utilizes conformal mapping and potential flow theory by restricting the problem to two-dimensions. Non-destructive inspection technology is our engineering application field. So far, we have proposed XFEM magnetic field analysis for two-dimensional internal defects [1]. In that method, we could obtain accurate solution by using the Joukowski mapping even with coarse mesh division. In this presentation, we will present a two-dimensional XFEM analysis that maps the enrichment function of straight-line cracks to kinked cracks and/or curved cracks. In these mappings, we use the power function of the complex numbers and use the linear-transformation (or Moebius-transformation). The feature of this presentation is to create enrichment functions by utilizing conformal mapping, limiting the problem to two dimensions. Since the nature of the enrichment function does not change after mapping, high accuracy can be expected. Also, the two-dimensional X and Y coordinates correspond to the real part and the imaginary part of the complex number respectively, and the operation of the complex number is performed in this research. We could obtain almost reasonable solutions in the numerical examples for verification. [1] S. Nakasumi and M. A. Schweitzer, Magnetostatic XFEM Analysis for Internal Multiple Cracks based on Joukowski Mapping, Proceedings of 12th World Congress on Computational Mechanics (WCCM12), 2016.

## Nonlinear parallel FEM analysis on thermal warpage of multilayered high-density wiring interposer

Shinji Nakazawa<sup>\*</sup>, Kazuya Goto<sup>\*\*</sup>, Gaku Hashimoto<sup>\*\*\*</sup>, Hiroshi Okuda<sup>\*\*\*\*</sup>, Naoki Iwasaki<sup>\*\*\*\*\*</sup>

<sup>\*</sup>Shinko electric industries co., ltd., <sup>\*\*</sup>PEXProCS, LLC., <sup>\*\*\*</sup>The university of Tokyo, <sup>\*\*\*\*</sup>The university of Tokyo, <sup>\*\*\*\*\*</sup>Shinko electric industries co., ltd.

### ABSTRACT

It is one of the most important issues to reduce the warpage of semiconductor package substrate (interposer), which is caused by the thermal loadings in IC mounting processes, from the viewpoints of connection reliability or product yield. To predict such the behavior of thermal warpage, the finite element analysis has been widely used at the stage of interposer designing and development. However, since a typical interposer for microprocessor has very fine wiring structure with dimensions of the order of several microns in the substrate of several tens of millimeters square, the number of finite element meshes required for the FEM analysis can reach up to several hundreds of million. Therefore, some approximation techniques such as the material homogenization method have been applied to reduce the number of finite element mesh. In our previous work [1], we showed large-scale finite element analyses of interposer warpage, where the finite element meshes were generated as high resolution as possible to recognize the wiring patterns; the maximum number of finite element was 210 million. However, all of our analyses in the above were done in the frame of the linear theory (infinitesimal deformation theory). Moreover, the temperature-dependency or the viscoelasticity, which are thought to be essential to understand the warpage behaviors especially when the temperature is higher than glass-transition temperature ( around 200 deg.C ), did not be taken into account. In this study, we have performed the large-scale nonlinear analysis of interposer warpage by using FrontISTR, which is an open-source, finite element analysis software that enables massively parallel computations. New point in this work is that viscoelasticity and geometric nonlinearity, which were ignored in our previous work[1], are included. Furthermore, our analysis will be compared with the measurement by means of the digital image correlation (DIC) method. [Reference] 1] Shinji Nakazawa, Naoki Iwasaki, Tatsuro Yoshida, Ryuichi Matsuki, Kazuya Goto, Gaku Hashimoto and Hiroshi Okuda, A Large-Scale Finite Element Analysis for Predicting Thermal Warpage of a Semiconductor Package Substrate, WCCM &&&& APCOM 2016, pp. 2492-2492, 2016.

## Numerical Analysis of Flows in Coating Processes

Jaewook Nam<sup>\*</sup>, J. Alex Lee<sup>\*\*</sup>, Matteo Pasquali<sup>\*\*\*</sup>, Heechan Jung<sup>\*\*\*\*</sup>

<sup>\*</sup>Seoul National University, <sup>\*\*</sup>Saint-Gobain Northboro, <sup>\*\*\*</sup>Rice University, <sup>\*\*\*\*</sup>Sungkyunkwan University

### ABSTRACT

Various parts of modern electronic devices, e.g., battery electrodes, solar cell panels, and mobile displays, contains multi-functional films. Continuous liquid coating processes can produce these films in fast and efficient manner. Coating liquids include various type, shape, and size of organic and inorganic particles. Due to these particles, the rheological characteristics of the coating liquids become complex. Therefore, one has to consider such rheological aspects into the design of coating apparatuses or devices. In this respect, computational fluid mechanics plays a vital role in the process design. In this presentation, we will cover two types of flows: a liquid-bridge break-up flow of polymeric solutions with free surfaces and highly loaded suspension flows inside channels, called coating die manifold. We proposed an efficient method for the time-stepping algorithm, trapezoidal rule based on finite difference interrupt for viscoelastic non-Newtonian flows of a liquid-bridge breakup phenomena. For highly-loaded suspension flows, we considered the shear-induced particle migration. This migration can affect the distribution of non-Brownian particles inside the flows that may lead to problematic situations including particle flocculation or coagulation that can cause coating defects. For the prediction of the particle distribution, we implemented the particle transport model by Phillips et al. (1992) in three-dimensional die manifold flows. Navier-Stokes equations and the particle transport equation are discretized by a space-time finite element method with Galerkin-least squares stabilization for large-scale computations. Using this computational approach, we will explain the diffusive particle fluxes under the non-homogeneous shear rate flows that typically encountered in the coating flows.

## A Forward Incremental Prestressing Method for Biological Membranes

Nitesh Nama<sup>\*</sup>, Miquel Aguirre<sup>\*\*</sup>, C Alberto Figueroa<sup>\*\*\*</sup>

<sup>\*</sup>University of Michigan, USA, <sup>\*\*</sup>Tecnalia Research & Innovation, Spain, <sup>\*\*\*</sup>University of Michigan, USA

### ABSTRACT

Computational techniques to simulate cardiovascular flows in three-dimensional models of arteries have attracted significant interest owing to their applications in disease research, medical device design, and surgical planning. To model the blood flow in compliant arteries, various fluid-structure interaction (FSI) methods such as Arbitrary Lagrangian-Eulerian methods, immersed methods, and Coupled Momentum Method have been employed. To reduce the computational costs while simulating large 3D FSI models of vasculature, a membrane formulation can be employed to model the deformation of the arteries. The membrane assumption for the arteries is reasonable in view of the long wavelength of the cardiac pulse compared to the diameters of arteries.<sup>1</sup> The patient-specific vessel geometry is typically obtained through in-vivo medical imaging techniques. These geometries are known to represent a deformed configuration under in vivo loading conditions, thereby necessitating knowledge of the current state of stress to perform computational study predicting accurate stress values. Inverse methods that rely on the computation of a stress-free configuration are unsuitable for membrane formulations owing to the instabilities and non-uniqueness in case of buckling during the calculation of stress-free configuration. An alternative to inverse methods is the forward incremental approach presented by Grytz and Downs<sup>2</sup> for 3D solids, where the state of stress is calculated in an accurate and unique manner. In this work, we adapt this methodology to biological membranes to determine the state of prestress in a medically-obtained vessel anatomy. We provide a description of the different configurations in curvilinear coordinates, the tangent vectors, and of the evaluation of a constitutive model from an unknown unloaded configuration. As in 3D solid formulation<sup>2</sup>, this methodology results in an equivalent Lagrangian description formulated onto the in-vivo reference configuration, thereby requiring minor modifications to a standard total Lagrangian forward membrane algorithm. We present results for a variety of constitutive models including the isotropic Neo-Hookean model as well as a four fiber-family constitutive model. Several benchmark problems are presented to verify the accuracy of the method. Furthermore, patient-specific geometries are used to assess the adequacy of the method for cardiovascular FSI computations. [1] Figueroa, C. A. et al., Computer methods in applied mechanics and engineering, 195(41), 5685-5706, 2006. [2] Grytz, R. and Downs, J.C., Computer methods in biomechanics and biomedical engineering, 16(7), pp.768-780, 2013.

## **Simulations of Shock Front Evolution in a Submicron Thick Nanocrystalline Aluminum: A Study of the Role of Grain Size in the Formation of Atomistic Defects**

Raju Namburu<sup>\*</sup>, Ramakrishna Valisetty<sup>\*\*</sup>, Arunachalam Rajendran<sup>\*\*\*</sup>, Avinash Dongare<sup>\*\*\*\*</sup>,  
Ianni James<sup>\*\*\*\*\*</sup>

<sup>\*</sup>US ARL, <sup>\*\*</sup>US ARL, <sup>\*\*\*</sup>University of Mississippi, <sup>\*\*\*\*</sup>University of Connecticut, <sup>\*\*\*\*\*</sup>Leidos

### **ABSTRACT**

The role of the grain size in designing nanocrystalline aluminum (nc-Al) for superior shock strength was investigated via the study of the Hugoniot elastic limit (HEL, or the shock precursor) decay under one dimensional strain condition using large scale molecular dynamics (MD) simulations†. For this purpose, shock fronts' evolution and shock fronts' progression were simulated at impact velocities in the range of 0.7 km/s to 1.5 km/s in a range of atom systems that span a length scale from the nano- to the sub-micron scale range. Spanning the nano-scale range were considered five 920 Å thick 20 million nc-al atom systems each with grains with an average size in the range of 60 Å to 180 Å. Spanning the sub-micron scale range were considered three 5000 Å thick 2 billion nc-al atom systems each with grains with an average size in the range of 180 Å to 1000 Å. The evolving shock front profiles were studied in detail via the averaged shock stress distributions in the shock fronts' travel direction and the HEL decay curves were generated by the shock stress rise behavior post-HEL. To further identify the compression process in the nano-grains, the atomistic defects evolving upstream under the rising shock fronts were identified and quantified using a crystal analysis algorithm and a twin dislocation identification method. The results showed that certain dislocation partials are strongly influenced by the elastic-plastic transition response past the HEL. The atomistic defects generated were very much dependent on the grain size with the lower grain size leading to more defects and more plasticity.

## Numerical Simulation of Crack Propagation Using CT Specimen under Low Cycle Fatigue

Yoshiki Namita<sup>\*</sup>, Yoshitaka Wada<sup>\*\*</sup>, Rekisei Ozawa<sup>\*\*\*</sup>

<sup>\*</sup>Kindai University, <sup>\*\*</sup>Kindai University, <sup>\*\*\*</sup>Kindai University

### ABSTRACT

Crack growth under the elastic-plastic fracture is an important issue of the structural integrity, because seismic wave causes low cycle fatigue in the engineering structure. Many researchers have worked for many experiments and numerical analyses, however obvious and general criterion cannot be found until now. In order to develop a three-dimensional fracture criterion, the fully automated and state-of-the-art FE crack growth simulation should be realized. In the numerical simulation system, there are three important processes which are generation of the model with crack, stable and accurate FE analysis and post-processing for fracture evaluation. Crack growth simulation requires each process to be stable and connected each other in the one system. On the other hand, experiment should be conducted to determine material properties such as cyclic stress strain curve, crack tip opening displacement, J integral and so on. In particular, determination of parameters for appropriate cyclic stress strain curve is very important to actual evaluation of seismic loading. In order to reproduce the fundamental experiment result of a CT specimen under low cycle fatigue, we have developed the mesh generation scheme with thumbnail crack shape for a CT specimen. The present work shows the result of contact analysis of a CT specimen at the low cycles, because contact behavior of crack surfaces occurs under the applied cyclic loading with stress ratio  $R = ?1$ . To show the effectiveness of the criterion using stress triaxiality and equivalent plastic strain along a crack front in the CT specimen, the conventional generation phase and application phase analyses are conducted. The work shows comparisons between experimental result and numerical simulation results. We discuss the effectiveness of the criterion using stress triaxiality and equivalent plastic strain for crack growth criterion under the low cycle fatigue.

## Fully-Resolved Simulation of Multiphase Fluid-Structure Interaction Problems Using a Constraint-Based Immersed Boundary Method on Adaptive Meshes

Nishant Nangia<sup>\*</sup>, Amneet Pal Singh Bhalla<sup>\*\*</sup>, Neelesh A. Patankar<sup>\*\*\*</sup>

<sup>\*</sup>Northwestern University, <sup>\*\*</sup>Lawrence Berkeley National Laboratory, <sup>\*\*\*</sup>Northwestern University

### ABSTRACT

Many industrial fluid flow problems involve the interaction between heavy, rigid objects and one or more fluid phases. Fictitious domain and immersed boundary methods for simulating fluid-structure interaction (FSI) have been gaining popularity in the past few decades because of their robustness in handling arbitrarily moving bodies on regular Cartesian meshes. One such technique is the constraint-based immersed boundary method (cIB), which involves an additional projection step to enforce a rigidity constraint within the solid body domain [1]. However, in cases where the density ratio between the solid and fluid is large and the inertia of the rigid object must be adequately simulated, the cIB method can suffer from numerical instabilities. In this work, we outline the formulation and development of a parallel, variable-coefficient, constraint-based immersed boundary method using adaptive mesh refinement. The variable density and viscosity of the flow field are handled implicitly using an unsplit, incompressible Navier-Stokes solver that uses a projection method based preconditioner [2]. This enables efficient and stable simulations of large density and viscosity ratio FSI problems. The numerical technique is validated using past experimental studies of multiphase particulate flows. Novel applications of this method include simulation of sports ballistics problems and self-propelled vehicle aerodynamics, in which the density ratio between the fluid and solid regions are more than three orders of magnitude. [1] Bhalla, A. P. S., Bale, R., Griffith, B. E., & Patankar, N. A. (2013). A unified mathematical framework and an adaptive numerical method for fluid-structure interaction with rigid, deforming, and elastic bodies. *Journal of Computational Physics*, 250, 446-476. [2] Cai, M., Nonaka, A., Bell, J. B., Griffith, B. E., & Donev, A. (2014). Efficient variable-coefficient finite-volume Stokes solvers. *Communications in Computational Physics*, 16(5), 1263-1297.

## **A Bayesian Interpretation of Kernel-Based Methods for Multifidelity Approximation**

Akil Narayan\*

\*University of Utah

### **ABSTRACT**

A recently developed technique for forward uncertainty quantification (UQ) uses the induced reproducing kernel Hilbert space from a low-fidelity parametric model as a tool to understand the parametric variability of a more expensive high-fidelity model. This has been the cornerstone of a multifidelity simulation technique that seeks to attain accuracy comparable to an expensive high-fidelity model with the cost of an inexpensive low-fidelity model. We show that this methodology, explicitly developed for forward UQ problems, has an interesting Bayesian interpretation by introducing suitable notions of prior and posterior distributions.

## Fluctuating Hydrodynamics Simulations of Hydrodynamic Instabilities at Meso- and Macro-scales

Kiran Narayanan\*, Ravi Samtaney\*\*

\*King Abdullah University of Science and Technology, \*\*King Abdullah University of Science and Technology

### ABSTRACT

Traditional deterministic hydrodynamic equations such as the compressible Navier-Stokes equations (CNS) describe macroscopic systems where the probabilistic effects of thermal fluctuations are negligible. However, there are systems in which thermal fluctuations can drive the macroscopic physical phenomenon; one such example is hydrodynamic instability at fluid-fluid interfaces where they affect the flow both quantitatively and qualitatively [1]. Here, we obtain numerical solutions of the two-fluid fluctuating compressible Navier-Stokes equations (FCNS) in order to study the effect of such fluctuations on the mixing behavior in the Richtmyer-Meshkov instability (RMI) and Kelvin-Helmholtz instability (KHI). FCNS are a system of stochastic partial differential equations that are a coarse-grained representation of microscopic dynamics, constitute a meso-level model of the system and provide a compromise between computational cost and the ability to capture thermal fluctuations. Their validity for non-equilibrium systems was derived by Espanol [2]. The numerical solver was developed in-house and verified using the equilibrium spectrum of fluctuations of hydrodynamic quantities. For RMI, we present results from simulations of three systems having length scales with decreasing order of magnitude ( $O(10^{-5})$ ,  $O(10^{-6})$ ,  $O(10^{-7})$  meters) that span from macroscopic to mesoscopic, with a corresponding increase of thermal fluctuations. Simulations show that for all systems, deterministic mixing behavior emerges as the ensemble-averaged behavior of several fluctuating instances, with the FCNS solution providing bounds on the growth rate of the amplitude of the mixing layer. Traditionally, a stochastic flux  $Z(x,t)$  is discretized using a regularization factor that scales as the inverse square root of  $(h*dt)$  for spatial interval  $h$ , time interval  $dt$ , with  $h$  greater than  $h_0$  where  $h_0$  produces the right equilibrium spectrum. For the mesoscale RMI systems simulated, it was desirable to use a cell size smaller than this limit in order to resolve the viscous shock. This was achieved by using a modified regularization factor that scaled as the inverse square root of  $(\max(h,h_0)*dt)$  with  $h_0$  being an integer multiple of  $h$  when  $h \leq h_0$ . For KHI, ensemble-averaged mixing behavior for similar length-scale systems will be presented. References [1] K. Kadau, C. Rosenblatt, J. L. Barber, T. C. Germann, Z. Huang, P. Carles, B. L. Holian, and B. J. Alder, "The Importance of Fluctuations in Fluid Mixing," Proc. Nat. Acad. Sci. U.S.A., vol. 104, pp. 7741–7746, 2007 [2] P. Español, "Stochastic differential equations for non-linear hydrodynamics," Physica A: Statistical Mechanics and its Applications, Vol. 248, No. 1-2, pp. 77–96, Jan 1998.

## DNS of Near-Wall Flame Propagation

Kosuke Narukawa<sup>\*</sup>, Yuki Minamoto<sup>\*\*</sup>, Masayasu Shimura<sup>\*\*\*</sup>, Mamoru Tanahashi<sup>\*\*\*\*</sup>

<sup>\*</sup>Tokyo Institute of Technology, <sup>\*\*</sup>Tokyo Institute of Technology, <sup>\*\*\*</sup>Tokyo Institute of Technology, <sup>\*\*\*\*</sup>Tokyo Institute of Technology

### ABSTRACT

Laminar flame speed is an important quantity for combustion analysis and turbulent combustion modeling. In a previous study [1], time-resolved CH chemiluminescence of methane-air flames impinging a wall were measured, and the flame displacement speed was estimated as a function of wall distance. They concluded that the flame displacement speed just before flame quenching corresponds to the laminar flame speed of a corresponding thermochemical condition. In this study, to explore the applicability of the above feature to experimental measurements of laminar flame speed, relationship between laminar flame speed and near-wall flame behavior is investigated under various conditions based on direct numerical simulations (DNS). Two-dimensional DNS of ignition combustion between two parallel walls are performed for methane, hydrogen, and n-heptane/air premixed flames under several mixture temperatures, wall temperatures and ignition positions. The mixture temperature is set to 300 K or 700 K, and the wall temperature is set to 300 K, 500 K or 700 K. An initial high-temperature region set in the center of the computational domain is given by a Gaussian function. The dependence of the results on the distance from ignition position to the wall is investigated by changing the computational domain. The distance from ignition position to the wall is 1.5 mm, 2.0 mm, 2.5 mm or 3.0 mm. In all cases, equivalence ratio and pressure are set to 1.0, 0.1 MPa respectively. Using the results of DNS, the flame front position nearest to the wall and defined by the point where the gradient of OH mass fraction takes maximum value, and the flame displacement speed defined by the temporal variation of this position are calculated. By estimating the flame speed under various conditions as a function of the distance from the wall, it is clarified that the near-wall flame propagation has unique characteristics and following results are obtained. (i) Under the conditions where the wall temperature equals unburnt gas temperature, the flame speed has a local minimum or inflection point near the wall, and this value corresponds to the laminar flame speed of the mixture. (ii) Similar trends are observed in near-wall flame speed variation regardless of mixture temperature, ignition position or fuels. Furthermore, the effect of the wall on the flame is investigated, and the mechanism for these characteristics is also discussed. References [1] Tsuzuki et al. , Proceedings of Thermal Engineering Conference, 2009, pp. 7-8.

## Feasibility of Myocardial Material Parameter Estimation from 2D Images

Anastasia Nasopoulou\*, David Nordsletten\*\*, Steven Niederer\*\*\*, Pablo Lamata\*\*\*\*

\*Department of Biomedical Engineering, King's College London, \*\*Department of Biomedical Engineering, King's College London, \*\*\*Department of Biomedical Engineering, King's College London, \*\*\*\*Department of Biomedical Engineering, King's College London

### ABSTRACT

Myocardial material parameter estimation is an essential step towards both the personalization of cardiac biomechanical models and the in vivo estimation of myocardial stiffness, a proposed clinical index of diagnostic and prognostic value. Currently the process requires the use of 3D cardiac imaging data, which -unlike the ubiquitous 2D ultrasound images- are costly and not widely available in clinical practice. Aiming to translate recent advances in cardiac modelling into the clinic, we develop in this study a method for myocardial material parameter estimation from 2D images, such as provided by 2D or 3D speckle tracking echocardiography. The proposed methodology relies on previous work [1], where an energy based cost function (CF) was introduced to address the inability of displacement/strain based CFs to uniquely confine the parameter space. In this study, a modified version of the CF is used based on the 'virtual works' principle (VWP) for more flexibility to adapt to the limited data, while the myocardial material behavior is described by a popular transversely isotropic model [2]. Using a combination of the modified CF and the VWP expressed at end diastole, our pipeline focuses on recovering two of the most inter-correlated parameters by keeping the remaining two exponential parameters fixed. To test the accuracy and robustness of the pipeline against model assumptions and data noise, two synthetic data sets were created from the passive inflation of a truncated ellipsoid, mimicking the availability of pressure recordings and 'long axis images' with either 3D or 2D displacement and deformation information. Using the proposed pipeline, the parameter estimation in the synthetic dataset recovered the ground truth values. A sensitivity analysis showed that the method was robust to offsets of the imaging plane from the axis of symmetry, when 3D deformation data is available. The most critical factor identified was the image quality, while model assumptions concerning the tissue microstructure (including the fixed exponential parameter values) had the least impact on results. Our study has demonstrated that accurate predictions of myocardial material parameters can be performed from 2D imaging data. In future work, the pipeline is applied to clinical data from heart failure patients. [1] Nasopoulou et al. Improved identifiability of myocardial material parameters by an energy-based cost function. *BMMB* (2017). [2] Guccione et al. Passive material properties of intact ventricular myocardium determined from a cylindrical model. *J Biomech Eng* (1991).

## Functionality of the Pelvic Floor after Vaginal Delivery with Episiotomy

Renato Natal\*, Dulce Oliveira\*\*, Marco Parente\*\*\*, Teresa Mascarenhas\*\*\*\*

\*INEGI, \*\*INEGI, \*\*\*INEGI, \*\*\*\*Hospital São João

### ABSTRACT

**Introduction** To increase the birth canal and prevent extensive vaginal tears, incisions in the perineal region were made. Currently, a policy of restrictive episiotomy is favored for spontaneous deliveries [1]. To identify the influence of episiotomy in the functionality of the pelvic floor, numerical simulations of vaginal deliveries in different fetal positions were performed based on the Finite Element Method. **Methods** In general terms, the childbirth model includes the most requested muscles of the pelvic floor region and the fetus. Two fetal positions were simulated, occipitoanterior (OA) and occipitoposterior (OP). Hyperelastic material models were used to describe the material behavior of the several structures of the model. **Results** As expected, the forces opposing the descent of the fetus are higher for deliveries with the fetus in OP position. Without episiotomy, the maximum value of force observed is around 20% higher in OP position. For deliveries with episiotomy, the forces reduction may be as high as 60% in OP position and greater than 50% in OA position. A lag between the moment of the peak force in the two positions is observed, which coincides with the moment when the pelvic diameters for the OP and OA positions are maximums. Regarding the widening of the incision, the highest values observed were for the episiotomies performed at 30°, which corresponds to the incisions that caused greater reductions in the values of the forces opposing the descent of the fetus. Analyzing the maximum principal stress along the lower portion of the muscles, it is verified that the insertion points in the symphysis pubis are the ones presenting the higher values, followed by the middle portion. The episiotomy at 30° is the closest to this middle region, which makes sense to be the one with the best results. Considering the medial portion, the stress values are higher in the rightmost portion. These results predict that, in this model, episiotomies performed on the right side would lead to better outcomes. **Conclusions** Fetal malposition (OP) induces greater extension of the muscles compared to normal position (OA), leading to increases of stretch. Also, the higher value of force required to achieve delivery might justify the increased need of surgical interventions. In mechanistic terms, episiotomy has proven to be a protective factor during delivery, reducing the risk of other pelvic floor injuries, and urogynecological complaints. **References** 1. Carroli G, Mignini L, (2009) In: Cochrane Database of Systematic Reviews, pp1-53.

## **A Novel Error Indicator and an Adaptive Refinement Technique Using the Scaled Boundary Finite Element Method**

Sundararajan Natarajan<sup>\*</sup>, Ean Tat Ooi<sup>\*\*</sup>, Pramod ALN<sup>\*\*\*</sup>, Song Chongmin<sup>\*\*\*\*</sup>

<sup>\*</sup>Department of Mechanical Engineering, Indian Institute of Technology-Madras, <sup>\*\*</sup>School of Engineering and Information Technology, Federation University Australia, VIC 3350, Australia., <sup>\*\*\*</sup>Department of Mechanical Engineering, Indian Institute of Technology-Madras, <sup>\*\*\*\*</sup>School of Civil and Environmental Engineering, University of New South Wales, Sydney, Australia.

### **ABSTRACT**

In this talk, an adaptive displacement based formulation based on the scaled boundary finite element method on quadtree meshes for linear elasticity problems is discussed. Within this framework, the elements with hanging nodes are treated as polygonal elements and thus does not require special treatment. The adaptive refinement is supplemented with a novel error indicator. The local error is estimated directly from the solution of the scaled boundary governing equations. The salient feature is that it does not require any stress recovery techniques. The efficacy and the robustness of the proposed approach is demonstrated with a few numerical examples from linear elasticity.

## **A Numerical Model for Quantifying the Reduction in the Structural Service Life of Flexible Pavements due to Dynamic Axle Loads**

Fermín Navarrina<sup>\*</sup>, Luis Ramírez<sup>\*\*</sup>, José París<sup>\*\*\*</sup>, Xesús Nogueira<sup>\*\*\*\*</sup>, Ignasi Colominas<sup>\*\*\*\*\*</sup>,  
Manuel Casteleiro<sup>\*\*\*\*\*</sup>, Manuel Ruiz<sup>\*\*\*\*\*</sup>, José R. Fernández-de-Mesa<sup>\*\*\*\*\*</sup>

<sup>\*</sup>University of La Coruna, <sup>\*\*</sup>University of La Coruna, <sup>\*\*\*</sup>University of La Coruna, <sup>\*\*\*\*</sup>University of La Coruna,  
<sup>\*\*\*\*\*</sup>University of La Coruna, <sup>\*\*\*\*\*</sup>University of La Coruna, <sup>\*\*\*\*\*</sup>University of La Coruna, <sup>\*\*\*\*\*</sup>University of La  
Coruna

### **ABSTRACT**

A numerical model for the fatigue analysis of flexible pavements considering the effects of dynamic axle loads is presented in this paper. The main objective of this work is to quantify the reduction in the structural service life of the pavement due to the rise of the dynamic axle loads exerted by the traffic, as the progressive deterioration of the road profile occurs. First, the procedure for the fatigue analysis of flexible pavements, as defined in the Spanish Standard 6.1-IC [1], is explained in detail. The implementation herein presented is specific for this Standard, but the underlying concepts are not restrictive, and the model can be easily adapted to fit the distinctive features of other regulations. Second, the concepts of accumulated damage and structural service life are formalized in mathematical terms. Next, dynamic axle loads are introduced, which leads to the definition of a suitable accumulated fatigue damage indicator that takes into account these effects. Dynamic axle loads are introduced in this formulation by means of a so-called effective dynamic load amplification factor. For the quantification of this factor, the Quarter-Car model is extended to allow for computing the time evolution of the dynamic axle load exerted by a heavy vehicle on the pavement [2]. The model is completed by adding a simple procedure for simulating how the road profile deteriorates over time. Finally, an application example is presented. [1] DGC / Dirección General de Carreteras, Secretaría de Estado de Infraestructuras. Norma 6.1--IC "Secciones de Firme" de la Instrucción de Carreteras. Orden FOM/3460/2003 de 28 de noviembre (BOE de 12 de diciembre de 2003). Centro de Publicaciones del Ministerio de Fomento, Gobierno de España, 2003. [2] F. Navarrina, L. Ramírez, J. París, X. Nogueira, I. Colominas, M. Casteleiro y J.R. Fernández-de-Mesa. Comprehensive Model for Fatigue Analysis of Flexible Pavements Considering Effects of Dynamic Axle Loads. Transportation Research Record: Journal of the Transportation Research Board, DOI: 10.3141/2524-11, No. 2524, pp. 110-118, Washington (2015).

## Recovery of the Contact Stress Field in the Cartesian Grid Finite Element Method (cgFEM)

José Manuel Navarro-Jiménez\*, Héctor Navarro-García\*\*, Enrique Nadal\*\*\*, Manuel Tur\*\*\*\*, Juan José Ródenas\*\*\*\*\*

\*Universitat Politècnica de València, \*\*Universitat Politècnica de València, \*\*\*Universitat Politècnica de València, \*\*\*\*Universitat Politècnica de València, \*\*\*\*\*Universitat Politècnica de València

### ABSTRACT

This paper proposes an adaptation of the SPR-C technique[1] (Superconvergent Patch Recovery[2] with constraints) for the evaluation of a recovered stress field at the contact area of mechanical components. In the context of the finite element method for the resolution of 2D linear elasticity problems, ref. [1] presented a procedure, based on the use of Lagrange multipliers, by means of which the polynomials used to describe the locally recovered stress field were enforced to satisfy the equilibrium and compatibility equations. In this work, we have extended the technique described in [1] to improve the stress field around the contact. To do this, and for the patches of elements involved in the contact, we simultaneously evaluate two stress fields (one for each of the contacting bodies) satisfying not only the previously mentioned equilibrium and compatibility equations but also the contact equilibrium equations. This is obtained by imposing the continuity of the normal and tangential stresses of the two stress fields along the contact surface. One of the most relevant characteristics of this work is that it has been developed within a Cartesian grid framework (cgFEM [3]) where the FE mesh is independent of the geometry. The numerical results show a considerable accuracy enhancement of the stress field at the contact area that improves the behaviour of the contact algorithm and its accuracy. Acknowledgements: The financial support to this work of Generalitat Valenciana (PROMETEO/2016/007) and the Spanish Ministerio de Economía, Industria y Competitividad (DPI2017-89816-R) is greatly acknowledged. REFERENCES [1] JJ Ródenas, M Tur, FJ Fuenmayor, A Vercher "Improvement of the superconvergent patch recovery technique by the use of constraint equations: The SPR-C technique". International Journal for Numerical Methods in Engineering 70, 705–727 (2007). [2] OC Zienkiewicz, JZ Zhu. "The superconvergent patch recovery and a posteriori error estimates. Part I: The recovery technique". International Journal for Numerical Methods in Engineering, 33, 1331-1364 (1992). [3] E Nadal, JJ Ródenas, J Albelda, M Tur, JE Tarancón, FJ Fuenmayor. Efficient Finite Element Methodology Based on Cartesian Grids: Application to Structural Shape Optimization. Abstract and Applied Analysis 2013, Article ID 953786, 19 pages (2013).

## Fracture Prediction in Patients with Skeletal Metastasis with CT-Based Rigidity Analysis

Ara Nazarian\*, Vahid Entezari\*\*, David Zurakowski\*\*\*, Nathan Calderon\*\*\*\*, John Hipp\*\*\*\*, Timothy Damron\*\*\*\*\*, Brian Snyder\*\*\*\*\*

\*BIDMC and HMS, \*\*BIDMC and HMS, \*\*\*CHB and HMS, \*\*\*\*BIDMC and HMS, \*\*\*\*\*Orthomet, \*\*\*\*\*SUNY Upstate, \*\*\*\*\*BIDMC and HMS

### ABSTRACT

Cancer patients are living longer due to new and aggressive treatments, yet at sites of skeletal metastasis patients experience significant complications. The dilemma for the physicians is to decide whether the metastatic tumor has weakened the bone such that pathological fracture is imminent. A multi-center, prospective, in-vivo study was conducted to identify significant predictors of physicians' treatment plan for skeletal metastasis based on clinical fracture risk assessments (Mirels score) and the proposed CT-based Rigidity Analysis (CTRA). One hundred and twenty four patients with 149 appendicular skeletal metastatic lesions were enrolled. Orthopaedic-oncologists were asked to select a treatment plan based on their initial risk assessment using Mirels method and follow up on patients over a 4-month period. Then, CTRA was performed on CT scans of the involved bones, and the results were provided to the enrolling physicians, who were asked to reassess their treatment plan. The pre- and post-CTRA treatment plans were compared to identify cases where treatment plan could be changed resultant from the CTRA report. Patient follow up resulted in 7 fracture cases, where the CTRA method was 100% sensitive and 90% specific, whereas Mirels method was 71% sensitive and 50% specific. Pain, lesion type and lesion size were significant predictors of the pre-CTRA plan. After providing the CTRA results, physicians changed their plan for 36 patients. CTRA results, pain and primary source of metastasis were significant predictors of post-CTRA plan. Lesion type and size along with pain level were relevant clinical information that influenced physician's plan for management of metastatic appendicular lesions. Physician's treatment plan and fracture risk prediction were significantly influenced by introduction of the CTRA results.

## **Roughness, Toughness and the Possibility of Crack Path Engineering**

Alan Needleman<sup>\*</sup>, Ankit Srivastava<sup>\*\*</sup>, Shmuel Osovski<sup>\*\*\*</sup>

<sup>\*</sup>Department of Materials Science & Engineering, Texas A&M; University, College Station, TX, <sup>\*\*</sup>Department of Materials Science & Engineering, Texas A&M; University, College Station, TX, <sup>\*\*\*</sup>Faculty of Mechanical Engineering, Technion - Israel Institute of Technology, Haifa, Israel

### **ABSTRACT**

Fracture surfaces of structural metals are rough and the statistics of that roughness are largely set by the material microstructure together with the nature of the imposed loading. A material's resistance to crack growth is also set by the same factors. Hence a basic question is: what is the relation, if any, between measures of the statistics of fracture surface roughness and measures of the material's crack growth resistance? Simulations of ductile fracture will be discussed that address this issue. The calculations are carried out within a continuum mechanics framework with a model of void nucleation, growth and coalescence incorporated into the constitutive relation. Simulations will be discussed that suggest the possibility that a material's crack ductile growth resistance can be significantly increased by suitably designing the microstructure to control the crack path. The results also suggest the possibility that suitably adding defects to a material can alter the crack path in a way that increases its ductile fracture resistance.

## A Comparison of Hertzian and Differential-variational Inequality Contact Models

Dan Negrut<sup>\*</sup>, Arman Pazouki<sup>\*\*</sup>, Michał Kwartka<sup>\*\*\*</sup>, Kyle Williams<sup>\*\*\*\*</sup>, William Likos<sup>\*\*\*\*\*</sup>, Radu Serban<sup>\*\*\*\*\*</sup>

<sup>\*</sup>University of Wisconsin-Madison, <sup>\*\*</sup>California State University, <sup>\*\*\*</sup>University of Wisconsin-Madison, <sup>\*\*\*\*</sup>University of Wisconsin-Madison, <sup>\*\*\*\*\*</sup>University of Wisconsin-Madison, <sup>\*\*\*\*\*</sup>University of Wisconsin-Madison

### ABSTRACT

We present and numerically compare two manifestly different contact models using a set of granular dynamics experiments. The first contact model, referred to herein as DEM-P from “discrete element method via penalty”<sup>1</sup>, is a force-displacement model that is commonly used in the soft matter physics and geomechanics communities. The second approach, called DEM-C from “complementarity”<sup>2</sup>, considers the grains perfectly rigid and enforces non-penetration via complementarity conditions; it is commonly used in robotics and computer graphics applications. Herein, we use a cone-complementarity formulation that formulates DEM-C as a global quadratic optimization problem subjected to conic constraints. DEM-P and DEM-C are manifestly unlike each other since they use different (1) approaches to model the frictional contact problem; (2) sets of model parameters to capture the physics of interest; and (3) classes of numerical methods to solve the differential equations that govern the dynamics of the granular material. Herein, we report numerical results for five experiments: shock wave propagation, cone penetration, direct shear, triaxial loading, and hopper flow, which we used to compare the DEM-P and DEM-C solutions. This experiments helped us reach two conclusions. First, both DEM-P and DEM-C are predictive; i.e., they predict well the macro-scale emergent behavior by capturing the dynamics at the micro-scale. Second, there is no clear winner insofar as handling granular dynamics is concerned. DEM-P runs into difficulties when handling complex geometries owing to its (1) ad-hoc approach to producing the friction and contact forces under these circumstances; and, (2) sensitivity to contact information; i.e., the geometrical or collision detection component, when small variations in contact information lead to sizable changes in forces. To a point, we found DEM-P insensitive to shearing rates, which could be increased, and to contact stiffness, which could be decreased, both by orders of magnitude. This lack of sensitivity can be traded for larger simulation step-sizes that led in some experiments to significant speedups over DEM-C. The DEM-P vs. DEM-C comparison was carried out using a public-domain, open-source software package called Chrono.

## Development of the CAVEMAN Human Body Model: Lower Extremity Injury Assessment in Underbody Blast Accelerative Loading Conditions

Ryan Neice<sup>\*</sup>, Matthew Panzer<sup>\*\*</sup>, Kevin Lister<sup>\*\*\*</sup>, Kent Butz<sup>\*\*\*\*</sup>, Chad Spurlock<sup>\*\*\*\*\*</sup>, Rajarshi Roy<sup>\*\*\*\*\*</sup>

<sup>\*</sup>University of Virginia, <sup>\*\*</sup>University of Virginia, <sup>\*\*\*</sup>Corvid Technologies, <sup>\*\*\*\*</sup>Corvid Technologies, <sup>\*\*\*\*\*</sup>Corvid Technologies, <sup>\*\*\*\*\*</sup>Corvid Technologies

### ABSTRACT

The use of improvised explosive devices (IED) against U.S. military vehicles in recent conflicts has led to an increased need for accurately predicting mounted warfighter injuries. The lower extremities are the most often injured region of the body in underbody blast (UBB) events. Computational injury assessment in conjunction with the use of experimental anthropomorphic test devices (ATD) in loading conditions similar to UBB events provides more comprehensive occupant safety analyses for military vehicles. A major benefit of computational injury assessment is its ability to describe soft tissue failures that are otherwise difficult to capture in experimental ATD testing. The Computational Virtual Experiment Man (CAVEMAN) is a detailed human body model focused on expanding injury prediction capabilities for skeletal and soft tissues. The CAVEMAN finite element model is based on a 50th percentile human male developed for use in high performance computing. Comparisons to PMHS experimental data have been performed with the CAVEMAN lower extremity model in order to validate its sub-injurious response (Butz, et al. 2017). Current efforts are focused on injury prediction capabilities with the CAVEMAN model as compared to an injurious PMHS experimental data set (Bailey 2016). In addition, a sensitivity study concerning biological variabilities such as positioning, material properties, and anatomical geometry was performed to understand how such parameters affect injury localization and severity in an underbody blast loading event. References: Butz, K., Spurlock, C., Roy, R., Bell, C., Barrett, P., Ward, A., Xiao, X., Shirley, A., Welch, C., and Lister, K. (2017). Development of the CAVEMAN Human Body Model: Validation of Lower Extremity Sub-Injurious Response to Vertical Accelerative Loading. Stapp Car Crash Journal, Vol. 61 Bailey, A. (2016). Injury Assessment for the Human Leg Exposed to Axial Impact Loading. University of Virginia, Department of Mechanical and Aerospace Engineering, PHD.



## Software-in-the-Loop based Optimization of Actuator/Sensor Placement for Active Vibration Control

Tamara Nestorovic\*, Atta Oveisi\*\*, Afshin Sattarifar\*\*\*

\*Ruhr-Universität Bochum, Mechanics of Adaptive Systems, \*\*Ruhr-Universität Bochum, Mechanics of Adaptive Systems, \*\*\*Ruhr-Universität Bochum, Mechanics of Adaptive Systems

### ABSTRACT

Modern engineering concepts and interdisciplinary development often require coupling of different techniques, methods and tools towards finding optimal solutions. Optimization is a crucial step in smart engineering structures development and design. One of the often addressed problems in smart structures is active vibration/noise control (AVC/ANC), which requires both the controller design expertise and structural dynamics modeling and characterization knowledge. While the control community on one hand often deals with mainly mathematically based development of novel controllers (state or output feedback based ones), state reconstruction and disturbance estimation, anti-windup compensators, and input/output filters, with implementation often restricted to abstract numerical examples or reduced order problems without real-world applications, the engineering community on the other hand requires implementation of such methods to different problems (among others AVC and ANC) ranging from civil structures to aerospace ones. This contribution aims at closing this gap by proposing a new Software-in-the-Loop (SiL) scheme which enables a control engineer to design AVC based on optimization of actuator/sensor placement on an approximation of a real-world application without requiring a very deep knowledge of the structural dynamics phenomena. The proposed SiL scheme is based on coupling structural dynamics modeling and controller design tools, i.e. the finite element (FE) package ABAQUS and MATLAB. The focal contribution of this coupling scheme is in adopting FORTRAN as a messenger between ABAQUS kernel and MATLAB engine. In contrast to the methods in the literature, this interconnection enables the user to call and execute functions within MATLAB in an online setting. Further coupling involves a Python script which defines the structural properties such as geometry, material and assembly of the CAE model, whereas the FORTRAN UAMP subroutine controls the MATLAB function execution. Sensor elements on a predefined set of nodes are specified in ABAQUS output variables, while the actuation is realized through the user-defined load amplitudes. UAMP subroutine determines the value of the user-defined amplitude (control signal) in feedback from the sensor variables. The novelty in establishing the feedback is defined at this stage, by forwarding the sensor values from UAMP subroutine to MATLAB engine. This procedure enables the use of functions in MATLAB and implementation of arbitrary control laws, which in turn define the optimization criteria with respect to actuator/sensor placement. In this contribution we show the implementation of the method on a benchmark AVC problem. Accordingly, all the benchmark problems in AVC can be efficiently investigated in this framework.

## Multiscale Elastography Using Multimodal Image Data Combined with Inverse Modeling

Corey Neu<sup>\*</sup>, Luyao Cai<sup>\*\*</sup>, Soham Ghosh<sup>\*\*\*</sup>

<sup>\*</sup>University of Colorado Boulder, <sup>\*\*</sup>Purdue University, <sup>\*\*\*</sup>University of Colorado Boulder

### ABSTRACT

Quantification of high resolution spatiotemporal motion, structural, and spatial changes in biological tissues are required to understand the mechanobiological regulations in physiological or pathological altered mechanical environments. Visualization of internal tissue and cellular displacements and strains require specialized, multiscale imaging techniques including displacements MRI or microscopy. However, displacement and strain information does not directly correlate with spatial distributions of stiffness, which are critical to the understanding pathology and deviations from normal. To overcome these limitations, we describe a general approach to quantitatively assess spatiotemporal strain and material properties in biological systems using an imaging and inverse modeling-based technique. We acquired displacement-sensitive image data for hydrogels, in situ ovine tibiofemoral joint cartilage, and single cells. We prepared complex, heterogeneous tissues or mimics, including layered agarose constructs of 2% and 4% w/v, and skeletally-mature ovine stifle (knee) cartilage. Deformation was computed in samples that were cyclically loaded within an MRI system. Additionally, we visualized deformation in nuclei of cardiomyocytes isolated from mouse embryos. We utilized finite element-based hyperelastic (e.g. neo-Hookean) constitutive formulations to account for complex 3D joint geometry, and topology optimization. The design variable was the relative density of each finite element, which was varied to minimize the absolute difference of the displacements at  $N$  discrete points between the simulation and the imaging data. The optimization formulation was solved using an iterative design process, where elemental relative densities were updated with the iteration until a stop criterion was satisfied, and scaled to the modulus at each location using known loading/boundary conditions. Distributions of the absolute stiffness in samples were derived from MRI/microscopy displacement data and topology optimization. The stiffness maps showed distinct differences between materials, with the averaged value for 2% and 4% agarose respectively as 5.4 kPa and 15.7 kPa. Heterogeneous stiffness distributions were also observed in ovine cartilage and cardiomyocyte nuclei, and related to structural characteristics. Combined imaging data with topology optimization allows for measurement of quasi-static elastography in biological tissues and cells over multiple length scales. Our results show stiffness maps that are robust to noise, but that also require careful attention to boundary condition settings, to ensure stability during the optimization process. This method may allow for the noninvasive measurement of tissue/cell stiffness following damage, as a promising functional imaging biomarker.

## **Fatigue Life Prediction by Extended Gurson Model for SAE 1045 and S460N Steels**

Raniere Neves<sup>\*</sup>, Lucival Malcher<sup>\*\*</sup>, Guilherme Ferreira<sup>\*\*\*</sup>

<sup>\*</sup>University of Brasília, <sup>\*\*</sup>University of Brasília, <sup>\*\*\*</sup>University of Brasília

### **ABSTRACT**

Several machines components and structures are subjected to cyclic loading and the phenomenon of progressive rupture, known as fatigue, can be analyzed. The study of fatigue is very important during the design of component because it is necessary to avoid sudden failures that may result in accidents and also avoid oversizing components so that it does not lose competitiveness. This contribution suggests fatigue life prediction for two different materials (SAE 1045 and S460N steels) by means of an iterative approach based on the evolution of the void volume fraction accounted for an extended Gurson model after each cycle of loading. Due to its characteristics, the traditional Gurson damage model (1977) can not be used to fatigue life prediction. The first limitation that model shows an unreal healing behavior for cases of cyclic axial loads, where all void growth generated during the tension step is cured during the compression step, therefore there is no evolution of damage variable cycle to cycle. The second limitation is the fact that the Gurson model does not account the void distortion during predominantly shear loads, so does not occur the evolution of the damage variable in this cases. In order to overcome both limitations, this paper proposes an extended Gurson model where an unrecovered parameter is added to the void growth law with the role of identifying by means of stress triaxiality whether the material is being tensioned or compressed and thus change the response of the material to avoid the total recovery of the damage generated during tension step and the paper also proposes the coupling of void shearing mechanism of damage proposed by Nahshon and Hutchinson (2008) to the Gurson model in order to account for damage in predominantly shear loads too. This contribution presents the validation of the proposed approach by means of the simulation of axial, torsional and axial torsional cyclic loads taken from the literature for SAE 1045 and S460N steels.

## Multi-Physics, Multi-scale Performance Assessment of Geological CO<sub>2</sub>

Pania Newell\*, Mario Martinez\*\*

\*University of Utah, \*\*Sandia National Laboratories

### ABSTRACT

Deep geological formations are considered as a potential tool for permanent storage of large amounts of carbon dioxide over long periods of time ( $10^3$ - $10^4$  years). Their overall performance is highly affected by various trapping mechanisms such as structural, capillary, solubility, and mineral mechanisms. The presence of faults, joints, pre- or newly-formed fractures and other mechanical discontinuities that range in scale from micro-cracks (micrometers) to fractures (10s-100s of meters) to faults (100s meters to km) affect the state of stress and influencing the structural trapping mechanisms. Opening/closure or generation of new fractures can alter the flow paths for injection or withdrawal of fluids. The magnitude of the pore pressure also depends on hydrological and geomechanical properties of rock formation, wellbore orientation, injection rate and injection schedule. In this presentation, we will address (i) geomechanical testing at core scale for material model calibration, (ii) impact of formation thickness, wellbore orientation, injection rate, presence of fault and pre-existing fractures within the caprock to highlight the importance of the spatial and temporal scales and coupled processes within geological formations. Moreover, our results indicates that the integration between experimental and numerical modeling is critical to understand the long-term behavior of geological carbon storage. Sandia National Laboratories is a multimission laboratory managed and operated by National Technology and Engineering Solutions of Sandia, LLC., a wholly owned subsidiary of Honeywell International, Inc., for the U.S. Department of Energy's National Nuclear Security Administration under contract DE-NA-0003525.

# DISCRETE ELEMENT MODELLING OF SLEEPER-BALLAST INTERACTION UNDER IMPACT LOADING

CHAYUT NGAMKHANONG<sup>1,2</sup> AND SAKDIRAT KAEWUNRUEN<sup>1,2</sup>

<sup>1</sup>Department of Civil Engineering, School of Engineering,  
University of Birmingham, Birmingham B152TT, United Kingdom  
Email address; cxn649@student.bham.ac.uk, s.kaewunruen@bham.ac.uk

<sup>2</sup>Birmingham Centre for Railway Research and Education, School of Engineering,  
University of Birmingham, Birmingham B152TT, United Kingdom

**Key words:** Impact Loading, Discrete Element Modelling, Sleeper, Ballast, Railway Track.

**Abstracts.** Generally, track structure experience impact load (also called “shock load”) due to the irregularities of either wheel or rail. The impact load, that may greatly exceed the static wheel load, are mainly caused by wheel/rail abnormalities such as poor weld geometry, rail corrugation, and rail defects like spalling, wheel burns and squats. Impact load is transient by nature which occurs over a short period with a high magnitude. This corresponds to the frequency range from 0 to 2000 Hz. In fact, ballast is a nonhomogeneous and discontinuities by nature. Based on literature, the conventional method, continuum modelling, cannot provide insight into the interaction of ballast particles. Hence, continuum modelling should be replaced by discrete element modelling (DEM) which has a finite number of ballast particles. The discrete element modelling is an approach to present the discontinuity of material. The ballast particles with various radii are modelled in LS-DYNA. The spherical shapes are modelled instead of polyhedral due to the lower cost of computational time and memory consumption. Even though the spherical model has limitation on the contact interlocking, this can be compensated by adopting the contact model. One bay ballasted track modelling has been conducted. The impact load associated with actual train load is applied on the rail. The interaction between sleeper and ballast are highlighted. Moreover, sleeper and ballast particle movement are presented. This study will provide greater insight into the ballast particle and the sleeper motion induced by impact load associated with actual train load.

## 1 INTRODUCTION

Railway ballast track, which has been widely used throughout the world, typically comprises rails, sleepers, fastening system, ballast, sub-ballast and subgrade. This type can be divided into two main components: superstructure and substructure. Superstructure, which is a multilayered construction supported by substructure, consists of rails, sleepers, fastening system and ballast. While, substructure includes sub-ballast and subgrade [1-2]. It is known that ballast is placed between superstructure and substructure. The duties of ballast are to transfer the load from superstructure to underlying structure, to provide stability of the track, to support sleepers

uniformly, to absorb noise and vibration, to provide drainage system etc [3-6]. It is noted that ballast is one of the prone area to experience deteriorations which lead to track deterioration.

Previously, it was believed that the continuum method was capable to solve all the engineering problems [7]. However, it has been proven that this method cannot be used to solve some problems as this is only useful for solving homogeneous material [8-10]. By nature, the interactions among ballast aggregate particles are mostly discontinuous. Ballast shapes are sharp, angular, complex, and irregular. Since railway ballast normally consists of large particles of typical size approximately 40-60 mm, it is difficult to treat such a material as a continuum. It can be seen in many literatures that this approach could not perform the particle behaviour and difficult to highlight any significant phenomena such as particles interaction, ballast fouling, ballast breakage etc. Thus, discrete element modelling (DEM) is an alternative method, which was firstly introduced for rock and soil materials [11]. This approach is a numerical method for computing the motion and effect of a large number of small particles with its interactions in a granular assembly. The discontinuous behaviour can also be included. DEM can provide insight into the micro-mechanical behaviour of railway ballast.

Railway track is usually subjected to dynamic impact load. Such load is a large magnitude applied over a short period. This may induce damage in railway track. It is noted that the typical impact load varies between 100kN to 750kN. Based on field works and many literatures [12-20], it can be seen that the dynamic impact loads are caused by the irregularities of wheel or rail as well as the resonance effect produced among the track components [1]. It should be also noted that the impact capacity of sleepers can be reduced due to the modification of their cross section [21-24] and time-dependent behaviour [25-27].

A three dimensional finite element model was firstly conducted using ANSYS [28-30]. This model was validated by full-scale experiment based on the European standard [31]. The three-dimensional finite element software LS-DYNA was then used to analyze the dynamic responses of single bay ballasted track. The model has been validated against experimental drop impact tests [32-34]. This study presents the dynamic responses and sleeper-ballast interaction under impact loading. The outcome of this study can help improve the understanding of ballast movement of each particle under impact loading.

## 2 MODELLING

In this study, finite element package LS-Dyna is used to analyze the dynamic response of single span ballasted track. The sleeper and rails are modelled by solid element with eight nodes with three degree of freedom (translation). Truss element is used to model the prestressing wires by assuming perfect bond between prestressing wires and concrete. It should be noted that truss element cannot resist bending moment and shear force. The modulus of elasticity of concrete ( $f_c$ ) was estimated based on AS3600 [35]. The material properties of each element are shown in Table 1.

Table 1 Material properties of ballasted track.

Parameters	Characteristic value	Unit
Rail		
Modulus of elasticity	200000	MPa
Density	7870	Kg/m <sup>3</sup>
Possion's ratio	0.25	
Sleeper		
Concrete		
Modulus of elasticity	98000	MPa
Density	2400	Kg/m <sup>3</sup>
Possion's ratio	0.2	
Prestressing wire		
Modulus of elasticity	200000	MPa
Density	7850	Kg/m <sup>3</sup>
Possion's ratio	0.25	
Rail pad		
Modulus of elasticity	1250	MPa
Density	960	Kg/m <sup>3</sup>
Possion's ratio	0.42	
Ballast		
Layer thickness	30	cm
Modulus of elasticity	1000	MPa
Density	2600	Kg/m <sup>3</sup>
Possion's ratio	0.3	
Diameter	20-50	mm
Spring constant (Tangential)	1	
Spring constant (Normal)	0.3	
Damping constant (Tangential)	0.7	
Damping constant (Normal)	0.4	
Friction coefficient	1	
Rolling friction coefficient	0.3	

The extended finite element model was calibrated using vibration data [30, 36]. The updated finite element model was then transferred to LS-Dyna [33, 34], as shown in Figure 3. The simulation results were achieved by assigning the initial velocity to the drop mass to generate an impact event, similarly to the actual drop tests.

The ballast particles were firstly generated and packed into the cubic element. The contacts between each particle were assigned in terms of spring and damper by keyword \*CONTROL\_DISCRETE\_ELEMENT. The friction coefficient can be also applied. The contacts between each component were assigned using keywords \*CONTACT\_AUTOMATIC\_SURFACE\_TO\_SURFACE and \*CONTACT\_AUTOMATIC\_NODES\_TO\_SURFACE. The friction coefficient between rails and sleepers, sleeper and ballast, were 0.3 and 0.3, respectively. The contact interactions were defined using keywords \*CONTROL\_DISCRETE\_ELEMENT. The contact parameters are shown in Table 1. The schematic contact between each particle is shown in Figure 1. It should be noted that the friction and rolling coefficient were applied into the contact between the ballast in order to compensate the disadvantage of spherical element.

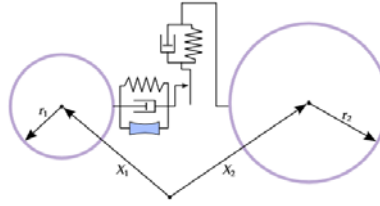


Figure 1 Schematic contact between each ballast particle [37].

It is noted that particle size varied between 20-50 mm were packed randomly into the concrete box, as shown in Figure 2. The gravity acceleration ( $9.81\text{m/s}^2$ ) was applied to the ballast, sleeper and rails before applying the velocity to the impactor. It should be noted that ballast, sleeper and rails fell down freely without constraint in any directions. The velocity of impactor was  $1.94\text{ m/s}$  which equivalent to the drop height  $0.2\text{ m}$  the test rig [32-34]. The modeling has been validated against experiment. It was found that the finite element model was fairly sufficient for use in predicting impact responses. The trends of peak acceleration responses are quite close to the experiment obtained [32-34], although there is certain phase and pulse duration differences.

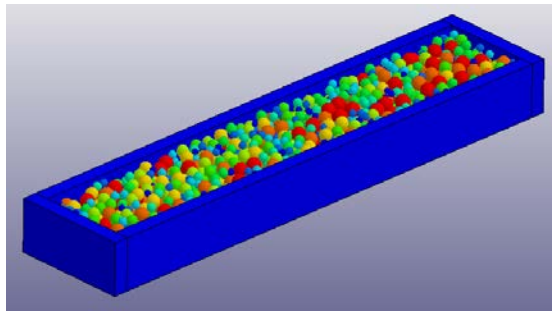


Figure 2 Various size of ballast packed into concrete box.

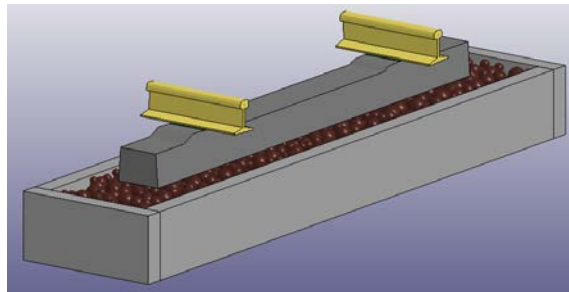


Figure 3 Finite element modelling of railway ballast track.

### 3 RESULTS AND DISCUSSIONS

The contact force between sleeper and ballast is shown in figure 4a. It is observed that about  $340\text{ kN}$  is the contact force between sleeper and ballast due to the applied velocities of drop mass of  $1.94\text{ m/s}$ . It is also noted the pulse durations is about  $2.6\text{ms}$ . While, the maximum sleeper/ballast contact force is about  $150\text{ kN}$ , as seen in figure 4b.

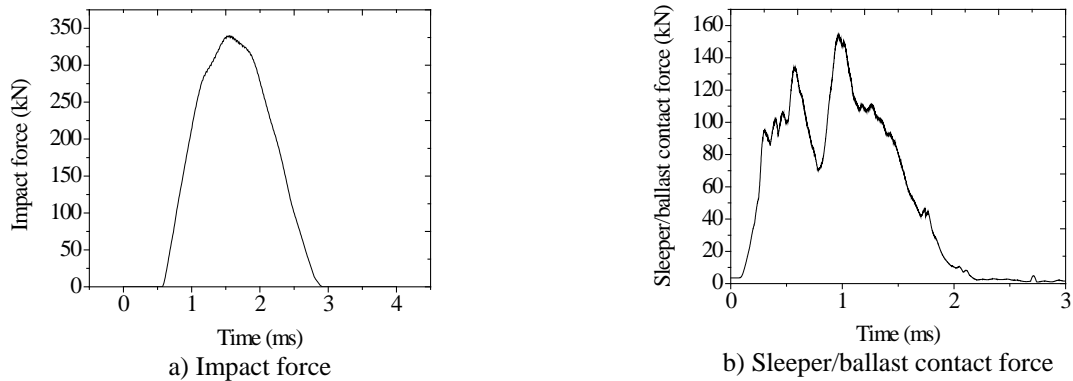


Figure 4 Contact force between sleeper and ballast.

Figure 5 presents the displacement contour at time of 0.64s and the displacement time history of sleeper at rail seat and mid-span. It should be noted that all components are in equilibrium within 0.5s after applying gravity acceleration. The result shows that the positive displacement is observed so that there is a slight uplift of sleeper at rail seat during unloading. The permanent displacement is also observed after all components are in equilibrium at about 0.9s due to the settlement and packing of ballast. The displacement of sleeper at rail seat (loaded side) is larger than that at mid span and another rail seat.

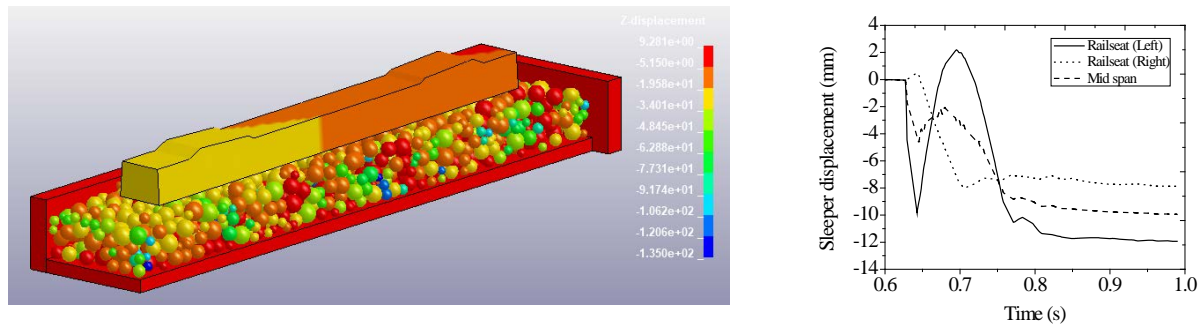
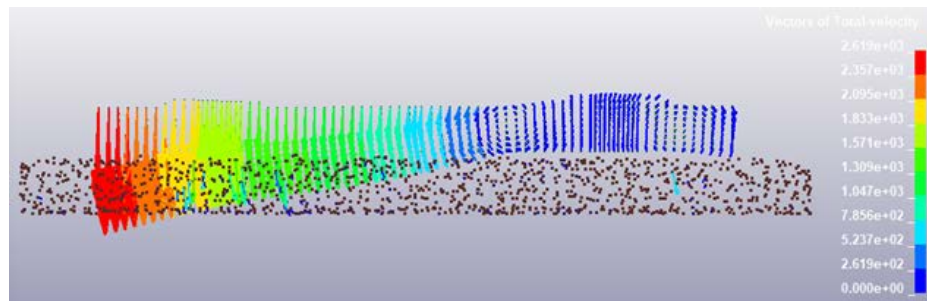
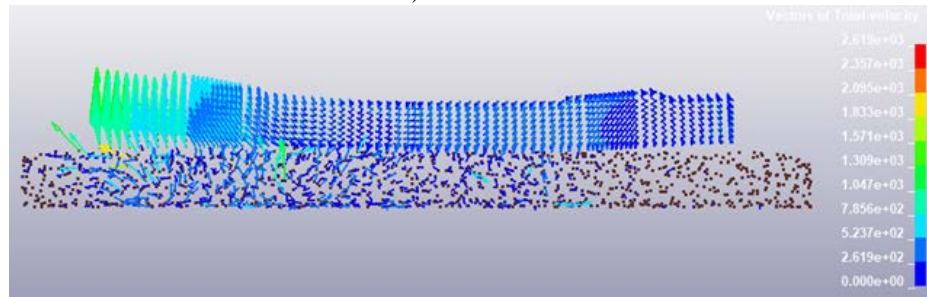


Figure 5 Vertical displacement contour and sleeper displacement time history.

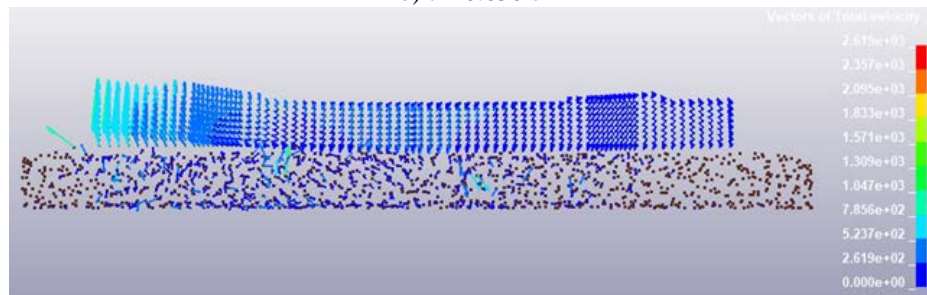
The movements of ballast particles and sleeper at each node are presented in terms of displacement vectors as shown in figure 6. Figure 6a displays the ballast and sleeper responses at the initial stage under gravity. Figure 6b-d shows the responses of ballast and sleeper under impact loading at each time step. It should be noted that the displacements contour and vector are cumulatively presented from the starting of applied gravity acceleration so that the displacements displayed are not due to only impact loading but also gravity at the first stage. Hence, figure 6 illustrate the node vector velocities of ballast and sleeper instead of displacement as it can show the behaviour at particular time. It is clearly seen that sleeper and ballast on loaded side moves down significantly and tends to lift up when unloading as previously describe. It is finally seen that ballast has a permanent settlement which lead to the permanent settlement of sleeper. These can be compared to the time history response obtained in figure 5.



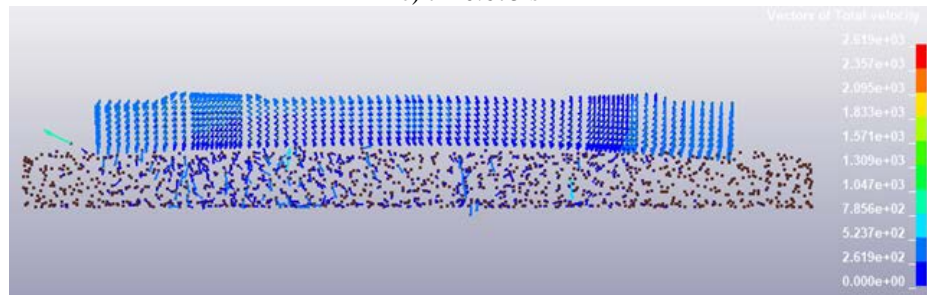
a)  $t = 0.625$  s



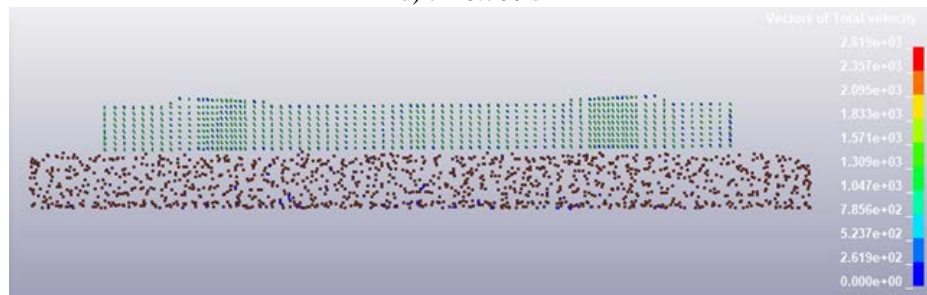
b)  $t = 0.650$  s



c)  $t = 0.675$  s



d)  $t = 0.700$  s



e)  $t = 0.100$  s

Figure 6 Velocity vectors of ballast and sleeper at each time.

It should be noted again that this study did not consider the lateral resistance of sleeper as we only consider the vertical movement. However, due to the random placement of various size of ballast, sleeper was not completely flatly placed on ballast bed. Also, in fact, longitudinal rail and fastening system can considerably constrain the movement of sleeper in longitudinal and transverse directions and they may also help reduce uplift effect.

#### **4 CONCLUSIONS**

Discrete element modelling (DEM) is an alternative method to take into account the nature of granular and heterogeneous materials. This method has been firstly used for granular material and then adapted to railway ballast. This method is very useful and powerful as it provides the multi scale mechanic behaviour and the movement of each ballast particle. A commercial finite element package, LS-Dyna, has been employed to extend the model for impact analysis and it has been validated against experimental drop impact tests. The spherical particle was employed since it can provide a better computational time and memory consumption than polyhedral. Although the simple spherical cannot provide insight into the real shape and particle contact, this can be fitted by adapting the proper contact coefficient between each particle. In fact, railway track normally experiences impact load, which is a shock load applied in short duration, due to the irregularities of either wheel or rail. It should be noted that the magnitude is much higher than static load. Thus, the vertical velocity of drop mass of 1.94 m/s associated with actual train loads was applied to the rail. It should be noted that this equivalent to about 340 kN. The results show that the maximum displacement occurred at rail seat under impact load while the displacement on another side of rail seat is lower than that at mid-span. The permanent deformation of sleeper is also observed. This is because ballast particles are packed and settled and then sleeper is pressed down into the ballast bed. Moreover, it is noted that uplift of the sleeper is observed during unloading. It should be noted that the relative uplifts of the sleepers tend to cause deteriorations of railway tracks over time, such as ballast breakage, excessive dilation and densification, which can cause further track differential settlements. In fact, ballast can be broken and crushed due to the impact load which leads to severe track degradation. However, this study did not consider ballast breakage. Hence, it is recommended to take into account the spherical cluster particle and ballast breakage under impact loading for further study.

#### **ACKNOWLEDGEMENTS**

The authors are sincerely grateful to the European Commission for the financial sponsorship of the H2020-RISE Project No. 691135 “RISEN: Rail Infrastructure Systems Engineering Network”, which enables a global research network that tackles the grand challenge of railway infrastructure resilience and advanced sensing in extreme environments ([www.risen2rail.eu](http://www.risen2rail.eu)) [<sup>38</sup>].

#### **REFERENCES**

- [1] Remennikov, A.M. and Kaewunruen, S. A review of loading conditions for railway track structures due to train and track vertical interaction. *Struct. Control. Health Monit.*

- (2008) 15(2):207-234.
- [2] Ngamkhanong, C., Kaewunruen, S. and Baniotopoulos, C. A review on modelling and monitoring of railway ballast, *Structural Monitoring and Maintenance*. (2017) 4(3):195-220. doi: 10.12989/smm.2017.4.3.195.
  - [3] Selig, E.T. and Waters, J.M. *Track Geotechnology and Substructure Management*, Thomas Telford Publishing, UK, (1994).
  - [4] Indraratna, B., Salim, W. and Rujikiatkamjorn, C., *Advanced Rail Geotechnology-Ballasted Track*, Taylor & Francis Group, London, UK, (2011).
  - [5] Remennikov, A.M. and Kaewunruen, S. Experimental load rating of aged railway concrete sleepers. *Eng. Struct.* (2014) 76(10):147-162.
  - [6] Kaewunruen, S. and Remennikov, A.M. Dynamic properties of railway track and its components: Recent findings and future research direction. *Insight: Non-Destructive Testing and Condition Monitoring*. (2010) 52(1):20-22.
  - [7] Nguyen, V., Duhamel, D. and Nedjar, B. A continuum model for granular materials taking into account the no-tension effect. *Mech. Mater.* (2003) 35:955-967.
  - [8] Alva-Hurtado, J.E. and Selig, E.T. Permanent strain behavior of railroad ballast. *Proceeding of the International Conference on Soil Mechanics and Foundation Engineering*. (1981) 1:543-546.
  - [9] Shenton, M. Ballast deformation and track deterioration. *Track technology*. (1985):253-265.
  - [10] Sato, Y. Japanese studies on deterioration of ballasted track. *Vehicle Syst. Dynam.* (1995) 24(1):197-208.
  - [11] Cundall, P.A. A Computer Model for Simulating Progressive, Large Scale Movements in Blocky Rock Systems. *International Symposium on Rock Fracture, I.S.R.M. Nancy, France*, (1971).
  - [12] Remennikov, A.M., Murray, M.H. and Kaewunruen, S. Reliability based conversion of a structural design code for prestressed concrete sleepers. *Proceedings of the Institution of Mechanical Engineers: Part F Journal of Rail and Rapid Transit*. (2012) 226(2):155-73.
  - [13] Wakui, H. and Okuda, H. A study on limit-state design for prestressed concrete sleepers. *Concrete Library of JSCE*. (1999) 33:1-25.
  - [14] Wang, N. Resistance of concrete railroad ties to impact loading. PhD Thesis, University of British Columbia, Canada, (1996).
  - [15] Gustavson, R. Structural behaviour of concrete railway sleepers. PhD Thesis, Department of Structural Engineering, Chalmers University of Technology, Sweden, (2002).
  - [16] Stevens, N.J. and Dux, P.F. A method of designing a concrete railway sleeper. International Patent No WO 2004/019772 A1, World Intellectual Property Organisation, International Bureau, (2004).
  - [17] Lilja, J., Preliminaries for probabilistic railway sleeper design. Licentiate Thesis, Chalmers Applied Mechanics, Chalmers University of Technology, Gothenburg, (2006).
  - [18] Leong, J. Development of a limit state design methodology for railway track. Master of Engineering Thesis, Queensland University of Technology, QLD, Australia, (2007).
  - [19] Kaewunruen, S., Remennikov, A.M. and Murray, M.H. Limit states design of railway concrete sleepers. *Proc. of ICE Transport Journal*. (2012) 164(TR1). doi: 10.1680/tran.9.00050
  - [20] Ngamkhanong, C., Kaewunruen, S. and Costa, B.J.A. State-of-the-Art Review of Railway Track Resilience Monitoring. *Infrastructures*. (2018) 3.

- [21] Ngamkhanong, C., Li, D. and Kaewunruen, S. Impact capacity reduction in railway prestressed concrete sleepers with vertical holes. IOP Conference Series: Materials Science and Engineering. (2017) 236(1).
- [22] Ngamkhanong, C., Kaewunruen, S. and Remennikov, A.M. Static and dynamic behaviours of railway prestressed concrete sleepers with longitudinal through hole. IOP Conference Series: Materials Science and Engineering. (2017) 251(1).
- [23] Ngamkhanong, C., Li, D. and Kaewunruen, S. Impact capacity reduction in railway prestressed concrete sleepers with surface abrasions. IOP Conference Series: Materials Science and Engineering. (2017) 245(3).
- [24] Ngamkhanong, C., Li, D., Kaewunruen, S. and Remennikov, A.M. Capacity Reduction in Railway Prestressed Concrete Sleepers due to Dynamic Abrasions. International Journal of Structural Stability and Dynamics. (2018). (Accepted)
- [25] Li, D., Ngamkhanong, C. and Kaewunruen, S. Influence of vertical holes on creep and shrinkage of railway prestressed concrete sleepers. IOP Conference Series: Materials Science and Engineering, (2017) 236(1).
- [26] Li, D., Ngamkhanong, C. and Kaewunruen, S. Time-dependent topology of railway prestressed concrete sleepers. IOP Conference Series: Materials Science and Engineering. (2017) 245(3).
- [27] Li, D., Ngamkhanong, C. and Kaewunruen, S. Influence of Surface Abrasion on Creep and Shrinkage of Railway Prestressed Concrete Sleepers. IOP Conference Series: Materials Science and Engineering. (2017) 245(3).
- [28] Kaewunruen, S. and Remennikov, A.M. Effect of a large asymmetrical wheel burden on flexural response and failure of railway concrete sleepers in track systems. Engineering Failure Analysis. (2008) 15(8): 1065-1075.
- [29] Kaewunruen, S. and Remennikov, A.M. Experimental simulation of the railway ballast by resilient materials and its verification by modal testing. Experimental Techniques. (2008) 32(4):29-35.
- [30] Kaewunruen, S. and Remennikov, A.M. Nonlinear finite element modeling of railway prestressed concrete sleeper. Proceedings of the 10th East Asia-Pacific Conference on Structural Engineering and Construction. (2006) 4:323-328.
- [31] British Standards Institute (BSI) European Standard BS EN13230 Railway applications. Track. Concrete sleepers and bearers. London, UK, (2016).
- [32] Kaewunruen, S. and Remennikov, A.M. Low-velocity impact analysis of prestressed concrete sleepers. Proceedings of the 23rd Biennial Conference of the Concrete Institute of Australia: Design, Materials, and Construction. Adelaide, Australia, (2007):659-668.
- [33] Kaewunruen, S. and Remennikov, A.M. Impact responses of prestressing tendons in railway concrete sleepers in high speed rail environments. Proceedings of the 5th Computational Methods in Structural Dynamics and Earthquake Engineering. May 25-27, Crete Island, Greece, (2015).
- [34] Kaewunruen, S., Remennikov, A.M. and Minoura, S. Dynamic responses of railway ultra-highstrength concrete sleepers under extreme impact loading. Proceedings of the 6th Computational Methods in Structural Dynamics and Earthquake Engineering. June 15-17, Rhodes Island, Greece, (2017).
- [35] Standards Australia. Design of concrete structures. Australian Standard: AS3600-2001. (2001).
- [36] Gamage, E.K., Kaewunruen, S., Remennikov, A.M. and Ishida, T. Toughness of Railroad

- Concrete Crossties with Holes and Web Openings. *Infrastructures*. (2017) 2(3). doi:10.3390/infrastructures2010003.
- [37] Livermore Software Technology Corporation (LSTC). *LS-DYNA KEYWORD USER'S MANUAL VOLUME I*. (2013).
- [38] Kaewunruen, S., Sussman, J.M. and Matsumoto, A. Grand challenges in transportation and transit systems. *Frontiers in Built Environment*. (2016) 2(4). doi:10.3389/fbuil.2016.00004.

## Performance of the Polygonal Finite Element Method in Modelling Complex Natural Structures

Tuan Ngo<sup>\*</sup>, Abdallah Ghazlan<sup>\*\*</sup>, Tuan Nguyen<sup>\*\*\*</sup>, Hung Nguyen-Xuan<sup>\*\*\*\*</sup>

<sup>\*</sup>University of Melbourne, <sup>\*\*</sup>University of Melbourne, <sup>\*\*\*</sup>University of Melbourne, <sup>\*\*\*\*</sup>Ho Chi Minh City University of Technology (Hutech)

### ABSTRACT

Well-organised polygonal structures have been observed in nature in many instances, such as polygonal brick and mortar found in nacreous seashells, functionally graded polygonal foams in porcupine quills and trabecular bone, arbitrary cellular structures in bamboo, beetle wing striations, and so on. These structures show unique structural configurations, which are effective under large deformations, and also in deflecting cracks and distributing damage. They can be approximated by voronoi diagrams, which is a powerful tool in computational geometry capable of generating complex and well-organised polygonal and polyhedral patterns by simply controlling a set of points. However, the loss in performance and accuracy in modelling complex natural structures is evident by the significant increase in elements introduced in the meshing process. In this study, the efficacy of the polygonal finite element method, which uses one element per voronoi polygon, is investigated in modelling the polygonal microstructure found nacre from mollusc shells, which can consist of millions of platelets. The voronoi diagram is generated using the well-known sweep line algorithm, which traverses a set of points and constructs the polygonal cells efficiently. The polygonal finite element method is benchmarked against the finite element method in ABAQUS and shown to significantly improve performance by reducing the computation time.

## Free Vibration of Cracked FG Plates Based on Strain-Gradient Theory

Hoang Nguyen<sup>\*</sup>, Elena Atroshchenko<sup>\*\*</sup>, Hung Nguyen-Xuan<sup>\*\*\*</sup>, Thuc Vo<sup>\*\*\*\*</sup>

<sup>\*</sup>Northumbria University, <sup>\*\*</sup>University of Chile, <sup>\*\*\*</sup>HCMC University of Technology, <sup>\*\*\*\*</sup>Northumbria University

### ABSTRACT

This study aims to investigate the free vibration responses of functionally graded (FG) cracked small-scale plates using the strain-gradient theory and the extended isogeometric analysis (XIGA). While the strain-gradient elasticity is employed to account for the size-dependent effects, the displacement fields of plate structures are described based on the refined plate theory (RPT). The simple strain-gradient theory with one additional length scale parameter, apart from Lamé's constants, is capable of effectively capturing the small-scale effects in nano/micro structures [1]. The RPT with four unknowns not only is able to improve the accuracy of the results for both thin and thick plates but also helps to describe the nonlinear distribution of the shear stress through the plate's thickness without using shear correction factor. The combination of SGE and RPT ends up requiring C2 elements, which causes difficulty if traditional finite element is involved to solve for approximate solutions. The isogeometric analysis (IGA) [2] is employed as a prominent numerical method to solve the problems that require higher-order elements. This recently developed method utilises the non-uniform rational B-splines (NURBS) functions to establish approximation functions and describe geometry domains simultaneously. In order to model the discontinuity at the cracks within the plates, the extended IGA with enrichment functions for crack path and crack tip is involved. The primary results for the free vibration of functionally graded plates show that the proposed approach is able to predict both the fracture behaviours and size-dependent effects well. It yields appropriate and reliable results in which the stiffness of the structures, consequently the fundamental frequency, is increased as the length scale ratio becomes larger. It also demonstrates that strain-gradient theory plays a significant role in the prediction of size-dependent effects of nano/micro structures which classical continuum theory could fail to capture. REFERENCES [1] R.D.Mindlin, Micro-structure in linear elasticity, *Archive for Rational Mechanics and Analysis*, 16, 51–78, 1964. [2] T.J.R. Hughes, J.A. Cottrell, Y. Bazilevs, *Isogeometric analysis: CAD, finite elements, NURBS, exact geometry and mesh refinement*, *Computer Methods in Applied Mechanics and Engineering*, 194, 4135-4195, 2005.

## **An Iterative Local Corrector Scheme for the Multiscale Finite Element Method**

Lam Nguyen<sup>\*</sup>, Dominik Schillinger<sup>\*\*</sup>

<sup>\*</sup>University of Minnesota, <sup>\*\*</sup>University of Minnesota

### **ABSTRACT**

Fine-scale features such as scale separation and periodicity are usually used to simplify simulations of heterogeneous materials and reduce the computational cost. Without these features, we need to fully resolve all microstructures to obtain accurate results, involving tremendous computational memory and time. The multiscale finite element method is one of the multiscale techniques that can be applied to this problem. Constraints on multiscale basis functions at element interfaces, however, prevent convergence to the fine-scale solution. In this work, we overcome this challenge by introducing an iterative corrector scheme which enables communication between fine-scale solutions across coarse element interfaces. In our approach, a first solution is found by using initial multiscale basis functions. The corrector scheme is then applied to improve the multiscale basis functions at element interfaces by solving local boundary problems in separate patches of coarse elements. The new multiscale basis is used to find a new multiscale solution. We repeat the procedure until reaching the desired accuracy. With this technique, we can solve large problems with significantly fewer degrees of freedom while retaining the same accuracy as the fully resolved discretization of the fine scale. In this talk, we briefly describe our method, discuss implementation aspects, and illustrate it with numerical examples.

## **Adaptive Isogeometric Collocation Method Based On Reproducing Kernel Meshfree Formulation For Large Deformation Frictional Contact Problems**

Nhon Nguyen\*, Kun Zhou\*\*

\*School of Mechanical and Aerospace Engineering, Nanyang Technological University, 50 Nanyang Avenue, Singapore 639798, Singapore, \*\*School of Mechanical and Aerospace Engineering, Nanyang Technological University, 50 Nanyang Avenue, Singapore 639798, Singapore

### **ABSTRACT**

Collocation has recently shown as a powerful alternative to Galerkin's method in the context of isogeometric analysis (IGA). In this method, the strong form of the governing differential equations of the problem is enforced at a set of discrete collocation points, equal in number to the control points. Isogeometric collocation (IGA-C) exhibits a strongly reduced computational cost when compared with Galerkin approaches while maintaining higher-order convergence rates. However, IGA has certain shortcomings in terms of numerical analysis. Because of the tensor-product form of non-uniform rational basis spline, the control points must belong to a structured grid, which causes an excessive overhead of control points with increasing refinement. In this work, adaptive IGA-C method based on reproducing kernel meshfree formulation for large deformation frictional contact problems are presented. The proposed reproducing kernel meshfree representation of IGA-C basis functions provides a reliable meshfree strategy which is flexible adaptive refinement. The shape functions in the refined regions can be naturally constructed in a straightforward meshfree manner. The consistency and independence of the shape functions required by the subsequent computational analysis are ensured by the consistency conditions of reproducing kernel meshfree formulation. Moreover, a large deformation contact formulation is subsequently developed and tested in the frictional setting, where collocation confirms the excellent performance already obtained for the frictionless case.

## **A Deterministic-stochastic Method for Computing the Boltzmann Collision Integral in $O(MN)$ Operations**

Truong Nguyen<sup>\*</sup>, Alexander Alekseenko<sup>\*\*</sup>, Aihua Wood<sup>\*\*\*</sup>

<sup>\*</sup>Wright State University, <sup>\*\*</sup>California State University, Northridge, <sup>\*\*\*</sup>Air Force Institute of Technology

### **ABSTRACT**

Abstract: We developed and implemented a numerical algorithm for evaluating the Boltzmann collision operator with  $O(MN)$  operations, where  $N$  is the number of the discrete velocity points and  $M \ll N$ . At the base of the algorithm is nodal-discontinuous Galerkin discretizations of the collision operator on uniform grids and a bilinear convolution form of the Galerkin projection of the collision operator. Efficiency of the algorithms is achieved by applying singular value decomposition compression of the discrete collision kernel and by approximating the kinetic solution by a sum of Maxwellian streams using a stochastic likelihood maximization algorithm. Accuracy of the method is established on solutions to the problem of spatially homogeneous relaxation. The method achieves more than ten fold speedup in comparison to the fully deterministic evaluation of the collision integral presented in [1,2].  
References: [1] A. Alekseenko and E. Josyula, Deterministic solution of the Boltzmann equation using a discontinuous Galerkin velocity discretization, in 28th International Symposium on Rarefied Gas Dynamics, 9-13 July 2012, Zaragoza, Spain, AIP Conference Proceedings, American Institute of Physics, 2012, 8. [2] A. Alekseenko and E. Josyula, Deterministic solution of the spatially homogeneous Boltzmann equation using discontinuous Galerkin discretizations in the velocity space, Journal of Computational Physics, 272 (2014), 170-188.

## Multiscale Modeling of Wave Propagation in Periodic Fluid-saturated Poroelastic Media

Vu-Hieu Nguyen<sup>\*</sup>, Eduard Rohan<sup>\*\*</sup>, Salah Naili<sup>\*\*\*</sup>

<sup>\*</sup>Laboratoire Modélisation et Simulation Multi Echelle, MSME UMR 8208 CNRS, Université Paris-Est, France,  
<sup>\*\*</sup>European Centre of Excellence, NTIS – New Technologies for Information Society Faculty of Applied Sciences,  
University of West Bohemia, Czech Republic, <sup>\*\*\*</sup>Laboratoire Modélisation et Simulation Multi Echelle, MSME UMR  
8208 CNRS, Université Paris-Est, France

### ABSTRACT

This work is motivated by the need for characterizing porous materials with heterogeneity at different scales, e.g. natural and artificial porous materials such as biological tissues, soils, rocks and foams. We aim to study the propagation of acoustic waves in periodic mixture of two fluid saturated poroelastic materials which exhibit the presence of heterogeneity at scales much larger than microstructure scales but much smaller than the wavelengths [1,2,3]. For describing the acoustic wave propagation in such materials, both porous materials at the mesoscale are modeled by using Biot's theory. Then, a two-scale homogenization scheme has been carried out for deriving the effective dynamic equations at the macroscale. Depending on the contrast between the permeability and the poroelastic coefficients of two phases, two different models have been derived. Finite element formulations were developed for computing the effective acoustic properties of the material at macroscopic scale from given mesoscale structural geometries. We also present a down-scale post-processing procedure for estimating the local dynamic responses at the mesoscale from solutions of homogenized medium at the macroscale. The proposed method is validated by considering a plane wave propagation problem in a half-space under harmonic excitations. The solutions obtained by using homogenized models are compared with the ones obtained by using a model which take into account all geometrical details at the mesoscale. The numerical validations showed that the high-contrast model can capture some phenomena which are not described by the standard homogenization treatment of a low contrast model. The domain of validity for high contrast model may also be determined. REFERENCES [1] Nguyen, V.-H., Rohan, E., & Naili, S. (2016). Multiscale simulation of acoustic waves in homogenized strongly heterogeneous porous media. *International Journal of Engineering Science*, 101, 92–109. [2] Rohan, E., Naili, S., & Nguyen, V.-H. (2016). Wave propagation in a strongly heterogeneous elastic porous medium: Homogenization of Biot medium with double porosities. *Comptes Rendus Mécanique*, 344(8), 569–581 [3] Rohan, E., Nguyen, V. H., & Naili, S. (2017). Numerical modelling of waves in double-porosity Biot medium. *Computers and Structures* (in press, DOI: 10.1016/j.compstruc.2017.09.003)

## Heat and Moisture Conduction and Hydrothermal Analysis in Laminated Plates Using Higher Order Zig-zag Theory

Ngoc Nguyen-Sy<sup>\*</sup>, Jaehun Lee<sup>\*\*</sup>, Maenghyo Cho<sup>\*\*\*</sup>

<sup>\*</sup>Seoul National University, <sup>\*\*</sup>Kyungnam University, <sup>\*\*\*</sup>Seoul National University

### ABSTRACT

This work developed higher order zig-zag theory to predict accurately the coupling hygroscopic-thermal-mechanical behaviors for viscoelastic composite laminated plates. All in-plane displacement, temperature, and moisture fields through the thickness are constructed by combining the locally linear zig-zag term and globally cubic polynomial distribution. The Laplace transform is employed to avoid such integration of the viscoelastic constitutive equation as well as improve accuracy and efficiency. All formulations are simplified in Laplace domain. The hydrothermal variation principle is employed to determine the temperature and moisture distributions through the thickness. Then, viscoelastic relaxation modulus with various hydrothermal shift factors in each layer are calculated in the general form of Prony series. The final numerical results of stresses and deformations are obtained by using inverse Laplace techniques. To demonstrate the efficiency and accuracy of the present theory, some numerical examples for long-term creep and relaxation processes are performed. The present theory is suitable for the predictions of coupled hygroscopic-thermal-mechanical behaviors for thick viscoelastic composite laminated plates.

## **An Adaptive Strategy Based on Conforming Quadtree Meshes for Kinematic Limit Analysis**

Hung Nguyen-Xuan\*

\*Hutech University, Ho Chi Minh City, Vietnam

### **ABSTRACT**

We propose a simple and efficient scheme based on adaptive finite elements over conforming quadtree meshes for collapse plastic analysis of structures. Our main interest in kinematic limit analysis is concerned with both purely cohesive-frictional and cohesive materials. It is shown that the most computational efficiency for collapse plastic problems is to employ an adaptive mesh strategy on quadtree meshes. However, a major difficulty in finite element formulations is the appearance of hanging nodes during adaptive process. This can be resolved by a definition of conforming quadtree meshes in the context of polygonal elements. Piecewise-linear shape functions in barycentric coordinates are used to approximate the velocity field. Numerical results prove the reliability and benefit of the present approach.

# NUMERICAL SIMULATION OF ICE LOADS IN THE PROCESS OF SHIP ICE COLLISION BASED ON NONLINEAR ELEMENT METHOD

Li Z.P.<sup>1</sup> Ni B. Y.<sup>1</sup> Yang D.<sup>2</sup> Han D. F.<sup>1</sup>

1. College of Shipbuilding Engineering, Harbin Engineering University, Harbin, China, 150001;  
Email address: nibaoyu@hrbeu.edu.cn
2. Wuhan Second Ship Design and Research Institute, Wuhan, China, 430205

**Key words:** ship, ice loads, collision, finite element method, nonlinearity.

**Abstract.** More and more ships are operating and will navigate in cold regions, particularly in the arctic route. The maneuverability of ship in level ice is complex no matter the ship is in straight motion or rotational motion. To study this complex, strong and nonlinear collision between ice and ship, nonlinear finite element method is adopted with appropriate ice material and failure modes. Numerical results are compared with that from empirical formula. On this basis, combined movement of an icebreaker including straight motion and rotational motion is studied and the characteristics of ice loads are discussed. The influences of forward and angular velocities are also analyzed.

## 1 INTRODUCTION

Along with global warming, the arctic route and resource exploration in Arctic areas are becoming more practical. As a result, more and more ships are operating and will navigate in cold regions. When a ship navigates in the Arctic area, its structural response and motion state are influenced by various external loads, including ice, winds, waves, and currents, etc. Among these external loads, the most important one may be the ice loads, which may induce severe dynamic structural response on the ship during the process of ship-ice collisions. When a ship is maneuvering in the level ice, the ship-ice interaction can be very complex. In the condition of straight-forward motion, due to the rake of the stem, the main force exerted on the ice sheet by the ship is the vertically downward force. As a result, the breaking mode of the ice sheet is bending failure mainly. However, when a ship turns in the level ice, the ice is extruded by the midship whose face is perpendicular to the ice sheet. Thus, the breaking mode of the ice sheet is compression failure mainly. The strong nonlinear impact between the ship and ice generates challenges on simulating the motion of the ship in the ice, especially in a rotational motion.

In numerical simulations, there has been researches on ship-ice collisions. Valanto (2007) [1] simulated the straight-forward resistance of a ship moving in level ice by establishing a three-dimensional finite element model of the ship. Numerical results were compared with the actual measured data and good agreement was achieved, which denotes their model can predict ice resistance well. Wang et al. (2008) [2] adopted commercial software MSC.DYTRAN to simulate the collision between LNG ships and crushable ice based on nonlinear finite element analysis. The results indicated that the ship structure under ice loads presented two major failure modes: the large plastic deformation and the local buckling. Su (2011) [3] developed a kind of ‘point-face’ contact algorithm to predict the ice loads on the ship surfaces. On this basis, the resistance and maneuverability of the ship were simulated by self-programming. Liu (2012) [4] developed a type of ice material and inserted it into commercial software LS-DYNA to analyze the collision between a ship and an iceberg. The iceberg was defined as a plastic material and the corrosion of the unit was used to simulate the growth of the cracks. Kim et al. (2013) [5] simulated the resistance performance of a cargo ship under the conditions of broken ice. The numerical simulated results were compared with the results of the non-frozen model ice test in a water tank in South Korea and the cut ice test in an ice tank in Canada, and good agreements were both achieved. Kajaste-Rudnitski & Kujala (2014) [6] adopted commercial software ABAQUS to simulate the three-degree-of-freedom motion of the ship in the level ice. The results showed that the ice breaking is a stochastic process and time history of ice loads present a series of high peaks with very short duration.

It can be seen that most researches concerned the collision process between ice and ship when the ship is in a straight-forward movement. Seldom work studied ice-ship collision when the ship in a rotational motion. However, in the actual voyage, ship usually needs to turn or move in a curvilinear motion. At that time, the side of hull squeezes the ice strongly, so the transverse loads increase a lot. To study this problem, based on the nonlinear finite element method, this paper sets up a three-dimensional finite element model of the ship and the ice to simulate the process of ice-ship collision when the ship in a rotational motion. The longitudinal and transverse load curves of the hull are obtained, and the effects of various parameters are analyzed, including tangential velocity and angular velocity of the ship.

## **2 MODELLING PRINCIPLES**

When a ship moves in the level ice, its bow breaks ice before the hull slides in the broken ice. The velocity of the ship is affected by the ice loads and may vary. However, in this paper, to simplify the simulation, we firstly assume that the ship is in a forced motion with a constant speed, whether the ship is in a straight motion or a rotational motion. Secondly, the effect of the water is assumed to be neglectable, considering the water load is small compared with the strong ice load. Under these assumptions, we consider a combined motion of the ship in the level ice. The ship moves straight forwards in a constant speed before turns in a constant angular velocity, so the velocity

**Li Z.P. Ni B. Y. Yang D. Han D. F.**

in the global coordinates can be expressed as follows:

$$\begin{cases} x = \\ y = 0 \end{cases} \quad (t \leq t_0, \text{ or in the straight motion}) \quad (1)$$

$$\begin{cases} x = \cos[\omega(t-t_0)] \\ y = \sin[\omega(t-t_0)] \end{cases} \quad (t > t_0, \text{ or in the rotational motion}) \quad (2)$$

where  $v$  is the given constant speed,  $\omega$  is the given angular velocity,  $t$  is the total time and  $t_0$  is the end moment of the straight motion. Only 3 degrees of freedom of the ship movement are allowed—surge( $x$ ), sway( $y$ ) and yaw ( $\varphi$ ). The origin of the local coordinates along with the body is fixed at the center of gravity of the ship, as shown in Fig.1, whose  $x$  axis points forwards,  $y$  axis points towards port and  $z$  axis points upwards. At the initial moment, the local coordinates coincide with the global coordinates.

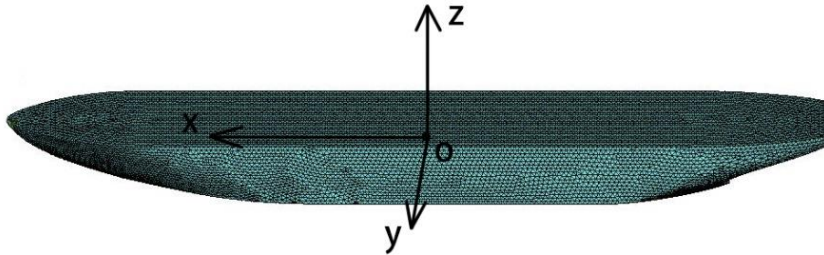


Figure1. Sketch of coordinates and finite element model of the ship

The length between perpendiculars of the ship is 147m, the beam of ship is 22.6m and the displacement is 18000DWT. The surface of the ship is meshed by triangular element, which is also shown in Fig. 1. The ship hull is presented as a rigid body. On the other hand, the main dimension of the level ice is 600m\*350m\*1m, and the boundary conditions of the ice is non-reflecting boundary. The material property of ice is simplified as Isotropic Elastic-Plastic with Failure model. When the stress or the strain of the element exceeds the set value in the finite element model, the element is invalid and will be deleted from the model. Ralston [7] first studied the yield conditions and plastic deformation of the failure of the ice, which proved the feasibility of ice materials by using the plastic theory. For ice, the principle of isotropic hardening is usually adopted to regulate the change rule of the yield function in the stress space after the material enters the plastic deformation. The von Mises yield criterion is used as the failure criterion of sea ice. The maximum plastic strain mode is used as the failure mode of materials, and the constant minimum pressure mode is used as the separation mode of materials [8].

**Li Z.P. Ni B. Y. Yang D. Han D. F.**

In this paper, the model parameters of the ice are taken as those in Table 1:

Table.1 Ice model characteristics

<i>RO</i> Kg/m <sup>3</sup>	<i>G</i> Gpa	<i>SIGY</i> Mpa	<i>ETAN</i> Gpa	<i>BULK</i> Gpa	<i>EPF</i>	<i>PRF</i> Mpa	<i>REM</i>	<i>TREM</i>
900	2.2	2.12	4.26	5.26	0.35	-4	0	0

where *RO* is the mass density, *G* is the shear modulus, *SIGY* is the yield stress, *ETAN* is the plastic hardening modulus, *BULK* is the bulk modulus, *EPF* is the plastic failure strain, *PRF* is the failure pressure, *REM* is the element erosion option, and *TREM* is the time interval for the element removal.

### 3 SOLUTION METHOD

The nonlinear finite element method is adopted to simulate the ice-ship collision process. The solution method is introduced briefly. The motion equation of the ship can be expressed as:

$$Ma_n = F_n^{ext} + \quad_n - F_n^{int} - \quad_n v_n \quad (3)$$

where *M* is the mass matrix;  $\quad_n$  is the damping matrix;  $a_n$  and  $v_n$  are the acceleration vector and velocity vector at time  $t_n$ , respectively;  $F_n^{ext}$  is the external force vector;  $\quad_n$  is the hourglass resistance;  $F_n^{int}$  is the internal force vector, which is the sum of unit internal force and contact force. Eq. (3) can be rewritten as:

$$a_n = M^{-1}(F_n^{ext} + \quad_n - F_n^{int} - \quad_n v_n) \quad (4)$$

The center difference method is used to update the velocity vector  $v_{n+1}$  and displacement vector  $d_{n+1}$  of the ship in the time domain as:

$$v_{n+\frac{1}{2}} = v_{n-\frac{1}{2}} + \Delta t_n a_n \quad (5)$$

$$d_{n+1} = d_n + v_{n+\frac{1}{2}} \Delta t_{n+\frac{1}{2}} \quad (6)$$

where it is assumed that the acceleration is constant throughout the time step. Thus, if the node position  $d_n$  and acceleration  $a_n$  of the time step  $n$  and the node speed  $v_{n-\frac{1}{2}}$  of time step  $(n-1/2)$  have been obtained, the node speed  $v_{n+\frac{1}{2}}$  of time step

$(n+1/2)$  and the displacement  $d_{n+1}$  of time step  $(n+1)$  can be solved by using Eqs. (5) and (6).

As we know, the central difference method is conditionally stable and the time step must be smaller than a critical value  $\Delta t^{crif}$  to keep it stable. In this paper, it is found that this critical time step can be taken as:

$$\Delta t^{crif} = \frac{l}{c} \quad (7)$$

based on the numerical experience, where  $l$  is the minimum height of the unit,  $c$  is the sound velocity of material. In this paper,  $\Delta t$  is taken as 0.9 times of  $\Delta t^{crif}$ .

## 4 RESULTS AND DISCUSSIONS

### 4.1 Validation of numerical model

In order to validate the numerical model, we assume the ship in a straight motion and compare the ice resistance obtained by the numerical simulation with the empirical formula proposed by Lindqvist (1989) [9]. The moving velocity of the ship is taken as  $=5\text{m/s}$ .

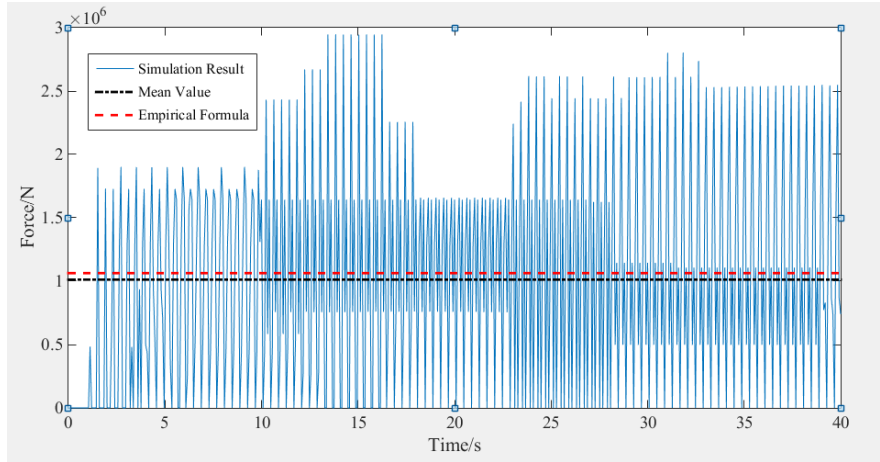


Figure 2. Comparison between results of numerical simulation and empirical formula

The comparison between results of numerical simulation and empirical formula is shown in Figure 2, where the fluctuate curve is calculated result with black dot-dash line as the mean value and the red broken line is the empirical-formula result. It can be seen that the average value of numerical simulation is very close to the value calculated by empirical formula. The result of empirical formula is 1.06MN and the average value of numerical simulation is 1.01MN, with a relative error 4.7%. Therefore, it can be considered that the numerical model is validated to some extent.

### 4.2 Analysis on ice loads

On the basis of the validation of numerical model, we consider the combined motion

**Li Z.P. Ni B. Y. Yang D. Han D. F.**

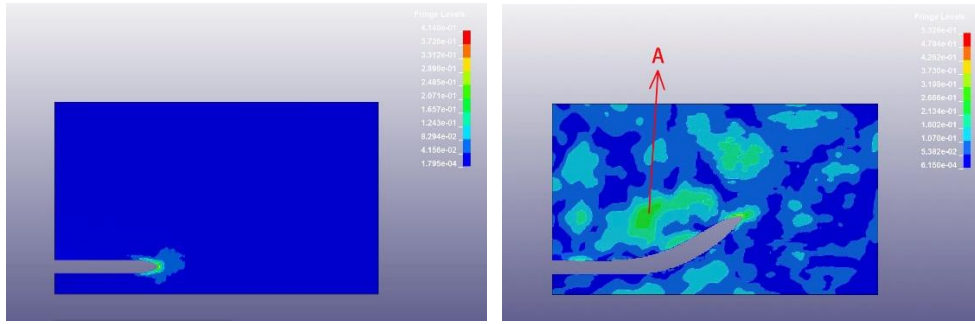
of the ship in the level ice as mentioned in section 2. When the ship is in the rotational motion, the ice loads in local coordinates and those in global coordinates have the relationships as below:

$$F_{long} = F_x \cos(\omega(t-t_0)) + F_y \sin(\omega(t-t_0)) \quad (8)$$

$$F_{trans} = -F_x \sin(\omega(t-t_0)) + F_y \cos(\omega(t-t_0)) \quad (9)$$

where  $F_{long}$  and  $F_{trans}$  are the longitudinal and transverse ice forces in the local coordinate system, respectively;  $F_x$  and  $F_y$  are the x-directional and y-directional ice forces in the global coordinate system, respectively.

In this section, we take  $v = 5\text{m/s}$ ,  $\omega = 1^\circ/\text{s}$  and  $t_0 = 40\text{s}$  as the example to discuss ice loads on the ship. Other parameters are taken same as section 2.



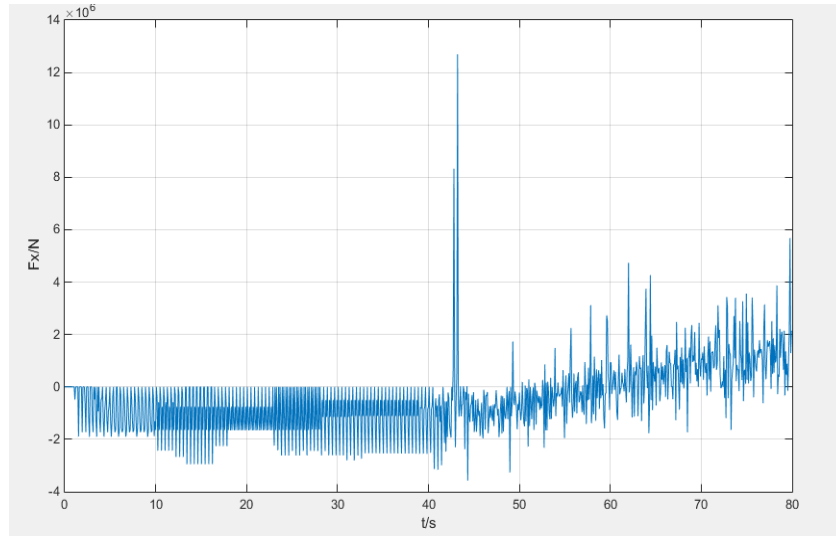
(a).  $t=40\text{s}$ .

(b).  $t=75.2\text{s}$

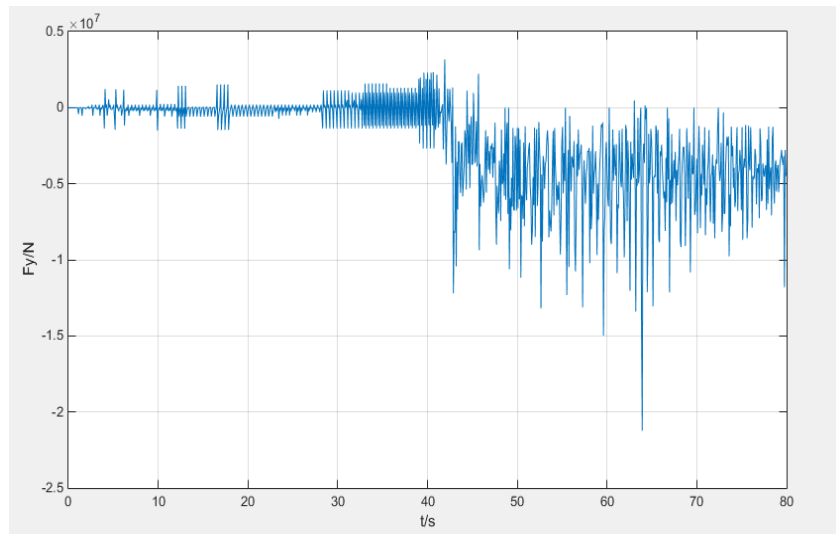
Figure 3. Von Mises stress contour on the level ice during ice-ship collision

Fig. 3 shows the trajectory of the ship and stress distribution on the level ice during ice-ship collision. Fig. 3 (a) and (b) correspond to straight forward and rotational stages, respectively. It can be seen in Fig.3 (a) that during the straight motion, the high-stress is mainly concentrated on the area near the bow. This is because the ice is extruded by the bow mainly and an ice channel whose width is a little wider than the ship beam is generated as a result. The rear part of the hull hardly contacts with the ice, so there is no stress almost. On the contrast, during the rotational motion, the stress presents a different distribution. There are two significant high-stress areas: one is in the area near the bow of the ship and the other is the area near the port of the ship. For the former, it can be understandable because the ship needs to open the channel like that in the straight motion stage. While for the latter, it is because the port of the ship contacts with and extrudes the ice in the inner side of the channel during its left constant-speed rotation. One may also notice there are also high-stress areas near the center of the turning circle. This phenomenon may be due to the ice material and failure mode adopted in this paper,

which will not be discussed here.



(a).  $F_x$



(b).  $F_y$

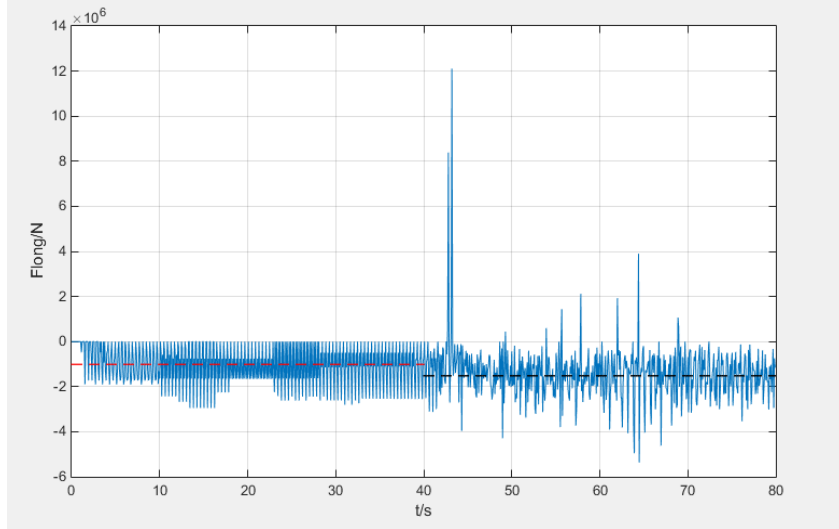
Figure 4 Time histories of the ice loads in the global coordinates

Time histories of ice loads  $F_x$  and  $F_y$  in the global coordinates are shown in the Fig. 4, where the first 40s corresponds to straight-forward motion. It can be seen from Fig. 4 that the time histories of ice loads present a series of high peaks with very short duration, which are the results of the transient and strong nonlinear ice-ship collision.

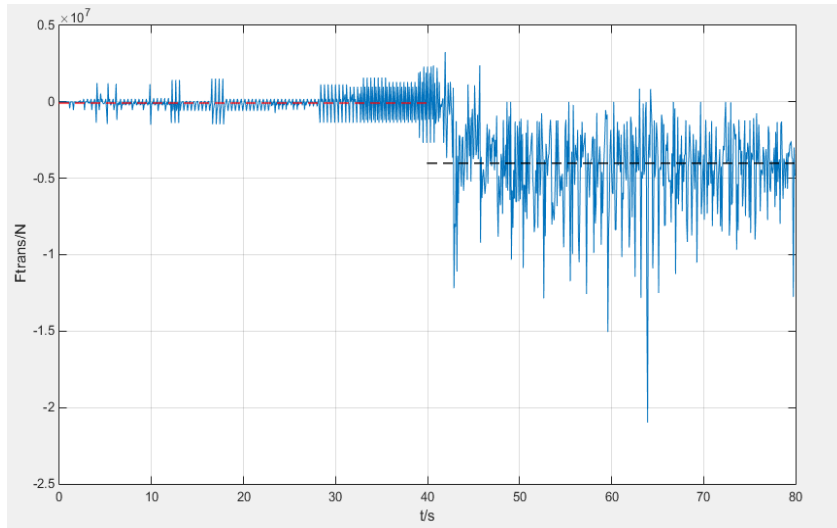
When the ship moves straight forward,  $F_x$  is always negative, which denotes the hull

**Li Z.P. Ni B. Y. Yang D. Han D. F.**

is subjected to the resistance of ice, while  $F_y$  fluctuates around zero with an average value near zero. When the ship begins to rotate around the  $Z$  axis, the global reaction  $F_x$  and  $F_y$  in the global coordinates become complex and it will be easier to analyze in the local coordinates fixed on the ship, as shown in Fig.5.



(a).  $F_{long}$



(b).  $F_{trans}$

Figure 5. Time histories of the ice loads in the local coordinates

Time histories of the ice loads  $F_{long}$  and  $F_{trans}$  in the local coordinates are shown

in the Fig. 5. The relationships between Figs.4 and 5 are Eqs. (8) and (9). The ice loads in the straight-forward motion stage in Fig.4 and Fig.5 are the same, so we just discuss the ice loads in the rotational motion stage. From Fig. 5 (a), it can be seen that the oscillation of  $F_{long}$  gets larger under the effects of the turning movement. However, the average resistance of ice in the rotational motion stage is just a little larger than that in the straight-forward motion stage, because of the same forward velocity. On the other hand,  $F_{trans}$  becomes much larger negative when the ship starts to turn as shown in Fig. 5 (b). This great force to the starboard is due to the extrusion of the ice between the hull and the inner channel when the ship is turning left, or inwards herein, which can also be seen in the stress contour shown in Fig.3 (b). In other words, the ice will prevent the ship from moving inwards when the ship turns.

### 4.3 Influence of different parameters

The ice loads in the case study have been analyzed as shown in Sec.4.2. On this basis, the influences of forward velocity and angular velocity will be discussed in this section. As mentioned above, many scholars have studied the collision process at straight-forward movement. Therefore, this section only analyzes the effect of parameters on the ice loads during the rotation stage.

#### 4.3.1 The effect of forward velocity

To study the effect of forward velocity, we keep angular velocity  $\omega = 1^\circ/s$  constant and change forward velocity from  $V = 2.5m/s$ , to  $V = 5m/s$  and then to  $V = 7m/s$ . The average longitudinal and the transverse ice loads of the ship in local coordinates at different forward velocities are shown in Fig. 6, where the minus denotes the force is opposite to the coordinate axis as discussed in Sec.4.2.

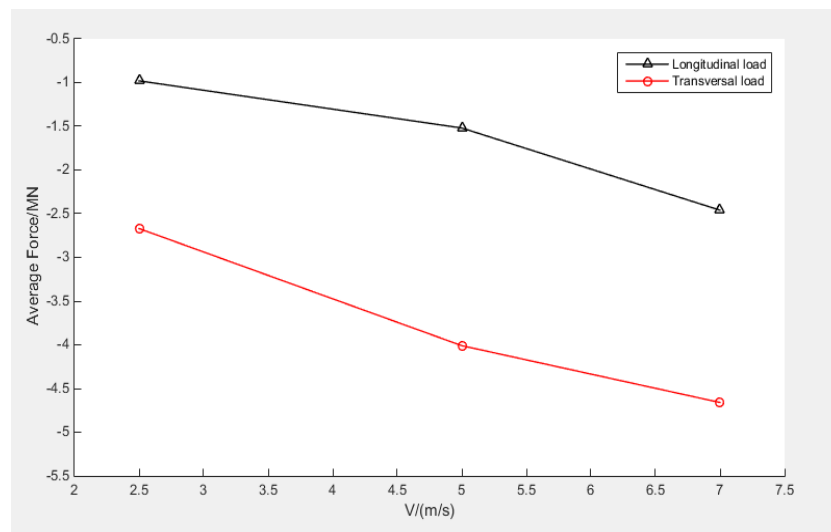


Figure 6. The change of ice loads with forward velocity ( $\omega = 1^\circ/\text{s}$ )

As can be seen from Fig. 6, both longitudinal and transverse ice loads increase significantly with forward velocity. In addition, the increase rate of the longitudinal force becomes larger than that of transverse force as the forward velocity rises. This can be predictable because the greater the forward velocity is, the severer the collision between the ice and ship is, particularly in longitudinal direction.

#### 4.3.2 The effect of angular velocity

To study the effect of angular velocity, we keep forward velocity  $V = 5\text{m/s}$  constant and change angular velocity from  $\omega = 0.4^\circ/\text{s}$ , to  $\omega = 1^\circ/\text{s}$  and then to  $\omega = 1.5^\circ/\text{s}$ . The average ice loads of the ship at different angular velocities are presented in Fig. 7.

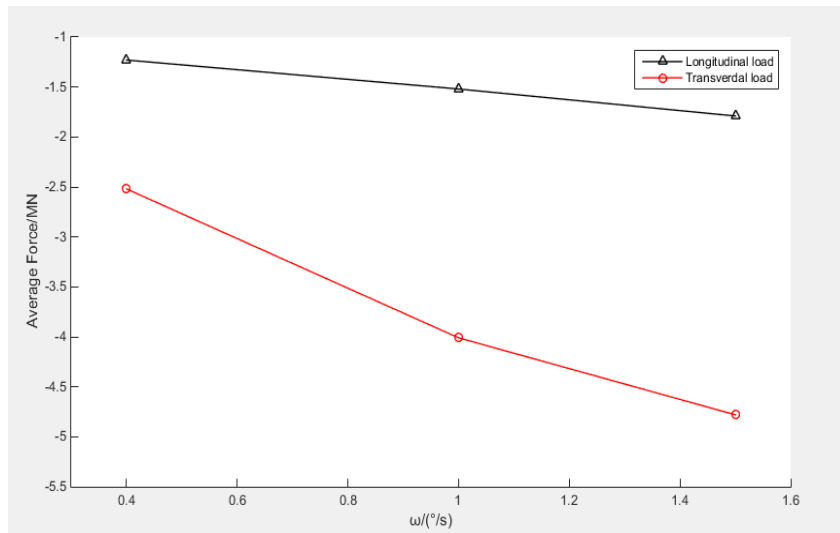


Figure 7. The change of ice loads with angular velocity ( $V = 5\text{m/s}$ )

It can be seen from Fig. 7 that both the longitudinal and transverse loads increase with the angular velocity, but it is obvious that the transverse load rises more rapidly. As one may know,  $V = \omega R$ , where  $R$  is the constant turning radius of the ship. When  $V$  remains and  $\omega$  rises, one can easily obtain  $R$  reduces. A smaller turning radius will, of course, cause a severer contact, extrusion and collision for a given length of the ship during rotation, particularly in transverse direction.

## CONCLUSIONS

In order to study the ice loads when the ship is moving in the level ice, the finite element method is adopted to simulate the motion of an ice-breaker under different movements. Main conclusions can be drawn from the numerical simulations:

- -Nonlinear finite element method is effective to study the transient and strong collision between ship and ice with appropriate ice material and failure modes. The ice loads present sawtooth configuration with large amplitudes and very high frequencies.

## Li Z.P. Ni B. Y. Yang D. Han D. F.

Its average loads in the straight motion is close to that obtained by the empirical formula.

- -Different from that only longitudinal ice resistance can be observed in the straight motion, both longitudinal and transverse loads can be obtained in the rotation motion. Transverse loads, which are caused by the extrusion between level ice and the side of the ship, prevent the ship from turning inwards.

- - Both absolute values of average longitudinal and transverse loads rise along with the increase of forward velocity or angular velocity. It is found that longitudinal ice loads rise more rapidly than transverse ones with forward velocity, while transverse ice loads rise more rapidly than longitudinal ones with angular velocity on the contrast.

## ACKNOWLEDGEMENTS

This work is supported by the National Key R&D Program of China (No. 2017YFE0111400), National Natural Science Foundation of China (Nos. 51639004, 51579054 and 11472088), the Fundamental Research Funds for the Central Universities (No. HEUCFG201811), the 111 Project in HEU, and Lloyd's Register Foundation through the joint centre involving University College London, Shanghai Jiaotong University and Harbin Engineering University, to which the authors are most grateful. Lloyd's Register Foundation helps to protect life and property by supporting engineering-related education, public engagement and the application of research.

## REFERENCES

- [1]. Valanto, P. Spatial distribution of numerically predicted ice loads on ship hulls in level ice. Report for Deliverable D6-3 of SAFEICE Project. (2007).
- [2]. Wang B, Yu H C, Basu R. Ship and Ice Collision Modeling and Strength Evaluation of LNG Ship Structure[C]// ASME 2008, International Conference on Offshore Mechanics and Arctic Engineering. 2008:121-6.
- [3]. Su B. Numerical Predictions of Global and Local Ice Loads on Ships[J]. Department of Marine Technology, 2011.
- [4]. Liu Z. Analytical and numerical analysis of iceberg collisions with ship structures[J]. Marin Teknologi, 2012.
- [5]. Kim M C, Lee S K, Lee W J, et al. Numerical and experimental investigation of the resistance performance of an icebreaking cargo vessel in pack ice conditions[J]. International Journal of Naval Architecture and Ocean Engineering, 2013, 5(1): 116-131.
- [6]. Kajaste-Rudnitski J., Kujala P. Ship propagation through ice field[J]. Rakenteiden Mekaniikka. (Journal of Structural Mechanics). 2014, 47(2):34-49.
- [7]. Ralston T D. Yield and plastic deformation in ice crushing failure: Preprint), ICSI/AIDJEX Symposium on Sea Ice--Processes and Models, Seattle, Washington, 1977.
- [8]. Hallquist J O. LS-DYNA Theory Manual[R]. California: Livermore Software Technology Corporation, 2006.

**Li Z.P. Ni B. Y. Yang D. Han D. F.**

[9]. Lindqvist G. A straightforward method for calculation of ice resistance of ships[J]. Performance, 1989.

## **A Hamiltonian-based Approach for Thermal Buckling of a Functionally Graded Magneto-electric Orthotropic Cylindrical Shell**

Yiwen Ni<sup>\*</sup>, Zhenzhen Tong<sup>\*\*</sup>, Shengbo Zhu<sup>\*\*\*</sup>, Xinsheng Xu<sup>\*\*\*\*</sup>

<sup>\*</sup>Dalian University of Technology; City University of Hong Kong Shenzhen Research Institute, <sup>\*\*</sup>Dalian University of Technology, <sup>\*\*\*</sup>Dalian University of Technology, <sup>\*\*\*\*</sup>Dalian University of Technology; City University of Hong Kong Shenzhen Research Institute

### **ABSTRACT**

The magneto-electro-elastic (MEE) shells with coupling effects are widely used in a variety of intelligent systems such as sensors and actuators. In practice, the MEE shell usually has a non-uniform distribution of stresses. The bonding agent may crack or peel off at low temperature or may creep at high-temperature which could lead to reliability and lifetime limitations. To avoid this, functionally graded (FG) MEE shells without any bonding agent have attracted much attention in recent years. Therefore, the study on dynamic behaviors of such shells is of serious consequence for their strength and safety designs. This paper aims to present a new analytical symplectic solution for thermal buckling of FG MEE orthotropic cylindrical shells. Though adopting the Reissner's shell theory and the symplectic mathematics, the governing equations of MEE medium involving mechanical, electrical and magnetic fields in the classical Lagrangian system is rebuilt in the Hamiltonian system. The high-order governing differential equation is reduced to a set of ordinary differential equations which can be analytically solved by the method of separation of variables. The thermal buckling problem is converted into solving of the symplectic eigenvalues and eigenfunctions. Critical thermal buckling loads are computed and presented in the numerical examples. Comparisons are presented to show the accuracy of the analytical solution procedure. A detailed parametric study is carried out to investigate the influences of the FGM magneto-electric properties and boundary conditions. Some new results are given also. The present study demonstrates that the general solutions of displacement, electric potential and magnetic potential highly depend on the computation parameters. The pre-determined general solution (e.g., trigonometric functions) used in the classical analytical method may lead to inappropriate results in some cases. In addition, the present accurate cylindrical shell model will provide more reasonable guidance to the design.

## Concurrently Coupled Peridynamics/Finite Element Simulation Based on Nonlocal Matching Boundary Condition

Clint Nicely\*, Dong Qian\*\*

\*Raytheon Space and Airborne Systems, \*\*The University of Texas at Dallas

### ABSTRACT

Peridynamics (PD) is a reformulation of the continuum theory based on an integro-differential formulation. With its unique capability in incorporating material length scale, there is a continuing interest in establishing multiscale computational methods that integrate PD with continuum scale simulation methods. In this presentation, a concurrent multiscale approach has been established to couple a stabilized non-ordinary peridynamics (SNOPD) with finite element method (FEM). In order to minimize the artificial wave reflection that is present within coupling methods a Non-Local Matching Boundary Condition (NMBC) is developed for treating the numerical peridynamic interface. The NMBC is cast in the form of a parameterized expression that involves the displacements and their higher-order time derivatives of peridynamic (PD) nodes at the numerical interface. Non-reflective and wave transmitting conditions are realized by zeroing the associated residual and its higher order derivatives that are functions of the dispersion relation at the particular wave length of interest. Both 1D and 2D versions of NMBCs have been established and it is shown that the 1st order NMBC for 2D SNOPD is applicable for both unidirectional and multidirectional waves. A bridging scale decomposition employing a projection approach is introduced in the concurrent multiscale discretization to realize a seamless information passage between the PD and FEM simulation. Multiple examples are given to demonstrate the effectiveness of the coupling method comparing a direct coupling, a coupling with only projection of the PD result, and finally a method using the projection and NMBC combined. These examples demonstrate the high effectiveness of the NMBC coupling approach.

## **A Stable Formulation of Resonant Maxwell's Equations in Cold Plasma**

Anouk Nicolopoulos\*, Bruno Després\*\*, Martin Campos Pinto\*\*\*

\*LJLL, \*\*LJLL/IUF, \*\*\*LJLL/CNRS

### **ABSTRACT**

A hybrid resonance phenomena is considered here for the heating of magnetic confinement fusion plasma. It is obtained sending high frequency electromagnetic waves into the plasma. Mathematically, it corresponds to a singular solution of the harmonic in time Maxwell's equations. Under some uniformity assumptions of the plasma, we work on the equations in 1D. The problem is that the equations are ill posed, meaning that there is no uniqueness of the solution. But the equations can be regularized introducing a small viscosity parameter to modelize the friction between ions and electrons. We then select the physical solution to our limit problem making that viscosity go to zero. From a numerical point of view, taking a small viscosity parameter is not satisfying as this small parameter should be linked to the discretization in space step. This is why we chose to characterize the limit solution. Constructing a family of manufactured functions based on the expected singularity of one over  $x$  of our electric field, energy relations on the scaled difference between the real electromagnetic fields and the manufactured ones have then been derived to construct a variational formulation for the limit problem. The formulation we obtained fits in the frame of classical mixed variational formulations, and its structure allows us to ensure its well-posedness, in the sense that there is a solution, which is unique. Furthermore, this formulation is stable in the sense that it is the limit of a mixed variational formulation for the viscosity problem. This feature is interesting for numerical simulations as the viscosity is of various orders of magnitude in a tokamak, and it also gives us additional information on the solution of our resonant equations. This work will be illustrated by numerical results using the finite element method to discretize these formulations. First in the X-mode case, meaning the heating wave sent into the plasma is of normal incidence, and which allows us to decouple the equations into two systems. Then in the mode-coupling case of oblique incidence.

# ULTRA-FAST, HIGH-FIDELITY COMPUTATIONAL FLUID DYNAMICS ON GPU FOR AUTOMOTIVE AERODYNAMICS

CHRISTOPH A. NIEDERMEIER\*, CARLO DEL BENE\*,  
CHRISTIAN F. JANSSEN†, BASTIAN SCHNEPF†,  
MARC RATZEL† AND THOMAS INDINGER\*

\*FluiDyna GmbH  
Edisonstr. 3  
85716 Unterschleißheim, Germany  
{christoph.niedermeier,carlo.del.bene,thomas.indinger}@fluidyna.de

†Altair Engineering GmbH  
Calwer Str. 7  
71034 Böblingen, Germany  
christian.janssen@altair.com, schnepf@altair.de, ratzel@altair.com

**Key words:** LBM, GPU, Automotive Aerodynamics.

**Summary.** In this work, we present the innovative commercial GPU-based Computational Fluid Dynamics (CFD) solver ultraFluidX. The software is based on the Lattice Boltzmann Method (LBM), which is explicit in time, hence inherently transient and which only requires nearest-neighbor information for each point of the computational grid. Therefore, LBM is a perfect match for the massively parallel architecture of GPUs and highly benefits from their tremendous computational power. Additionally, ultraFluidX can make use of multiple GPUs through an efficient implementation based on CUDA-aware MPI. The software thereby achieves unprecedented turnaround times of just a few hours for transient flow simulations of fully detailed production-level passenger and heavy-duty vehicles. This work features simulations of the DrivAer model, a generic, publicly available vehicle geometry that was developed by the Chair of Aerodynamics and Fluid Mechanics at the Technical University of Munich and which is widely used for testing and validation purposes nowadays.

## 1 INTRODUCTION

The optimization of aerodynamic properties of a vehicle plays a crucial role in the automotive design process. In the case of interurban travel, the biggest portion of the driving resistance is induced by aerodynamic drag. Moreover, there are other secondary goals, such as driving stability and ride comfort, that are influenced by the vehicle's aerodynamics. For such a sophisticated level of aerodynamic optimization, it is very important to have as much knowledge as possible about the flow field around the vehicle under consideration. This can only be achieved through a CFD simulation, where the full three-dimensional information can be easily extracted from the

numerical results in contrast to, e.g., wind tunnel testing. The flow field in such a case is very complex and highly unsteady, and the corresponding CFD simulations must be fully transient and highly resolved to capture all relevant physical effects. This was posing a big challenge for automotive OEMs so far, because such simulations based on pure CPU systems are typically constraint by available computational resources and in general also very expensive. The situation now changes drastically with GPU-based CFD, where well-suited methods like LBM can achieve turnaround times of just a few hours for the aforementioned use cases.

## 2 ULTRAFLUIDX

The current contribution is based on the commercial GPU-based CFD solver ultraFluidX. ultraFluidX is developed by Fluidyna GmbH, a wholly-owned subsidiary of Altair Engineering. The main motivation for the development of the code is to introduce higher fidelity models, fully transient analyses, small turnaround times and low total cost to automotive OEMs around the world. ultraFluidX is based on the Lattice Boltzmann Method, which is explicit in time, hence inherently transient and which only requires nearest-neighbor information for each point of the computational grid. Therefore, ultraFluidX highly benefits from the tremendous computational power of the massively parallel architecture of GPUs and can additionally make use of multiple GPUs through an efficient implementation based on CUDA-aware MPI. The solver thereby achieves unprecedented turnaround times of just a few hours for transient flow simulations of fully detailed production-level passenger and heavy-duty vehicles.

ultraFluidX uses a recent, highly accurate LBM collision operator based on Cumulants [1-3], which is accompanied by an LBM-consistent Smagorinsky LES model [4] and a wall modeling technique based on the work of Malaspinas & Sagaut [5] and Wang & Moin [6]. The Cartesian LBM base mesh is combined with an octree-based grid refinement. Starting from a relatively coarse Cartesian background grid, the mesh is consecutively refined towards the obstacle surface. Between each refinement level, the mesh spacing is reduced by a factor of 2. The first refinement levels are typically defined via axis-aligned bounding boxes, higher refinement levels closer to the geometry are either based on custom user-defined volumes or defined via geometry offsets. Kinks and thin parts are fully resolved in the volumetric preprocessing. Moreover, the appropriate physical modeling is selected automatically inside tight gaps and cavities. Representative production-level volume meshes are generated within the order of one hour.

In addition, the code contains several enhanced features for automotive applications. These features typically come with additional computational overhead, which has to be considered in the performance evaluation and in comparison to other available software packages. ultraFluidX nevertheless achieves a parallel strong scaling efficiency of more than 80% for a realistic production-level case even when using these enhanced features [7], which include, but are not limited to, porous media zones, support for moving floors (single- and five-belt systems), static floors with boundary layer suction, rotating wheel models (straightforward wall-velocity boundary conditions or more advanced MRF and overset grid approaches) and automatic convergence detection. The code also features advanced post-processing capabilities, such as window averaging, spatial drag/lift contributions, probe output and section cut output.

### 3 DRIVAER MODEL WITH ENGINE BAY FLOW

The DrivAer model [8] was introduced by Heft et al. [9] to address the need for a generic geometry for investigations of automotive aerodynamics that is somewhere in between rather simple, academic models like the Ahmed body and very complex, production-level vehicle geometries of automobile manufacturers. The original DrivAer model already featured different rear end and underbody designs, however, it was only available in mock-up configuration and hence missing the possibility to include flow through the engine bay. Therefore, Wittmeier & Kuthada [10] lately presented an update with additional underhood flow to make the model even more realistic. This model was then used by Collin et al. [11] in their recent work, where they performed both wind tunnel tests and numerical simulations of the 40% scale open cooling notchback model using perforated aluminum sheets with different opening ratios to mimic different radiator properties. Below, we will compare some of the results from these wind tunnel tests with numerical results obtained with ultraFluidX.

#### 3.1 Case setup

The simulations are performed with the 40% scale DrivAer open cooling notchback model with open wheelhouses and closed rims using a rectangular computational domain with a constant-velocity inlet, slip walls at the sides as well as at the top and a non-reflecting outlet. Additionally, Figure 1 shows the mixed boundary conditions that are used at the ground of this numerical wind tunnel to account for the moving belt system and the passive boundary layer scoop that were used for the experiments by Collin et al. [11] at the Technical University of Munich.

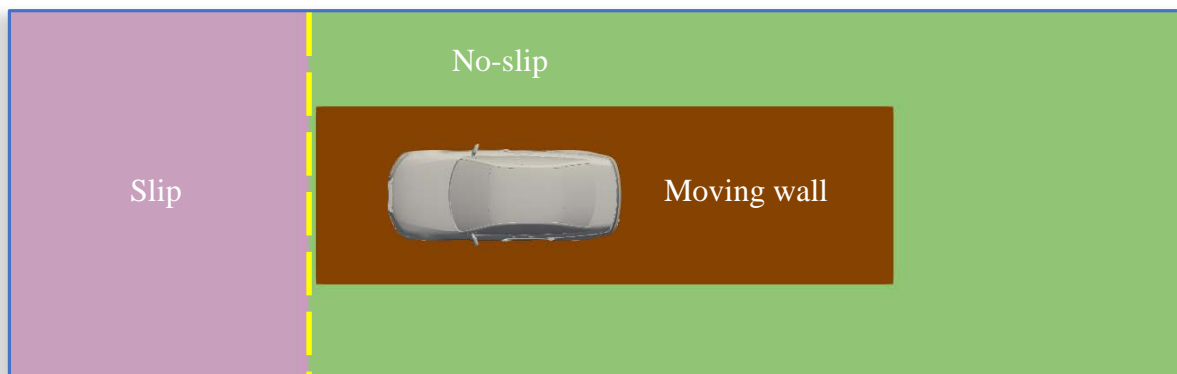


Figure 1: Boundary conditions at the wind tunnel ground.

The inlet velocity is 44 m/s and the density, temperature and kinematic viscosity of the air are assumed to be 1.135 kg/m<sup>3</sup>, 27.6 °C and 0.0000163 m<sup>2</sup>/s, respectively. Three different cases with opening ratios ( $A_o/A_c$ ) of 12.3%, 19.7% and 28.3% for the perforated aluminum sheets are simulated. For doing so, each of the respective pressure drop curves provided by Collin et al. [11] is converted into viscous and inertial resistances that have to be provided as input parameters to the porous media zones in ultraFluidX.

A mixture of axis-aligned bounding boxes, user-defined volumes and geometry offsets is used to refine the computational grid in relevant areas like the wake, the engine bay and sensitive regions along the surface. The minimum grid size at refinement level 7 is 0.6 mm and the grid overall consists of 156.6 million voxels with 57.5 million so-called fine equivalents, Figure 2 shows the computational grid in the y-normal symmetry plane of the wind tunnel.

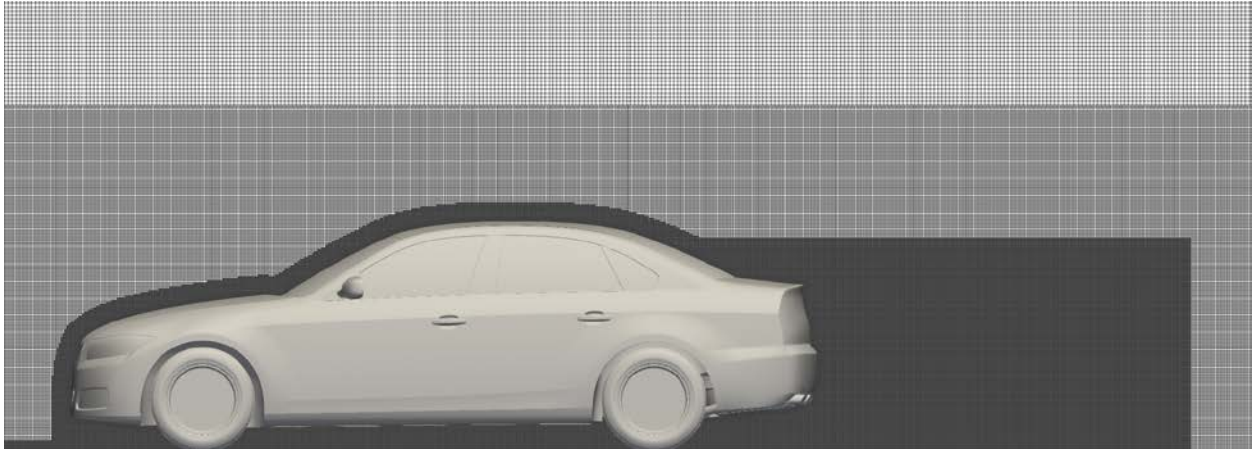


Figure 2: Computational grid in the y-normal symmetry plane of the wind tunnel.

The physical simulation time is 1.276 s, which corresponds to 30 flow passes over the vehicle. Additionally, the simulations are run at twice the original Mach number, which is a common technique for LBM to reduce the necessary number of iterations if only the aerodynamic properties are of interest.

### 3.2 Numerical results and performance

The simulations are performed on an NVIDIA DGX-1 with eight NVIDIA Tesla V100 GPUs, where they exhibit an overall performance of 2,208 million node updates per second (MNUPS), so 276 MNUPS per GPU. This results in a computation time of only 4.7 h with the case setup as mentioned above. If we also take into account the meshing time of 0.8 h, the total turnaround time is just 5.5 h.

A short time-to-solution is of course only beneficial if the solution is also accurate. Figure 3 shows the instantaneous velocity magnitude in the y-normal symmetry plane of the wind tunnel. Even small turbulent structures, e.g., in the wake region, are clearly visible, meaning that both the spatial as well as the temporal resolution of the simulation are sufficient to capture such effects. However, the most interesting quantities for an aerodynamic analysis are usually still the deltas between the drag and lift coefficients due to certain changes of the vehicle geometry or the simulation parameters. These deltas are then usually used to assess if a design change or an attachment part like, e.g., a spoiler has the desired aerodynamic effect.

In this work, we use the deltas between different opening ratios to analyze if ultraFluidX can predict the same trends for the drag, front lift and rear lift coefficients that were measured in the wind tunnel by Collin et al. [11]. For doing so, we use the opening ratio of 12.3% as a baseline

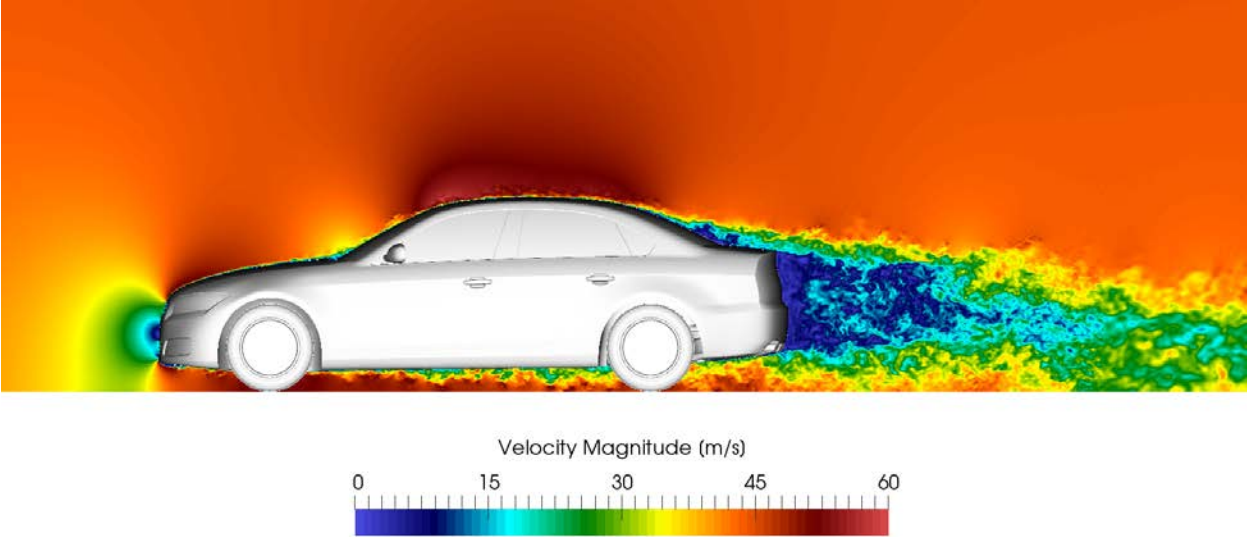


Figure 3: Instantaneous velocity magnitude in the y-normal symmetry plane of the wind tunnel.

and compare the deltas that we get for 19.7% and 28.3%. Figure 4 shows the deltas of the drag coefficient and the ultraFluidX results exhibit an excellent agreement to the deltas measured by Collin et al. [11] within less than 1 count, which means that the difference is less than 0.001. A similar observation can be made in Figure 5 for the deltas of the front lift coefficient, which almost exactly match for the opening ratio of 19.7% and still only differ by approx. 2 counts for 28.3%. Figure 6 finally shows the deltas of the rear lift coefficient, the agreement for 19.7% with a deviation of approx. one count is also excellent, just the difference for 28.3% is higher and reaches a maximum value of 6 counts. However, this is still within a reasonable range and the especially the trend from 12.3% to 19.7% and 28.3% is correctly captured for all coefficients, which is very important for a consistent evaluation of parameter changes.

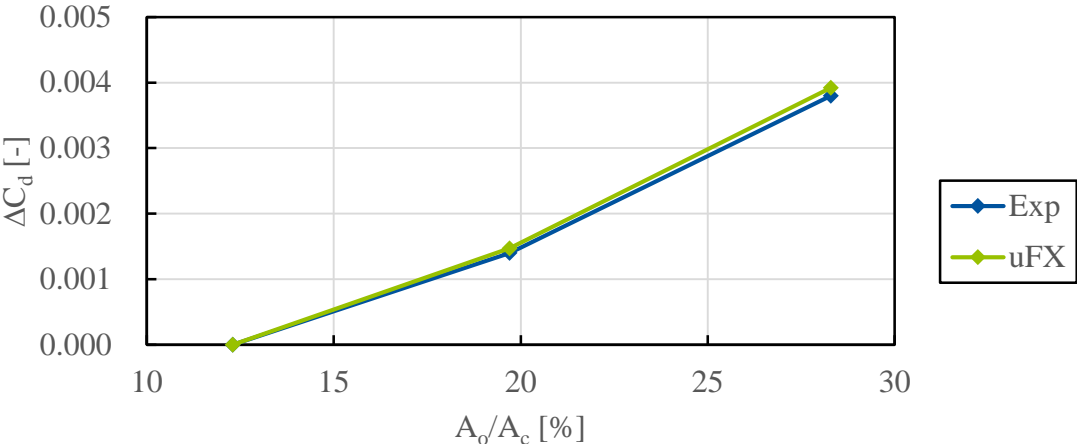


Figure 4: Deltas of the drag coefficient w.r.t. an opening ratio of 12.3% obtained with ultraFluidX (uFX) and compared with reference data by Collin et al. [11] (Exp).

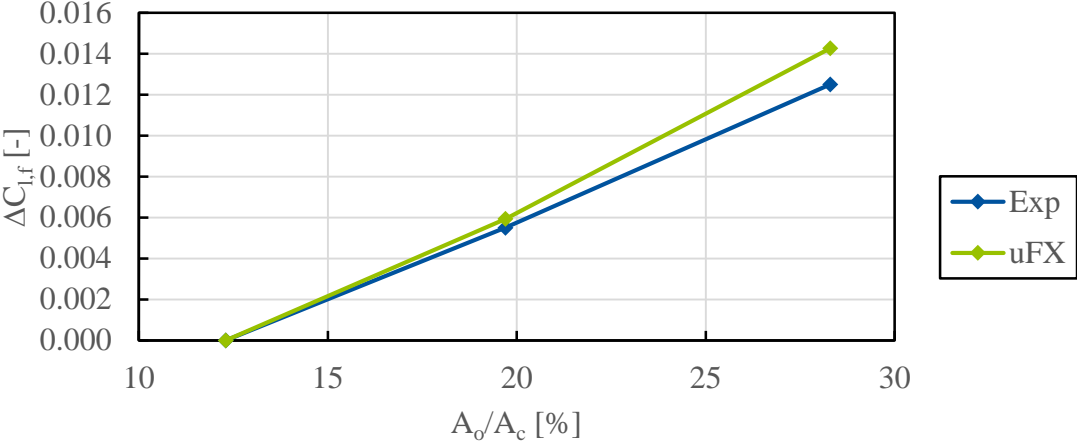


Figure 5: Deltas of the front lift coefficient w.r.t. an opening ratio of 12.3% obtained with ultraFluidX (uFX) and compared with reference data by Collin et al. [11] (Exp).

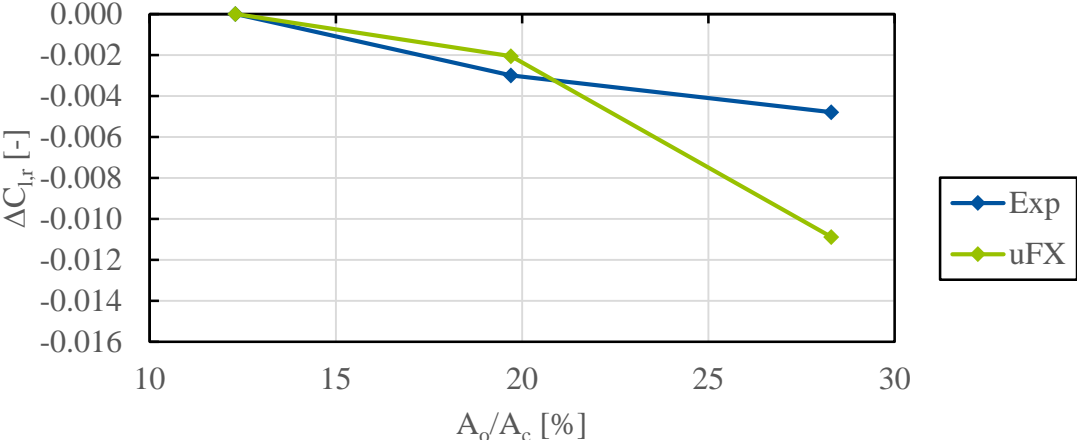


Figure 6: Deltas of the rear lift coefficient w.r.t. an opening ratio of 12.3% obtained with ultraFluidX (uFX) and compared with reference data by Collin et al. [11] (Exp).

#### 4 SUMMARY AND CONCLUSION

In this work, we presented the innovative commercial GPU-based CFD solver ultraFluidX and used it to perform simulations of the recently updated 40% scale DrivAer notchback model with engine bay flow. Drag and lift trends compared to experimental reference data can be reproduced very well within just 5.5 h of total wall time per simulation, while the maximum resolution of the grid is as high as 0.6 mm and the total size of the case is more than 150 million voxels. Therefore, by using an advanced LBM collision operator and by leveraging the massively parallel architecture

of GPUs, ultraFluidX can deliver accurate, fully transient results within unprecedented turnaround times of just a few hours on a single compute node. This creates completely new possibilities for automotive OEMs to use even highly resolved, high-fidelity simulations for simulation-driven design processes on a daily basis.

## REFERENCES

- [1] Geier, M., Schönherr, M., Pasquali, A., & Krafczyk, M. (2015). The cumulant lattice Boltzmann equation in three dimensions: Theory and validation. *Computers & Mathematics with Applications*, 70(4), 507-547.
- [2] Geier, M., Pasquali, A., & Schönherr, M. (2017). Parametrization of the cumulant lattice Boltzmann method for fourth order accurate diffusion part I: Derivation and validation. *Journal of Computational Physics*, 348, 862-888.
- [3] Geier, M., Pasquali, A., & Schönherr, M. (2017). Parametrization of the cumulant lattice Boltzmann method for fourth order accurate diffusion Part II: Application to flow around a sphere at drag crisis. *Journal of Computational Physics*, 348, 889-898.
- [4] Malaspinas, O., & Sagaut, P. (2012). Consistent subgrid scale modelling for lattice Boltzmann methods. *Journal of Fluid Mechanics*, 700, 514-542.
- [5] Malaspinas, O., & Sagaut, P. (2014). Wall model for large-eddy simulation based on the lattice Boltzmann method. *Journal of Computational Physics*, 275, 25-40.
- [6] Wang, M., & Moin, P. (2002). Dynamic wall modeling for large-eddy simulation of complex turbulent flows. *Physics of Fluids*, 14(7), 2043-2051.
- [7] Niedermeier, C. A., Janßen, C. F., & Indinger, T. (2018, June). Massively-parallel Multi-GPU Simulations for Fast and Accurate Automotive Aerodynamics. In *7th European Conference on Computational Fluid Dynamics*.
- [8] Technical University of Munich. DrivAer Model. Retrieved from <http://www.drivaer.com>
- [9] Heft, A. I., Indinger, T., & Adams, N. A. (2012). *Introduction of a new realistic generic car model for aerodynamic investigations* (No. 2012-01-0168). SAE Technical Paper.
- [10] Wittmeier, F., & Kuthada, T. (2015). Open grille DrivAer model-first results. *SAE International Journal of Passenger Cars-Mechanical Systems*, 8(2015-01-1553), 252-260.
- [11] Collin, C., Müller, J., Islam, M., & Indinger, T. (2017, September). On the Influence of Underhood Flow on External Aerodynamics of the DrivAer Model. In *FKFS Conference* (pp. 201-215). Springer, Cham.

## **Extreme-Scale Unstructured-Grid CFD Algorithms for a Many-Core Landscape**

Eric Nielsen<sup>\*</sup>, Justin Luitjens<sup>\*\*</sup>, Aaron Walden<sup>\*\*\*</sup>, Mohammad Zubair<sup>\*\*\*\*</sup>

<sup>\*</sup>NASA Langley Research Center, <sup>\*\*</sup>NVIDIA Corp, <sup>\*\*\*</sup>NASA Langley Research Center, <sup>\*\*\*\*</sup>Old Dominion University

### **ABSTRACT**

We explore the transition of an unstructured-grid CFD code from a flat MPI model to a shared-memory model suitable for a many-core landscape. Included are node-level studies of computationally intensive CFD kernels on the Intel Xeon Phi Knights Landing, NVIDIA Pascal P100, and NVIDIA Volta V100 architectures. Performance comparisons are shown, and scaling studies on several modern supercomputing systems including the new IBM Power9/NVIDIA V100 system located at Oak Ridge National Laboratory known as Summit are also included. Meshes with billions of elements are used to demonstrate GPU performance equivalent to over one million Xeon cores.

## Coupled Finite Element Analysis Model of Structural and Electrical Coupled Analysis for Electrical Contact Resistance

Tomoya Niho<sup>\*</sup>, Hiroyuki Kuramae<sup>\*\*</sup>, Daisuke Ishihara<sup>\*\*\*</sup>, Tomoyoshi Horie<sup>\*\*\*\*</sup>

<sup>\*</sup>Kyushu Institute of Technology, <sup>\*\*</sup>Osaka Institute of Technology, <sup>\*\*\*</sup>Kyushu Institute of Technology, <sup>\*\*\*\*</sup>Kyushu Institute of Technology

### ABSTRACT

Electrical contact resistance plays important role in melting and bonding of interface between steel sheets for resistance spot welding. Although many researchers have proposed theoretical models of electrical contact resistance[1], microscale structural and electrical coupled finite element analysis is required to evaluate electrical contact resistance because its characteristics depend on the real contact surface, elasto-plastic large deformation contact, electric current and temperature. In this study, we discuss a microscale structural and electrical coupled finite element analysis for the electrical contact resistance[2]. In this analysis, the structural analysis with elasto-plastic, large deformation and contact effect is performed using measured surface based finite element analysis model and temperature dependent material properties. Deformed shape obtained by the structural analysis is used for the electrical analysis considering temperature dependent electrical resistivity. In the microscale electrical contact resistance analysis, statistically similar representative volume element (SS-RVE) size and mesh resolution are important to obtain the accurate results. On the other hand, the large computational cost is required for 3D coupled analysis. The electrical contact resistance analyses are performed to discuss the SS-RVE size, mesh resolution and computational cost. The electrical contact resistance analyses are performed for 270 MPa grade, 440 MPa grade and 980 MPa grade tensile strength steel sheets to confirm the validity of the proposed analysis method. The dependency of the electrical contact resistance on the contact pressure and the temperature are compared with that of Babu's model[3] and experimental results from the viewpoint of these path dependencies. [1] M. Hamedi and M. Atashparva. A Review of Electrical Contact Resistance Modeling in Resistance Spot Welding. *Welding in the World*, Vol. 61, No. 2, pp. 269 - 290, 2017. [2] T. Niho, K. Kubota, H. Aramaki, H. Kuramae, D. Ishihara and T. Horie, Microscale Electrical Contact Resistance Analysis for Resistance Spot Welding, *Proceedings of VII International Conference on Computational Methods for Coupled Problems in Science and Engineering 2017*, pp. 1152-1158, 2017. [3] S.S. Babu, M.L. Santella, Z. Feng, B.W. Riemer, and J.W. Cohron, Empirical Model of Effects of Pressure and Temperature on Electrical Contact Resistance of Metals, *Science and Technology of Welding and Joining*, Vol. 6, No. 3, pp. 126-132, 2001.

## Geometry Optimization of Nitinol Stent Design: Comparing Old and New Design Using Finite Element Method

Dalibor Nikolic\*, Igor Saveljic\*\*, Nenad Filipovic\*\*\*

\*BioIRC - Research and Development Center for Bioengineering, \*\*BioIRC - Research and Development Center for Bioengineering, \*\*\*Faculty of Engineering University of Kragujevac

### ABSTRACT

**OBJECTIVE** In-stent restenosis struct shape and thickness have significant impact, especially if stent was implanted in the small arteries. In this paper author suggest novel approach for better geometry stent modeling – topology optimization process on existing stent design. For evaluation of the topology optimization and mechanical performance of nitinol stents and comparing differences between old design (non-optimized) and new optimized design the finite element method was used. The Z-shaped closed-cell self-expanding stent type for testing was used. This type of stent is most common in clinical practice. For better understanding of the mechanical process inside of the stent device for researcher is very important to simulate them and compare the results. **METHOD** Geometrically of stent model was used from Palmaz-Schatz first stent model. Finite element method (FEM) was performed assuming that the stents device used for this research were made by laser cutting, from tube form, by application of expanding and crushing force. The behavior of two different stent models was analyzed: old Palmaz-Schatz design and optimized design obtained based on the results from topology optimization of the Palmaz-Schatz design. Palmaz-Schatz stent geometry is a very simple geometry with enormous potential for modification this is the main reason why this geometry was used in this research. **RESULTS** By compering of simulation result between old Palmaz-Schatz and new modern and optimized design, it can be noticed that maximal stress and strain are much lower on the modern design model than on the old design model. Also, from distribution of stress and strain conclusion could be made that the old design has a lot of problematic positions with stress and strain concentration. **CONCLUSION** Performed simulation on stent models show that the new modern design has better clinical behavior due to lower contacting surface, higher radial resistive strength and much better superplastic behavior. Optimization process based on two optimization rules: minimization of the model volume and retention (or increase) of the maximal strain of the basic model.

## Dynamic Analysis of B-train Articulated Vehicle

Barbieri Nilson\*, Rubem Melo\*\*, Key Lima\*\*\*

\*PUCPR, \*\*PUCPR, \*\*\*PUCPR

### ABSTRACT

The new Brazilian Regulations 210 and 211/2006 of the CONTRAN, had authorized the circulation of new Cargo Vehicles Combinations. Because their major load capacity, the numbers of these new models grew quickly, mainly b-trains, road-trains and semi-trailers with spaced axles. Certainly representative of a cargo vehicles evolution because the increase of productivity that provide and for the reduction of the costs and pollution with the road cargo transport, these new models must be observed about their characteristics of handling and security. Because the number of articulations, these combinations have specific phenomenon that affect their handling. Among them, the most important is the "rearward amplification". In consequent of this rear amplification, the last unit is exposed to highest lateral acceleration, and can rollover, taking with it other vehicles of combination. The semi-trailers with spaced axles have higher resistance to maneuvering that can bring tires wear and need higher friction demand in the tractor-vehicle during the maneuvers. A revision about the characteristics is necessary for the evolution of the vehicles project, roads design and traffic signs. There is also the necessity to include specific instructions for the drivers. In this work, the dynamic behavior of a b-train vehicle with liquid cargo is analyzed. The vehicle is subjected to evasive maneuvers and the vibration data is obtained through four accelerometers positioned along the vehicle. The liquid cargo is varied from 100, 80, 60 and 40% of the total capacity. The results evidential the phenomenon slosh through the variation in the loads of the wheels. Mathematical models use high order nonlinear polynomials to adjust system parameters. The results show great agreement between the numerical and experimental values of the lateral accelerations.

## **A Boundary Integral Equation (BIE) Method for Modeling Flow Through Non-deformable Porous Medium Using Brinkman Equation in Terms of Non-primitive Variables**

Chandra Shekhar Nishad<sup>\*</sup>, Anirban Chandra<sup>\*\*</sup>, Timir Karmakar<sup>\*\*\*</sup>, Raja Sekhar G.P.<sup>\*\*\*\*</sup>

<sup>\*</sup>Indian Institute of Technology Kharagpur, India, <sup>\*\*</sup>Indian Institute of Technology Kharagpur, India, <sup>\*\*\*</sup>Indian Institute of Technology Kharagpur, India, <sup>\*\*\*\*</sup>Indian Institute of Technology Kharagpur, India

### **ABSTRACT**

In this work, we propose a new boundary element technique for steady two-dimensional viscous incompressible Newtonian flow through non-deformable porous medium. We assume that the porous medium is isotropic and homogeneous, and utilize Brinkman equation to model the fluid flow. There are mainly two approaches to solve Brinkman equation using boundary integral methods, one in terms of primitive variables, namely velocity and traction (also known as Brinkmanlet formulation) and another in terms of non-primitive variables, namely stream function-vorticity variables (in case of two-dimensional or three-dimensional axisymmetric flows). Boundary integral formulation for Brinkman flows in terms of primitive variables is well known and available in the literature ([1], [2]). As per the knowledge of the authors, there does not exist any boundary integral formulation so far for two-dimensional Brinkman flows in terms of non-primitive variables, namely stream function-vorticity variables. Moreover, it is always advantageous to have an alternative approach which is efficient and easy to implement. In this context, first we present boundary integral equation (BIE) method for 2D Brinkman equation in terms of the non-primitive variables namely, stream-function and vorticity variables. Subsequently, a test problem namely, the lid-driven porous cavity over a unit square domain is presented to assert the accuracy of our BEM code. We observe that the rate of convergence increases with increasing Darcy number. Finally, we discuss an application of our proposed method to flows through porous wavy channel, which is a problem of significant interest in the microfluidics, biological domains and groundwater flows. For low Darcy number the streamlines follow the curvature of the wavy channel and no circulation occurs irrespective of the wave-amplitude, while for high Darcy number the flow circulation occurs near the crest of the wavy channel (when the wave-amplitude is large enough), which in many cases promotes the convective mixing and may prevent the leakage of carbon dioxide and support storage safety ([3]). References: [1]. Feng, J., Ganatos, P., Weinbaum, S.: Motion of a sphere near planar confining boundaries in a Brinkman medium. *Journal of Fluid Mechanics* 375, 265–296 (1998) [2]. Pozrikidis, C.: A study of linearized oscillatory flow past particles by the boundary-integral method. *Journal of Fluid Mechanics* 202, 17–41 (1989) [3]. Karmakar, T., Raja Sekhar, G.P.: A note on flow reversal in a wavy channel filled with anisotropic porous material. In: *Proc. R. Soc. A*, vol. 473, p. 20170193. The Royal Society (2017)

## Implicit Particle-in-cell Formulation for Fluid-Structure Interaction Simulations with Hard Solid

Koji Nishiguchi<sup>\*</sup>, Rahul Bale<sup>\*\*</sup>, Shigenobu Okazawa<sup>\*\*\*</sup>, Makoto Tsubokura<sup>\*\*\*\*</sup>

<sup>\*</sup>RIKEN Advanced Institute for Computational Science, <sup>\*\*</sup>RIKEN Advanced Institute for Computational Science, <sup>\*\*\*</sup>University of Yamanashi, <sup>\*\*\*\*</sup>RIKEN Advanced Institute for Computational Science, Kobe University

### ABSTRACT

An implicit particle-in-cell method using a fixed Eulerian mesh and a set of Lagrangian particles is proposed to simulate fluid-structure interaction (FSI) problems. The authors have been developing a full Eulerian scheme for solid dynamics [1]. A full Eulerian method, however, cannot avoid the numerical dissipation of material interfaces and history-dependent variables of structures due to the advection. Even if a high-order advection scheme is adopted, material interfaces become diffusive gradually with time. To retain the sharp interface, K. Sugiyama et al. [2] proposed the particle-in-cell method for FSI simulations of flexible neo-Hookean tube flows in axisymmetric cylindrical coordinates. In this study, we propose a novel implicit particle-in-cell formulation using a fixed Cartesian mesh in order to relax limitation of small time increment in FSI simulations with hard solid such as metal materials. In the present method, the unified equation of motion for fluid and structure [3] is computed on the fixed Cartesian mesh. To avoid numerical dissipation of material interfaces and history-dependent variables of solid, Lagrangian particles represent the solid region and carry history-dependent variables such as solid deformation tensor. For an implicit time-integration for relaxing the time restriction stemming from an elastic wave, we assume the linear approximation using a fourth-order Jacobian tensor of hyperelastic stress tensor [4]. To verify the present approach, several numerical examples of FSI problem with hard solid will be demonstrated in the presentation. [1] K. Nishiguchi, S. Okazawa, M. Tsubokura: Multi-material Eulerian finite element formulation for pressure-sensitive adhesives, *International Journal for Numerical Methods in Engineering*, accepted, 2017. [2] K. Sugiyama, N. Nagano, S. Takeuchi, S. li, S. Takagi, Y. Matsumoto: Particle-in-cell method for fluid-structure interaction simulations of neo-Hookean tube flows, *Theoretical and Applied Mechanics Japan*, 59, 245-256, 2011. [3] K. Sugiyama, S. li, S. Takeuchi, S. Takagi, Y. Matsumoto: A full Eulerian finite difference approach for solving fluid-structure coupling problems, *Journal of Computational Physics*, 230(3), 596-627, 2011. [4] S. li, K. Sugiyama, S. Takeuchi, S. Takagi, Y. Matsumoto: An implicit full Eulerian method for the fluid-structure interaction problem, *International Journal for Numerical Methods in Fluids*, 65(1-3), 150-165, 2011.

## **Preliminary Investigation for Robust Topological Design Considering Nonlinear Structural Behavior**

Takayuki Nishino<sup>\*</sup>, Takashi Kyoya<sup>\*\*</sup>, Junji Kato<sup>\*\*\*</sup>

<sup>\*</sup>TOHOKU university, <sup>\*\*</sup>TOHOKU university, <sup>\*\*\*</sup>TOHOKU university

### **ABSTRACT**

Most studies on topology optimization find the optimum solution deterministically under a prescribed and unchanged boundary condition. However, in reality, uncertainty such as disturbances or errors in boundary conditions often occurs: this may degrade the structural performance or cause a serious structural problem if the optimized structure is sensitive with respect to the uncertainty. For this reason, the development of robust topology optimization considering an uncertainty is demanded. Many of the previous studies, however, deal with the conventional stiffness maximization problem assuming a linear elastic body, which is not related to a serious structural problem such as buckling. With this background, the present study addresses preliminary investigation for robust topology optimization to avoid a serious structural problem. One of the important uncertainties may be deviation from a prescribed loading condition, such as errors in loading angle, location and magnitude. These uncertainties and their influences onto the nonlinear structural response will be discussed in this study.

## **A Stochastic Analysis of Tensile Ductile Fracture for Polypropylene Solids**

Koh-hei Nitta<sup>\*</sup>, Chun-yao Li<sup>\*\*</sup>

<sup>\*</sup>Institute of Science and Engineering, Kanazawa University, <sup>\*\*</sup>Graduate School of Natural Science and Technology, Kanazawa University

### **ABSTRACT**

Tensile fracture data from over 100 tensile tests of a polypropylene showed Gaussian distribution functions of fracture time and strength. With increasing tensile speed, the mean and deviation of fracture time decreased whereas those of toughness were independent of the tensile speed. We found a stochastic differential equation for predicting the fracture time under tension and the strength distribution can be determined uniquely from the stochastic equation.

## Atomistic Simulation Study on Ultrasound-driven Aggregation Mechanism of Ceramic Nanoparticles

Xinrui Niu<sup>\*</sup>, Zijian Yao<sup>\*\*</sup>, Hao Zhang<sup>\*\*\*</sup>

<sup>\*</sup>City University of Hong Kong, <sup>\*\*</sup>City University of Hong Kong, <sup>\*\*\*</sup>University of Alberta

### ABSTRACT

Nanoparticles (NPs) and their assemblies have been widely for many applications such as nanocomposites, nano medicines, microfluidic devices et al. Methods to assemble NPs have attracted considerable amount of research interests. Ultrasonication is a widely adopted method to treat NPs. The original goal was to break down NP agglomerations but later the method was demonstrated able to assemble NPs. Although ultrasound-driven NP assemblies have been observed experimentally, its formation mechanism is still unclear. This talk reports a recent effort to investigate mechanism of ultrasound driven NP aggregation. The work suggested that the NPs can be aggregated by partial melting of the NPs induced by the ultrasound driven collision. Critical aggregation velocity of NP under ultrasonication was estimated by molecular dynamics (MD) simulation. This work not only explained the phenomena observed in experiments but also indicates a possible novel method to assemble ceramic NPs through which ceramic NPs are aggregated through ultrasonication in standard ambient environment without any additional heat source or chemical treatment. Meanwhile, by predicting formation velocities of three different types of interparticle bondings, this work provided guidance to control and/or optimize the dispersion and/or aggregation of NPs, which could benefit the development of NP assembling technique.

## **Models and Finite Element Simulations of Nonlinear Electro-Thermo-Mechanical Problems with Application to the Shape Memory Polymer Medical Devices**

Innocent Niyonzima\*, Jacob Fish\*\*

\*Columbia University, \*\*Columbia University

### **ABSTRACT**

Biomaterial implants, especially intelligent biomaterials have gained considerable attention in the biomedical community thanks to their ability to change physical properties (morphing, structural rigidity, etc.) when subjected to external stimuli such as temperature, pH, humidity, electromagnetic fields, etc. These materials are increasingly used for a large number of biomedical applications such as prevention and cure of coronary heart disease and stroke, ophthalmological applications, biosensors and drug delivery systems (S. K. Bhatia. "Biomaterials for clinical applications". Springer Science & Business Media, 2010). Among intelligent materials, shape memory polymers have a very promising future because they can be chosen biocompatible and biodegradable. For applications inside the human body, contactless control can be achieved by the addition of electric and/or magnetic particles that can react to electromagnetic fields, thus leading to a composite biomaterial. The difficulty of developing accurate numerical models for intelligent materials results from their multiscale nature and from the coupling of physical phenomena. This coupling involves electromagnetic, thermal and mechanical problems (C. Miehe et al., "Homogenization and multiscale stability analysis in finite magneto-electro-elasticity. Application to soft matter EE, ME and MEE composites". Comput. Methods Appl. Mech. Eng., 300 : 294–346, 2016). This research work will contribute to the multi-physical modelling of a shape memory polymer material used as a medical stent. The stent is excited by electromagnetic fields produced by a coil which can be wrapped around a failing organ. In this paper we develop Lagrangian formulations for the coupled electro-thermo-mechanical problem using the electric potential to solve the electric problem. The formulations are then discretized and solved using the finite element method. In the extended paper, the theoretical multi-physical model will be thoroughly detailed and the results will be validated by comparison with the experimental results present in the literature.

## **An Accurate and Well-Conditioned Conformal Decomposition Finite Element Method for Many Materials**

David Noble\*

\*Sandia National Laboratories

### **ABSTRACT**

Enriched finite element methods such as the Generalized Finite Element Method (GFEM), the eXtended Finite Element Method (XFEM), and the Conformal Decomposition Finite Element Methods (CDFEM) are powerful tools for multi-material problems. To capture the discontinuities across material interfaces, these methods introduce enrichment in the elements that contain multiple materials. Additional unknowns are assigned to the mesh entities (elements, nodes, sides, or edges) that are associated with these interfacial elements, and additional equations are formulated. However, as an interface comes arbitrarily close to background mesh nodes, the resulting equations may become linearly dependent. This problem is exacerbated when many materials intersect an element. To circumvent this issue, practitioners have omitted the enrichment in elements that intersect only a small fraction of material. In this way, the interface is snapped to the nodes of the background mesh. This approach incurs an error in the geometry to gain better conditioning. CDFEM is an enriched finite element method that can be used to describe discontinuous physics across material interfaces. Level sets are used to describe the domain of each material. Nodes are added at the intersection of each level set surface with the edges of the input mesh, and a conforming mesh is generated automatically. This allows the physics code to describe either weak or strong discontinuities across material interfaces using standard finite element methods. CDFEM can also produce poorly conditioned systems of equations when the interfaces come close to the background mesh nodes. This can be addressed by snapping the interface to the nearest node. However, this snapping introduces an error in the location of the interface. In the current work, an alternate approach is taken that removes the poor conditioning without introducing an error in the interface location. When an edge is crossed near one of its ends, the nearest node of the edge is moved to the crossing, instead of moving the crossing to the node. For simulations with many materials, the material interfaces may meet producing material intersection points, curves, and surfaces. In that case, the background mesh nodes are preferentially snapped to material interfaces that consist of a point, then curves, then surfaces. This approach improves the quality of the resulting decomposed meshes and produces systems of equations with dramatically better conditioning. The resulting system of equations is readily solved using traditional linear solvers. The method is described further and the improvement in the matrix conditioning is quantified. \*Sandia National Laboratories is a multimission laboratory managed and operated by National Technology and Engineering Solutions of Sandia, LLC, a wholly owned subsidiary of Honeywell International, Inc., for the U.S. Department of Energy's National Nuclear Security Administration under contract DE-NA0003525.

## A Damage to Crack Transition Framework for Ductile Materials Accounting for Stress Triaxiality

Ludovic Noels<sup>\*</sup>, Julien Leclerc<sup>\*\*</sup>, Ling Wu<sup>\*\*\*</sup>, Van Dung Nguyen<sup>\*\*\*\*</sup>

<sup>\*</sup>University of Liege, <sup>\*\*</sup>University of Liege, <sup>\*\*\*</sup>University of Liege, <sup>\*\*\*\*</sup>University of Liege

### ABSTRACT

Predicting the entire ductile failure process is still a challenge task since it involves different processes: damage first diffuses before localizing, eventually leading to a micro-crack initiation and propagation. On the one hand, discontinuous approaches can describe localised processes such as crack propagation but fail in capturing diffuse damage evolution. On the other hand, continuous approaches such as continuum damage models are suited for diffuse damage modelling, but cannot represent properly physical discontinuities. In this work both approaches are combined in a hybrid implicit non-local damage model combined with an extrinsic cohesive law in a discontinuous Galerkin finite element framework [1]. The implicit non-local damage model reproduces the initial diffuse damage stage without mesh-dependency. Upon transition at void coalescence or intensive plastic localisation, a crack is introduced using a cohesive band model. Contrarily to cohesive elements, cohesive band models capture in-plane stretch effects, and thus account for stress triaxiality [2]. Indeed, by considering a band of small but finite thickness ahead of the crack surface, the strain field inside this band is evaluated from the neighbouring strains and from the cohesive jump [2]. Then, an appropriate damage model is used to compute the stress-state inside the band and the cohesive traction forces on the crack lips. The approach is first applied in the case of elastic damage for which the band thickness is evaluated to ensure the energetic consistency of the damage to crack transition with respect to purely non-local continuum damage mechanics [1]. Then, the scheme is formulated to the case of a non-local porous-plastic damage Gurson model. In particular, the law governing void growth accounts for shear effects, while the void coalescence mechanism, hence the damage to crack transition criterion, is predicted using the Thomason model [3]. [1] Leclerc J., Wu L., Nguyen V.D., Noels L. Cohesive band model: a cohesive model with triaxiality for crack transition in a coupled non-local implicit discontinuous Galerkin/extrinsic cohesive law framework. *Int. J. for Num. Methods in Eng.* (2017): In press. [2] Remmers J. J. C., de Borst R., Verhoosel C. V., Needleman A. The cohesive band model: a cohesive surface formulation with stress triaxiality. *Int. J. Fract.* 181 (2013). [3] Benzerga A.A., Leblond J.-B., Needleman A., Tvergaard V. Ductile failure modelling. *Int J Fract* 201 (2016).

## Topology Optimization Applied to Pumps with Turbulent Flows

Luís Fernando Nogueira de Sá\*, Emílio C. N. Silva\*\*

\*Polytechnic School of University of São Paulo, \*\*Polytechnic School of University of São Paulo

### ABSTRACT

The design of pumps by using topology optimization method is a powerful approach to improve these devices. When considering flow machines that operate at high rotations there are regions where the flow detaches from the blade and turbulence characteristics are present. The flow in the rotor of these machines have a considerably influence of their topology (Romero, 2014) and can be optimized to attend different design requirements. In this work we explore the topology optimization applied to rotors under turbulent flows by using the density method. The rotor is modeled in a rotary frame and the RANS equations coupled with the Spalart-Allmaras turbulence model are used. We use different material models between the constitutive equations, in a similar way as the work of Yoon (2016). The objective function used is the viscous energy dissipation (Borrvall and Peterson, 2003). The problem is implemented in the FEniCS environment with dolfin-adjoint and the Ipopt optimizer. At the present the flow is solved with arbitrary properties. Finally, blade topologies are presented and compared computationally with a traditional straight blade. Borrvall T, Petersson J (2003). Topology optimization of fluids in Stokes flow. *Int J Numer. Methods Eng* 41(1):77–107 Romero JS, Silva ECN (2014). A topology optimization approach applied to laminar flow machine rotor design. *Comput Methods Biomech Biomed Engin* 279:268–300 Yoon, Gil Ho (2016). Topology optimization for turbulent flow with Spalart–Allmaras model. *Computer Methods in Applied Mechanics and Engineering*, 303:288-311

## Numerical and Analytical Investigation of a Phase Field Model for Ductile Fracture

Timo Noll\*, Charlotte Kuhn\*\*, Ralf Müller\*\*\*

\*University of Kaiserslautern, \*\*University of Kaiserslautern, \*\*\*University of Kaiserslautern

### ABSTRACT

In phase field models for fracture a scalar valued order parameter describes the state of the material in terms of fracture on a fixed finite element mesh. Thus, in contrast to conventional fracture models, where cracks are described by sharp surfaces, computationally expensive remeshing and/or techniques are not necessary. In this contribution a phase field model for ductile fracture with linear isotropic hardening is presented. An energy functional consisting of an elastic energy, a plastic dissipation potential and a Griffith type fracture energy constitutes the model. The application of an unaltered radial return algorithm [1] on element level is possible due to the choice of an appropriate coupling between the nodal degrees of freedom, namely the displacement fields and the crack fields. The degradation function accomplishes the mentioned coupling by reducing the stiffness of the material and the plastic contribution of the energy density in broken material. Furthermore, to solve the global system of differential equations comprising the balance of linear momentum and the quasi-static Ginzburg-Landau type evolution equation, the application of a monolithic iterative solution scheme becomes feasible. Analytic considerations are presented demonstrating, that if the conventional, quadratic degradation function is used, the nominal plastic material parameters do not coincide with the effective parameters of the model and a reinterpretation of the parameters is necessary in order to relate simulation results to experimental data [2]. On the other hand, if certain cubic degradation functions [3], are used such a distinction between effective and nominal parameters is not necessary. Furthermore, the meaning of the fracture resistance, a model parameter stemming from the underlying brittle fracture model [4] is considered in context of ductile fracture and regarding its influence on e.g. the fracture strain compared to a plastic threshold function. In numerical examples, it is studied in how far the findings of the 1D considerations can be applied to the 3D cases. REFERENCES [1] J.C. Simó and T.J.R. Hughes, Computational Inelasticity, Interdisciplinary Applied Mechanics (Springer Berlin, New York, Heidelberg), 1998. [2] C. Kuhn, T. Noll, R. Müller, "On phase field modeling of ductile fracture", GAMM-Mitt., 39, 35-54 (2016). [3] C. Kuhn, A. Schlüter, R. Müller, "On degradation functions in phase field fracture models ", Comp. Mater. Sci., 108, 374-384 (2015). [4] C. Kuhn and R. Müller, "A continuum phase field model for fracture", J. Eng. Fract. Mech., 77, 3625-3634 (2010).

## Multiscale Estimation of Effects of Coastal Vegetation in Consideration of Breakage and Washout During Tsunami

Reika Nomura<sup>\*</sup>, Shuji Moriguchi<sup>\*\*</sup>, Shinsuke Takase<sup>\*\*\*</sup>, Kenjiro Terada<sup>\*\*\*\*</sup>

<sup>\*</sup>Tohoku University, <sup>\*\*</sup>Tohoku University, <sup>\*\*\*</sup>Hachinohe Institute of Technology, <sup>\*\*\*\*</sup>Tohoku University

### ABSTRACT

This study presents a multiscale analysis method to estimate the positive and negative effects of coastal forests in consideration of the breakage and the washout of constituent trees by an incoming tsunami. More specifically, the proposed method is designed to characterize both the disaster mitigation effect and the washout risk of a coastal forest by performing numerical analyses under various conditions. To this end, we separate the coastal forest into two spatial scales; micro- and macro-scales. That is, the domain containing several trees is defined as a micro-structure, whereas the overall forest is a macrostructure. Numerical analyses are conducted for the micro-structure to characterize the macroscopic effects on the tsunami force/energy. A porosity model is employed to transmit the micro-scale information to the macro-scale in the scale-up evaluation process. That is, by regarding the coastal forest as a porous medium at the macro-scale, we expect that the overall flow resistance can be characterized by the mechanical behavior at the micro-scale. Thus, the proposed method can be recognized as a sort of homogenization methods. Based on the results of the micro-scale analyses, the flow resistance of the porous medium is defined as a function of not only the fluid velocity and the flow depth, but also the damage variable, which represents the degree of damage of trees during a tsunami. Since the damage variable develops according to the amount of trees breakage, the washout trees are described as a source of equivalent mass density advected to the overall flow. In numerical analyses, the stabilized Finite Element Method [1] is employed to solve the Navier-Stokes equation containing a porosity-related drag term, which is an alternative to the classical roughness coefficients modeling in the shallow water equation [2]. Several case studies are conducted and the numerical results are compared to the laboratory experiments for the validation. It is thus demonstrated that both assessments of mitigation effect of coastal forests and risk caused by the washout trees can be made for a whole coastal region with relatively low computational cost. [1] Tezduyar, T.E.: Stabilized finite element formulations for incompressible flow computations: Adv. Appl. Mech. 28, 1-44(1991) [2] Harada, K., Imamura, F.: Effects of coastal forest on tsunami hazard mitigation—a preliminary investigation, Tsunamis, Springer Netherlands, 279-292(2005)

## **Anisotropic Multi-Component Topology Optimization Method for Composite Shell Structures**

Tsuyoshi Nomura<sup>\*</sup>, Kazuhiro Saitou<sup>\*\*</sup>, Yuqing Zhou<sup>\*\*\*</sup>

<sup>\*</sup>Toyota Research Institute of North America, <sup>\*\*</sup>University of Michigan, <sup>\*\*\*</sup>University of Michigan

### **ABSTRACT**

This paper discusses about multi-component topology optimization for structures made of anisotropic materials, typically, fiber reinforced composite materials. The proposed method is capable of designing a variety of types of structures which are comprised by multiple components made of anisotropic materials. The topology of both the entire structure and each component is optimized by the conventional density design variables. The component is optimally divided under given constraints. In addition to that, the orientation distribution of the anisotropic material in each component is also optimized by means of anisotropic topology optimization. One major application field of this method is design of composite shell structures. Conventionally, this type of problem is formulated as a multi-material topology optimization problem, that is, a problem to find the optimal material distribution in an extended design domain. The most successful method for this problem is the discrete material optimization (DMO). As similar to isotropic topology optimization, the materials to be used in the design are given, a priori. For a composite shell structure design problem, they are given as a discrete set of options, such as, 0, 45, 90, 135 degrees. However, the selection of the discrete set severely affects the performance of the structure, and it is difficult to select the optimal angle option set beforehand. Another type of method for the composite shell structure design problem is based on continuous fiber angle optimization or anisotropic topology optimization. These types of methods handle topology optimization as a continuous angle field or a vector field distribution optimization problem; therefore, the orientation angle is optimized without any restriction. In addition to that, it is also capable of deriving designs with a discrete set of options by penalizing intermediate angles, but still, prescribed discrete options must be provided beforehand. The proposed method can solve this problem without a prescribed option set. The method is based on multi-component topology optimization and anisotropic topology optimization. The method optimizes the orientation distribution without any restriction, thanks to the nature of anisotropic topology optimization. To obtain a discrete angle design, it constraints the maximum allowed curvature in each component. The component partitioning occurs by this constraint up to the maximum allowed number of components. Therefore, it can provide discrete angle designs with the optimal angle for each component without a prescribed discrete set of options. Several numerical examples are provided in the presentation to show the usefulness of the proposed method.

## 3-dimensional Topology Optimization with Supershapes

Julián Norato\*

\*Assistant Professor, University of Connecticut

### ABSTRACT

We present a method for the topology optimization of 3-dimensional structures made by the union of geometric primitives represented via supershapes. In two dimensions, supershapes are a generalization of hyperellipses that allow for different symmetries and thus can render not only circles and ellipses, but (approximately) any polygon. In three dimensions, the spherical product can produce sweeps of 2-dimensional supershapes in order to generate extruded and revolved solids. A distinct advantage of this parameterization is that it allows individual shapes to morph into several primitives via a single mathematical representation (the superformula). Being able to render a design made of primitives combined via Boolean operations is advantageous because that is exactly how most CAD programs build a solid model. The low-dimensional design representation thus constructed facilitates several aspects of the production process, such as providing convenient datum features for fabrication and assembly, specifying production tolerances and performing inspection of dimensional quality. To perform the analysis and optimization, we wish to retain one of the major advantages of classical topology optimization methods, namely the use of a fixed grid. To this end, we employ the geometry projection method to smoothly map the supershapes onto a density field discretely defined on the fixed grid. As customary, this field is used to define an ersatz material to perform the primal and sensitivity analyses. Unlike previous work by our group, where only a union of solid shapes is performed, in this work shapes can also be subtracted via a generalization of the geometry projection. We demonstrate the effectiveness of our method with several compliance minimization problems.

## Stabilized and Multiscale Methods for Free Surface Flow Problems

Leo Nouveau<sup>\*</sup>, Guglielmo Scovazzi<sup>\*\*</sup>, Alex Main<sup>\*\*\*</sup>

<sup>\*</sup>Duke University, <sup>\*\*</sup>Duke University, <sup>\*\*\*</sup>Duke University

### ABSTRACT

Embedded boundary methods obviate the need for continual re-meshing in many applications involving rapid prototyping and design. Unfortunately, many finite element embedded boundary methods for incompressible flow are also difficult to implement due to the need to perform complex cell cutting operations at boundaries, and the consequences that these operations may have on the overall conditioning of the ensuing algebraic problems. We present a new, stable, and simple embedded boundary method, which we call “shifted boundary method” (SBM), that eliminates the need to perform cell cutting. Boundary conditions are imposed on a surrogate discrete boundary, lying on the interior of the true boundary interface. We then construct appropriate field extension operators, with the purpose of preserving accuracy when imposing the boundary conditions. We demonstrate the SBM applied to several free surface flow problems.

## The Biomimetic Method for Shape Optimization in 3D Elasticity

Michał Nowak\*, Antoni Zochowski\*\*, Jan Sokolowski\*\*\*

\*Chair of Virtual Engineering, Poznan University of Technology, Poland, \*\*Systems Research Institute of the Polish Academy of Sciences, Poland, \*\*\*Institut Elie Cartan, Laboratoire de Mathématiques Université Henri Poincaré, France

### ABSTRACT

This paper presents a new biomimetic approach to the structural design. The trabecular bone adapts its form to mechanical loads and is able to form lightweight but very stiff structures. In this sense, it is a problem (for the Nature) similar to the structural optimization. The remodeling phenomenon with strain energy density equalization on the trabecular bone surface assumption could be described from the stiffness point of view [1]. In the paper the structural optimization with shapes parameterization by the assumed energy density on the structural surface will be discussed. The structural optimization system based on shape modification using shape derivative [2] will be presented. The stiffest design is obtained by adding or removal material on the structural surface in the virtual space. The assumed value of the strain energy density on the part of the boundary subjected to modification could be related to the material properties. Change in the assumed value of the strain energy density results in change of the structural form – topology and volume. In general the problem of stiffest design (compliance minimization) has no solution. If the volume of the object is increasing, the compliance is decreasing. Thus, in the standard approach to the energy based topology optimization the additional constraint has to be added. Usually the volume of the material is limited. In the presented approach instead of imposing volume constraint the shapes are parameterized by the assumed energy density, which may be predicted from the yield criteria. The domain independence, functional configurations during the process of optimization and possibility to solve multiple load problems are the unique features of the biomimetic method, useful in mechanical design. To illustrate the algorithm functionality, the problem of determining the optimal internal wing structure will be discussed. For the purpose of aircraft wing design the numerical environment combining simultaneous structural size, shape, and topology optimization based on aeroelastic analysis was developed [3]. The optimal internal wing structure resulting from aeroelastic computation with different angles of attack will be presented. [1] Nowak M., Sokolowski J. Zochowski A., Justification of a certain algorithm for shape optimization in 3D elasticity, *Struct Multidiscipl Optim*, doi 10.1007/s00158-017-1780-7, 2017 [2] Sokolowski J., Zolesio J., *Introduction to shape optimization. Shape Sensitivity Analysis*. Springer, 1992 [3] Gawel D., Nowak M., Hausa H. et al., New biomimetic approach to the aircraft wing structural design based on aeroelastic analysis, *Bull. Pol. Ac.: Tech.* 65(5), pp. 741-750, 2017

## Computational Modelling of Thermoplastic Behaviour of Inconel 718 in Application to Laser-Assisted Bending of Thin-Walled Alloy Tubes

Zdzislaw Nowak\*, Marcin Nowak\*\*, Ryszard Pecherski\*\*\*, Krzysztof Wisniewski\*\*\*\*, Jacek Widlaszewski\*\*\*\*\*, Piotr Kurp\*\*\*\*\*

\*Institute of Fundamental Technological Research, Polish Academy of Sciences, \*\*Institute of Fundamental Technological Research, Polish Academy of Sciences, \*\*\*Institute of Fundamental Technological Research, Polish Academy of Sciences, \*\*\*\*Institute of Fundamental Technological Research, Polish Academy of Sciences, \*\*\*\*\*Institute of Fundamental Technological Research, Polish Academy of Sciences, \*\*\*\*\*Kielce University of Technology

### ABSTRACT

At present, nickel based alloys are broadly used in the aerospace industry due to their excellent corrosion resistance and high mechanical properties. Laser-assisted tube bending process is a promising manufacturing process because of its ability to produce forms and shapes that cannot be achieved by mechanical bending. Laser bending is particularly suitable for the high hardness and brittle materials, such as nickel alloys, ceramics and cast iron. An experimental investigation of the Inconel 718 alloy is used in validation of the constitutive model. The multi-axial constitutive model accounts for the strength-differential behaviour under uniaxial tension/compression [1-3]. It encompasses softening phenomena as well as the coupling between temperature and strains, both of them observed in experiments. Bending of thin-walled tubes in a specially designed device is studied. Mechanical loading and simultaneous heating of the material by a moving laser beam are introduced in a controlled manner to obtain the required deformation. The current paper is focused on numerical simulations to provide more insight into the laser bending process of the Inconel 718 tubes. A 3D thermomechanical analysis model is developed in the FE code ABAQUS. The temperature, stress and deformation fields during thermo-mechanical loading of tubes are determined in a sequentially coupled thermo-mechanical analysis. Laser beam is modelled as a surface heat flux using the dedicated DFLUX procedure. The temperature field is then used as a thermal load in the static general step, together with an external mechanical load. The tube is discretized using the C3D8R. For the steel rollers with horizontal and vertical axes, the R3D4 element is used. The process of tube bending is controlled by the displacement of the piston rod, while the thrust force is the resulting value. References 1. Iyer S. K., Lissenden C. J., Multi-axial constitutive model accounting for the strength-differential in Inconel 718, *Int. J. Plasticity*, 19, 2055–2081, 2003. 2. Vadillo G., Fernandez-Saez J., Pecherski R. B., Some applications of Burzynski yield condition in metal plasticity, *Materials and Design*, 32, pp.628-635, 2011. 3. Pecherski R. B., Szeptynski P., Nowak M., An extension of Burzynski hypothesis of material effort accounting for the third invariant of stress tensor, *Archives of Metallurgy and Materials*, 56 (2), pp. 503-508, 2011.

## Modeling Brain Tissue Degradation through Continuum Damage Mechanics

Lise Noël\*, Ellen Kuhl\*\*

\*Stanford University, \*\*Stanford University

### ABSTRACT

Human brain is extremely sensitive to environmental changes and can exhibit different behaviors depending on the nature of the received stimuli. Undergoing large deformation over short time scale, the brain is unable to adapt to its environment. It is subject to damage and presents an inelastic material behavior. Modeling brain tissue degradation could lead to a better understanding of the mechanisms involved in neurodamage and neurodegeneration associated with various pathologies ranging from traumatic brain injuries to Alzheimer's disease. The basics of continuum damage mechanics (Kachanov 1958) can be adapted to describe damage in soft biological tissues. These ones are generally modeled as hyperelastic rubberlike materials, for which the stress-strain relation is established through a stored strain energy function. Material degradation can be accounted for by defining the damaged stored strain energy as a damage weighted function of the elastic stored strain energy. Directly impacting the material behavior, damage is represented by a scalar variable (if isotropic) that evolves from 0 for a virgin material to 1 for a complete failure. The material stress-strain curve is dependent on the loading history and damage is characterized resorting to a damage loading function. Assuming that damage is strain driven, its growth can be described by an evolution law including history dependency through an internal variable recording the largest strain state reached during the loading process. This work focuses on the role of mechanics in neurodamage. To model brain tissue damage, the mechanical model assumes finite strains and an hyperelastic constitutive material behavior based on an Ogden energy type. Degradation is introduced following continuum damage mechanics and the damage evolution law is calibrated with experimental results found in the literature (Franceschini et al. 2006, Goriely et al. 2015). The developed method is applied to two dimensional structures discretized resorting to the finite element method and the damage process is solved using Newton's method. Regular and arbitrary 2D structures, obtained from human brain medical imaging techniques, are considered. Kachanov, L. M., On creep rupture time. *Izvestiya Akademii Nauk SSSR. Otdelenie Tekhnicheskikh Nauk*, 8:26-31, 1958. Franceschini G., Bigoni D., Regitnig P. and Holzapfel G.A., Brain tissue deforms similarly to filled elastomers and follows consolidation theory. *Journal of the Mechanics and Physics of Solids*, 54:2592-2620, 2006. Goriely A., Budday S. and Kuhl E., *Neuromechanics: From Neurons to Brain*. In *Advances in Applied Mechanics*, 48:79-139, 2015.

## **A Time-multiscale Model Reduction Technique for Nonlinear Problems Involving High Number of Cycles**

David Néron<sup>\*</sup>, Pierre Ladevèze<sup>\*\*</sup>, Shadi Alameddin<sup>\*\*\*</sup>, Mainak Bhattacharyya<sup>\*\*\*\*</sup>, Amélie Fau<sup>\*\*\*\*\*</sup>, Udo Nackenhorst<sup>\*\*\*\*\*</sup>

<sup>\*</sup>ENS Paris-Saclay, <sup>\*\*</sup>ENS Paris-Saclay, <sup>\*\*\*</sup>Leibniz Universität Hannover, <sup>\*\*\*\*</sup>Leibniz Universität Hannover, <sup>\*\*\*\*\*</sup>Leibniz Universität Hannover, <sup>\*\*\*\*\*</sup>Leibniz Universität Hannover

### **ABSTRACT**

The simulation of the mechanical response of structures subjected to cyclic loadings for a large number of cycles remains a challenge. The goal of this work is to develop a dedicated computational scheme for fatigue computations in problems involving nonlinear material behaviors described by internal variables. The focus is on the Large Time Increment (LATIN) method coupled with the PGD model reduction technique. This method has already been introduced in the 90s in this context but a new version, more robust, is proposed herein taking in particular into account the progress done recently. More, unilateral damage is considered here for the first time. In that scheme, a two-time-multiscale approach is proposed, that consists in computing the quantities of interest only at particular predefined cycles called the "nodal cycles" and using a suitable interpolation to estimate their evolution at the intermediate cycles. The proposed framework is exemplified for a structure subjected to cyclic loading, where, combined to visco-plasticity, damage is considered to be isotropic and micro-defect closure effects are taken into account. The combination of these techniques reduce the numerical cost drastically and allows to create virtual S-N curves for large number of cycles.

## A Complete Model of Metal Additive Manufacturing: Requirements and Progress

Patrick O’Toole\*, Vu Nguyen\*\*, Paul Cleary\*\*\*, Peter Cook\*\*\*\*, Sharen Cummins\*\*\*\*,  
Gary Delaney\*\*\*\*\*, Dayalan Gunasegaram\*\*\*\*\*, Anthony Murphy\*\*\*\*\*, Matthew  
Sinnott\*\*\*\*\*, Mark Styles\*\*\*\*\*

\*CSIRO, \*\*CSIRO, \*\*\*CSIRO, \*\*\*\*CSIRO, \*\*\*\*\*CSIRO, \*\*\*\*\*CSIRO, \*\*\*\*\*CSIRO, \*\*\*\*\*CSIRO, \*\*\*\*\*CSIRO,  
\*\*\*\*\*CSIRO

### ABSTRACT

Metal additive manufacturing based on powder-bed fusion processes is becoming increasingly important production method. The technology has several advantages over conventional methods, for example in the manufacture of components having complex geometries and of custom-designed parts. The physical phenomena that occur in these processes are highly transient and difficult to monitor. Very challenging experiments requiring expensive sensing equipment are usually needed to obtain the data required for process understanding and improvement. Computational modeling of powder-bed fusion processes is therefore important from several points of view. These include obtaining an improved understanding of the phenomena occurring in the process, optimization of process parameters and component designs, and prediction of component properties. In the long term, it is foreseen that modeling will play an important role in qualification of components and in assisting process control. Several physical processes have to be considered to develop a complete model. These include the raking of the powder bed surface, the transfer of energy from the laser or electron beam to the metal, the melting and solidification of the powder, the flow of liquid metal in the melt pool, the heat transfer from the melt pool to the surrounding powder and solid metal, the evolution of the microstructure of the component, and the residual stress and deformation of the component. A further complication is that many of the processes are interdependent. The physical processes occur on very different length and time scales, and their treatment requires the use of different computational techniques. We are modeling powder bed raking using the discrete element method, and have obtained results for different particle shapes and sizes. We are applying two techniques, computational fluid dynamics and smoothed particle hydrodynamics, to treat the melt pool phenomena. A semi-empirical approach has been used to predict microstructure evolution, and we are now implementing the phase field method to obtain more detailed insights. The residual stress and deformation caused by the non-uniform heat fluxes is being modeled with the finite element method; the results obtained depend critically on the constitutive model that is used to describe the metal’s thermomechanical properties. This paper discusses the rationale for developing a complete model, progress in developing the sub-models of the different physical processes at the disparate scales, and the framework that is envisaged to handle the interdependencies of the sub-models to allow the development of a predictive model of the full additive manufacturing process.

## Explicit Dynamics IGA : LR B-Spline Implementation in the Radioss Solver

Matthieu OCCELLI\*, Salim BOUABDALLAH\*\*, Lionel MORANCAY\*\*\*, Thomas ELGUEDJ\*\*\*\*

\*LaMCoS / Altair Engineering France, \*\*Altair Engineering France, \*\*\*Altair Engineering France, \*\*\*\*LaMCoS

### ABSTRACT

Isogeometric analysis has shown to be a very promising tool for an integrated design and analysis process [1]. A challenging task is still to move IGA from a proof of concept to a convenient design tool for industry and this work contributes to this endeavor. This communication deals with the implementation of IGA concept into Radioss explicit code in order to address crash and stamping simulation applications. To this end, the necessary ingredients to a smooth integration of IGA in a traditional finite element code have been identified and adapted to the existing code architecture. First, a solid NURBS element has been developed in Radioss and then, an existing contact interface has been extended in order to work seamlessly with both NURBS and Lagrange finite elements, using a node to surface formulation. Some academic and simple industrial cases will be presented to show the obtained results and the relevance of the retained solution. Mesh refinement is the third ingredient added to this integration, as local refinement is needed for solution approximation and for patch connection. After comparing it with several existing refinement methods such as Hierarchical B-Splines (HBS) and Truncated Hierarchical B-Splines (THBS) in term of additional data requirements and implementation aspects, we implemented the approach of locally refined B-Splines (LRBS) [3]. This approach is validated on industrial benchmarks, for validation cases conventionally used for industrial codes like stamping and drop test. REFERENCES [1] J.A. Cottrell, T.J.R. Hughes and Y. Bazilevs, Isogeometric Analysis: Toward integration of CAD and FEA, John Wiley &amp;amp; sons, 2009. [2] L. Piegl and W. Tyler, The NURBS book, 2nd ed., Springer, 1997. [3] K.A. Johannessen, T. Kvamsdal and T. Dokken, Isogeometric analysis using LR B-splines, Comput. Methods Appl. Mech. Engrg, 269, 471-514, 2014.

## Modal Synthesis for Sloshing Modeling. Reduced Order Model and Summation Rule

Roger OHAYON\*, Jean-Sebastien SCHOTTE\*\*

\*Conservatoire National des Arts et Metiers (CNAM), Paris, France, \*\*ONERA, The French Aerospace Lab., France

### ABSTRACT

The application of modal synthesis methods to the modeling of the coupling between a deformable structure and a quiescent fluid was the subject of many works [Morand & Ohayon (1995)]. Although this approach is limited to the study of the low amplitude vibrations of a coupled fluid-structure system, it has the advantage of allowing the efficient construction of reduced models, useful for an intuitive frequency analysis of the coupling between both sub-systems. In particular, it permits to generalize the representation method of a sloshing fluid by equivalent mechanical systems (mass-spring or pendulum) to cases of deformable tanks with complicated geometrical shapes [Schotté & Ohayon (2009)]. Starting from a pressure formulation for the fluid and a decomposition of its response on the modal basis of its sloshing modes, completed by some particular quasi-static solutions, the reduced coupled equations of the fluid-structure system are established and a summation rule concerning the various fluid mass operators is exposed. The interest of this approach is illustrated by comparison with the classical mass-spring or pendulum approach. Finally, an extension of this model, to take the capillarity effects into account, is tackled with the aim to adapt this approach to the case of fluid-structure systems in micro-gravity (for satellite applications) [El-Kamali, Schotté & Ohayon (2011), Ohayon & Soize (2016)].

References Morand & Ohayon (1995): Fluid-Structure Interaction: Applied Numerical Methods, Wiley Schotté & Ohayon (2009): Various modelling levels to represent internal liquid behavior in the vibratory analysis of complex structures, CMAME, 198: 1913-1925 El-Kamali, Schotté & Ohayon (2011): Three-dimensional modal analysis of sloshing under surface tension, IJNMF, 65: 87-105 Ohayon & Soize (2016): Nonlinear model reduction for computational vibration analysis of structures with weak geometrical nonlinearity coupled with linear acoustic liquids in the presence of linear sloshing and capillarity, Computers & Fluids, 141: 82-89

## **A Generic Metallurgical Phase Transformation Framework Applied to Additive Manufacturing Processes**

Victor Oancea\*, Qi Zhang\*\*, Jiawen Xie\*\*\*, Tyler London\*\*\*\*

\*Dassault Systemes SIMULIA Corp., Johnston, RI, USA, \*\*Brown University/Dassault Systemes SIMULIA Corp.,  
\*\*\*Dassault Systemes SIMULIA Corp., \*\*\*\*TWI Ltd, Cambridge, UK

### **ABSTRACT**

While significant progress has been made in the last few years, the reliability of AM manufactured parts is often questionable as they suffer from manufacturing defects and hence subpar strength/fatigue life. Like in many other fields before, numerical methods are sought to provide insight into the process and help accelerate progress in raising the quality of AM parts, including predicting thermal evolutions, part distortions and residual stresses. In metal applications, assessing the amount of unfused powder, melt pool volumes, grain growth, and metallurgical phase transformations are often of interest. Ultimately, process-controlled microstructures can lead to superior designs and desirable mechanical properties. In previous work, a highly customizable general simulation framework was demonstrated and validated for a wide spectrum of additive manufacturing processes (laser and electron beam powder bed fabrication, direct energy deposition, arc welding, polymer extrusion, ink jetting ) as implemented on the Dassault Systemes 3DX Platform based on new FE technology implemented in Abaqus. The framework allows for: 1) arbitrary meshes of CAD representations; 2) exact specification in time and space of processing conditions (e.g., powder addition, laser trajectories, dwell times, etc.); 3) precise tracking of the progressive raw material addition to each element in the mesh via complex geometric computations; 4) precise integration of the moving energy sources (e.g., laser, electron beams, arc welds, high temperature polymer extrusion) and; 5) automatic computation of the continuously evolving convection and radiation surfaces. In the current work, in conjunction with the general simulation framework above, we are introducing a generic metallurgical phase transformation framework applicable to arbitrary metal alloys. The framework accounts for phase transformations (physical state changes) from stock feed (e.g., powder) via melting/vaporization/solidification followed by metallurgical solid state phase transformations induced by either rapid heating/cooling events associated with typical 3D printing sequences but also with slower rate temperature evolutions as associated with heat treatment applications. The user defines in a systematic fashion all possible transformations that can take place via a parent-children paradigm (e.g., austenite to martensite); the temperature conditions when transformations can occur with associated TTT/CCT diagrams; and whether the transformations are reversible, diffusional/non-diffusional. The framework predicts temperature evolutions, calibrates JMA/KM models, and predicts phase transformations during print and heat treatment. Grain growth and aspect ratio assessment models are also included. A few verification/validation exercises for two different alloys are presented

## **New Application Domains for the Variational Multiscale Method**

Assad Oberai\*

\*University of Southern California

### **ABSTRACT**

One of Prof. Hughes's lasting contribution to the field of computational mechanics is the Variational Multiscale Method (VMS). The variational multiscale method was developed as a tool to derive numerical methods for solving partial differential equations. In this context, it has been applied to a large class of problems that include incompressible and compressible fluid flow, MHD and turbulence modeling. However, more recently, its applications in other areas have emerged. These include PDEs with stochastic parameters, discrete reduced order models, goal-oriented error estimates, and phase change problems. In this talk, I will begin with a brief description of the variational multiscale method, and then discuss its application in these new areas.

## **An Accelerated Molecular Dynamics Study of Yield Stress of Ultrafine-grained Metals**

Shigenobu Ogata\*

\*Osaka University

### **ABSTRACT**

Plastic deformation and yielding of nanocrystalline metals is mostly governed by a dislocation nucleation from grain boundaries. A newly developed accelerated molecular dynamics simulation method computes temperature and strain-rate dependent yield stress, which is corresponding to a stress of onset of dislocation nucleation from grain boundaries. Since the accelerated molecular dynamics allows to analysis very rare events, the yield stress is computed over very wide ranged strain rate,  $10^{-4}$  to  $10^{10}$  1/s, which never be covered by conventional molecular dynamics simulation methods. In addition, the accelerated molecular dynamics reveals a mechanism transition and strong stress, temperature and strain-rate dependencies of the dislocation nucleation events. At stress levels up to 90% of the ideal dislocation nucleation stress, atomic shuffling at the E structural unit in a grain boundary acts as a precursor to dislocation nucleation, and eventually a single dislocation is nucleated. At very high stress levels near the ideal dislocation-nucleation stress, a multiple dislocation is collectively nucleated. In these processes, the activation free energy and activation volume depend strongly on temperature. The strain-rate dependence of the critical nucleation stress shows that the mechanism transition from the shuffling-assisted dislocation-nucleation mechanism to the collective dislocation-nucleation mechanism occurs during the strain rate increasing.

# **HYBRID MORI-TANAKA/FINITE ELEMENT METHOD: AN EFFICIENT HOMOGENIZATION OF COMPOSITE MATERIALS WITH VARIOUS REINFORCEMENT SHAPE AND ORIENTATION**

WITOLD OGIERMAN\*

\*Institute of Computational Mechanics and Engineering,  
Faculty of Mechanical Engineering, Silesian University of Technology  
ul. Konarskiego 18A, Gliwice, Poland  
witold.ogierman@polsl.pl; <http://www.icme.polsl.pl/>

**Key words:** Homogenization, Mori-Tanaka method, Composite materials, Micromechanics

**Abstract.** The main goal of this study is to use the hybrid Mori-Tanaka/Finite element homogenization method for determination of effective properties of composite materials reinforced with particles of arbitrary shape. Mori-Tanaka homogenization method, that is based on Eshelby's fundamental solution, provides very efficient solution. On the other hand, it has got several limitations, for example it allows to consider only ellipsoidal shape of the reinforcement. A hybrid Mori-Tanaka/Finite element method can overcome the limitations of standard Mori-Tanaka approach. In this case mean field relations between per phase stresses and strains are combined with numerical solution of the equivalent inclusion problem by the finite element method. The numerical model of equivalent inclusion problem requires very simple geometry containing single inclusion and embedding matrix. An influence of size of the embedding matrix on the strain concentration tensor has been investigated by considering different volume fractions of the single inclusion and comparing the obtained results with analytical solution. The accuracy of hybrid M-T/FE method has been verified by performing direct FE homogenization based on the representative volume element containing substantial number of inclusions.

## **1 INTRODUCTION**

Effective properties of composite materials corresponding to the material behavior at the macroscale can be determined by using homogenization procedures. Methods of homogenization allow to take into account an influence of microstructural features on the effective material properties. One way of using homogenization is to solve a boundary value problem (BVP) by using numerical methods like finite element method (FEM) [1, 2, 3] or boundary element method (BEM) [4, 5, 6]. In this case the macroscopic quantities are computed as volume averages of the microscopic quantities over the representative volume element (RVE). The RVE can be defined as a volume of heterogeneous material that is sufficiently large to be statistically representative of the composite [7]. Therefore, the RVE must include a sufficient number of the composite inhomogeneities like fibers, particles ect. On the other hand, the RVE should be small enough to provide reasonable computational cost. The RVEs corresponding to composites containing inclusions of complex shape and orientation distribution typically require taking into account large number of

inhomogeneities that makes the computational homogenization time consuming. Another group of homogenization methods is based on the Eshelby's fundamental solution [8]. In this case several different approaches can be distinguished like for example self-consistent schemes [9] and Mori-Tanaka method [10]. In particular, the Mori-Tanaka (M-T) method found wide popularity in analysis of composite materials due to good predictive capabilities and low computational cost [11]. Tucker and Liang [12] studied different mean field methods and recommend the M-T method as the best choice for estimating the stiffness of aligned short-fiber composites. M-T method can be also used in modeling of composites with misaligned inclusions by using the orientation averaging procedure [13]. On the other hand, Eshelby's solution is limited to the case of the ellipsoidal shape of inclusions only. However, the numerical solution of equivalent inclusion problem, instead of using the Eshelby's tensor, allowing the M-T method to be extended so as to involve the arbitrary shapes of the inhomogeneities. Therefore, usage of hybrid Mori-Tanaka/Finite element (M-T/FE) method can overcome the limitations of standard M-T approach. In this case mean field relations between per phase stresses and strains are combined with numerical solution of the equivalent inclusion problem by the finite element method (in standard M-T method Eshelby's tensor is used in this case). This approach is generally more computationally effective than direct analysis of RVE by the FEM, as it requires very simple geometrical model containing single inclusion and embedding matrix. The feasibility and effectiveness of the hybrid approach has been presented by Bradshaw et al. [14] who investigated the influence of nanotube waviness on effective properties of nanotube reinforced composite. Klusemann et al. [15] analyzed different shapes of reinforcing particles however authors restricted their calculations to the plane strain conditions. Three dimensional models corresponding to the fiber reinforced composites have been developed by Srinivasulu et al. [16], authors reported good agreement between results obtained by hybrid method and pure numerical solution. Brassart et al. [17] developed hybrid approach that accounts for elastic-plastic material behavior. In the present work, hybrid M-T/FE method is applied in modeling of effective elastic properties of composites reinforced with particles of arbitrary shape, as an example composite reinforced with cubic particles is presented. An influence of size of the embedding matrix on the accuracy of the obtained results has been investigated. The accuracy of hybrid M-T/FE method has been verified by performing direct FE homogenization based on the RVE containing substantial number of inclusions.

## 2 HYBRID HOMOGENIZATION METHOD

The Mori-Tanaka approach provides the effective stiffness tensor  $C^{EFF}$  by the following expression:

$$C^{EFF} = C_m + f_i(C_i - C_m)A[(1 - f_i)I + f_iA]^{-1}, \quad (1)$$

where  $C_m$  and  $C_i$  are isotropic stiffness tensors of matrix and inclusion respectively,  $f_i$  is volume fraction of inclusions,  $A$  is strain concentration tensor,  $I$  is identity tensor [10]. The strain concentration tensor relates the average strain in the inclusion  $\varepsilon_i$  to the far field strain (macro strain)  $\varepsilon$ :

$$\begin{bmatrix} \varepsilon_{11}^i \\ \varepsilon_{22}^i \\ \varepsilon_{33}^i \\ \varepsilon_{23}^i \\ \varepsilon_{13}^i \\ \varepsilon_{12}^i \end{bmatrix} = \begin{bmatrix} A_{11} & A_{12} & A_{13} & A_{14} & A_{15} & A_{16} \\ A_{21} & A_{22} & A_{23} & A_{24} & A_{25} & A_{26} \\ A_{31} & A_{32} & A_{33} & A_{34} & A_{35} & A_{36} \\ A_{41} & A_{42} & A_{43} & A_{44} & A_{45} & A_{46} \\ A_{51} & A_{52} & A_{53} & A_{54} & A_{55} & A_{56} \\ A_{61} & A_{62} & A_{63} & A_{64} & A_{65} & A_{66} \end{bmatrix} \begin{bmatrix} \varepsilon_{11} \\ \varepsilon_{22} \\ \varepsilon_{33} \\ \varepsilon_{23} \\ \varepsilon_{13} \\ \varepsilon_{12} \end{bmatrix}. \quad (2)$$

The strain concentration tensor for the M-T method depends on the Eshelby's tensor  $S$  as follows:

$$A = [S(C_m^{-1}C_l - I) + I]^{-1}. \quad (3)$$

The principle of the hybrid method is replacement of strain concentration tensor expressed by the equation 3 by strain concentration tensor determined numerically. Therefore, the numerical solution of equivalent inclusions problem is required. The equivalent inclusion problem is connected with analysis of single inclusion embedded in an infinite matrix. Numerical model approximates the infinite medium by rectangular prism whose finite dimensions are large enough in comparison with the size of the inclusion. In order to obtain the strain concentration tensor by using numerical method six FE simulations have to be performed by prescribing displacement boundary conditions that enforce the unit strains as follows (superscript denotes the analysis number):

$$\varepsilon^{(1)} = \begin{bmatrix} 1 \\ 0 \\ 0 \\ 0 \\ 0 \\ 0 \end{bmatrix}, \quad \varepsilon^{(2)} = \begin{bmatrix} 0 \\ 1 \\ 0 \\ 0 \\ 0 \\ 0 \end{bmatrix}, \quad \varepsilon^{(3)} = \begin{bmatrix} 0 \\ 0 \\ 1 \\ 0 \\ 0 \\ 0 \end{bmatrix}, \quad \varepsilon^{(4)} = \begin{bmatrix} 0 \\ 0 \\ 0 \\ 1 \\ 0 \\ 0 \end{bmatrix}, \quad \varepsilon^{(5)} = \begin{bmatrix} 0 \\ 0 \\ 0 \\ 0 \\ 1 \\ 0 \end{bmatrix}, \quad \varepsilon^{(6)} = \begin{bmatrix} 0 \\ 0 \\ 0 \\ 0 \\ 0 \\ 1 \end{bmatrix}. \quad (4)$$

At the post processing stage of the finite element computations the strains inside the inclusion  $\varepsilon_i$  are averaged in the following way:

$$\langle \varepsilon^i \rangle = \frac{1}{V^i} \int_{V^i} \varepsilon^i dV^i \quad (5)$$

where  $V^i$  is volume of the inclusion. The volume averaging is performed for each strain component, due to assumption of the unit macro strains (equation 4) the components of strain concentration tensor  $A$  are directly regarded as  $\langle \varepsilon^i \rangle$ . An influence of the rectangular prism size (embedding matrix) on the strain concentration tensor has been investigated by considering different volume fractions of single spherical inclusion. The numerical solution has been compared with analytical result for spherical inclusion which is achieved by substituting the Eshelby's tensor whose nonzero components are given by [18]:

$$\begin{aligned}
S_{11} = S_{22} = S_{33} &= \frac{7-5\nu}{15(1-\nu)}, \\
S_{12} = S_{23} = S_{31} = S_{13} = S_{21} = S_{32} &= \frac{5\nu-1}{15(1-\nu)}, \\
S_{44} = S_{55} = S_{66} &= \frac{4-5\nu}{15(1-\nu)},
\end{aligned} \tag{6}$$

to the equation 3. In case of numerical model fine finite element mesh consisting of hexahedral elements have been applied. View on one-eighth of model containing inclusion whose volume fraction is 0.001 is presented in Fig.1a and corresponding finite element mesh is presented in Fig. 2b. During the analysis the following elastic constants related to the matrix and inclusion have been taken into account:  $E_m=70$  GPa,  $\nu_m=0.30$ ,  $E_i=415$  GPa,  $\nu_i=0.16$  which are typical for aluminum alloy and silicon carbide.

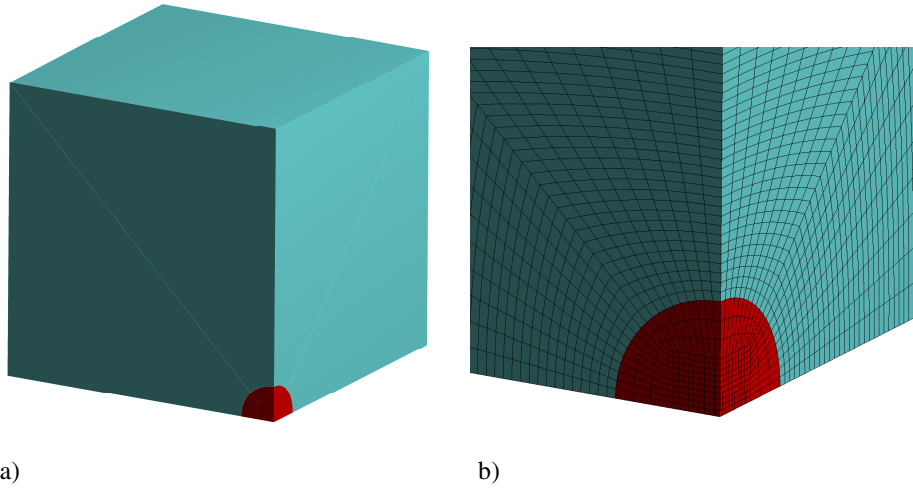


Figure 1. Model of equivalent inclusion problem involving spherical inclusion: a) view on the one-eighth of the model, b) detailed view on the finite element mesh

The error of numerical solution of equivalent inclusion problem has been quantified by comparing the components of strain concentration tensor determined analytically and numerically:

$$\chi_{ij} = \frac{|A_{ij}^{ANA} - A_{ij}^{NUM}|}{A_{ij}^{ANA}} 100\% \tag{7}$$

The dependence of the volume fraction of the single inclusion on the error  $\chi_{ij}$  is presented in Fig. 2 (due to isotropic behavior only  $A_{11}$  and  $A_{12}$  components are compared).

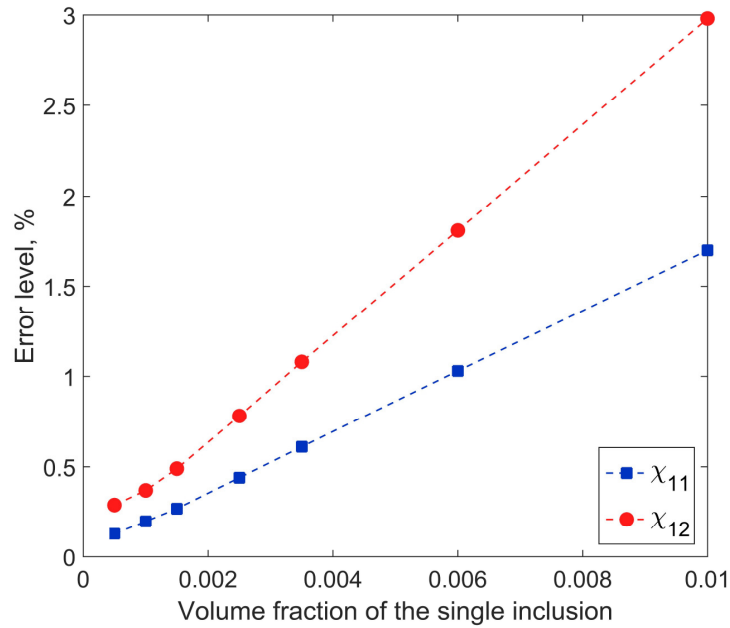


Figure 2. Dependence of the volume fraction of the single inclusion on the error of numerical solution of equivalent inclusion problem

Analysis of the Fig. 2 lead to conclusion that 0.001 volume fraction of the single inclusion provides good approximation of the equivalent inclusion problem. Strain concentration tensors computed analytically and numerically involving 0.001 volume fraction of single inclusion have the following form respectively:

$$A^{ANA} = \begin{bmatrix} 0.31203 & 0.04085 & 0.04085 & 0.00000 & 0.00000 & 0.00000 \\ 0.04085 & 0.31203 & 0.04085 & 0.00000 & 0.00000 & 0.00000 \\ 0.04085 & 0.04085 & 0.31203 & 0.00000 & 0.00000 & 0.00000 \\ 0.00000 & 0.00000 & 0.00000 & 0.27117 & 0.00000 & 0.00000 \\ 0.00000 & 0.00000 & 0.00000 & 0.00000 & 0.27117 & 0.00000 \\ 0.00000 & 0.00000 & 0.00000 & 0.00000 & 0.00000 & 0.27117 \end{bmatrix}, \quad (8)$$

$$A^{NUM} = \begin{bmatrix} 0.31264 & 0.04070 & 0.04070 & 0.00000 & 0.00000 & 0.00000 \\ 0.04070 & 0.31264 & 0.04070 & 0.00000 & 0.00000 & 0.00000 \\ 0.04070 & 0.04070 & 0.31264 & 0.00000 & 0.00000 & 0.00000 \\ 0.00000 & 0.00000 & 0.00000 & 0.27170 & 0.00000 & 0.00000 \\ 0.00000 & 0.00000 & 0.00000 & 0.00000 & 0.27170 & 0.00000 \\ 0.00000 & 0.00000 & 0.00000 & 0.00000 & 0.00000 & 0.27170 \end{bmatrix}. \quad (9)$$

### 3 ANALYSIS OF REINFORCEMENT OF ARBITRARY SHAPE

One of the main goals of this study is to use the hybrid homogenization method for determination of effective properties of composite materials reinforced with particles of arbitrary shape. This section presents the results obtained for cubic particles. The results obtained by using hybrid homogenization method are compared with pure numerical solution based on the direct finite element (FE) analysis of representative volume element (RVE) containing substantial number of inclusions. The numerical model of equivalent inclusion problem has been formulated in a way described in section 2 by considering single cubic inclusion of volume fraction 0.001 (Fig. 3) and the same elastic constants as previously.

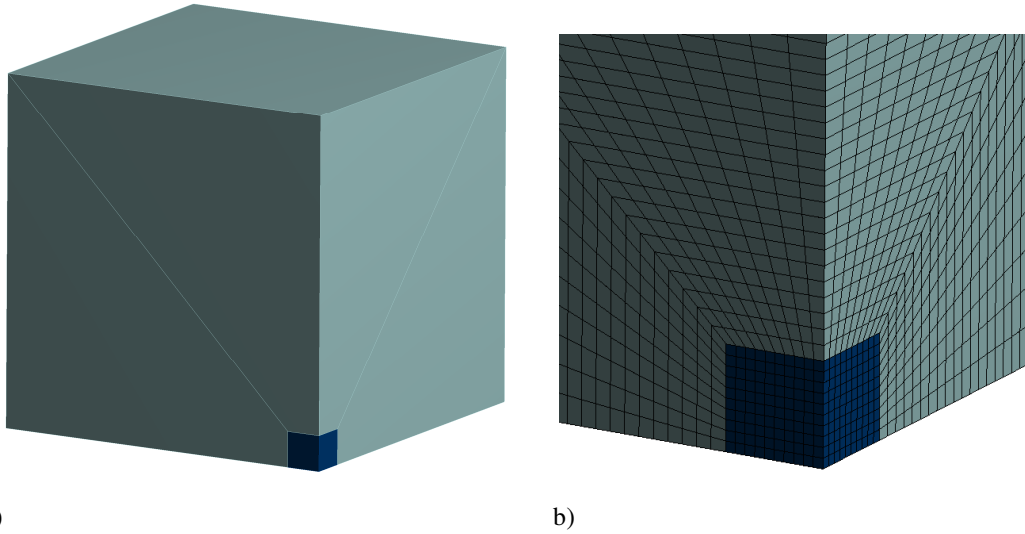


Figure 3. Model of equivalent inclusion problem involving cubic inclusion: a) view on the one-eighth of the model, b) detailed view on the finite element mesh

Strain concentration tensor obtained for cubic inclusion is given by:

$$A^{NUM\_CUBE} = \begin{bmatrix} 0.34391 & 0.03273 & 0.03273 & 0.00000 & 0.00000 & 0.00000 \\ 0.03273 & 0.34391 & 0.03273 & 0.00000 & 0.00000 & 0.00000 \\ 0.03273 & 0.03273 & 0.34391 & 0.00000 & 0.00000 & 0.00000 \\ 0.00000 & 0.00000 & 0.00000 & 0.28037 & 0.00000 & 0.00000 \\ 0.00000 & 0.00000 & 0.00000 & 0.00000 & 0.28037 & 0.00000 \\ 0.00000 & 0.00000 & 0.00000 & 0.00000 & 0.00000 & 0.28037 \end{bmatrix}. \quad (10)$$

The effective stiffness tensor determined in terms of tensor  $A^{NUM\_CUBE}$  exhibit cubic symmetry. For example, effective stiffness tensor obtained for 0.2 volume fraction of particles has the following form:

$$C = \begin{bmatrix} 122.326 & 46.544 & 46.544 & 0.000 & 0.000 & 0.000 \\ 46.544 & 122.326 & 46.544 & 0.000 & 0.000 & 0.000 \\ 46.544 & 46.544 & 122.326 & 0.000 & 0.000 & 0.000 \\ 0.000 & 0.000 & 0.000 & 36.876 & 0.000 & 0.000 \\ 0.000 & 0.000 & 0.000 & 0.000 & 36.876 & 0.000 \\ 0.000 & 0.000 & 0.000 & 0.000 & 0.000 & 36.876 \end{bmatrix}. \quad (11)$$

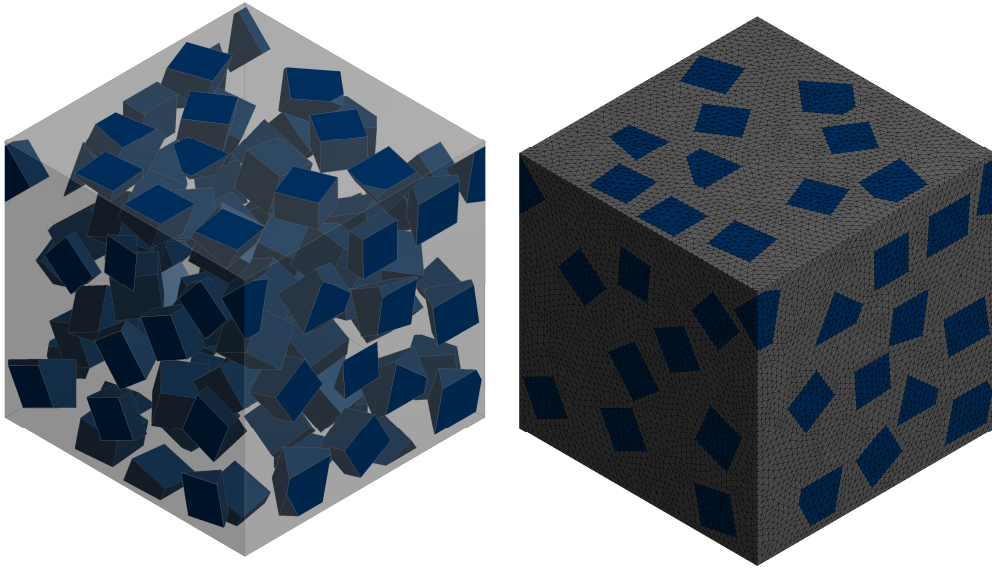
However, in many cases, particle reinforced composites contain the inclusions which are distributed randomly hence the material is characterized by isotropic symmetry. Therefore, the orientation averaging procedure has been employed to model the random orientation of cubic particles. The effective stiffness tensor of the material with random orientation of the inclusions can be determined by integration over the unit sphere:

$$C^{RANDOM} = \int_{\theta=0}^{\pi} \int_{\varphi=0}^{2\pi} C(\theta, \varphi) \psi(\theta, \varphi) \sin \theta d\theta d\varphi, \quad (12)$$

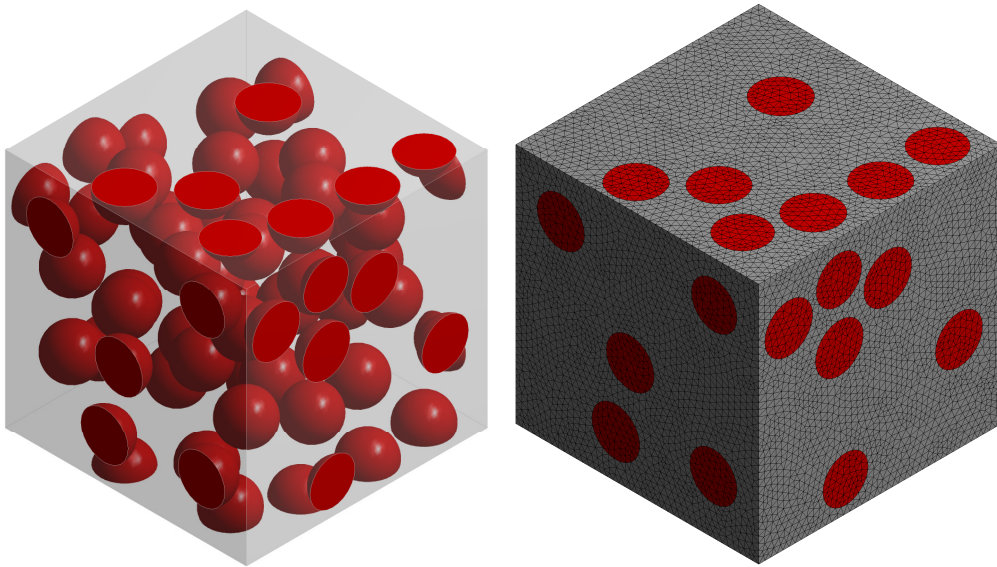
where  $\theta$  and  $\varphi$  are spherical angles,  $C(\theta, \varphi)$  is transformed stiffness tensor determined in terms of tensor  $A^{NUM\_CUBE}$ ,  $\psi(\theta, \varphi)$  is orientation distribution function [19, 20]. The stiffness tensor obtained after orientation averaging which represents the material with randomly oriented cubic particles of volume fraction 0.2 is given by:

$$C^{RANDOM} = \begin{bmatrix} 121.514 & 46.950 & 46.950 & 0.000 & 0.000 & 0.000 \\ 46.950 & 121.514 & 46.950 & 0.000 & 0.000 & 0.000 \\ 46.950 & 46.950 & 121.514 & 0.000 & 0.000 & 0.000 \\ 0.000 & 0.000 & 0.000 & 37.282 & 0.000 & 0.000 \\ 0.000 & 0.000 & 0.000 & 0.000 & 37.282 & 0.000 \\ 0.000 & 0.000 & 0.000 & 0.000 & 0.000 & 37.282 \end{bmatrix}. \quad (13)$$

Afterwards the direct FE homogenization has been performed on the basis of the representative volume elements (RVE) whose exemplary models are presented in Fig. 4-5. During the direct FE homogenization periodic boundary conditions [1] have been applied in order to enforce the unit strains in the similar way to the equation 4. In this case tetrahedral finite elements with quadratic shape functions have been used where the nodes on opposite faces of the RVE model are consistent that makes application of periodic boundary conditions convenient. Cubic and spherical shapes of the reinforcement have been studied involving four different volume fractions: 0.1, 0.15, 0.20, 0.25 hence eight different cases have been studied.



a) b)  
Figure 4. RVE containing cubic inclusions used in direct FE homogenization: a) geometrical model, b) finite element mesh



a) b)  
Figure 5. RVE containing spherical inclusions used in direct FE homogenization: a) geometrical model, b) finite element mesh

For example, effective stiffness tensors obtained after direct FE homogenization corresponding to the materials reinforced with cubic and spherical particles of volume fraction 0.2 have the following form:

$$C^{FE\_CUB} = \begin{bmatrix} 122.751 & 46.975 & 46.466 & -0.328 & 0.103 & -0.017 \\ 46.975 & 122.482 & 46.435 & -0.104 & -0.065 & -0.125 \\ 46.466 & 46.435 & 123.008 & 0.135 & 0.039 & 0.198 \\ -0.328 & -0.104 & 0.135 & 38.170 & -0.004 & -0.042 \\ 0.103 & -0.065 & 0.039 & -0.004 & 37.718 & 0.036 \\ -0.017 & -0.125 & 0.198 & -0.042 & 0.036 & 37.615 \end{bmatrix}, \quad (14)$$

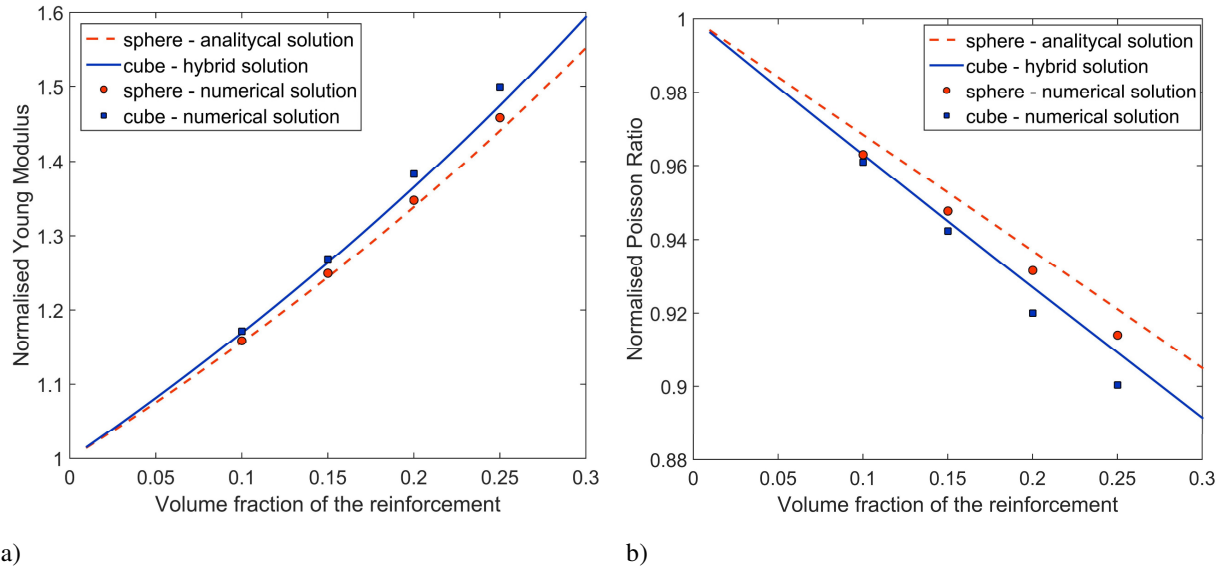
$$C^{FE\_SPH} = \begin{bmatrix} 120.653 & 46.666 & 46.702 & 0.055 & -0.104 & 0.134 \\ 46.666 & 120.430 & 46.801 & 0.090 & 0.019 & 0.098 \\ 46.701 & 46.800 & 120.289 & -0.054 & 0.010 & 0.159 \\ 0.055 & 0.090 & -0.054 & 36.826 & 0.215 & -0.012 \\ -0.104 & 0.019 & 0.010 & 0.215 & 36.822 & -0.028 \\ 0.134 & 0.098 & 0.160 & -0.012 & -0.028 & 36.947 \end{bmatrix}. \quad (15)$$

The obtained stiffness tensors do not exhibit the isotropic symmetry exactly therefore in order to extract the effective Young modulus and Poisson ratio the procedure of the best isotropic approximation of elastic anisotropies discussed by Cavallini [21] has been applied. The result of approximation is given by the following stiffness tensors:

$$C^{FE\_CUB\_ISO} = \begin{bmatrix} 122.566 & 46.716 & 46.716 & 0.000 & 0.000 & 0.000 \\ 46.716 & 122.566 & 46.716 & 0.000 & 0.000 & 0.000 \\ 46.716 & 46.716 & 122.566 & 0.000 & 0.000 & 0.000 \\ 0.000 & 0.000 & 0.000 & 37.925 & 0.000 & 0.000 \\ 0.000 & 0.000 & 0.000 & 0.000 & 37.925 & 0.000 \\ 0.000 & 0.000 & 0.000 & 0.000 & 0.000 & 37.925 \end{bmatrix}, \quad (16)$$

$$C^{FE\_SPH\_ISO} = \begin{bmatrix} 120.456 & 46.724 & 46.724 & 0.000 & 0.000 & 0.000 \\ 46.724 & 120.456 & 46.724 & 0.000 & 0.000 & 0.000 \\ 46.724 & 46.724 & 120.456 & 0.000 & 0.000 & 0.000 \\ 0.000 & 0.000 & 0.000 & 36.866 & 0.000 & 0.000 \\ 0.000 & 0.000 & 0.000 & 0.000 & 36.866 & 0.000 \\ 0.000 & 0.000 & 0.000 & 0.000 & 0.000 & 36.866 \end{bmatrix}. \quad (17)$$

Normalized effective Young moduli and Poisson ratios have been determined on the basis of effective stiffness tensors, Fig. 6 presents results obtained by using: analytical solution for spherical inclusion, hybrid solution for cubic inclusion and pure numerical (FE) solution for both analyzed shapes of the inclusions. The effective properties are expressed in terms of volume fraction of the reinforcement.



a) b)  
Figure 6. Effective material constants in terms of the reinforcement volume fraction: a) normalized Young modulus, b) normalized Poisson ratio

#### 4 CONCLUSIONS AND FURTHER WORK

The work presents the hybrid Mori-Tanaka/Finite element (M-T/FE) homogenization method which allowed to determine the effective properties of composite materials reinforced with particles of arbitrary shape. The method is efficient, as it requires the numerical solution of equivalent inclusion problem involving very simple geometry. An influence of size of the embedding matrix on the strain concentration tensor has been investigated by considering different volume fractions of the single inclusion and comparing the obtained results with analytical solution. Carried out computations showed that single inclusion of volume fraction 0.001 allows to approximate the equivalent inclusion problem properly. The effective stiffness tensor determined for cubic inclusion exhibit the cubic symmetry and therefore the orientation averaging procedure has been applied to obtain the effective stiffness tensor corresponding to material reinforced with randomly oriented cubic particles. The accuracy of obtained results has been verified by performing direct FE homogenization based on the RVE containing substantial number of inclusions. The error of hybrid solution related to the direct FE results is increasing with increasing volume fraction of the inclusions. The hybrid solution underestimates the effective Young moduli and overestimates the effective Poisson ratios. A similar situation is present in case of analytical solution for spherical inclusion. Further work will focus on different shapes of inclusions and orientation distributions. In order to reduce the error of M-T/FE method in case of intermediate volume fractions of the reinforcement a double inclusion approach [22, 23] will be applied. While this paper focuses on linear-elastic material behavior only, the future work will be devoted to extension of M-T/FE method for nonlinear composites.

#### ACKNOWLEDGEMENT

The research for this paper was financially supported by the National Science Centre, Poland (Grant No. UMO-2016/21/N/ST8/01119)

**REFERENCES**

- [1] Segurado, J. and Llorca, J. A numerical approximation to the elastic properties of sphere-reinforced composites. *J. Mech. Phys. Solids.* (2002) 50:2107–2121.
- [2] Kouznetsova, V., Brekelmans, W.A.M. and Baaijens, F.P.T. Approach to micro-macro modeling of heterogeneous materials. *Comput. Mech.* (2001) 27:37–48.
- [3] Burczyński, T., Kuś, W. and Brodacka, A. Multiscale modeling of osseous tissues. *J. Theor. Appl. Mech.* (2010) 48:855–870.
- [4] Kamiński, M. Boundary element method homogenization of the periodic linear elastic fiber composites. *Eng. Anal. Bound. Elem.* (1999) 23:815–823.
- [5] Fedeliński, P., Górski, G., Czyż, T., Dziatkiewicz, G. and Ptaszny, J. Analysis of effective properties of materials by using the boundary element method. *Arch. Mech.* (2014) 66: 19–35.
- [6] Ptaszny, J. Accuracy of the fast multipole boundary element method with quadratic elements in the analysis of 3D porous structures. *Comput. Mech.* (2015) 56:477–490.
- [7] Kanit, T., Forest, S., Galliet, I., Mounoury, V. and Jeulin, D. Determination of the size of the representative volume element for random composites: Statistical and numerical approach. *Int. J. Solids Struct.* (2003) 40:3647–3679.
- [8] Eshelby, J.D. The determination of the elastic field of an ellipsoidal inclusion, and related problems. *Proc. R. Soc. Lond. A. Math. Phys. Sci.* (1957) 241:376–396.
- [9] Benveniste, Y. Revisiting the generalized self-consistent scheme in composites: Clarification of some aspects and a new formulation. *J. Mech. Phys. Solids.* (2008) 56: 2984–3002.
- [10] Benveniste, Y. A new approach to the application of Mori-Tanaka's theory in composite materials. *Mech. Mater.* (1987) 6:147–157
- [11] Sadowski, P., Kowalczyk-Gajewska, K. and Stupkiewicz, S. Consistent treatment and automation of the incremental Mori–Tanaka scheme for elasto-plastic composites. *Comput. Mech.* (2017) 60:1–19.
- [12] Tucker, I.C. and Liang, E. Stiffness predictions for unidirectional short-fibre composites: review and evaluation. *Compos. Sci. Technol.* (1999) 59:655–671.
- [13] Ogierman, W. and Kokot, G. A study on fiber orientation influence on the mechanical response of a short fiber composite structure. *Acta Mech.* (2016) 227:173–183.
- [14] Bradshaw, R.D., Fisher, F.T. and Brinson, L.C. Fiber waviness in nanotube-reinforced polymer composites-II: Modeling via numerical approximation of the dilute strain concentration tensor. *Compos. Sci. Technol.* (2003) 63:1705–1722.
- [15] Klusemann, B., Böhm, H.J. and Svendsen, B. Homogenization methods for multi-phase elastic composites with non-elliptical reinforcements: Comparisons and benchmarks. *Eur. J. Mech. A/Solids.* (2012) 34:21–37.
- [16] Srinivasulu, G., Velmurugan, R. and Jayasankar, S. A hybrid method for computing the effective properties of composites containing arbitrarily shaped inclusions. *Comput. Struct.* (2015) 150:63–70.
- [17] Brassart, L., Doghri, I. and Delannay, L. Homogenization of elasto-plastic composites coupled with a nonlinear finite element analysis of the equivalent inclusion problem. *Int. J. Solids Struct.* (2010) 47:716–729.
- [18] Mura, T. *Micromechanics of defects in solids*, Martinus Nijhoff Publishers, Dordrecht (1987)

- [19] Doghri, I. and Tinel, L. Micromechanics of inelastic composites with misaligned inclusions: Numerical treatment of orientation. *Comput. Methods Appl. Mech. Eng.* (2006) 195, 1387–1406.
- [20] Ogierman, W. and Kokot, G. Homogenization of inelastic composites with misaligned inclusions by using the optimal pseudo-grain discretization. *Int. J. Solids Struct.* (2017) 113–114:230–240.
- [21] Cavallini, F. The best isotropic approximation of an anisotropic Hooke's law. *Bollettino di Geofisica Teorica ed Applicata* (1999) 40: 1-18.
- [22] Lielens, G. *Micro–Macro Modeling of Structured Materials*. PhD thesis (1999) Universite' Catholique de Louvain, Belgium.
- [23] Friebel, C., Doghri, I. and Legat V. General mean-field homogenization schemes for viscoelastic composites containing multiple phases of coated inclusions. *Int. J. Solids Struct.* (2006) 43:2513–2541.

## **An Efficient Many-core Implementation of Non-overlapping Domain Decomposition Methods**

Masao Ogino\*

\*Nagoya University

### **ABSTRACT**

To solve complex problems in science and industrial applications, the finite element analysis with large-scale unstructured mesh has been widely used on parallel computers. Moreover, the iterative methods such as Krylov subspace method has been usually adopted for solving the large-scale system of the linear equation. However, solving large-scale linear systems from actual problems suffer from slow convergence rate. Therefore, numerical methods having both robust convergence and scalable parallel efficiency are in great demand. The domain decomposition method (DDM) is well known as the iterative substructuring method, and is an efficient approach for parallel finite element methods. As an implementation of the DDM, the hierarchical domain decomposition method (HDDM) [1] has high scalability on distributed-memory parallel computers. As a preconditioner for the non-overlapping DDM, the balancing domain decomposition (BDD) method [2] have robust convergence for the number of subdomains and is expected to be high convergence rate compared to conventional preconditioners. This study focuses on an implementation of the non-overlapping DDM and the BDD method. Especially, parallel scalability of many-core CPUs and multi-GPUs is investigated by using the BDD method based on the HDDM. Moreover, an efficient linear solver of subdomain-interior problems is investigated. To indicate that our system has both robust convergence and high parallel efficiency, some numerical results are demonstrated on the Fujitsu PRIMEHPC FX100 consisting of 32-core CPU and a supercomputer consisting of multi-CPU and multi-GPU. [1] Yagawa, G. and Shioya, R. (1994) Parallel finite elements on a massively parallel computer with domain decomposition, *Computing Systems in Engineering*, 4, 495-503. [2] Mandel, J. (1993) Balancing domain decomposition, *Communications on Numerical Methods in Engineering*, 9, 233-241.

## Numerical Investigations on Pattern Formation in Surface Earthquake Faults

Kenji Oguni\*, Sayako Hirobe\*\*

\*Keio University, \*\*Keio University

### ABSTRACT

Surface earthquake faults due to underground strike slip often show a typical echelon fault pattern on the top surface of the embedded soil. This typical echelon fault pattern is called Riedel shear. Based on the observations from model experiments for Riedel shear using a box of sand, the twist of the fault surface growing from the strike-slip at the bottom could be suspected as the fundamental source of the periodical pattern of the Riedel shear. On the other hand, experiments using transparent gelatin specimen show that Riedel shear is the consequence of the consecutive choice of the bifurcated solution. These experimental observations with contradicting appearances prevent us from the complete explanation of the mechanism behind Riedel shear. The purposes of this study are to simulate Riedel shear caused by strike-slip faults and to identify the governing mechanism of the Riedel shear. The periodical pattern formation observed in Riedel shear implies the importance of bifurcation in the governing mechanism of this phenomenon. Therefore, numerical analysis method with the capacity of the fracture-induced bifurcation analysis is required. For this purpose, PDS-FEM (particle discretization scheme finite element method) has been employed and elasto-dynamic analysis of a plate of homogeneous elasticity subject to strike-slip at the bottom surface has been carried out as the simplest model of the Riedel shear. The periodical echelon fault pattern generated by numerical simulation shows reasonable agreement with the Riedel shear observed in sandbox experiment in its size, orientation, and pitch. The detail investigation of the internal structure of the numerically generated faults has revealed the formation process of the Riedel shear. The Riedel shear starts from the segmentation of the straight strike-slip line into short echelon faults with small twist, then, as the cracks evolve upwards, these short segments undergo consecutive bifurcation with alternative choice of the growing segments. As this process proceeds, the cracks reach to the top surface, the twist angle of the cracks increases, and the number of the cracks decreases as the consequence of the consecutive bifurcation.

## Mitigation of Boundary Effect in Nonordinary State-based Peridynamics by Addition of Mirroring Nodes

Seong Eun Oh\*, Jung-Wuk Hong\*\*

\*Korea Advanced Institute of Science and Technology, \*\*Korea Advanced Institute of Science and Technology

### ABSTRACT

In this research, the boundary effect of the nonordinary state-based peridynamics (PD) in the displacement controlled simulation is investigated and mitigated by adding mirroring nodes along the boundary. The peridynamic variables at each node are collectively calculated using the configurations and variables at neighboring nodes within its horizon [1]. If there exists an intersection between a certain horizon and the boundary, the domain within the horizon is not completely spherical, yielding inaccurate estimation of tensors and state variables. In order to mitigate this boundary effect, virtual nodes are deployed by mirroring the interior nodes residing within the body with respect to the boundary. In specific, the shape tensors of the peridynamic nodes that have incomplete spherical horizons are calculated by considering both the interior peridynamic nodes and the mirrored virtual nodes. For the calculation of the force states, the displacements of the peridynamic nodes in the body are extrapolated to the virtual nodes anti-symmetrically, and the interacting forces between the interior nodes and the virtual nodes are added to the nodal forces. In order to validate the proposed methodology, displacement-controlled simulations are carried out by exerting axial elongation and shear deformation on the left and right sides of a solid cube. For different horizons ( $1\delta$ ,  $2\delta$  and  $3\delta$ ), the numerical results from the proposed mirroring method are compared with the results from the original nonordinary state-based peridynamics, and the differences are investigated. The proposed methodology yields more accurate results than the original methodology, especially around the boundary. [1] Silling, S.A., Epton, M., Weckner, O., Xu, J., Askari, E., 2007. Peridynamic states and constitutive modeling. *Journal of Elasticity* 88, 151-184.

## **Extension of Quantitative Phase-field Simulations to Prediction of Macrosegregation Based on Machine Learning**

Munekazu Ohno\*

\*Hokkaido University

### **ABSTRACT**

Segregation arises during alloy solidification. It is generally classified into microsegregation on a dendritic scale and macrosegregation on an ingot scale. Prediction of macrosegregation requires precise description of microsegregation during dendritic growth. Several analytical models were developed for prediction of microsegregation and they have played an important role in making progress in understanding the microsegregation behavior. Effects of microstructural change and multicomponent diffusion are the important factors to be taken into account for better description and prediction of microsegregation behavior. The phase-field model is a powerful tool to describe microstructural evolution processes in alloy solidification. Importantly, quantitative phase-field model (Q-PFM), which is formulated based on the thin-interface limit, enables us to carry out quantitative description and prediction of microstructural evolution processes. However, the early developed Q-PFMs are applicable to alloy systems without diffusion in the solid phase(s) and therefore these models cannot be utilized for the analysis of microsegregation. In order to describe the microsegregation behavior, Q-PFM was extended by our group to deal with alloy systems with diffusion in the solid in multicomponent alloys. In this talk, we show that Q-PFM enables highly accurate prediction of microsegregation behavior in Fe-Mn and Al-Cu alloy systems. Several simulation models have been proposed for prediction of macrosegregation. The improvement of accuracy of the early developed models requires the improvement of microsegregation calculation in these models in which the details of microstructural change are not taken into account. In this study, we propose the macrosegregation model in which the microsegregation behavior predicted by Q-PFM is introduced by means of machine learning.

## Edge Wrinkle or Crease in Very Thin Rectangular Plates under Gravity

Akira Ohta<sup>\*</sup>, Hideo Koguchi<sup>\*\*</sup>

<sup>\*</sup>Niigata Institute of Technology, <sup>\*\*</sup>Niigata Institute of Technology

### ABSTRACT

A precise position control of glass substrates is required in a process of manufacturing an organic electroluminescence display. The precise position of glass is the most important process, which determines the definition of the display. Recently, glass substrates tend to be larger every year to increase a productive efficiency. The thickness of the glass substrate reduces every year since a market demands thinner end products. Furthermore, material of the substrate is required to be replaced except glass. In the manufacture process, multiple deformation modes in the glass substrate are frequently observed. In a deformation mode, when the glass substrate is pushed up by a finger from the bottom and release the finger, the deformation mode of the substrate varies stably. When a different place in the substrate is pushed up with a finger in the same manner, the plate becomes stable at the different shape. We can simulate this phenomenon in a computer and real manufacture process. We will present a mechanism of occurrence for multiple deformation modes and the relationship of thickness, elasticity, the size and the density of the substrate. When a thin plate is supported only at side edges, the center area of the plate deflects due to gravity, the side edge is dragged along the side and compressed. When compressive stress exceeds a critical value, buckling occurs at the side edges. The local buckling occurs in a part of the thin plate, that is, buckling does occur in the whole plate. This local buckling is the cause of multiple unstable deformation. In a production site, it is required that multiple unstable deformation never occurs. A method for calculating a occurrence limit of phenomenon is needed. We would like to present a method for calculation. Furthermore, it is investigated that the buckling occurs under what kind of condition using this method. Here, the ratio of the thickness and the area of the plate is referred to as the degree of thin plate. The ratio of the stiffness and the density of the plate is referred to as a specific stiffness. The occurrence limit of the unstable deformation will be shown using these ratios.

## UMMDp and UMMDr: Unified User Subroutine Libraries for Nonlinear Material Models in Advanced Finite Element Applications

Kai Oide<sup>\*</sup>, Hideo Takizawa<sup>\*\*</sup>, Takashi Terajima<sup>\*\*\*</sup>, Junji Yoshida<sup>\*\*\*\*</sup>, Toshihiko Kuwabara<sup>\*\*\*\*\*</sup>

<sup>\*</sup>Mechanical Design & Analysis Corporation, <sup>\*\*</sup>Nippon Institute of Technology, <sup>\*\*\*</sup>Meiji Rubber & Chemical CO., LTD, <sup>\*\*\*\*</sup>University of Yamanashi, <sup>\*\*\*\*\*</sup>Tokyo University of Agriculture and Technology

### ABSTRACT

With the spread of commercial finite element software, numerical simulation has become widely used throughout many fields, not only in advanced industrial applications, as a method for solving practical problems. Appropriate solutions for daily routine design work can easily be identified using the extensive analytical functions of these software programs. For example, large displacement problems, large strain problems, and contact problems are becoming common tasks for general design engineers. However, in nonlinear material application fields, if more advanced problems are attempted, material models that are not prepared in default analysis options are needed. Analysts have to customize the available options in finite element programs, and prepare material constants through appropriate material testing. These kinds of technical processes require professional knowledge and skills, and are therefore not yet widely available. The Japan Association for Nonlinear Computer Aided Engineering (JANCAE), a non-profit organization, has held lectures twice a year for four days each since 2001 to provide training on theories and technology related to nonlinear simulation; more than 3000 people have participated so far. Over the last decade, it has held working groups during which participants have developed and verified two user-subroutine libraries: the Unified Material Model Driver for Plasticity (UMMDp) for anisotropic yield functions, and the Unified Material Model Driver for Rubber (UMMDr) for modeling rubber materials. These working groups were established to provide a multidisciplinary forum for steel researchers, rubber researchers, design engineers, and software engineers to collaborate through the medium of advanced finite element codes. The UMMDp contains a subroutine library that includes practically recognized anisotropic yield functions (e.g. Yoshida's 6th-order polynomial, Barlat's Yld2000-2d and Yld2004, Banabic's BBC2008). In UMMDr, a subroutine library combines the isochoric components of hyperelastic models (e.g. a stretch-based model such as Ogden, Shariff, and an invariants-based model such as Mooney Rivlin.), damage models (e.g. Simo, Miehe, Ogden-Roxburgh), visco-elastic models (e.g. Simo, Holzappel, Reese-Govindjee), and the volumetric components of the hyperelastic models. Both subroutine libraries provide multi-port capabilities that can be used with commercial finite element software, such as Abaqus, ADINA, ANSYS, LS-DYNA and MSC.Marc. Moreover, new material models can be added to both subroutine libraries. Each subroutine is verified with basic tests, and both libraries are verified with one elements test and multiple practical tests. This paper introduces the development of the UMMDp and UMMDr, and discusses some verification methods and example simulations.

# A FUNDAMENTAL STUDY ON DAMAGE DETECTION BASED ON DEEP LEARNING USING DATA OBTAINED FROM SHAKE TABLE TESTS OF A STEEL FRAME

KAZUYA OKA\*, KENTA WATANABE\*, MASAYUKI KOHIYAMA\*,  
TAKUZO YAMASHITA†, KAZUTOSHI MATSUZAKI‡, AND YUJI MORI‡

\*Graduate School of Science and Technology, Keio University  
3-14-1 Hiyoshi, Kohoku-ku, Yokohama 223-8522, Japan  
kazuyaoka@a8.keio.jp

†National Research Institute for Earth Science and Disaster Resilience  
3-1 Tennodai, Tsukuba-shi, Ibaraki, 305-0006, Japan

‡Mizuho Information & Research Institute, Inc.  
2-3 Kanda-Nishikicho, Chiyoda-ku, Tokyo 101-8443, Japan

**Key words:** Damage Identification, Deep Learning, Structural Health Monitoring, Brace,  
Steel Frame, Shaking Table Test

**Abstract.** To employ neural networks in structural health monitoring, a large volume of training data is required. The data can be obtained by a generative learning method based on high-precision simulation of seismic responses. We investigate appropriate machine learning parameters such as the numbers of layer nodes in a deep neural network and the number of epochs for training. Response records measured in shaking table tests of a steel frame structure are used as training, validation, and test data. Our results show that response data of only the translational component can achieve high accuracy of damage pattern classification. Regarding the length of response data, clear difference is not observed in two durations of 1 s and 2 s. We propose a method to detect unlearned damage pattern data using the Mahalanobis distance.

## 1 INTRODUCTION

Structural health monitoring (SHM) systems have not been extensively applied to existing buildings, and it is expected to improve damage estimation accuracy of these systems. Some SHM systems employ a neural network (NN); many studies have been conducted on damage detection using NN. For example, with respect to the NN input data, Ferregut et al.<sup>[1]</sup> used resonance frequency and Choi and Kwon<sup>[2]</sup> used responses measured by strain gauges and acceleration sensors for the truss bridge under traffic vibrations. Chang et al.<sup>[3]</sup> used modal parameters such as natural periods and mode shapes, and Lee et al.<sup>[4]</sup> used mode vectors of a

linear model. However, these studies performed damage detection based on linear responses rather than nonlinear responses, which are often observed under strong ground motion.

To consider nonlinear responses, Lautour and Omenzetter<sup>[5]</sup> predicted damage indices by numerical simulations using a nonlinear finite element method, and Derkevorkian et al.<sup>[6]</sup> also took a nonlinear response into account and proposed a time-marching framework to predict damage from the change. Rafiei and Adeli<sup>[7, 8]</sup> proposed a global and local SHM system that can detect damage using only ambient vibrations of high-rise building structures before damage occurs. However, these methods cannot detect damage of individual members, such as columns, beams, and braces.

Recently, Abdeljaber et al.<sup>[9]</sup> developed a method to detect damage of individual members through deep learning of distribution from raw acceleration responses of random vibrations for damage patterns. In addition, Zhang et al.<sup>[10]</sup> presented a machine learning framework using peak plastic hinge rotation obtained from a nonlinear response analysis of a four-story and three-span reinforced-concrete building under simulated ground motion. These studies use the acceleration of all joints; therefore, it is necessary to develop systems that can be applied to models installed with less sensors.

To overcome problems in the field of SHM described above, we use the shaking table test data of a steel structure and nonlinear responses at a limited number of joints to train deep NN. We analyze the identification accuracy of damage patterns. Additionally, we propose and verify a detection method of unlearned damage pattern data.

## 2 OUTLINE OF THE SHAKING TABLE TEST

In this research, response records measured in the shaking table tests of a steel frame structure are used as training, validating, and test data instead of response data simulated by E-Simulator, a high-precision finite element analysis software. The test specimen (Fig. 1) is a small-scale model of a four-story steel frame structure with a longitudinal direction width of 12 m, a transverse direction width of 6 m, and a height of 14 m. The test specimen has a height of 1.157 m and a first natural period of 0.21 s. We install four braces in the second story of the specimen and assume eight different damage patterns of the braces, as shown in Fig. 2, which are simulated by relaxing the turn buckle of the braces before shaking. We prepare simulated ground motions for horizontal uniaxial shaking; an example of input waves is shown in Fig. 3. The simulated ground motions are synthesized based on a modified method for design ground motion prescribed by the Notification of Building Standard Law of Japan, which uses time-domain envelope functions, design acceleration response spectrum, and random phases. Approximately 100 different simulated ground motions with small to large amplitudes and short to long durations are input to the specimen with each state of damage. We install inertial measurement units, M-G550-PC made by Seiko Epson Corporation, throughout the specimen and measure three translational acceleration components and three angular velocity components with a sampling frequency of 500 Hz.

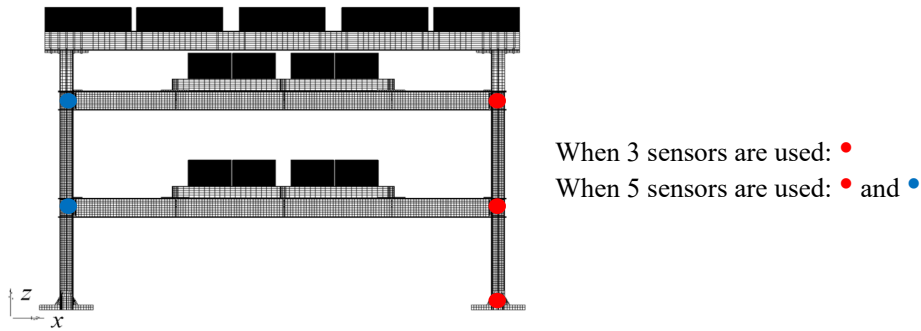


**Figure 1.** The test specimen and sensor location used in the study

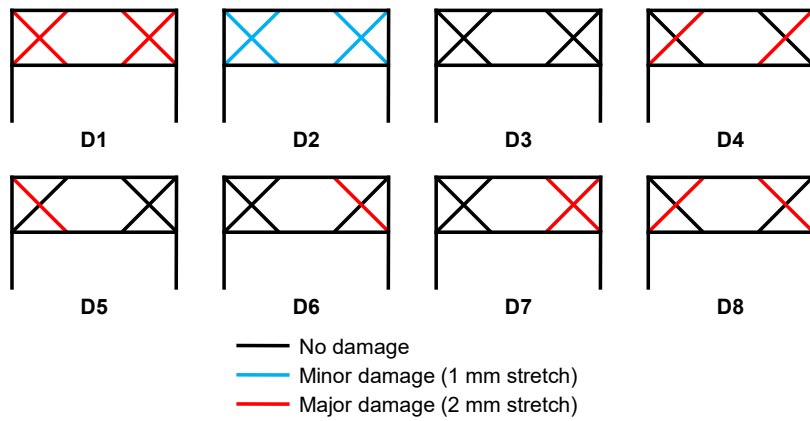


**Figure 2.** Damage patterns of braces

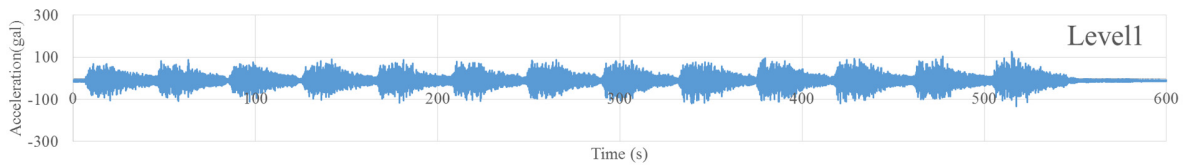


**Figure 3.** An example of simulated ground motion input in a shaking table test

### 3 ANALYSIS ON ACCURACY OF DAMAGE PATTERN IDENTIFICATION

We identify damage patterns of the specimen using the damage pattern identification system based on a multi-layer NN, which was developed by the National Research Institute for Earth Science and Disaster Resilience and Mizuho Information & Research Institute. For data input of NNs, a sample is a raw measurement record divided and extracted with a time length of 1 s or 2 s (two cases), which is 5 or 10 times that of the first natural period, 0.21 s, of a specimen without braces. The input dataset is randomly divided into two groups, one for training and the other for validation, and cross validation is performed.

To clarify hyper-parameters that improve the accuracy of damage pattern identification, accuracies are compared among different combinations of the components of the measurement records, the number of middle layers nodes, the sample length, and the number of training epochs. The number of sensors used is three or five (two cases), as shown in Fig. 1. We fixed the number of middle layers of NNs to three, and three cases of the numbers of middle layers nodes are compared: (100, 50, 25), (500, 250, 125), and (1000, 500, 250), values are ordered from the middle layer closest to the input layer. Two cases of the sample length, 1 s and 2 s, are compared.

Figure 4 shows the learning curves representing the relationship between the number of training epochs and the accuracy rate, i.e., a fraction of the number of samples with a damage pattern correctly identified over the total number of samples, for the case of the highest accuracy. A blue curve shows the average accuracy rate of the training data and a red curve is that of the cross-validation data. To reduce computation time, the average accuracy rate of the cross-validation data is calculated sparsely. When comparing two curves, the red curve decreases at the epoch size of 100 due to overfitting. Among the compared hyper-parameter combinations, the highest accuracy is achieved when there are three sensors, three components (only the translational acceleration component in the  $x$ -axis direction), the middle layer nodes (500, 250, 125), the sample length is 1 s, and the number of learning epochs is ninety. The cross-validation results at the hyper-parameter combination are shown in Table 1. The average accuracy rate is 88%.

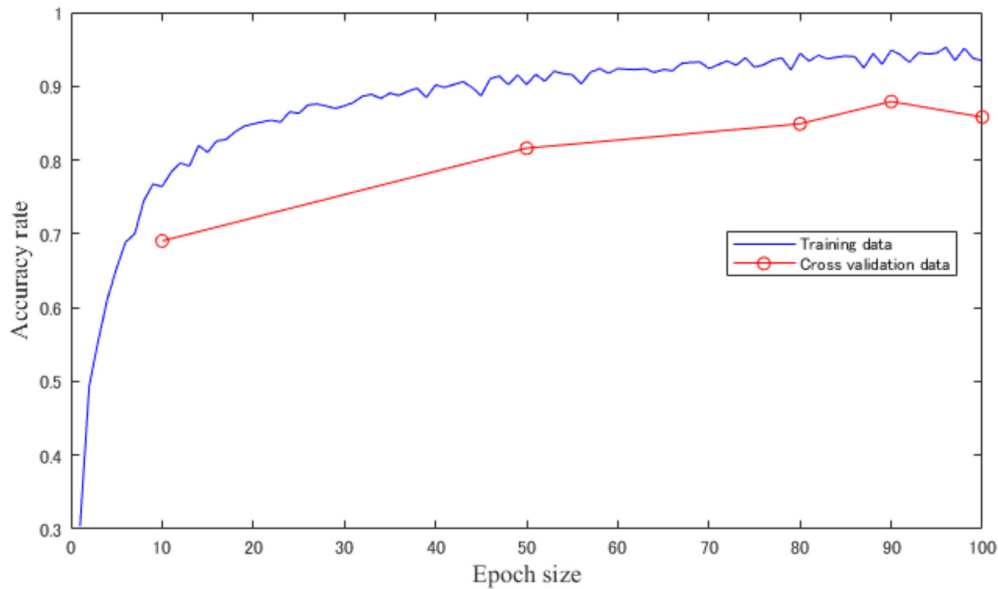


**Figure 4.** Relation between training epoch size and accuracy rates

**Table 1.** Cross-validation results with three sensors, one component, middle layers nodes (500, 250, 125), a sample length of 1 s, and 90 learning epochs.

		Damage pattern in experiment (true value)								Total
		D1	D2	D3	D4	D5	D6	D7	D8	
Cross validation result	D1	5099	1595	23	13	0	0	5	9	6744
	D2	1476	4987	6	27	0	0	3	7	6506
	D3	4	2	6532	7	18	6	0	0	6569
	D4	6	11	1	5919	36	15	257	133	6378
	D5	0	0	32	43	6195	448	10	1	6729
	D6	0	0	5	14	341	5969	87	20	6436
	D7	2	1	1	347	10	150	5795	502	6808
	D8	13	4	0	230	0	12	443	5928	6630
Total		6600	6600	6600	6600	6600	6600	6600	6600	52800
Accuracy rate		0.773	0.756	0.990	0.897	0.939	0.904	0.878	0.898	0.879

#### 4 METHOD TO DETECT SAMPLE DATA OF UNLEARNED DAMAGE PATTERNS

We consider the input space of the output layer node, and detect unlearned damage pattern data at Mahalanobis distance, as shown in Figure 5. Therefore, the detection criterion of the unlearned pattern is given as

$$\sqrt{(\mathbf{x}_n - \boldsymbol{\mu}^k)^T (\mathbf{X}^k)^{-1} (\mathbf{x}_n - \boldsymbol{\mu}^k)} > \theta_\alpha^k \text{ for all } k \text{ and } n (k = 1, 2, \dots, K; n = 1, 2, \dots, N) \quad (1)$$

where  $\mathbf{x}_n = (x_{n,1}, x_{n,2}, \dots, x_{n,K})^T$  is the input of the node in the output layer of sample  $n$ ;  $K$  is the number of learned damage patterns, and  $N$  is the number of test samples. Let  $\mathbf{x}_m^k = (x_{m,1}^k, x_{m,2}^k, \dots, x_{m,K}^k)^T$  ( $k = 1, 2, \dots, K; m = 1, 2, \dots, M_k$ ) be the input of the node in the output layer of the training sample  $m$  whose damage pattern is  $k$  (where  $M_k$  is the number of training samples of damage pattern  $k$ ), the component of the average value  $\boldsymbol{\mu}^k = (\mu_1^k, \mu_2^k, \dots, \mu_K^k)^T$  ( $k = 1, 2, \dots, K$ ) of  $\mathbf{x}_m^k$  is  $\mu_i^k = (1/M_k) \sum_{m=1}^{M_k} x_{m,i}^k$ , and the covariance matrix  $\mathbf{X}^k = (X_{ij}^k | i, j = 1, 2, \dots, K)$  has  $X_{ij}^k = (1/M_k) \sum_{m=1}^{M_k} (x_{m,i}^k - \mu_i^k)(x_{m,j}^k - \mu_j^k)$ . By setting the significance level  $\alpha$  of detection, and for each damage pattern, searching a sample of the  $\alpha$ -quantile point counted from a point where the Mahalanobis distance is far from the training data distribution, the threshold  $\theta_\alpha^k$  is defined by the distance.

#### 5 VERIFICATION OF DETECTION METHOD

We conducted a verification test of the proposed method to detect sample data of unlearned damage patterns. First, we used damage patterns D1 to D8 as training data, and new data were obtained by inverting the sensor location and sign of the measurement records as data of an unlearned damage pattern. As a result, all the 660 samples were detected as “unlearned” at the significance level  $\alpha = 5\%$ .

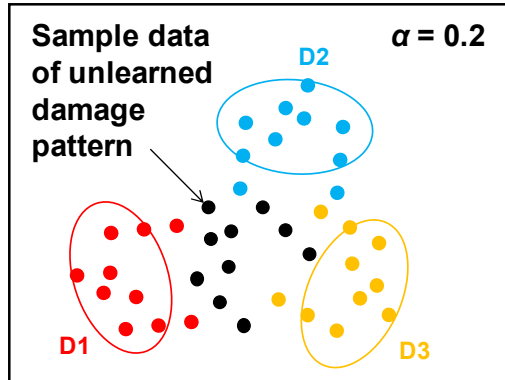


Figure 5. A method to detect sample data of unlearned damage patterns

A different dataset was also investigated; we used D1, D3, D4, D5, D6, and D8 as training data, and D7 as an unlearned damage pattern. It was observed that the samples detected as unlearned at  $\alpha = 5\%$  was 0 out of 660. Eleven of 660 were detected as unlearned at  $\alpha = 25\%$ . In the proposed method, classification accuracy will decrease when training data of learned damage patterns do not follow a normal distribution in the space of the input values of the output layer nodes. Therefore, it is necessary to improve the method.

## 6 CONCLUSIONS

The accuracy of damage pattern classification based on a deep NN was analyzed using response records of a shaking table experiment as training and test data. It was confirmed that the average accuracy rate was approximately 88% under the condition that the sample length was 1 s, which is about five times the natural period of the target structure, and the number of installed sensors was one per layer. We constructed a method of detecting unlearned damage pattern data using the Mahalanobis distance. The classification accuracy significantly varied depending on the learned damage pattern; therefore, improvement of the method is needed in the future.

## REFERENCES

- [1] Ferregut, C.M., Osegueda, R.A., and Ortiz, J. Artificial neural networks for structural damage detection and classification. *Proc. SPIE*. (1995) 2446:68–80.
- [2] Choi, M-Y. and Kwon, I-B. Damage detection system of a real steel truss bridge by neural networks. *Proc. SPIE*. (2000) 3988:295–306.
- [3] Chang, C.C., Chang, T.Y.P., and Xu, Y.G. Structural damage detection using an iterative neural network. *J. Intell. Mater. Syst. Struct.* (2000) 11:32–42.

Kazuya Oka, Kenta Watanabe, Masayuki Kohiyama, Takuzo Yamashita, Kazutoshi Matsuzaki, and Yuji Mori

- [4] Lee, J.J., Lee, J.W., Yi, J.H., Yun, C.B., and Jung, H.Y. Neural networks-based damage detection for bridges considering errors in baseline finite element models. *J. Sound Vib.* (2005) 280:555–578.
- [5] De Lautour, O.R. and Omenzetter, P. Prediction of seismic-induced structural damage using artificial neural networks. *Eng. Struct.* (2009) 31:600–606.
- [6] Derkevorkian, A., Hernandez-Garcia, M., Yun, H.-B., Masri, S.F., and Li, P. Nonlinear data-driven computational models for response prediction and change detection. *Struct. Control Health Monit.* (2015) 22:273–288.
- [7] Rafiei, M. H. and Adeli, H. A novel machine learning-based algorithm to detect damage in high-rise building structures. *Struct. Des. Tall Special Buildings* (2017) 26:1400. <https://doi.org/10.1002/tal.1400>.
- [8] Rafiei, M.H. and Adeli, H. A novel unsupervised deep learning model for global and local health condition assessment of structures. *Eng. Struct.* (2018) 156:598–607.
- [9] Abdeljaber, O., Avci, O., Kiranyaz, S., Gabbouj, M., and Inman, D.J. Real-time vibration-based structural damage detection using one-dimensional convolutional neural networks. *J Sound Vib.* (2017) 388:154–170.
- [10] Zhang, Y., Burton, H.V., Sun, H., and Shokrabadi, M. A machine learning framework for assessing post-earthquake structural safety. *Struct. Saf.* (2018) 72: 1–16.

## Parameter Estimation during Solidification of Metals based on Data Assimilation

Yukimi Oka<sup>\*</sup>, Munekazu Ohno<sup>\*\*</sup>, Tomohiro Takaki<sup>\*\*\*</sup>, Yasushi Shibuta<sup>\*\*\*\*</sup>, Kiyotaka Matsuura<sup>\*\*\*\*\*</sup>

<sup>\*</sup>Hokkaido University, <sup>\*\*</sup>Hokkaido University, <sup>\*\*\*</sup>Kyoto Institute of Technology, <sup>\*\*\*\*</sup>The University of Tokyo, <sup>\*\*\*\*\*</sup>Hokkaido University

### ABSTRACT

It is essential for production of casts with high quality to control the solidification microstructures. However, it is difficult to clarify the formation process of solidification microstructure in detail, because the solidification process is a multi-physics problem involving thermo-solutal diffusion and fluid dynamics. Moreover, it is generally not possible to directly observe the dynamics of solidification by experimental approaches. Therefore, computational studies have contributed to understanding of such a complicated solidification process and predicting of solidification microstructure. A phase-field method is a method of choice in simulating the dendrite structure, which is typical growth morphology in solidification of metals. In order to predict solidification microstructure precisely by the means of phase-field simulation, physical parameters must be determined accurately. Especially, solid-liquid interfacial energy and its anisotropy largely affect the morphology of the dendrite structure. Hence, it is indispensable to use accurate values of these interfacial properties. However, it is difficult and/or cumbersome to determine interfacial properties by means of experimental methods. Although calculation methods for interfacial properties based on molecular dynamics (MD) simulations have been developed, the application of these methods is limited to the equilibrium state. Also, it is not easy to calculate accurate values of interfacial energy and its anisotropy even by MD simulations. Therefore, it is very important to develop a reliable method for estimation of interfacial properties in both equilibrium and non-equilibrium states. In this study, data assimilation is utilized for the estimation of interfacial properties at the solid/liquid interface during solidification of metals. The data assimilation is a method based on Bayesian inference developed in the field of data science. In this study, the data assimilation is employed for estimation of interfacial properties of the phase-field simulation. The applicability of the data assimilation to the estimation of interfacial properties at the solid/liquid interface during solidification of metal is systematically investigated on the basis of the twin experiment.

## **CAE Simulation in OMRON Co. And My Idea about CAE Using “Big Data” and AI**

Hiroshi Okada\*

\*OMRON

### **ABSTRACT**

Omron Corp. has worked extensively to improve product development process utilizing CAE. However, the market requests are more demanding for higher quality, improved functionality, smaller dimension and appropriate delivery time. Moreover, the market is requesting Omron Corp. to develop the product which can be used safely with severe environmental impact. At first, I explain how Omron Corp. uses CAE for the many different field problems such as structural and thermal problems in the development process of our industrial products. Next, I will explain how Omron Corp. will extend CAE to make use of AI and Big Data Analytics. The extended CAE includes AI technology, especially Deep Learning with Neural Network, which can be used for the regression of complex design space (Big Data) generated by extensive parametric simulations. Last, I will explain how Omron Corp. will utilize the extended CAE for the future in order to satisfy the market requests.

## Computations of Fracture Mechanics Parameters for 3D Arbitrary Shaped Crack in Welded Joint and Functionally Graded Material

Hiroshi Okada<sup>\*</sup>, Tatsuro Ishizaka<sup>\*\*</sup>, Masahiro Ono<sup>\*\*\*</sup>, Yasunori Yusa<sup>\*\*\*\*</sup>

<sup>\*</sup>Tokyo University of Science, <sup>\*\*</sup>Tokyo University of Science, <sup>\*\*\*</sup>Tokyo University of Science, <sup>\*\*\*\*</sup>Tokyo University of Science

### ABSTRACT

In this presentation, the formulations and the computations of fracture parameters, such as the stress intensity factors and the energy release rates for 3D arbitrary shaped crack in welded joint and functionally graded material are discussed. Welded joints and functionally graded materials have common features such that the mechanical properties have continuous and discontinuous spatial variations. Furthermore, residual stresses generally develop in welded joints. Classical ways to compute the fracture parameters often assume the material to be homogeneous. The weld residual stresses are not assumed. In the present investigation, a series of related developments to perform realistic 3D fracture mechanics analyses have been carried out. First, the use of general finite element program with the quadratic tetrahedral element along with an automatic mesh generation technique based on the constrained Delaunay tessellation technique was proposed (Okada et al. [1]). Then, methodologies to compute the J and the interaction integrals (Daimon and Okada [2]) were presented. They are presently extended to the problems of welded joints (Nose et al. [3]). We assume that residual stresses are present but the prior strain histories are not known. Furthermore, mechanical properties have spatial variations. The key issues are in the treatments on additional terms arising due to the spatial changes of mechanical properties and the existence of residual stress. To make all the methodologies tractable for application engineers, only a general purpose finite element program with the automatic meshing technique is used. The J- and the interaction integral evaluations are carried out as their post processes by separate software. In the presentation, the discussions on the additional terms, their numerical treatments and their numerical results are presented. Acknowledgements: A part of present research was supported by JSPS (Japan Society for the Promotion of Science) Grant-in-Aid for Scientific Research (C) No.16K05988. The support is acknowledged. References: [1] H. Okada, H. Kawai, T. Tokuda, Y. Fukui, Fully automated mixed mode crack propagation analyses based on tetrahedral finite element and VCCM (virtual crack closure-integral method), *International Journal of Fatigue*, Vol. 50, pp. 33-39, 2013. [2] R. Daimon, H. Okada, Mixed-mode stress intensity factor evaluation by interaction integral method for quadratic tetrahedral finite element with correction terms, *Engineering Fracture Mechanics*, Vol. 115, pp. 22-42, 2014. [3] M. Nose, H. Amano, H. Okada, Y. Yusa, A. Maekawa, M. Kamaya, H. Kawai, Computational crack propagation analysis with consideration of weld residual stresses, *Engineering Fracture Mechanics*, Vol. 182, pp. 708-731, 2017.

## DES of Pulsatile Turbulent Flow Through a Double 90° Bend Pipe for Flow Analysis of an Automotive Exhaust System

Junichi Oki<sup>\*</sup>, Haruna Yanagida<sup>\*\*</sup>, Yukika Kuga<sup>\*\*\*</sup>, Ryo Yamamoto<sup>\*\*\*\*</sup>, Kazuhiro Nakamura<sup>\*\*\*\*\*</sup>,  
Hideaki Yokohata<sup>\*\*\*\*\*</sup>, Keiya Nishida<sup>\*\*\*\*\*</sup>, Yoichi Ogata<sup>\*\*\*\*\*</sup>

<sup>\*</sup>Hiroshima University, <sup>\*\*</sup>Mazda Motor Corporation, <sup>\*\*\*</sup>Hiroshima University, <sup>\*\*\*\*</sup>Mazda Motor Corporation,  
<sup>\*\*\*\*\*</sup>Mazda Motor Corporation, <sup>\*\*\*\*\*</sup>Mazda Motor Corporation, <sup>\*\*\*\*\*</sup>Hiroshima University, <sup>\*\*\*\*\*</sup>Hiroshima  
University

### ABSTRACT

The present study focuses on pulsatile turbulent flow that is encountered in an exhaust system of an internal combustion engine. Whereas most of numerical studies related to exhaust flows have used Reynolds-averaged Navier-Stokes modeling even though such a flow is highly unsteady [1,2], our numerical simulation is performed using detached-eddy simulation (DES) [3] capable of calculating with a coarser spatial resolution close to the wall compared with large-eddy simulation approach. The flow configuration and condition are determined from our pulsatile flow rig with a square-sectioned S-shaped test section comprising a double 90° bend. The inlet boundary condition for the velocity and the outlet boundary condition for the pressure are respectively set based on the measured data with a hot-wire anemometer and a piezoelectric pressure sensor, resulting in a Reynolds number of 36,400 and a Womersley number of 59.9. The numerical result is validated against the experimental data obtained from the phase-locked stereo PIV conducted in the pipe cross sections located downstream of the bends. The comparisons show good agreement between the numerical and experimental results in terms of the phase-averaged secondary and axial velocities. The DES can capture the Dean-type secondary vortices downstream of the first bend and the Lyne-type vortices developing through the double bend. This implies that our numerical simulation is capable of accurately predicting the development process of the turbulent flow through the straight pipe as well as the bend under the pulsatile condition, because the inflow velocity distribution to the bend plays a significant role in the secondary flow formation. This study improves the understanding of pulsatile turbulent flow structures in bends through the computation, and confirms the capability of the DES approach for industrial application. [1] Jeong S.-J. (2014) A full transient three-dimensional study on the effect of pulsating exhaust flow under real running condition on the thermal and chemical behaviour of closed-coupled catalyst. *Chemical Engineering Science*, Vol. 117, pp. 18-30. [2] Rao H.K.S., S. Raviteja, Kumar G.N. (2017) Computational Analysis of Unsteady Flow in Turbine Part of Turbocharger. In: Saha A., Das D., Srivastava R., Panigrahi P., Muralidhar K. (eds) *Fluid Mechanics and Fluid Power – Contemporary Research. Lecture Notes in Mechanical Engineering*. Springer, New Delhi. [3] Spalart P.R., Jou W-H., Strelets M., Allmaras S.R. (1997) Comments on the feasibility of LES for wings, and on a hybrid RANS/LES approach. First AFOSR International Conference on DNS/LES.

## **3D Vertex Modeling and Computational Simulations of Multicellular Dynamics**

Satoru Okuda\*

\*PRESTO, Japan Science and Technology Agency

### **ABSTRACT**

Multicellular dynamics have a key role in determining the macroscopic behaviors of living tissues in development, homeostasis, and disease. Such multicellular dynamics emerge from the integration of mechanical cell behaviors in three-dimensional (3D) space, such as cell deformation, movement, division, and apoptosis. Typical examples of 3D multicellular dynamics are epithelial deformations in morphogenesis and collective cell migration in cancer metastasis. However, while such 3D multicellular dynamics is fundamental to general soft tissue dynamics, little is about how individual cell behaviors are spatiotemporally coordinated in the macroscopic level. To simulate such 3D multicellular dynamics, we have developed a versatile 3D vertex model framework. Here, we show the mathematical framework of the model and its applications to morphogenesis.

## Mechanism of Strain Softening Predicted by an Extended Flory-Rehner Model for Swollen Elastomers

Dai Okumura<sup>\*</sup>, Shoji Shimizu<sup>\*\*</sup>, Takafumi Mano<sup>\*\*\*</sup>

<sup>\*</sup>Osaka University, <sup>\*\*</sup>Nagoya University, <sup>\*\*\*</sup>Nagoya University

### ABSTRACT

In this study, we investigate the ability of two scaling exponents to describe swelling-induced strain softening of elastomers. Two scaling exponents are included in the extended version of the Flory-Rehner (F-R) model [1], and are introduced into elastic strain energy functions that are separated into deviatoric and volumetric components [2]. The two scaling exponents are used to adjust the swelling effects on the Young's modulus and osmotic pressure of swollen elastomers, resulting in the ability to describe swelling-induced strain softening under uniaxial and biaxial deformations [2]. Swelling-induced strain softening can be related with strain localization followed by swelling-induced rupture. In Gee's experiments [3], natural rubbers exhibited swelling-induced rupture when a small extension was applied in good solvents. This tendency was successfully predicted when the two scaling exponents were determined based on experiments [2]. To investigate the detailed mechanism, mechanical properties such as the Young's modulus and Poisson's ratio are explicitly derived from linear perturbation analysis of the extended F-R model. This derivation is performed by considering an arbitrary deformation state. The onset point of swelling-induced strain softening are analysed using the combination of the explicit expressions of the mechanical properties. It is found that swelling-induced strain softening can be caused with negative Poisson's ratio, which appears under deformation states at equilibrium swelling and that it depends on the combination of the two scaling exponents. References [1] Flory, P.J., Rehner, J., "Statistical mechanics of cross-linked polymer networks II. swelling", *The Journal of Chemical Physics*, Vol.11, page 521-526 (1943). [2] Okumura, D., Kondo, A., Ohno, N., "Using two scaling exponents to describe the mechanical properties of swollen elastomers", *Journal of the Mechanics and Physics of Solids*, Vol.90, page 61-76 (2016). [3] Gee, G., "The interaction between rubber and liquid. X. some new experimental tests of a statistical thermodynamic theory of rubber liquid systems", *Transactions of Faraday Society*, Vol.42, page B033-B044 (1946).

## **A Marginalized Unscented Kalman Filter for Efficient Parameter Estimation with Applications to Finite Element Models**

Audrey Oliver\*, Andrew Smyth\*\*

\*Columbia University, \*\*Columbia University

### **ABSTRACT**

This paper focuses on the problem of combined state/parameter estimation in dynamical systems with many degrees of freedom, for instance finite element models, using measured data from the system and nonlinear Bayesian filtering techniques for the estimation. An efficient nonlinear Kalman filtering technique is developed (marginalized UKF), based on a combination of extended Kalman filtering for state estimation and unscented filtering for parameter learning. While extended filtering requires computations of Jacobians, which might become cumbersome in large dimensional cases, unscented filtering is a gradient-free method that requires only function evaluations of the forward problem and could thus be combined with an external FE software. However, the number of required function evaluations grows linearly with the number of states, rendering this approach computationally cumbersome when considering FE models with many degrees-of-freedom. Instead, the algorithm presented herein implements the principle of marginalization to the unscented transform to conveniently combine extended and unscented filtering. The algorithm can then take advantage of the fact that Jacobians of the system equations with respect to the dynamic states, required in extended Kalman filtering, can be easily related to outputs of the finite element analysis such as the tangent stiffness matrix of the finite element model, thus greatly facilitating the use of extended filtering with respect to the dynamic states. In this talk we will first review basics of Bayesian filtering for combined state/parameter estimation, then we will present the specifics of the marginalized UKF and how it can be used to solve for inverse problems in finite element analysis. We will then demonstrate the applicability of this algorithm to perform efficient parameter estimation using simulated data from different types of finite element models. Systems which exhibit linear or nonlinear behaviors with respect to both the states and/or the parameters will be considered.

## BDDC Methods for the Simulation of High Temperature Superconductors

Marc Olm<sup>\*</sup>, Santiago Badia<sup>\*\*</sup>, Alberto Martín<sup>\*\*\*</sup>

<sup>\*</sup>Technical University of Catalonia, CIMNE, <sup>\*\*</sup>Technical University of Catalonia, CIMNE, <sup>\*\*\*</sup>Technical University of Catalonia, CIMNE

### ABSTRACT

In this work, we present numerical results using BDDC methods for preconditioning the systems arising from finite element discretizations of the time-domain quasi-static approximation of Maxwell's equations with Nédélec (or edge) elements of arbitrary order. First, we show the scalability of the proposed schemes on a set of academical linear problems with a highly scalable implementation based on overlapped multilevel task implementation in FEMPAR. Next, in order to model the behaviour of High Temperature Superconductors (HTS), resistivity is assigned a stiff power law depending on the magnetic field itself, introducing a strong nonlinearity. On the other hand, a constant resistivity value is kept in a large dielectric region, which completely surrounds the superconducting device. A h-adaptive meshing technique customized for Nédélec elements leads to a smart mesh coarsening in the dielectric region, where no results of interest are found but nevertheless it allows us to impose realistic external conditions far away from the HTS sample. Then the problem is linearized with a Newton-Raphson scheme, and nonlinear convergence is boosted with a line search technique. Finally, our BDDC preconditioners are composed with Krylov-subspace iterative methods to solve the linearized problems arising at every nonlinear iteration. References [1] S. Badia, A. Martín and J. Principe. A Highly Scalable Parallel Implementation of Balancing Domain Decomposition by Constraints. *SIAM Journal on Scientific Computing*, 36(2):C190–C218, 2014. doi:10.1137/130931989 [2] M. Olm, S. Badia, and A. Martín. Simulation of high temperature superconductors and experimental validation. arXiv:1707.09783 [physics], 2017.

## **A Blended Force-based Atomistic-to-continuum Coupling Method for Multilattice Materials**

Derek Olson\*, Xingjie Li\*\*

\*Rensselaer Polytechnic Institute, \*\*University of North Carolina--Charlotte

### **ABSTRACT**

Atomistic-to-continuum coupling methods are a general class of methods which combine nonlocal atomistic models of materials with a local continuum mechanics description. Recently, the blended-force based quasicontinuum method, which operates by smoothly blending atomistic and continuum forces over a blending (or transition region), has been proposed and analyzed for general multilattice crystals. In this talk, we survey recent developments in applying the force-based quasicontinuum method to 2D materials for which out-of-plane behavior including bending is incorporated into the model. This results in changes to both the formulation of the method and the analysis.

## On the Three-dimensional Simulation of Endocytosis

Yannick A. D. Omar<sup>\*</sup>, Amaresh Sahu<sup>\*\*</sup>, Kranthi K. Mandadapu<sup>\*\*\*</sup>, Roger A. Sauer<sup>\*\*\*\*</sup>

<sup>\*</sup>RWTH Aachen University, <sup>\*\*</sup>University of California, Berkeley, <sup>\*\*\*</sup>University of California, Berkeley, <sup>\*\*\*\*</sup>RWTH Aachen University

### ABSTRACT

During endocytosis, an important mode of intercellular trafficking, cells form invaginations by internalizing parts of the plasma membrane to transport cargo into the cell. Endocytic events are mediated through a protein coat, which attaches to the outer membrane of the cell. The protein's structure induces curvature into the cell membrane, which thus forms an invagination and subsequently a bud which carries the material to be transported. When the neck of the bud is sufficiently constricted, scission occurs at the bud's neck and a vesicle is formed. Lipid bilayers are usually modeled as liquid shells which do not have any shear resistance in their in-plane directions (Sahu et al., 2017). There are few non-axisymmetric continuum studies on lipid bilayers available and axisymmetry has also commonly been assumed for continuum simulations of endocytosis. In contrast, we will review a recently developed, three-dimensional, C1-continuous Finite Element formulation (Sauer et al., 2017) with which non-axisymmetric simulations of endocytosis have been conducted. Further, we will discuss potential numerical pitfalls of lipid bilayer simulations. For endocytosis, we find that axisymmetric solutions in the high tension regime can only be regarded as metastable states. We show that small perturbations, either of numerical or physically-motivated type, are sufficient to trigger nonaxisymmetric shapes. Furthermore, we identify several parameters that determine the stability of axisymmetric solutions such as the surrounding tension, viscous dissipation, and shape of the protein coat. In the low surface tension regime, we find, similar as in the axisymmetric setup, closed buds with a constricted neck. However, the newly obtained shapes show a bud that is twisted relative to the flat lipid bilayer. Additionally, we present a newly observed transition from constricted buds to elongated tubes at relatively low surface tensions. These newly obtained shapes will be put in perspective using experimental data. Based on that comparison, the physical and physiological implications of nonaxisymmetry in lipid bilayers, such as the existence of a spontaneous Gaussian curvature, will be presented. Finally, we will critically evaluate the material formulation, in particular with respect to the protein coat model, and will discuss alternative modeling approaches. Sauer, R. A., Duong, T. X., Mandadapu, K. K., & Steigmann, D. J. (2017). A stabilized finite element formulation for liquid shells and its application to lipid bilayers. *Journal of Computational Physics*, 330, 436-466. Sahu, A., Sauer, R. A. & Mandadapu, K. K. (2017). Irreversible thermodynamics of curved lipid membranes. *Physical Review E* 96, 042409.

## Computing Stochastic Stress Intensity Factors as a Result of Uncertain Material Properties by Generalized Polynomial Chaos

Netta Omer<sup>\*</sup>, Zohar Yosibash<sup>\*\*</sup>

<sup>\*</sup>Afeka College of Engineering, Tel-Aviv, Israel, <sup>\*\*</sup>Tel Aviv University, Ramat Aviv, Israel

### ABSTRACT

Realistic material properties, as the Young modulus  $E$  and Poisson ratio  $\nu$  (isotropic materials), are measured by experimental observations and are inherently stochastic. Having their stochastic representation  $E(\omega)$  or  $\nu(\omega)$  where  $\omega$  is a random variable, we investigate the elastic solution of the stochastic elasticity system in the vicinity of a crack tip. An efficient method is presented to compute the stress intensity factors (SIF) and eigenfunctions by generalized polynomial chaos (GPC) [1], at a fraction of the computational cost compared to Monte Carlo simulations. We show that the stochastic asymptotic displacements are compound of a series of stochastic eigenpairs (with deterministic eigenvalues and stochastic eigenfunctions) multiplied by a stochastic polynomial representation of the Edge Stress Intensity Functions (ESIFs). The stochastic eigenpairs are computed explicitly and the stochastic ESIFs are computed numerically using the Quasi Dual Function Method (QDFM). The stresses, on the other hand, are represented in an asymptotic series so that the stochastic behavior is only manifested in the SIF. The GPC is used to compute the stochastic SIF from deterministic finite element solutions. As an example we consider either the stochastic Young modulus or the Poisson ratio to be given as random variable with a normal distribution. We present numerical examples of the computation of the stochastic eigenpairs, ESIFs and the SIF. These functions are obtained using deterministic finite element analyses [2] as a series of Hermite polynomials in the stochastic space. Monte Carlo simulations are used to demonstrate the efficiency of the proposed methods. References [1] Dongbin Xiu, Numerical methods for stochastic computations: A spectral method approach, Princeton University Press, 2010. [2] Neta Omer and Zohar Yosibash, On the path independency of the point-wise J-integral in three-dimensions, Int J Fracture, 136, pp. 1 - 36, 2005

## An Imaged-based Fluid Structure Coupling Investigation on the Hemodynamic Origin of Intraluminal Thrombus Formation

ChiWei Ong<sup>\*</sup>, ChoonHwai Yap<sup>\*\*</sup>, Foad Kabinejadian<sup>\*\*\*</sup>, Fei Xiong<sup>\*\*\*\*</sup>, Fangsen Cui<sup>\*\*\*\*\*</sup>, Pei Ho<sup>\*\*\*\*\*</sup>, HwaLiang Leo<sup>\*\*\*\*\*</sup>

<sup>\*</sup>Biofluid Mechanics Research Laboratory, Department of Biomedical Engineering, National University of Singapore, Singapore, <sup>\*\*</sup>Cardiovascular Biomechanics and Ultrasound Laboratory, Department of Biomedical Engineering, National University of Singapore, Singapore, <sup>\*\*\*</sup>Department of Biomedical Engineering, Tulane University, New Orleans, USA, <sup>\*\*\*\*</sup>Biofluid Mechanics Research Laboratory, Department of Biomedical Engineering, National University of Singapore, Singapore, <sup>\*\*\*\*\*</sup>Institute of High Performance Computing, A\*STAR, Singapore, Singapore, <sup>\*\*\*\*\*</sup>Department of Cardiac, Thoracic & Vascular Surgery, National University Health System, Singapore, <sup>\*\*\*\*\*</sup>Biofluid Mechanics Research Laboratory, Department of Biomedical Engineering, National University of Singapore, Singapore

### ABSTRACT

Intraluminal thrombus (ILT) has been shown to be associated with the growth of aneurysm. However, the underlying factors that generate ILT are still unclear. We hypothesize that formation of ILT under the influence of unusual and unfavorable hemodynamic patterns is subjected to the patient-specific geometry. Three cases of thoracic aortic aneurysms (TAA) were reconstructed using retrospective CT images in the present study. Only one case developed ILT, and for this case, simulation was conducted with the removal of ILT to understand the hemodynamics origin of the ILT formation. It was observed in ILT case that an unusual and interesting stationary vortex near the aortic isthmus at the proximal end of the aneurysm, not observed for the other cases. This vortex exerted elevated stresses on blood particles and trapped them in recirculation, before dispersing them into the ILT locality during early diastole. The exposure of the aortic wall to blood elements under fluid-induced stress may be one factor that contribute to the formation of the ILT. Further simulations were performed to understand the factors leading up to the formation of this stationary vortex. It was found that the sharp curvature at the aortic isthmus was the primary factor causing this stationary vortex while reduction of vascular curvature prevented its formation. Reduction of the size of the aneurysm delayed the vortex formation, and shortened the duration of the vortex's existence. On the other hand, our study showed that shifting the location of aneurysm distally did not significantly alter the recirculation and particle dispersion dynamics, although it relocated the vortex to the proximal end of aneurysm.

## Development of a Fully Parallelized Code for Phase Field Simulation of Microstructure Evolution in Solid Oxide Fuel Cell Electrodes

Junya Onishi<sup>\*</sup>, Zhenjun Jiao<sup>\*\*</sup>, Naoki Shikazono<sup>\*\*\*</sup>

<sup>\*</sup>Institute of Industrial Science, The University of Tokyo, <sup>\*\*</sup>Institute of Industrial Science, The University of Tokyo,  
<sup>\*\*\*</sup>Institute of Industrial Science, The University of Tokyo

### ABSTRACT

Solid oxide fuel cell (SOFC) has gathered much attention as a next-generation power generation system because of its high conversion efficiency, low emissions, fuel flexibility, and so on. SOFCs consist of a porous cathode and anode electrodes, and a solid oxide electrolyte, which is used as a conductor of oxygen ions. The use of the solid oxide electrolyte requires very high operating temperature, typically between 500 and 1000 degree Celsius. As a result, capillary-driven microstructure evolution, such as grain growth and coarsening of material particles, is observed at both electrodes. It is of critical importance to predict this microstructure evolution because it highly influences the performance of SOFCs, through the density of triple phase boundary and the tortuosity of each phase. To predict the long-time behavior of microstructure evolution observed in a typical SOFC anode, which is composed of nickel phase and yttria-stabilized zirconia, some of the authors have developed a numerical model based on the phase field approach and have successfully simulated the morphological change of the nickel phase [Z. Jiao and N. Shikazono, Journal of The Electrochemical Society, 161 F577-F582 (2014)]. However, the total period achieved in their simulation is not sufficiently long for the purpose of assessing the performance degradation in practical applications. Furthermore, it is not clear if the computational grid is fine enough to resolve all relevant structures of grains and particles. These limitations are mainly due to the programming model and the numerical algorithm used in their code. In this research, we develop a highly scalable code for simulating the large-scale and long-time behavior of microstructure evolution with sufficient grid resolution. To do this, firstly, we employ a finite difference method to discretize the governing equations, instead of a spectral method adopted in the previous study. This employment of the finite difference method is intended to avoid communication overhead in large-scale parallel computation. Next, we introduce a hybrid programming model (MPI and OpenMP) for parallelization. In the parallelization, the computational domain is decomposed into sub-domains, and each sub-domain is assigned to one MPI process. To reduce the communication overhead, we implement a communication hiding algorithm for exchanging halo data and evaluate its impact on the parallel performance. Additionally, in the thread parallelization, we investigate the effects of decomposition strategy, including block decomposition and cyclic decomposition. Currently, it is confirmed that the developed code achieves 95% weak scaling parallel efficiency on 32,768 K-computer nodes.

## Element-wise Selective Smoothed Finite Element Method for 10-node Tetrahedral Elements in Large Deformation Problems

Yuki Onishi<sup>\*</sup>, Ryoya Iida<sup>\*\*</sup>, Kenji Amaya<sup>\*\*\*</sup>

<sup>\*</sup>Tokyo Institute of Technology, <sup>\*\*</sup>Tokyo Institute of Technology, <sup>\*\*\*</sup>Tokyo Institute of Technology

### ABSTRACT

A novel 10-node tetrahedral (T10) FE formulation that overcomes the shear/volumetric locking, spurious zero-energy modes, pressure checkerboarding, and reaction force oscillation issues is proposed. The proposed method utilizes the selective reduced integration technique and the smoothed finite element method (S-FEM)[1] with T10 element subdivision[2]. In contrast to the conventional Selective S-FEMs[3], this method applies the strain smoothing technique only within each element and thus never across the elements. Each T10 element is divided into 12 subelements of 4-node tetrahedra (T4) with 1 dummy node at the element center framed by 30 edges. The deformation gradient of each subelement is then given in the manner of the standard T4 element. The hydrostatic stress on each element is derived with the weighted mean of all the 12 subelements. On the other hand, the deviatoric stress on each subelement is derived with the edge-based S-FEM from subelements to edges followed by the cell-based S-FEM from edges to subelements. The stress integration is then performed in the manner of the selective reduced integration to obtain the nodal internal force. This formulation is regarded as an element-wise S-FEM; therefore, it is capable to be introduced as a user-defined add-on element of the general-purpose FE codes such as ABAQUS in contrast to the conventional S-FEMs. Moreover, this formulation is a purely displacement-based formulation, which means it can be directly applied to not only static implicit analyses but also dynamic implicit/explicit analyses. Several example analyses including complex shapes, large deformation, nearly incompressible materials and contact problems reveal that our method has superior accuracy and stability in comparison to the conventional T10 formulations. [1] G.R. Liu et al., &quot;Smoothed Finite Element Methods&quot;, CRC Press. [2] J.T. Ostien et al., &quot;A 10-node composite tetrahedral finite element for solid mechanics&quot;, IJNME, 2016. [3] Y. Onishi et al., &quot;A locking-free selective smoothed finite element method using tetrahedral and triangular elements with adaptive mesh rezoning for large deformation problems&quot;, IJNME, 2014.

## Scientific Workflow Tailored for Capacity Computing of Product Design

Kenji Ono\*, Tomohiro Kawanabe\*\*

\*Research Institute for Information Technology, Kyushu-University, \*\*Advanced Institute for Computational Science,  
RIKEN

### ABSTRACT

Design paradigm of industrial products has been changing along with the progress of computer power and computational methodologies. The capacity computing is one of the effective approach to exploit vast amount of distributed parallel computational resources, which drastically changes the design paradigm of industrial products, however, demanding the mechanism of the efficient management and execution for many simulation cases to be performed. For specific purpose of design, e.g., the robust design or the optimization, engineers explore the solution space formed from the obtained simulation results and try to find suitable parameters. Scientific workflow system is the promising and essential infrastructure to proceed the capacity computing and is providing the function such as the description of flow of tasks on web user interface, automation of task flow, reuse of the workflow, management of tasks, control of task on a remote machine, resilience from errors, tracking of task, and provenance. This paper introduces the novel workflow system developed with the modern information technology widely used and its application examples.

## Membrane Rotors: from Euler Vorticity Dynamics to Quasi-geostrophic Flows

Naomi Oppenheimer<sup>\*</sup>, Michael Shelley<sup>\*\*</sup>

<sup>\*</sup>Flatiron Institute at the Simons Foundation, <sup>\*\*</sup>Flatiron Institute at the Simons Foundation

### ABSTRACT

We show that the dynamics of rotors embedded in a quasi 2D membrane exhibit a power law transition in their interactions, from Euler fluid at small distances ( $1/r$ ), to quasi-geostrophic at large distances ( $1/r^2$ ). We derive a Hamiltonian for a discrete system of rotors and describe the conserved quantities. We develop a coarse-grained description for a density field of rotors. Theory and simulations for both the discrete and the continuous cases are presented. Although the membrane rotors are both driven and embedded in a viscous system, they show strong resemblance to vorticity in an ideal fluid. We discuss the analogies and the differences. references: P. Lenz, J.-F. Joanny, F. Ju ?licher, and J. Prost, 2004. Eur. Phys. J. E 13, 379–390 D. Cordoba, M A. Fontelos, A. M. Mancho, and J. L. Rodrigo, 2005. PNAS 102, 5949-5952



## Development of hp-Adaptive H(curl)-conforming Approximation Spaces for Photonic Waveguide Analysis

Francisco Orlandini<sup>\*</sup>, Philippe Devloo<sup>\*\*</sup>, Hugo Figueroa<sup>\*\*\*</sup>

<sup>\*</sup>FEEC - State University of Campinas, <sup>\*\*</sup>FEC - State University of Campinas, <sup>\*\*\*</sup>FEEC - State University of Campinas

### ABSTRACT

A hierarchical strategy for creating H(curl)-conforming elements is introduced in the context of a Finite Element Method (FEM) scheme for modal analysis of photonic waveguides. The hierarchical H(curl)-conforming elements are used for the transversal component of the electric field, coupled with scalar H(1) elements for its longitudinal component. The Nédélec elements of the first kind were chosen for this work, and the easy integration with p-adaptivity schemes motivated the hierarchical construction of the FE basis. The application of hp-adaptivity schemes leads to a reduction of the computational effort, still obtaining high accuracy in the dispersion parameters with a significant decrease in the resultant generalized eigenvalue problem size. Curved geometries are dealt with using the Piola mapping, allowing the analysis of complex intricate geometries without increase of the computational effort, since both the basis functions and their curl are calculated directly in the reference element. Since the Nédélec elements naturally allow the analysis of inhomogeneous waveguides and the precise imposition of tangential boundary conditions, the present scheme is able to deal with the complex geometries and the interfaces between materials with contrasting properties present in the field of photonic waveguides. Different numerical examples in increasing complexity are used to demonstrate the features of the strategy, and finally an example with a Photonic Crystal Fiber illustrates the accuracy and the generalized eigenvalue problem size when dealing with a scenario requiring hp-adaptivity for high precision on the dispersion parameters.

## Conservative Corrected FEM for Free Surface Frictional Flows

Pablo Ortiz<sup>\*</sup>, Jorge Molina<sup>\*\*</sup>

<sup>\*</sup>University of Granada, Spain, <sup>\*\*</sup>University of Granada, Spain

### ABSTRACT

Abstract Simulation of natural flows requires a proper numerical approach for the dynamics on the dry–wet interface, avoiding spurious residuals during front propagation and computing proper celerity of the wavefront. Errors due to mass and momentum imbalances during interface propagation are associated with the method employed in partially wet cells, with the criteria to specify wet or dry computational cells, and with the treatment of terms coming from correction procedures. In recent years we introduced a finite element model to simulate shallow flows with dry fronts (e.g.[1]), extending the formulation to flows coupled with erodible–non erodible sediment interfaces [2]. The method is developed by integrating a high order continuous finite element procedure with a conservative sign-preserving correction. Corrected continuous model has an inherent solution for the motion of interfaces, and does not need extensive modifications to compute flooding and evolutionary beds. The incorporation of relevant sources could produce high order conservation errors in the solution by standard flux correction procedure. In this work we present an extended conservative finite element method based on flux limiters with improved conservation properties after correction. We introduce applications of the procedure to severe frictional flows, such as experiments of dam–break flow type problems over erodible and non–erodible beds, and scrutinize propagation and conservation properties of the improved corrected method. Acknowledgements This work was supported by the MICIIN Grant #BIA-2015-64994-P (MINECO/FEDER) References [1] P.Ortiz, “Non oscillatory continuous FEM for transport and shallow water flows”, *Comput. Methods Appl. Mech. Engrg.*, 223-224, 55–69 (2012). [2] P. Ortiz, J. Anguita, M. Riveiro, “Free surface flows over partially erodible beds by a continuous finite element method”, *Environ. Earth Sci.*, 74, 7357–7330 (2015).

## **The Virtual Element Decomposition: A New Paradigm for Developing Convergent and Stable Meshfree Galerkin Methods**

Alejandro Ortiz-Bernardin\*

\*Universidad de Chile

### **ABSTRACT**

In the numerical solution of partial differential equations, meshfree Galerkin methods are numerical methods that use a cloud of nodes for domain discretization. Smooth nonpolynomial basis functions are constructed using this nodal discretization. Even though these methods do not need an underlying mesh for construction of the nodal basis functions, they require a mesh to perform the numerical integration of the Galerkin weak form integrals. Due to the nonpolynomial character of the meshfree nodal basis functions, there exist inaccuracies in the numerical integration that affect the consistency and stability of the method. This work presents a new paradigm for developing consistent and stable meshfree Galerkin methods: via the virtual element decomposition, the numerical integration issue is tackled in such a way that consistency and stability of the numerical solution are ensured by construction. Linear and quadratic consistency will be discussed along with new possibilities for developing consistent and stable nodal integration techniques. Some numerical examples are presented to demonstrate the performance of the method.

## Universal Fragment Descriptors for Predicting Properties of Inorganic Crystals

Corey Oses<sup>\*</sup>, Olexandr Isayev<sup>\*\*</sup>, Cormac Toher<sup>\*\*\*</sup>, Eric Gossett<sup>\*\*\*\*</sup>, Alexander Tropsha<sup>\*\*\*\*\*</sup>,  
Stefano Curtarolo<sup>\*\*\*\*\*</sup>

<sup>\*</sup>Duke University, <sup>\*\*</sup>University of North Carolina at Chapel Hill, <sup>\*\*\*</sup>Duke University, <sup>\*\*\*\*</sup>Duke University,  
<sup>\*\*\*\*\*</sup>University of North Carolina at Chapel Hill, <sup>\*\*\*\*\*</sup>Duke University

### ABSTRACT

Although materials discovery has historically been driven by a laborious trial-and-error process, knowledge-driven materials design can now be enabled by the rational combination of Machine Learning methods with materials databases. Here, data from the AFLOW repository for ab initio calculations [1] is combined with Quantitative Materials Structure-Property Relationship models to predict important properties: metal/insulator classification, band gap energy, bulk/shear moduli, Debye temperature, and heat capacities. The accuracy of the predictions compares well with the quality of the training data for virtually any stoichiometric inorganic crystalline material, as well as with the available thermo-mechanical experimental data. The universality of the approach is attributed to the construction of the descriptors: Property-Labeled Materials Fragments [2]. While the models are trained on the full suite of properties available in the AFLOW repository, the predictions require only minimal structural input, allowing straightforward implementations of simple heuristic design rules. Access to these models and their predictions is streamlined through the development of an open RESTful API, available online at [aflow.org/aflow-ml](http://aflow.org/aflow-ml) [3], facilitating easy integration into any application workflow. [1] C. Toher, C. Oses, et al., The AFLOW Fleet for Materials Discovery, submitted arXiv:1712.00422 (2017). [2] O. Isayev, C. Oses, C. Toher, E. Gossett, S. Curtarolo, and A. Tropsha, Universal fragment descriptors for predicting properties of inorganic crystals, Nature Communications 8, 15679 (2017). [3] E. Gossett, C. Toher, C. Oses, O. Isayev, F. Legrain, F. Rose, E. Zurek, J. Carrete, N. Mingo, A. Tropsha, and S. Curtarolo, AFLOW-ML: A RESTful API for machine-learning predictions of materials properties, submitted arXiv:1711.10744 (2017).

## **Spatial-Temporal Nonlocal Homogenization Model for Transient Wave Propagation in Periodic Viscoelastic Composites**

Caglar Oskay\*, Ruize Hu\*\*

\*Vanderbilt University, \*\*Vanderbilt University

### **ABSTRACT**

Wave propagation in manufactured composite materials has received increasing research interest over the past decade due to the opportunities for achieving favorable dynamic properties within targeted frequency ranges (e.g., acoustic band gaps). Phononic crystals and acoustic metamaterial demonstrate significant potential in many novel engineering applications, such as cloaking, acoustic diode and blast mitigation. These materials exhibit unique wave propagation and attenuation patterns possible through the design of the microstructure and constituent material properties. It has been recently recognized that employing viscoelastic materials could significantly expand the possibilities for these materials by leveraging the interactions between material damping and heterogeneity induced dispersion, such as shifting the stop band to lower frequencies and enhancing wave attenuation. We present a spatial-temporal nonlocal homogenization model for transient wave propagation in composites accounting for wave dispersion and attenuation due to material heterogeneity and damping. The proposed model is formulated through asymptotic homogenization with higher order corrections incorporated to extend the applicability of the homogenization theory to shorter wavelength regime. A homogenization model that is nonlocal in both space and time is consistently derived with all model parameters directly computed from the microstructure equilibrium. A reduced order model is then proposed for efficient transient wave propagation analysis. The reduced model retains the dispersive character of the original nonlocal model through the effective stiffness tensor. A Hybrid Laplace Transform/Isogeometric Analysis (HLT/IGA) is developed to solve the macroscale momentum balance equation, which provides high convergence rate for high frequency wave propagation simulation. Transient wave propagation in two-dimensional domain with periodic elastic and viscoelastic microstructures is investigated and the proposed models were verified against direct numerical simulations. The key contributions of our work are: (1) the proposed model captures the wave dispersion in the first pass band and stop band; (2) all the model parameters are computed directly from the microscale equilibrium as an off-line process.

## **Strain-Rate and Temperature Effects in Ductile Damage and Element Removal Threshold and Its Influence in FEM Orthogonal Cutting Simulations**

Juan Camilo Osorio Pinzon\*, Juan Pablo Casas Rodriguez\*\*, Sepideh Abolghasem\*\*\*, Edgar Alejandro Marañón Leon\*\*\*\*, Niyireth Alicia Porras Holguin\*\*\*\*\*

\*Universidad de los Andes, \*\*Universidad de los Andes, \*\*\*Universidad de los Andes, \*\*\*\*Universidad de los Andes, \*\*\*\*\*Universidad de los Andes

### **ABSTRACT**

Orthogonal cutting processes for ductile materials imposes severe plastic deformation, which involves ductile material failure at high strain-rates and the accompanying temperature rise. Plastic constitutive model parameters, ductile damage initiation parameters, damage evolution and damage threshold are directly affected by the complicate interactions among the thermomechanical conditions during the cutting process. During FEM simulation element removal threshold and damage threshold are needed to perform an accurate cutting simulation taking into account plastic, thermodynamic and damage effects in the workpiece, since reasonable parameters estimation can potentially lead to reliable solutions for cutting force, thrust force, temperature rise and residual stress among others. This study presents the experimental results for damage threshold and critical damage values for various strain - rate and temperature conditions using two different test devices: a conventional quasi-static test apparatus and a drop weight impact test (DWIT) adapted for tensile tests, covering strain rate values from 0.01/s to 10/s. Relationship between material damage threshold and critical damage value with strain – rate and temperature rise are presented, as well as, its effects during orthogonal cutting FEM simulation and accurate chip thickness prediction. Simulations with different damage parameters are presented and compared with previous works to verify convergence as well as, experimental results to show the importance of accurate damage parameter determination in cutting force prediction using numerical simulations.

## How to Choose a Length Scale?

Shmuel Osovski\*

\*Technion - Israel Institute of Technology

### ABSTRACT

The continuing efforts in improving the mechanical properties of structural alloys have led to a variety of materials with multiple characteristic length scales resulting from the underlying microstructure. A successful attempt at modeling the process of ductile fracture in such materials requires the implementation of the relevant microstructural length scale into the numerical models. As length scales in a given material system can vary drastically, it is impossible to explicitly represent all of them. As such, it is necessary to choose the relevant microstructural feature, which in turn can be identified based on experimental data. Recently it was suggested that the microstructural length scale, which has dictated the fracture process, could be extracted from fractured samples through a statistical analysis of the fracture surface. Here, we will present a detailed analysis on the statistical features of fracture surface roughness parameters obtained from 3D FE simulations with several microstructural features. The material is modeled using an elastic visco-plastic constitutive relation for a progressively cavitating solid, and each microstructural feature is allowed to accumulate damage through a different set of parameters. The propensity of each microstructural feature to fail is varied systematically with respect to the others and the resulting fracture surfaces are compared. The applicability of such an analysis in identifying the dominant microstructural feature, dictating the crack growth process, will be discussed with relation the experimental capabilities.

## Mathematical Model Connecting Biological Processes and Physical Chemistry of Hydroxyapatite Formation in Bone Tissue

Borys Ostapienko\*, Svetlana V. Komarova\*\*

\*McGill University, Department of Biomedical Engineering, \*\*Department of Biomedical Engineering, Faculty of Medicine and Faculty of Dentistry, McGill University, Shriners Hospital for Children-Canada

### ABSTRACT

Mathematical Model connecting Biological processes and Physical chemistry of Hydroxyapatite formation in Bone tissue Borys Ostapienko, Svetlana V. Komarova Department of Biomedical Engineering, Faculty of Medicine and Faculty of Dentistry, McGill University, Montreal, Quebec; Shriners Hospital for Children-Canada, Montreal, Quebec Abnormal mineralization of bone matrix results in severe clinical problems including bone deformities and fractures, such as observed in osteogenesis imperfecta and vitamin D deficiency. To better understand the physicochemical processes occurring during bone mineralization, we have developed a mathematical model that examines hydroxyapatite mineral formation on collagen matrices. The model describes biological components of bone mineralization in the form of kinetics of collagen matrix maturation, turnover of mineralization inhibitors and formation of nucleators. Chemical reactions occurring between  $\text{Ca}^{2+}$ ,  $\text{PO}_4^{3-}$  and  $\text{OH}^-$  ions in the aqueous phase as well as hydroxyapatite precipitation as single solid phase mineral are accounted for in kinetic reactions, mass balance and electro-neutrality requirements. We examined the roles of biological processes in generating normal and abnormal mineralization patterns characterized using two outcome measures: mineralization lag time and degree of mineralization. Model parameters describing inhibitor homeostasis most effectively changed the mineralization lag time, while a parameter describing the rate of matrix maturation was found to increase both the mineralization lag time and the degree of mineralization. When the effect of physicochemical factors, including ion concentrations, pH and temperature, was examined, we found a more prominent effect of varying  $[\text{PO}_4^{3-}]$  compared to  $[\text{Ca}^{2+}]$  on mineralization kinetics, as well as a significant effect of changing pH in the physiological range. This model can be applied for qualitative predictions of genotype/phenotype relationship for bone mineralization, and adapted to study physiological and pathological calcification of other tissues, including formation of kidney stones and vascular calcification.

## Exponential Integrators

Alexander Ostermann\*

\*University of Innsbruck, Austria

### ABSTRACT

In recent years there has been a considerable progress in the construction, analysis and implementation of new types of time discretization schemes for evolution equations. In this talk we will concentrate on exponential methods, a class of integrators which dates back to the late 1950ies. We start with a historical account on these methods and emphasize their relation to linearly implicit time integration, an alternative approach which was developed concurrently. The larger part of the talk, however, is devoted to recent developments. In particular, we will touch upon applications of exponential integrators in computational mechanics. Exponential integrators rely on an appropriate linearization of the vector field and employ the exponential and related functions of the Jacobian of this linearization. The efficient evaluation of the action of such matrix functions on vectors is of paramount importance for getting competitive schemes. This topic will also be addressed in the talk.

## **Implementation of Modular Plasticity Models for Hyperelastic Material Response Including Coupled Damage**

Jakob Ostien<sup>\*</sup>, William Scherzinger<sup>\*\*</sup>, Brian Lester<sup>\*\*\*</sup>, Brandon Talamini<sup>\*\*\*\*</sup>

<sup>\*</sup>Sandia National Laboratories, <sup>\*\*</sup>Sandia National Laboratories, <sup>\*\*\*</sup>Sandia National Laboratories, <sup>\*\*\*\*</sup>Sandia National Laboratories

### **ABSTRACT**

As a foundational technology in the engineering practice of modeling the large deformation of ductile metals up to and including failure, accurate models for constitutive response and efficient implementation into finite element codes remains a challenge. The purpose of this talk is to discuss implementation details for a class of hyperelastic plasticity models applicable for a family of yield surfaces and rate dependent models. The choice of finite deformation strain tensor facilitates direct comparison to the more broadly established hypoelastic versions of the models. Emphasis is placed on formulation, numerical integration, and verification of the algorithms. Efficacy of the models will be demonstrated on engineering applications and coupled damage formulations will be highlighted against two Sandia Fracture Challenge scenarios. Sandia National Laboratories is a multi-mission laboratory managed and operated by National Technology & Engineering Solutions of Sandia, LLC., a wholly owned subsidiary of Honeywell International, Inc., for the U.S. Department of Energy's National Nuclear Security Administration under contract DE-NA0003525.

## Tensor-Valued Random Fields for Continuum Physics

Martin Ostoja-Starzewski<sup>\*</sup>, Anatoliy Malyarenko<sup>\*\*</sup>

<sup>\*</sup>University of Illinois at Urbana-Champaign, <sup>\*\*</sup>Mälardalen University

### ABSTRACT

Continuum mechanics/physics typically involves fields of dependent quantities (temperature, displacement, stress...) and those of constitutive response (conductivity, stiffness...). In each case, there is a random field taking values in a linear space of tensors of a fixed rank: hence, a tensor-valued random field (TRF). First, we discuss most general and explicit representations of correlation functions of 2nd, 3rd, and 4th rank TRFs, which are wide-sense stationary and statistically isotropic having anisotropic realizations [MEMOCS 2(2), 209-231, 2014; ZAMP 67(3), 20, 2016; J. Elast. 127(2), 269-302, 2016]. Next, we examine the consequences for TRFs in 2d and 3d problems of classical continuum mechanics: velocity field in incompressible fluids, heat flux in steady-state heat conduction, or stress in quasi-static continuum mechanics. By extension, this leads to a study of consequences in stochastic micropolar theories [Math. Mech. Solids 20(4), 418-432, 2015]. Finally, we report what TRFs may arise if they are to represent most general constitutive responses in 2d or 3d heat conduction, (visco-thermo)elasticity, piezoelectricity, damage mechanics, or wave propagation [Adv. Appl. Mech. 49, 111-211, 2016]. By micro-physics and micro-mechanics arguments, such TRFs should be employed as input into stochastic partial differential equations or stochastic finite elements, instead of the commonly assumed locally isotropic (i.e. scalar) random fields.

## Automated Feature Recognition of 3D CAD Models for Pre-and Post-Processing of CAE

Koji Otani\*, Kazuyuki Mikami\*\*

\*Integral Technology Co., Ltd., \*\*Integral Technology Co., Ltd.

### ABSTRACT

It is time consuming to create FEM models for simulation and to analyze the simulation results especially when dealing with large assembly models. To create FEM mesh for input CAD models ensuring a certain quality of simulation result, it is important to follow specific mesh rules as simulation results may vary depending on the input FEM mesh. As large-scale modeling in FEM analysis increases, the importance of being able to create adequate FEM mesh for the input CAD models automatically is growing. This paper describes a method to recognize various features of 3D CAD models to create mesh according to mesh rules and to make post-processing efficient. In pre-processing step, recognizing features of input CAD models and generating mesh satisfying the detailed mesh rules automatically help to reduce manual mesh modifying work dramatically. In post-processing step, the recognized feature data makes it easier to analyze the simulation result by showing the result for each feature that is recognized. The feature recognition data can be post processed by linking recognized feature data and created FEM mesh data. To recognize specific features of input CAD models, we used characteristics of each face of the input CAD models, face type data that is calculated from the characteristics, combination of faces, and cross sectional shapes of the faces. This algorithm is capable of recognizing features of both mid-surface models such as sheet metal parts and solid models such as cast or resin parts. The features that we recognize with this algorithm include 2D/3D simple holes, stepped holes, steps on plane, embosses, beads, flanges, fillet flows, chamfers, corner fillets, ribs, grooves, gear teeth, and screws. After recognizing these features, FEM mesh for each feature can be generated with the information on the feature data and the mesh rules that are embedded and controlled by external control files. With this feature recognition algorithm, we achieved to recognize and create mesh meeting mesh rules in pre-processing step. In post-processing step, we proposed to link the recognized feature data and mesh data to analyze simulation results more efficiently.

## Automated Simulation Model Preparation with Machine Learning

Steven Owen\*, Timothy Shead\*\*, Shawn Martin\*\*\*

\*Sand, \*\*Sandia National Laboratories, \*\*\*Sandia National Laboratories

### ABSTRACT

We propose using machine learning to reduce the bottleneck in the engineering analyst workload. We discuss a potential rich new area of research where current machine learning methods can be applied to model preparation tasks such as defeating, resolution of dirty geometry and decomposition for hex meshing while maintaining high confidence in results. Because of the engineering judgment involved in these tasks, there can be wide ranges of good and bad solutions for any given problem, with bad solutions leading to inaccurate or misleading results and suboptimal engineering decisions. In order to effectively move the state-of-the-art towards full automation, analysts must have high confidence that the models created using automatic solutions are at least as good as the models they would otherwise build on their own. We believe that machine learning can prove useful in accomplishing this goal, providing algorithms that can reproduce the choices made by expert analysts. To accomplish this, the tasks now currently performed by analysts can be identified and used to train machine learning models, by capturing and labelling operations performed by experts using existing software tools as part of the model preparation process. We introduce an initial proof-of-concept environment, extending Sandia's Cubit geometry and meshing toolkit to utilize machine learning methods. In this software, geometric operations that are most likely to be effective for handling particular geometric characteristics of a CAD model are presented to the user. The ability to easily preview, execute, undo or even ignore the suggested operations are made available through an interactive user interface. Since the suggested solutions are based on previous training data, they draw upon the expertise of past users in similar simulations, while respecting the engineering judgment of the current user. While machine learning is widely used in text, image, audio, and video analysis, there has been little research on the application of machine learning to model preparation for simulation. Many important questions on how to use machine learning in this domain remain unexplored. In this talk we also introduce several open questions that need to be explored in order for machine learning techniques to be effectively applied in model preparation tasks. \*Sandia National Laboratories is a multi-program laboratory managed and operated by Sandia Corporation, a wholly owned subsidiary of Lockheed Martin Corporation, for the U.S. Department of Energy's National Nuclear Security Administration under contract DE-AC04-94AL85000

## **A Game Theoretic Approach to Numerical Approximation and Algorithm Design**

Houman Owhadi\*

\*Caltech

### **ABSTRACT**

This talk will cover interplays between Game Theory, Numerical Approximation and Gaussian Process Regression. We will illustrate this interface between statistical inference and numerical analysis through problems in multiscale analysis, the design of fast solvers, the identification of operator adapted wavelets, and computation with dense kernel matrices. This talk will cover joint work with F. Schäfer, C. Scovel, T. Sullivan and L. Zhang.

## **Design Optimization Under Uncertainty Using Polynomial Chaos Expansions and Conditional Value-At-Risk**

Geoffrey Oxberry\*

\*Lawrence Livermore National Laboratory

### **ABSTRACT**

Recent advances in additive manufacturing have enabled the manufacture of parts of almost any shape. Although topology optimization searches this large design space systematically, deterministic problem formulations assume that boundary conditions (e.g., loads for structural physics), material properties, and the correspondence between designed part and manufactured part (e.g., geometric variability) are known. In practice, these assumptions are violated, and deviations from assumptions can affect substantially design performance. To compensate for uncertainties in topology optimization problem formulations, we present a stochastic programming approach to topology optimization that incorporates the effects of known uncertainties, and represent these uncertainties using polynomial chaos expansions. We compare traditional mean-standard-deviation approaches with the  $x\%$  conditional value-at-risk, which is the average over the  $x\%$  of worst cases (average-worst-case), arguing that the latter better compensates for worst-case events when uncertainties are skewed. We also compare the polynomial chaos expansion approach to computing the mean, standard deviation, and conditional value-at-risk directly via deterministic quadrature, and to computing these quantities using Monte Carlo sampling.

## **A Second-order in Time Approximation of Fluid-structure Interaction Problem**

Oyekola Oyekole\*, Catalin Trenchea\*\*, Martina Bukac\*\*\*

\*University of Notre Dame, \*\*University of Pittsburgh, \*\*\*University of Notre Dame

### **ABSTRACT**

Fluid-structure interaction (FSI) problems arise in many applications, such as aerodynamics, geo-mechanics and biomedical engineering. They are characterized by highly non-linear coupling between two different physical phenomena. As a result, the development of robust numerical algorithms is a subject of intensive research. Since coupled FSI problems give rise to large and ill-conditioned systems of algebraic equations, partitioned methods have often been used to split the coupled problem into smaller and better-conditioned sub-problems. However, in applications where the density of the structure is comparable to the density of the fluid (such as the interaction between blood and arterial walls), classical partitioned schemes suffer from instabilities known as the added mass effect. In this case, the development of stable, non-iterative numerical schemes for FSI problems is challenging – even for first-order accurate solution techniques. We propose and analyze a novel, second-order accurate in time, partitioned method for the interaction between an incompressible, viscous fluid and a thin, elastic structure. The proposed numerical method is based on the Crank-Nicolson discretization scheme, which is used to decouple the system into a fluid sub-problem and a structure sub-problem. The scheme is loosely coupled, and therefore at every time step, each sub-problem is solved only once. Energy and a priori error estimates for a fully discretized scheme using finite element spatial discretization are derived. We prove that the scheme is stable under a CFL condition, second-order convergent in time and optimally convergent in space. We also present two numerical examples that support the theoretically obtained results. Using realistic parameter values for blood flow in a human common carotid artery, our simulation results demonstrate that the proposed scheme is stable and accurate when applied to problems related to blood flow modeling.

## **Turbulence-resolving Two-Phase Flow Simulations of Current Supported Turbidity Flows over Erodible and Non-erodible Beds**

Celalettin Ozdemir\*, Sahar Haddadian\*\*

\*Louisiana State University, \*\*Louisiana State University

### **ABSTRACT**

Although their existence was discovered more than two decades ago, wave- and current-supported turbidity currents (WCSTC) are now considered to be a major carrying agent that shapes the submarine geomorphology and deliver sediment from its source to its sink in the deep ocean with growing evidence. These flows are usually very thin at the seafloor and their occurrence is episodic which make their observation in the field very hard with the available sensor technology. To that end, turbulence-resolving two-phase flow simulations of WCSTC can be considered as virtual experiments to understand the full range of mechanisms that are responsible for and/or affect these currents. In this study, we present the culmination of two-phase, turbulence-resolving simulations, i.e. Direct Numerical Simulations (DNS), of alongshore current-supported fine sediment turbidity currents across mild bathymetric slopes. This type of flows exhibits rich hydrodynamic features because the flow is forced by both a non-uniform density difference due to suspended sediment concentration and a constant pressure gradient. Here, we analyze the alongshore current supported turbidity currents under two boundary conditions. First, suspended sediments are considered to be wash load. Second, we allow sediment mass exchange at the bottom boundary by using Krone-Partheniades type of erosion formula. Our results show a competition between sediment-induced density stratification and the horizontal flow created by the sediment-induced density difference to dampen and generate turbulence, respectively. Our numerical simulations also provide significant insights on how to model these turbidities in regional-scale models which will then be used to estimate the location of mud depocenters and the dynamics of submarine geomorphology such as in the clinoform development at the continental margin.

## Time Integration Schemes for Transient Problems with Enhanced Stability and Accuracy via Finite Increment Calculus (FIC)

Eugenio Oñate\*

\*International center for Numerical Methods in Engng (CIMNE), Barcelona, Spain

### ABSTRACT

The Finite Increment Calculus (FIC) (sometimes termed “finite calculus”) was proposed by Oñate [1] as a conceptual framework for deriving stabilized numerical methods for solving problems in mechanics for situations where numerical methods typically fail (i.e. high Peclet/Reynolds numbers and incompressible situations). The essence of the FIC approach lays in solving the modified form of the governing differential equations in mechanics obtained by writing the equations for balance of heat, momentum and mass in a space-time domain of finite size, and not in a domain of infinitesimal size, as it is usually done. The FIC governing equations involve the balance domain dimensions. The merit of the FIC equations is that they are a natural starting point for deriving stabilized numerical schemes [1-5]. In the presentation it is shown that the FIC equations in time are the starting point for deriving new explicit and implicit time integration schemes with increased stability and accuracy. Examples of the promising features of the FIC-Time approach for solving more efficiently and accurately a number of transient problems in mechanics are given. References [1] Oñate, E. Derivation of stabilized equations for numerical solution of advective-diffusive transport and fluid flow problems. *Comp. Meth. Appl. Mech. Eng* 151(1-2), 233–265 (1998). [2] Felippa C. A. and Oñate E., Nodally exact Ritz discretizations of 1D diffusion-absorption and Helmholtz equations by variational FIC and modified equation methods, *Computational Mechanics*, Vol. 39, pp. 91 - 111, 2007 [3] Oñate E., Miquel J. and Nadukandi P., An accurate FIC-FEM formulation for the 1D advection-diffusion-reaction equation, *Computer Methods in Applied Mechanics and Engineering*, Vol. 298, pp. 373-406, 2016 [4] Oñate E., Miquel J. and Nadukandi P., Accurate FIC-FEM formulation for the multidimensional steady-state advection–diffusion–absorption equation, *Comput. Meth. Appl. Mech. Eng.*, Vol 327, 352-368, 2017 [5] Felippa, C.A., Oñate, E., Idelsohn, S.R. , Variational Framework for FIC Formulations in Continuum Mechanics: High Order Tensor-Derivative Transformations and Invariants, *Archives of Comput. Meths.in Engng*, 10.1007/s11831-017-9245-0, 45 pp, 2018.

## Experimental Characterisation and Constitutive Modelling of the PC/ABS Polymeric Blend

Fernando P. B. Macedo\*, Shenghua Wu\*\*, Daniel de Bortoli\*\*\*, Francisco M. A. Pires\*\*\*\*

\*INEGI - Instituto de Ciência e Inovação em Engenharia Mecânica e Engenharia Industrial; FEUP - Faculdade de Engenharia da Universidade do Porto, \*\*INEGI - Instituto de Ciência e Inovação em Engenharia Mecânica e Engenharia Industrial, \*\*\*INEGI - Instituto de Ciência e Inovação em Engenharia Mecânica e Engenharia Industrial, \*\*\*\*FEUP - Faculdade de Engenharia da Universidade do Porto

### ABSTRACT

Keywords: Mechanics of Solid Polymers; Amorphous Polymers; Polymer Blends; Constitutive Modelling. Abstract. Polymeric blends are widely used in industrial applications in order to improve the mechanical performance and physical specifications of the individual constituents [1]. A case of interest is the ternary amorphous Polycarbonate/ABS blends – although neat PC has high ductility, thermal stability and durability, it lacks in high notch-sensitivity and fracture toughness, properties that are highly improved by the addition of ABS, a rubber-toughened polymer [2]. It is known that the fracture behaviour of rubber toughened polymers is governed by matrix shear yielding and crazing, interconnected with cavitation of the rubber particles. In this work, several experimental tests are performed to study the deformation behaviour of PC/ABS with different volume fractions of the blend constituents under different stress states, strain rates and temperatures. After that, a constitutive formulation framework was proposed, based on Gearing and Anand model [3], to describe the mechanical behaviour of PC/ABS blends. The proposed constitutive model accounts for the plastic deformation mechanisms described above (shear yielding, crazing, and cavitation) and is implemented within an implicit integration scheme. A representative set of numerical examples is analysed covering a wide range of parameters of the model. The predictions of the model are appraised against an experimental set of results obtained by our group. REFERENCES: [1] Helbig, M.; van der Giessen, E.; Clausen, A.H.; Seelig, T. (2016). Continuum-micromechanical modeling of distributed crazing in rubber-toughened polymers. *European Journal of Mechanics and Solids*, 57, 108-120. [2] Greco, R.; Astarita, M.F.; Dong, L.; Sorrentino, A. (1994). Polycarbonate/ABS blends: Processability, thermal properties, and mechanical and impact behavior. *Advances in Polymer Technology*, 13 (4), 259-274. [3] Gearing, B.P.; Anand, L. (2004). Notch-sensitive fracture of polycarbonate. *International Journal of Solids and Structures*, 41, 827-845.

## **Circumventing the Solution of Inverse Problems in Mechanics through Deep Learning**

Dhruv PAtel<sup>\*</sup>, Assad Oberai<sup>\*\*</sup>, Adriana Vega<sup>\*\*\*</sup>, Raghav Tibrewala<sup>\*\*\*\*</sup>, Li Dong<sup>\*\*\*\*\*</sup>

<sup>\*</sup>Rensselaer Polytechnic Institute, <sup>\*\*</sup>University of Southern California, <sup>\*\*\*</sup>City University of New York, <sup>\*\*\*\*</sup>Indian Institute Technology, Chennai, <sup>\*\*\*\*\*</sup>University of Texas, Austin

### **ABSTRACT**

Recent studies have demonstrated that images of mechanical heterogeneity of a tumor, and its nonlinear elastic response can be used to distinguish benign tumors from their malignant counterparts. These images of the linear and nonlinear parameters of tissue are typically obtained by using a measured displacement field and solving a complicated inverse elasticity problem. In this talk we circumvent the step of solving the inverse problem by using the displacement measurements as direct input to a deep convolutional neural net, and training it to directly classify tumors based on their heterogeneity and nonlinear elastic response. We explore the use of transfer learning in this context as a means to work with a reduced training data set, and also examine the characteristics of the trained model to understand the process through which the CNN extracts features from the raw displacement images.

## Voronoi Tessellation with ShaPo

Joachim POUDEIROUX\*, Florian CHEVASSU\*\*, Marc CHAREST\*\*\*, Mack KENAMOND\*\*\*\*,  
Mikhail SHASHKOV\*\*\*\*\*

\*Kitware SAS, \*\*Kitware SAS, \*\*\*LANL, \*\*\*\*LANL, \*\*\*\*\*LANL

### ABSTRACT

Voronoi meshes are polygonal or polyhedral meshes that have properties that are appreciated in many scientific fields like computational fluid dynamics or geo-physics. In the particular context of the implementation of Reconnection-Based ALE family of methods at LANL, we are developing a cross platform C++ software library called ShaPo. This tool produces Voronoi meshes from a domain defined by a set of complex boundaries (convex or non-convex, simply or multi-connected) and user defined set of seeds. ShaPo integrates different algorithms to generate, in serial or in parallel, 2D and 3D Voronoi meshes with different properties, and it provides a complete API to retrieve the full connectivity of the generated meshes. In this talk we will present the core algorithms of ShaPo and expose the common pitfalls of the development of a Voronoi tessellation algorithm which can seem straightforward in theory but appears to be very complex to implement in practice, especially if you consider reliability, robustness and speed. We will also explain our algorithm to compute the tessellation in a MPI parallel context and how we establish the global mesh connectivity. Finally we will detail an important feature of ShaPo which is its capability to remesh a subregion of an existing unstructured mesh with a Voronoi tessellation and reconstruct the full mesh connectivity.

## A Mid-frequency Method to Model Coupled Vibro-acoustic Response of a Railway Track

Guillaume PUEL<sup>\*</sup>, Raphaël CETTOUR-JANET<sup>\*\*</sup>, Pierre-Etienne GAUTIER<sup>\*\*\*</sup>, Andrea Barbarulo<sup>\*\*\*\*</sup>

<sup>\*</sup>CentraleSupélec, <sup>\*\*</sup>CentraleSupélec, <sup>\*\*\*</sup>SYSTRA, <sup>\*\*\*\*</sup>CentraleSupélec

### ABSTRACT

With metropolis and transport grid densification, the result of vibro-acoustic impact assessment has a pivotal role in rail network expansion. Indeed, for railway neighbors, the pass-by train noise is a key issue. One of the main source is the rolling noise: Roughness on the wheel and rail surface produce an imposed displacement on the both last. This last one generates vibrational response of wheels and the railway track and their acoustic radiation. The frequency range is 50-5000 Hz In this work, a vibro-acoustic model of the ballasted railway track is presented. For vibrational response, analytical models (beam, mass, springs, ...) and finite elements do not allow to simulate correctly the behavior of the track. In this work, a generic element is simulated. It is constituted of a piece of rail and a half sleeper at the both ends. Semi-analytical finite element method (SAFEM) is used to simulate this element. This method use a FEM mesh in the cross section and analytical formulation in the third dimension. Consequently, it allows to reduce computation time while taking account the 3 dimensions of the model. Infinite part and periodicity between supports are simulated using Floquet theorem and injecting the force produced by the support at the ends of the generic element. However, this technique suffers from numerical problems which imposed an adaptive algorithm. The second-order Arnoldi method (SOAR) is used before solving the SAFEM equation. This reduction allows to eliminate critical values that induce numerical problems. Moreover, the orthogonal basis created by this method allows improving the robustness of the algorithm. This method is validate thanks a comparison with experimental results. For acoustic radiation, high frequency simulation prevent using conventional techniques (FEM, BEM, ...) . This impose to use mid frequency technics. Railway track geometry can be decomposed into big cavities. Consequently, the Variational theory of complex ray is particularly well adapted to this case. The principal features of VTCR approach are the use of a weak formulation of the acoustic problem, which allows to consider automatically boundary conditions between sub-domains. Then, the use of an integral repartition of plane waves in all the direction allow to simulate the acoustic field. The unknowns of the problem are their amplitudes. This method well assessed for closed domain has been extended to open domain and coupled to vibrational response. Comparison with FEM simulation at low frequency allow to validate the method.

## Temperature Induced Structural Instabilities in Two-dimensional Buckled Honeycomb Systems

Alejandro Pacheco-Sanjuán\*, Salvador Barraza-Lopez\*\*

\*Universidad Técnica Federico Santa María, \*\*University of Arkansas

### ABSTRACT

Non-linear deformations and phase changes in 2D buckled honeycomb crystals are analyzed by First-principles molecular dynamics simulations and discrete differential geometry. Unlike graphene, Silicene (Si) and Germanene (Ge) are not absolutely planar, but have buckled heights of 0.44 Å and 3.97 Å respectively. The low buckled (LB) configurations for these two structures exhibit positive frequencies for the phonon dispersion and therefore it is considered to be stable. At high temperatures, these systems are excited so they can cross the energy barrier and locally shift the positions of atoms from the LB to the high buckled (HB) state, generating a pattern of linear defects. Abrupt changes in the local geometry of Si and Ge are detected at a critical temperature  $T_c$  well below the melting point  $T_m$ . Distributions of the invariants for the local curvature and metric tensors are computed and compared for temperatures below and above  $T_c$  for both structures. Dynamical changes at  $T_c$  are also detected by the frequency shifting of non-linear modes in the power spectra. The geometrical analysis shows that this local disorder arises when nearest neighboring atoms are reassigned when the system is thermally excited at temperatures greater than  $T_c$ .

## **Numerical Simulation of Fuel Rod Vibrations Induced by Turbulence in the Vicinity of the Fuel Assembly Inlet Zone**

Julien Pacull<sup>\*</sup>, Yasmail Akariouh<sup>\*\*</sup>, Valérie Biscay<sup>\*\*\*</sup>, Serge Delafontaine<sup>\*\*\*\*</sup>, Pierre Badel<sup>\*\*\*\*\*</sup>

<sup>\*</sup>Framatome, <sup>\*\*</sup>Framatome, <sup>\*\*\*</sup>CEA, <sup>\*\*\*\*</sup>CEA, <sup>\*\*\*\*\*</sup>EDF

### **ABSTRACT**

This work pertains to the safety and performance analysis of fuel assembly components (i.e. fuel rods) of pressurized water reactor nuclear plants. Inside the reactor core of pressurized water reactors, fuel assemblies experience significant thermal, hydraulic, and irradiation loads during operation. These loads may induce large scale fuel rod oscillations that might result in fuel rod cladding fretting wear or fuel assembly motions that may contribute to significant assembly fretting. To address the flow induced vibrations of fuel rods subjected to the most generic form of excitation from turbulence-induced fields, a new nonlinear structural model is proposed. The model is constructed by beams with six degrees of freedom simulating the response of a single fuel rod subjected to a turbulent flow field. Mechanical non-linearities originate from the relative motion of the fuel rod cladding with respect to its supports, which becomes prominent especially for irradiated fuel for which the grid spring relaxation leads to degraded supporting conditions. Impacts and sliding motion can be derived from the simulations to support subsequent fretting wear risk assessment. The excitation field is generated by high fidelity unsteady CFD simulations, which are performed on a geometry representative of the fuel assembly components. As a post-treatment of the flow simulation, the Power Spectral Density of the fluctuating pressure is computed, to serve directly as excitation input for the nonlinear fuel rod model with no further empirical adjustment needed. This numerical tool is used to simulate the turbulent-induced vibrations of fuel rods in the vicinity of the bottom nozzle. In that zone, the flow complex topology is driven primarily by the axial flow jet coming through the holes in the lower core plate, combined with the hydraulic redistribution stemming from the bottom nozzle. The rod vibration amplitude and frequencies are compared with experimental data obtained from a full-scale fuel assembly testing in order to validate the prediction capability of the analytical tool.

## **Sensitivity Analysis and Optimization of Transient Responses**

Narayanan Pagaldipti\*, Shaobin Liu\*\*

\*Altair Engineering, Inc., \*\*Altair Engineering, Inc.

### **ABSTRACT**

Sensitivity Analysis and Optimization of Transient Responses Narayanan Pagaldipti and Shaobin Liu Altair Engineering, Inc. 2030 Main Street, Suite 100, Irvine, California 92614, USA E-mail: pagaldip@altair.com Dynamic analyses of engineering systems are conducted in the frequency domain (frequency response analysis) and the time domain (transient response analysis). Altair OptiStruct1, a leading commercial Computational Mechanics and Design Optimization software, supports these analyses extensively and offers accurate, efficient and innovative solutions not only for Noise, Vibration and Harshness (NVH) applications but also in the broad CAE space and Multidisciplinary Design Optimization (MDO). OptiStruct is the established leader in topology, sizing and shape optimization for many applications. For dynamic applications, design optimization is supported for natural frequencies, frequency response displacements, stresses, Equivalent Radiated Power (ERP) and also for transient analysis using the Equivalent Static Load method (ESL Method). This paper will present recent developments for supporting transient responses directly in design optimization. The motivation is to rigorously capture the stiffness, inertial and damping effects in the sensitivity calculations along with the time integration of the transient analysis. Unlike the ESL Method, this rigorous approach is better equipped to offer robust designs, albeit at an increased computational price. Both direct and adjoint sensitivity methods will be covered with the latter being a necessity for supporting topology optimization. Peak transient responses will be automatically considered in the optimization formulation without requiring the design engineer to specify any specific time instants or geometric locations for the response evaluations. Several design studies based on this implementation will be presented to validate its robustness, efficiency and practical use. Comparative studies against the more efficient ESL Method will also be conducted to establish the robustness of the new, more rigorous method. References: 1. Altair OptiStruct 2017: Users Guide. Altair Engineering, Inc., Troy, Michigan.

## Reduced Order Modeling for Uncertainty Quantification of the Cardiac Function

Stefano Pagani<sup>\*</sup>, Andrea Manzoni<sup>\*\*</sup>, Alfio Quarteroni<sup>\*\*\*</sup>

<sup>\*</sup>École polytechnique fédérale de Lausanne, <sup>\*\*</sup>Politecnico di Milano, <sup>\*\*\*</sup>Politecnico di Milano

### ABSTRACT

A growing number of biomedical applications are bringing new challenges dealing with the integration of high-dimensional and complex data (possibly affected by uncertainty) within mathematical models built on partial differential equations (PDEs). The mathematical and numerical modeling of the cardiovascular system requires a huge amount of data when trying to reproduce both physiological and pathological behaviors. Often partially missing, these data show a considerable intra- and extra-subject variability and are inevitably hampered by uncertainty, e.g., in (i) the computational domain, (ii) physical parameters and (iii) boundary conditions, among others. These are the main reasons behind the very rapid growth of applications of uncertainty quantification (UQ) methods to cardiovascular problems in the past decade, in view of both model calibration and personalization -- that is, the adaptation of model inputs to subject-specific conditions. Forward UQ problems are strictly related to the task of parametric studies, multi-scenario and sensitivity analyses, whereas backward UQ problems involve parameter (and state) estimation and data assimilation. In particular, Bayesian methods provide a rigorous framework for the solution of backward UQ problems. Sampling algorithms, such as the Markov chain Monte Carlo (MCMC) or the (ensemble) Kalman filter, enable to estimate the distribution of quantities of interest (model parameters, state of a system) from noisy (non)-invasive clinical measurements. Numerical strategies for UQ problems in this context involve the approximation of PDEs for several (usually, order of thousands) input parameter values, thus making high-fidelity, or full-order, techniques (e.g. the finite element method) ill-suited, despite the constant growth of computer resources available. Reduced-order models (ROMs) such as the reduced basis (RB) method, are emerging methodologies in the UQ framework since they are aimed at reducing the computational complexity entailed by the repeated solution of PDEs. In this talk we show how to take advantage of ROM techniques to treat forward and backward propagation of uncertainty in relevant problems dealing with cardiac electrophysiology and electromechanics.

## Identification of Nonlinear Parameters of a Nuclear Fuel Rod

Brian Painter<sup>\*</sup>, Marco Amabili<sup>\*\*</sup>, Stanislas Le Guisquet<sup>\*\*\*</sup>, Prabakaran Balasubramanian<sup>\*\*\*\*</sup>,  
Kostas Karazis<sup>\*\*\*\*\*</sup>

<sup>\*</sup>AREVA NP Inc, <sup>\*\*</sup>McGill University, <sup>\*\*\*</sup>McGill University, <sup>\*\*\*\*</sup>McGill University, <sup>\*\*\*\*\*</sup>AREVA NP Inc.

### ABSTRACT

In Pressurized Water Reactors (PWRs), fuel assemblies are made up of fuel rods, long slender tubes filled with uranium pellets, bundled together using spacer grids. These structures are subjected to fluid-structure interaction, due to the flowing coolant surrounding the fuel assemblies inside the core, coupled with large-amplitude vibrations in the case of external seismic excitation. Therefore, understanding the nonlinear response of the structure, and, particularly, its dissipation, is of paramount importance for the choice of safety margins, in the design of fuel assemblies, to ensure their functionality and safety in the worst external condition scenarios. To model the nonlinear dynamic response of fuel rods, the identification of the nonlinear stiffness and damping parameters is required. A tool based on the harmonic balance method was developed to identify these parameters from the experimentally obtained force-response curves, considering one-to-one resonance phenomenon present in axisymmetric structures such as cylindrical tubes and shells. To validate the tool, it was applied to the reference case of a circular cylindrical shell filled with water, which revealed an increase of damping with the excitation amplitude. More recently, the more realistic case of a single fuel rod with clamped-clamped boundary conditions was investigated by applying harmonic excitation at various force levels in the presence of a surrounding fluid. The nonlinear parameters including damping were extracted from experimental results by means of the adapted tool. An increase in damping with excitation amplitude has been shown according to earlier studies.

## **An Elasto-plastic Dynamic Response Analysis of E-Defense Large-scale Experiment on Soil-underground Structure Interaction**

Mahendra Kumar Pal\*, Takuzo Yamashita\*\*, Shintaro Ohno\*\*\*, Atsushi Iizuka\*\*\*\*

\*National Institute for Earth Science and Disaster Resilience (NIED), Japan, \*\*National Institute for Earth Science and Disaster Resilience (NIED), Japan, \*\*\*Kajima Corporation, Japan, \*\*\*\*Kobe University, Japan

### **ABSTRACT**

In this study, an elasto-plastic dynamic response analysis of Soil-Structure Interaction (SSI) specimen, with an aim to validate the numerical results of E-Simulator, is presented. A large-scale soil-underground structure specimen was tested against multiple seismic waves [1], to assimilate a comprehensive understanding of SSI. Specimen is comprised of two inclined layers of soil-strata, two vertical shafts, two horizontal shield tunnels and one cut-and-cover tunnel interconnecting the shafts. All structural component and soil-layers of specimen are discretized using solid 3-Dimensional linear tetrahedral elements to generate a high fidelity finite element model of test specimen. Interface between soil and structures is modeled using conforming mesh. To achieve conforming mesh, soil mesh around the structures is adaptively refined with an aim to generate mesh, which is compatible with high-resolution meshes of structures. Soil laminar container is modeled using rigid-body elements with linear interpolatory constraints. Modified Cam-Clay model [3] has been employed to simulate nonlinear behaviour of soil, in which cyclic plasticity, development of anisotropy and collapsibility of soil-structure are modelled using extended sub-loading surface, rotational hardening and super-loading surface, respectively. Dynamic response analysis of the detailed FE model of the specimen is analysed using E-Simulator. E-simulator [3] is in-house high performance parallel finite element (FE) package developed at-and-by E-Defense to reproduce the damage mechanism of buildings and civil structures against seismic loading. Acceleration and displacement time history responses of numerical simulation at various critical locations of specimen are compared with those of experiment. A comparative study of profiles of curvature, rotation and displacement along depth of specimen is also demonstrated. The obtained numerical results are in reasonable agreement with the E-Defense large-scale experiment. A torsional deformation of cut-and-cover tunnel is also reported. Keywords: Soil-Structure-Structure Interaction, Large-scale Shake Table Test, Underground Structures, Modified Cam-Clay Model, E-Simulator, E-Defense. References: 1) Yohsuke Kawamata, Manabu Nakayama, Ikuo Towhata, Susumu Yasuda, "Dynamic behaviour of underground structure in E-Defense shaking experiment", Soil dynamics and earthquake engineering, 82, pp. 24-39, 2016. 2) Shintaro Ohno, "Elasto-plastic constitutive models derived from non-linear description of soil contractancy", Doctoral thesis submitted to Tokyo Institute of Technology Japan, 2006. 3) Takuzo Yamashita, Muneo Hori, Koichi Kajiwara. "Petascale Computation for Earthquake Engineering", Computing in Science and Engineering, 13(4), pp.44-49, 2011

## Tunable Dynamic Response in Tensegrity Based Lattices

Raj Kumar Pal<sup>\*</sup>, Massimo Ruzzene<sup>\*\*</sup>, Julian Rimoli<sup>\*\*\*</sup>

<sup>\*</sup>Georgia Institute of Technology, <sup>\*\*</sup>Georgia Institute of Technology, <sup>\*\*\*</sup>Georgia Institute of Technology

### ABSTRACT

Tensegrity-based lattices exhibit mechanical properties very distinct from their constituent materials due to their geometry, topology and nonlinear interaction between the members. They also have potential to exhibit significant tunability in their dynamic properties by varying the cable prestrain. As the prestrain increases, the bars buckle leading to a change in the effective stiffness. We investigate the linear wave properties of such tunable tensegrity-based beams, plates and solids, where the basic building block is a truncated octahedron. We show the presence of three distinct stages of dynamic behavior as the cable prestrain is varied, with sharp transitions in wave speeds between them. These transitions are analogous to phase transitions in condensed matter systems, and lead to qualitative change in wave response. For example, we show that, in a range of cable prestrains, tensegrity solids exhibit dilational response, where the shear waves travel faster than pressure waves. Our dispersion analyses are verified by detailed numerical simulations. This work provides a robust and simple framework for developing tunable tensegrity-based periodic media in three dimensions.

## **Nonlinear Static Analysis of a Celestial Icosahedron Vacuum Lighter Than Air Vehicle**

Anthony Palazotto\*, Kyle Moore\*\*

\*Air Force institute of technology, \*\*Air Force Institute of technology

### **ABSTRACT**

The idea of a lighter than air vehicle (LTAV) which uses an internal vacuum to achieve buoyancy has been around since the 17th century, but advancements in engineering and manufacturing processes are just now allowing for this concept to be feasible. Research on vacuum LTAVs has been conducted at AFIT since 2013. A new design for such a vehicle, called the Celestial Icosahedron design, was proposed by Brian Cranston in 2016 as part of his PhD dissertation but has not yet been analyzed as thoroughly as previous designs. The design itself is composed of 9 intersecting, circular hoops made of a carbon nanotube (CNT) composite, spaced out and revolved at 45 degree increments. The frame is covered by a thin membrane-like, Graphene skin. The research for this particular design followed that of previous AFIT designs. The research includes a boundary condition study of the frame in order to ensure symmetry, as well as a comparison of different sized designs (variation of diameter) with the goal of achieving the smallest possible structure (diameter less than 3 feet). The structure's nonlinear static response to a loading condition that is representative of sea-level pressure was analyzed using the Finite Element Analysis (FEA) program, Abaqus including adoptive stabilization. Spherical stresses and displacements show the level of material and structural nonlinearity based on the various boundary conditions. Matlab is used in order to optimize both the size and the weight to buoyancy ratio of the structure. The frame of the structure has been built using additive manufacturing. A small, feasible design is to be implemented in the intelligence, surveillance, and reconnaissance (ISR) field with an emphasis on cramped urban environments. Future research will include a comparison of different structural materials, further optimization and dynamic response including instability.

## Flow Diverter Treatment Outcome of Intracranial Aneurysms is Associated with Blood Flow Modifications: In Silico Computational Analysis of Clinical Cases

Nikhil Paliwal<sup>\*</sup>, Robert Damiano<sup>\*\*</sup>, Jason Davies<sup>\*\*\*</sup>, Adnan Siddiqui<sup>\*\*\*\*</sup>, Hui Meng<sup>\*\*\*\*\*</sup>

<sup>\*</sup>Mechanical and Aerospace Engineering, Toshiba Stroke and Vascular Research Center, University at Buffalo,

<sup>\*\*</sup>Mechanical and Aerospace Engineering, Toshiba Stroke and Vascular Research Center, University at Buffalo,

<sup>\*\*\*</sup>Neurosurgery, Toshiba Stroke and Vascular Research Center, University at Buffalo, <sup>\*\*\*\*</sup>Neurosurgery, Toshiba Stroke and Vascular Research Center, University at Buffalo, <sup>\*\*\*\*\*</sup>Mechanical and Aerospace Engineering,

Neurosurgery, Toshiba Stroke and Vascular Research Center, University at Buffalo

### ABSTRACT

Introduction Flow diverters (FDs) are the preferred treatment modality for endovascular treatment of intracranial aneurysms (IAs). Densely woven stent-meshes structure of FDs disrupt blood flow within the aneurysm to induce pro-thrombotic conditions, and serves as a scaffold for endothelial ingrowth and arterial remodeling. Despite good clinical success of FDs, complications like incomplete occlusion and post-treatment rupture have been reported.[1] In silico analysis of FD-treated IA patients can shed light on the contrasting hemodynamics in different clinical outcomes. To that end, this study aims to investigate differences in hemodynamics in patients with completely and partially occluded IAs after FD-treatment. Methods Patients with following criteria were included in this study: (1) sidewall aneurysm at the ICA treated using one FD, (2) pre-treatment images and 6-month follow-up available. Patients were divided into "occluded" and "residual" groups based on their 6-month clinical outcome. Images were segmented to obtain patient-specific IA models. Virtual stenting workflow[2] was used to recapitulate the clinical FD deployment in each IA. CFD was performed on the untreated and virtually-treated IA geometries using STAR-CCM+ (CD-adapco, Melville, NY) under physiological flow conditions, with blood modeled as Newtonian (density: 1056 kg/m<sup>3</sup>, viscosity: 0.0035 Pa-s). Time-averaged reductions in shear rate (SR), aneurysmal average velocity (AAV), wall shear stress (WSS) and inflow rate (IR) were calculated for each case. A two-tailed Student's t-test was performed for statistically significant differences in hemodynamic parameters between the groups. Results Thirty-eight IAs in 35 patients fulfilled the inclusion criteria and were included in the study. At 6-month clinical follow-up, 27 aneurysms were occluded and 11 aneurysms were patent (residual). IAs in the occluded group had higher hemodynamic reductions than the residual group. IR was significantly different between the two groups with a p-value of 0.04. SR, AAV and WSS showed no significant difference between the groups. Discussion Our results shows higher flow reduction in successfully occluded IAs at 6-month follow-up. This is in accordance with previous findings that larger hemodynamic reductions are associated with successful occlusion of FD-treated IAs.[3] Statistically significant differences in IR between the groups implies that higher flow reductions at the aneurysmal neck may be required for complete occlusion of FD-treated sidewall IAs. Large prospective studies are required to confirm our findings, and develop statistical models for a priori prediction of the occlusion outcome of FD-treated IAs. References 1. Siddiqui et al., Neurosurgery, 2012 2. Paliwal et al., CMBME, 2016 3. Ouared et al., JNIS, 2016

## **Schwarz Alternating Implicit Enrichment Methods for Analysis of Kirchhoff-Love Plate Model with Angular Corners**

Birce Palta\*

\*The University of North Carolina at Charlotte

### **ABSTRACT**

We develop numerical methods for analysis of Kirchhoff-Love plate model with angular corners. Even though this thin plate model has no boundary layer problems, we have to handle fourth order partial differential equations whose finite element approach requires smoother basis functions. It is known that Isogeometric Analysis (IGA) can effectively handle this type of problems whenever plate is a simple convex domain. However, IGA with single patch encounters difficulties in dealing with irregular shaped polygonal plates. In literatures, for analysis of thin plates with angular corners, multi-patches approaches, discontinuous Galerkin method (DGA), penalty methods, domain decomposition methods (DDM), and so on, are suggested. In this paper, in order to handle thin plate model with singularities, we introduce implicitly enriched Galerkin method combined with smooth flat-top partition of unity functions. Unlike XFEM, this approach does not have singular integral problems. For the cases where multi-patches are necessary, we combine DDM and implicitly enriched Galerkin method. Numerical examples show effectiveness of the proposed methods in dealing with cracked and L-shaped plates.

## **On the Numerical Study of Ballistic Performance of Multi-ply Woven Fabrics**

Emre Palta<sup>\*</sup>, Howie Fang<sup>\*\*</sup>

<sup>\*</sup>The University of North Carolina at Charlotte, <sup>\*\*</sup>The University of North Carolina at Charlotte

### **ABSTRACT**

Studies on ballistic performance of woven fabrics possess considerable importance because woven fabrics are one of the most commonly used materials for soft body armor equipment. The ballistic impact performance of single-ply woven fabrics has been widely evaluated both experimentally and numerically in literature. Although a soft body armor equipment is always made of multi-ply woven fabrics, there are few experimental and numerical studies dealing with multi-ply woven fabrics. In this study, a multi-scale numerical modeling technique was developed to evaluate in detail the ballistic performance of multi-ply woven fabrics. The multi-scale modeling technique was validated against experimental data and was found to reduce computational expense while maintaining adequate solution accuracy. The multi-scale models of four multi-ply woven fabric targets with three, five, seven, and ten plies, respectively, were created and used in the evaluation of the ballistic performance of multi-ply woven fabrics in terms of ballistic limits, transverse displacements, and perforation mechanism.

# OPTIMIZED STRATEGIC TASK ALLOCATION FOR THE MITIGATION OF OFF NOMINAL EVENTS IN THE FUTURE AIR TRAFFIC MANAGEMENT SYSTEM

**Roberto Palumbo and Edoardo Filippone**

\*CIRA, Italian Aerospace Research Center  
Via Maiorise  
Capua (CE), 81043 Italy  
r.palumbo@cira.it; www.cira.it

**Key words:** ATM performance; resilience engineering; optimal path search; task allocation.

## 1 INTRODUCTION

The growing density of air transportation operations and airspace users, has increased the complexity of the Air Traffic Management (ATM) system. For this reason, in recent years international programs, such as SESAR in Europe and NextGEN in the US, are developing new operational concepts to redesign and reorganize the ATM system in a more efficient way improving capacity, efficiency and safety, thus avoiding the increase of costs, delays and emissions as well as the increase of workload of air traffic controllers. More specifically the goal is to fulfil the performance expectations expressed in the 11 Key Performance Areas defined by ICAO plus Human Performance [1]. To this end, the new and future air traffic management paradigms will focus on:

- increasing the level of automation of the system (to reduce workload)
- moving toward a network centric approach to information sharing (to improve situational awareness)
- moving toward time-based operations (to increase sector capacity).

In the context of this future highly automated system, disruptive events will call for an efficient re-allocation of tasks and authority sharing between humans and automated systems in order to mitigate the degradation of performance caused by the off-nominal condition. Recently, the ATM research community is giving more and more attention to the concept of resilience as a possible way to analyze the capabilities of the ATM system to recover an acceptable level of performance when non-nominal conditions occur. In fact the original definition of resilience comes from the material science domain where it is considered a property of a system that describes its ability to return to its original state (at some later time), after the removal of a [deforming] stress. In 2009, EUROCONTROL has given a specific interpretation of resilience in the context of air traffic management. In fact according to Ref. 2,

resilience is “the intrinsic ability of a system to adjust its functioning prior to, during, or following changes and disturbances, so that it can sustain required operations under both expected and unexpected conditions”. This definition, while explaining well the desired behavior of a resilient ATM system, it does not, however, provide a quantitative framework to evaluate the resilience of the ATM system. Recently, the SESAR JU E2.21 SAFECORAM (Sharing of Authority in Failure/Emergency Condition for Resilience of Air traffic Management) project, introduced a quantitative methodology to measure the level of resilience of the ATM system based on the concept of tasks re-allocation and authority sharing between humans and systems within the future ATM system (year 2050) [3, 4]. The following sections will describe the methodological approach developed in the SAFECORAM project, together with some applications from different operational perspectives.

## 2 SAFECORAM METHODOLOGY

The SAFECORAM definition of resilience is based on a quantitative measure of the global performance of the ATM system. To quantify resilience, it is therefore necessary to define the meaning of global performance. The global performance of the ATM system can be thought as the fulfilment of the aforementioned performance expectations in the 11 Key Performance Areas (KPAs) defined by ICAO plus Human Performance. With reference to Figure 1a, if we are able to assign a performance level to each KPA, then we could interpret the yellow area, as the global performance of the ATM system at a given state. When an off-nominal condition occurs, the ATM system can no longer perform in its nominal conditions and its global performance will inevitably change. Of course the ATM system reacts to the disturbance applying a set of mitigation tasks and actions that are aimed at restoring the nominal level of performance (i.e. the original yellow area) as much as possible. This residual level of global performance is what SAFECORAM defines as the resilience of the system. Therefore an ATM system is more resilient the more it is able to reorganize itself towards the most similar state with respect to the reference (nominal) one.

It is important to remark that not all mitigation strategies are alike. Different mitigation strategies may recover different levels of global performance (Figure 1b). This means that among all the possible sets of mitigation actions suitable to face the disruptive event, some of them are better at minimizing performance loss. In other words, it is possible to define an optimization problem aimed at maximizing the resilience of the system (i.e. minimize performance loss). This optimization is based on the optimal re-allocation of tasks between different ATM actors, in order to preserve the highest possible level of residual performance of the system when an off-nominal condition occurs.

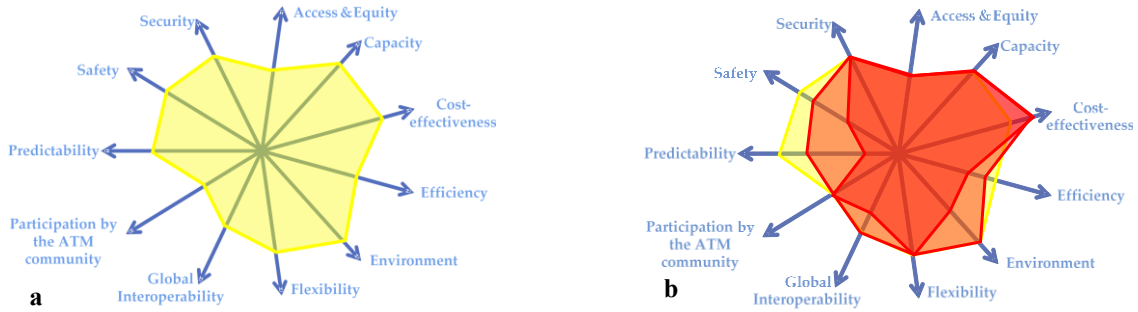


Figure 1. Global Performance of the system (a). Residual global performance in off-nominal conditions (b).

Therefore, to quantify the global performance of the ATM system in nominal and off-nominal conditions it is necessary to provide:

- a methodology to quantify the performance levels of the KPAs and how they are degraded once the off-nominal condition occurs;
- a methodology to establish the best re-allocation of tasks.

### 2.1 Scenario Based Approach

The SAFECORAM methodology was derived following a scenario based approach. This means that the methodology was developed starting from the definition and analysis of several ATM scenarios. Basically, a scenario represents a description of a set of nominal and non-nominal situations affecting the ATM system. In SAFECORAM, the objective of a scenario is to explore alternative behaviors of the system when an off-nominal condition is triggered.

In Section 3, we will describe an explanatory case study scenario (developed with the help of ATM operational experts) which is very useful to understand the application of the SAFECORAM approach.

In general, the approach consists of several steps (see Figure 2): first of all, the ATM scenario is described in nominal conditions, then a disturbance is considered leading to off-nominal conditions and possible different task reallocation strategies are analyzed. These strategies are then evaluated and optimized in terms of global performance yielding the best mitigation strategy which finally defines the resilience of the system.

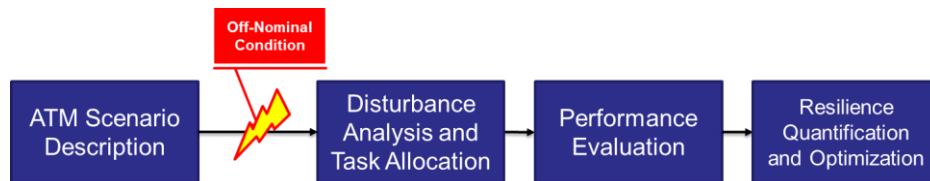


Figure 2. The SAFECORAM methodology steps.

### 3 CASE STUDY SCENARIO

Before describing the details of the case study scenario it is important to state some basic assumptions:

- the framework is the future ATM system (year 2050): this means that the SESAR ConOps are fully deployed, the ATM system is highly automated and Remotely Piloted Aerial Systems (RPAS) and Personal Air Transportation Systems (PATS) (with their related infrastructure) are fully integrated as airspace users;
- the stochastic nature of the events that can affect the scenarios is not taken into account.

#### 3.1 Scenario Description

The scenario consists of four en-route airplanes that according to their flight plan have to cross a specific air sector and 4 airplanes that depart from an airport inside that same air sector. Nominally the four en-route airplanes fly their assigned 4D trajectory contract crossing the specific air sector, and the departing four airplanes depart from the airport inside the air sector. The unexpected event that triggers the application of a mitigation strategy is the fact that the airspace sector is affected by a temporary GNSS unavailability that impairs the navigation systems of the vehicles.

#### 3.2 Disturbance Analysis and Task Allocation

In general, the scenario description may be broken down into a flow of tasks and actions performed by the actors of the scenario. The nominal flow is the set of tasks and actions that describes the nominal execution of the scenario and guarantees the nominal global performance.

When the off-nominal condition occurs, there are several task reallocation alternatives and different flows of actions that may be performed to mitigate the effect of the disturbance. Each of these alternatives determine different paths characterized by a different, yet degraded level of global performance. Comparing the degraded global performances of each alternative flow with the nominal global performance, it is possible to identify the mitigation strategy which minimizes performance loss.

Figure 3 shows the task breakdown identified for this case study scenario. Basically the ACC Manager must decide how to deal with the off-nominal condition inside the specific air sector, either closing the sector (deviating the en-route airplanes and grounding the departing ones) or allowing only a limited number of airplanes through the airspace sector (either departing or crossing the area).

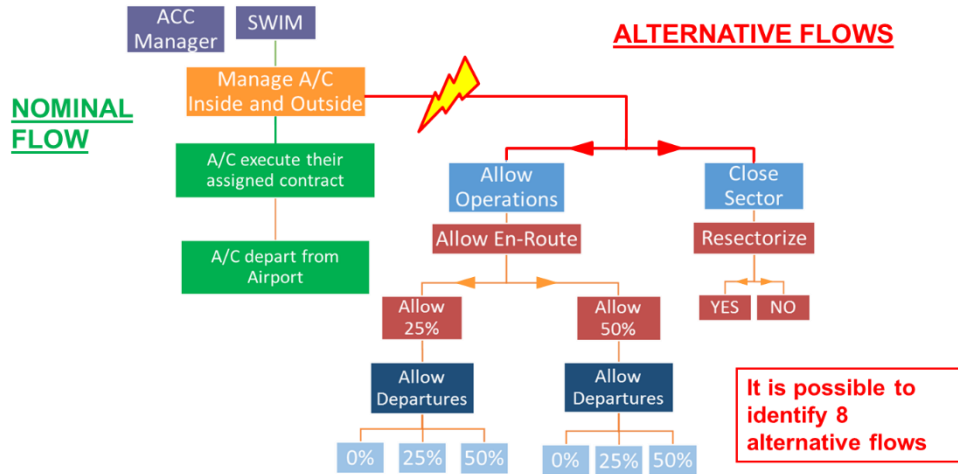


Figure 3. Nominal flow and alternative mitigation strategies for the Case Study.

### 3.3 Global Performance Evaluation and Optimization

As it can be seen, eight possible alternative flows can be identified. Now, in order to evaluate the global performance of the system for each of these alternative flows, we consider a quantitative evaluation of the performance in certain KPAs through the use of specific Key Performance Indicators (KPIs). Specifically:

- K1 - efficiency (fuel burn);
- K2 - efficiency (delay);
- K3 - environment (emissions);
- K4 - capacity (throughput).

In general, once the nominal flow and the off-nominal flows are completely described, it is possible to analyze and optimize the performance through the use of graph theory results. As a matter of fact both the nominal flow and the alternative flows may be represented in the form of weighted directed acyclic graphs (DAGs), in which vertices are tasks whose contribution to performance degradation is weighted along the connecting edges [4].

A computer program written in Java maps the graph and finds the task reallocation strategies (which are all of the possible paths of the graph) with their associated level of global performance. Given a path distance function  $d(\cdot)$  between the nominal task flow and the alternative ones, it is possible to quantify resilience as the shortest path which is basically the one that minimizes performance loss. Specifically – in line with Figure 1b – we have chosen as distance function the difference between the areas that are generated by the performance levels expressed by the KPIs for all of the possible mitigation strategies [3,4].

### 3.4 Results

In this specific case study we have obtained the graph shown in Figure 4 and the results shown in Figure 5. As it can be seen, the more the global performance area of the off-nominal strategies is close to the nominal one, the more the system is resilient.

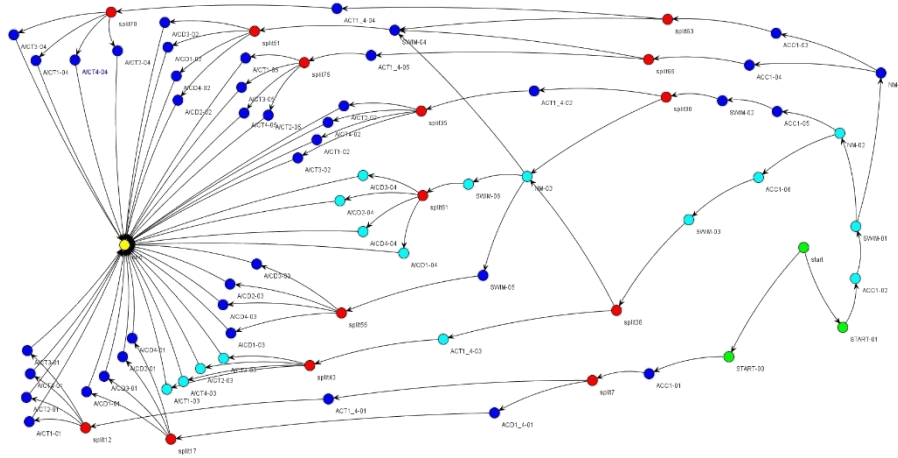


Figure 4. Generated DAG graph for the Case Study.

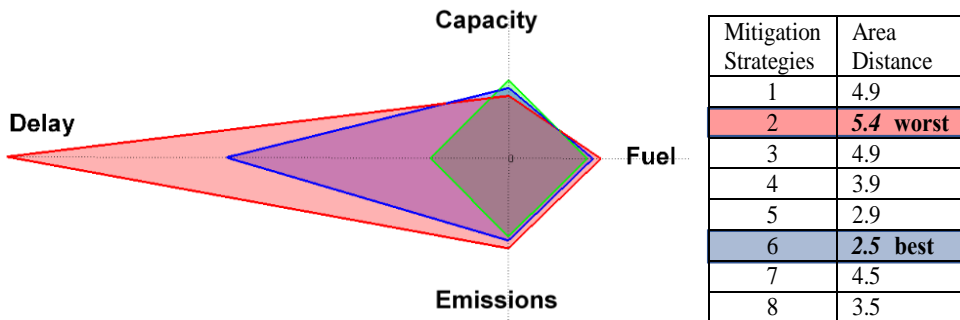


Figure 5. Results of the resilience optimization for the Case Study.

As seen, the analysis of this Case Study is quite straightforward and – in principle – it does not need a computational approach. However, the analysis of different scenarios throughout the development of the SAFECORAM project has demonstrated that the system can become extremely complex and impossible to treat without a computational approach and graph theory results.

## 4 SAFECORAM METHODOLOGY AS A DECISION SUPPORT TOOL

While the methodology defined in the SAFECORAM project is mainly oriented at defining an operational way to quantify the resilience of the future ATM system, it can also be employed as a decision-support tool in performance optimization analyses related to ATM contexts.

In this section, we use the SAFECORAM approach as a cost-benefit analysis tool for airlines dealing with potential flight cancellations or replanning due to a volcanic ash cloud. This idea – which is still currently work in progress – stems from the well-known volcanic ash aviation crisis of 2010, one of the most common actual events referred in ATM resilience studies.

### 4.1 The 2 1 Volcanic Ash Aviation Crisis

Between April and May 2010, the European airspace was massively disrupted by the eruption of the Icelandic volcano Eyjafjallajökull which caused the presence of a large cloud of fine ash drifting south east. In fact many national aviation authorities, following the “zero ash tolerance” regulation advised by ICAO (because of the threat posed by ash to aircraft engines) and relying on the ash cloud forecast carried out by the Volcanic Ash Advisory Centre in London, decided to shut-down many air sectors for days, grounding thousands of flights and millions of passengers, causing huge economic losses to airlines and airports. As a matter of fact, during the ash crisis, several airlines conducted a number of independent flight tests and safety assessments demonstrating the limitations of the precautionary “zero ash tolerance” criterion in areas where the ash concentration was lower than  $2 \text{ mg/m}^3$  [5]. As a consequence, after some pressure from the airlines and in agreement with jet engine experts, ICAO decided to raise the threshold for dangerous ash concentration and a new safety code was roughed out. Specifically, any ash concentration:

- higher than  $2 \text{ mg/m}^3$ , is a no-fly zone;
- between  $2 \text{ mg/m}^3$  and  $0.2 \text{ mg/m}^3$ , requires airlines to take extra precautions
- below  $0.2 \text{ mg/m}^3$  is considered no threat at all.

This new regulation allowed most of the airspace to be reopened. In fact in the aftermath of the crisis, EUROCONTROL ultimately decided that, “while each individual state remains responsible for deciding whether or not to impose restrictions on flights in its airspace, [...] decisions to perform flights in airborne contamination (such as ash or sand), should be made by airlines, based on the conclusions of their safety risk assessment” [6].

### 4.2 Simulated Ash Cloud Scenario Description

The objective of this section is to describe and analyze an ash cloud crisis scenario similar to the one of 2010. This study will show how the SAFECORAM approach can be used as a cost-benefit analysis tool that may help to find the best mitigation strategy in terms of economic damage caused by ash cloud flight disruptions.

As study reference scenario, we consider a one-day flight schedule of a generic low-cost airline operating a B737-800 fleet from London, UK, to several European cities.

In the nominal strategy, 14 daily flights are carried out nominally (see Figure 6) and the airline expenses for each flight are the nominal reference costs.

We then consider two consecutive days of ash cloud crisis. We assume the following:

- the post 2010 ash crisis regulation holds, therefore the ash cloud is divided into three areas with high, medium and low levels of ash concentration. Areas with concentration levels higher than  $2 \text{ mg/m}^3$  are considered no fly zones, while areas with levels below  $0.2 \text{ mg/m}^3$  are totally safe;
- areas with medium concentration levels are assumed to have a homogeneous value of  $1.1 \text{ mg/m}^3$  and are all safe to cross, however the airline is faced with additional maintenance costs [7];
- the vertical distribution of the ash cloud is uniform between FL200 and FL350 while its horizontal distributions (in the 2 days) slightly resemble those observed on April 18-19, 2010 [5];
- the ash cloud topology for each day is not a function of time, i.e. the cloud is constant across the day of operation.

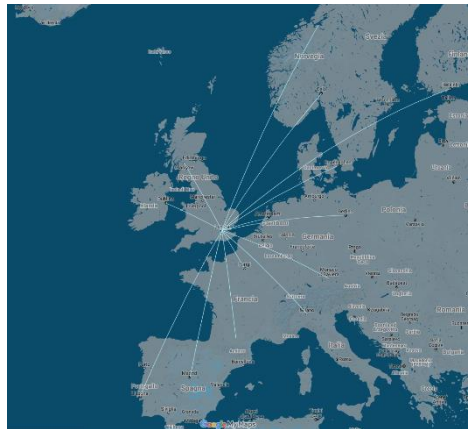


Figure 6. Route structure of the generic low-cost airline considered in the Scenario.

### 4.3 Disturbance Analysis and Task Allocation

As far as the mitigation strategies are concerned, we assume that for each flight of the day the airline can decide:

- to cancel the flight, or
- to fly directly to the destination (modifying as little as possible the trajectories that should intersect no-fly zones), or

- to deviate the flight in order to reduce as much as possible the flight time within the medium concentration ash cloud.

These options have all different impacts on the overall flight costs.

#### 4.4 Global Performance Evaluation and Optimization

In fact the KPI used in this analysis is the overall cost that the airline has to face in order to tackle the flight operations in each day of the crisis. The overall cost is then normalized with respect to the nominal case (i.e. flights carried out nominally without any contingency measure due to the ash cloud).

Degradation of the KPI is brought about by costs due to additional flight time when rerouting the airplane to avoid the ash cloud, and to additional maintenance when crossing the medium concentration ash cloud.

The determination of flight costs has been carried out collecting data from different literature sources [<sup>8,9</sup>] relative to the B737 type of aircraft. Delay costs and cancellation costs were taken from [<sup>9,10</sup>]. All costs were expressed in terms of dollars per block hour. No literature references were found on the cost of maintenance due to flights within ash clouds of medium concentration. However, according to Ref. 7, the maximum tolerable exposure dose to volcanic ash of a turbine engine before mandatory engine inspection is around  $15\text{g}\cdot\text{s}/\text{m}^3$ . From this piece of information, assuming that the cloud has a constant concentration of  $1.1\text{mg}/\text{m}^3$ , we were able to draw some conclusions on the additional costs of maintenance per flight hour within the cloud, as this process reduces the time interval between routinary engine inspections.

Using these data and assuming (realistically) constant average speed for each flight, we were able to determine the cost of each flight per day for the three different aforementioned alternative airline choices.

#### 4. Results

Analyzing the resulting decision tree it is possible to determine the most convenient flight management for both days of operations.

Figure 7 shows the route structure assuming that all flights during Day 1 (above) or Day 2 (bottom) are either direct (left) or deviated (right). On Day 1 some routes are not disrupted by the ash cloud, while some routes marked as DIRECT are slightly deviated to avoid the high density ash cloud. In both ash cloud situations there are some flights that must be cancelled since their destination is not reachable without crossing the no-fly zone.

Table 1 and Table 2 summarize the resulting flight management schedule in the best case (lowest economic damage) and worst case (highest economic damage). The tables report the Cost KPI for each flight (normalized with respect to the nominal cost of that flight) and also a Best and Worst Total Cost Index which is the total cost of the day of operations normalized to the overall nominal cost of the same day. It can be seen that on both days, although the total

cost to the airline will obviously grow, there are mitigation strategies that generate a total cost lower than 1.5 times the nominal cost, while other (worse) strategies could cost up to more than twice the nominal cost.

DAY 1		Best Management		Worst Management		
Route	Flight Status	Cost KPI		Flight Status	Cost KPI	
LHR-CDG	DIRECT	3.21	Not Affected	DEVIATED	6.82	
LHR-AMS	DEVIATED	1.23		CANCELED	3.61	
LHR-DUB	DIRECT	1.00		DIRECT	1.00	
LHR-GLA	DIRECT	1.00		DIRECT	1.00	
LHR-MAD	DIRECT	1.30		DEVIATED	2.40	
LHR-SXF	DEVIATED	1.02		CANCELED	2.13	
LHR-CPH	DIRECT	1.00		DIRECT	1.00	
LHR-OSL	CANCELED	1.95		Unreachable	CANCELED	1.95
LHR-LIN	DIRECT	1.63		CANCELED	2.13	
LHR-LIS	DIRECT	1.21		Unreachable	DEVIATED	1.63
LHR-HEL	CANCELED	1.38		CANCELED	1.38	
LHR-MUC	DIRECT	1.46		CANCELED	2.23	
LHR-TLS	DIRECT	1.78		Unreachable	DEVIATED	3.16
LHR-TRD	CANCELED	1.56		CANCELED	1.56	
<b>Best Total Cost Inde</b>				<b>1.43</b>		
<b>Worst Total Cost Inde</b>				<b>2.</b>		

Table 1. Day 1: Most convenient and least convenient flight planning (in terms of economic damage).

DAY 2		Best Management		Worst Management		
Route	Flight Status	Cost KPI		Flight Status	Cost KPI	
LHR-CDG	DIRECT	1.62	Unreachable	CANCELED	4.70	
LHR-AMS	DEVIATED	1.10		CANCELED	3.61	
LHR-DUB	DIRECT	1.39		CANCELED	3.33	
LHR-GLA	CANCELED	2.93		CANCELED	2.93	
LHR-MAD	DIRECT	1.17		DEVIATED	1.79	
LHR-SXF	DEVIATED	1.07		CANCELED	2.13	
LHR-CPH	DIRECT	1.46		CANCELED	2.13	
LHR-OSL	DIRECT	1.25		DEVIATED	2.51	
LHR-LIN	DIRECT	1.55		DEVIATED	5.21	
LHR-LIS	DIRECT	1.17		CANCELED	1.38	
LHR-HEL	DIRECT	1.29		DEVIATED	1.53	
LHR-MUC	DIRECT	1.48		DEVIATED	2.87	
LHR-TLS	DIRECT	1.36		DEVIATED	3.61	
LHR-TRD	DIRECT	1.22		DEVIATED	2.33	
<b>Best Total Cost Inde</b>				<b>1.3</b>		
<b>Worst Total Cost Inde</b>				<b>2. 1</b>		

Table 2. Day 2: Most convenient and least convenient flight planning (in terms of economic damage).

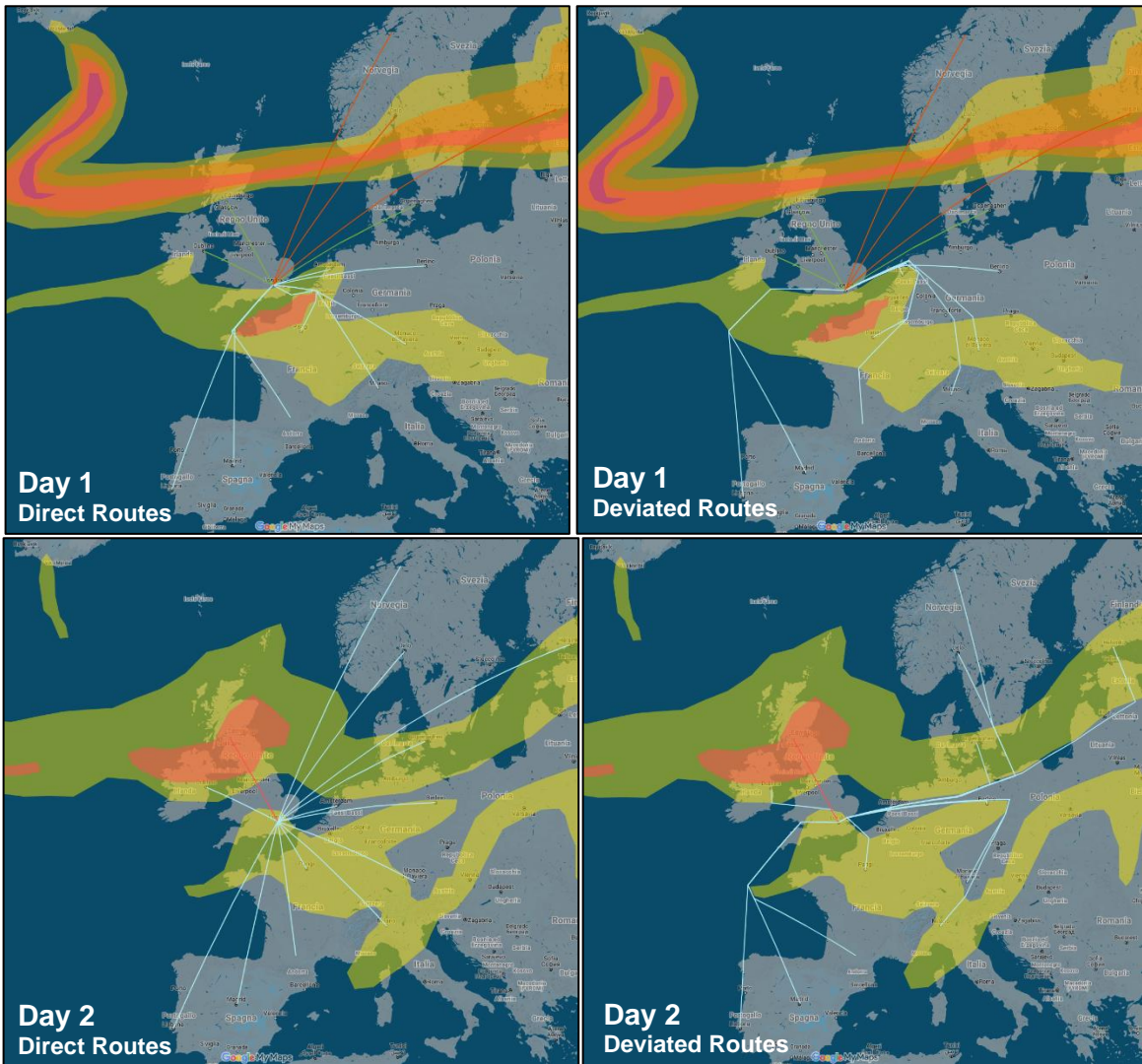


Figure 7. Direct and deviated routes considered in the Scenario.

## CONCLUSIONS

This work describes the SAFECORAM approach, a methodology to quantify and optimize the ATM system resilience. The application of this approach to realistic case studies demonstrated the consistency of the methodology. In fact in non-nominal conditions that could disrupt, locally or extensively, the ATM system operability, the proposed approach allows to

select the proper task allocations that optimize the recovery of the global performance of the ATM system. We have also employed the SAFECORAM methodology as a support-decision tool in a cost-benefit analysis for a generic airline, evaluating a volcanic ash crisis kind of scenario, using a cost index as Key Performance Indicator.

Future work will expand this approach to consider the full ATM performance framework, merging several KPIs related to different key performance areas.

## REFERENCES

- [1] Graham, R., Pilon, N., Tabernier, L., Koelman, H. and Ravenhill, P., Performance framework and influence model in ATM, Digital Avionics Systems Conference, IEEE/AIAA (2009).
- [2] EUROCONTROL, A white paper on resilience engineering for ATM, Report of the Project Resilience Engineering for ATM (2009).
- [3] Palumbo, R., Filippone, E., A Quantitative Approach to Resilience Engineering for the Future ATM System: Case Studies Results, 12th USA/Europe Air Traffic Management Research and Development Seminar (2017).
- [4] Filippone, E., Gargiulo, F., Errico, A., di Vito, V. and Pascarella, D., Resilience management problem in ATM systems as a shortest path problem, *J. Air. Tra. Man.* (2016) 56:57-65.
- [5] Folch, A., Costa, A., Basart, S., Validation of the FALL3D ash dispersion model using observations of the 2010 Eyjafjallajökull volcanic ash clouds, *Atmos. Environ.* (2012) 48:165-183.
- [6] EUROCONTROL, What has changed for aviation in dealing with volcanic ash since 2010?, retrieved from <http://www.eurocontrol.int/articles/what-has-changed-aviation-dealing-volcanic-ash-2010>
- [7] Clarkson, R., Simpson, H., Maximising Airspace Use During Volcanic Eruptions: Matching Engine Durability against Ash Cloud Occurrence, STO-MP-AVT-272 (2017).
- [8] Aviation Week, July 30, 2012.
- [9] EUROCONTROL, Standard Inputs for EUROCONTROL Cost-Benefit Analyses (2015).
- [10] Cook, A., Tanner, G., Jovanović, R., Lawes, A., The Cost of Delay to Air Transport in Europe – Quantification and Management, 13th Air Transport Research Society World Conference (2009).

## Data-driven Discovery of Closure Models

Shaowu Pan<sup>\*</sup>, Karthik Duraisamy<sup>\*\*</sup>

<sup>\*</sup>University of Michigan, Ann Arbor, <sup>\*\*</sup>University of Michigan, Ann Arbor

### ABSTRACT

In this work, we discover closures for reduced-dimensional dynamical systems using data from high-dimensional dynamical systems. In contrast to parameter estimation or function reconstruction, the entire evolution operator of the closure term is extracted from data. Inspirations for the closure are derived from the Mori-Zwanzig formalism of statistical mechanics, which is a formal procedure to address coarse-graining of multi-scale problems. A key characteristic feature of this approach is that the closed lower-dimensional system is capable of emulating the non-Markovian character of the true reduced-dimensional dynamics. For Machine learning, we pursue global features (via non-linear regression) and local approaches (via neural networks), and the limitations of both approaches are discussed. Applications will be demonstrated in reduced order models of transport PDEs.

## **A Consistent Adaptive-resolution Meshless Method**

Wenxiao Pan<sup>\*</sup>, Wei Hu<sup>\*\*</sup>, Guannan Guo<sup>\*\*\*</sup>, Xiaozhe Hu<sup>\*\*\*\*</sup>

<sup>\*</sup>University of Wisconsin-Madison, <sup>\*\*</sup>University of Wisconsin-Madison, <sup>\*\*\*</sup>University of Wisconsin-Madison, <sup>\*\*\*\*</sup>Tufts University

### **ABSTRACT**

We seek to accelerate and increase the size of simulations for fluid-structure interactions (FSI) by using adaptive resolutions in the spatial discretization of the equations governing the time evolution of systems displaying two-way fluid-solid coupling. To this end, we propose an adaptive-resolution smoothed particle hydrodynamics (SPH) approach, in which spatial resolutions adaptively vary according to a recovery-based error estimator of velocity gradient as flow evolves. The second-order consistent discretization of spatial differential operators is employed to ensure the accuracy of the proposed method. The convergence, accuracy, and efficiency attributes of the new method are assessed by simulating different flows. In this process, the numerical results are compared to the analytical and finite element solutions. We anticipate that the proposed adaptive-resolution method will enlarge the class of SPH-tractable FSI applications.

## **Lattice Type Model in Fracture Analysis of Cementitious Materials: A Brief Review on Achievements and Developments During the Past 30 Years**

Zichao Pan<sup>\*</sup>, Rujin Ma<sup>\*\*</sup>, Airong Chen<sup>\*\*\*</sup>, Dalei Wang<sup>\*\*\*\*</sup>

<sup>\*</sup>Department of Bridge Engineering, Tongji University, <sup>\*\*</sup>Department of Bridge Engineering, Tongji University,  
<sup>\*\*\*</sup>Department of Bridge Engineering, Tongji University, <sup>\*\*\*\*</sup>Department of Bridge Engineering, Tongji University

### **ABSTRACT**

The lattice model is a discrete model that is typically used to simulate the fracture process of brittle materials such as mortar and concrete. This review briefly summarizes the most important achievements of the lattice model in fracture mechanics during the past 30 years. The lattice type models can be generally divided into (1) lattice spring model (LSM), and (2) lattice beam model (LBM), where the classical LSM can only simulate a fixed Poisson's ratio. This problem can be solved by using (1) extra nodal DOFs, (2) extra shear springs, (3) extra nonlocal energy parameters, and (4) higher dimensional normal springs. The lattice model has already been successively applied in simulations of fracture processes of different materials including mortar and concrete, and under different loads. The innovative areas of future research in reference to the use of the lattice model in engineering practice include constitutive relations, failure criteria, anisotropic material modeling and efficient computing techniques to expand its use and range of applications.

## A Probabilistic Model for Aircraft Freeplay Dynamics

J. Panchal<sup>\*</sup>, H. Benaroya<sup>\*\*</sup>, S. Mottaghi<sup>\*\*\*</sup>

<sup>\*</sup>Rutgers University, <sup>\*\*</sup>Rutgers University, <sup>\*\*\*</sup>William J. Hughes Technical Center, FAA

### ABSTRACT

A probabilistic approach is developed to model the potentially unstable dynamics, known as flutter, of airfoils due to nonlinearities in the behavior of the coupled fluid-structural system. One source of nonlinearity is freeplay, which is a regime where stiffness is zero or almost zero. There is a break in the stiffness force around zero displacement or rotation. The literature on this is substantial. It is generally agreed that this freeplay nonlinearity lowers the flutter onset velocity, and typically introduces a limit cycle oscillation mode of flutter. While not necessarily divergent, this behavior can significantly accelerate the accumulation of structural fatigue damage and degrade controllability. Experimental, as well as computational and analytical studies have explored this behavior. Regimes of instability have been mapped. Damping-driven hysteretic behavior has been identified, as well as snap-through behavior. Reduced-order models have been derived based on classical aerodynamic theory, for sub- and transonic regimes. These reduced-order models generally allow one or two structural degrees of freedom, depending on the allowable motion of the airfoils. Cubic spring hardening nonlinearity is common. In many instances the aerodynamic force and moment are assumed to be linear. Damping is rarely included in the analytical models. Most analyses are deterministic, with a few including aerodynamic turbulence in the model, in which cases random responses are examined, where it appears that there is a coupling between the nonlinearity and the random external excitation. Current regulatory guidance is based on relatively old data on structural models that no longer closely resemble today's aircraft. There is much interest in deriving a better understanding of this phenomenon due to the seriousness of its impact on safety, reliability and maintenance. Our work is based on the development of stochastic dynamic models for the above phenomena. Based on experimental evidence, there appear to be substantial variabilities in the parameters that define the freeplay, as well as the regimes of structural response, in particular, the onset of instabilities. We believe that the freeplay characterization is not only nonlinear, but also stochastic in loading as well as in system properties. The freeplay region likely changes with age. System parameters, including damping, in principle, need to reflect random changes in parameter values with time. We present our modeling efforts.

## An Irving-Kirkwood Based Homogenization Procedure for Thermomechanical Continua

Sushrut Pande<sup>\*</sup>, Panayiotis Papadopoulos<sup>\*\*</sup>, Robert Taylor<sup>\*\*\*</sup>

<sup>\*</sup>University of California, Berkeley, <sup>\*\*</sup>University of California, Berkeley, <sup>\*\*\*</sup>University of California, Berkeley

### ABSTRACT

This talk presents a homogenization procedure to model material behaviour for thermomechanical continua. The procedure [1] is derived using an approach inspired by Irving and Kirkwood [2] which only homogenizes extensive quantities namely mass, linear momentum and energy. In conjunction with continuum balance laws, expressions are derived for the macroscopic stress and heat flux in terms of microscopic quantities. The procedure is compared with the classical energy-conserving Hill-Mandel condition. The talk will also describe the implementation of this procedure using a continuum-to-continuum FE<sup>2</sup> solution - whereby every material point is associated with an RVE (representative volume element) which represents the underlying microstructure. An RVE boundary-value problem is solved at the microscale and the results are homogenized to obtain macroscopic quantities. The two scales are linked by means of Lagrange multiplier constraints, which indirectly impose various kinds of boundary conditions on the RVE at the microscale which will be discussed. Some numerical examples which illustrate the application of this procedure to practical problems will also be presented. References: [1] Mandadapu, K.K., Sengupta, A., Papadopoulos, P. A homogenization method for thermomechanical continua using extensive physical quantities. Proc. R. Soc. A., 486, pp 1696--1757, 2012. [2] Irving, J.H., Kirkwood, J.G. The statistical mechanical theory of transport processes. IV. The equations of hydrodynamics. J. Chem. Phys., 18, pp. 817--829, 1950.

## **A Numerical Algorithm for the Solution of the Fluid-Structure Interaction Problem in the Corneal Air Puff Test**

Anna Pandolfi<sup>\*</sup>, Andrea Montanino<sup>\*\*</sup>, Maurizio Angelillo<sup>\*\*\*</sup>

<sup>\*</sup>Politecnico di Milano, <sup>\*\*</sup>Politecnico di Milano, Italy, <sup>\*\*\*</sup>Universita' di Salerno, Italy

### **ABSTRACT**

The air puff test is a clinical exam commonly used in ophthalmology to determine the intraocular pressure (IOP), the pressure exerted on the cornea by the fluid filling the anterior chamber of the eye. The test consists in applying a rapid and localized air jet pulse on the anterior surface of the cornea, provoking a transient local change of sign of the mean curvature: the level of external pressure exerted by the air jet when the cornea is locally flattened is correlated to IOP. More recently, the air puff test has been regarded as a possible tool to retrieve patient-specific material parameters of the corneal structure. In this respect, the numerical modelling of the air puff test has assumed interest, in view of conducting inverse analyses correlating medical images and numerical simulations, that can provide information about the material parameters of the corneal material and finally, a more accurate patient specific model of the eye, a goal of great interest in refractive surgery. From the mechanical side point of view, the air puff test is a Fluid-Structure Interaction (FSI) problem, due to the mutual interaction between the corneal deformation and changes in the pressure load due to fluid movement. In this work we present an algorithm for the simulation of the FSI problem of the air puff test. For the numerical simulation we use a staggered approach, consisting in the use of two different solvers for the two subdomains, allowing to preserve the advantages of each solver. In particular, we use a finite element code for the solid elastic problem of the cornea, already used in [1], and a meshless method for the fluid domain [2], using a Lagrangian formulation, particularly suitable for fluid-dynamic problems with moving boundaries. The coupling between subdomains is made through an iterative Dirichlet-Neumann algorithm, following the formulation already used in [3] for the axis-symmetric case. The results we present confirm the computational efficiency of the numerical approach in dealing with the corneal-humor aqueous interaction, and provide useful information for the determination of the mechanical properties of the corneal tissue. [1] Pandolfi, A. and Manganiello, F. &quot;A model for the human cornea: constitutive formulation and numerical analysis.&quot; BMMB 5.4(2006):237-246. [2] Asprone, D., et al. &quot;A Modified Finite Particle Method: Multi-dimensional elasto-statics and dynamics.&quot; IJNME 99.1(2014):1-25. [3] Montanino, A., et al., &quot;Modelling with a meshfree approach the cornea-aqueous humor interaction during the air puff test.&quot; JMBBM 77(2018):205-216.

## Minimal Worst-Case Stress Microstructure Design

Julian Panetta<sup>\*</sup>, Denis Zorin<sup>\*\*</sup>

<sup>\*</sup>École Polytechnique Fédérale de Lausanne (EPFL), <sup>\*\*</sup>New York University

### ABSTRACT

The power of modern additive fabrication technologies to rapidly and inexpensively manufacture special-purpose customized objects has spurred the development of computational tools for designing objects to meet specific performance goals. However, many such design goals--for instance, achieving particular deformations under applied forces--require precise control of the fabrication material's elastic properties beyond the capabilities of even advanced multi-material 3D printers. Furthermore, many behaviors are impossible to achieve with ordinary fabrication materials (e.g., negative Poisson's ratios). Several recent works address this limitation by using periodic microstructures to emulate a large space of elastic materials. This approach to tailoring material properties is a perfect fit for additive fabrication, which can produce parts of arbitrary complexity at a cost proportional to only the material consumed. Unfortunately, one significant problem blocks practical applications: the structures tend to feature thin joints that concentrate stress, leading to plastic deformation or fracture. My talk addresses this problem; I describe how to design microstructures that minimize stress, thereby improving the resulting metamaterials' robustness in practice. First, I introduce an efficient, exact solution to the worst-case stress analysis problem for periodic microstructures. Because microstructures behave like general-purpose materials, it is most natural and computationally efficient to build a single complete metamaterial library up-front instead of re-solving the microstructure design problem in the inner loop of each macroscopic design optimization. Consequently, the specific loads a microstructure will experience are unknown during its design. To ensure that every microstructure in the library is robust in generic use, we must design each to withstand its worst-case load: the load most likely to induce failure at any given point. I show that, for several different stress-based failure criteria (e.g., maximum principal stress or von Mises stress), determining a periodic structure's worst-case loads can be formulated as solving an inexpensive tensor eigenvalue problem for each point in the structure. Next, I introduce a method to design microstructures that experience minimal worst-case stresses while producing a wide range of elastic material properties. The design problem is formulated as a parametric shape optimization and incorporates constraints to ensure manufacturability on 3D printers without support structure. Finally, I demonstrate how the worst-case stress reductions achieved by the method (typically a reduction factor of roughly 5x) translate into practical robustness improvements visible in lab tests on 3D printed samples. [1] Panetta, J., Rahimian, A., Zorin, D. 2017. Worst-case Stress Relief for Microstructures. ACM Trans. Graph. 36, 4 (July), 122:1--122:16.

## Strength Distributions of Brittle Heterogenous Materials and Its Scale Effects on Stochastic Simulations of Fracture

Sze Dai Pang\*

\*National University of Singapore

### ABSTRACT

It has been well accepted that the probability distribution function of structural strength follows the Gaussian distribution for ductile materials by virtue of the central limit theorem of the theory of probability while it follows the Weibull distribution for brittle materials by virtue of the weakest-link theory of probability. Recently, it has been shown that the probability distribution function of structural strength for brittle heterogenous materials lies somewhere between Gaussian and Weibull distributions and depends on type of loading, structure size and geometry (Bažant and Pang, 2006; Le et al. 2011). In fact, it has been argued theoretically and matched experimentally that the probability distribution function of these quasibrittle materials comprises of a Gaussian distribution with a transition to Weibull distribution at the tail probabilities. The point of transition is largely dependent on the size of the representative volume element (RVE) and the number of equivalent RVEs in the structure. The coefficients of variation for the Weibull and Gaussian distribution segments are found to be dependent on the stress distribution and redistribution within the RVE and size of the RVE. A proper treatment will necessitate a probability distribution function that can reproduce the Gaussian distribution at small size limit and Weibull distribution at large size limit. Such is the probability distribution function proposed by Bažant and Pang (2006) which is size dependent and also relies on the knowledge of the size and statistical property of each RVE. When the FE mesh coincides with the size of the RVE, the material strength can be treated as brittle with its random field being sampled from the proposed probability distribution function which would have accounted for the stress redistribution with the RVE. In most cases, the size of the FE mesh does not correspond to the size of the RVE and this inevitably leads to a scale effect on the probability distribution of strength which is further complicated by the stress redistribution (having the effect of sharing the loads analogous to extending the Gaussian core). The scaling of the probability distribution ought to lead to mesh objectivity in FE simulations which is investigated in this study. REFERENCES Bažant, Z.P., and Pang, S.-D. (2006). Proc. of the National Academy of Sciences 103(25), 9434-9439. Le, J.-L., Bažant, Z.P., and Bažant, M.P. (2011). Journal of the Mechanics and Physics of Solids 59, 1291-1321.

## Robust Hex-Dominant Mesh Generation Using Field-Guided Polyhedral Agglomeration

Daniele Panozzo\*

\*New York University

### ABSTRACT

While hexahedral meshes are generally preferred for solving nonlinear partial differential equations, automatic techniques capable of producing them robustly are still out of reach despite three decades of extensive research dedicated to this topic. Hexahedral-dominant meshes strike a good balance: they are easier to generate, since they can contain a small number of irregular elements, while offering good numerical properties. Building upon the 2D instant meshing (IM) approach, we introduce a novel algorithm to efficiently, robustly, and automatically create field-aligned hex-dominant meshes. The first part of the talk will cover a quaternionic representation for a volumetric cross-field, which will guide the edge alignment of the hex-dominant mesh. When paired with a hierarchical accelerations structure, this representation enables us to interpolate user-defined constraints, while naturally aligning to shape features. The volumetric cross-field is used to define a position field encoding the position of the nodes of the hex-dominant mesh. The second part of the talk will complete the pipeline, providing a robust extraction algorithm guaranteed to extract a compatible manifold mesh from any field-aligned parameterization — it is designed to work with local parameterizations that are characteristic of the output produced by the IM technique, but it can also be applied to any global parameterization generated by other means. The algorithm uses a sequence of local topological operations to collapse and split edges, faces, and polyhedra of the input mesh, eventually converting the input tetrahedral mesh into a hex-dominant output mesh. Topological invariants are checked before each operation, and only those preserving the invariants are executed, which ensures that both genus and manifoldness of the input are preserved throughout this process. While the two contributions are independently useful in existing meshing pipelines, they have been designed together to extend the IM pipeline to the volumetric cases. Combined, they lead to a simple, robust, automatic, and scalable pipeline that automatically remesh a benchmark composed of 106 meshes, with no user-interaction and no parameter tweaking.

## **Introduction to Geometry Processing and Field-Aligned Mesh Generation**

Daniele Panozzo<sup>\*</sup>, Denis Zorin<sup>\*\*</sup>, Leif Kobbelt<sup>\*\*\*</sup>

<sup>\*</sup>NYU, <sup>\*\*</sup>NYU, <sup>\*\*\*</sup>NYU

### **ABSTRACT**

Introductory comments on MS 812 topic.

## Flaw Tolerance of Architected Metamaterials

Panos Pantidis<sup>\*</sup>, Andrew Gross<sup>\*\*</sup>, Katia Bertoldi<sup>\*\*\*</sup>, Simos Gerasimidis<sup>\*\*\*\*</sup>

<sup>\*</sup>PhD Candidate, University of Massachusetts, Amherst, <sup>\*\*</sup>Post-Doctoral, Harvard University, Boston, USA,  
<sup>\*\*\*</sup>Professor, Harvard University, Boston, USA, <sup>\*\*\*\*</sup>Assistant Professor, University of Massachusetts, Amherst

### ABSTRACT

Recent advancements in the area of bio-inspired lattice-truss metamaterials have allowed the design and fabrication of new lightweight materials with unique and tunable properties. High fabrication rates may though result in a higher probability of producing defects, whereas the term 'defect' is utilized to describe the presence or absence of a member-strut in the lattice-truss topology. This work constitutes a systematic approach to examine and identify the mechanical properties of defected architected meta-materials. Using advanced nonlinear finite element techniques, a variety of bending- and stretching-dominated topologies are investigated under quasi-static compression and their characteristic mechanical properties such as the effective elastic modulus, the yield stress and the damage propagation path of the failure mode are assessed. The randomness of the defect spatial distribution for a given defect percent is accounted for through exhaustive sampling using Monte Carlo simulations, and the evolution of the mechanical properties is monitored as the total defect percent increases in magnitude. Additional idealizations of cluster defect scenarios are conducted, providing insight on the behavior of the different topologies when voids exist within their domain. The impact of fixed boundary conditions in finite defected tessellation sizes versus infinite defected periodic geometries is also investigated. The experimental part of this work is conducted using the two-photon lithography approach, an advanced additive manufacturing technique capable of printing polymer struts with sub-micron cross-sectional dimensions. Representative specimens of intact and defected metamaterials topologies are fabricated and they are compared to the numerical results, providing a detailed picture of the actual behavior of defected lattice-truss materials at different connectivity levels.

## **Defect Generation and Nanostructure Deformation during Focused Ion Beam Processes of Nanomaterials**

Chun-Wei Pao\*, Cheng-Lun Wu\*\*

\*Research Center for Applied Sciences, Academia Sinica, Taiwan, \*\*Research Center for Applied Sciences, Academia Sinica, Taiwan

### **ABSTRACT**

Focused ion beam (FIB) is a versatile tool with applications across disciplines ranging from optoelectronic devices, metamaterials, bioimaging, and even to archaeology. Nevertheless, the nanoscale machining precision of FIB is often accompanied by damages to the nanostructures due to energetic ion beam bombardment. In this talk, we will present our recent works on studying the nanostructure deformation as well as defect generation mechanisms during FIB processes using a series of large-scale molecular dynamics (MD) simulations. We will focus on two subjects: 1) the mechanisms leading to FIB-induced self-fold behavior of nanostructures, and 2) defect generation and suppression during FIB patterning of 2D materials. We will reveal that mass transport from ion beam irradiation is responsible for the nanostructure self-folding, and the constrained scattering of atoms from 2D materials is the primary source of damage to 2D materials during FIB patterning. Hence, by understanding the mechanisms behind nanostructure deformation and defect generation during FIB processes, it is possible to fabricate nanostructures with complicated geometries, as well as patterning 2D materials with nanoscale precision using FIBs.

## Consistent Bayesian Updating for Multiscale Analysis Using Subset Simulation

Vissarion Papadopoulos<sup>\*</sup>, Marios Impraimakis<sup>\*\*</sup>, Dimitris Giovanis<sup>\*\*\*</sup>, Ioannis Kalogeris<sup>\*\*\*\*</sup>

<sup>\*</sup>National Technical University of Athens, <sup>\*\*</sup>National Technical University of Athens, <sup>\*\*\*</sup>Johns Hopkins University, <sup>\*\*\*\*</sup>National Technical University of Athens

### ABSTRACT

Bayesian updating is a powerful method to learn and calibrate models with data and observations, facts that is of utmost importance in multiscale problems with uncertain microscale status like very random and hard predicted nanocomposite behavior. In this work BUS (Bayesian Updating with Structural reliability methods) with SuS (Subset Simulation) in a multiscale environment is employed to compute the posterior distribution of microscale random parameter in a framework that microscale with mesoscale and microscale with macroscale pair models converge into each experimental data simultaneously. More specific, every sample cluster of every subset within SuS in this parallel double problem forced to agree with the other one. In the end, the samples in the final subset (posterior samples in Bayesian terms) have the best agreement with experimental data. This methodology is very promising for nanomaterial reinforced composites which have big uncertainty range with quite unexpected measurements and really large number of parameter. It is a gainful direction for engineering practice and non-costly experimental investigations, being concurrently quite appropriate for every multiscale modeling applications.

## Enhanced Computational Techniques for Improving the Performance of Isogeometric Analysis

Manolis Papadrakakis<sup>\*</sup>, George Stavroulakis<sup>\*\*</sup>, Dimitrios Tsapetis<sup>\*\*\*</sup>, Manos Trypakis<sup>\*\*\*\*</sup>,  
Christos Gritzalis<sup>\*\*\*\*\*</sup>, Alex Karatarakis<sup>\*\*\*\*\*</sup>

<sup>\*</sup>Institute of Structural Analysis and Antiseismic Research, National Technical University of Athens, Greece,

<sup>\*\*</sup>Institute of Structural Analysis and Antiseismic Research, National Technical University of Athens, Greece,

<sup>\*\*\*</sup>Institute of Structural Analysis and Antiseismic Research, National Technical University of Athens, Greece,

<sup>\*\*\*\*</sup>Institute of Structural Analysis and Antiseismic Research, National Technical University of Athens, Greece,

<sup>\*\*\*\*\*</sup>Institute of Structural Analysis and Antiseismic Research, National Technical University of Athens, Greece,

<sup>\*\*\*\*\*</sup>Microsoft Corporation, Seattle, USA

### ABSTRACT

Due to high regularity across mesh elements, isogeometric analysis (IGA) achieves higher accuracy per degree of freedom and improved spectrum properties, among others, compared with finite element analysis. However, this inherent feature of isogeometric analysis increases the density of the stiffness matrix and requires more elaborate numerical integration schemes for its computation. Furthermore, the augmented continuity of the shape functions in IGA results in greater bandwidth and overlapping of the resulting matrices, raising the computational cost of solving the corresponding linear systems of equations. For these reasons, both the assembly of the stiffness matrix and the solution of the resulting algebraic equations in isogeometric analysis is a computationally demanding task, which needs special attention in order to be affordable for real-world applications. In this paper we address the computational demanding task of assembling the stiffness matrix using the standard element-wise Gaussian quadrature. A novel approach is proposed for the formulation of the stiffness matrix which exhibits several computational merits, among them, its amenability to parallelization and the efficient utilization of the graphics processing units (GPU) to drastically accelerate computations. In addition, an efficient, scalable and load balanced solution algorithm is proposed that combines the advantages of the preconditioned conjugate gradient (PCG) algorithm and domain decomposition methods (DDM) by introducing a preconditioner based on the isogeometric tearing and interconnecting (IETI) solution method. The proposed preconditioner circumvents the dependency between domain subdivisions and patches that IETI imposes, decoupling load balancing and scalability properties from the model geometry. Numerical examples demonstrate the efficiency of the proposed handling of matrix assembling and solution algorithm, when compared to other matrix assembling schemes and previously presented domain decomposition methods. As a result, the proposed methodologies enables minimization of the computational cost for solving demanding problems with IGA and thus widens its applications in large-scale real life applications. [1] A. Karatarakis, P. Karakitsios, M. Papadrakakis, GPU Accelerated Computation of Isogeometric Analysis Stiffness Matrix, *Comput. Methods Appl. Mech. Engrg*, 269, 334-355, 2014. [2] M. Papadrakakis, G. Stavroulakis, A. Karatarakis, A New Era in Scientific Computing: Domain Decomposition Methods in Hybrid CPU-GPU Architectures, *Comput. Methods Appl. Mech. Engrg*, 200, 1490-1508, 2011. [3] S. Kleiss, C. Pechstein, B. Juttler, S. Tomar, IETI – Isogeometric Tearing and Interconnecting, *Comput. Methods Appl. Mech. Engrg*, 247-248, 201-215, 2012.

## Identifying Far From Equilibrium Microstructures in Crystal Plasticity and Other Crackling Noise Phenomena

Stefanos Papanikolaou\*

\*West Virginia University

### ABSTRACT

When far from equilibrium, many-body systems display behavior that strongly depends on the initial conditions. A characteristic such example is the phenomenon of plasticity of crystalline and amorphous materials that strongly depends on the material history. In plasticity modeling, the history is captured by a quenched, local and disordered flow stress distribution. While it is this disorder that causes avalanches that are commonly observed during nanoscale plastic deformation, the functional form and scaling properties have remained elusive. In this presentation, a generic formalism is developed for deriving local disorder distributions from field-response (log stress/strain) timeseries in models of crackling noise. We demonstrate the efficiency of the method in the hysteretic random-field Ising model and also, models of elastic interface depinning that have been used to model crystalline and amorphous plasticity. We show that the capacity to resolve the quenched disorder distribution improves with the temporal resolution and number of samples. Moreover, we demonstrate how this method may apply to nanoindentation of FCC crystals.

## **A Unified Framework for Multiscale Modeling Using the Mori-Zwanzig Formalism and the Variational Multiscale Method**

Eric Parish<sup>\*</sup>, Karthik Duraisamy<sup>\*\*</sup>

<sup>\*</sup>University of Michigan, Ann Arbor, <sup>\*\*</sup>University of Michigan, Ann Arbor

### **ABSTRACT**

We describe a paradigm for multiscale modeling that combines the Mori-Zwanzig (MZ) formalism of Statistical Mechanics with the Variational Multiscale (VMS) method of Hughes. The MZ-VMS approach leverages both VMS scale-separation projectors as well as phase-space projectors to provide a systematic modeling framework that is applicable to non-linear partial differential equations. Spectral as well as continuous and discontinuous finite element methods are considered. The framework leads to a formally closed equation in which the effect of the unresolved scales on the resolved scales is non-local in time and appears as a convolution or memory integral. The resulting non-Markovian system is used as a starting point for model development. We discover that unresolved scales lead to memory effects that are driven by an orthogonal projection of the coarse-scale residual and inter-element jumps. It is further shown that an MZ-based finite memory model is a variant of the well-known adjoint-stabilization method. For hyperbolic equations, this stabilization is shown to have the form of an artificial viscosity term. We further establish connections between the memory kernel and approximate Riemann solvers.

## **Computational Design of Quantum Spin Hall-Based Phononic Topological Insulators**

Harold Park<sup>\*</sup>, S.S. Nanthakumar<sup>\*\*</sup>, Xiaoying Zhuang<sup>\*\*\*</sup>, Timon Rabczuk<sup>\*\*\*\*</sup>

<sup>\*</sup>Boston University, <sup>\*\*</sup>Leibniz University Hannover, <sup>\*\*\*</sup>Leibniz University Hannover, <sup>\*\*\*\*</sup>Bauhaus-University Weimar

### **ABSTRACT**

We present a new topology optimization framework to design phononic topological insulators based on electronic quantum spin hall-based principles. We discuss the methodology, and show numerical examples demonstrating the resulting phononic topological insulators.

## Prediction of Quasi-static Yield of Amorphous Epoxy Polymers Using Temperature Accelerated Molecular Dynamics

Hyungbum Park<sup>\*</sup>, Byungjo Kim<sup>\*\*</sup>, Maenghyo Cho<sup>\*\*\*</sup>, Joonmyung Choi<sup>\*\*\*\*</sup>

<sup>\*</sup>Seoul National University, <sup>\*\*</sup>Seoul National University, <sup>\*\*\*</sup>Seoul National University, <sup>\*\*\*\*</sup>Samsung electronics Co.

### ABSTRACT

It has been challenging to derive the quasi-static dynamic responses of amorphous polymer systems in the molecular dynamics (MD) simulations, since it demands tremendous computational costs owing to the inherent short timestep of MD simulations. In an efforts to derive the quasi-static mechanical response of amorphous polymer, we propose a temperature accelerated approach using the physical equivalence of time and temperature involving the yield behaviors of polymer system. Herein, quasi-static yield behaviors of amorphous epoxy polymers are predicted using the stress-strain relationship of various elevated temperatures. To predict the yield stress at low strain rate which cannot be explored with classical MD environment, a method to construct Eyring's plot is proposed by quantifying the correlation between increasing temperature and decreasing strain rate. In this study, the obtained results reveal that the strain rate sensitivity of reduced yield stress is getting lower with increasing temperature. This observation opens an avenue for constructing the Eyring's plot toward the low rate condition by sequential shifting of yields at elevated temperature. The predicted quasi-static yield stress of epoxy polymers is validated with the experimental literature, showing good agreement each other. The proposed acceleration approach provides a good way to design of amorphous polymer based materials enabling the estimation of quantitatively comparable constitutive equation to the experimental tests.

## Use of Perimeter Control for Geometrically Complex Structures in Topology Optimization

Jaejong Park<sup>\*</sup>, Alok Sutradhar<sup>\*\*</sup>, Jami J Shah<sup>\*\*\*</sup>, Glaucio H Paulino<sup>\*\*\*\*</sup>

<sup>\*</sup>The Ohio State University, <sup>\*\*</sup>The Ohio State University, <sup>\*\*\*</sup>The Ohio State University, <sup>\*\*\*\*</sup>Georgia Institute of Technology

### ABSTRACT

Perimeter control emerged into topology optimization to alleviate the common numerical instabilities. For instance, solution space employing checkerboard can be discarded during the optimization process by introducing the upper bound on the perimeter. Earlier research efforts in filters and basic projection functions in topology optimization also attempts to reduce the topological complexity that leads to a reduction of the perimeter. However, some design problems demand a high level of geometric complexity with large perimeter value. Simulating designs found in nature requires a solution to have complex internal structures with lots of holes. For instance, stress shielding phenomenon between bone and the implant is of immense importance in the implant design industry. The inherent property mismatch between the bone and implant material can be reduced by designing them with fine members interconnected in a complex manner. Conventional topology optimization formulated as density distribution problem cannot achieve this goal without additional restrictions. In this work, this is attained by confining a lower bound on the perimeter. By restricting the design space by means of the perimeter, intricate design features can be obtained. Three different bone regions with well-known physical loadings are selected to illustrate the efficacy of the method, i.e., femur, calcanium, and midface. Additionally, we observed the perimeter value and the pattern of the initial distributions play a vital role in obtaining natural looking structural members with various curvatures. We also witnessed the initial material distribution is required to have a sufficient perimeter value to avoid excessive islanding. The desired structural complexity can also be obtained by manipulating the target perimeter. The approach demonstrates great potential in engineering problems that requires geometric complexity to cope with uncertainties in the design domain and to promote reliable structure options with high porosity. Issues with aforementioned stress shielding and inadequate mass transfer in medical implant industry could be tackled with the technique described in this work.

## A Study on Selective Bivariate Dimension Reduction Method for Efficient Reliability Analysis

Jeongwoo Park\*, Ikjin Lee\*\*

\*KAIST, \*\*KAIST

### ABSTRACT

As reliability of engineering systems under uncertainty becomes more important in various industries due to global competitive market situation, a safer and more reliable product design to satisfy consumers' needs is required. To satisfy these requirements, there have been various attempts to accurately and efficiently compute the product reliability, which is obtained from reliability analysis and used as a probabilistic constraint of reliability-based design optimization. Among various reliability analysis methods, analytical reliability analysis methods such as the first-order reliability method (FORM), the second-order reliability method (SORM), and the most probable point based dimension reduction method (MPP-based DRM) are available. Reliability analysis using MPP-based DRM, the most recently proposed method, has advantages of the FORM and SORM in terms of efficiency and accuracy. However, the reliability analysis using the MPP-based univariate DRM does not obtain high accuracy because it does not consider the cross-term of the performance function. To increase the accuracy, the MPP-based bivariate DRM can consider the cross-term, but the efficiency decreases as the number of integration points required increases as the dimension of the performance function increases. The main objective of this paper is to develop an efficient methodology for the MPP-based bivariate DRM by using the subspaces considering cross-term. In the proposed method, a partial F-test is introduced to evaluate cross-term and the axial sensitivity. The MPP search points are used in this process, no additional function evaluation is required. In the partial F-tests, F-values and p-values are suggested as criteria to assess sensitivity, the variables selected in the cross-term direction are applied to the bivariate DRM, and the variables selected in the axial direction are increased in the number of integration points of the Gaussian quadrature integration method. Since the partial F-test suggests the application direction of the DRM and the number of integration points, the proposed method can present selection criteria of FORM, univariate DRM, and bivariate DRM for each variable. Several numerical examples demonstrate the improvement of the accuracy and the efficiency of the probability of failure estimation and the feasibility of partial F-tests. Reference [1] Lee, I., Choi, K.K., Du, L. and Gorsich, D., Inverse analysis method using MPP-based dimension reduction for reliability based design optimization of nonlinear and multi-dimensional systems, *Computer Methods in Applied Mechanics and Engineering*, 198(1), p.14–27, 2008. [2] Geladi, P., and Kowalski, B.R., Partial least-squares regression: a tutorial, *Analytica chimica acta*, 185, p.1-17, 1986.

## **Partitioned Symmetric Formulation and Solution Algorithms of Thermoelastic Interaction Problems**

K. C. Park<sup>\*</sup>, Carlos Felippa<sup>\*\*</sup>, Charbel Farhat<sup>\*\*\*</sup>

<sup>\*</sup>University of Colorado, <sup>\*\*</sup>University of Colorado, <sup>\*\*\*</sup>Stanford University

### **ABSTRACT**

A partitioned formulation of transient coupled thermoelastic problems is presented, which yields a four-field symmetric set of partitioned governing equations. The present formulation can be reduced to conventional two-field non-symmetric coupled thermoelastic equations as a special case, thus validating the present partitioned formulation. A key feature of the present formulation is the addition of the constraint enforcement of energy exchanges between the elastic body and the thermal conduction body, each of which occupying the same volume space. The variational formulation of the elastic body and the thermal conduction part is independently constructed as if they are uncoupled. Various solution algorithms are suggested including explicit-implicit, implicit-implicit time integration strategies.

## Multiscale Modelling Framework for Predicting Mechanical Properties of Concrete

S.M. Park<sup>\*</sup>, Bezawit Haile<sup>\*\*</sup>, D.W. Jin<sup>\*\*\*</sup>, B.J. Yang<sup>\*\*\*\*</sup>, H.K. Lee<sup>\*\*\*\*\*</sup>

<sup>\*</sup>Korea Advanced Institute of Science and Technology, <sup>\*\*</sup>Korea Advanced Institute of Science and Technology, <sup>\*\*\*</sup>Korea Advanced Institute of Science and Technology, <sup>\*\*\*\*</sup>Korea Institute of Science and Technology, <sup>\*\*\*\*\*</sup>Korea Advanced Institute of Science and Technology

### ABSTRACT

Cement concrete is the most widely employed construction material, while its heterogeneous nature, i.e., presence of multiple phases such as unreacted clinkers, hydrates, aggregates and pores at various length scales, makes modelling approaches extremely difficult. The present study summarizes a portion of a work conducted by Haile et al. [1], which proposes a multiscale modelling framework for predicting mechanical properties and durability of cementitious materials. The elastic properties of various phases present in a cement paste (e.g., silicate and aluminate hydrates) are calculated by considering molecular dynamics, while the phase assemblage is predicted by coupling Parrot and Killoh's hydration kinetic model [1] and a thermodynamic modelling approach. This information is carried forward to a micromechanics model, in which the different phases present are considered as inhomogeneous inclusions, in order to predict the mechanical properties of concrete at macroscale. The modelling strategy, its perspectives, and validation with experimental results reported in the literature will be discussed in detail. Acknowledgement This study was supported by the National Research Foundation (NRF) of the Korean government (Ministry of Science&amp;amp;amp; ICT) [Grant No. 2017R1A5A1014883] through Smart Submerged Floating Tunnel System Research Center. References [1] Haile, B.F, Jin, D.W., Yang, B.J., Park, S.M. and Lee, H.K. (2018). Multiscale modelling framework for predicting mechanical properties of cementitious composites, in preparation. [2] Parrot L.J. and Killoh D.C. (1984). Prediction of cement hydration, Proc. Br. Ceram. Soc. No. 35, pp. 41.

## Design Optimization for Loading Arm of LNG Bunkering System Considering Dynamic Behavior

Sanghyun Park<sup>\*</sup>, Jaewon Oh<sup>\*\*</sup>, Dongho Jung<sup>\*\*\*</sup>, Hong-Gun Sung<sup>\*\*\*\*</sup>, Cheonhong Min<sup>\*\*\*\*\*</sup>, Tae Hee Lee<sup>\*\*\*\*\*</sup>, Su-gil Cho<sup>\*\*\*\*\*</sup>

<sup>\*</sup>Korea Research Institute of Ships & Ocean Engineering, <sup>\*\*</sup>Korea Research Institute of Ships & Ocean Engineering, <sup>\*\*\*</sup>Korea Research Institute of Ships & Ocean Engineering, <sup>\*\*\*\*</sup>Korea Research Institute of Ships & Ocean Engineering, <sup>\*\*\*\*\*</sup>Korea Research Institute of Ships & Ocean Engineering, <sup>\*\*\*\*\*</sup>Hanyang University, <sup>\*\*\*\*\*</sup>Korea Research Institute of Ships & Ocean Engineering

### ABSTRACT

The LNG bunkering system means a technique for supplying Liquefied Natural Gas (LNG) fuel to a ship in a stably and efficiently. Since liquefied cargoes, such as crude oil and natural gas, have inherent risk of accident such as fire or explosion, it is very important to transfer it safely to ship. In offshore, the loading arm, which is composed of pipe, is mechanically controlled and used for LNG transport because of its high stability. In this study, therefore, the design optimization of the loading arm is carried out for the safe transfer to the ship supplied from the LNG carrier. First of all, the loading arm should keep the center of gravity stable from the stationary mode to the operation mode in the 5K condition (meaning the distance between ship and ship) and minimize the reaction force acting on each joint part structurally. Secondly, the most important operating condition is when injecting fuel of the loading arm. The hydraulically actuated loading arm should not be damaged at the connection of the Quick Connect/Disconnect Couplers (QC/DC) with the moored ship. Since the behavior of ship cannot be precisely controlled, the reaction force acting on the fastening part of the QC/DC must be minimized. In this regard, the loading arm is a multi-objective optimization problem and to find the optimal weight of dual-type counterweight. Finally, we perform design verification of the loading arm based on optimized result. The loading arm should be satisfied with the required requirements in EN 1474 for the design. EN 1474 considers various loading conditions and environmental loading conditions, such as dead load, earthquake load, fluid load, thermal load, wind load.

## Subsurface Applications for Peridynamics

Michael Parks\*

\*Sandia National Laboratories

### ABSTRACT

Peridynamics is a nonlocal reformulation of continuum mechanics that is suitable for representing fracture and failure, see [1, 2] and the references therein. Better understanding and control of the subsurface is important to the energy industry for improving productivity from reservoirs. We motivate and explore two relevant subsurface applications for peridynamics. The first involves solving inverse problems in heterogeneous and fractured media, which may be useful in characterizing subsurface stress-state conditions [3]. The second involves the study of fracture initiation and growth from propellant-based stimulation of a wellbore [4]. Simple models and proof-of-concept numerical studies are presented. [1] S. A. Silling, Reformulation of elasticity theory for discontinuities and long-range forces, *J. Mech. Phys. Solids* 48, (2000), 175-209. [2] S. Silling, M. Epton, O. Weckner, J. Xu, and E. Askari, Peridynamic states and constitutive modeling, *J. Elasticity* 88, (2007), 151-184. [3] D. Turner, B. van Bloemen Waanders and M.L. Parks, Inverse problems in heterogeneous and fractured media using peridynamics, *Journal of Mechanics of Materials and Structures*, 10(5), pp. 573-590, 2015. [4] R. Panchadhara, P.A. Gordon, and M.L. Parks, Modeling propellant-based stimulation of a borehole with peridynamics, *International Journal of Rock Mechanics and Mining Sciences*, 93, pp. 330-343, 2017.

## Reproducing Kernel Enhanced Peridynamics

Marco Pasetto\*, J. S. Chen\*\*

\*University of California, San Diego, \*\*University of California, San Diego

### ABSTRACT

Peridynamics is a nonlocal reformulation of continuum mechanics in which balance laws are computed through integration rather than differentiation [1]. For this reason, the peridynamic theory does not require any assumptions on the spatial differentiability of the displacement fields and remains valid in the presence of displacement discontinuities. Peridynamics is thus directly applicable to problems involving material failure and damage. The two most common discretization methods for peridynamic models used in engineering problems are the Finite Element method, based on a weak formulation and a meshfree method, based on nodal integration of the strong form. The former is computationally expensive and limited by the need of adapting the mesh to track evolving cracks. The latter approach discretizes peridynamic domains by a set of nodes, each associated with a nodal cell with a characteristic volume, leading to a particle based description of continuum systems. The behavior of each particle is then considered representative of its cell, limiting the convergence rate to first-order [2]. This work proposes the use of a meshfree Reproducing Kernel (RK) approximation [3] to the field variables in the peridynamic equations in order to increase the order of convergence of peridynamic numerical solutions. In this work, the peridynamic framework and the RK approximations are reviewed, the proposed approach is presented and the improved convergence rates in static peridynamic problems obtained using the proposed method is shown through numerical examples. REFERENCES [1] Silling, S.A., "Reformulation of elasticity theory for discontinuities and long-range forces", *Journal of the Mechanics and Physics of Solids*, 48, 175-209, 2000. [2] Seleson, P., Littlewood, D.J., "Convergence studies in Meshfree Peridynamics", *Computers and Mathematics with Applications*, 71, 2432-2448, 2016. [3] Chen, J. S., Pan, C., Wu, C. T., and Liu, W. K., "Reproducing Kernel Particle Methods for Large Deformation Analysis of Nonlinear Structures", *Computer Methods in Applied Mechanics and Engineering*, 139, 195-227, 1996.

## Isogeometric Residual Minimization (iGRM)

Maciej Paszynski<sup>\*</sup>, Marcin Los<sup>\*\*</sup>, Victor Calo<sup>\*\*\*</sup>, Ignacio Muga<sup>\*\*\*\*</sup>

<sup>\*</sup>AGH University, Krakow, Poland, <sup>\*\*</sup>AGH University, Krakow, Poland, <sup>\*\*\*</sup>Curtin University, Perth, Western Australia, <sup>\*\*\*\*</sup>University of Valparaiso, Chile

### ABSTRACT

The residual minimization methods allow finding the best possible approximation in the trial space while increasing the test space. The residual minimization method allows stabilizing the numerical simulations of challenging computational problems. The isogeometric analysis (IGA) is a modern rapidly growing numerical method integrating Computer Aided Design (CAD) with Computer Aided Engineering (CAE) [1]. The IGA allows to perform the computations directly on B-splines and NURBS, and the computations can be integrated with CAD tools, such as AutoCAD. The alternating directions method (ADS) introduced in 1960 [2] deals with finite difference simulations for time-dependent problems. Due to its linear computational cost, it is used nowadays to deal with difficult computational problems on parallel machines. The ADS has been recently used [3] for fast solution of the isogeometric L2 projection problem in the context of IGA. The method has also been applied for explicit dynamics simulations of different physical phenomena expressed as a sequence of isogeometric L2 projections [4]. In this talk we present a new computational method for a stable, accurate solution of stationary and time-dependent problems, which we call Isogeometric Residual Minimization (iGRM) method, with the following unique features: 1) Linear computational cost  $O(N)$  of the direct solver solution; 2) Unconditional stability of the implicit time integration scheme; 3) Unconditional stability in the spatial domain. This method mixes benefits of the Discontinuous Petrov-Galerkin method (DPG), the Isogeometric Finite Element Method (IGA-FEM), and Alternating Direction solvers (ADS). We verify our method on some computational problems, including the advection skew to the mesh, Ericsson problem, two- and three-dimensional propagation of pollutant from a chimney. For all these problems we present a superior convergence of the iGRM stabilization. We also emphasize that our method is not problem specific, and thus switching from one problem to another is straightforward. [1] J. A. Cottrell, T. J. R. Hughes, Y. Bazilevs, *Isogeometric Analysis: Toward Unification of CAD and FEA*, John Wiley and Sons, (2009) [2] G. Birkhoff, R.S. Varga, D. Young, Alternating direction implicit methods, *Advanced Computing* 3 (1962) 189–273. [3] L. Gao, V.M. Calo, Fast Isogeometric Solvers for Explicit Dynamics, *Computer Methods in Applied Mechanics and Engineering*, 274 (1) (2014) 19-41. [4] M. Los, M. Wozniak, M. Paszynski, A. Lenharth, M. A. Hassan, K. Pingali, IGA-ADS: Isogeometric analysis FEM using ADS solver, *Computer & Physics Communications* 217 (2017) 99-116. The work has been supported by National Science Centre, Poland grant no. 2017/26/M/ST1/00281

## **A Study of Approximation Error in Eulerian Hydrocodes**

Parth Patel\*, David Littlefield\*\*

\*The University of Alabama at Birmingham, \*\*The University of Alabama at Birmingham

### **ABSTRACT**

In this study we examine a number of approximations in the formulation of hydrocodes. These approximations were borne out of an original requirement for the code to run as fast as possible – i.e. with accuracy being secondary to speed. Many of these approximations originated from the 1970's when computers were slow and memory was at a premium. Although speed and memory are not as much of an issue today, these approximations are still used to formulate the hydrocodes. In this study, the effect of these approximations is examined systematically. The lumped mass approximation is a simplification to the consistent mass formulation and is routinely used in hydrocodes. While this approximation is computationally efficient, the consistent mass formulation is the most accurate (and computationally expensive) option. There are other levels of approximation between these two extremes that trade off computational efficiency for accuracy. As is shown in this work, some of these result in tridiagonal systems which are very computationally efficient to solve. Linear finite elements are also used pervasively in hydrocodes. Like the lumped mass approximation, the use of linear elements was borne out of the requirement for computational efficiency and not accuracy. Surprisingly, linear elements are still used routinely today, despite their numerous accuracy issues such as realistic representation of geometry and the need for hourglass stabilization. In this work higher order finite elements, including quadratic and cubic elements, are examined. Special attention is placed on quadrature order used in integration and its effect on overall accuracy. The 2D version of ALEAS (Arbitrary Lagrangian-Eulerian Adaptive Solver), an in-house ALE research code, is used in this work. The Taylor impact test is used as the benchmark problem to assess and quantify the effect of higher order approximations in Eulerian hydrocodes.

## 3-D Conditional Hyperbolic Quadrature Method of Moments for Dilute Gas-particle Flows

Ravi Patel\*, Olivier Desjardins\*\*, Rodney Fox\*\*\*

\*Cornell University, \*\*Cornell University, \*\*\*Iowa State University

### ABSTRACT

Although dilute gas-particle flows are common in many industrial processes, efficient and faithful simulation of such flows remains a challenge. When the particle phase is in a regime with finite Stokes and Knudsen numbers, the dynamics may stray far from equilibrium and require a more complete kinetic description to capture than is assumed with commonly used hydrodynamic techniques. To reduce the computational cost of integrating the full kinetic equation, moment methods transform the kinetic equation to evolution equations for a set of moments of the number density function (NDF). Quadrature based moment methods (QBMM) solve the resulting closure problem by constructing a NDF comprised of weighted Dirac deltas from a given set of moments. It has been shown that QBMM in conjunction with kinetic based finite volume schemes maintain realizable sets of moments during transport [1]. However previous QBMM either fail to maintain the strict hyperbolicity of the kinetic equations or use alternatives to Dirac delta functions that restrict the sets of moments that can be reconstructed. The conditional hyperbolic quadrature method of moments (CHyQMOM) has recently been introduced as a QBMM that maintains both the strict hyperbolicity of the kinetic equation and the Dirac delta representation of the NDF [2]. In this talk, we present the 3-D extension to CHyQMOM and results from simulations of particle-laden flows using CHyQMOM. Comparing with benchmark Lagrangian simulations, we demonstrate that CHyQMOM is capable of capturing the complex dynamics resulting from non-equilibrium effects in gas-particle flows. [1] V. Vikas, Z. J. Wang, A. Passalacqua, and R. O. Fox. Realizable high-order finite-volume schemes for quadrature-based moment methods. *J. Comput. Phys.*, 230(13):5328–5352, 2011. [2] R. O. Fox, F. Laurent, and A. Vie. Conditional Hyperbolic Quadrature Method of Moments for Kinetic Equations. hal-01632813, 2017.

## Data-driven Homogenization Technique for Mechanical Property Prediction in Composite Materials

Mehtab Pathan<sup>\*</sup>, Sathiskumar Anusuya Ponnusami<sup>\*\*</sup>, Borja Erice<sup>\*\*\*</sup>, Nik Petrinic<sup>\*\*\*\*</sup>

<sup>\*</sup>University of Oxford, <sup>\*\*</sup>University of Oxford, <sup>\*\*\*</sup>University of Oxford, <sup>\*\*\*\*</sup>University of Oxford

### ABSTRACT

This research aims to explore the potential of data science and machine learning techniques following Bessa et al. [1], in developing a model to predict the mechanical properties of composite materials using their geometric (microstructural) and constituent properties. Numerical homogenisation techniques are utilised to extract effective properties of a composite material. Subsequently, a training database is created by analyses of large set of Representative Volume Elements (RVE) with varying parameters involving size and spatial distribution of the reinforcing phases as well as the constituent material properties. Elastoplastic constitutive models involving damage are used for the material behaviour of the matrix phase while the reinforcement phase is assumed to be linear elastic. Periodic boundary condition is enforced on the analysed RVEs and a case of transverse tensile loading is considered. Each analysed RVE and its calculated effective properties are correlated with a 'microstructural fingerprint' i.e. a combination of its geometric and constituent material parameters. The geometric parameters of the microstructures are quantified using a variety of spatial descriptive metrics (see [2]) such as the pair-correlation function, Ripley's K-function etc. as well as the reinforcement volume fraction. Thus a complete mapping of microstructural features to the computed effective property is established. Subsequently, supervised machine learning techniques are then applied to this dataset with an aim to develop a model to predict effective properties of an arbitrary, user-defined microstructure. Exploratory data analysis is used to highlight the underlying relationships between independent predictors i.e. microstructural features and the computed effective properties. The effectiveness of the developed machine learning model is then validated using high-fidelity finite element simulations. Finally, an inverse problem is solved using optimization techniques in order to find an optimal microstructure for a given set of material parameters and for a user defined property (stiffness, yield stress, ultimate stress).  
Keywords: Composites, Machine learning, Optimization, Microstructure, Data Science  
References  
1. Bessa, M.A., Bostanabad, R., Liu, Z., Hu, A., Apley, D.W., Brinson, C., Chen, W., Liu, W.K., 2017. A framework for data-driven analysis of materials under uncertainty: Countering the curse of dimensionality. *Computer Methods in Applied Mechanics and Engineering* 320, 633–667.  
2. Niezgoda, S. R., Yabansu, Y. C. & Kalidindi, S. R., 2011. Understanding and visualizing microstructure and microstructure variance as a stochastic process. *Acta Materialia* 59, 6387–6400.

## Hybrid Finite Element Strategy for Simulation of Coupled Electro/Magneto-Thermoelastic Interactions in Microsystems

Kunal Patil\*, Chandrashekhar Jog\*\*

\*Indian Institute of Science (IISc), Bangalore, India, \*\*Indian Institute of Science (IISc), Bangalore, India

### ABSTRACT

An efficient numerical solution strategy for problems involving multiple energy domains is of importance not only for predicting the underlying coupled behaviour, but also for subsequent optimization. Many applications in Micro-Electro-Mechanical Systems (MEMS) or dielectric elastomers etc. involve chunky structural geometries in combination with thinner elements such as beams, plates or shells etc., and subjected to strongly or weakly interacting fluid, thermal, electric or magnetic forces. Computational modelling of such multi-physical systems using Finite Elements (FE) have to deal with the challenges posed by the 'locking' phenomenon associated with the use of standard displacement based finite elements, while modelling small aspect ratio geometries and incompressible materials, and the problem of spurious stress oscillations while modelling thermoelastic coupling. The problems of locking and spurious thermal stress oscillations were circumvented using the Hybrid FE strategy in the context of coupled electro-elasticity [1], and coupled thermoelasticity [2]. In this work, we discuss the non-trivial extension of the Mixed/Hybrid FE strategy for modelling monolithically the non-linear coupled electro/magneto-thermoelastic behaviour for microsystems. The efficacy of the developed computational strategy is demonstrated using several numerical examples, with an emphasis on predicting accurately the onset of static and dynamic pull-in instabilities associated with microsystems. References [1] Jog C, Patil KD. A hybrid finite element strategy for the simulation of mems structures. *International Journal for Numerical Methods in Engineering* 2016; 106(7):527–555. [2] Jog C, Gautam G. A monolithic hybrid finite element strategy for nonlinear thermoelasticity. *International Journal for Numerical Methods in Engineering* 2017; 112(1):26–57.

# **An Immersed Interface Finite Element Method for the Analysis and Design of Multi-Material Systems**

Mayuresh Patil\*

\*Virginia Tech

## **ABSTRACT**

Design of multi-material systems involve the optimal placement of multiple materials within a base material. The optimal design takes the form of a shape or interface design problem. Large number of interface design variables require the use of gradient based optimization which need interface sensitivities, i.e., the effect of change in interface on the performance of the material. There are two computational issues with interface design using current discrete or continuum shape sensitivity analyses: remeshing at each design iterations and the need for either mesh Jacobian sensitivities (domain velocity form) or solution gradients (boundary velocity form). An alternate way to design multi-materials systems is the use of immersed interface method for analysis. The present effort is focused on developing and presenting an immersed interface method based on the splitting of material constitutive law along the interface and normal to it. This leads to a solution that converges to the exact multi-material solution as the number of finite elements are increased. To verify the results of the multi-material immersed interface finite element method a multi-material patch test is developed. It is shown that the proposed approach satisfies the multi-material patch test which guarantees convergence of the analysis. Finally, the method is used to calculate the sensitivities of the analysis solution to interface change. Future work will focus on using the analysis and sensitivity computation based on the present method for optimal design of multi-material systems.

## **Integrating the Use of Multiple Models Based on Complex Mass Flows**

Abani Patra\*

\*University at Buffalo, SUNY

### **ABSTRACT**

In this talk, we will outline recent work on integrating the use of multiple models based on different rheological assumptions to improve predictive power when modeling complex flows where the ideal rheology is hard to determine a priori or changing in the course of the flow as a result of entrainment or deposition. We begin by a careful statistical analysis of major extant models to establish the most significant factors arising from different rheological assumptions. These can then be put together in a problem specific manner to produce predictive simulations that exploit all the models.

## Wave Motion in an Elastically Connected Double Beam Using Super-convergent Finite Element Formulation

Shweta Paunikar\*, Srinivasan Gopalakrishnan\*\*

\*Indian Institute of Science, \*\*Indian Institute of Science

### ABSTRACT

Adhesively bonded metallic and composite joints are an inseparable part of today's aerospace industry. Wave propagation across such joints is an effective way of monitoring their health for delamination and aging. In this work, a new semi-analytical double beam element is developed to model wave propagation characteristics of a bonded joint. A double beam element is constituted of two parallel Timoshenko beam-rod elements connected to each other by continuously distributed vertical elastic springs. Different values of spring stiffness are used to simulate different levels of adhesion, which is required for monitoring the health of adhesive bond between the two beams. First order shear deformation theory is used for assessing the displacement field, namely, axial, transverse, and shear components each for top and bottom beams. Six coupled equations governing dynamic interactions between two parallel beams are obtained. While using conventional finite elements, discrete springs modelling the elastic layer must have stiffness values depending on the node spacing, sometimes even having negative stiffness values. Therefore, a new set of stiffness values needs to be found for each frequency and mesh refinement. This tedious nature of finite element modelling is the motivation for developing a novel, simpler and more accurate formulation for elastically coupled beams. In this formulation, the exact solutions to the static part of the axial-flexure-shear coupled governing equations are obtained. The exact interpolating functions ensure the exactness of stiffness matrix, thus largely reducing the error in approximation in comparison with finite element method. The order of interpolating function of transverse displacement, thus obtained, is one order higher than that of the beam slope. As a result, the beam element has super-convergent properties and is free from shear locking. Hence, obtaining the wave propagation behaviour in elastically coupled metallic and symmetric or asymmetric composite beams accurately and within a short time is possible with this double beam element. This approach also makes it feasible to model various level of bonding in beams by varying stiffness values of the spring. Consequently, more accurate models for health monitoring of adhesively bonded metallic or composite joints can be developed with this element.

## Joint Image Segmentation and Registration Based on a Dynamic Level Set Approach Using Hierarchical B-splines

Aishwarya Pawar<sup>\*</sup>, Yongjie Zhang<sup>\*\*</sup>, Cosmin Anitescu<sup>\*\*\*</sup>, Timon Rabczuk<sup>\*\*\*\*</sup>

<sup>\*</sup>Carnegie Mellon University, <sup>\*\*</sup>Carnegie Mellon University, <sup>\*\*\*</sup>University of Weimar, <sup>\*\*\*\*</sup>University of Weimar

### ABSTRACT

We present an efficient approach for joint image segmentation and nonrigid registration based on a level set formulation. Joint image segmentation and registration is an efficient tool as it incorporates automatic structural analysis into the image processing framework. This method has shown an improved performance as compared to carrying out the segmentation and registration methods separately [1,2]. Unlike previous approaches, the implicit level set function defining the segmentation contour and the spatial transformation that maps the deformation for the image registration are both defined using C2 continuous hierarchical B-splines. This joint level set framework uses a variational form of an atlas-based segmentation together with a nonrigid registration method which can compute large deformations with cubic splines. The minimization of the variational form is accomplished by dynamic evaluations on a set of successively refined adaptive grids at multiple image resolutions. The improvement in the description of the segmentation result using higher order splines leads to a better accuracy of both the image segmentation and registration process. The performance of the proposed method is demonstrated on 2D synthetic and medical images to show the advantages of the proposed method as compared to other joint segmentation and registration methods. Keywords: joint image registration and segmentation, adaptive refinement, level set framework, partial differential equation models, hierarchical B-splines, dynamic scheme REFERENCES: [1] A. Pawar, Y. J. Zhang, C. Anitescu, Y. Jia, T. Rabczuk. DTHB3D\_Reg: Dynamic Truncated Hierarchical B-Spline Based 3D Nonrigid Image Registration. Communications in Computational Physics, 23(3):877-898, 2018. [2] A. Pawar, Y. Zhang, Y. Jia, X. Wei, T. Rabczuk, C. L. Chan, C. Anitescu. Adaptive FEM-based Nonrigid Image Registration Using Truncated Hierarchical B-splines. A Special Issue of FEF 2015 in Computers and Mathematics with Applications, 72:2028-2040, 2016.

## Application of the Concept of Virtual Material for the Design of Additive Manufacturing Processes of Open Cell Foams

Piotr Pawlowski\*, Ryszard Pecherski\*\*, Marcin Nowak\*\*\*, Zdzislaw Nowak\*\*\*\*, Marek Sklodowski\*\*\*\*\*

\*Institute of Fundamental Technological Research Polish Academy of Sciences, \*\*Institute of Fundamental Technological Research Polish Academy of Sciences, \*\*\*Institute of Fundamental Technological Research Polish Academy of Sciences, \*\*\*\*Institute of Fundamental Technological Research Polish Academy of Sciences, \*\*\*\*\*Institute of Fundamental Technological Research Polish Academy of Sciences

### ABSTRACT

The subject of the presented paper is the model based on a digital microstructure called also virtual material, in particular open cell foams characterised with the skeleton formed of convex or re-entrant cells. The study is based on the following hypothesis: Computed Tomography analysis of polyurethane foam with convex or re-entrant cells provides an adequate basis for the computational reconstruction of a “virtual cellular material.” It enables one to simulate numerically the thermomechanical processes for assumed properties of the skeleton material. The hypothesis is based on visible similarity in the structure of convex or re-entrant cells of the observed polyurethane and metallic cellular materials that are reported in many papers discussed in [1]. The virtual foam structure is derived from the real polyurethane foam specimens produced and studied in [2] with use of computed tomography images implementing the procedures described in [1]. The additive manufacturing (AM) methods used for metallic materials mostly require numerical models composed of large sets of 2-D slices of the 3-D structural model. The necessary steps of computational design and pre-processing of additive manufacturing of open cell foams are discussed, including voxel-based and smoothed geometry generation algorithms, positioning and supporting in the working volume of the AM system, slicing, and post-processing. To demonstrate the feasibility of the study, the open-cell multifunctional structures were manufactured, which can be used as e.g., crush-resistant heat exchangers, heat capacitors, etc. The structures were produced using selective laser melting process in the powder bed fusion technology using aluminium and maraging steel powders. References 1. R.B. Pecherski, M. Nowak, Z. Nowak, Virtual metallic foams. Application for dynamic crushing analysis, International Journal for Multiscale Computational Engineering, 15, 431-442, 2017. 2. A. Streck, Production and study of polyether auxetic foam, Mech. Control, 29,78–87, 2010.

## Towards a Hybrid Multi-fluid/PIC Plasma Capability

Roger Pawlowski<sup>\*</sup>, John Shadid<sup>\*\*</sup>, Edward Phillips<sup>\*\*\*</sup>, Sidafa Conde<sup>\*\*\*\*</sup>, Stephen Bond<sup>\*\*\*\*\*</sup>,  
Eric Cyr<sup>\*\*\*\*\*</sup>, Sean Miller<sup>\*\*\*\*\*</sup>, Matthew Bettencourt<sup>\*\*\*\*\*</sup>

<sup>\*</sup>Sandia National Laboratories, <sup>\*\*</sup>Sandia National Laboratories, <sup>\*\*\*</sup>Sandia National Laboratories, <sup>\*\*\*\*</sup>Sandia National Laboratories, <sup>\*\*\*\*\*</sup>Sandia National Laboratories

### ABSTRACT

Plasma physics systems are often simulated by either a continuum approach (e.g. magnetohydrodynamics or multi-fluid plasma models) or a charged particle description (e.g. Boltzmann equation). Particle-in-cell (PIC) methods are typically applied to solve the Boltzmann equation that is the fundamental equation for the distribution function describing particle motion in the presence of electromagnetic fields. As the plasma density and collisional interaction increases, PIC becomes intractable to simulate directly due to the large number of particles required. In this case, fluid PDE models such as the single fluid magnetohydrodynamics (MHD) and multi-species fluid models are often utilized. In transition regions certain problems may require a hybrid model that combines the fluid and PIC descriptions for tractability. This presentation describes an initial effort to couple a finite element (FE) multi-species fluid model to a PIC description. The multi-fluid model consists of continuity, momentum and energy equations for each species coupled to Maxwell's equations for the electromagnetic field. The equations are discretized using the continuous Galerkin FE method with a compatible basis to enforce the electric field (edge basis) and magnetic field (face basis) involutions from Maxwell's equations. The resulting set of fluid equations contains a wide range of multiple time and length-scale physical mechanisms, producing a stiff system. To evolve the coupled kinetic-PIC / fluid system for the time scales of interest, we explore the use and development of IMplicit-EXplicit (IMEX) Runge-Kutta time integration methods and pursue initial comparisons with operator split methods. For robustness, efficiency, and scalability the implicit nonlinear fluid physics are solved using a Newton-Krylov method with a GMRES linear solve and an approximate block factorization preconditioner. Algebraic multigrid is applied within the blocks. Code verification problems will be presented to assess accuracy and efficiency of the algorithm.

## Multilevel Hierarchy of Shear Banding in Viscoplastic Flow and Failure

Ryszard Pecherski\*

\*Institute of Fundamental Technological Research, Polish Academy of Sciences, Warsaw, Poland

### ABSTRACT

Experimental observations show that inelastic deformation of metals is often produced as an effect of competing mechanisms of crystallographic glide, twinning and micro-shear banding. The micro-shear bands are observed as concentrated shear zones in the form of transcrystalline layers of the thickness of the order 0.1  $\mu\text{m}$ . It has been observed that the change of the mechanism of inelastic deformation has strong influence on ductile failure processes in different length scales. Therefore, the identification and elucidation of physical mechanisms that are responsible for initiation, growth and evolution of micro-shear bands is of fundamental importance for understanding the macroscopic behaviour of metallic materials, [1]. A new physical model of multilevel hierarchy and evolution of shear bands is proposed with use of the analysis of recent state of the art of the investigations carried on different levels of observations: uni-axial and bi-axial mechanical tests enhanced with digital image correlation method and in-situ tests with use of electron microscopy as well as atom probe tomography in relation with ab initio and molecular dynamics computational simulations. The difficulties with application of a direct multiscale integration scheme are discussed and an original idea of an extension of the representative volume element concept with use of the known theory of the propagation of the singular surfaces of microscopic velocity field is proposed, [2]. A new formulation of the description of rate of shear strain generated by multilevel hierarchy of shear bands is formulated in the workflow integration approach, in which information from molecular simulation at different levels flows into the decision process, [3]. [1] R.B. Pecherski, Macroscopic effects of micro-shear banding in plasticity of metals, *Acta Mechanica*, 131, pp 203–224, (1988). [2] R.B. Pecherski, Finite deformation plasticity with strain induced anisotropy and shear banding, *Journal of Materials Processing Technology*, 60, pp. 35-44, (1996). [3] G. Goldbeck, Foreword, in: *Industrial Applications of Molecular Simulations*, M. Meunier (ed.), CRC Press, Taylor & Francis Group, Boca Raton, (2012).

## Efficient Reduced Coupling of PDEs Based on Weak Transmission Conditions

Luca Pegolotti<sup>\*</sup>, Simone Deparis<sup>\*\*</sup>

<sup>\*</sup>École polytechnique fédérale de Lausanne, <sup>\*\*</sup>École polytechnique fédérale de Lausanne

### ABSTRACT

We present a non-conforming domain decomposition method based on weakly imposed transmission conditions. The continuity of the global solution is enforced by Lagrange multipliers defined over the interfaces of adjacent subdomains. The method falls into the class of primal hybrid methods [1], which include also the well-known mortar method [2]. In contrast with the mortar method, we discretize the space of basis functions at each interface independently of the discretization of the two adjacent domains. The advantages of this choice are twofold. Firstly, the accuracy of the coupling can be tuned accordingly to the specific application, because the continuity of the global solution and its normal derivatives at the interface depends on the richness – i.e. the number of basis functions – of the space of Lagrange multipliers. Secondly, the global solution is independent of any partition of the subdomains into master and slave domains, which, in the mortar method, must be done a priori. Being a non-conforming method, applications of our approach include e.g. the solution of problems with finite element spaces built on non-conforming meshes or with different polynomial degrees, or the coupling of solutions obtained using otherwise incompatible methods such as the finite element method, the spectral element method and isogeometric analysis. The method can be also used to couple solutions obtained on reduced basis spaces. We explore some of these possibilities with numerical experiments. [1] D. Boffi, F. Brezzi, M. Fortin. Mixed finite element methods and applications, Springer (2013) [2] C. Bernardi. A new nonconforming approach to domain decomposition: the mortar element method, Nonlinear partial equations and their applications (1989)

## Multifidelity Monte Carlo Estimation with Adaptive Low-Fidelity Models

Benjamin Peherstorfer\*

\*University of Wisconsin-Madison

### ABSTRACT

Multifidelity Monte Carlo (MFMC) estimation combines low- and high-fidelity models to speedup the estimation of statistics of the high-fidelity model outputs. MFMC optimally samples the low- and high-fidelity models such that the MFMC estimator has minimal mean-squared error for a given computational budget. In the setup of MFMC, the low-fidelity models are static, i.e., they are given and fixed and cannot be changed and adapted. We introduce the adaptive MFMC (AMFMC) method that splits the computational budget between adapting the low-fidelity models to improve their approximation quality and sampling the low- and high-fidelity models to reduce the mean-squared error of the estimator. Our AMFMC approach derives the quasi-optimal balance between adaptation and sampling in the sense that our approach minimizes an upper bound of the mean-squared error, instead of the error directly. We show that the quasi-optimal number of adaptations of the low-fidelity models is bounded even in the limit case that an infinite budget is available. This shows that adapting low-fidelity models in MFMC beyond a certain approximation accuracy is unnecessary and can even be wasteful. Our AMFMC approach trades-off adaptation and sampling and so avoids over-adaptation of the low-fidelity models. Besides the costs of adapting low-fidelity models, our AMFMC approach can also take into account the costs of the initial construction of the low-fidelity models ("offline costs"'), which is critical if low-fidelity models are computationally expensive to build such as reduced models and data-fit surrogate models. Numerical results demonstrate that our adaptive approach can achieve orders of magnitude speedups compared to MFMC estimators with static low-fidelity models and compared to Monte Carlo estimators that use the high-fidelity model alone.

## A Mesoscale-based Homogenization Study of Sand

Gerald Pekmezi\*, David Littlefield\*\*

\*The University of Alabama at Birmingham, \*\*The University of Alabama at Birmingham

### ABSTRACT

In recent years, renewed research effort has been directed toward characterizing soils in transient applications. The main approach favored towards that end, has been to use one of many “cap” models derived from Mohr-Coulomb failure theory. In addition to a friction-based yielding stress like Mohr-Coulomb, typically such models incorporate a pressure cap. More advanced three-phase models also take into account the great difference in soil response with degree of saturation through “effective” stress. Effective stress isolates the stress in the solid skeleton of the material, from the bulk behavior. One such model, the Hybrid Elastic Plastic (HEP) model has been used extensively to model soils subjected to energetic, highly-transient phenomena using hydrocodes, a class of explicit computational packages geared toward such phenomena. Geomaterials such as soils, differ from other common engineering materials like metals, polymers, and many composites, in that the fundamental evolution of the underlying structure may reasonably be considered to occur at a higher scale, i.e. at the mesoscale rather than the microscale. This offers a somewhat unique opportunity to be able to characterize the underlying structural evolution of the material, and use that characterization to inform a general constitutive framework to model the behavior of a wide spectrum of soils under a range of pressures and distortional transient loading conditions. In the current work, experimental and laboratory data of a poorly graded sand previously modeled using the HEP model, is used to explore the internal evolution of the sand by carrying out particle-based simulations of the behavior at the mesoscale. These simulations are used to conduct a homogenization study of the granular subdomain. This is done in order to 1) identify the threshold at which the transition from discrete mesoscale to the Representative Volume Element (RVE) occurs, and 2) to quantify the uncertainty associated with discretization below that threshold. Additionally, the mesoscale results are used to formulate an effective stress model that matches the behavior observed in the particle-based simulations. This new effective stress model is then compared with the predictions of the sand behavior from the HEP model.

## Combining Tetrahedra into Valid Finite-Element Hexahedral Cells

Jeanne Pellerin<sup>\*</sup>, Amaury Johnen<sup>\*\*</sup>, Jean-François Remacle<sup>\*\*\*</sup>

<sup>\*</sup>Université catholique de Louvain, <sup>\*\*</sup>Université catholique de Louvain, <sup>\*\*\*</sup>Université catholique de Louvain

### ABSTRACT

To generate automatically hex-dominant meshes for general domains, indirect methods take advantage of the existence of tetrahedral mesh generation algorithms and combine tetrahedra in hexahedra, prisms and pyramids. Existing indirect methods rely on a small set of predefined patterns of subdivision of the hexahedron into tetrahedra. However these patterns do not account for the whole range of valid finite-element hexahedron geometries since the patterns are limited to hexahedra with planar faces. Valid cells, i.e. which have a strictly positive Jacobian, have bilinear faces by definition, may be quite distorted and/or non-convex. We describe an algorithm that overcomes this limitation and identifies all combinations of tetrahedra into valid finite element hexahedral cells. All combinations of eight vertices of a tetrahedral mesh which are candidates to define a valid hexahedron are generated in a first step. The tetrahedra are computed in a second step. The core of the algorithm is a combination generator which efficiency is drastically improved by tests discarding invalid hexahedra as early as possible. We reach 300,000 potential hexahedra computed per second on a laptop. Our algorithm does not depend on any pattern and is actually able to discover new patterns that are compared using an edge-colored graph formalism. We have discovered more than a hundred patterns that do correspond to valid hexahedral cell geometries. Our unexpected result includes the ten previously used patterns. It shows how the complexity of tetrahedral meshes propagates to indirect meshing methods. We exhibit subdivisions of hexahedral cells valid for finite-element computation into up to fourteen tetrahedra without additional vertices. We further study the discovered patterns in terms of occurrence, maximum quality and show how these values are linked to the point set quality for hexahedral meshing and on the tetrahedral mesh chosen.

## Multiscale Modeling of a Red Blood Cell Passing through the Human Spleen

Zhangli Peng\*, Huijie Lu\*\*

\*University of Notre Dame, \*\*University of Notre Dame

### ABSTRACT

We developed a boundary integral formulation to study a red blood cell (RBC) squeezing through a submicron slit under prescribed inlet and outlet pressures. The motivation of this study is to investigate splenic filtrations of RBCs and corresponding in vitro mimicking microfluidic devices, during which RBCs regularly pass through inter-endothelial slits with a width less than 1 micrometer. We first derived the boundary integral equations of a RBC immersed in a confined domain with both Neumann and Dirichlet boundary conditions, and gave the explicit matrix forms of equations and numerical procedures to solve these equations. In addition, we also developed accurate treatments of nearly singular integrals and corner singularities, which are especially important in this fluid-structure interaction study with strong lubrication. After validations against analytical and experimental results, we explored the membrane tension, shear deformation, and bilayer-cytoskeletal interactions under various conditions. We systematically studied the effects of pressure drop, volume-to-surface-area ratio, internal viscosity, and membrane stiffness on RBC deformation and internal stress. The numerical methods developed will not only be important for understanding RBCs physiology and diseases related to splenic filtration, but also be useful for studying elastic capsules, vesicles, and other cells squeezing small slits in drug delivery and extravasation.

## Preconditioning the Virtual Element Method

Micol Pennacchio<sup>\*</sup>, Silvia Bertoluzza<sup>\*\*</sup>, Daniele Prada<sup>\*\*\*</sup>

<sup>\*</sup>CNR-IMATI, Pavia, Italy, <sup>\*\*</sup>CNR-IMATI, Pavia, Italy, <sup>\*\*\*</sup>CNR-IMATI, Pavia, Italy

### ABSTRACT

The Virtual Element Method [1] is a quite recent discretization framework which can be viewed as an extension of the Finite Element Method. The Virtual Element Method allows to easily handle meshes consisting of very general shaped polygonal or polyhedral elements, while keeping simplicity in implementation as far as accuracy and stability of the resulting numerical schemes. However, in order to make the method more competitive, it is also necessary to deal with the efficient solution of the associated linear system of equations, and, in particular, to provide good preconditioners. Here we deal with a Domain Decomposition approach [2] and we focus on a non overlapping domain decomposition method: the Dual-Primal Finite Element Tearing and Interconnecting (FETI-DP) method. We prove polylogarithmic condition number bounds in two [3] and three dimensions, independent of the number of subdomains, the mesh size, and jumps in the diffusion coefficients. Numerical results validate the theory. [1] L. Beirão da Veiga, F. Brezzi, L.D. Marini, A. Russo: The hitchhiker guide to the Virtual Element Method, *Math. Models Methods Appl. Sci.*, Vol. 24, 1541-1573, (2014). [2] A. Toselli, O. Widlund: *Domain Decomposition Methods - Algorithms and Theory*. Springer Series in Computational Mathematics volume 34, 2005. [3] S. Bertoluzza, M. Pennacchio, D. Prada: BDDC and FETI-DP for the Virtual Element Method. *Calcolo*, 54(4), 1565-1593, (2017),

## TWO-DIMENSIONAL CHAPEAU FUNCTION RECURSION RELATIONS

SOGOL PIRBASTAMI\*, DARRELL W. PEPPER\*

\*University of Nevada, Las Vegas  
4505 S Maryland Pkwy,  
NV, Las Vegas, USA  
Sogol.pirbastami@unlv.edu

\*University of Nevada, Las Vegas  
4505 S Maryland Pkwy,  
NV, Las Vegas, USA  
Darrell.pepper@unlv.edu

**Key words:** Finite Element, Chapeau Function, Strongly Implicit Procedure

**Abstract.** In this study, a simple Galerkin-based finite element approach is used to solve the advection-diffusion equations in two-dimensional. The finite element method (FEM) is a powerful technique that is commonly used for solving complex engineering problems. However, the implementation of the FEM in two or Three-dimensional problems can be computationally expensive. A simple finite element algorithm based on the bilinear triangular, bilinear quadrilateral and Quadratic Lagrangian approximation is employed to discretize the 2D convection-diffusion equations. This algorithm is an extension of the 1D Chapeau (linear element) technique which employed a tridiagonal recursion expression common to the classical central finite-difference approach. In this case, the global matrix now becomes penta-diagonal (for 2D). Hypermetrics and the natural coordinate system are used to transform the integral expressions. Then, integrating and assembling the set of relations over the  $i$ th node within the patch of four bilinear elements (similar to assembling the one-dimensional linear chapeau function), a recursion relation is established for the 2D equations. The transient term is finally approximated in a forward-in-time difference, and the assembly becomes complete. The FEM algorithm is validated by applying the method to a simple problem in a two-dimensional square and Strongly Implicit Procedure (SIP) method used as a solver.

### INTRODUCTION

The most commonly used numerical techniques used in Computational Fluid Dynamics (CFD) simulations are the finite difference (FDM), finite volume (FVM), and finite element (FEM) methods. Due to the mathematical robustness and flexibility of the finite element method, the FEM is popular for solving the general class of transport equations. However, the implementation of the FEM in 2 or 3-dimensions can be computationally expensive.

In this study a simple Galerkin-finite element recursion-based algorithm for the 2-D general transport equation is examined. The algorithm is based on integrating and assembling eight bilinear triangular elements, 4 bilinear quadrilateral elements, or one Lagrangian quadratic quadrilateral element over the  $i^{\text{th}}$  node within the patch of 9 nodes. A recursion relation is established which can be solved using the strongly implicit method (SIP) instead of a more direct Gaussian elimination matrix solver, i.e., the global matrix. The purpose of this method is to speed up the computational time while eliminating the issue of minimizing global bandwidth associated with global matrix assembly[4].

Pepper and Baker [1] used linear basis functions for each element in a simple finite element algorithm (chapeau function) to derive the 1-D advection-diffusion transport equation. Hypermatrices and natural coordinates were employed to evaluate the integral forms of the algorithm and then assembly was conducted over two adjacent elements, creating a tridiagonal recursion relation which resembles a central FDM. Multidimensional problems were solved using time splitting for the 2D/3D equations, i.e., treating the discretized equations as a series of 1D algorithms. Long and Hicks [8] used the 1D chapeau function to model atmospheric boundary layer flow, and found that the method produced fourth order accuracy and stable solutions. For transient problems in 2D and 3D, Marchuk's time splitting method was employed.

Pepper et al [5] studied quasi-Lagrangian cubic-spline and chapeau-function (Galerkin) methods for general dispersion models. Both methods showed more accurate results and stability compared to finite difference methods. Both methods used low storage and were simple to code. In simple advection with uniform discretization, the chapeau function showed 4<sup>th</sup> order accuracy but in unequal mesh spacing, the cubic spline had slightly lower dispersion errors. The chapeau function method is based on the use of linear basis functions, or hat-shaped (chapeau) expressions in 1-D.

## FINITE ELEMENT ALGORITHM OF 2D CHAPEAU FUNCTION

In a conventional Galerkin approach, the weighting functions are set equal to the basis functions, converting a PDE into a series of algebraic equations. The general 2D transport equation can be discretized using either 2D triangular elements or quadrilateral elements and then assembled over eight triangular elements, four quadrilateral elements, or one quadratic Lagrangian quadrilateral element, consecutively, to establish a set of recursion relations.

*eneral transport e uation*

$$\frac{\partial c}{\partial t} + \nabla(Vc) - \nabla \cdot (D(\nabla c)) = S \quad (1)$$

For simplicity, we consider the source term, S, to be zero and define c as a scalar transport, e.g. temperature.

The 1D chapeau function is described in Pepper and Baker [1]. The linear shape function and weighted residual method are used for two consecutive elements. After assembly (creating a 3x3 global matrix), the recursion relation for the  $i^{\text{th}}$  node can be established:

*inear shape function*

$$N_{i-1} = \frac{x_i - x}{\Delta x} \quad (2)$$

$$N_i = \frac{x - x_{i-1}}{\Delta x} \quad (3)$$

The approximation for linear function can be expressed as:

$$c = N_{i-1} * c_{i-1} + N_i * c_i \quad (4)$$

*Weighted residual method for 1D:*

$$\int W. \left( \frac{dc}{dt} + u * \frac{dc}{dx} - D * \left( \frac{d^2c}{dx^2} \right) \right) \quad (5)$$

when W=N. Thus, the integral relation for the 1D element spanning nodes i-1 to i can be written as

$$\int N_i * N_{i-1} dx. \left\{ \begin{matrix} c^i - 1 \\ c^i \end{matrix} \right\} + U * N_i \int N_i. \frac{dN_{i-1}}{dx} dx. \left\{ \begin{matrix} c^i - 1 \\ c^i \end{matrix} \right\} D * \int \frac{dN_i}{dx} \frac{dN_{i-1}}{dx}. \left\{ \begin{matrix} c^i - 1 \\ c^i \end{matrix} \right\} = 0 \quad ( )$$

The integral terms are similarly evaluated for elements spanning i to i+1. Thus, for the two adjacent linear elements,

For  $\Delta x_- = x_i - x_{i-1}$

$$\frac{\Delta x_-}{6} \begin{bmatrix} 2 & 1 \\ 1 & 2 \end{bmatrix} * \left\{ \begin{matrix} c^i - 1 \\ c^i \end{matrix} \right\} + \frac{-1}{2} \begin{bmatrix} -1 & 1 \\ -1 & 1 \end{bmatrix} * \left\{ \begin{matrix} c^i - 1 \\ c^i \end{matrix} \right\} + \frac{-1}{\Delta x_-} \begin{bmatrix} 1 & -1 \\ -1 & 1 \end{bmatrix} * \left\{ \begin{matrix} c^i - 1 \\ c^i \end{matrix} \right\} = 0 \quad (7)$$

For  $\Delta x_+ = x_{i+1} - x_i$

$$\frac{\Delta x_+}{6} \begin{bmatrix} 2 & 1 \\ 1 & 2 \end{bmatrix} * \left\{ \begin{matrix} c^i - 1 \\ c^i \end{matrix} \right\} + \frac{-1}{2} \begin{bmatrix} -1 & 1 \\ -1 & 1 \end{bmatrix} * \left\{ \begin{matrix} c^i - 1 \\ c^i \end{matrix} \right\} + \frac{-1}{\Delta x_+} \begin{bmatrix} 1 & -1 \\ -1 & 1 \end{bmatrix} * \left\{ \begin{matrix} c^i - 1 \\ c^i \end{matrix} \right\} = 0 \quad (8)$$

Assembling the two adjacent elements in a global matrix,

$$\frac{1}{6} \begin{bmatrix} 2\Delta x_- & \Delta x_- & 0 \\ \Delta x_- & 2\Delta x_- + 2\Delta x_+ & \Delta x_+ \\ 0 & \Delta x_+ & 2\Delta x_+ \end{bmatrix} * \left\{ \begin{matrix} c^i + 1 \\ c^i \\ c^i - 1 \end{matrix} \right\} + \frac{1}{2} \begin{bmatrix} -1 & 1 & 0 \\ -1 & 0 & 1 \\ 0 & -1 & 1 \end{bmatrix} * \left\{ \begin{matrix} c^i + 1 \\ c^i \\ c^i - 1 \end{matrix} \right\} + \frac{1}{6} \begin{bmatrix} \frac{1}{\Delta x_-} & \frac{-1}{\Delta x_-} & 0 \\ \frac{-1}{\Delta x_-} & \frac{1}{\Delta x_-} + \frac{1}{\Delta x_+} & \frac{-1}{\Delta x_+} \\ 0 & \frac{-1}{\Delta x_+} & \frac{1}{\Delta x_+} \end{bmatrix} * \left\{ \begin{matrix} c^i + 1 \\ c^i \\ c^i - 1 \end{matrix} \right\} = 0 \quad (9)$$

The recursion relation in 1D is obtained by stripping out the central expression within the global matrix, i.e.,

$$\frac{1}{6} * (C'_{i-1} + 4C'_i - C'_{i+1}) + \frac{U}{2 * \Delta x} (C_{i+1} - C_{i-1}) - \frac{K}{\Delta x^2} (C_{i+1} - 2C_i + -2C_{i-1}) = 0 \quad (10)$$

For 2D, the shape functions bilinear triangular and quadratic elements are used. Employing isoparametric transformations and applying Galerkin's weighted residual method, the 2D recursion relation for bilinear elements and triangular elements are shown:

$$\int_{-a}^a \int_{-b}^b F(x, y) dx dy = \int_{-1}^1 \int_{-1}^1 f(\xi, \eta) |J| d\xi d\eta \quad (11)$$

$$[M]\dot{c} + [F]c - [K]c = s \quad (12)$$

$$[M] \text{ Mass matrix} \quad (13)$$

$$[F], [K] \text{ Stiffness matrix} \quad (14)$$

$$[M]\dot{c} = \int_{-1}^1 \int_{-1}^1 \frac{\partial c}{\partial t} \cdot Ni dx dy = \int_{-1}^1 \int_{-1}^1 [Ni \cdot Nj |J| d\xi d\eta] \left[ \frac{\partial ci}{\partial t} \right] \quad (15)$$

$$[F]c = \int_{-1}^1 \int_{-1}^1 \left[ (u \cdot Ni \cdot Ni \frac{\partial Nj}{\partial x} + v \cdot Ni \cdot Ni \frac{\partial Nj}{\partial y}) |J| d\xi d\eta \right] [ci] \quad (16)$$

$$[K]c = \int_{-1}^1 \int_{-1}^1 \left[ D * \left( \frac{\partial Nj}{\partial x} \frac{\partial Nj}{\partial x} + \frac{\partial Nj}{\partial y} \frac{\partial Nj}{\partial y} \right) |J| d\xi d\eta \right] [ci] \quad (17)$$

After establishing the global matrices for a patch consisting of 8 bilinear triangular elements, 4 bilinear quadrilateral elements, and one Lagrangian quadratic quadrilateral element, a set of recursion relations for the  $T_{ij}$  node can be established.

The set of finite element expressions, defined over a rectangular subspace and formulated using chapeau basis functions, can be interpreted as integrated averaged finite difference approximations. After applying Galerkin's method, integrating by parts, and using isoparametric transformations, we obtain the equations as follows:

2D bilinear triangular elements:

$$\begin{aligned} & \frac{1}{36} * [(3C'_{i+1j+1} + 3C'_{i-1j-1} + 3C'_{i+1j} + 3C'_{i-1j} + 3C'_{ij+1} + 3C'_{ij-1}) + 54 C'_{ij}] + \frac{U}{6 * \Delta x} * [(C_{i+1j+1} - C_{i-1j} + \\ & 2C_{i+1j} - 2C_{i-1j} + C_{i+1j} - C_{i-1j-1})] + \frac{V}{6 * \Delta y} [(C_{i-1j} - C_{i-1j-1} + 2C_{ij+1} - 2C_{ij-1} + C_{i+1j+1} - C_{i+1j})] + \\ & \frac{K}{\Delta x^2} [(-C_{i-1j-1} + 2C_{ij} - C_{i+1j+1})] + \frac{K}{\Delta y^2} [(-C_{ij+1} + 2C_{ij} - C_{ij-1})] = 0 \quad (19) \end{aligned}$$

2D bilinear quadrilateral elements:

$$\begin{aligned} & \frac{1}{9} * [(C'_{i-1j+1} + C'_{i+1j+1} + C'_{i-1j-1} + C'_{i+1j-1}) + 4(C'_{i+1j+1} + C'_{i-1j} + C'_{i+1j} + C'_{ij-1}) + 52 C'_{ij}] + \frac{U}{6 * \Delta x} * \\ & [(2C_{i+1j+1} - 2C_{i-1j+1} + 8C_{i+1j} - 8C_{i-1j} + 2C_{i+1j-1} - 2C_{i-1j-1})] + \frac{V}{6 * \Delta y} [(2C_{i-1j+1} - 2C_{i-1j-1} + 8C_{ij+1} - \\ & 8C_{ij-1} + 2C_{i+1j+1} - 2C_{i+1j-1})] + \frac{K}{6 * \Delta x^2} [(-4C_{i-1j} + 8C_{ij+1} - 4C_{i+1j} - C_{i-1j} + 2C_{ij} - C_{i+1j} - C_{i-1j-1} + 2C_{ij-1} - \\ & C_{i+1j-1})] + \frac{K}{6 * \Delta y^2} [(-C_{i-1j+1} + 2C_{i-1j} - C_{i-1j-1} - 4C_{ij+1} + 8C_{ij} - 4C_{ij-1} - C_{i+1j+1} + 2C_{i+1j} - C_{i+1j-1})] = 0 \quad (20) \end{aligned}$$

2D Quadratic Lagrangian quadrilateral element:

$$\begin{aligned} & \frac{1}{225} * [(C'_{i-1j+1} + C'_{i+1j+1} + C'_{i-1j-1} + C'_{i+1j-1}) + 8(C'_{i+1j+1} + C'_{i-1j} + C'_{i+1j} + C'_{ij-1}) + 16 C'_{ij}] + \frac{U}{45 * \Delta x} * \\ & [(16C_{i+1j+1} - 16C_{i-1j+1} + 128C_{i+1j} - 128C_{i-1j} + 16C_{i+1j-1} - 16C_{i-1j-1})] + \frac{V}{45 * \Delta y} [(16C_{i-1j+1} - 16C_{i-1j-1} + \\ & 128C_{ij+1} - 128C_{ij-1} + 16C_{i+1j+1} - 16C_{i+1j-1})] + \frac{K}{45 * \Delta x^2} [(-8C_{i-1j} + 16C_{ij+1} - 8C_{i+1j} - 64C_{i-1j} + 128C_{ij} - \\ & 64C_{i+1j} - 8C_{i-1j-1} + 16C_{ij-1} - 8C_{i+1j-1})] + \frac{K}{45 * \Delta y^2} [(-8C_{i-1j+1} + 16C_{i-1j} - 8C_{i-1j-1} - 64C_{ij+1} + 128C_{ij} - \\ & 64C_{ij-1} - 8C_{i+1j+1} + 16C_{i+1j} - 8C_{i+1j-1})] = 0 \quad (21) \end{aligned}$$

### Basis Functions

The general 2D bilinear element configurations are shown in Fig. 1. Notice that the triangular element array permits either a 9-node configuration or a 5-node configuration.

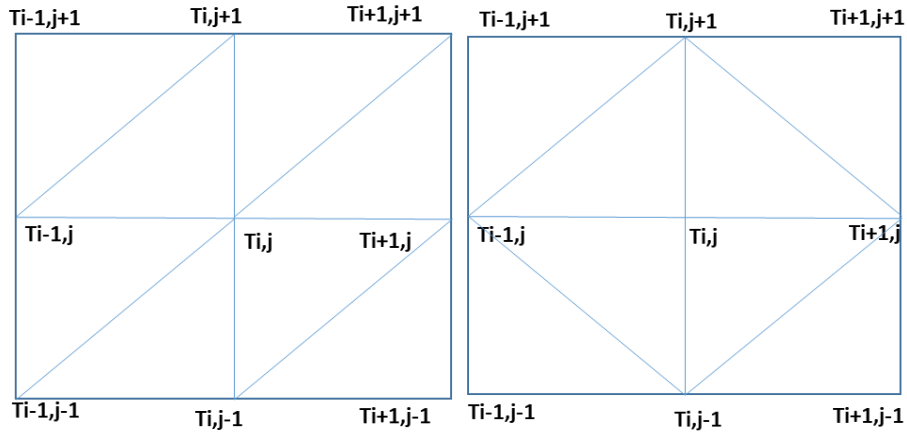


Figure 1. Basis Function-Triangular element

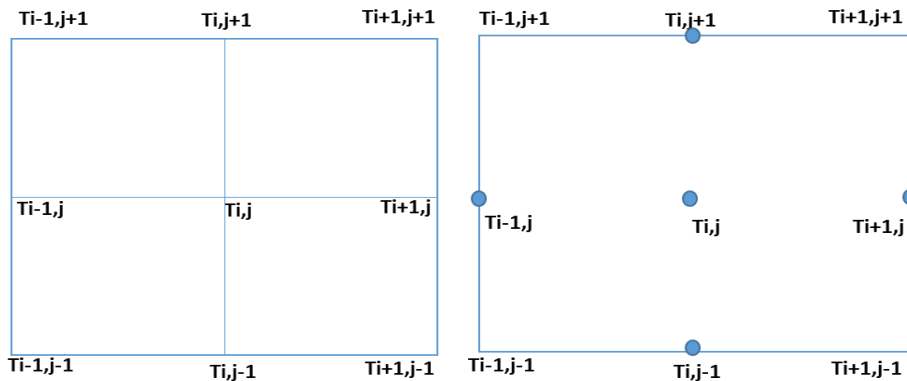


Figure 2. Basis Function-Quadrilateral element

## STRONGLY IMPLICIT PROCEDURE

For large algebraic systems, conventional solvers and direct solvers are computationally expensive. In the one-dimensional chapeau function study by Pepper and Baker [1], the ADI method was used to solve a set of tridiagonal matrices. In this study, SIP (Strongly Implicit Procedure) is considered for the penta-diagonal matrices but modified since we have 9 diagonal stripes in the overall matrix structure. While SIP was developed to solve 2-D transport equations, the overall SIP solution modifies the 5-stripe matrix into a 9-stripe matrix, hence involving the 9 nodes obtained from the triangular or quadrilateral patch. SIP has been shown to produce fewer iterations and lower computational cost compared to ADI conventional methods [Stone, 1968]. The SIP method decomposed the original matrix into upper and lower triangular matrices, i.e.

$$[A]x = B \quad (22)$$

$$[A + M]x = [A + M]x - ([A]x - B) \quad (23)$$

$$[A + M] = [L][U] \quad (24)$$

$$[L][U] * \{\delta\}^{n+1} = \{R\}^n \quad (25)$$

$$[V]^{n+1} = [U] * \{\delta\}^{n+1} \quad (26)$$

$$[L][V]^{n+1} = \{R\}^n \quad (27)$$

$$[U] * \{\delta\}^{n+1} = \{V\}^{n+1} \quad (28)$$

[A+M] is a modified matrix that can be decomposed to L and U matrices. This method can be applied to 5-stripe penta-diagonal matrices (produced in a 2D central FDM discretization). In this study, we employ the modified SIP (MSIP) used by Schneider and Zedan [4] to resolve the 9-diagonal matrix[2,6,7].

## APPLICATION AND RESULTS

In this simulation, a simple 2D domain (1 x 1) was used with a source established near the lower left corner. A simple diffusion test was first run, followed by an advection test, and then the combination of the two. The time dependent transport equation was solved for a 5 x 5 rectangular domain which was discretized into 32 triangular elements, 25 rectangular bilinear elements and 4 Lagrangian elements. Here we assume velocity  $U=V=1$  and diffusion coefficient  $\alpha_x = \alpha_y = 1$  and also  $\Delta y = \Delta x$  (constant) with fluxes set to zero at the outer boundaries.

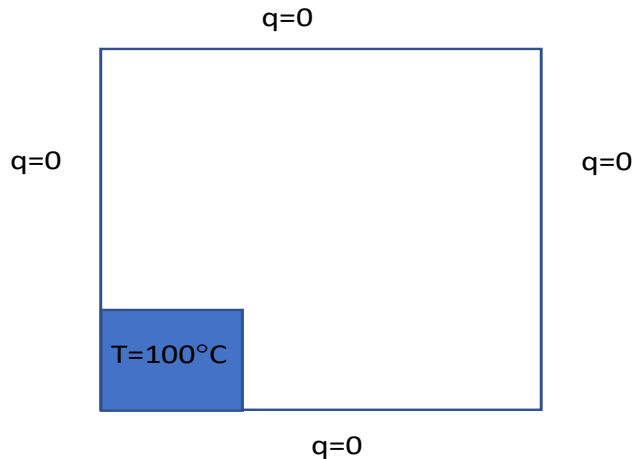


Figure3. Application Domain

Both a conventional FEM assembly (global matrix method) and SIP were used to solve the 2-D general transport equation. For a square patch of 5 by 5 rectangular elements, results from both conventional method and MSIP are shown in Fig. 4,5 for the triangular elements and in Fig. 6,7 for the bilinear quadrilateral and Lagrangian quadratic elements. While a little dispersive noise is observed in the simulations, the errors associated with the numerical methods are very low in the diffusion simulations, but become more noticeable as the advection terms become more dominant. Table 1 lists the CPU times (running on a 64-bit, 12GB Ram PC) for the various simulations. All programming was conducted using MATLAB. After almost 400 iteration for various simulation the residual become less than residual was less than  $1e^{-4}$  for time step of 0.1(s).

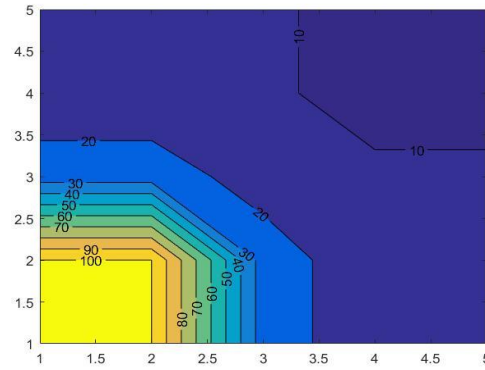
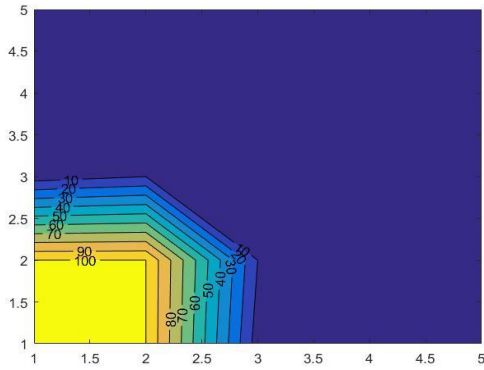
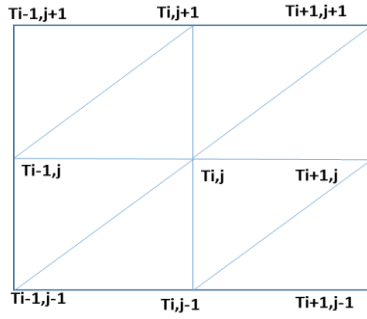
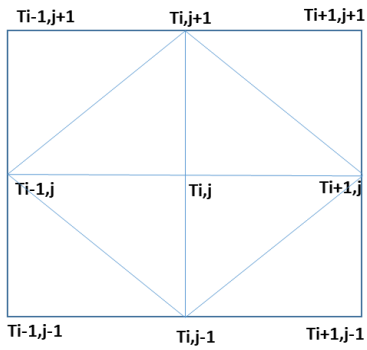


Figure4.

Left, Triangular-32 elements-conventional. Right, Triangular-32 elements-MSIP



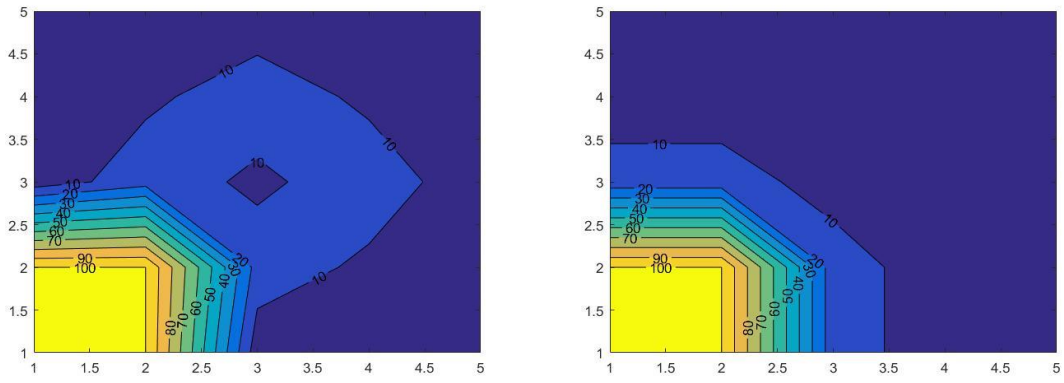


Figure5. Left, Triangular-32 elements-conventional method. Right, Triangular-32 elements-MSIP

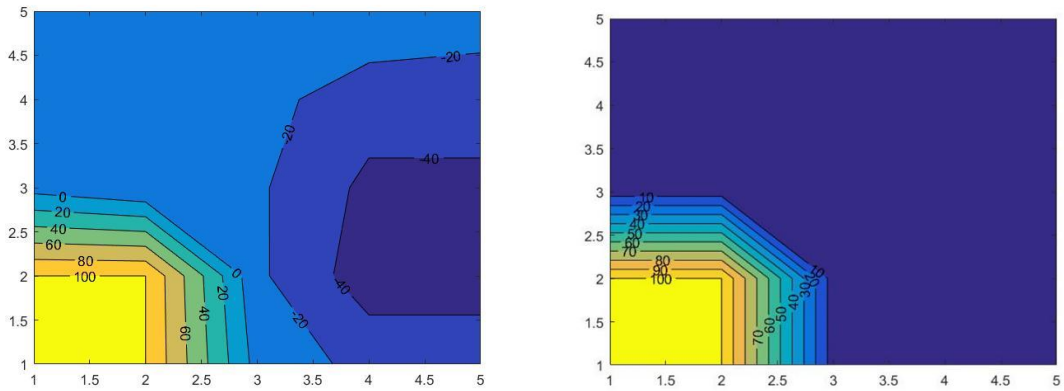
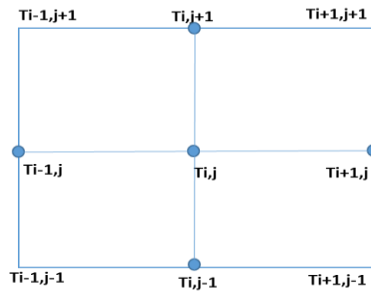


Figure6. Left, Bilinear-25 elements-conventional. Right, Bilinear-25 elements-MSIP

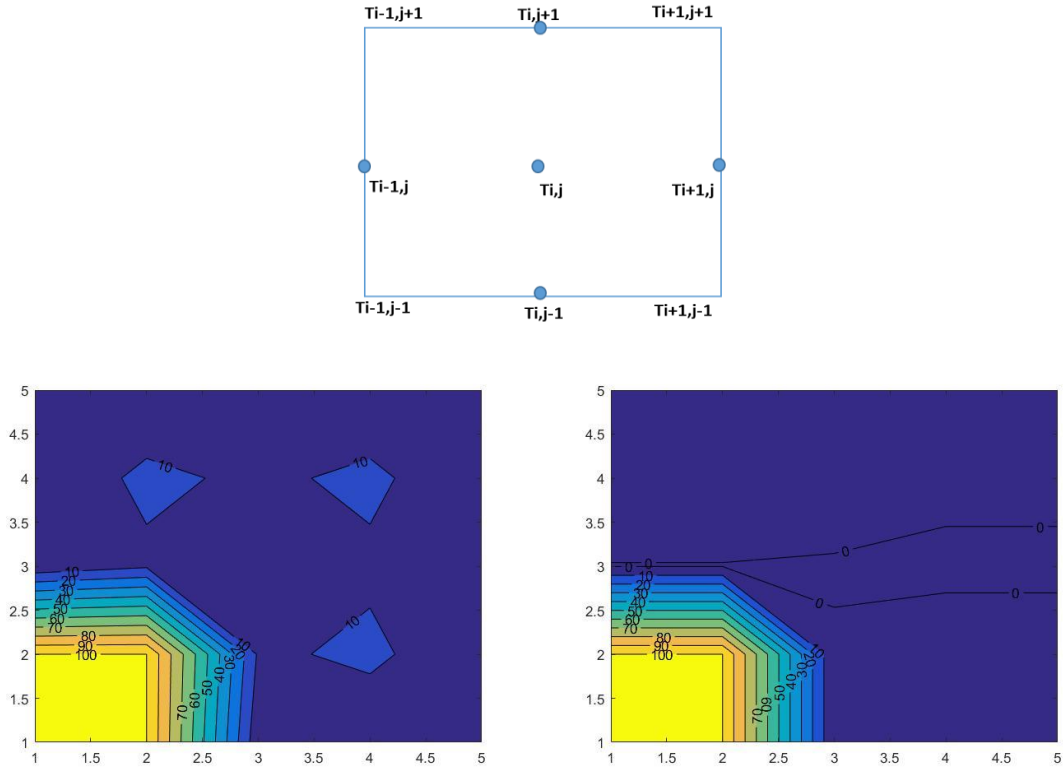


Figure7.Left,Lagrangian-25elements- Conventional. Right, Lagrangian-25elements- MSIP

Table 1. Comparison of CPU times

Shape function	Conventional (time, s)	MSIP (time, s)
Triangular(1)	5.5 (S)	1.4 (S)
Triangular(2)	5.4 (S)	1(S)
Bilinear	0.5 (s)	0.1(s)
Lagrangian	1.2(s)	0.2(s)

### Conclusions

The MSIP method is significantly faster than the conventional solution approach and provides a means for solving an implicit equation involving 5 (or 9) unknown nodal values. By establishing a recursion expression for a series of element patches, a conventional finite element method employing either triangular or quadrilateral elements can be converted into a pseudo finite difference approximation. This eliminates the need for renumbering global node numbers in order to minimize global bandwidth. While values using the Chapeau function approach provide values close to conventional FEM results, there is a slight loss in numerical accuracy. However, the use of 2D Chapeau functions provides a very convenient and easy methodology to resolve problem domains more routinely solved using conventional finite element techniques.

## References

- [1] Pepper, D.W. and Baker, A.J. A SIMPLE ONE-DIMENSIONAL FINITE-ELEMENT ALGORITHM WITH MULTIDIMENSIONAL CAPABILITIES, Numerical Heat Transfer, vol 2, 1979, pp 81-95.
- [2] Halada L., Lucká M. A Parallel Strongly Implicit Algorithm for Solving of Diffusion Equations. In: Zinterhof P., Vajteršic M., Uhl A. (eds) Parallel Computation. ACPC 1999. Lecture Notes in Computer Science, vol 1557, Springer, Berlin, Heidelberg, 1999.
- [3] P. E. Long and D. W. Pepper , A Comparison of Six Numerical Advection Schemes for Calculating the Advection of Atmospheric Pollution , Proc. AMS 3d Symp. Atmospheric Turbulence Diffusion and Air Quality, Raleigh, N.C., Oct. 19–22 , 1976 , pp. 181 – 187 .
- [4] Diersch, H. and Heidelberg, S. FEFLOW - Finite Element Modeling of Flow, Mass and Heat Transport in Porous and Fractured Media, Springer, (2018).
- [5] Pepper, D., Kern, C. and Long, P. Modeling the dispersion of atmospheric pollution using cubic splines and chapeau functions. Atmospheric Environment, 1979.
- [6] Azevedo, J.L.T., Durst, F., Pereira, J.C.F., Comparison of strongly implicit procedures for the solution of the fluid flow equations in finite difference form, Applied Mathematical Modelling, 1988
- [7] Schneider, G. E., Zedan, M., A MODIFIED STRONGLY IMPLICIT PROCEDURE FOR THE NUMERICAL SOLUTION OF FIELD PROBLEMS, Numerical Heat Transfer, 1981
- [8] Long P. E., Shaffer W. A., Kemper J. E. and Hicks F. J. The state of the Techniques Development Laboratory's boundary layer model, 1977.

## Modeling Abrasive Wear by the Discrete Elements Method

Franco Perazzo\*, Rainald Löhner\*\*

\*Universidad Técnica Federico Santa María, \*\*George Mason University

### ABSTRACT

The discrete elements method (DEM) is a computational method used to describe the movement of a large number of particles of different sizes and shapes, which interact through a contact model. Among other applications, the DEM is used as an effective way of addressing engineering problems to model the behavior of granular materials, mechanics of dust and rocks. In the field of mining, the DEM has been used mainly to predict the trajectory of the material inside SAG mills and in chutes of mineral transfer [1]. Within the applications of interest in this area, there is also the modeling of wear. There are many processes where wear limits the life of equipment, affecting its productivity and operating costs. However, no calculations that predict the wear of the enclosing walls have been performed to date. After an extensive review of the literature, a methodology to predict wear via DEM and phenomenological wear models has been developed. The decision was taken to use Archard's model [2], one of the simplest yet most accurate models proposed to date in the context of DEMs. The Archard model was used to predict the rate and the wear pattern on a structural steel plate A37-24 ES under different granulometry conditions of copper ore. One of the key stages is the correct characterization of the granular medium in order to be able to calibrate the numerical model. The numerical results obtained to date show a correct behavior with respect to the experimental values, which allows to establish that the model can to predict the phenomenon of abrasive wear and to compute realistic wear patterns. [1] P. Cleary, Modelling comminution devices using DEM; Int. J. Numer. Anal. Methods Geomech. 25, 83–105, 2001. [2] J.F. Archard, Contact and Rubbing of Flat Surfaces; J. Appl. Phys. 24, 981-988, 1953.

## **Effects of Microstructural and Production Inhomogeneities on the Macroscopic Behavior of Dual Phase Steels**

Semih Perdahcioglu\*, Erkan Asik\*\*, Ali Torkabadi\*\*\*, Ton Van den Boogaard\*\*\*\*

\*University of Twente, \*\*University of Twente, \*\*\*University of Twente, \*\*\*\*University of Twente

### **ABSTRACT**

It is well established that microstructural inhomogeneities such as crystal orientations, grain boundaries and second phase particles play a direct role on the macroscopic mechanical behavior of materials. The statistical distribution of these inhomogeneities however is equally important as it results in a microscopic distribution of mechanical quantities such as strain and stress fields. Using a lower order gradient enhanced crystal plasticity approach and realistic but computer generated microstructures representing a class of multiphase steels the effect of material as well as production induced inhomogeneity distributions is studied. The adopted crystal plasticity framework is rate-independent elastoplastic with gradient enhancement enforced at the finite element mesh using a staggered approach that makes it applicable directly to many commercial software packages efficiently. The production route is simulated by generating solid state phase transformations with volumetric mismatch which results in local stress fields as well as GNDs. Further steps in production such as discrete rolling operations are applied as simplified boundary conditions on the same RVE. It is shown that many relevant macroscopic phenomena such as anelasticity and Bauschinger effect can be observed when a sufficiently accurate mechanical history of the material is taken into account in terms of stress and GND distributions. Furthermore a Mean-Field homogenization approach is adopted to incorporate these distributions in a statistical manner in order to reproduce the aforementioned phenomena directly using simple phenomenological constitutive models for material fractions. To this end, a multiphase self-consistent elastoplastic framework is utilized. The results show that the distributions that occur as a result of production deformations as well as microstructural inhomogeneities play a significant role in dictating the macroscopic behavior of this class of materials.

## Physics Informed Neural Networks

Paris Perdikaris\*, Maziar Raissi\*\*

\*University of Pennsylvania, \*\*Brown University

### ABSTRACT

We introduce physics informed neural networks – neural networks that are trained to solve supervised learning tasks while respecting any given law of physics described by general nonlinear partial differential equations. In this two part treatise, we present our developments in the context of solving two main classes of problems: data-driven solution and data-driven discovery of partial differential equations. Depending on the nature and arrangement of the available data, we devise two distinct classes of algorithms, namely continuous time and discrete time models. The first form a new class of data-efficient spatio-temporal function approximators, while the latter allow the use of arbitrarily accurate Runge-Kutta time stepping schemes with up to 500 stages. Their effectiveness is demonstrated through a collection of classical problems in fluids, quantum mechanics, and reaction-diffusion systems.

## **Advances in the Approximation Theory for Functional Reconstructions Using GMLS and Applications to Meshless Discretization of Differential Equations**

Mauro Perego<sup>\*</sup>, Paul Kuberry<sup>\*\*</sup>, Pavel Bochev<sup>\*\*\*</sup>, Peter Bosler<sup>\*\*\*\*</sup>, Nathaniel Trask<sup>\*\*\*\*\*</sup>, Kara  
Peterson<sup>\*\*\*\*\*</sup>

<sup>\*</sup>Sandia National Laboratories, <sup>\*\*</sup>Sandia National Laboratories, <sup>\*\*\*</sup>Sandia National Laboratories, <sup>\*\*\*\*</sup>Sandia  
National Laboratories, <sup>\*\*\*\*\*</sup>Sandia National Laboratories, <sup>\*\*\*\*\*</sup>Sandia National Laboratories

### **ABSTRACT**

In this talk we present existence and approximation results for the reconstruction of a few classes of linear functionals, including differential and integral functionals, using the Generalized Moving Least Square (GMLS) method. These results extend or specialize classical GMLS theoretical results, and they rely both on the classic approximation theory for finite elements and on existence/approximation results for scattered data. In particular, we will consider the reconstruction of vector fields in Sobolev spaces and, more in general, the reconstruction of differential k-forms. We show how these results can be applied, in a rather straightforward way, to a variety of meshless schemes such as staggered stable discretizations for local/nonlocal diffusion and elasticity problems.

## **A Mixed-Mode Delamination Model Accounting for Large Openings and Fiber-Bridging**

Umberto Perego\*, Federica Confalonieri\*\*

\*Politecnico di Milano, \*\*Politecnico di Milano

### **ABSTRACT**

When large openings or extensive fiber-bridging phenomena are involved, classical cohesive models formulated under the assumption of small relative displacements often fail to predict the delamination growth. In the presence of large openings, the rotational equilibrium of the cohesive element is not satisfied [1], while the development of large scale fiber-bridging sensibly enhances fracture energy [2]. This effect, mainly governed by the normal opening, has been experimentally observed in several DCB tests performed on fiber-reinforced composites and is described in terms of R-curves, expressing the progressive growth of the toughness up to a steady-state value. In this work the isotropic damage cohesive model formulated in [3] under the assumption of small openings is extended to properly model both the cases of small and large openings and the presence of large-scale bridging or interfacial fibrillation. The considered cohesive model is specifically conceived for the case of mixed-mode delamination with variable mode ratios. Since the fiber bridging is mainly induced by mode I loading conditions, two distinct traction-separations laws are introduced for Mode I and II. A classical bilinear traction-separation law is adopted in pure Mode II, while the traction separation law in pure Mode I is, instead, characterized by a trilinear softening branch, consisting of an initial linear branch, followed by a plateau and by a second linear branch up to complete decohesion. Assuming that the fiber bridging occurs when the plateau is reached allows formulating a simple activation criterion that can be generalized also to mixed-mode conditions. To account for the transition from small to large openings, the classical interface element is substituted with a fibril element, whose constitutive behaviour is defined such that no discontinuity in the dissipated energy or in the transmitted cohesive tractions is introduced. As shown in [2], this kind of elements is able to account for large openings in a consistent way, since the interface tractions and openings are colinear. [1] Vossen, Schreurs, van der Sluis, Geers, On the lack of rotational equilibrium in cohesive zone elements, *Computer Methods in Applied Mechanics and Engineering*, 254, 146-153 (2013) [2] Dávila, Rose, Camanho, A procedure for superposing linear cohesive laws to represent multiple damage mechanisms in the fracture of composites, *International Journal of Fracture*, 158, 211-223 (2009) [3] Confalonieri, Perego, A mixed-mode cohesive model for delamination with isotropic damage and internal friction, *Proceedings of the sixth ECCOMAS Thematic Conference on the Mechanical Response of Composites* (2017)

## **Buckling of Viscoplastic Bingham Fluid Filaments under Compression Stresses**

Anselmo Pereira<sup>\*</sup>, Mehdi Khalloufi<sup>\*\*</sup>, Elie Hachem<sup>\*\*\*</sup>, Romain Castellani<sup>\*\*\*\*</sup>, Rudy Valette<sup>\*\*\*\*\*</sup>

<sup>\*</sup>Université Paris Sciences et Lettres (PSL), MINES ParisTech, Centre de Mise en Forme de Matériaux (CEMEF), 1 Rue Claude Daunesse, 06904 Sophia Antipolis, France, <sup>\*\*</sup>Université Paris Sciences et Lettres (PSL), MINES ParisTech, Centre de Mise en Forme de Matériaux (CEMEF), 1 Rue Claude Daunesse, 06904 Sophia Antipolis, France, <sup>\*\*\*</sup>Université Paris Sciences et Lettres (PSL), MINES ParisTech, Centre de Mise en Forme de Matériaux (CEMEF), 1 Rue Claude Daunesse, 06904 Sophia Antipolis, France, <sup>\*\*\*\*</sup>Université Paris Sciences et Lettres (PSL), MINES ParisTech, Centre de Mise en Forme de Matériaux (CEMEF), <sup>\*\*\*\*\*</sup>Université Paris Sciences et Lettres (PSL), MINES ParisTech, Centre de Mise en Forme de Matériaux (CEMEF), 1 Rue Claude Daunesse, 06904 Sophia Antipolis, France

### **ABSTRACT**

Fluid buckling instabilities represent a major source of irregularities for several industrial and natural processes such as container filling, glass plate fabrication and folding of geological structures. Despite some recent and significant works regarding such instabilities in Newtonian fluids, the buckling of non-Newtonian materials remains scarcely explored in the literature. In the present work, we analyse through scaling laws and direct numerical simulations the buckling of filaments of a viscoplastic Bingham fluid compressed at constant velocity by two parallel plates. Under low gravity conditions (the Laplace pressure exceeds the hydrostatic pressure), three regimes are observed for slender filaments: a first one driven by the capillary force and during which there is no deflection and a folding regime that is dominated by the compressive viscous force and for which the inertia is negligible, as found by Le Merrer, Quéré and Clanet [PRL 109, 064502 (2012)]; and a twist/coil regime appearing at larger Reynolds number. Introducing a yield stress induces localization that restricts the buckled flow dimensions. Our main results are summarized in a four-dimensional phase diagram whose axes are a slenderness parameter, capillary number, Reynolds number and Bingham number.

## An Asynchronous Task-Based Parallelization Strategy for Multiscale Solid Mechanics

J. Antonio Perez<sup>\*</sup>, Jeremiah Wilke<sup>\*\*</sup>, David Littlewood<sup>\*\*\*</sup>, Janine Bennett<sup>\*\*\*\*</sup>, David Hollman<sup>\*\*\*\*\*</sup>, Jonathan Lifflander<sup>\*\*\*\*\*</sup>

<sup>\*</sup>University of New Mexico and Sandia National Laboratories, <sup>\*\*</sup>Sandia National Laboratories, <sup>\*\*\*</sup>Sandia National Laboratories, <sup>\*\*\*\*</sup>Sandia National Laboratories, <sup>\*\*\*\*\*</sup>Sandia National Laboratories, <sup>\*\*\*\*\*</sup>Sandia National Laboratories

### ABSTRACT

Concurrent multiscale approaches for solid mechanics combine the use of a low-cost macroscale model, applied over the bulk of the domain, with a high-cost, high-fidelity model operating at a lower length scale. This combination of modeling approaches with vastly different computational expenses and memory requirements greatly complicates the management of tasks within a parallel simulation code. Recent work in Asynchronous Many-Task (AMT) scheduling provides a framework for multiscale mechanics that addresses this complexity through a task-based programming model and a flexible, highly-scalable runtime environment. In this presentation, we explore the use of the DARMA AMT programming model within a FE-squared multiscale mechanics code [1]. The FE-squared approach, which associates independent mesoscale finite-element problems with material points in the macroscale model, is naturally compatible with AMT scheduling on next-generation, heterogeneous computing platforms. We first review the implementation of a traditional parallelization strategy based on direct application of the MPI programming model, which illustrates the challenges of parallelization and provides a performance baseline. We then present an alternative parallelization approach based on AMT. In this approach, the software design follows a paradigm that compartmentalizes work in a set of tasks with explicitly-defined interdependencies. Applied in combination with an overdecomposition strategy, the task-based model enables the AMT runtime to execute work asynchronously and to migrate work among hardware resources to accommodate load-balancing requirements that may evolve over time. We present example simulations for single-scale and multiscale solid mechanics that span a range of computational expense and load-balancing requirements. Results obtained using AMT scheduling are compared against those obtained using traditional parallelization to illustrate both the advantages and the challenges associated with AMT scheduling for computational mechanics. [1] J. Bennett, M. Bettencourt, R. Clay, H. Edwards, M. Glass, D. Hollman, H. Kolla, J. Lifflander, D. Littlewood, A. Markosyan, S. Moore, S. Olivier, J. Perez, E. Phipps, F. Rizzi, N. Slattengren, D. Sunderland, and J. Wilke. ASC ATDM level 2 milestone #6015: Asynchronous many-task software stack demonstration. Report SAND2017-9980, Sandia National Laboratories, Albuquerque, NM and Livermore, CA, 2017.

## Stochastic Partial Linearization Approach for Nonlinear Reduced Order Models of Thin Panels

Ricardo Perez<sup>\*</sup>, Benjamin Smarslok<sup>\*\*</sup>, Marc Mignolet<sup>\*\*\*</sup>

<sup>\*</sup>Universal Technology Corporation, <sup>\*\*</sup>U.S. Air Force Research Laboratory, <sup>\*\*\*</sup>Arizona State University

### ABSTRACT

Finite element analysis (FEA) of the dynamic response of aircraft panels in extreme aeroacoustic environments requires substantial computational resources, which has led to numerous research efforts on the development of nonlinear reduced order models (ROMs). ROMs reduce the finite element model to a low-order system of nonlinear modal-like equations which can be integrated in the time domain [1]. Although much more computationally efficient than FEA, it may still be expensive to build and solve the ROM equations of motion for large structures (i.e., built-up panels) owing to the large number of nonlinear terms involved [2]. The proposed approach seeks to further reduce the computational cost by building a sparse ROM that only includes the nonlinearity in the dominant modes of the basis. The methodologies stem from previous observations that only a subset of the modes in the basis are dominant [2], while the rest of them respond significantly less to the loading or are parametrically excited by nonlinear coupling with the most important modes. Yet, the contributions of the non-dominant modes cannot simply be ignored without unduly affecting the accuracy of the predictions. Their small level of response has however suggested that the nonlinear terms involving them may be neglected, a process referred to here as partial linearization. The selection of the number of dominant modes can be made as aggressively or conservatively as desired (i.e., as many or as few) leading to a varying tradeoff between degree of accuracy of the solution and computational cost. The solution approximation error introduced by this process is recognized as an epistemic uncertainty, which is modeled by randomizing the linear stiffness terms of the non-dominant modes. The nonparametric stochastic approach [3] is adopted for this modeling and its uncertainty level is estimated using maximum likelihood estimation. The approach is verified on the ROM of a 96,000 degrees-of-freedom, 9-bay panel, where significant computational gains are observed for dynamic simulations. [1] Mignolet, M.P., Przekop, A., Rizzi, S.A., and Spottswood, S.M., "A Review of Indirect/Non-Intrusive Reduced Order Modeling of Nonlinear Geometric Structures," *Journal of Sound and Vibration*, Vol. 332, 2013. [2] Perez, R., Wang, X.Q., and Mignolet, M.P., "Non-Intrusive Structural Dynamic Reduced Order Modeling for Large Deformations: Enhancements for Complex Structures," *Journal of Computational and Nonlinear Dynamics*, Vol. 9, 2014. [3] Soize, C., "Stochastic linearization method with random parameters for SDOF nonlinear dynamical systems: prediction and identification procedures," *Probabilistic Engineering Mechanics*, Vol. 10, 1995.

## **Bayesian Identification of the Random Elasticity Field of a Heterogeneous Microstructure**

Guillaume Perrin\*, Christian Soize\*\*

\*cea, \*\*Université Paris-Est

### **ABSTRACT**

This paper presents a statistical inverse method for identifying the mechanical properties of a heterogeneous microstructure, which is modeled by a random elastic media. To this end, several experimental tests are performed on a series of specimens made of the same material. For each experiment, the applied force field is supposed to be imposed, and the induced displacement field is measured on the contours of the specimens only. In parallel, for given properties of the random media, it is possible to simulate independent realizations of the elasticity random field, and to approximate (using the Finite Element Method) the displacements that are induced by the experimental force field. Based on the comparison of the statistical properties of the displacement fields on the contours of the specimens in the experimental and the simulated cases, a method is thus proposed to identify the most likely properties of the random media characterizing the heterogeneous microstructure (such as the mean elasticity field, the dispersion and the correlation lengths). It should be noted that the elasticity field is not a real-valued random field, but a tensor-valued random field, and that the different components of this random field cannot be identified separately due to algebraic constraints. Additionally, the quantity of interest on which the identification procedure is based is not a scalar, but a high-dimension vector. This requires the introduction of dedicated reduction techniques. Last but not least, the number of code evaluations that is generally required for the identification procedure can quickly become burdensome. To circumvent this problem, statistical extrapolation techniques and iterative procedures will be presented to maximize the precision of the identification at a reduced computational cost. Validations of the procedure are eventually presented using simulated data in two and three dimensions.

## Modeling of Laser Powder Bed Fusion Additive Manufacturing Using The eXtended Discrete Element Method (XDEM)

Bernhard Peters<sup>\*</sup>, Mehdi Baniasadi<sup>\*\*</sup>, Maryam Baniasadi<sup>\*\*\*</sup>

<sup>\*</sup>Université du Luxembourg, <sup>\*\*</sup>Université du Luxembourg, <sup>\*\*\*</sup>Université du Luxembourg

### ABSTRACT

The production of parts via laser powder bed fusion additive manufacturing (LPBF-AM) of metallic powders is growing exponentially. LPBF-AM involves complex physical processes such as the laser interaction with the bed, powder bed melting, solidification, the melt formation, and Marangoni effect. The bed structure can significantly affect the local heat transfer, fluid formation, and the porosity distribution. The shape and surface of the transient fluid flow along with its internal porosity distribution will form the final product. Therefore, the final product quality is a strong function of all the above-mentioned parameters. In order to be able to model the bed structure along with the melt formation, the combined continuous-discrete methods are of interest. The eXtended Discrete Element Method known as XDEM [1,2] an advanced numerical tool based on discrete-continuous concept able to address the thermophysical phenomena involved during laser powder bed fusion is presented. Within this platform, the continuous phases such as gas and liquid phases are coupled to the discrete entities such as powders through mass, momentum and energy exchange. It can predict the position, temperature distribution and phase change for each particle in conjunction with each fluid phases' temperature, velocity, and volume fraction. In this contribution, the XDEM is used as an alternative approach for laser powder bed fusion additive manufacturing of metallic powders. To this aim, a bed of powders is constructed and a moving heat source representing the laser will melt the exposed powders and the melt phase will form. In this concept, the melting and shrinking of the powders, as well as the formation of the melt pool and heat transfer, are well studied. References [1] Mehdi Baniasadi, Maryam Baniasadi, Bernhard Peters, Coupled CFD-DEM with Heat and Mass transfer to Investigate the Melting of a Granular Packed Bed, doi:10.1016/j.ces.2017.12.044. [2] Bernhard Peters, Gabriele Pozetti, Flow characteristics of metallic powder grains for additive manufacturing, The European Physical Journal Conferences, 2017, doi:10.1051/epjconf/201714013001.

# **A Divergence-Conforming Hybridized Discontinuous Galerkin Method for the Incompressible Reynolds Averaged Navier-Stokes Equations**

Eric Peters\*, John Evans\*\*

\*University of Colorado Boulder, \*\*University of Colorado Boulder

## **ABSTRACT**

We introduce a hybridizable discontinuous Galerkin method for the incompressible Reynolds Averaged Navier-Stokes equations coupled with the Spalart-Allmaras one equation turbulence model for the scalar eddy viscosity. With a special choice of velocity and pressure spaces for both element and trace degrees of freedom, we arrive at a method which returns point-wise divergence-free velocity fields and properly balances momentum and energy at an element-level. We further demonstrate how to directly enforce a non-negativity constraint on the eddy viscosity field without loss of accuracy through the intelligent utilization of constrained optimization. Finally, we examine the use of different polynomial degrees and meshes for the flow and turbulence variables to most efficiently represent the flow field (which is typically smooth) and the eddy viscosity (which is typically rough). As is standard with hybridized discontinuous Galerkin methods, static condensation can be employed to remove the element degrees of freedom and thus dramatically reduce the global number of degrees of freedom. Numerical results illustrate the effectiveness of the proposed methodology both in the case of no turbulence model as well as in the case of the Spalart-Allmaras turbulence model.

## Explicit Partitioned Methods for Multiphysics Coupling

Kara Peterson<sup>\*</sup>, Pavel Bochev<sup>\*\*</sup>, Paul Kuberry<sup>\*\*\*</sup>

<sup>\*</sup>Sandia National Laboratories, <sup>\*\*</sup>Sandia National Laboratories, <sup>\*\*\*</sup>Sandia National Laboratories

### ABSTRACT

Complex multiphysics applications often require the efficient and stable coupling of individual codes or separately meshed regions through non-matching interfaces. A characteristic example of this type of coupling occurs between atmospheric and ocean codes in global Earth system models where conservation of fluxes as they are passed between the different code discretizations is crucial. In this talk we describe an explicit Lagrange multiplier-based interface coupling method and its application to advection-diffusion equations and to a simplified ocean/atmosphere system. To obtain a Lagrange multiplier formulation that is fully compatible with explicit time integration we consider a coupling condition which enforces the continuity of the time derivatives of the states across the interface. Assuming that the initial data are continuous across the interface, this alternative coupling condition implies continuity of the state while enabling a fully explicit treatment. For the explicit partitioned method we compute the Lagrange multiplier directly and use it for boundary data in partitioned solves on each domain. Numerical results for advection-diffusion equations demonstrate the stability of the formulation and second-order convergence in both the advection and diffusion dominated regimes.

## DPG Multigrid Solvers for High Frequency Time-harmonic Wave Propagation Problems

Socratis Petrides\*, Leszek Demkowicz\*\*

\*Institute for Computational Engineering and Sciences, UT Austin, \*\*Institute for Computational Engineering and Sciences, UT Austin

### ABSTRACT

We present a novel adaptive DPG multigrid (MG) solver for the solution of high-frequency wave propagation problems in both two and three space dimensions. In stark contrast to traditional MG methods, this solver operates only on the trace variables defined on the mesh skeleton. Since trace variables supported on new faces created upon h-refinements have no predecessors, coarse grid basis functions have no fine grid representatives. Thus, an auxiliary mesh is constructed by statically condensing these trace variables. Therefore, communication between meshes involves both an inclusion and a Schur complement extension operator. True to the DPG spirit, this solver is applicable to a general class of second order problems, cast in any DPG formulation. However, in this talk we focus on high-frequency wave propagation problems with localized solutions (e.g. simulation of Gaussian beams). For very large wavenumbers,  $h_p$ -adaptivity is crucial in order to keep the computational cost and the memory requirements under control. The DPG unconditional mesh-independent discrete stability and its built-in error indicator provide efficient and reliable adaptive mesh refinements starting from very coarse meshes. The need for iterative solvers, comes from the fact that the problem has to be solved several times throughout the adaptive procedure. Employing a direct solver, at every adaptive step is far from optimal and unnecessary. We use the aforementioned multigrid technology as a preconditioner for the Conjugate Gradient method. The resulting iterative solution scheme is employed in order to produce partially converged solutions, accurate enough to drive the adaptive refinements. Our results show convergence in terms of iterations at a rate independent of the mesh and the wavenumber. The efficacy of the above construction (in the two-grid case) has already been demonstrated for high-frequency acoustics problems in 2D in [1]. [1] Petrides, S. and Demkowicz, L. (2017). An Adaptive DPG Method for High Frequency Time-harmonic Wave Propagation Problems. Comput. Math. Appl.

## **An Experimental and Numerical Study of Deformation and Decohesion Mechanisms During Peel Testing of a Laminate Packaging Material**

Simon Pettersson<sup>\*</sup>, Stephen Hall<sup>\*\*</sup>, Jonas Engqvist<sup>\*\*\*</sup>, Håkan Hallberg<sup>\*\*\*\*</sup>, Nils Toft<sup>\*\*\*\*\*</sup>

<sup>\*</sup>Lund University, <sup>\*\*</sup>Lund University, <sup>\*\*\*</sup>Lund University, <sup>\*\*\*\*</sup>Lund University, <sup>\*\*\*\*\*</sup>Tetra Pak Packaging Solutions AB

### **ABSTRACT**

The material used in packages for the food and dairy industries comprise multiple laminate layers, each serving different purposes in preserving and protecting the package content and by providing the appropriate package rigidity during handling. Already during package manufacturing and filling, the package material is subject to large deformations and a range of thermal and chemical processes that sometimes cause delamination between the laminate layers. This, in turn, can lead to a reduced product shelf lifetime and unsatisfactory package performance. In addition, controlled delamination can also be a required material property, for example in the case of package folding or opening mechanisms. Aspects like these emphasize a great need for increased understanding of adhesion and for the ability to predict adhesion properties of different packaging materials and under different handling conditions. In order to quantify the delamination strength, more or less standardized peel tests are often employed. In such tests, a laminate layer is partly separated to provide the peel arm which is pulled off from the substrate layer(s) at a constant angle. The required peel force is measured along with the peel arm deformation and provides a measure of the delamination strength of the laminate package material. However, the measured force is not only the force component required to separate the layers, but it is also due to deformation of the peel arm and possibly also additional deformation mechanisms in the substrate layer(s). Therefore, not only the cohesive bond between individual laminate layers, but also the properties of the individual laminate layers themselves must be properly characterized. In the present work, peel test experiments have been conducted and the peel force and displacement as well as the peel arm geometry have been monitored. The same peel test has also been studied by numerical simulations using a cohesive zone modeling framework. The influence of the cohesive model formulation and the choice of constitutive model for the peel arm material are investigated in relation to the experimental observations and different delamination mechanisms are observed.

## Computational Modelling of Carotid Atherosclerotic Plaque Formation and Development on Patient-specific Geometries

Estefania Peña<sup>\*</sup>, Patricia Hernández<sup>\*\*</sup>, Myriam Cilla<sup>\*\*\*</sup>, Miguel A. Martínez<sup>\*\*\*\*</sup>

<sup>\*</sup>Aragón Institute of Engineering Research (I3A), University of Zaragoza, Zaragoza, Spain; CIBER de Bioingeniería, Biomateriales y Nanomedicina (CIBER-BBN), Zaragoza, Spain, <sup>\*\*</sup>Mechanical Engineering Department, University of Zaragoza, Zaragoza, Spain, <sup>\*\*\*</sup>1. Centro Universitario de la Defensa. Academia General Militar, Spain; Aragón Institute of Engineering Research (I3A). University of Zaragoza, Spain; Centro de Investigación Biomédica en Red de Bioingeniería Biomateriales y Nanomedicina (CIBER-BBN), Spain, <sup>\*\*\*\*</sup>Aragón Institute of Engineering Research (I3A), University of Zaragoza, Zaragoza, Spain; CIBER de Bioingeniería, Biomateriales y Nanomedicina (CIBER-BBN), Zaragoza, Spain

### ABSTRACT

Atherosclerosis is the process in which atheroma plaques are built up in the walls of the arteries causing narrowing, hardening of the arteries and loss of elasticity. Cyclic stretch, laminar and oscillatory shear stress, effects of vessel compliance, curvature, pulsatile blood flow or cardiac motion are considered the main triggers of atherosclerosis initiation. The location of atherosclerosis is associated with flow separation and turbulence. Therefore, many studies have identified haemodynamic shear stresses as an important determinant of endothelial function and phenotype in atherosclerosis disease. We propose a mathematical model of atheroma plaque initiation and early development in carotid arteries. Our current approach is on the process on plaque initiation and intimal thickening rather than in severe plaque progression and rupture phenomena. This model uses the Navier–Stokes equations and Darcy’s law for fluid dynamics, convection–diffusion–reaction equations for modelling the mass balance in the lumen and intima, and the Kedem–Katchalsky equations for the interfacial coupling at membranes, i.e. endothelium. The volume flux and the solute flux across the interface between the fluid and the porous domains are governed by a three-pore model. The main species and substances which play a role in early atherosclerosis development have been considered in the model, i.e. LDL, oxidized LDL, monocytes, macrophages, foam cells, smooth muscle cells, cytokines and collagen. This model has been applied to model the plaque formation patient-specific geometries of carotid artery where the atherosclerotic plaque has been removed in order to validate the mathematical framework. Our results for plaque localization correspond to low shear stress zone and the plaque location is compared with the patient-specific geometries with atheroma. References M. Cilla, E. Peña, and M. A. Martínez. Mathematical modelling of atheroma plaque formation and development in coronary arteries. *J. R. Soc. Interface* 11:201308661–2013086616, 2014. U. Olgac, V. Kurtcuoglu, and D. Poulikakos. Computational modeling of coupled blood-wall mass transport of LDL: effects of local wall shear stress. *Am. J. Physiol. Heart Circ. Physiol.* 294(2):909–919, 2008. Acknowledgements Support from the Spanish Ministry of Economy and Competitiveness through the research projects DPI2016-76630-C2-1-R.

## Layer-specific Failure Mechanics of Thoracic and Abdominal Aorta and Related Constitutive Modeling

Juan A. Peña<sup>\*</sup>, Miguel A. Martínez<sup>\*\*</sup>, Estefanía Peña<sup>\*\*\*</sup>

<sup>\*</sup>Department of Management and Manufacturing Engineering, Faculty of Engineering and Architecture University of Zaragoza, Spain, <sup>\*\*</sup>Aragón Institute of Engineering Research (I3A), Mechanical Engineering Department University of Zaragoza, Spain, <sup>\*\*\*</sup>Aragón Institute of Engineering Research (I3A), Mechanical Engineering Department University of Zaragoza, Spain

### ABSTRACT

Mechanical force at the tissue level leads to local stress concentrations within the tissue, and, if high enough, starts damaging it at specific spots. In healthy tissues at physiological stress levels, healing continuously repairs such defects to maintain the tissue's structural integrity. Despite increasing experimental and analytical efforts to investigate failure-related irreversible effects of soft biological tissue, the underlying mechanisms are still poorly understood. The goal of this study was characterize the failure properties of the intact wall and each separated layer (intima, media and adventitia) of the descending thoracic and infrarenal abdominal aorta and to test the hypothesis that the failure properties of layer-separated thoracic arteries differ depending on arterial location in the aorta (Peña et al. 2015). To test this hypothesis, we performed uniaxial tests to study the mechanical behavior of both intact and layer-separated porcine aortic tissue samples taken from descending thoracic and infrarenal abdominal aorta until complete failure. The damage behavior required a continuum damage theory commonly used to describe the softening of soft tissues under large deformations. The structural model here presented was built within the framework of nonlinear continuum mechanics (Calvo et al. 2007). Tissue damage was simulated considering different damage behaviors for the matrix and the fibers. We reported values of constitutive parameters using the damage model that can be used by biomedical engineers for investigating better therapies and developing artery-specific devices

References Calvo, B., Peña, E., Martínez, M.A., Doblaré, M., 2007. An uncoupled directional damage model for fibered biological soft tissues. Formulation and computational aspects. *Int. J. Numer. Meth. Eng.* 69, 2036–2057. Peña, J.A., Martínez, M.A., Peña, E., 2015. Layer-specific residual deformations and uniaxial and biaxial mechanical properties of thoracic porcine aorta. *J. Mech. Behav. Biomed.* 50, 55–69.

Acknowledgements Support from the Spanish Ministry of Economy and Competitiveness through the research projects DPI2016-76630-C2-1-R and the Instituto de Salud Carlos III (ISCIII) through the CIBER initiative.

## Incremental POD and Custom Integration Schemes for Hyper-reduced Automotive Crash Analysis

Pierre Phalippou<sup>\*</sup>, Piotr Breitkopf<sup>\*\*</sup>, salim bouabdallah<sup>\*\*\*</sup>, pierre villon<sup>\*\*\*\*</sup>

<sup>\*</sup>Altair/UTC, <sup>\*\*</sup>UTC, <sup>\*\*\*</sup>Altair, <sup>\*\*\*\*</sup>UTC

### ABSTRACT

Industrial usage of numerical math-based tools such as the finite element method may in some applications become prohibitive due to the computational cost. This is particularly true in the automotive sector when optimizing the shape of a vehicle in crash situations. Model Order Reduction addresses this issue. Most model order reduction methods rely on the construction of a reduced basis to project the model on. The Proper Orthogonal Decomposition (POD) builds a modal basis from solution observations called snapshots. Data are in a first stage taken from full order model runs and then processed in a so-called 'off-line phase' to give the reduced basis which is then used to build the reduced model. Some difficulties arise in the POD. In industrial applications, the data generated in the observation phase may become huge and hard to manipulate. Moreover, the computational cost for post-processing this data may as well explode. Another issue concerns the numerical integration schemes, i.e. the position of numerical integration points and the integration weights. The incremental Singular Value Decomposition originates from streamed visual content. This method is based on rank one modifications of a given matrix decomposition. In the POD framework it allows post-processing observations as soon as they are available. This method leads to memory savings and possible computational savings during the 'off-line phase', as data are not kept in memory and redundant or nonrelevant observations are automatically rejected by the method. Another benefit of this method is the ease to manipulate the POD basis by adding new observations or removing others. For the integration of internal forces, we propose a reduced integration scheme, with integration sites and weights obtained as the solution of a Linear Programming problem. This allows us to add to the training set additional constraints such as an exact integration of monomials or of other explicit base functions. The proposed approach has been implemented in ALTAIR's solver RADIOSS<sup>®</sup> and applied to a structural impact problem. Results regarding computation time, developed features such as estimation of the Reduced Basis error of approximation as well as visual representations illustrate this work. The presentation will focus on the integration of such approach in the whole reduction process, highlighting the attractiveness of the method as well as the required developments to make the whole reduction process incremental.

## **The Web Force-Field (WebFF) Project: Ontology Based Force-field Repository for Soft Materials at Multiple Levels of Granularity**

Frederick Phelan Jr.\*, Huai Sun\*\*

\*NIST, \*\*Shanghai Jiao Tong University

### **ABSTRACT**

In this talk, we will describe WebFF, an open and extensible force-field repository, designed to support the Materials Genome Initiative (MGI) for organic and related soft materials. The repository is built using the NIST Materials Data Curation System (MDCS). The MDCS has a web-based interface built on top of the RESTful API and a NoSQL database system to support ontology based database descriptions using XML schema. Users interact with the repository through two main portals. The Data Curation Portal supports upload of published force-field data with appropriate metadata descriptors to support provenance based data sharing. New datasets may be curated interactively or using a python based toolset to upload large datasets en masse. The User Portal supports search for curated force-field data based on the metadata descriptors and download in a number of common formats. The initial release of the repository will feature a number of integrated XML schemas. The first schema supports Class I organic force-fields in such as OPLS, Amber and CHARMM style representations. The second supports Class II style force-fields such as CFF, PCFF, COMPASS and TEAMFF. We have also developed a schema for representing a wide range of coarse-grained force-field data ranging from united-atom style models to tabulated potentials. The methods, requirements and goals of force-field data sharing, and the plan for extending the initial repository to include other classes of force-field data will also be described.

## Modeling the Nonlinear Response of Complex Periodic Truss Lattices Using a Modified Quasicontinuum Method

Greg Phlipot\*, Dennis Kochmann\*\*

\*California Institute of Technology, \*\*ETH Zurich

### ABSTRACT

Recently, there has been significant interest in periodic truss lattices down to the micro- and nanoscales, but the computational modeling of these metamaterials remains a challenge due to the fine scale of the truss architecture and the resulting large numbers of truss members to be modeled. In this talk, we model periodic truss lattices using an extension of the quasicontinuum (QC) method [1]: a multiscale tool originally designed to significantly reduce the computational cost of atomic lattice simulations, which has recently been extended to model simple (Bravais) truss lattices and fiber networks with inelasticity and failure [2]. The QC method is a set of interpolation and energy approximation rules that allows for full resolution of the microstructure to be obtained in areas of interest, while drastically reducing the number of degrees of freedom by coarse-graining in areas requiring less resolution. We present results from a new, fully-nonlocal formulation of the QC method capable of modeling the nonlinear response of more general three-dimensional periodic truss (multi)lattices that uses an optimal summation rule [3] to approximate the total energy of the system. Corotational beam elements are used to capture the geometric nonlinearities on the microscale, while the degrees of freedom of the beams are linearly interpolated in coarse-grained regions. Adaptive mesh refinement is also used, which allows us to expand the fully-resolved region as necessary to accurately capture local nonlinear phenomena. Importantly, this approach does not rely upon a separation of scales and is thus a powerful tool to bridge across scales in a concurrent manner. References: [1] E.B. Tadmor, R. Phillips, M. Ortiz, &quot;Mixed atomistics and continuum models of deformation in solids&quot;, *Langmuir*, v. 12, p. 4529-4534, 1996. [2] L.A.A. Beex, R.H.J. Peerlings, M.G.D. Geers, &quot;A multiscale quasicontinuum method for dissipative lattice models and discrete networks&quot;, *Journal of the Mechanics and Physics of Solids*, v. 64, p. 154-169, 2014. [3] J. S. Amelang, G. N. Venturini, and D. M. Kochmann, &quot;Summation rules for a fully nonlocal energy-based quasicontinuum method,&quot; *J. Mech. Phys. Solids*, 2015.

## **An Adaptive Method to Verify the Lack of Collision Between Solid Bodies in a 2D Incompressible Viscous Flow**

Marco Picasso<sup>\*</sup>, Samuel Dubuis<sup>\*\*</sup>, Peter Wittwer<sup>\*\*\*</sup>

<sup>\*</sup>Institute of Mathematics, EPFL, Switzerland, <sup>\*\*</sup>Institute of Mathematics, EPFL, Switzerland, <sup>\*\*\*</sup>Department of Theoretical Physics, University of Geneva, Switzerland

### **ABSTRACT**

Our goal is to check numerically a Theorem of Hillairet (Communications in Partial Differential Equations 32(9) 2007) which states that a solid body falling in a constant-density incompressible viscous fluid cannot reach the bottom of the cavity in finite time. A penalty method is used to formulate the fluid flow problem in the whole cavity, thus avoiding the solid-liquid interface to be tracked explicitly. However, an adaptive method in space and time is advocated, the error indicators in space and time being derived on simplified problems. Space adaptivity requires the use of anisotropic finite elements. Numerical experiments indeed show that the solid body does not reach the bottom of the cavity in finite time.

## Strain Control via Level Set Topology Optimization: An Energy Harvesting Application

Renato Picelli<sup>\*</sup>, Carol Featherston<sup>\*\*</sup>, H. Alicia Kim<sup>\*\*\*</sup>, John McCrory<sup>\*\*\*\*</sup>, Scott Townsend<sup>\*\*\*\*\*</sup>,  
Stephen Grigg<sup>\*\*\*\*\*</sup>

<sup>\*</sup>Cardiff University, <sup>\*\*</sup>Cardiff University, <sup>\*\*\*</sup>Cardiff University / University of California, San Diego, <sup>\*\*\*\*</sup>Cardiff University, <sup>\*\*\*\*\*</sup>Cardiff University, <sup>\*\*\*\*\*</sup>Cardiff University

### ABSTRACT

Topology optimization has been previously applied to manipulation of displacements (compliant mechanisms) and failure (stress isolation), but not to strain control. This work formulates a level set topology optimization method to strain integral functions, thus facilitating the manipulation of strain in a specified region of a structure (sub-structure). A general shape sensitivity analysis is developed herein, with the sub-structure considered fixed and the external structure variable. Such a scenario finds use in the design of structural supports for strain-based sensors without a need to optimize the sensor material itself, e.g., piezoelectric skins. Numerical results demonstrate effective strain minimization/maximization for a range of directions. An application of the method to the design of a cantilever beam for use in vibrational energy harvesting is presented. The piezoelectric device is located in the sub-structure, with the surrounding beam shape designed to maximize the strain caused by ambient vibrations in a predefined frequency range. Experimental results show excellent agreement regarding location of natural frequencies and relative magnitude of harvested power.

## A Practical Finite Element Method to Include Osmotically Induced Prestretch\Prestress in Image-Driven Simulations of Cartilage

David M. Pierce<sup>\*</sup>, Xiaogang Wang<sup>\*\*</sup>, Thomas S.E. Eriksson<sup>\*\*\*</sup>, Tim Ricken<sup>\*\*\*\*</sup>

<sup>\*</sup>University of Connecticut, <sup>\*\*</sup>University of Connecticut, <sup>\*\*\*</sup>FOI – Swedish Defense Research Agency, <sup>\*\*\*\*</sup>Stuttgart University

### ABSTRACT

Medical imaging, e.g. MRI, is generally performed in vivo, hence finite element (FE) models constructed from medical images of cartilage represent geometries under Donnan osmotic loading even when the articulating joint is physically unloaded. Thus, an osmotically induced stretch/stress exists prior to constructing the geometry of the FE model, and we refer to it as prestretched/prestressed. When applying classical modeling approaches to patient-specific simulations of cartilage a theoretical inconsistency arises: the in-vivo imaged geometry (used to construct the model) is not an unloaded, stress-free reference configuration. Furthermore, cartilage specimens removed from the joint and placed into a physiological bathing solution, are commonly in this equilibrium state, and thus mechanical testing commonly occurs on prestretched/prestressed specimens. If one assumes that the resulting experimental data begin from a stress-free reference configuration when fitting nonlinear constitutive models that include osmotic swelling (to obtain material parameters) the fitted stress-strain relationship (parameters) obtained will actually describe a different behavior. The objectives of this study are two-fold: (1) to establish practical computational method to include osmotically induced prestretch in image-driven simulations of cartilage; and (2) to investigate (by apply the new methods) the influence of considering the prestretched/prestressed state when fitting fiber-reinforced, biphasic (swelling) constitutive models of cartilage. Towards objective (1) we extend our recent constitutive model for cartilage (Pierce et al., 2016, JMBBE 15:229-244) to include the mechanical effects of osmotic pressure, and determine the prestretched/prestressed state within the solid matrix induced by osmotic loading in the (imaged) initial configuration of the FE model using the backward displacement method (Bols et al., 2013, JCAM 246:10-17) prior to solving boundary value problems of interest. We compare results from simulations with/without including osmotic contributions. Towards objective (2) we fit our new constitutive model for cartilage with/without considering osmotic contributions and considering different initial configurations, and compare the resulting stress-stretch responses and parameters. Our results highlight the importance of determining the prestretched/prstressed state within the solid matrix induced by osmotic loading in the imaged configuration prior to solving boundary value problems of interest. With our new constitutive model and modeling methods, we hope to improve the fidelity of FE-based, patient-specific biomechanical simulations of joints and cartilage. Improved simulations can provide medical researchers with new information often unavailable in a clinical setting, information that may contribute to better insight into the pathophysiology of cartilage diseases. With our new fitting approach, we can also better fit available experimental data.

## The Comparison of Parametric and Non-Parametric Estimation of an Uncertainty for Parameters of a Modified Surface Layer

Jacek Pietraszek<sup>\*</sup>, Norber Radek<sup>\*\*</sup>, Renata Dwornicka<sup>\*\*\*</sup>

<sup>\*</sup>Cracow University of Technology, <sup>\*\*</sup>Kielce University of Technology, <sup>\*\*\*</sup>Cracow University of Technology

### ABSTRACT

The quantitative estimation of an uncertainty is one of the most important issues in the industrial statistics, especially in the design of experiment (DoE) being a source of specific experimental schemes for a quick and effective knowledge acquisition. The classic parametric approach based on the normal distribution is usually applied however it is only very rough approximation of data obtained from the real tests. Since Efron's papers [1, 2], the bootstrap approach is well recognized method for non-parametric estimation of distributions and their statistics including confidence intervals, especially for relatively small datasets where reliable selection of the particular family of distributions is not possible. Decade later, Owen proposed [3] another non-parametric approach based on Wilks's theorem, subsequently extended to the non-parametric maximum likelihood estimation method (NPMLE). The authors conducted the real experiment on a surface layer coated by a wear-resistant material (WC-Cu) and next modified by a laser beam impulse. The modified material is very important for a mechanical engineering and machining due to a longer life-time of parts, especially for friction pairs. The analyzed dataset contained many mechanical and geometrical properties of a such layer, hardness and friction among them. The comparison a classic parametric model and non-parametric approach was performed. The obtained non-parametric results were generally consistent with parametric however some significant differences were observed. The main advantage was the rejection of the arbitrary assumption on a distribution shape. The paper presents obtained results, their discussion, conclusions and guidelines for future works. References: 1. B. Efron: Bootstrap Methods: Another Look at the Jackknife. The Annals of Statistics 7, 1979, pp. 1–26. 2. B. Efron: Bootstrap confidence intervals for a class of parametric problems. Biometrika 72, 1985, pp. 45-58. 3. A.B. Owen: Nonparametric Likelihood Confidence Bands for a Distribution Function. Journal of the American Statistical Association 90, 1995, pp. 516-521.

## Prediction of Distribution of Microstructural Parameters in Steels Described by Differential Equations with Recrystallization Term: Two Possible Approaches.

Maciej Pietrzyk<sup>\*</sup>, Paweł Morkisz<sup>\*\*</sup>, Piotr Oprocha<sup>\*\*\*</sup>, Paweł Przybyłowicz<sup>\*\*\*\*</sup>, Danuta Szeliga<sup>\*\*\*\*\*</sup>, Jan Kusiak<sup>\*\*\*\*\*</sup>

<sup>\*</sup>AGH University of Science and Technology, <sup>\*\*</sup>AGH University of Science and Technology, <sup>\*\*\*</sup>AGH University of Science and Technology, <sup>\*\*\*\*</sup>AGH University of Science and Technology, <sup>\*\*\*\*\*</sup>AGH University of Science and Technology, <sup>\*\*\*\*\*</sup>AGH University of Science and Technology

### ABSTRACT

The high strength and elongation of DP (Dual Phase) steels are due to combination of soft ferrite with hard martensite. These steels, however, are characterised by large gradients of properties, which cause poor local formability. Contrary, steels with a more heterogeneous microstructure have superior formability. This leads to a question: is it possible to achieve more balanced properties of multiphase steels by tailoring microstructure gradients? More detailed models of the microstructure are required to answer this question. A hypothesis was made that application of the distribution functions of various internal variables will allow to predict gradients of final product properties. The objective of the paper was to investigate the possibility of multiscale modelling of microstructure evolution based on distribution functions. Thermomechanical FE code was used to describe the macro scale during hot forming. A differential equation describing evolution of dislocation populations was considered as the first approach in the micro scale. This equation is based on K-M model [1] with the dynamic recrystallization introduced in [2]. Numerical solutions of this equation assuming average dislocation density is frequent in the literature. The present work aims at description of evolution of dislocation populations by distribution function and choice of parameters which assure consistency with real process. From mathematical point of view, we look for accurate description of associated Frobenius-Perron operator, representing evolution of densities when considered system evolves in time (see [3]) following the macro scale results. Due to the recrystallization, the underlying differential equation has discontinuous righthand side. Two approaches were considered to deal with this problem. First is to regularize the vector field via sigmoid function and then to apply suitable numerical method for stiff equations. The second is to use Filippov's framework (e.g. see [4]) for discontinuous differential equations together with appropriate numerical scheme based on time stepping or event detection. These two strategies and their utility from material science point of view were compared. Prediction of distribution of microstructural parameters is the main output of the paper.

1. Mecking H., Kocks U.F., Acta Metallurgica, 29, 1981, 1865-1875.
2. Sandstrom R., Lagneborg R., Acta Metallurgica, 23, 1975, 387-398.
3. Lasota A., Mackey M. C., Chaos, fractals, and noise. Stochastic aspects of dynamics. Applied Mathematical Sciences, 97. Springer-Verlag, New York, 1994.
4. Filippov, A. F. Differential equations with discontinuous righthand sides. Mathematics and its Applications (Soviet Series), 18. Kluwer Academic Publishers Group, Dordrecht, 1988.

## **Stabilized Monolithic FEM for Cahn-Hilliard/Navier-Stokes Equations on Anisotropic Unstructured Meshes**

Franck Pigeonneau<sup>\*</sup>, Youssef Mesri<sup>\*\*</sup>, Rudy Valette<sup>\*\*\*</sup>, Elie Hachem<sup>\*\*\*\*</sup>

<sup>\*</sup>Mines-Paristech, CEMEF, <sup>\*\*</sup>Mines-Paristech, CEMEF, <sup>\*\*\*</sup>Mines-Paristech, CEMEF, <sup>\*\*\*\*</sup>Mines-Paristech, CEMEF

### **ABSTRACT**

Two-phase flows are involved in a large range of industrial processes for which the interfacial dynamics plays an important role on the overall behavior. It is particularly true in boiling devices for which the wetting properties on wall are crucial to determine the occurrence of the nucleation process. To investigate this kind of problems, phase-field or diffusive interface approach is chosen to describe the dynamics of two immiscible fluids. Four fields are involved: two for the phase-field (order parameter and chemical potential) and two for the fluid dynamics (pressure and velocity). To solve the Cahn-Hilliard equation which is a bi-harmonic non-linear equation, a coupled method is used to solve two second-order equations stabilized when advection is dominant. When the order parameter and the chemical potential are known, the Navier-Stokes equations are solved using a mixed-formulation stabilized with variational multiscale method. An anisotropic mesh adaptation is also implemented to capture accurately the interface dynamics. The numerical solver is applied to study the capillary rising in a tube, or the drop spreading on a substrate. A comparison with numerical results or with experimental data previously published is provided.

## Multiscale Modeling of Notched Composites under Compression with Improved Shear Toughening Through Nano-reinforcement

Evan Pineda<sup>\*</sup>, Gregory Odegard<sup>\*\*</sup>, Hashim Al Mahmud<sup>\*\*\*</sup>, Matthew S. Radue<sup>\*\*\*\*</sup>, Sorayot Chinkanjanarot<sup>\*\*\*\*\*</sup>, William Pisani<sup>\*\*\*\*\*</sup>

<sup>\*</sup>NASA Glenn Research Center, <sup>\*\*</sup>Michigan Technological University, <sup>\*\*\*</sup>Michigan Technological University, <sup>\*\*\*\*</sup>Michigan Technological University, <sup>\*\*\*\*\*</sup>Michigan Technological University, <sup>\*\*\*\*\*</sup>Michigan Technological University

### ABSTRACT

Nano-reinforcement can be utilized to improve the properties of traditional carbon fiber reinforced polymers (CFRPs). One critical design parameter for CFRP structures is the open hole compression (OHC) strength. As the specimen is compressed, initially misaligned fibers rotate, inducing shear stress in the matrix. The shear stress acts to degrade the stiffness of the matrix through micro-cracking which permits further rotation. The interaction between matrix damage and fiber rotation leads to an instability wherein the fibers buckle and a kink band is formed. Thus, OHC failure is a result of micro buckling of the fibers which is primarily governed by the shear toughness of the polymer matrix. As such, nano-particles can be utilized to improve the shear toughness of the matrix, and hence increase the OHC strength of the material system. In this work, graphene nano-platelets (GNPs) are mixed into the resin system to produce nano-reinforced composite panels. The CFRP/GNP materials exhibited an improved shear toughness as compared to the baseline CFRP system. Neat resin, CFRP, and CFRP/GNP experiments are used to characterize the multiscale progressive damage analysis (MPDA) models. The MPDA model includes five disparate length scales ranging from the nano-scale up to the laminate scale. Numerous analytical, semi-analytical and numerical are integrated into the MPDA framework to provide predictions of the OHC strength of CFRP and CFRP/GNP. Molecular dynamics (MD) is used predict the elastic properties of a representative volume element (RVE) of a GNP with epoxy at the nano-scale. The generalized method of cells (GMC) is used to bridge the nano and continuum scales by modeling a repeating unit cell of epoxy with the appropriate volume fraction of GNP. The nonlinear behavior of the matrix is modeled using the multi-axial mixed-mode continuum damage mechanics (MMCDM) model, and the MD simulations are used to provide the properties of the homogenized GNP-epoxy subcell. An analytical technique is used to average the non-linear response of the GNP-epoxy RUC over all possible physical orientations of GNP within the matrix. MMCDM is then used to capture the non-linear response of the homogenized GNP-epoxy matrix in an additional GMC model containing a carbon fiber and GNP-epoxy matrix. Finally, Schapery theory (ST) is used to predict shear micro-cracking in the matrix of OHC specimens. The MPDA predictions indicate that the addition of a very small percentage of GNP may lead to a substantial increase in the OHC strength of the composite.

## Computational Homogenization of Heterogeneous Materials in the Presence of Contact Interactions

Rodrigo Pinto Carvalho\*, Thiago Doca\*\*, Igor Rodrigues Lopes\*\*\*, Francisco Andrade Pires\*\*\*\*

\*Institute of Science and Innovation in Mechanical and Industrial Engineering, \*\*Department of Mechanical Engineering, Faculty of Technology, University of Brasilia, \*\*\*Institute of Science and Innovation in Mechanical and Industrial Engineering, \*\*\*\*Institute of Science and Innovation in Mechanical and Industrial Engineering

### ABSTRACT

In past decades, the need to accurately predict the constitutive behavior of complex materials by explicitly taking into account their properties at finer physical scales has gained considerable attention and, with the increasing advent of computing capacity, nowadays the field of Multi-Scale computational modeling has become a well-established discipline among the field of computational mechanics. In particular, the analysis of a microscopic Representative Volume Elements (RVE) to investigate the impact of microstructure properties on the homogenized macroscopic response has been extensively exploited within many different applications. The main purpose of the present contribution is to further extend the numerical modeling capacity at the micro-scale by incorporating contact mechanics within a finite deformation computational homogenization framework. Specifically, contact interactions are modeled by using the well-known dual Mortar method combined with a semi-smooth Newton method [1,2]. In order to evaluate the algorithm, the constitutive behavior of a two-phase composite with debonded inclusions is analyzed and the numerical results compared with existing analytical solutions [3]. References: [1] Hüeber, S., Stadler, G., & Wohlmuth, B. I. (2008). A primal-dual active set algorithm for three-dimensional contact problems with Coulomb friction. *SIAM Journal on Scientific Computing*, 30(2), 572-596. [2] Gitterle, M., Popp, A., Gee, M. W., & Wall, W. A. (2010). Finite deformation frictional mortar contact using a semi-smooth Newton method with consistent linearization. *International Journal for Numerical Methods in Engineering*, 84(5), 543-571. [3] Zhao, Y. H., & Weng, G. J. (1996). Plasticity of a two-phase composite with partially debonded inclusions. *International Journal of Plasticity*, 12(6), 781-804.

## Dynamics of Porous FG Curved Beams with Uncertain Parameters

Marcelo Piovan\*, Lucas Digiorgio\*\*

\*Universidad Tecnologica Nacional, FRBB, \*\*Universidad Tecnologica Nacional, FRBB

### ABSTRACT

This article deals with the stochastic dynamics of curved beams constructed with ceramic and metallic materials that vary in a given functional form. The construction process of this type of structures conducts to the presence of porosity in its domain. The porosity and a non-constant curvature radius may be source of uncertainties in the dynamic behavior. The beam model is deduced in the context of common variational principles, incorporating shear flexibility, variable curvature. It serves as a mean deterministic approach to the studies on stochastic dynamics and uncertainty quantification, which are the main objective of the present article. The uncertainty quantification procedure considers the employment of random variables to characterize the uncertainty in material or geometric properties such as elasticity moduli and/or density of the material constituents, curvature radius of the beam, porosity parameters, among others. The probability density functions of the random variables are derived appealing to the Maximum Entropy Principle. Then the probabilistic model is constructed with the basis of the deterministic model and both discretized with finite element approaches. Once the probabilistic model constructed, the Monte Carlo Method is employed to perform statistical realizations. Numerical studies are carried out to show the main advantages of the modeling schemes employed, as well as to quantify the propagation of the uncertainty in the dynamics of curved FG beams.

## **Comparison of Structural Properties of Bare-metal Stents versus Bioresorbable Stents**

Sogol Pirbastami\*, Darrell Pepper\*\*

\*University of Nevada, Las Vegas, \*\*NCACM, University of Nevada Las Vegas

### **ABSTRACT**

Stents are wire loop shaped devices placed in coronary artery to provide short term support to open the narrowed or obstructed coronary artery and repair the blood passage for flow. Over the last decade, numerous types of stents have been developed. The first generation of stents was bare-metal, which are still in use today. However, the main drawback is that they remain permanently inside the body and increase the risk of restenosis and in-stent thrombosis. Also, this type of stent cannot be used for pediatric patients due to the limitations associated with vessel growth. The next generation of stents was coated with drug-eluting material to decrease the thrombosis, but the stent would still remain in the vessel as a bare metal stent. The new generation of stents is bioresorbable, where the blood flow is restored and the arterial wall is remodeled, and gradually degrades and becomes reabsorbed by the body. Since the new generation of stents is in the early stage of development, additional studies are still required to provide information about their mechanical properties, material composition, design, and performance. In this study, a computational model is developed for both bare-metal and bioresorbable stents, and their mechanical properties examined with regards to shear stresses and deformations in straight and curved vessels. Inserting a stent in a tortuous coronary artery can produce high shear stresses at both ends of the stent, impacting the shape of the artery. Deformation in metal stents is less than in bioresorbable stents. Over the long term, the bioresorbable stent conforms to the shape of the curved artery and applies less stress to surrounding tissues. The metal stent can create a tear in the arterial wall, resulting in restenosis. In this study, the COMSOL Multiphysics finite element code is used to investigate the wall shear stresses and the deformations to the tissues and artery walls. Results indicate that the bioresorbable stent is more flexible and conforms more readily to the shape of an arterial wall, producing lower stress levels than bare-metal stents.

## Simulation of a Proposed FSI Validation Case

Jonathan Pitt\*

\*The Pennsylvania State University

### ABSTRACT

A new validation test case for low-frequency, large amplitude deformation Fluid-Structure Interaction (FSI) codes is proposed, and simulations of the experiment are presented. This validation case extends previous benchmarks in the literature, by providing high Reynolds number, turbulent, three-dimensional experimental and computational data for FSI algorithms and solution methods comparison. The proposed case consists of a flexible flag attached to a vertically mounted square rod immersed in fully developed pipe flow. This flow is created in the test section of Penn State's twelve-inch water tunnel loop facility. As the flow passes over the square rod, vortices are generated which subsequently excite the flag and cause it to oscillate. The deformation of the flag is the key metric used for experiment-simulation comparison, similar to the two-dimensional laminar computational benchmark of Turek and Hron [1]. A high-resolution simulation of the proposed experiment is performed using an FSI solver previously developed at Penn State [2]. This solver implements a partitioned, overset grid enabled ALE-based method for the solution of tightly coupled FSI problems. In particular, overset meshes are attached to the immersed deformable structure, and permitted to move independently of the static background mesh. The overset grid capability is the enabling technology to allow large deformation of body fitted meshes, required to capture the turbulent boundary phenomena, without the need to re-mesh or distort the grid beyond usability. This approach also allows for simplified meshing of complex geometries, and a reduced domain size for mesh motion calculations, providing for significant reductions in computational cost. Comparison of computational results to experimental measurements are presented. [1] S. Turek and J. Hron. "Proposal of Numerical Benchmarking of Fluid-Structure Interaction Between and Elastic Object and Laminar Incompressible Flow", Fluid-Structure Interaction, Vol. 53, pp. 371–385, 2006. [2] S. T. Miller, R. L. Campbell, C. W. Elsworth, J. S. Pitt, and D. A. Boger. "An Overset Grid Method for Fluid-Structure Interaction", World Journal of Mechanics, Vol. 4, No. 7, pp. 217–237, 2014.

## Yield Surfaces for Heterogeneous Materials Using a Multi-Scale Approach

José Julio de Cerqueira Pituba\*, Wanderson Ferreira Santos\*\*

\*Federal University of Goiás, \*\*Federal University of Goiás

### ABSTRACT

This work deals with numerical simulation of the mechanical behavior of materials composed of heterogeneous ductile microstructures using a multi-scale approach considering plasticity processes and phase debonding. Due to few studies about yield surfaces of metal matrix composites (MMC) with weak interfaces presented in the literature, the major goal of this work is to propose yield surfaces for metal matrix composites reinforced by rigid inclusions. All simulations in this section have been performed by employing the computational homogenization under the plane stress assumption in small strain regime. The average stress is obtained by imposing the macro-strain over the RVE and subsequently solving the microscopic initial boundary value problem for the defined boundary condition assumed [1]. The yield surfaces are obtained for Representative Volume Elements (RVEs) of materials presenting perfectly bonded inclusions and phase debonding in the interface zone. The matrix is considered an ideally plastic material governed by von Mises model, whereas the interface zone is modeled by means contact and fracture constitutive models incorporated in a proposed finite element [2]. Also, RVEs containing different distributions and volume ratios of voids are analyzed. Considering the phase debonding, for compressive loadings the RVE behaves like RVE with perfectly bonded inclusions whereas for tension loadings the RVE presents a behavior quite similar to the one with voids. On the other hand, the concentration of voids in the RVE decreases its mechanical strength. [1] Fernandes, G.R., Pituba J.J.C., Souza Neto, E.A. (2015b). FEM/BEM formulation for multi-scale analysis of stretched plate, *Engineering Analysis with Boundary Elements* 54: 47-59. [2] Pituba, J.J.C., Fernandes, G.R., Souza Neto, E.A. (2016). Modelling of cohesive fracture and plasticity processes in composite microstructures. *Journal of Engineering Mechanics* 142: 04016069.1-04016069.15.

## **Dissipative Particle Dynamics for Soft Matter Simulations**

Igor Pivkin\*

\*Institute of Computational Science, USI Lugano, Switzerland

### **ABSTRACT**

Particle-based methods have been extensively used to study many biophysical systems in recent years. Dissipative Particle Dynamics (DPD) is a Lagrangian method that was originally proposed as a coarse-grained version of Molecular Dynamics. The popularity of this method is due to several essential properties. First, DPD provides an accurate hydrodynamics due to mass and momentum conservation. It also allows to model complex interactions between particles representing fluid, solid walls and soft matter in a unified way by defining proper DPD interaction parameters. Finally, DPD is a scale-free method meaning that it can be used for modeling processes on different length scales, from nanometers to microns and above. In this talk, we will present DPD models for soft matter applications, including modeling of cells in complex flow domains.

## Multiscale Method with Patches for the Solution of Linear Parabolic Equations with Localized Uncertainties

Florent Pled<sup>\*</sup>, Anthony Nouy<sup>\*\*</sup>, Mathilde Chevreuril<sup>\*\*\*</sup>

<sup>\*</sup>Université Paris-Est, Laboratoire Modélisation et Simulation Multi Echelle, MSME UMR 8208 CNRS, <sup>\*\*</sup>Université de Nantes, Laboratoire de Mathématiques Jean Leray, UMR 6629 CNRS, <sup>\*\*\*</sup>Université de Nantes, Ecole Centrale Nantes, Institut de Recherche en Génie Civil et Mécanique, GeM UMR 6183 CNRS

### ABSTRACT

Uncertainty quantification in computational engineering is nowadays an essential step to perform the robust design of mechanical systems. Analyzing the propagation of localized uncertainties in computational models allows for robust predictions of the model response with respect to the input uncertainties. Such uncertainties may represent either natural variabilities in the material properties or epistemic variabilities due to a lack of knowledge in the geometry, the boundary or initial conditions. Traditional monoscale approaches based on local refinement or enrichment techniques can be relatively difficult to implement in the existing commercial softwares and computationally demanding for solving high-dimensional stochastic problems. Consequently, concurrent multiscale approaches based on substructuring, domain decomposition or multigrid methods have been proposed to tackle large-scale engineering applications and perform stochastic computations of multiscale problems. A multiscale method has been recently introduced in [1] for solving linear elliptic equations with localized uncertainties and extended to a wider class of semi-linear elliptic equations with localized uncertainties and non-linearities in [2]. It relies on a decomposition of the domain into several subdomains of interest (called patches) containing the sources of uncertainties and possible non-linearities, and a complementary subdomain. A global-local iterative algorithm is then introduced to compute the multiscale solution and calls for the solution of a sequence of linear global problems (with deterministic operators and uncertain right-hand sides) over a deterministic domain, and (non-)linear local problems (with uncertain operators and right-hand sides) over the patches. In this work, the method is extended to linear parabolic equations with localized uncertainties. The convergence of the iterative algorithm is analyzed. The proposed multiscale approach allows for considering independent computational models, adapted discretization spaces and solvers for both types of problems. The stochastic local problems are solved using sampling-based approaches along with adaptive sparse approximation methods [3] to efficiently compute sparse representations of high-dimensional stochastic local solutions with arbitrarily-high accuracy. The performances of the multiscale method are illustrated on a transient linear advection-diffusion-reaction stochastic problem with localized random material heterogeneities. [1] M. Chevreuril, A. Nouy, and E. Safatly. A multiscale method with patch for the solution of stochastic partial differential equations with localized uncertainties. *CMAME*, 255:255–274, 2013. [2] A. Nouy and F. Pled. A multiscale method for semi-linear elliptic equations with localized uncertainties and non-linearities. *ESAIM: M2AN*, submitted, 2017. [3] A. Chkifa, A. Cohen, R. DeVore, and C. Schwab. Sparse adaptive Taylor approximation algorithms for parametric and stochastic elliptic PDEs. *ESAIM: M2AN*, 47(1):253–280, 2013.

## Electronic Structure Calculations with Bezier-extraction-based Isogeometric Analysis

Jiri Plešek<sup>\*</sup>, Robert Cimrman<sup>\*\*</sup>, Matyáš Novák<sup>\*\*\*</sup>, Jiri Vackar<sup>\*\*\*\*</sup>, Miroslav Tuma<sup>\*\*\*\*\*</sup>, Radek Kolman<sup>\*\*\*\*\*</sup>

<sup>\*</sup>Institute of Thermomechanics, The Czech Academy of Sciences, <sup>\*\*</sup>New Technologies Research Centre, University of West Bohemia, <sup>\*\*\*</sup>New Technologies Research Centre, University of West Bohemia, <sup>\*\*\*\*</sup>Institute of Physics, The Czech Academy of Sciences, <sup>\*\*\*\*\*</sup>Institute of Computer Science, The Czech Academy of Sciences, <sup>\*\*\*\*\*</sup>Institute of Thermomechanics, The Czech Academy of Sciences

### ABSTRACT

We present an application of isogeometric analysis based on Bézier extraction in electronic structure calculations [1]. A computational strategy [2] for non-periodic electronic structures based on the density functional theory, environment-reflecting pseudopotentials and the isogeometric analysis with Bézier extraction has been developed and tested. The approach is especially suitable for calculating the total energy and its derivatives, particularly for evaluation of atomic forces based on the Hellmann-Feynman theorem. In the contribution, we present convergence properties of this numerical method in electronic structure calculations [3]. The results are compared with results obtained by the finite element method based on the Lagrangian shape functions. Acknowledgements to projects: CSF 17-12925S. MEYS CZ.02.1.01/0.0/0.0/15\_003/0000493 (Plešek, Kolman) under AV0Z20760514 and MEYS CZ.02.1.01/0.0/0.0/15\_0 03/0000358. REFERENCES [1] R.M. Martin, *Electronic Structure: Basic Theory and Practical Methods*, Cambridge University Press, (2005). [2] R. Cimrman, M. Novák, R. Kolman, M. Tuma and J. Vackar, Isogeometric analysis in electronic structure calculations, *Math. Comput. Simul.*, vol. 145, p. 125-135, 2018. doi: 10.1016/j.matcom.2016.05.011 [3] R. Cimrman, M. Novák, R. Kolman, M. Tuma, J. Plešek and J. Vackar, Convergence study of isogeometric analysis based on Bézier extraction in electronic structure calculations, *Applied Mathematics and Computation*, vol. 319, p. 138-152, 2018. <http://dx.doi.org/10.1016/j.amc.2017.02.023>

## Progress on an MPI+X Scalable, Multiscale GFEM for Large-scale Simulations

Julia Plews\*, Matthew Mosby\*\*

\*Sandia National Laboratories, \*\*Sandia National Laboratories

### ABSTRACT

This presentation will demonstrate recent progress toward a data-parallel generalized finite element method with global-local enrichment functions (GFEMgl) for large-scale, multiscale computational mechanics problems. The GFEMgl simultaneously resolves fine-scale (e.g., crack- or material-scale) and coarse-scale (e.g., component- or structural-scale) physics in interdependent local and global boundary value problems. Local solutions are inserted into the global basis as enrichment functions to achieve strong coupling of fine- and coarse-scale response without sacrificing fine-scale fidelity. The embarrassing parallelism of GFEMgl local problems has led to promising scalability on shared memory computers while maintaining good accuracy relative to direct simulation [1,3]. However, scalable algorithms for the next generation of manycore high-performance computing platforms must exploit a combination of distributed parallel communication and on-node thread, or MPI+X, parallelism. This talk will focus on a new MPI-parallel version of the GFEMgl with particular emphasis on strategies for task-parallelism similar to [2] and minimizing communication of fine-scale data across compute nodes. REFERENCES [1] D.-J. Kim, C. Duarte, and N. Sobh. Parallel simulations of three-dimensional cracks using the generalized finite element method. *Computational Mechanics*, 47(3):265–282, 2011. [2] M. Mosby and K. Matous?. Computational homogenization at extreme scales. *Extreme Mechanics Letters*, 6:68–74, 2016. [3] J. Plews and C. Duarte. Bridging multiple structural scales with a generalized finite element method. *International Journal for Numerical Methods in Engineering*, 102(3–4):180–201, 2015.

## **Preston-Tonks-Wallace (PTW) Model Parameterization of Gamma (FCC) - Cerium**

JeeYeon Plohr\*

\*Los Alamos National Laboratory

### **ABSTRACT**

Cerium (Ce) is an scientifically interesting material for which there are seven allotropies; it goes through phase transformation between alpha and gamma phases via localization/delocalization of f electron with a large volume collapse; the liquid phase has a larger volume than solid phase in low pressure regime (less than 3GPa), and it has a critical point at low pressure/temperature. As part of an effort to have a better material model parameters for Ce, we have fitted the Preston-Tonks-Wallace (PTW) viscoplasticity model [1]. In doing so, we have used a newly generalized thermoelasticity model that provides the analytic expressions of shear modulus and melt curve [2]. The experimental data needed were provided by Russian Federal Nuclear Center (RFNC) where the split Hopkins bar tests were performed for seven sets of strain rate and temperature regimes from which stress-strain data were extracted, and we have used them to find the best fitting PTW model parameters. However, due to the lack of large strain data, there remains a big uncertainty in selecting the parameters. [1] D. L. Preston, D. L. Tonks, and D. C. Wallace, Model of Plastic Deformation for Extreme Loading Conditions, J. Appl. Phys. 93 (2003), 211-220 [2] L. Burakovsky, J. N. Plohr, S. K. Sjue, and D. J. Luscher, Thermoelasticity Model for Cerium, in preparation.

## **A Micromorphic Computational Homogenization Framework for Heterogeneous Materials**

Leong Hien Poh\*

\*National University of Singapore

### **ABSTRACT**

The first-order computational homogenization approach is restricted to problems where the macro characteristic length scale is much larger than the underlying RVE. In this contribution, focusing on matrix-inclusion composites, a novel computational homogenization framework is proposed such that standard continuum models at the micro-scale translate onto the macro-scale to recover a micromorphic continuum. Departing from the conventional FE2 framework where a macroscopic strain tensor characterizes the average deformation within the RVE, our formulation introduces an additional macro kinematic field to characterize the average strain in the inclusions. The two macro kinematic fields, each characterizing a particular aspect of deformation within the RVE, thus provide critical information on the underlying rapid fluctuations. The net effect of these fluctuations, as well as the interactions between RVEs, are next incorporated naturally into the macroscopic virtual power statement through the Hill-Mandel condition to recover a micromorphic continuum at the macro-scale. The length scale parameter associated with the higher-order term characterizes the nonlocal interaction between neighbouring micro-mechanisms, which in turn provides a regularization effect and enables an accurate prediction of the size-effect. The excellent performance of the proposed homogenization approach is illustrated by benchmarking its predictions against reference DNS solutions. Considering a shear wave loading problem, it is shown that the homogenized micromorphic model adequately captures the material responses, even in the absence of a clear separation between the loading wavelength and the RVE size. Specific choices for the decomposition of kinematic fields, as well as the boundary conditions adopted, will also be elaborated.

## **Coupling MD with Phase Field Models: Atomistically Informed Free Energy Representation for Applications in Organic Electronics**

Balaji S Sarath Pokuri<sup>\*</sup>, Shi Li<sup>\*\*</sup>, Sean Ryno<sup>\*\*\*</sup>, Chad Risko<sup>\*\*\*\*</sup>, Baskar Ganapathysubramanian<sup>\*\*\*\*\*</sup>

<sup>\*</sup>Iowa State University, <sup>\*\*</sup>University of Kentucky, <sup>\*\*\*</sup>University of Kentucky, <sup>\*\*\*\*</sup>University of Kentucky, <sup>\*\*\*\*\*</sup>Iowa State University

### **ABSTRACT**

Phase field based simulation strategies have been shown to be quite useful in exploring process-structure relationships for solvent based fabrication of organic electronics. The free energy functional predominantly contains the specifications of the material system. Standard free energy functional representations are simplistic. However, with the increasing complexity of the molecular structure (conjugated, diverse side groups, anisotropic) of the materials that are currently being developed and utilized, standard Flory-Huggins type parametrization may be insufficient. This is further exacerbated by the need to accurately model multi component systems (consisting of donor, acceptor, solvent, solvent additives). In this work, we tackle this problem through an atomistically-driven construction of the free energy of representative material systems. The free energy construction is formally represented as a regression problem using a finite number of MD simulations. MD calculations of free energy are performed using the 2PT method with all-atom MD simulations. In order to minimize the number of MD simulations, we use a Bayesian optimization approach to intelligently sample the configuration space to spawn MD simulations. Under assumptions of smoothness of the free energy, we can provide rigorous bounds on the number of MD simulations required to construct the free energy functional (given an error threshold). We illustrate the framework through a few examples of increasing complexity.

## **Search for the Optimum Simple Computational Model of the Turbine Bladed Disk**

Pavel Polach\*

\*Research and Testing Institute Plzen

### **ABSTRACT**

Motivation for introducing this paper is the topical application of the method using the rotational periodicity of the structure at calculating natural vibration characteristics of the steam turbine bladed disk with continuous binding, in this case in the form of an integral shrouding and in the middle of the blade with the tie-boss connection. Part of the shroud and part of the tie-boss are the integral parts of the blade. Blades are free at non-rotating bladed disk. Blades of the advanced design are continuously coupled in the zone of the shroud and in the tie-boss zone by the blades untwist caused by the centrifugal forces acting at the turbine rotation. The method used for the calculation of natural frequencies and mode shapes rotational periodicity of the structure supposes that the finite periodic system (in this case of the bladed disk with the continuous binding) is composed of the definite number of identical parts – subsystems. The subsystem discretization (in this case using the finite element method) will be performed in such a way that it may be coupled to their left-side and right-side adjacent subsystems in identical number of points in identical degrees of freedom. Mathematically, this approach to the problem formulation leads to assembling and solving the matrix difference equations. This method does not enable to model real contact properties. The contact must be modeled by the flexible connection. Stiffness of the connection in the zones of adjoining blades contact was tuned at turbine operational speed (i.e. at 3000 rpm) in such a way that the values of calculated natural frequencies might come as near as possible to the values of the measured natural frequencies. Calculated value of the first natural frequency associated to mode shape with zero nodal diameter appears to be problematic. It differs from the measured natural frequency associated to mode shape with zero nodal diameter by 30 per cent. The paper deals with searching for the approach to the creation of the model of the steam turbine bladed disk with continuous binding that would improve the compliance of this natural frequency with the measured natural frequency.

## **Branched Covering Surfaces – New Shapes, New Materials and New Processes**

Konrad Polthier\*

\*FU Berlin

### **ABSTRACT**

The classic geometric view on smooth surfaces hardly fits to the complex and often multiscale physical surface shapes in nature and, nowadays, in industrial applications. In this talk we will introduce a new class of surface shapes derived from classic complex analysis. Multivalued functions and differential forms naturally lead to the concept of branched covering surfaces and more generally of branched covering manifolds in the spirit of Hermann Weyl's book "The Idea of a Riemann Surface " from 1913. We will illustrate and discretize basic concepts of branched (simplicial) covering surfaces starting from complex analysis and surface theory up to their recent appearance in geometry processing algorithms and artistic mathematical designs. Applications will touch discrete and differential based surface modeling, image and geometry retargeting, optimal surfaces, and novel weaved geometry representations with serious industrial applications.

## Acceleration in Molecular Dynamics Simulations Using Phase Space Sampling

Mauricio Ponga\*

\*University of British Columbia

### ABSTRACT

Molecular Dynamics (MD) simulations have proven to be a useful tool to understand many phenomena at the nanoscale. Although the capabilities of MD simulations for predicting properties of systems with great accuracy, many limitations still hamper widespread usage of this technique. One such limitation is the time scale that can be simulated. Since MD needs to resolve the phonon vibrations of atoms and molecules, the critical time for conditional stability -the maximum time step that can be taken in order to maintain stability in the system- in the simulations is a fraction of this frequency. This, in turn, gives a critical time step of the order of  $1 \text{ fs} = 10^{-15} \text{ sec}$ . The restriction in the timescale places several limitations in the total time that can be modeled with MD and, therefore, the loads and deformation are usually applied at exceedingly large rates that do not represent most of the everyday working condition of systems and components. In this work, we propose a new technique for sampling the free-energy and time acceleration of atomic systems. The new technique is based on the concept of macroscopic evolution of systems at finite temperature and acceleration of rare events by phase space sampling at accelerated rates. We show how the free energy of the system and the average atomic forces for a given temperature can be computed by making a separation of slow-fast variables of motion and subsequent phase average. Thus, the evolution of the free-energy at the desired temperature computed in terms of the macroscopic variables of the system can be sampled at a much higher rate with the aid of an artificial large temperature leading to an accelerated sampling technique. We use this idea to accelerate the dynamics of the system and the transition rate of rare events. Several validation cases are studied to show the acceleration of MD simulations in relevant problems of interest such as dislocation climb, vacancy diffusion, and vacancy cluster collapse in dislocation cores.

## A Mortar Finite Element Approach for Modeling Point, Line and Surface Contact

Alexander Popp\*, Philipp Farah\*\*, Wolfgang A. Wall\*\*\*

\*Bundeswehr University Munich, \*\*Technical University of Munich, \*\*\*Technical University of Munich

### ABSTRACT

In this contribution, a new approach for investigating finite deformation frictional contact problems with a special emphasis on non-smooth geometries such as sharp corners and edges is presented [1]. The contact conditions are separately enforced for point contact, line contact and surface contact by employing three different sets of Lagrange multipliers and, as far as possible, a variationally consistent discretization approach based on mortar finite element methods. The discrete Lagrange multiplier unknowns are eliminated from the system of equations by employing so-called dual or biorthogonal shape functions. For the combined algorithm, no transition parameters are required and the decision between point contact, line contact and surface contact is implicitly made by the variationally consistent framework, which has not been possible until now with any other mortar-based approach from the literature [2]. One core ingredient of the proposed formulation for non-smooth contact geometries is a suitable modification of the discrete Lagrange multiplier spaces for line contact and surface contact in the vicinity of non-smooth geometric entities such as vertices and edges, respectively. If, for example, a line contact element in 2D is connected to a vertex, the vertex node would carry both a discrete line Lagrange multiplier and a discrete point Lagrange multiplier. Thus, partition of unity would not be guaranteed anymore. In order to recover consistency, the line Lagrange multiplier shape functions have to be modified in the vicinity of the vertex node. It should be pointed out that such modifications are quite well-established in mortar finite element methods in the context of so-called crosspoints, which arise when multiple subdomains meet at one point [3]. Similar modifications of the Lagrange multiplier shape functions have also been devised for 3D surface contact. In addition, a novel static condensation procedure for dual (biorthogonal) mortar methods is presented that allows for removing all discrete Lagrange multiplier degrees of freedom from the global system of equations at negligible computational costs. [1] P. Farah, W. A. Wall, and A. Popp. A mortar finite element approach for point, line and surface contact. *International Journal for Numerical Methods in Engineering*, accepted for publication, 2017. [2] A. Popp, A. Seitz, M. W. Gee, and W. A. Wall. Improved robustness and consistency of 3D contact algorithms based on a dual mortar approach. *Computer Methods in Applied Mechanics and Engineering*, 264:67-80, 2013. [3] B. I. Wohlmuth. Variationally consistent discretization schemes and numerical algorithms for contact problems. *Acta Numerica*, 20:569-734, 2011.

## Orthogonality Constrained Gradient Reconstruction for the Super-convergent Computation of Stress Intensity Factors

Roberto Porcù<sup>\*</sup>, Maurizio M. Chiaramonte<sup>\*\*</sup>

<sup>\*</sup>Princeton University, <sup>\*\*</sup>Princeton University

### ABSTRACT

The accurate prediction of crack propagation requires the careful computation of the Stress Intensity Factors (SIFs) to determine whether the crack propagates, as well as its direction of propagation. The Stress Intensity Factors are a measure of the stress divergence near the crack tip and can be computed through the evaluation of linear and continuous functionals, termed Interaction Integrals functionals [1]. The argument of the latter is the gradient of the displacement field of the deforming elastic solid, a quantity that is often approximated using finite element methods. As the error in the computation of the SIF is bound by the error in the approximation of the displacement gradient, we propose a novel gradient reconstruction technique to enhance the accuracy of the computed SIFs. The salient feature of the proposed approach is that, by recognizing that the convergence properties of linear and continuous functionals are strongly tied to a Galerkin-orthogonality-like condition of its argument, we perform an orthogonality constrained gradient reconstruction. We will showcase that the proposed approach for gradient recovery preserves the super-convergent property of the reconstructed gradient and further, unlike previous methods, it enhances the convergence of linear functionals of the reconstructed gradient. We will combine this novel technique with Mapped Finite Element Methods [2], a finite element method for the optimal approximation of problems on cracked domains, to compute super-convergent SIFs. We will showcase that, by combining the aforementioned technologies, the SIFs can be computed to arbitrary orders of accuracy without any considerable computational overburden. References [1] M. M. Chiaramonte, Y. Shen, L. M. Keer, and A. J. Lew. Computing stress intensity factors for curvilinear cracks. *Int. Journal For Numerical Methods in Engineering*, Submitted, 2015. [2] Maurizio M. Chiaramonte, Yongxing Shen, and Adrian J. Lew. Mapped finite element methods: High-order approximations of problems on domains with cracks and corners. *International Journal for Numerical Methods in Engineering*, 2017.

# IDENTIFICATION OF POROUS STRUCTURE PARAMETERS USING AN ARTIFICIAL IMMUNE SYSTEM

ARKADIUSZ POTERALSKI\* AND JACEK PTASZNY†

Institute of Computational Mechanics and Engineering  
Silesian University of Technology  
Konarskiego 18A, 44-100 Gliwice, Poland

\*arkadiusz.poteralski@polsl.pl, †jacek.ptaszny@polsl.pl  
www.icme.polsl.pl

**Key words:** Porous Structure, Identification, Artificial Immune System, Computational Homogenization, Linear Elasticity.

## 1 INTRODUCTION

Optimization and identification by using artificial immune systems (AIS) are interesting and give good results methods in comparison to other global optimization algorithms. Intensive research on the development of such algorithms in application to optimization and identification problems has been carried out in recent years [1]. The paper presents an application of the fast multipole boundary element method (FMBEM) coupled with artificial immune system (AIS) to the identification of a porous structure. Shape and orientation of ellipsoidal voids in a porous material are identified. 3D representative volume elements (RVE) of linear elastic porous materials are modelled by the FMBEM, that requires only the discretization of the boundary. The RVE contains uniformly distributed identical cavities. For this RVE effective elastic constants are calculated. This paper is organized as follows. In Section 2, the AIS is briefly reviewed. In Section 3, the numerical example of identification of a porous structure is presented. Finally, concluding remarks are given in Section 4.

## 2 ARTIFICIAL IMMUNE SYSTEM

The artificial immune systems (AIS) are developed on the basis of a mechanism discovered in biological immune systems. An immune system is a complex system which contains distributed groups of specialized cells and organs. The main purpose of the immune system is to recognize and destroy pathogens - fungi, viruses, bacteria and improper functioning cells. The lymphocytes cells which play a very important role in the immune system are divided into several groups of cells (two main groups are: B and T cells). The B cells contain antibodies, which could neutralize pathogens and are also used to recognize pathogens. The B cells are produced in the bone marrow in long bones. The B cells undergoes a mutation process to achieve big diversity of antibodies. The T cells mature in thymus and only T cells

recognizing non self cells are released to the lymphatic and the blood systems. There are also other cells like macrophages with presenting properties, the pathogens are processed by a cell and presented by using MHC (Major Histocompatibility Complex) proteins.

The recognition of a pathogen is performed in a few steps. In the first stage, the B cells or macrophages present the pathogen to a T cell using MHC the T cell decides if the presented antigen is a pathogen. The T cell gives a chemical signal to B cells to release antibodies (figure 1).

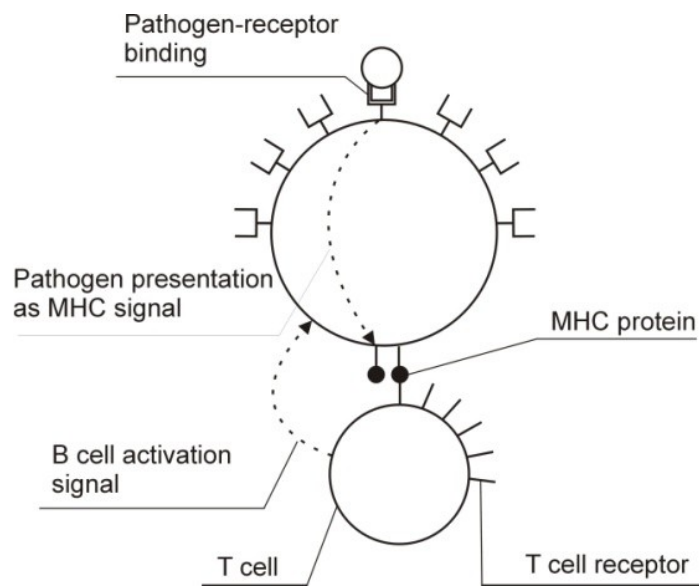


Figure 1. The recognition of a pathogen

A part of stimulated B cells goes to a lymph node and proliferate (clone). A part of the B cells changes into memory cells, the rest of them secrete antibodies into blood (figure 2a). The secondary response of the immunology system in the presence of known pathogens is faster because of memory cells. The memory cells created during primary response, proliferate and the antibodies are secreted to blood (figure 2b). The antibodies bind to pathogens and neutralize them. Other cells like macrophages destroy pathogens. The number of lymphocytes in the organism changes, while the presence of pathogens increases, but after attacks a part of the lymphocytes is removed from the organism.

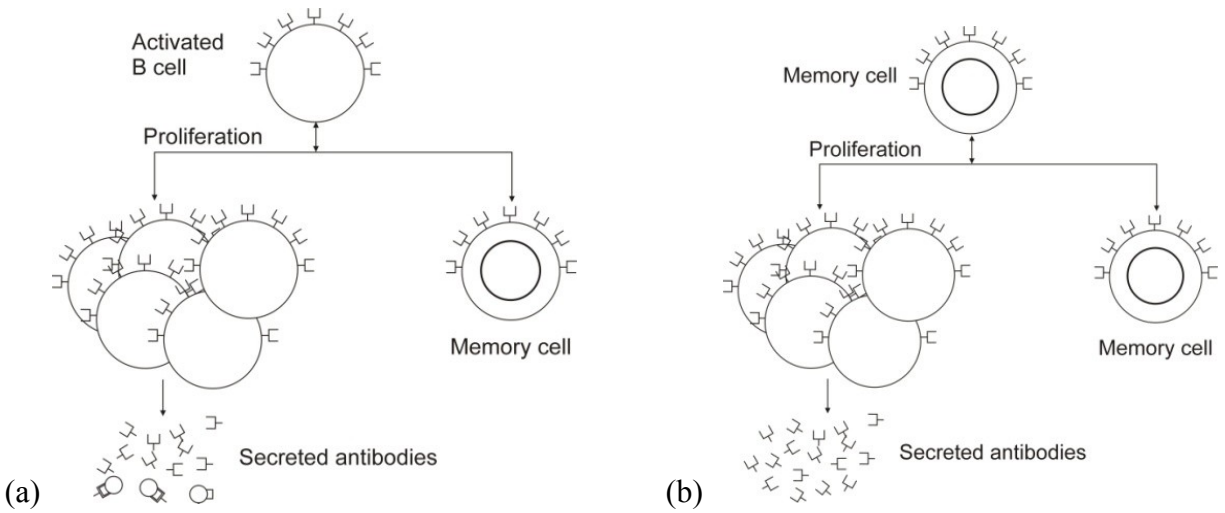


Figure 2. The proliferation of the a) B cells and b) memory cells

The artificial immune systems [2,3] take only a few elements from the biological immune systems. The most frequently used are the mutation of the B cells, proliferation, memory cells, and recognition by using the B and T cells. The artificial immune systems have been used to many optimization or identification problems [4] where the unknown global optimum is the searched pathogen. The memory cells contain design variables and proliferate during the optimization process. The B cells undergo mutation are created from memory cells. The B cells evaluate and better ones exchange memory cells. In this version of artificial immune system the crowding mechanism is used. Using this operator the diverse between memory cells is forced. A new memory cell is randomly created and substitutes the old one, if two memory cells have similar design variables. The crowding mechanism allows finding not only the global optimum but also other local ones.

The figure 3 presents the flowchart of an artificial immune system. In the first stage of AIS the memory cells are created randomly. In the next stage the memory cell are proliferated and mutated creating new B cells. The number of clones created by each memory cell is determined by the memory cells objective function value (the objective function for each B cell is evaluated). The selection process exchanges some memory cells for better B cells. The selection is performed on the basis of the geometrical distance between each memory cell and B cells (measured by using design variables). The crowding mechanism removes similar memory cells. The similarity is also determined as the geometrical distance between memory cells. The process is iteratively repeated until the stop condition is fulfilled. The stop condition can be expressed as the maximum number of iterations.

The optimization process using artificial immune system is controlled by several parameters [5,6]:

- the number of memory cells,
- the number of clones,
- the probability of occurrence of a crowding mechanism (crowding factor) ,
- the probability of Gaussian mutation

The settings of individual parameters of the artificial immune system affect the efficiency of the optimization process. Therefore, it is important to properly select the parameters of AIS. In general, the settings of these parameters is dependent from the scientist's experience. For each new problem we have to search the new and the best parameters of AIS.

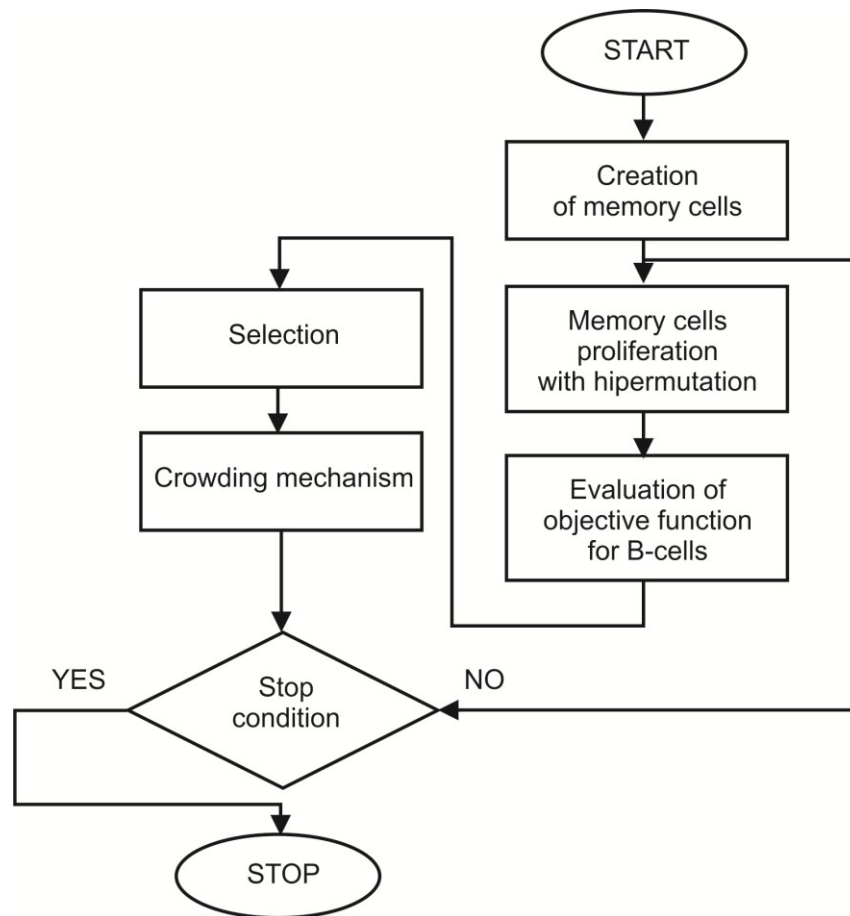


Figure 3. An artificial immune system

### 3 NUMERICAL EXAMPLE

Shape and orientation of ellipsoidal voids in a porous material are identified. A representative volume element (RVE) is modeled and effective elastic constants are calculated. The RVE contains uniformly distributed identical cavities. The shape and orientation of single cavity is defined by five parameters that are identified, namely  $a$ ,  $b$ ,  $\alpha$ ,  $\beta$  and  $\gamma$ . First two parameters describe the shape of single cavity and refer to ellipsoid radii in  $x_1$  and  $x_2$  directions. The parameters are defined as:

$$a = \frac{2a'}{A} \cdot 100\%, \quad b = \frac{2b'}{A} \cdot 100\%, \quad (1)$$

where  $a'$  and  $b'$  are absolute values of the ellipsoid radii, and  $A$  is the dimension of a cubic region containing single cavity. The third radius,  $c'$ , that is shown in Figure 4a, is dependent on  $a'$  and  $b'$ , and is calculated to preserve constant porosity value of 10%. The three other parameters indicate the Euler angles that define the orientation of a single cavity in the  $x_3$ - $x_1$ - $x_2$  convention. In this convention, the void is rotated by the angles  $\alpha$ ,  $\beta$  and  $\gamma$  respectively. As a result of the rotation, the ellipsoid symmetry axes, that are initially the  $x_i$  axes (figure 4a), become  $x'''_i$  ( $i = 1, 2, 3$ ) as shown in figure 4b. The description of identified parameters with bounds for box constraints is summarized in table 1.

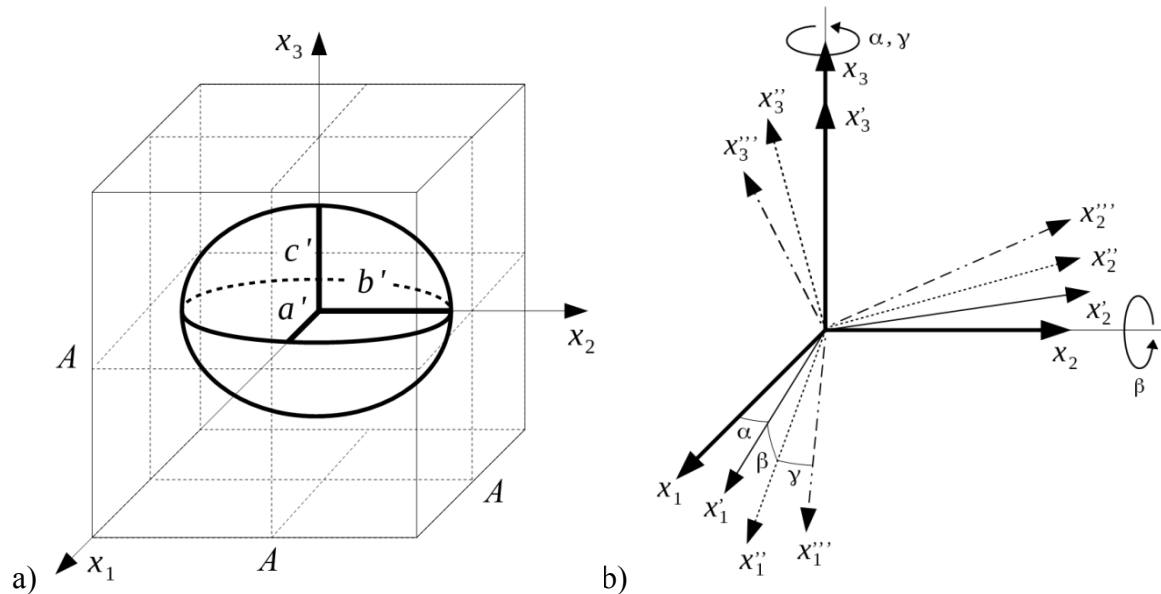


Figure 4. Parameters of single spheroidal cavity: a) initial orientation of the symmetry axes  $x_i$ , b) orientation of the rotated cavity symmetry axes  $x'''_i$

Table 1. Description of the void parameters

Parameter	Meaning	Unit	Lower bound	Upper bound
$g_1$	$a$	%	45	90
$g_2$	$b$	%	45	90
$g_3$	$\alpha$	deg	0	90
$g_4$	$\beta$	deg	0	45
$g_5$	$\gamma$	deg	0	90

The analysed RVE contains  $4 \times 4 \times 4$  (64) cavities. On the external boundary, displacement boundary conditions are applied to evaluate the matrix of effective elastic constants of the porous material  $\mathbf{C}$  [7]. The external boundary is a cube with side length equal of  $4 \times A = 1$  mm. The properties of the solid linear elastic material are Young's modulus  $E = 200$  GPa and Poisson's ratio  $\nu = 0.3$ . The RVE is modelled by the fast multipole boundary element method with 8-node Serendipity boundary elements [8, 9]. In this method, only the boundaries are discretized. For the generation of cavities, a boundary element mesh for single cavity is scaled, rotated, translated and duplicated. The number of degrees of freedom (DOF) of the model is 69 510. Probably, the number of DOF for corresponding finite element model would be by order of magnitude higher [10].

In the identification problem, the following cost function is minimized:

$$f(\mathbf{g}) = \frac{\|\log \mathbf{C}(\mathbf{g}) - \log \mathbf{C}^{\text{tet}}(\mathbf{g}^0)\|}{\|\log \mathbf{C}(\mathbf{g}^0) - \log \mathbf{C}^{\text{tet}}(\mathbf{g}^0)\|}, \quad (2)$$

where  $\mathbf{C}(\mathbf{g})$  is the matrix of the material with pores described by the vector  $\mathbf{g} = [g_1, g_2, g_3, g_4, g_5]^T$ .  $\mathbf{g}^0$  is a reference vector that describes the identified pore geometry. It is equal to  $\mathbf{g}^0 = [46, 46, 0, 0, 0]^T$ . Because  $\mathbf{C}(\mathbf{g}^0)$  is a numerical solution of a boundary value problem in the micro scale, it is not ideally symmetric. By taking into account the pore shape and orientation, it is assumed that the elastic matrix exhibits the tetragonal symmetry. Thus, the matrix  $\mathbf{C}^{\text{tet}}(\mathbf{g}^0)$  is introduced that is the Euclidean projection of the matrix  $\mathbf{C}(\mathbf{g}^0)$  onto this type of symmetry. The cost function (2) involves the log-Euclidean norm that possesses the property that it is invariant under inversion. The norm was applied in [11] to the problem of finding the closest elasticity tensor to a tensor obtained from experiments. The form of function (2) allows one to evaluate the relative distance between the current elastic matrix of  $\mathbf{g}$  and the idealized (symmetrized) matrix of  $\mathbf{g}^0$ , with respect to the distance between the matrix of  $\mathbf{g}^0$  and its symmetric projection. The function takes its minimal value  $\min[f(\mathbf{g})] = 1$  for  $\mathbf{g} = \mathbf{g}^0$ . Typical structures with corresponding cost function values are shown in figures 5a and 5b. The reference structure is shown in figure 6a.

The identification problem is solved by using the AIS described in Section 2. Parameters of the method are given in table 2. The stop criterion was set as 10 iterations. 10 test were performed and their results are listed in table 3. The identified structure is shown in figure 6b. It is shown, that the identified parameters are close to the reference structure, although the found values of  $\alpha$  and  $\gamma$  are not equal to zero. It is caused by the fact, that for the considered structure, any change of these angles does not influence the void shape if  $\beta = 0$ . For the best identified solution  $\mathbf{g}^*$ , denoted by  $\mathbf{5}^*$  in table 3,  $g_4(\beta)$  is less than one degree.

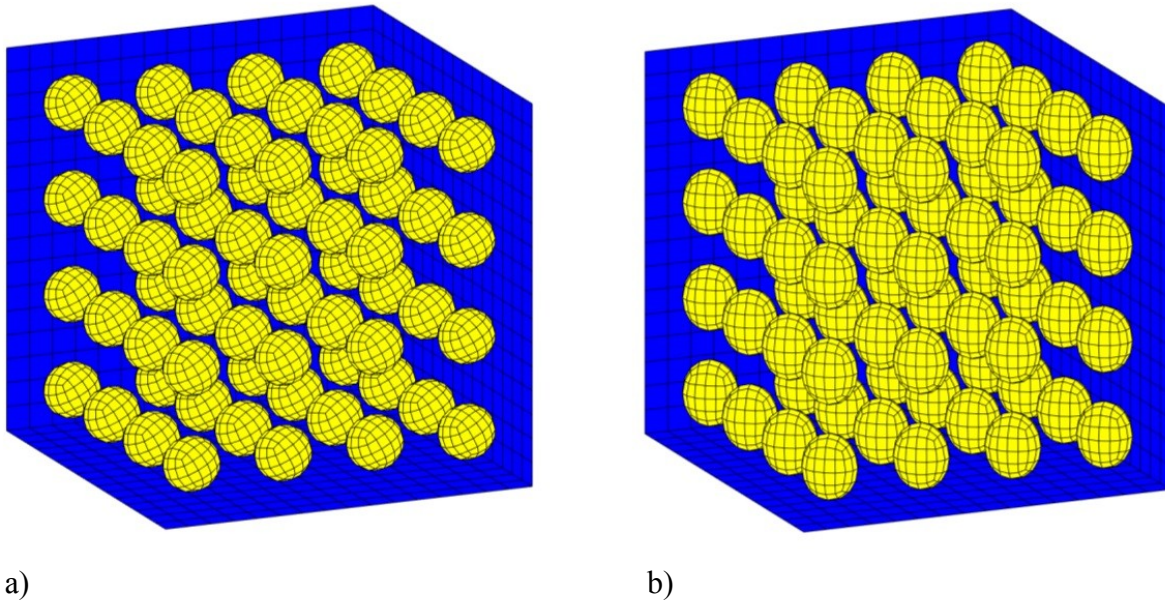


Figure 5. Typical RVEs with 64 voids corresponding to:

a)  $\mathbf{g}=[59.8, 56.7, 27.1, 26.9, 77.3]^T, f(\mathbf{g}) = 150.4$

b)  $\mathbf{g}=[57.8, 47.1, 15.8, 0.1, 36.7]^T, f(\mathbf{g}) = 91.3$

Table 2. AIS parameters

No. of design variables	No. of memory cells	No. of clones	Crowding factor	Gaussian mutation
5	8	5	0.5	0.5

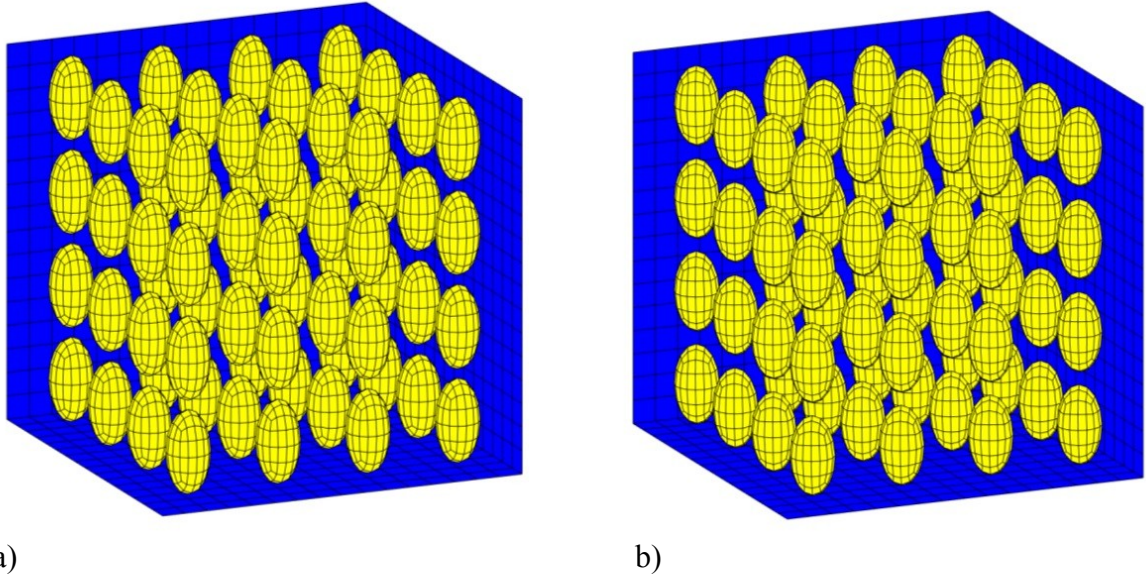


Figure 6. RVEs corresponding to: a) reference  $\mathbf{g}^0 = [46, 46, 0, 0, 0]^T$ ,  $f(\mathbf{g}^0) = 1$ ,  
 b) identified  $\mathbf{g}^* = [46.7, 47.4, 26.8, 0.7, 36.7]^T$ ,  $f(\mathbf{g}^*) = 14.6$

Table 3. Identification results

Test no.	$g_1$	$g_2$	$g_3$	$g_4$	$g_5$	$f(\mathbf{g})$
1	53.7	49.7	78.7	1.4	47.0	73.1
2	51.0	50.7	45.0	7.6	48.0	72.6
3	50.4	51.7	61.9	15.1	55.6	84.3
4	47.2	49.4	77.4	2.7	89.0	33.6
<b>5*</b>	<b>46.7</b>	<b>47.4</b>	<b>26.8</b>	<b>0.7</b>	<b>36.7</b>	<b>14.6</b>
6	48.2	48.3	90	4.8	22.8	33.0
7	50.2	49.8	62.0	14.4	22.9	69.3
8	47.2	46.9	85.0	5.7	68.8	24.9
9	56.3	52.4	63.5	11.5	29.8	108.6
10	57.3	48.5	30.8	3.8	74.3	92.8

## 4 CONCLUSIONS

- An AIS was applied to the identification of ellipsoid pore geometry (shape and orientation) in a porous material with periodic microstructure, on the basis of its overall elastic matrix. The cost function involved the log-Euclidean metric for the measurement of the distance between the current solution and the referenced (searched) structure. To the computational homogenization, the FMBEM was applied.
- The FMBEM allowed us to only discretize the boundary and made the model preparation easy in comparison to the usually applied FEM [4]. The log-Euclidean norm involved in the cost function allowed for identification of both dimensions and orientation of the ellipsoidal cavities.
- The preliminary results show that the proposed approach can be applied to the optimization of material microstructure of other porous materials, composites, etc. This can be achieved by the minimization of the elastic distance between an optimized structure and a desired tensor of effective elastic constants. The desired tensor can be characterized e.g. by maximized moduli, specific ratio of moduli, etc.
- Efficiency of the proposed method can be improved by distributing computations or using hybrid global optimization algorithm, like hybrid artificial immune system [12].

## ACKNOWLEDGEMENTS

The scientific research was funded by National Science Centre, Poland, grant no. 2015/19/B/ST8/02629.

## REFERENCES

- [1] de Castro L.N. and Von Zuben F.J.: Learning and optimization using the clonal selection principle, IEEE Transactions on Evolutionary Computation, Special Issue on Artificial Immune Systems (2002) 6,3:239-251.
- [2] Wierzchoń S.T. Sztuczne systemy immunologiczne. Teoria i zastosowania (Artificial Immune Systems. Theory and Applications). EXIT, Warszawa (2001) (in polish).
- [3] Ptak M. and Ptak W. Basics of Immunology. Jagiellonian University Press, Cracow, (2000).

- [4] Poteralski A., Szczepanik M., Beluch W. and Burczyński T. Optimization of composite structures using bio-inspired methods. *Artificial intelligence and soft computing*. ICAISC (2014) 8468:385-395.
- [5] Poteralski A. Optimization of mechanical structures using artificial immune algorithm. *Beyond Databases, Architectures, and Structures*. *Communications in Computer and Information Science* (2014) 424:280-289.
- [6] Poteralski A. Data processing in immune optimization of the structure. *Beyond Databases, Architectures, and Structures (BDAS)*. *Communications in Computer and Information Science* (2015)521:309-319.
- [7] Zohdi, T.I. and Wriggers, P. *An Introduction to Computational Micromechanics*. Springer (2008).
- [8] Ptaszny, J. Accuracy of the fast multipole boundary element method with quadratic elements in the analysis of 3D porous structures. *Comput. Mech.* (2015) 56: 477–490.
- [9] Ptaszny, J. Parallel fast multipole boundary element method applied to computational homogenization. *AIP Conference Proceedings* (2018) 1922: 140003. DOI 10.1063/1.5019145.
- [10] Ptaszny, J., and Hatlas, M. Evaluation of the FMBEM efficiency in the analysis of porous structures, *Eng. Computation*. (2018) 35: 843-866.
- [11] Moakher, M. and Norris, A.N. The closest elastic tensor of arbitrary symmetry to an elasticity tensor of lower symmetry, *J. Elasticity* (2006) 85: 215–263.
- [12] Poteralski A. Hybrid artificial immune strategy in identification and optimization of mechanical systems. *Journal of Computational Science* (2017) 23:216–225.

## Property Prediction and Damage Modeling in Ultra High Temperature Ceramics Using the Material Point Method

Stefan Povolny<sup>\*</sup>, Gary Seidel<sup>\*\*</sup>, Carolina Tallon Galdeano<sup>\*\*\*</sup>

<sup>\*</sup>Virginia Tech, <sup>\*\*</sup>Virginia Tech, <sup>\*\*\*</sup>Virginia Tech

### ABSTRACT

Ultra high temperature ceramics (UHTCs) show promise for use in material systems operating in extreme environments, such as leading edges on hypersonic aerospace vehicles. Enabling the design of such systems necessitates developing an understanding of UHTC properties and behavior. Experimental characterization is an option, but can be difficult and expensive when emulating hypersonic operating conditions where temperatures regularly exceed 2000 °C. This motivates a need for computational UHTC characterization, which is the main subject of this manuscript. The specific material system being characterized was produced with a manufacturing technique intended to introduce multiscale porosity. It is desired to predict effective material properties (such as elastic modulus and thermal conductivity) along with material behavior (such as damage initiation and propagation) as a function of porous microstructure variations, and to correlate computational results with experimental ones. Various physical phenomena are anticipated to be relevant in this problem. Examples include damage initiation and propagation during compressive loading, large deformations and rotations due to buckling of slender microstructure features, and extensive self-contact. In lieu of the finite element method (FEM), which is the typical choice for property prediction of solids, the material point method (MPM) is proposed as an appropriate tool to capture the aforementioned phenomena and thus adequately model the behavior of the highly porous material. The MPM discretizes a body using particles and incrementally updates their states by interpolating to a background grid to solve relevant equations of motion. The resulting hybrid Eulerian-Lagrangian nature of the method is often touted as its primary advantage, as it allows it to capture large deformation behavior without needing to worry about mesh degradation. Furthermore, the single-valued nature of the particles' velocity/displacement fields in the original MPM allows for automatic treatment of non-slip contact. Although the non-slip aspect is non-physical, having some contact treatment provides a starting point to explore UHTC behavior under high compressive loads. In this work, an MPM and continuum damage approach will be applied towards the modelling of large scale compression and fracture of porous ceramic microstructures in order to obtain effective mechanical properties. In addition, MPM will be used to capture changes in the effective thermal properties at various levels of damage. Future work will take advantage of more sophisticated kernel-based and multi-field treatments for contact and fracture that already exist in the literature.

## XFEM/AMR Coupling for Efficient Crack Patterns Analyzes

Benoit Prabel\*, Clémentine Jacquemoud\*\*

\*Den-Service d'études mécaniques et thermiques (SEMT), CEA, Université Paris-Saclay, F-91191, Gif-sur-Yvette, France, \*\*Den-Service d'études mécaniques et thermiques (SEMT), CEA, Université Paris-Saclay, F-91191, Gif-sur-Yvette, France

### ABSTRACT

In some situations, multiple cracks may exist and interact in structures. Taking them into account in a “traditional” finite element analysis may be cumbersome as a fine and conforming mesh representing the crack pattern is needed. When the crack pattern is a parameter of the simulation (in term of number of cracks, size and location), the engineer has to build complex procedures that are generally not generic to the whole range of possible situations. Hence, it is proposed in this paper to develop a methodology combining XFEM (eXtended Finite Element Method) and AMR (Adaptative Mesh Refinement) for the study of stationary interacting cracks in 2 or 3 dimensions, in both linear and nonlinear fracture mechanics context. The declination of this approach implemented in Cast3M to the implicit/explicit crack description and to the enrichment strategy is deeply explained. Also integration technique compatible with crack propagation in history-dependent material is adopted. In the present paper only two main examples are considered to point out the benefit of the method. First the 2D case of a periodic crack pattern with a parametric description of its size and tilt angle is presented. The numerical results obtained feed a cohesive model for combined mode I+III crack propagation [1]. The proposed procedure is demonstrated to be more efficient than standard finite element analysis : time spent by engineer for the numerical model definition is far lower and the computation is possible for a wider range of parameter. Refining the mesh locally enables to maintain the computational time reasonable for a very good accuracy. Then the 3D case of multiple cracks in a nonlinear material will be discussed. This example is representative of the mechanical analysis undertaken to assess potential interaction between quasi-laminar or tilted cracks. In particular XFEM/AMR coupling is shown to be directly applicable to 3D non-linear case for complex crack geometry, saving time and effort of discretization, and thus allowing the modelling of numerous cracks configurations. Numerical results are directly validated by associated experiments. Extension to crack propagation is an undergoing work discussed in [2]. [1] Leblond, J. B., Lazarus, V., & Karma, A. (2015). Multiscale cohesive zone model for propagation of segmented crack fronts in mode I+ III fracture. *International Journal of Fracture*, 191(1-2), 167-189. [2] Gibert, G., Prabel, B., & Jacquemoud, C. (2018). XFEM/AMR coupling for crack propagation in inelastic media. 13th World Congress on Computational Mechanics (WCCM).

## Virtual Element Modeling of the Perfusion of the Lamina Cribrosa

Daniele Prada<sup>\*</sup>, Silvia Bertoluzza<sup>\*\*</sup>

<sup>\*</sup>Istituto di Matematica Applicata e Tecnologie Informatiche "Enrico Magenes", <sup>\*\*</sup>Istituto di Matematica Applicata e Tecnologie Informatiche "Enrico Magenes"

### ABSTRACT

In this study, we theoretically investigate blood perfusion of the lamina cribrosa, a collagen structure located in the optic nerve head that plays a critical role in ocular pathologies, especially glaucomatous optic neuropathy [1]. The lamina is modeled as a porous material where capillaries are viewed as isotropically distributed pores in a solid matrix comprising collagen, elastin, extracellular matrix and neural tissue. The permeability tensor of the lamina is isotropic and homogeneous with a scalar value that is estimated according to the volume averaging method. We test this method on a morphologically-based micro structural model of the lamina using the Virtual Element Method (VEM) for the solution of the averaging closure problems. After estimating the permeability, blood pressure and perfusion velocities are approximated by a mixed virtual element space [2]. In view of coupling this three dimensional model with a zero dimensional model accounting for systemic factors that influence the local perfusion, a boundary condition of integral type is used [3]. Simulated distributions of blood pressure and perfusion velocity within the lamina are quantitatively close to realistic data. These results, together with the high flexibility that VEM allows in the treatment of complex geometries, suggest that VEM is a promising candidate for modeling the perfusion of the lamina cribrosa. [1] D. Prada, A. Harris, G. Guidoboni, B. Siesky, A. M. Huang, J. Arciero, Autoregulation and neurovascular coupling in the optic nerve head. *Surv Ophthalmol*, Vol. 61:2, pp. 164-186, 2016. [2] L. Beirao da Veiga, F. Brezzi, L. D. Marini, A. Russo,  $H(\text{div})$  and  $H(\text{curl})$  conforming virtual element methods. *Numer Math*, Vol. 133, 303-332, 2016. [3] S. Bertoluzza, G. Guidoboni, R. Hild, D. Prada, C. Prud'homme, R. Sacco, L. Sala, M. Szopos, An implementation of HDG methods with Feel++ and application to problems with integral boundary conditions. Manuscript in preparation, 2017.

## Interface Thickness Effect on Impact Induced Failure in Energetic Material using Cohesive Finite Element Method

Chandra Prakash<sup>\*</sup>, Emre Gunduz<sup>\*\*</sup>, Vikas Tomar<sup>\*\*\*</sup>

<sup>\*</sup>Purdue University, <sup>\*\*</sup>Purdue University, <sup>\*\*\*</sup>Purdue University

### ABSTRACT

Energetic materials are susceptible to unwanted detonation due to the hot-spot formation, which may be triggered by defects occurred due to impact or shock. One of the main factors that can contribute to this type of defect is the failure initiated at the interfaces. Examples include failure at interfaces such as those between Hydroxyl-terminated polybutadiene (HTPB)-Ammonium Perchlorate (AP) in an example energetic material. In order to analyze the hot-spot behavior of energetic materials, a better understanding the impact behavior of interfaces is important. It has been shown that by coating the binder-particle interface with a low-density polymer can considerably lower the shock sensitivity of energetic materials. Interface size and composition also depend on the type of matrix, particle, binding agent, mixing time, etc. One way to change the interface composition is to add a binding agent to the matrix-particle mixture. In this work, we study the effect of interface thickness on the impact behavior of a single particle HTPB-AP material. A power law viscoplastic constitutive model is used in the simulation which is obtained from a dynamic impact experiment. Stress-strain-strain rate data was fitted in order to obtain constitutive behavior of interfaces, particle, and matrix. The experiments were conducted with indenter of radius  $1\mu\text{m}$  on the interfaces with varying amount of binding agent Tepanol. Results show that interfacial properties are affected by the rate of loading and are also dependent upon the binding agent. Stress maps are obtained near the interface using In-situ Mechanical Raman Spectroscopy to analyze the changes in the stress distribution around interfaces for different loads till failure. The stress required for the delamination of the interface is called the interface strength. A bilinear cohesive zone model parameters were obtained from the consideration of local stress during failure and the cohesive energy required for delamination of AP from HTPB matrix. Effect of binding agent on the interface strength is found to be quite significant. The cohesive zone parameters and the viscoplastic model obtained from the experiment were then used in the cohesive finite element method to simulate the delamination between the matrix and the particle due to high-speed impact.

## Peridynamics Applied to Deformation and Damage Sensing in Polymer Bonded Explosive Materials

Naveen Prakash\*, Gary Seidel\*\*

\*Los Alamos National Laboratory, \*\*Virginia Tech

### ABSTRACT

Peridynamics, a recently developed non-local theory of continuum mechanics is gaining momentum as a novel method to model complex phenomena in solids such as the crack initiation, branching and propagation. The non-local nature of peridynamic equations allows one to overcome issues such as mesh dependent results and ill conditioned matrices. Peridynamic equations have also been extended to model multiphysics problems such as heat diffusion, coupled thermomechanics, fluid flow, corrosion among others. Polymer bonded explosives are complex materials susceptible to damage in low velocity impact events during transportation and handling, which can weaken the material in addition to the possibility of accidental ignition. Therefore to maintain reliability and efficacy, it is important to monitor in real time, the structural health of the material for safe transportation and handling [1]. It is proposed that dispersing carbon nanotubes within the binder phase will allow for in-situ structural health monitoring owing to the unique piezoresistive properties of nanocomposites [2]. In this work, a computational electromechanical framework based on peridynamics is used to investigate the strain and damage sensing properties of nanocomposite bonded explosive materials (NCBX) [3]. The peridynamics computational framework allows in capturing key deformation mechanisms like interface debonding and granular fracture which are important in assessing the piezoresistive response in the damage regime. The computational results presented in this work indicate that there is promise for in - situ monitoring of granular energetic materials based on the piezoresistive properties of nanocomposites which may prove to be advantageous over current methods. Some ongoing work with respect to including temperature effects, generating PBX/PBS microstructures and calibrating peridynamic model parameters will also be presented. Refs: 1. Han D K, Pecht M G, Anand D K and Kavetsky R 2007 Energetic material/systems prognostics Reliability and Maintainability Symposium, 2007. RAMS'07. Annual 59–64 (IEEE). 2. Sengezer, Engin C., and Gary D. Seidel. "Structural health monitoring of nanocomposite bonded energetic materials through piezoresistive response." *AIAA Journal* (2017): 1-14. 3. Prakash, Naveen, and Gary Don Seidel. "Effects of microscale damage evolution on piezoresistive sensing in nanocomposite bonded explosives under dynamic loading via electromechanical peridynamics." *Modelling and Simulation in Materials Science and Engineering* (2017).

## **A Configurational Energy Criterion Using Discrete Dislocation Plasticity for the Prediction of Fatigue Crack Nucleation Sites in Ni Superalloys**

Nikoletta Prastiti<sup>\*</sup>, Zebang Zheng<sup>\*\*</sup>, Fionn Dunne<sup>\*\*\*</sup>, Daniel Balint<sup>\*\*\*\*</sup>

<sup>\*</sup>Imperial College, <sup>\*\*</sup>Imperial College, <sup>\*\*\*</sup>Imperial College, <sup>\*\*\*\*</sup>Imperial College

### **ABSTRACT**

High-performance nickel-based superalloys commonly find application as safety critical rotatory components in the automotive, power and aerospace industries due to their exceptional mechanical properties. This kind of application involves cyclic loading and therefore, the dominating failure mechanism is fatigue. The stage of crack nucleation during fatigue may consume a considerable fraction of the life of an engineering component compared to that for crack propagation. In addition, the former is not as well understood, in the sense of obtaining useful quantitative predictions of safe component lifetimes and therefore leading to highly conservative and expensive safe-life component design. The key for accurate quantitative predictions lies in the mechanistic understanding of crack nucleation. A new stored energy criterion [1] that has been established and used within a crystal plasticity framework to predict the location of fatigue crack nucleation sites, has been reproduced in a more fundamental way using a discrete dislocation methodology [2] that explicitly represents the dislocations and dislocation pile ups in regions that could potentially act as fatigue crack nucleation sites. Integrated experimental, characterisation and computational crystal plasticity studies in Ni single and oligo crystals [3] were used for the critical appraisal of the new discrete dislocation approach which showed satisfactory qualitative agreement. References [1] Wan, V. V. C., D. W. MacLachlan, and F. P. E. Dunne. &quot;A stored energy criterion for fatigue crack nucleation in polycrystals.&quot; International Journal of Fatigue 68 (2014): 90-102. [2] Van der Giessen, Erik, and Alan Needleman. &quot;Discrete dislocation plasticity: a simple planar model.&quot; Modelling and Simulation in Materials Science and Engineering 3.5 (1995): 689. [3] Chen, Bo, Jun Jiang, and Fionn PE Dunne. &quot;Microstructurally-sensitive fatigue crack nucleation in Ni-based single and oligo crystals.&quot; Journal of the Mechanics and Physics of Solids 106 (2017): 15-33.

## The Mechanical Response and Failure of Al-TiB<sub>2</sub> Composites Produced by Spark Plasma Sintering: A Multi-Scale Computational Study

Elad Priel<sup>\*</sup>, Brigit Mittelman<sup>\*\*</sup>, Nir Trabelsi<sup>\*\*\*</sup>, Nissim Navi<sup>\*\*\*\*</sup>, Noa Bitton<sup>\*\*\*\*\*</sup>, Or Rahamim<sup>\*\*\*\*\*</sup>, Shlomo Haroush<sup>\*\*\*\*\*</sup>, Shmuel Hayun<sup>\*\*\*\*\*</sup>, Nachum Frage<sup>\*\*\*\*\*</sup>

<sup>\*</sup>Shamoon College of Engineering, <sup>\*\*</sup>Shamoon College of Engineering & NRCN, <sup>\*\*\*</sup>Shamoon College of Engineering, <sup>\*\*\*\*</sup>Shamoon College of Engineering & NRCN, <sup>\*\*\*\*\*</sup>NRCN, <sup>\*\*\*\*\*</sup>Ben-Gurion University of the Negev, <sup>\*\*\*\*\*</sup>NRCN, <sup>\*\*\*\*\*</sup>Ben-Gurion University of the Negev, <sup>\*\*\*\*\*</sup>Ben-Gurion University of the Negev

### ABSTRACT

Aluminum matrix composites (AMC) are highly attractive structural materials due to their high strength to weight ratio. Mechanical properties of AMC can be tailor made to suite a specific application, by controlling the particle volume fraction, size and distribution. A good control of these parameters can be achieved by using a powder metallurgy approach. In the present study, AMC specimens were fabricated by Spark Plasma Sintering (SPS) of a mixture of Al and TiB<sub>2</sub> powders with 0-15% volume fraction of TiB<sub>2</sub>. Uniaxial compression of cylindrical specimens and Small Punch Test (SPT) experiments were conducted to examine the mechanical response and failure modes of the composite in both compression and bi-axial tension loading modes. A multi-scale finite element framework was used to investigate the relation between the micro-structure and mechanical properties of the composites. First, macro-scale models were used in conjunction with the compression and SPT experiments to determine the effective constitutive response. Next, micro-scale models of representative volume elements (RVE&amp;amp;amp;amp;amp;apos;s) were constructed from Scanning Electron Microscopy (SEM) images of the sintered material. Computational homogenization methods were used to determine the effective properties derived from the micro-structure as well as to investigate failure modes within the micro-scale. Finally, the effective mechanical properties derived from the RVE computations were compared to the effective properties derived from the macro-scale analysis. This comparison provides insight on the role of particle-matrix interactions in the resulting effective mechanical properties and failure modes.

## **Determining Critical Scenarios of Porosity in the Fatigue Behavior of Additively Manufactured IN 718 via Crystal Plasticity**

Veerappan Prithvirajan\*, Michael Sangid\*\*

\*Purdue University, \*\*Purdue University

### **ABSTRACT**

Selective laser melting (SLM) can be used to fabricate components for aerospace applications, in order to realize several advantages that are well documented. However, prior to their use in safety critical components, the failure mechanisms have to be well understood, especially for the unique defects within SLM materials. The focus of our work is on the influence of porosity towards fatigue behavior of a Ni-based super alloy, IN 718, produced by SLM. A fatigue crack in a SLM IN718 microstructure may either initiate at a crystallographic feature (grain boundary, triple points, etc.) or at a pore, and this depends on multiple factors like grain attributes, grain neighbor interactions, pore size and pore interactions. In our work, a crystal plasticity based framework is developed to identify the critical porosity, which quantifies the scenarios of the crack initiating at the pore rather than the crystallographic features. 3D virtual microstructures are developed based on the characterization of SLM IN718 and are used as input to crystal plasticity finite element (CP-FE) simulations. Damage indicator parameters (DIPs) such as the plastic strain accumulation, elastic stress anisotropy, resolved shear stress and triaxiality, obtained from the CP-FE simulations are used to identify the most probable locations of crack initiation. Pores are added to the microstructure instantiations in a systematic manner by varying the size, location, and proximity between pores. The critical pore size is defined as the size beyond which the crack nucleation transitions from crystallographic features to the pore vicinity, which is determined to be 20 microns with respect to an average grain size of 48 microns . This work is beneficial in qualifying SLM materials given the natural porosity inherent to the manufacturing process, by reducing the number of fatigue experiments. Additionally, this study informs the choice of non-destructive evaluation methods and subsequent post-processing steps.

## Improving the Efficiency of a Surge Model via Adaptive Mesh Resolution

Jennifer Proft\*

\*The University of Texas at Austin

### ABSTRACT

Storm-induced waves and flooding can be predicted using the computational model ADCIRC+SWAN modeling system for storm surge applications such as mapping of floodplain flood risk and forecasting of storm surge and inundation. This modeling system has been shown to be efficient in parallel computing environments. It is implemented on static meshes and with a static parallelization, and thus it does not evolve as a storm approaches and inundates a coastal region. This implementation can be inefficient when large portions of the mesh remain dry during the simulation. We improve the parallel implementation of ADCIRC by using large-scale adaptivity, in which a mesh is refined by incorporating entire portions of another, higher-resolution mesh. Instead of subdividing an individual element, we will increase resolution by adding elements from a pre-existing mesh that has been well-validated. This technology will decrease the computational cost and better utilize the available resources. We show developed technologies to improve the efficiency of ADCIRC+SWAN simulations, thus allowing for more model runs in ensemble-based design applications, and for faster simulations in time-sensitive applications such as operational forecasting.

## **A Multi Level Moving Particles Method for Uncertainty Quantification and Reliability Analysis**

Carsten Proppe\*

\*Dept. of Engineering Mechanics, Karlsruhe Institute of Technology

### **ABSTRACT**

Markov Chain Monte Carlo simulation methods allow estimating small failure probabilities efficiently, even for problems that involve a high-dimensional vector of input random variables. Subset simulation can be considered as the most prominent method in this class. In subset simulation, the failure probability is computed as the telescoping product of larger probabilities that require sampling from conditional distributions. Recently, a generalization of subset simulation in the sense of particle methods has been proposed [1], where a threshold is associated to each sample, samples are moved to new positions in the design space and the number of moves for the initial samples to reach the failure region are counted and yield an estimator for the failure probability, which is of comparable accuracy and efficiency as the subset simulation estimator. The algorithm allows for an easy parallel implementation. Just as for subset simulation, sampling from conditional distributions is required when moving a particle. In most practical applications, the limit state function is approximated numerically to a certain level  $h$ . In order to obtain an efficient simulation algorithm, it is necessary to balance the statistical error and the numerical error. In this presentation, we propose a multi level moving particles simulation method that balances both errors by computing a telescoping sum of estimates for the number of moves. For each term in the telescoping sum, it is necessary to compute as corrector the difference of the number of moves for each initial sample with two consecutive accuracy levels using the same random numbers in the Markov Chain Monte Carlo simulation. For the multi level moving particles method, the sample variance decreases with decreasing numerical error. Thus, the number of samples that has to be evaluated with high accuracy is reduced compared to a single level computation. Therefore, the proposed algorithm is very efficient for problems where highly accurate evaluations of the limit state function are necessary and require a tremendous computational effort. References: [1] C. Walter: "Moving particles: A parallel optimal Multilevel Splitting method with application in quantiles estimation and meta-model based algorithms". In: Structural Safety 55 (2015), pp. 10–25.

## Goal-oriented Formulation of Boundary-value Problems for Accurate Estimation of Quantities of Interest

Serge Prudhomme<sup>\*</sup>, Kenan Kergrene<sup>\*\*</sup>, Marc Laforest<sup>\*\*\*</sup>, Ludovic Chamoin<sup>\*\*\*\*</sup>

<sup>\*</sup>École Polytechnique Montréal, <sup>\*\*</sup>École Polytechnique Montréal, <sup>\*\*\*</sup>École Polytechnique Montréal, <sup>\*\*\*\*</sup>École Normale Supérieure de Paris-Saclay

### ABSTRACT

We will present in this talk a mathematical formulation of boundary-value problems aiming at constructing finite element or model reduction approximations for accurate estimation of quantities of interest. The main idea is to reformulate a boundary-value problem as a minimization problem that involves inequality constraints on the error in the goal functional so that the resulting model is capable of delivering quantities of interest within some prescribed tolerance. Chaudhry et al. [1] have proposed a similar method in which constraints are imposed via a penalization approach. However, an issue with that approach is concerned with the selection of suitable penalization parameters. Our goal in this work aims at circumventing this difficulty by enforcing the inequality constraints through Lagrange multipliers [2]. We will also show how to design an adaptive strategy to construct adapted meshes based on a posteriori error estimates. Such a paradigm represents a departure from classical goal-oriented approaches in which one computes first the finite element solution and then adapts the mesh by controlling the error with respect to quantities of interest using dual-based error estimates. The proposed formulation will be extended to the construction of reduced models using the so-called proper generalized decomposition (or low-rank approximation) method. Numerical examples will be presented in order to demonstrate the efficiency of the approach. References: [1] J.H. Chaudhry, E.C. Cyr, K. Liu, T.A. Manteuffel, L.N. Olson, L. Tang, Enhancing least-squares finite element methods through a quantity-of-interest, *SIAM J. Numer. Anal.* 52 (6), 3085–3105 (2014). [2] K. Kergrene, S. Prudhomme, L. Chamoin, M. Laforest, A new goal-oriented formulation of the finite element method, *Comput. Methods Appl. Mech. Engrg.* 327, 256–276 (2017).

## Soil-structure Interaction in Masonry Arch Bridges: A Hybrid Approach

Bora Pulatsu<sup>\*</sup>, Ece Erdogmus<sup>\*\*</sup>, Paulo B. Lourenço<sup>\*\*\*</sup>

<sup>\*</sup>PhD Candidate, <sup>\*\*</sup>Professor, <sup>\*\*\*</sup>Professor

### ABSTRACT

Masonry structures constitute a large portion of the architectural heritage, transportation system and residential buildings all around the world. Therefore, understanding their structural behavior has a crucial role in avoiding excessive amount of interventions and preserving the historical characteristics of those structures. However, it has been a challenge for engineers to analyze masonry structures, due to its composite and highly non-linear nature. This problem becomes even more complicated in masonry arch bridges when soil-masonry interaction is considered to capture structural behavior. In present research, up-to-date numerical modeling strategies are combined, so called discrete and finite element methods in the framework of discrete element modeling (DEM), in which equations of motions are solved by an explicit finite-difference method. To achieve that, masonry units are modeled as distinct blocks, which interact along their boundaries, whereas backfill material is considered as a continuous medium consisting of tetrahedral finite elements. There is no mortar assumed to replicate dry-joint masonry which has zero cohesion and tensile strength at the joints. The contact forces are calculated depending on the stiffness and amount of inter-penetration between blocks. The goal of this study is to demonstrate the interaction between backfill and masonry under static loads in three-dimensions, including development of damage and crack propagation. In this context, a published experimental study is utilized to validate proposed methodology. Further, the influence of the constitutive properties of contact parameters such as normal stiffness, shear stiffness, cohesion and friction angle, are investigated by sensitivity analysis. The results of the analysis indicated that presented approach captures soil-structure interaction and provides insight into the masonry arch bridge behavior by taking the advantage of both computational methods.

## Trimming Methods in Isogeometric Analysis

Riccardo Puppi<sup>\*</sup>, Annalisa Buffa<sup>\*\*</sup>, Rafael Vazquez Hernandez<sup>\*\*\*</sup>

<sup>\*</sup>EPFL, <sup>\*\*</sup>EPFL, <sup>\*\*\*</sup>EPFL

### ABSTRACT

Trimming is one of the most fundamental tools in Computer Aided Design (CAD) that allows the construction of complex geometries. At the same time it constitutes a source of difficulty in the interplay between CAD and the numerical analysis of PDEs. When the superfluous surface areas are cut away, the visualization of the resulting surface changes, but its mathematical description remains unchanged. It turns out that we have to deal with elements unfitted with the boundary, making the research for efficient quadrature rules and the imposition of boundary conditions a challenge. Moreover there are basis functions, whose support has been cut, affecting the conditioning of the related linear system. In this regard, ideas from the Cut-FEM literature come to help. For the sake of simplicity and in order to be able to provide rigorous mathematical proofs, we confine our attention to the Laplace equation. In particular we study methods based on a modification of the weak form, e.g. Nitsche's method, enriched with suitable stabilizations. We present a stabilized method which delivers optimal accuracy and is parameter free. This stabilization needs to be coupled with ad-hoc preconditioners to restore good condition numbers of the underlying systems. Finally, numerical tests in the Matlab code GeoPDEs (<http://rafavzqz.github.io/geopdes/>) are provided to confirm our theoretical results. [1] Erik Burman. Ghost penalty. *Comptes Rendus Mathématique*, 348 (21), pp. 1217-1220, 2010. [2] Jaroslav Haslinger and Yves Renard A New Fictitious Domain Approach Inspired by the Extended Finite Element Method. *SIAM Journal on Numerical Analysis*, 47 (2), pp. 1474-1499, 2009.

## Investigation in Stable Symmetric or Two-pass Contact Algorithms

Michael Puso<sup>\*</sup>, Jerome Solberg<sup>\*\*</sup>

<sup>\*</sup>Lawrence Livermore National Laboratory, <sup>\*\*</sup>Lawrence Livermore National Laboratory

### ABSTRACT

It's become common practice to apply the mortar contact approach in production applications due to its robustness and its recent appearance in most of the major commercial code applications. It is typically the clear choice when a single-pass (slave-master) contact algorithm is tractable. Of course, there are many situations where it becomes less attractive, particular when self-contact can occur. For most commercial codes, the only consistent schemes available would be the penalized two-pass mortar scheme or deprecated Lagrange multiplier constraint scheme. Potential approaches for stable symmetric algorithms are few. One method approaches the self-contact problem using the single-pass contact approach augmented with a binary tree that attempts to choose unique (nodal) contact pairs to avoid redundancy [1]. Lately, the Nitsche approach as in [e.g. 2] has been given more attention although it is not clear how this would perform in an explicit finite element setting. Here we present a stabilized two-pass mortar scheme and evaluate its performance against the canonical single-pass method. Comparison to other symmetric approaches along with potential techniques to alleviate computational cost will also be discussed. [1] B Yang, TA Laursen, "A large deformation mortar formulation of self-contact with finite sliding", Computer Methods in Applied Mechanics and Engineering, 198 (47), 3656-3669, (2009) [2] R Mlika, Y Renard, F Chouly, "An unbiased Nitsche's formulation of large deformation frictional contact and self-contact". ", Computer Methods in Applied Mechanics and Engineering, 325 (1), 265-288, (2017).

## Multiphysics Problems for Viscoelastic Contact Mechanics

Carmine Putignano\*, Giuseppe Carbone\*\*

\*Politecnico di Bari, \*\*Politecnico di Bari

### ABSTRACT

Lubrication between soft viscoelastic solids has crucial peculiarities that only very recently have started to be investigated by the lubrication science community. Indeed, in the last decades, massive research efforts have been dedicated to understand the role of non-Newtonian lubricants, but very little has been done to get what occurs when the lubricated solids are not linearly elastic, but exhibit a different rheology. However, such a topic is acquiring an increasingly marked prominence: all the biological cases, where the so-called soft lubrication occurs, are only examples of situations where the solids into contact cannot be considered linearly elastic. This work contains an innovative numerical methodology to assess the lubrication regime occurring between a rigid sphere and a linear viscoelastic layer. In detail, an explicit finite difference scheme is coupled to a Boundary Element solver in order to study the viscoelastic lubrication without any limitation in terms of material properties, geometry and viscosity. The results and, specifically, the film thickness, the contact pressure and, ultimately, the friction force show marked differences in comparison with classic lubrication theory. Indeed, we observe that the film thickness minimum moves from the flow outlet to the inlet, where consistently we found a maximum for the fluid pressure. This can be explained only accounting for the actual viscoelastic rheology of the contacting bodies. Finally, we notice that such results have been validated by means of experiments specifically developed to deal with soft matter.

## Algebraic Decomposition as a Variance Reduction and Multiscale Coupling Technique

Jean-Philippe Péraud\*, Nicolas Hadjiconstantinou\*\*

\*Corning Incorporated, \*\*Massachusetts Institute of Technology

### ABSTRACT

Stochastic particle methods, such as direct Monte Carlo simulations, are very well suited to the solution of kinetic equations because they lend themselves to intuitive simulation methods that handle the advection process elegantly and require no grid-based discretization. For problems characterized by small deviations from equilibrium, which are very common, if not prevalent, at the nanoscale (e.g. small Mach number flow), computational savings of several orders of magnitude (4 to 8 depending on the problem [1]) can be achieved by simulating only the deviation from the nearby equilibrium state [1, 2]. This algebraic decomposition of the distribution function into an equilibrium and a non-equilibrium part can be viewed as a control-variate variance-reduction technique, in which the (large) uncertainty associated with the evaluation of the equilibrium part of the distribution function is removed with no approximation. The remaining uncertainty, associated with the (small) non-equilibrium part of the distribution, scales with the signal, leading to a constant signal to noise ratio and a method that can capture arbitrarily small deviations from equilibrium at constant cost. [1] In other words, deviational Monte Carlo methods use significantly fewer computational particles for the same resolution, or alternatively, provide significantly improved resolution, compared to traditional Monte Carlo methods for the same computational cost. In fact, by limiting the use of computational resources to regions where deviations from a known state occur, these methods function as hybrid multiscale methods which employ different descriptions in different regions of the computational domain in order to reduce the computational cost associated with multiscale problems [1,2]. Deviational methods will be presented and discussed using examples from both nanoscale gas flow and solid-state heat transfer. For the case of phonon transport, we show that additional computational savings can be obtained by using a kinetic-type of Monte Carlo simulation with no time discretization [3]. We will also discuss adjoint methods for further accelerating problems which require fine resolution in small regions of phase space [3]. References: [1] Péraud, J-P. M. and N.G. Hadjiconstantinou, "Efficient Simulation of Multidimensional Phonon Transport Using Energy-based Variance-reduced Formulations," *Physical Review B*, 84, 205331, 2011. [2] Radtke, G.A., J-P. M. Péraud and N.G. Hadjiconstantinou, "On Efficient Simulations of Multiscale Kinetic Transport," *Philosophical Transactions of the Royal Society A*, 371, 20120182, 2013. [3] Péraud, J-P.M., C.D. Landon, and N.G. Hadjiconstantinou, "Monte Carlo Methods for Solving the Boltzmann Transport Equation," *Annual Reviews of Heat Transfer*, 17, 205-265, 2014.

## Phase-field Modeling for Crack Propagation in Bio-inspired Composites

heeyeong jeong\*

\*Korea Advanced Institute of Science and Technology

### ABSTRACT

In nature highly stiff and highly tough materials are found in living organism's body due to evolution in harsh environment. Such materials have less stress concentration near crack tips even when cracks exist in the material. Also their crack paths are lengthened by deflection, which increases the toughness of material. Here, crack phase-field modeling was utilized to investigate behavior of cracks in bio-material. crack phase-field simulation can model crack propagation in bio-material more properly than previous crack propagation simulation. Through crack phase-field modeling, we found that high toughness of bio-material can be achieved by difference between young's modulus within material. we investigated staggered plates structure in nacre and structure of haverisan system in bone. toughness increase was observed in both structures.

## **Study of Vibration Analysis of Automotive Seating Seat**

heeyong jung\*

\*Hyundai-dyamos

### **ABSTRACT**

The purpose of this study is to develop of vibration analysis of automotive seating seat. In the paper, test results show that variation of natural frequency according to the conditions of frame, seat assembly and seating. Using the test results and FE dummy, it made a finite element model similar test results. Also the equivalent FE model was developed for the FE dummy to reduce the analysis time. Topics of interest include, but are not limited to: - Vibration analysis of automotive seating seat - Equivalent model - Reduced analysis time

## A Parallel Shared-Memory Implementation of an Overlay Grid Method

nicolas le goff\*, franck ledoux\*\*, jean-christophe janodet\*\*\*

\*Commissariat à l'énergie atomique et aux énergies alternatives, \*\*Commissariat à l'énergie atomique et aux énergies alternatives, \*\*\*Université d'Évry-Val-d'Essonne

### ABSTRACT

Some overlay grid methods [OW08] take a cartesian grid or an adaptively refined grid carrying materials volume fraction data as an input and produce an unstructured mesh with pure cells as an output. This can be used in particular when the geometry is not explicitly known, or in an intercode context where two simulation codes are executed one after the other, the first one providing the data needed to build the input of the second one. We have implemented an overlay grid method that relies on the Bulk-Synchronous Parallelism (BSP) model and a threadsafe mesh data structure. By adopting a BSP, parallel regions are gathered in steps where data consistency must then be ensured at the beginning and the end of each step. In our mesh data structure, a basic set of operations such as mesh entity creation and destruction is designed with threadsafe properties, while data races still have to be managed by the developer. We extended our data structure GMDS [FL08], a C++ Generic Mesh Data Structure that allows the developer to select the mesh entities and connectivities his algorithm requires on-the-fly, using the Kokkos [Ko] programming model and its containers in order to provide the needed threadsafe functionalities. The performance and scalability of our implementation were measured on the Haswell processor as well as the Xeon Phi manycore architecture for several examples. [OW08] S. Owen, M. Staten and M. Sorensen. Parallel Hex Meshing from Volume Fractions. 17th International Meshing Roundtable (2008) [FL08] F. Ledoux, J.-C. Weill and Y. Bertrand. GMDS: a Generic Mesh Data Structure. 17th International Meshing Roundtable (2008) [Ko] <https://github.com/kokkos>

## Minimising Stress Concentration around the Voids by Location Optimisation

dedao liu<sup>\*</sup>, Louis N. S. Chiu<sup>\*\*</sup>, Chris Davies<sup>\*\*\*</sup>, wenyi yan<sup>\*\*\*\*</sup>

<sup>\*</sup>Monash University, <sup>\*\*</sup>Monash University, <sup>\*\*\*</sup>Monash University, <sup>\*\*\*\*</sup>Monash University

### ABSTRACT

Structural optimisation has experienced fast development during the past decades. It plays a vital role in component designs. Three major aspects, size optimisation, shape optimisation and topology optimisation are included in structural optimisation. The three aspects correspond to the size, shape, and topology of design features. However, it should be noted that in between shape and topology, the location information of design feature has not been clearly stated. For a design feature with given shape and size, its location can be defined as the location of its characteristic point, such as its centroid. The location of design feature also has a significant effect on the stress distribution in the component. And such "location optimisation" is believed to be useful especially in additive manufacturing. In traditional manufacturing, a component's complexity is usually constrained by the accessibility of tools in processes including cutting, drilling etc. In additive manufacturing, however, this kind of constraints can be removed and it's much easier to build complex features such as internal voids to reduce the component weight. The locations of these internal voids need to be optimised to minimise stress concentration. A random search method with hill-climbing algorithm has been used to solve this "location optimisation" problem in this paper. Case studies have achieved stress minimization via such "location optimisation".

## Effect of the Clamping Force on Stress Redistribution for a CFRP Interference-fit Bolted Joint

ping liu<sup>\*</sup>, kaifu zhang<sup>\*\*</sup>, yuanxin duan<sup>\*\*\*</sup>

<sup>\*</sup>NWPU IN CHINA, <sup>\*\*</sup>NWPU IN CHINA, <sup>\*\*\*</sup>NWPU IN CHINA

### ABSTRACT

Carbon fiber reinforced polymer (CFRP) composites as a typical kind of multilayers material have widely been applied on the primary structure of airplanes due to the relentless pursuit of the lighter weight and higher performance. The joint is often the weakest area in a composite structure and the bolted joint. Compressive residual stresses induced by interference-fit installation can reduce the effective hoop stress in the vicinity of the fastener hole and cause significant improvement in fatigue life of the composite joints. The clamping force along the axial direction produced by the nut and bolt head screw in assembly process, which has a significant influence on the strength of the composite structure. In the interference-fit installation process, the effect of the clamping force combining with the interference compressive force, the stress will redistribution for the composite bolted joints after the nut fastening stage. In this paper, the theoretical model of the stress distribution in the vicinity of the hole was established based on the consideration of the interference-fit amount and the clamping force. The influence of the change of the interference amount and the clamping force on the stress redistribution was studied by combining the results of the finite element simulation. Through these analyses, the following conclusions can be drawn. ? Quadratic function distribution model of the axial compressive stress in the clamping region was constructed by the hydrodynamic semi-inverse method. The compressive stress has a maximum value at the boundary of the whole wall, and then the value decreases gently to zero at the boundary of the clamping area. The amplitude and range were related to clamping force, taper angle, effective extrusion ratio coefficient and so on. ? The equivalent transformation equation of the axial compressive deformation for the perimeter of the hole was deduced based on the equivalent anisotropy of the composite material. And the radial stress distribution equation around the hole was established taking the amount of interference-fit and clamping force into account. ? Comparing the results of finite element simulation with theoretical calculation, the validity of the analytical model was verified. The influence of the interference-fit amount and clamping force on the stress distribution were analyzed. It is found that when the small interference-fit amount and big pre-tightening force occurs, stress distribution appears &quot;peak shift&quot;, that is, the wave crests/troughs deviates from coordinate axis and move closer to the middle.

## First Principle Based Multi-scale Modeling to Predict Bondline Strength of Co-cured Composite-metal Joints

xianfeng ma<sup>\*</sup>, Bozhi Heng<sup>\*\*</sup>, Stephanie TerMaath<sup>\*\*\*</sup>

<sup>\*</sup>The University of Tennessee, Knoxville, <sup>\*\*</sup>The University of Tennessee, Knoxville, <sup>\*\*\*</sup>The University of Tennessee, Knoxville

### ABSTRACT

Compared to traditional composite-metal joints such as bolts or rivets that usually cause unacceptable damage in hybrid structure design, the emerging co-cured composite-metal joints are attractive as they avoid damage to load bearing fibers, reduce stress concentrations in substrates, and thus are less prone to fatigue and do not suffer from the manufacturing pitfalls associated with fabrication of bolted joints. [1] However, evaluating the damage propagation and potential joint failure of co-cured composite-metal joints has been challenging since the bondline failure is non-visible and difficult to detect. [2,3] Therefore, improved understanding of the bondline physics is critical to resulting desired structural performance and reliable inspection schedules for bondline damage. In this work, we present our effort to integrate quantum-mechanical based calculation and microscale simulation to develop a first principle based multi-scale modeling framework for understanding the bondline behavior of co-cured composite-metal joints. Electronic and atomic structure calculations within the formulation of density functional theory (DFT) are performed to determine the equilibrium structure and properties (lattice constants, bulk/shear moduli, and elastic constants) of each component in the joint systems. [4] Based on the obtained material constants, the microscale level study on the bondline strength is carried out through peridynamics theory, [5] a theory of mechanics that extends classical continuum solid mechanic to include discrete particles and growing cracks. We demonstrated the capability of our approach through the Aluminum substrates co-cured to E-glass/Epoxy composite joints system, where we established the correlation between the composite layer structures and the corresponding bondline behavior for the joints under service loading like bending, uniaxial tension, and low velocity impact. The approach enables us to discover the optimal design parameters of the composite-metal co-cured joints with maximum performance. References: [1] S. A. Ucsnik and G. Kirov, Mater. Sci. Forum 690, 465 (2011). [2] B. Heng and S. C. TerMaath, AIAA SciTech Forum, 2018. [3] T. J. Truster and A. Masud, Comput. Mech. 52, 499 (2013). [4] X. Ma and H. Xin, Phys. Rev. Lett. 118, 36101 (2017). [5] S. A. Silling and R. B. Lehoucq, Adv. Appl. Mech. 44, 73 (2010).

## **Macro-zone Size Effect in Polycrital Alloys Compute with FFT-based Crystal Elastic-Visco-Platic Simulations of Structured Polycrystal**

Azdine nait-ali\*, Samuel Hémery\*\*

\*Institut Pprime, \*\*Institut Pprime

### **ABSTRACT**

In this study, we want to define the effects of the "crystal microstructure" of the deformation and plasticity mechanisms of Titanium alloys. Numerical modeling of the elastic stress field in a real Ti-6Al-4V microstructure was performed using the FFT technique. We have observed a strong influence of the microstructure gradient on the mechanical fields and therefore on the critical stress of the solved shear stress (CRSS). In a first study, we simulate a virtual aggregate while maintaining the morphology of the grains of the initial material and especially of the same structure . Conservation of the grains morphology in order to separate the effects of the morphology of the effects of the crystallographic orientations. The 3D calculations based on FFT allowed us to estimate an influence distance of the macrozone. We highlight the influence of the texture of local crystals, as well as the effect of the "real" macrozone present in the study material. A second study, we try to highlight the influence of the morphology of the macrozone on the mechanical fields and on the CRSS. We modify the size (volume) by creating a spherical macrozone, and varying the orientation of the ellipsoid. This information aims to highlight an effect of macrozone too often overlooked in the literature, is based on a house code of the elastic-visco-plate model based on FFT.